Materials Science
of Synthetic Membranes

Materials Science
of Synthetic Membranes

Douglas R. Lloyd, EDITOR

The University of Texas at Austin

Based on a symposium sponsored by
the Division of Polymeric Materials
Science and Engineering
at the 187th Meeting
of the American Chemical Society,
St. Louis, Missouri, April 9–11, 1984

ACS Symposium Series

M. Joan Comstock, *Series Editor*

Advisory Board

FOREWORD

The ACS SYMPOSIUM SERIES was founded in 1974 to provide
a medium for publishing symposia quickly in book form. The
format of the Series parallels that of the continuing ADVANCES
IN CHEMISTRY SERIES except that in order to save time the
papers are not typeset but are reproduced as they are sub-
mitted by the authors in camera-ready form. Papers are re-
viewed under the supervision of the Editors with the assistance
of the Series Advisory Board and are selected to maintain the
integrity of the symposia; however, verbatim reproductions of
previously published papers are not accepted. Both reviews
and reports of research are acceptable since symposia may
embrace both types of presentation.

PREFACE

MEMBRANE SCIENCE has recently received considerable attention. Membranes for industrial separations, therapeutic medical applications, and controlled release, as well as membrane barriers for packaging, have all moved from the laboratory bench to the world of commerce. Forecasts call for additional applications and expanded markets in the future. However, for membranes to proceed beyond the present level of success, further advances must be made in the materials science of membranes. The objective of this book is to compile state-of-the-art reviews of several aspects of the materials science of synthetic membranes. It is hoped that this compilation will serve as a useful reference regarding past and present developments, and that it will provide the impetus for future advances in membrane materials science.

The 21 chapters that comprise this volume were contributed upon the invitation of the editor. Prior to publication, the manuscripts were subjected to peer review and revised accordingly. This volume is the product of considerable effort on the part of the authors, the reviewers, my editorial assistant Robert Fabrize, Robin Giroux of the American Chemical Society Books Department, and Betty Friedrich who typed six chapters. To each of these people I express my deepest gratitude. I also wish to thank Eric Lee for his assistance in organizing the symposium and for chairing two of the four sessions.

This book is dedicated to my past, present, and future graduate students; it is my pleasure to be associated with these fine people. Finally, but above all, this book is dedicated to my wife Linda, in appreciation of her patience and encouragement.

DOUGLAS R. LLOYD
The University of Texas at Austin
Austin, TX 78712

August 1984

ix

Membrane Materials Science

An Overview

DOUGLAS R. LLOYD

Department of Chemical Engineering, Separations Research Program, Center for Polymer Research, The University of Texas at Austin, Austin, TX 78712

Material science aspects of synthetic polymeric membranes are presented in this survey. The objective is to place each of the subsequent chapters of this volume into proper perspective. Therefore, frequent reference is made to the accompanying chapters and, where necessary, to alternative information sources. By way of introduction, this chapter considers in turn: material selection, material characterization and evaluation, membrane preparation, membrane characterization and membrane evaluation. Membrane module design and manufacture, transport phenomena and process performance are introduced in the discussion only as they pertain to membrane materials science. Following this introduction, the various chapters of this volume are previewed.

Membrane science is a phrase that encompasses a vast array of topics (1). The common thread that ties together the various aspects of membrane science is that each one deals to some extent with *the study of permeation and permeable media.* More specifically, the permeable medium or *membrane is a phase* between two phases. The role of the membrane may be either to change the composition of a solution on the basis of relative permeation rates (membrane separation processes), to physically or chemically modify the permeating species (ion-exchange membranes and biofunctional membranes), to conduct electric current, to prevent permeation (packaging and coating) or to regulate the rate of permeation (controlled release). Functionally, membranes may be either *passive* or *reactive* depending upon the membrane's ability to alter the chemical nature of the permeating species. Membranes can also be categorized as being either *neutral* or *charged* according to their ionic nature. Structurally, membranes can be categorized as being either *non-porous* (that is, membranes in which the membrane phase is continuous, such as dense polymeric films and liquid

membranes) or *porous* to various extents (for example, porous
polymeric films in which both the polymer matrix and the void
spaces are continuous. Further categorization according to the
porous structure of these co-continuous membranes is discussed
below under the heading "Membrane Preparation"). The various
chapters in this book discuss the materials science of synthetic
polymeric membranes for separations, conductive membranes and
reactive membranes.

     Membrane performance is often measured by the ability of the
membrane to prevent, regulate or facilitate permeation. The rate
of permeation and the mechanism of transport depend upon the
magnitude of the driving force, the size of the permeating molecule
relative to the size of the available permanent or dynamic
transport corridor and the chemical nature (dispersive, polar,
ionic, etc.) of both the permeant and the polymeric membrane
material.

     Membrane science can arbitrarily be divided into seven
intimately related categories: material selection, material
characterization and evaluation, membrane preparation, membrane
characterization and evaluation, transport phenomena, membrane
module design and process performance. This chapter and those to
follow emphasize the materials science aspects of synthetic
polymeric membranes; that is, the selection, characterization and
evaluation of membrane materials as well as the preparation,
characterization and evaluation of membranes. Transport phenomena,
membrane module design and process performance enter the discussion
only as these topics pertain to materials science.

Material Selection. In designing a membrane, one must first
determine the physicochemical nature of the permeants (gas, vapor,
liquid, solid; dispersive, polar, ionic; reactive, inert; physical
size and shape). The membrane scientist then has *two
materials science controls* over permeation: *membrane material
selection* and *membrane preparation procedures*. Membrane material
selection allows control over the nature and magnitude of the
permeant-membrane physicochemical interactions. Choice of membrane
material also determines the packing density and segment mobility
of the polymer chains which comprise the solid regions of the
membrane. Membrane preparation procedures determine membrane
morphology and the extent to which physical considerations, such as
steric hindrance, influence the rate of permeation. Together,
material selection and membrane preparation procedures influence
the mechanism of transport, membrane stability and membrane
performance.

     In the past, membrane material selection for gas separations
(2) and liquid separations has often followed either an Edisonian
or a common sense approach. For example, almost every polymer that
can be formed into a film has been characterized in terms of gas
permeability (at least for a few common gases). In this volume,
Chern et al. (3) and Lloyd and Meluch (4) discuss membrane material
selection in terms of physicochemical interactions for gas mixture
separations and liquid mixture separations, respectively. Hoehn
(5) presents similar arguments for membrane material selection in
general. In comparison to the wide variety of polymers investigated

for their gas transport properties, the number of polymers studied
for their liquid transport properties is somewhat limited. However,
a survey of recent literature and patents (4) indicates that an
ever-increasing number of polymers, copolymers and blends are being
considered as potential membrane materials for liquid mixture
separations. It is interesting to compare the number of materials
which have reached commercialization for liquid separations and gas
separations. Lloyd and Meluch (4) list in excess of twenty-seven
polymers, copolymers and blends currently being used for liquid
separation membranes. However, only polysulfone and a variety of
cellulose acetates and silicone based polymers have attained
commercial success for gas mixture separations (6).

In addition to the guidelines suggested by Chern et al. (3)
and by Lloyd and Meluch (4), Ward et al. (7) point out that
biocompatibility and sterilizability need to be considered when
selecting membrane materials for therapeutic applications.

Each of these chapters (3-7), plus the chapter by Cadotte (8),
demonstrates that one can molecularly engineer polymer chemical
structures to obtain membrane materials which theoretically can
achieve the desired control over permeability. Alternatively,
the ideas developed (3-5) can simply serve as criteria by which one
can select, from a list of available polymers, those membrane
materials with the greatest potential for achieving the desired
control over permeability.

Material Characterization and Evaluation. Physicochemical
considerations can be useful in membrane material selection.
However, it would be beneficial if one could experimentally verify
that the proper choice has been made prior to undertaking the often
difficult tasks of membrane preparation and characterization. In
addition, it is frequently beneficial to have fully characterized
the polymer prior to forming the membrane.

In this context, *material characterization* refers to obtaining
information related to the intrinsic properties of the polymer
rather than structural or physical properties of the membrane which
is to be subsequently formed from the polymer. It is often useful
to characterize the polymer in terms of the following: molecular
architecture or bulk properties (molecular weight characteristics,
degree of branching, chemical functionality and, if necessary,
copolymer or blend composition), polymer solution properties
(polymer swellability, polymer solubility and solution viscosities),
thermal properties (glass transition temperature and crystal melting
temperature), chemical stability and, if appropriate,
biocompatibility. Physical properties of the polymers, such as
mechanical strength and extent of crystallization, often depend
upon sample preparation procedures and are ultimately reflected in
the properties of the membrane. As such, they are discussed below
under the heading of Membrane Characterization and Evaluation.

Lloyd and Meluch (4) summarize several methods of evaluating
potential membrane materials for liquid separations without
actually preparing membranes. They point out that once a membrane
or film has been formed, it is often difficult to distinguish the
intrinsic properties of the polymer from the structural
characteristics of the membrane, which are themselves dependent

upon preparation procedures. Therefore, they emphasize those
methods which characterize membrane materials in terms of their
physicochemical interactions with small molecules, without
requiring the formation of membranes or dense films. Similar
procedures (for example, inverse gas chromatography) can be used to
characterize the physicochemical interactions which occur during
gas and vapor transport.

Membrane Preparation. The ability of a membrane to regulate
permeation lies not only in the selection of an appropriate
membrane material, but also in the physical structure of the
membrane. The physical structure and the physical properties of a
membrane can be directly related to membrane preparation procedures.
     Depending upon the membrane preparation procedure and based on
information obtained from membrane characterization, membranes are
often classified as having one of the following structures:
     (i) *Non-porous, Dense or Homogeneous.* These membranes consist
of closely packed polymer chains with a uniform, continuous packing
density throughout the system. The void spaces between
macromolecules, and thus the corridors for transport, are beyond
the current level of optical and electron microscopic resolution.
Transport through these intersticial spaces is often discussed in
terms of dynamic free volume and energy requirements for polymer
segmental motion. That is, the transport mechanism is considered
to be one of dissolution in the "liquid" or "swollen" membrane
phase and diffusion down the chemical potential gradient.
The properties of dense films are often equated with the intrinsic
properties of the bulk polymer. However, this comparison must be
made with caution because chain packing, and thus transport
properties, may be dependent upon thermal history or solution
history during film preparation and upon the attainment of
equilibrium prior to characterization. Dense films can be prepared
by melt extrusion, compression molding or solution casting.
     (ii) *Porous or Heterogeneous.* In contrast to the dense membranes
in which the polymer forms essentially a continuous phase, porous
membranes are comprised of co-continuous phases of polymer and
interconnecting voids that serve as transport corridors. Depending
on the size of the voids and the interactions which occur during
transport, the mechanism of transport may be considered as one of
convection, diffusion or a combination of these mechanisms. The
size and distribution of these voids vary with membrane preparation
procedure and are somewhat arbitrarily distinguished as *finely
porous, microporous* and *macroporous.* Alternatively (9), the terms
ultragel and *microgel* have been suggested to indicate membranes of
different pore size; "ultra" indicating smaller pores (0.1-0.5 μm),
"micro" indicating larger pores (1-2 μm). The exact pore size or
range of pore sizes that are described by these various terms are
poorly defined and differ from author to author. Porous membranes
may be *symmetric* (that is, uniformly porous throughout the
structure), *anisotropic* (that is, pore size varies continuously in
one direction) or *skinned.* In this review, the terms *skinned* and
asymmetric are used interchangeably to describe membranes which
consists of a *thin, relatively dense layer* supported by a
porous support layer. Symmetrically porous membranes often retain

solutes and suspended matter within the membrane structure; thus,
the term depth filter is used to describe these membranes. On the
other hand, highly anisotropic and skinned membranes reject solutes
and suspended matter at the surface; thereby avoiding membrane
clogging or blinding problems. Consequently, skinned, and to a
lesser extent anisotropic, membranes have become the membranes of
choice for liquid phase and gas phase separations.
    Since permeation is inversely related to membrane thickness,
the advantage of the skinned membrane over the homogeneous membrane
lies in the extreme thinness of the skin (typically < 1.0 μm), and
thus the ability to achieve high fluxes without any loss in
selectivity. Whether the skin layer of a membrane is dense or
finely porous often depends on the method of membrane preparation.
Skin layers deposited from solution or plasma onto a porous support
(8,10), especially those intended for gas separations, are probably
homogeneous. Skin layers resulting from phase inversion processes
(9,11,12) may be finely porous or dense, depending upon casting
solution composition, casting conditions and post-formation thermal
or chemical treatments. The presence or absence of pores,
especially below the level of electron microscope resolution,
continues to be a point of debate. Regardless of origin or
structure, it is this skin which exerts the greatest influence over
the permeation properties of the membrane. The skin and the porous
support layer may be comprised of the same material and produced in
one casting operation. In this case, the asymmetric membrane may
be referred to as an *integrally-skinned microgel* or an *integrally-
skinned ultragel* depending on the size of the pores in the support
layer. Alternatively, the skin and the support may be comprised of
different materials and produced in separate steps. These
nonintegrally-skinned structures are referred to as *composite
membranes* (8) or *dynamic membranes* (10) depending on the method by
which and the time at which the skin is deposited on the support
layer. Porous and asymmetric membranes are typically produced via
a *phase inversion* process (9,11-13). The asymmetry and *porosity*
(that is, *pore size, pore size distribution* and *pore volume*)
of the final solidified gel are directly related to the structure
of the metastable "solution" immediately prior to gelation
(6,9,11-13).
    Often a post-formation treatment is used to improve membrane
performance characteristics by physically or chemically modifying
the membrane (6,9,11). One example of a physical modification is
the thermal annealing of cellulose acetate membranes. The effect
of this thermal treatment on the physical structure of the membrane
is alternatively viewed as increasing the crystallinity or
decreasing the porosity. Perhaps a combination of these effects
occurs. In either case, the result is a decrease in flux and an
increase in solute rejection with increasing temperature and
duration of the thermal treatment. An example of a chemical
modification is the sulfonation of hydrophobic membrane materials
to increase hydrophilicity and thus increase water permeability
(14). Usually these post-formation treatments are conducted prior
to mounting the membrane in the membrane module. However,
Grodzinsky and co-workers (15) have reported that the physical
structure of a variety of charged polymeric membranes can be

temporarily and controllably altered after mounting the membrane in
the module. By imposing an electric field on the membrane, the
authors found that it is possible to modify the permeation rates of
both charged and neutral species. Presumably the applied electric
field causes the transport corridors to change in size due to
electrostatic interactions within the membrane matrix.

When discussing membrane preparation, not only must the
physical structure be considered, but one must also consider the
membrane form or shape. In an effort to combat concentration
polarization and membrane fouling and to maximize the membrane
surface area per unit module volume, membranes are produced in the
form of *flat sheets* (used either in plate-and-frame or spiral wound
modules), supported and unsupported *tubes*, and *hollow fibers*.
Although much of the technology associated with membrane development
and membrane production is closely guarded as proprietary
information, some of the details are beginning to appear in the
literature (6,9–13,16–20).

Membrane Characterization and Evaluation. Following the selection,
characterization and evaluation of the material and the preparation
of the membrane, the next steps are to characterize the membrane in
terms of physical properties and to evaluate the membrane in terms
of performance.

In this context, *membrane characterization* refers to obtaining
information about the physical structure of the membrane phase and
characteristics of the bulk polymer. Pusch and Walch (21) have
critically reviewed the commonly used techniques to investigate
porous structure (pore size, pore size distribution, pore volume,
anisotropy, etc.) and molecular structure (rubbery versus glassy,
crystallinity, chain segment arrangement and mobility, etc.).
Their list of methods for characterizing the porous structure
includes microscopy, low-angle X-ray scattering, bubble point
determination, mercury intrusion, fluid permeation measurements and
molecular weight cut-off determinations. For characterizing the
bulk polymer properties, Pusch and Walch list low-energy neutron
scattering and diffraction, X-ray scattering and diffraction,
infra-red absorption, nuclear magnetic resonance, thermomechanical
analysis, differential thermoanalysis, differential scanning
calorimetry, as well as gas permeation and sorption methods. For
membranes that are used in an aqueous environment, the structure of
the water within the membrane can be characterized via water
sorption isotherms, nuclear magnetic resonance, infra-red
absorption and by determining the heat capacity of the water within
the membrane. These water-structure studies provide insight into
the porous nature of the membrane and into the strength of the
water-membrane interactions. In relating membrane structure to
permeability, Pusch and Walch (21) make extensive use of an
excellent collection of electron photomicrographs. In this volume
Kyu (22) critically evaluates the techniques available for
characterizing ion-exchange membranes in terms of polymer structure
and functionality.

Frequently, only the properties of the skin layer of
asymmetric membranes are of importance, because the skin layer is
considered to play a dominant role in determining membrane

performance. In this volume, Smolders and Vugteveen (23) as well
as Zeman and Tkacik (24) present a number of techniques for
characterizing the porous structure of the skin layer of
ultrafiltration membranes.

    Membrane evaluation may refer to determining the ability of
the membrane to achieve its desired function; for example, to
separate the components of a mixture. Alternatively, membrane
evaluation may refer to identifying a suitable application for an
existing membrane. A survey of the literature reveals that there
are few standard procedures for evaluating membrane performance.
This lack of uniformity in evaluation procedures, plus the
inability to confidently predict performance under a specific set
of operating conditions on the basis of experiments conducted under
different conditions, restricts comparisons of available membranes
and performance data. Therefore, membrane performance must be
evaluated for each application under the conditions of use.
Depending on the specific membrane application, membrane evaluation
might include measurements of flux, rejection or separation factor,
ion-exchange capacity, membrane functionality or activity, membrane
degradation (physical and chemical), membrane fouling, membrane
compaction, release rates and barrier properties. These membrane
properties are directly related to the choice of membrane material,
the membrane preparation procedures and the final application
conditions.

Overview of This Volume

The various chapters in this book address the topics of material
selection, characterization and evaluation as well as membrane
preparation, characterization and evaluation. At the expense of
neglecting membranes for applications such as controlled release
and impermeable barriers, this book focuses on synthetic membranes
for separation processes as well as active membranes and conductive
membranes. While many of the concepts developed herein can be
extrapolated to other applications, the interested reader is
referred elsewhere for specific details (for example, controlled
release (25-30), coating and packaging barriers (31-33), contact
lenses (34,35), devolatilization (36), ion-selective membrane
electrodes (37-42) and membranes in electrochemical power sources
(43)).

Membrane Material Selection and Evaluation. Chern et al. (3) and
Lloyd and Meluch (4) propose possible approaches to the problem of
selecting the appropriate membrane material to separate gas
mixtures and liquid mixtures, respectively. Chern et al. discuss
membrane permeation and separation in terms of thermodynamic
solubility and kinetic mobility of the permeant gases in the
polymer phase and how each of these is influenced by the molecular
structure of the glassy polymeric membrane material. Correlations
that apply in the absence of strong plasticization or swelling
interactions between the penetrant gases and the membrane are
discussed in terms of inherent polymer and penetrant properties to
rationalize the solubility and mobility contributions to the
permselection process. Advantages of focusing on "mobility

selection" rather than "solubility selection" are emphasized by
these authors. They point out how the chemical nature of the
polymer, and thus polymer segmental motion and packing, can be used
to select membrane materials for gas mixture separations. The
authors suggest that a loosely packed glassy polymer with
sufficient cohesive energy and a rigid plasticization-resistant
backbone is ideally suited to achieve both high flux and high
selectivity. Structurally modified poly(aryl ethers), polyimides,
polyamides, polycarbonates, polyesters and polyurethanes appear to
be likely candidates to attain these goals. Chern et al. (3)
suggest that modification of the above simple concepts are
necessary when one or more of the permeants plasticizes the
membrane material. The authors discuss these and other
"environmental" considerations and the importance of evaluating the
membranes under final useage conditions.

     In contrast to the separation of relatively inert gas
mixtures, the separation of liquid mixtures is strongly influenced
by both the effective size of the permeants and the chemical
interactions which occur within the membrane phase. That is, both
thermodynamic solubility or partitioning and kinetic mobility or
transport are directly influenced by physical as well as chemical
factors. Lloyd and Meluch (4) discuss membrane material selection
in terms of the effective size of the permeants relative to each
other and relative to the size of the membrane transport corridor.
The transport corridor size is subsequently related to polymer
molecular structure and membrane preparation procedures. In this
sense, the discussion closely resembles that of Chern et al. (3).
However, Lloyd and Meluch add the often more significant factor of
chemical interactions near and within the membrane phase. The
authors demonstrate the possibility of selecting an appropriate
membrane material on the basis of the dispersive, polar and
hydrogen-bonding character of both the available membrane materials
and the solution components to be separated. Having selected an
appropriate membrane material on this thermodynamic basis, membrane
performance is ultimately related to the kinetics of transport
through the physical structure of the membrane, which in turn is
related to membrane preparation procedures. Lloyd and Meluch also
discuss methods for characterizing and evaluating membrane
materials prior to membrane formation.

     Hoehn (5) reviews the development of aromatic polyamide
(aramid), polyamide-hydrazide, polyhydrazide and polyimide
membranes for liquid and gas phase separations. Hoehn discusses
the structure-property relationships of these membranes in terms of
polymer chemical composition (primary or Level I characteristics),
in terms of steric effects resulting from chain packing and chain
flexibility (secondary or Level II) and in terms of membrane
morphology, such as asymmetry, anisotropy and skinning (Levels III
and IV). It is Level I that Lloyd and Meluch (4) use to establish
their material selection index on the basis of dispersive, polar
and hydrogen bonding considerations. Structure Level II is beyond
the level of detection via electron microscopy, and determines the
size of the transport corridor in dense membranes and the skin
layer of asymmetric membranes. As such, Hoehn's Structure Level II
can be related to the corridor size parameter identified by Lloyd

and Meluch (4) and to the mobility selectivity discussed by Chern
et al. (3). Levels I and II are intrinsic properties of the
polymer; Levels III and IV represent physical structure
characteristics on a microscopic level and are dependent upon
membrane preparation procedures for integrally- and nonintegrally-
skinned membranes, respectively. As such, Structure Level III
relates to the chapters by Finken (6), Kesting (9), Strathmann
(11), Kamide and Manabe (12), Hiatt et al. (13) and Cabasso (44),
while Level IV relates to the chapters by Cadotte (8), Spencer
(10), Cabasso (44) and Lee et al. (45).

     Ward, Feldhoff and Klein (7) demonstrate that in addition to
some demanding separation performance requirements (which are
primarily attributable to membrane preparation procedures and
transport mechanisms), therapeutic applications such as
hemodialysis, hemofiltration and plasmapheresis impose some unique
material selection restrictions. Specifically, one must consider
protein adsorption, biocompatibility (that is, thrombogenicity,
complement activation and toxicity) and the sterilizability of the
membrane. In selecting a membrane material for any of these
therapeutic liquid separations, the biocompatibility and
sterilizability restrictions must be considered in addition to the
guidelines established by Lloyd and Meluch (4). Thrombogenicity
and complement activation are directly related to the
physicochemical interactions between the polymer and the various
components of blood. Toxicity is related to the chemical
functionality of the polymer or any residual low molecular weight
compounds in the polymer. Sterilizability is a function of both
the thermal properties of the polymer, such as glass transition
temperature and crystalline melting temperature, and the chemical
stability of the polymer to ethylene oxide exposure and gamma
irradiation. Additional requirements of optical clarity and
biodegradability must also be taken into account in selecting
membrane materials for other applications such as contact lenses
and controlled release devices, respectively. Ward et al. review
several membrane materials currently in use for therapeutic liquid
separations and discuss their advantages and disadvantages for
specific applications. The authors also point out that for
continued growth in the use of membranes for therapeutic liquid
separations a better understanding of blood-membrane physicochemical
interactions is required. This knowledge would be of great value
in predicting biocompatibility, and thus in selecting membrane
materials. The authors also point out the need to refine membrane
preparation procedures to more accurately control pore size and to
produce membranes of narrow pore size distribution.

     In the biomedical applications outlined by Ward et al. (7),
more so than in any other separation application of synthetic
polymeric membranes, the goal is to mimic natural membranes.
Similarly, the development of liquid membranes and biofunctional
membranes represent attempts by man to imitate nature. *Liquid
membranes* were first proposed for liquid separation applications by
Li (46-48). These liquid membranes were comprised of a thin liquid
film stabilized by a surfactant in an emulsion-type mixture. While
these membranes never attained widespread commercial success, the
concept did lead to *immobilized or supported liquid membranes*. In

these membranes, the transport occurs in a stationary liquid phase
which has been fixed within a porous membrane for purposes of
stability. A variety of techniques have been used to support the
liquid membrane phase including immobilization within porous inert
"membranes" (for example, common filter paper, nitrocellulose
filters, cellulose acetate films and hollow fibers, track-etched
polycarbonate membranes, polytetrafluoroethylene membranes,
polyvinyl chloride membranes and polypropylene membranes such as
those discussed by Hiatt et al. (13)) as well as within ion-
exchange membranes and between two relatively dense films in the
form of a "sandwich." In any of these forms, the membranes can be
used for either gas or liquid mixture separations.
     Way, Noble and Bateman (49) review the historical development
of immobilized liquid membranes and propose a number of structural
and chemical guidelines for the selection of support materials.
Structural factors to be considered include membrane geometry (to
maximize surface area per unit volume), membrane thickness (<100
μm), porosity (>50 volume %), mean pore size (<0.1 μm), pore size
distribution (narrow) and tortuosity. The amount of liquid
membrane phase available for transport in a membrane module is
proportional to membrane porosity, thickness and geometry. The
length of the diffusion path, and therefore membrane productivity,
is directly related to membrane thickness and tortuosity. The
maximum operating pressure is directly related to the minimum pore
size and the ability of the liquid phase to wet the polymeric
support material. Chemically the support must be inert to all of
the liquids which it encounters. Of course, final support
selection also depends on the physical state of the mixture to be
separated (liquid or gas), the chemical nature of the components to
be separated (inert, ionic, polar, dispersive, etc.) as well as the
operating conditions of the separation process (temperature and
pressure). The discussions in this chapter by Way, Noble and
Bateman should be applicable the development of *immobilized or
supported gas membranes* (50).

Membrane Formation, Modification and Production. Kesting (9),
Strathmann (11), Kamide and Manabe (12), Hiatt et al. (13) and
Finken (6) all address the important subjects of membrane formation
mechanisms and membrane production processes, including post
formation treatments and modifications. In each chapter, the
emphasis is on membrane preparation via a *phase inversion process*.
To paraphrase Kesting (9), the phase inversion process is one in
which a homogeneous polymer solution is converted or inverted into
a three-dimensional macromolecular network or gel comprised of
solid polymer regions and intervening voids. That is, a
homogeneous solution *decomposes* into a two-phase system comprised
of a solid, polymer-rich phase forming the rigid membrane structure
and a liquid, polymer-poor phase forming the voids. The common
thermodynamic feature of all phase inversion processes is that the
free energy of mixing of the polymer system must be negative under
certain conditions of temperature and composition. That is, the
system must have a miscibility gap over a defined temperature and
concentration range. The cause of the phase inversion or phase
separation may be either a change in solution composition or a

change in solution temperature. Kesting distinguishes between a *dry* or *complete evaporation process*, a *wet* or *combined evaporation-diffusion process* and a *thermal process*. This distinction is based on the procedure used to achieve the phase inversion; that is, the cause of the precipitation and solidification of the polymer. Each of these variations of the phase inversion process, plus the closely related *polymer assisted phase inversion process*, is discussed in terms of the mechanism of membrane formation, membrane structural characteristics (*anisotropy* versus *asymmetry* or *skinning*, and structural irregularities) and membrane production considerations.   Some of the topics discussed by Kesting in this comprehensive review are subsequently elaborated upon in greater detail elsewhere in this volume; for example, membrane formation mechanism (11,12), membrane production (11), thermal phase inversion (13) and composite or nonintegrally-skinned membranes (8,10).

Strathmann (11) explores further the details of the phase-inversion membrane formation mechanism and the influence of process variables.   Concentrating on the wet phase inversion process, Strathmann discusses membrane formation by making use of three-component equilibrium phase diagrams. Recognizing that the phase-inversion process is actually a nonequilibrium process and thus difficult to describe in thermodynamic terms, Strathmann emphasizes the kinetic factors (diffusivities, driving forces, viscosity, etc.) which govern phase inversion. The major process variables considered are the choice of polymer and its concentration, the choice of solvent or solvent system, the choice of precipitant or precipitant system and the precipitation temperature. Extensive use is made of electron microscopy and optical microscopy in relating these membrane preparation process variables to membrane performance and the structure of the porous support layer. Strathmann demonstrates that through proper control of the process variables listed above the same membrane structure can be prepared from various polymers and that the same polymer can be used to prepare various membrane structures. The rate of precipitation is shown to have a direct influence on the structure of the porous support layer: slow precipitation produces a "sponge" structure; fast precipitation produces "finger-like" macrovoids. The rate of precipitation is related to the polymer concentration in the casting solution, the chemical similarity of the polymer-solvent, polymer-precipitant and solvent-precipitant pairs, the precipitant temperature, the diffusivities of the solvent and precipitant in the nascent membrane during gelation, the method of introducing the precipitant (vapor or liquid), the presence of additives in the precipitation medium and the resistance to solvent-precipitant exchange offered by any existing skin layer. Strathmann briefly discusses the effects of evaporation prior to precipitation and the effects of post-formation treatments such as annealing.

Relying heavily on their established expertise in the field of polymer solution thermodynamics, Kamide and Manabe (12) take a more detailed look at the mechanism of phase-separation which occurs during membrane formation. In this context, phase separation is the process which takes place during phase inversion. A theory is developed which allows for the prediction of pore characteristics

in a membrane cast from solution. According to this theory,
provided that the initial polymer concentration is smaller than an
established critical level, the phase-separation process yields a
polymer-rich phase which becomes a small primary particle. Primary
particles subsequently aggregate to form the larger secondary
particles which eventually form the membrane pore walls. The
authors point out that this nucleation-and-growth model differs
from the spinodal decomposition model proposed by other authors.
The theory developed by Kamide and Manabe allows them to model the
primary-to-secondary particle growth process and to predict final
pore size and pore size distribution. Experimental studies using
electron microscopy to evaluate membrane structure were carried out
to substantiate their predictions.

In reviewing phase inversion membrane preparation, Kesting (9)
referred to the thermal phase inversion process as perhaps the most
universally applicable method. Strathmann (11) refers to the
process as the simplest procedure for obtaining microporous
membranes. In this process, a homogeneous polymer solution at
an elevated temperature is converted to a two-phase system by a
decrease in temperature rather than by changing the solution
composition. The resulting phase-separation process may be one of
liquid-liquid separation followed by either polymer solidification
or crystallization (13) or one of simultaneous polymer
crystallization and solidification (51). The pore-forming latent
solvent is subsequently extracted to produce a porous structure.
Hiatt et al. (13) discuss the production of microporous membranes
via thermally-induced liquid-liquid separation followed by polymer
crystallization. They demonstrate that the pore structure of these
membranes is dependent upon a number of controllable parameters
including choice of polymer, polymer concentration, choice of pore-
former and rate of solution cooling. The authors demonstrate the
significance of these variables in preparing porous membranes of
high molecular weight polypropylene and low molecular weight
polyvinylidene fluoride. For example, polypropylene membranes cast
from N,N-bis-(2-hydroxyethyl) tallow amine are shown to assume
either an "open cell" structure or a "lacy" structure. In this
case, a slow cooling induces a nucleation-and-growth mechanism to
produce the macroporous open cell structure. A fast cooling induces
spinodal decomposition to produce the microporous lacy structure
which may even possess a skin layer. On the other hand, membranes
made from polyvinylidene fluoride and carbitol acetate solutions
produce either a structure of "polymer spheres" supported by a
tight skin or a structure of "polymer leaves" stacked on a more
open skin. The spherical structure results from either slow cooling
or high polymer concentrations. The polymer leaf structure results
from rapid cooling and low polymer concentrations. The membranes
produced via thermal phase inversion have proven useful for
controlled release, air filtration, plasmapheresis, depyrogenation
and cross-flow microfiltration. They should also prove useful as
liquid membrane supports.

Post-formation chemical, thermal and physical treatments are
often used to modify the performance characteristics of membranes.
Finken (6) presents recent results from his studies on thermal and
physical modifications of integrally-skinned cellulosic blend

membranes for gas mixture separations. Freeze drying and the sublimation temperature were shown to influence membrane performance (flux and separation). Similarly, thermal annealing and the annealing temperature influence membrane performance. Finally, a proprietary solvent exchange and subsequent drying treatment was also shown to influence membrane performance.

In addition to the phase-inversion processes described by Kesting (9), Strathmann (11), Kamide and Manabe (12) and Hiatt et al. (13), a number of alternative membrane preparation processes exist. Of these alternative processes only two are presently used to produce commercial skinned membranes. Specifically, these nonintegrally-skinned membranes are referred to as *composite membranes* (8) and *dynamic membranes* (10) depending on the method of formation and the capability to replace or renew the skin layer. A major advantage of nonintegrally-skinned membranes is the ability to produce the skin layer from a polymer different than that used for the porous support. This is significant in that the two layers serve different purposes and thus have different requirements. The skin layer governs the separation and flux properties. Therefore, it should be chemically similar to the preferentially transported species (4) and the polymer molecules should be capable of close packing. On the other hand, the porous layer serves as a rigid, compaction-resistant support and should be chemically inert. In both composite and dynamic membranes, the skin layer is deposited on a porous support (usually polysulfone for composite membranes and stainless steel, carbon or ceramic for dynamic membranes). The porosity of the support layer can have a direct influence on the preparation and performance of these nonintegrally-skinned membranes. The number and frequency of the pores at the top of the porous support should be as great as possible to assure adequate binding of the skin to the support. The pore size should be as small as possible to minimize the distance between points of support for the deposited skin layer. In preparing composite membranes the skin layer is either laminated, dip-coated, polymerized from a plasma or interfacially polymerized from solution prior to membrane module fabrication (spiral wound or hollow fiber). On the other hand, the skin layer in a dynamic membrane is desposited in a pre-existing membrane module (usually tubular). Since the skin layer of dynamic membranes is stabilized by ionic cross-linking at best, it can be controllably removed and a new one deposited as desired.

Cadotte (8) presents a comprehensive review of the development of the composite membrane with emphasis on the pros and cons of the four preparation methods mentioned above and on the polymer chemistry involved. Cadotte points out that while each of the four methods continues to receive some attention, the interfacial polymerization method appears to be the most versatile. This method can be used to produce skin layers from polyamines, polyimines, polyurethanes, polyesters and other polymers. Elsewhere in this volume, Lee and co-workers (45) discuss the advantages and problems associated with using these composite membranes for ethanol-water separations via counter-current reverse osmosis. Also, Cabasso (44) discusses double-layer composite membranes.

Following a brief review of the development of dynamic membranes and an overview of the current state of the art, Spencer (10) discusses dynamic polyblend membranes. In particular, he looks at the influence that polymer selection and membrane preparation procedures have on membrane performance. Dynamic membranes composed of a poly(acrylic acid)/basic polyamine blend deposited on a ZOSS (hydrous zirconium oxide on stainless steel) ultrafiltration membrane are discussed. Their hyperfiltration or reverse osmosis properties are compared to the more traditional ZOPA (zirconium oxide plus poly(acrylic acid)) membrane.

Another non-integrally skinned membrane worthy of note is the coated membrane developed by the research group at Monsanto (52,53). The interesting points of distinction between the composite membranes discussed by Cadotte (8) and Monsanto's Prism membranes are the role of the skin and the role of the support layer. The skin layer of composite membranes as described by Cadotte controls flux and separation by serving as a semi-permeable barrier. The support layer acts primarily as a substrate for the skin; any influence that the support layer has on flux and separation is secondary. On the other hand, the coated skin layer in the Monsanto membrane is a highly permeable, relatively non-selective polymer used primarily to plug any defects in the already existing skin layer of the hollow fiber membrane. By imposing this additional resistance to pore flow, the coated skin forces the gases to permeate the polymer which comprises the hollow fiber. Consequently, the hollow fiber supporting the coated skin controls the flux and separation. The Monsanto membranes are discussed in this volume by Finken (6) and Kesting (9).

The search for alternative reverse osmosis membrane materials resulted in not only the emergence of new materials but also new membrane module designs and membrane preparation procedures. Specifically, workers at Dow (54-56) and DuPont (57,58) developed techniques for solution-spinning and melt-spinning hollow fiber membranes. In this volume, Hoehn (5) reviews the development of these membranes at DuPont. Cadotte (8) discusses the formation of composite hollow fiber membranes, including those developed at Albany International Research Company. Lee et al. (45) consider an interesting application of these membranes. Finken (6) and Kesting (9) present brief discussions of the coated hollow fiber membranes developed at Monsanto. Cabasso (44) provides a brief overview of four topics of current interest to those involved in the development of hollow fiber membranes. The topics referred to by Cabasso are: (i) methods of characterizing the development of morphology during wet-spinning, (ii) the use of double-layer composite membranes for gas separations, (iii) the characterization of stress-induced crystallization, and (iv) the use of ion-exchange hollow fibers for alcohol-water separations (a topic closely related to the chapter by Lee et al. (45)).

A number of procedures exist for preparing non-skinned membranes of either the symmetric or the anisotropic type (5,59). Finken (6) describes a procedure referred to as the Langmuir-Blodgett technique which was first used to produce extremely thin

dense films for gas separations by Ward and co-workers (60). Langmuir-Blodgett films have had only limited commercial success for separation processes; however, Aizawa (61) points out in this volume that these mono- and multilayer thin films have found extensive use for simulating natural or biological membranes. In his classic monograph on synthetic polymeric membranes (59), Kesting describes a number of other membrane preparation procedures and membrane structures. While many of these have never advanced beyond the level of laboratory curiosities, a few have attained commercial success. *Sintered* membranes, *nuclear track-etched* polycarbonate microfiltration membranes by Nuclepore Corp. (62), stretched polyolefin Celgard membranes by Celanese Corp. (63,64) and stretched polytetrafluoroethylene Gore-Tex membranes by W. L. Gore and Assoc., Inc. (65) have all proven to be commercially successful microfiltration and/or air filtration membranes. *Charged mosaic* membranes continue to be investigated for possible use in piezodialysis (66). *Ionotropic gels* in which the gel contains a resin or a resin precurser of one charge and the pores contain resin of the opposite charge (67) and *latex-polyelectrolytes* (68) appeared to hold the most promise as charged mosaic membranes; however, piezodialysis has never come to fruition as a method of desalination.

Membrane Characterization. Smolders and Vugteveen (23) and Zeman and Tkacik (24) discuss a number of methods for determining the physical characteristics of skinned ultrafiltration membranes. Smolders and Vugeveen (23) make use of a gas adsorption/desorption method, thermoporometry and selective permeation of aqueous dextran and aqueous polyethylene glycol solutions analyzed via liquid chromatography. Pore volume and pore size distribution are calculated from the hysteresis loop in the sorption/desorption studies. Cumulative and differential pore volumes are likewise obtained by observing the shift in melting or freezing temperature in thermograms for water in the pores. By comparing the molecular weight distribution of dextran and polyethylene glycol in the feed with that in the permeate, a fractional rejection curve is generated. When used in conjunction with the classical molecular weight cut-off curve, a more complete representation of membrane pore size is obtained. The authors use a combination of these techniques to characterize the skin layer of ultrafiltration membranes of various materials in terms of mean pore size (as small as 1.5 nm) and pore size distribution. Zeman and Tkacik (24) also make use of nitrogen sorption/desorption studies and the selective permeation or fractionation of aqueous dextran solutions to estimate the pore size characteristics of polysulfone ultrafiltration membranes. In addition, high resolution scanning electron microscopy, SEM, (90,100X magnification) is used to obtain a "visual" representation of the membrane structure. Analysis of the photomicrographs yielded pore size distributions that are adequately represented by log-normal functions and which show reasonable agreement between predicted and observed dextran rejection. The pore sizes estimated on the basis of gas sorption/desorption studies were significantly larger than those suggested in the SEM studies; therefore, the authors conclude that the sorption studies provide

information about the porous support layer rather than the skin
layer. The techniques used by these authors, as well as those
reviewed by Pusch and Walch (21), provide valuable insight into the
mechanism of membrane formation and thus may assist membrane
scientists in developing better membranes. However, many of these
techniques do not characterize the membrane under the conditions of
application; for example, the ultrafiltration membranes (23,24) are
dried prior to gas sorption studies and microscopy. Therefore,
caution must be exercised in interpreting the results of these
characterization methods and relating them to membrane performance
and transport mechanisms.

The transport corridors of some membranes are too small to be
directly characterized by the techniques mentioned in the previous
paragraph. Notably, the transport corridors of ion-exchange
membranes and the skin layer of reverse osmosis and gas separation
membranes are so small as to spark considerable controversy
regarding the mechanism of transport in these membranes. Krause
(69) proposes an *interpenetrating microphase model* for transport
through ion-exchange membranes and the skin layer of reverse
osmosis membranes. In this model, the membrane consists of two
co-continuous, interpenetrating microphases—a feature confirmed by
Kyu (22). Water, ions and the principle hydrogen-bonding groups of
organic permeants are transported through a water-swollen,
hydrophilic microphase. Small organic molecules without major
hydrogen-bonding groups and the hydrophobic portions of other
molecules permeate the hydrophobic microphase. Partition
coefficients and diffusivities for a number of organic solutes in
cellulose acetate membranes are correlated using the solubility
parameters of only the hydrophobic portions of both the membrane
polymer and the organic permeant.

Way et al. (49) point out that *ion-exchange membranes* or
ionomeric membranes can be used as support materials for
immobilized liquid membranes. Of course, these membranes have a
variety of other applications which capitalize on their ability to
exchange either cations or anions (70,71). Ion-exchange membranes
are highly swollen gels carrying either a fixed positive charge
(anion exchange membrane) or a fixed negative charge (cation
exchange membrane). These membranes can be prepared by dispersing
a conventional ion-exchange resin within a polymer matrix, by
casting a film from an ionomeric polymer or by chemically modifying
an existing non-ionic polymer film. The most common fixed anions
in cation-exchange membranes are sulfonic and, to a lesser extent,
carboxylic. Phosphoric, phosphinic and selenic groups have also
been used. Anion-exchange membranes have been made with fixed
quaternary ammonium, quaternary phosphonium and teriary sulfonium
groups. Since the basic groups are not entirely stable, most of
the advances in ion-exchange membranes have been in the development
of cation-exchange membranes. The performance of these membranes
depends on the nature and density of the fixed ionic groups as well
as the mechanical and chemical stability of the polymer matrix.
Kyu (22) summarizes the properties and structure of perhaps the
most important class of ion-exchange membranes; that is,
perfluorinated ion-exchange membranes. A review of the properties
and structure of earlier ion-exchange membranes can be found

elsewhere (72). Kyu demonstrates how the structure of these
membranes can be investigated through the use of wide-angle and
low-angle scattering studies as well as spectroscopic and
microscopic studies. Physical and ion-exchange properties are
characterized via stress relaxation, dielectric relaxation and
dynamic mechanical studies. Because each of these methods of
investigation probe a different aspect of the membrane, Kyu
suggests that a variety of these techniques must be combined to
obtain a satisfactory representation of the membrane and its
capabilities.

Membrane for Specific Applications. Lee and co-authors (45)
discuss the selection and development of membranes for separating
ethanol and water. A process design referred to as countercurrent
reverse osmosis, CCRO, was used to investigate the problems of high
osmotic pressures associated with concentrated alcohol solutions.
Because of the high alcohol concentrations that result and the CCRO
mode of operation, not only does the choice of membrane material
become critical (that is, Structure Levels I and II defined by
Hoehn), but so does the asymmetric structure of the membrane
(Structure Levels III and IV). In CCRO, a portion of the
concentrated feed is circulated to mix with the permeate on the low
pressure side of the membrane. To attain good mixing of these two
solutions and to facilitate the diffusion of the alcohol to the low
pressure side of the membrane skin, the porous support layer must
have an open structure. For this purpose, thin film composite
membranes proved to be best. Lee and co-workers report that
composite membranes in which the skin layer is formed via the
polymerization of a monomeric amine perform better than composite
membranes in which the skin is formed by *in situ* cross-linking of
prepolymer (8). Presumably the later technique for composite
membrane preparation produces a gel which hinders diffusion within
the porous sublayer. These workers also concluded that the hollow
fiber membrane conformation is preferred because it facilitates
circulation on the low pressure side.
      Wagener (73) discusses electrically conductive membranes or
electromembranes. The purpose of these membranes is to achieve
control over permeation of charged species by presenting an
electric potential barrier. Thus, separation is to be accomplished
on the basis of electrochemical interactions rather than or in
addition to on a size distinction basis. These membranes differ
from ion-exchange membranes in that no ions are exchanged during
permeation. An additional application for electromembranes is in
the area of membranes for chemical communication, as discussed in
this volume by Aizawa (61). Wagener describes alternative methods
for the preparation of electromembranes by utilizing the porous
membranes described by Hiatt et al. (13) and polyacetylene chemistry
followed by an iodine or a $NOPF_6$ doping. Wagener demonstrates that
the amount and type of dopant as well as the choice of polymer from
which the porous membrane is made each play a role in determining
the conductive properties of the electromembrane. Polymers which
do not contain active hydrogens were found to make the best porous
support materials. For example, polyethylene and polyvinylidene
fluoride served as useful porous substrates while nylon-6 failed to

yield suitable electromembranes. This is apparently due to the
influence that the membrane material has during the acetylene
polymerization, rather than any effect the porous polymer might
have during transport. Electromembranes with conductivities in the
range 10^{-2} to 10^{1} ohm^{-1} cm^{-1} were produced.

     Closing out this volume, Aizawa ([61](61)) presents a comprehensive
review of *biofunctional synthetic membranes*. These membranes
represent another attempt by man to mimic natural or biological
membranes. In this case not only are chemical compounds separated
but they are often chemically modified while being transported in
the membrane. Aizawa notes that the original attempts to mimic
biological membranes resulted in the incorporation of biologically
active molecules in planar bilayer lipid membranes and liposomes;
both of which are liquid membranes. As mentioned above in
discussing the chapter by Way et al. ([49](49)), these relatively weak,
noncovalent assemblies were not stable and found limited practical
use. More recently techniques have been developed to permit the
immobilization of biologically active molecules within synthetic
polymeric membranes. The most common techniques of immobilization
are covalent bonding to the support matrix and entrapment within
the pores of the support matrix. Aizawa reviews three
classifications   of   biofunctional   synthetic   membranes:
biocatalytic, energy-transducing and information-transducing.
Under each of these three headings, he discusses historical
development, the molecular mechanism that occurs in the biological
membrane which the synthetic membrane is trying to mimic, the
methodology of membrane preparation and current trends in the
research and development of these membranes.

Summary

In preparing this volume of the ACS Symposium Series, the editor
and the authors have concentrated their efforts on the materials
science of synthetic membranes. In doing so, it was necessary to
limit discussions of other, equally important, aspects of membrane
science. Specifically, we have focused on synthetic polymers
serving as either membranes or membrane supports. Readers with an
interest in the materials science of inorganic membranes (metallic,
ceramic and glass ([74](74)) as well as precipitation ([75](75)) membranes),
gas membranes ([50](50)) and natural biological membranes ([76](76)) are
referred to the literature. Readers with an interest in transport
modelling, process design and optimization, membrane applications
and the economics of membrane processes are referred to the
literature cited in this overview and elsewhere in this volume.
Each chapter of this volume is designed to present the state of the
art at the time of final manuscript preparation (early 1984), to
provide an appreciation of the materials science of synthetic
membranes and to encourage further developments in these areas. An
understanding of the concepts presented herein can facilitate the
selection of better membrane materials, the preparation of better
membranes, the modelling of membrane transport and the improvement
of membrane separation processes.

Literature Cited

1. For example, see the variety of topics covered in the following: (a) Maku (journal of the Membrane Society of Japan). (b) Journal of Membrane Science. (c) Meares, P., Ed. "Membrane Separation Processes"; Elsevier: Amsterdam, 1976. (d) Turbak, A. F., Ed. "Synthetic Membranes, Vol. I and II"; American Chemical Society: Washington, D.C., 1981. (e) Starzak, M. E. "The Physical Chemistry of Membranes"; Academic Press: New York, 1984.
2. Stern, S. A. In Reference 1(c).
3. Chern, R. T.; Koros, W. J.; Hopfenberg, H. B.; Stannett, V. T. In "Materials Science of Synthetic Membranes"; Lloyd, D. R., Ed.; American Chemical Society: Washington, D.C., 1985.
4. Lloyd, D. R.; Meluch, T. B. *ibidem.*
5. Hoehn, H. H. *ibidem.*
6. Finken, H. *ibidem.*
7. Ward, R. A.; Feldhoff, P. W.; Klein, E. *ibidem.*
8. Cadotte, J. *ibidem.*
9. Kesting, R. E. *ibidem.*
10. Spencer, H. G. *ibidem.*
11. Strathmann, H. *ibidem.*
12. Kamide, K.; Manabe, S. *ibidem.*
13. Hiatt, W. C.; Vitzthum, G. H.; Wagener, K. B.; Gerlach, K.; Josefiak, C. *ibidem.*
14. Lloyd, D. R.; Gerlowski, L. E.; Sunderland, C. D., Wightman, J. P.; McGrath, J. E.; Iqbal, M.; Kang, Y. In Reference 1(d).
15. Eisenberg, S. R.; Grodzinsky, A. J. J. Memb. Sci. 1984, 19, 173-194.
16. Sourirajan, S., Ed. "Reverse Osmosis and Synthetic Membranes"; NRCC Press: Ottawa, Canada, 1977; Chapters 15-17.
17. Keller, P. R., Ed. "Membrane Technology and Industrial Separation Techniques"; Noyes Data Corp.: Park Ridge, N.J., 1976.
18. Scott, J., Ed. "Desalination of Seawater By Reverse Osmosis"; Noyes Data Corp.: Park Ridge, N.J., 1981.
19. Scott, J., Ed. "Hollow Fibers: Manufacture and Application"; Noyes Data Corp.: Park Ridge, N.J., 1981.
20. Baum, B.; Holley, W.; White, R. A. In Reference 1(c).
21. Pusch, W.; Walch, A. J. Memb. Sci. 1982, 10, 325-360. Angew. Chemie Intern. Edn. 1982, 21, 660-685.
22. Kyu,T. In "Materials Science of Synthetic Membranes"; Lloyd, D. R., Ed.; American Chemical Society: Washington, D.C., 1985.
23. Smolders, C. A.; Vugteveen, E. *ibidem.*
24. Zeman, L.; Tkacik, G. *ibidem.*
25. Baker, R. W., Ed., "Controlled Release of Bioactive Materials"; Academic Press: New York, 1980.
26. Chandrasekaran, S., Ed. "Controlled Release Systems"; AIChE Symp. Series No. 206, 1981.
27. Johnson, J. C., Ed. "Sustained Release Medications"; Noyes Data Corp.: Park Ridge, N.Y., 1980.
28. Lewis, D. H., Ed. "Controlled Release of Pesticides and Pharmaceuticals"; Plenum Press: New York, 1981.

29. Das, K. G., Ed. "Controlled-Release Technology"; Wiley: New York, 1983.
30. Roseman, T. J.; Mansdorf, S. Z., Ed. "Controlled Release Delivery Systems"; Marcel Dekker: New York, 1983.
31. Lee, W. M. Polym. Eng. Sci. 1980, 20, 65-69.
32. Gordon, G. A.; Ravve, A. ibidem 70-77.
33. Swaroop, N.; Gordon, G. A. ibidem 78-81.
34. Refogo, M. F. In "Encyclopedia of Chemical Technology, Vol. 6"; Wiley Interscience: New York, 1979.
35. Refogo, M. F. In "Encyclopedia of Polymer Science and Technology, Vol. 1"; Interscience: New York, 1979.
36. Biesenberger, J. A.; Sebastian, D. H. "Principles of Polymerization Engineering"; Wiley: New York, 1983; Chapter 6.
37. Lakshminarayanaiah, N. "Membrane Electrodes"; Academic Press: New York, 1976.
38. Bloch, R.; Lobel, E. In Reference 1(c).
39. Buck, R. P. CRC Critical Reviews in Analytical Chemistry 1976, 5, 323-420.
40. Buck, R. P.; Thompsen, J. C.; Melroy, O. R. In "Ion-Selective Electrodes in Analytical Chemistry"; Freiser, H., Ed.; Plenum Press: New York, 1978.
41. Buck, R. P. Sensors and Actuators 1981, 1, 197-260.
42. Covington, A. K., Ed. "Ion Selective Electrode Methodology"; CRC Press: Boca Raton, Florida, 1979.
43. Lee, J. A.; Maskell, W. C.; Tye, F. L. In Reference 1(c).
44. Cabasso, I. In "Materials Science of Synthetic Membranes"; Lloyd, D. R., Ed.; American Chemical Society: Washington, D.C., 1985.
45. Lee, K. L.; Babcock, W. C.; Bresnahan, P. A. ibidem.
46. Li, N. N. Ind. Eng. Chem. Proc. Des. Devel. 1971, 10, 215-221.
47. Li, N. N. AIChE J. 1971, 17, 459-463.
48. Cahn, R. P.; Li, N. N. In Reference 1(c).
49. Way, J. D.; Noble, R. D.; Bateman, B. R. In "Materials Science of Synthetic Membranes"; Lloyd, D. R., Ed.; American Chemical Society: Washington, D.C., 1985.
50. Imai, M.; Furusaki, S.; Miyauchi, T. Ind. Eng. Chem. Proc. Des. Devel. 1982, 21, 421-425.
51. Shipman, G. H.; Kinzer, K. E.; Tabar, R. J. private communication, June 1984.
52. Henis, J.M.S.; Tripodi, M. K. J. Memb. Sci. 1981, 8, 233-246.
53. Henis, J.M.S.; Tripodi, M. K. U.S. Patent 4,230,463 Oct. 28, 1980.
54. Mahon, H. I. U.S. Patent 3,228,876 1966; U.S. Patent 3,228,877 1966.
55. McLain, E. A. U.S. Patent 3,422,008 1969.
56. McLain, E. A.; Mahon, H. I. U.S. Patent 3,423,491 1969.
57. Richter, J. W.; Hoehn, H. H. U.S. Patent 3,567,632 1971.
58. Beasley, J. K. Desalination 1977, 22, 181-189.
59. Kesting, R. E. "Synthetic Polymeric Membranes"; McGraw-Hill: New York. 1971.
60. Ward, W. J.; Browall, W. R.; Salemme, R. M. J. Memb. Sci. 1976, 1, 99-108.

61. Aizawa, M. In "Materials Science of Synthetic Membranes";
    Lloyd, D. R., Ed.; American Chemical Society: Washington,
    D.C., 1985.
62. Fleischer, R. L.; Price, P. B.; Walker, R. M. <u>Sci. Amer.</u> 1969,
    220, 30-39.
63. Bierenbaum, H. S.; Isaacson, R. B.; Druin, M. L.; Plovan, S.
    G. <u>Ind. Eng. Chem. Prod. Res. Devel.</u> 1974, 13, 2-9.
64. Sarada, T.; Sawyer, L. C.; Ostler, M. I. <u>J. Memb. Sci.</u> 1983,
    15, 97-113.
65. Gore, R. W. U.S. Patent 3,953,566 1976; U.S. Patent 3,962,153
    1976.
66. Leitz, F. B. In Reference 1(c).
67. Ditter, J. F.; Kesting, R. E. Office of Saline Water Rpt.
    Contract No. 14-30-3128, U.S. Dept. Interior, 1973.
68. Leitz, F. B.; Shorr, J.; Sims, K.; Spencer, S.; Carlson, D.
    Office of Saline Water Rpt. No. 988; U.S. Dept. Interior,
    1974.
69. Krause, S. In "Materials Science of Synthetic Membranes";
    Lloyd, D. R., Ed.; American Chemical Society: Washington,
    D.C., 1985.
70. Eisenberg, A.; Yeager, H. L., Eds. "Perfluorinated Ionomer
    Membranes"; American Chemical Society: Washington, D.C.,
    1982; Chapters 14 to 19.
71. Flett, D. S., Ed. "Ion Exchange Membranes"; Ellis Harwood
    Ltd.: Chichester, G.B., 1983.
72. Solt, G. S. In Reference 1(c).
73. Wagener, K. B. In "Materials Science of Synthetic Membranes";
    Lloyd, D. R., Ed.; American Chemical Society: Washington,
    D.C., 1985.
74. Hwang, S.-T.; Kammermeyer, K. "Membranes in Separations";
    Wiley-Interscience: New York, 1975; Chapter XVI.
75. Ayalon, A. <u>J. Membr. Sci.</u> 1984, 20, 93-102.
76. Bittar, E. E., Ed. "Membrane Structure and Function, Vol. 1
    and 3"; Wiley: New York, 1980.

Material Selection for Membrane-Based Gas Separations

R. T. CHERN, W. J. KOROS[1], H. B. HOPFENBERG, and V. T. STANNETT

Department of Chemical Engineering, North Carolina State University, Raleigh, NC 27650

High membrane permselectivity for a gas mixture is well-known to correlate with low permeability of the desired product through the membrane. Exceptions to this rule exist, however, and this suggests the possibility of improved membranes for a number of important applications. This paper suggests possible polymer structural changes which may allow control over the magnitudes of permeabilities and selectivities. These suggestions result from considering the permeability and selectivity in terms of their separate thermodynamic solubility and kinetic mobility contributions. The two contributions vary markedly with changes in the polymer structure and correlate with variations in penetrant and polymer physical properties. The feasibility of developing extremely selective high flux membrane materials is explored in terms of these correlations. The potential for such developments is shown to be fairly high for cases in which the permeant molecule is substantially more compact than the nonpermeant molecule if the resulting mobility advantage is not eliminated by a large solubility advantage favoring the nonpermeant. Several important examples of such systems are discussed including H_2/CH_4 and CO_2/CH_4. A short discussion of approaches to assess membrane materials for resistance to attack by components in the process stream is also presented.

Membrane-based gas separations have emerged as important chemical engineering unit operations for hydrogen recovery from purge and recycle streams (1-4) and for carbon dioxide and water removal from natural and land fill gases (5-9). Using asymmetric structures in high surface area modules permits the use of higher selectivity, lower permeability glassy polymers in the place of rubbery materials.

[1] Current address: The Center for Energy Studies, The University of Texas at Austin, Austin, TX 78712.

The first generation of gas separators has achieved an impressive penetration into markets traditionally dominated by cryogenic, chemical and physical sorption processes. Competition from these processes is strong. Membranes with higher permeabilities, selectivities and resistance to penetrant attack are required to meet challenges from these traditional processes and to permit expansion into additional application areas.

Although no commercial examples exist currently in the gas separation field, thin film composite membranes such as those pioneered by Cadotte and co-workers (10) may ultimately permit the use of novel materials with unique transport properties supported on standard porous membranes. Therefore, the focus in this paper will be on suggesting a basis for understanding differences in the permeability and selectivity properties of glassy polymers. Presumably, if such materials prove to be difficult to fabricate into conventional monolithic asymmetric structures, they could be produced in a composite form. Even if thin film composite structures are used, however, the chemical resistance of the material remains an important consideration. For this reason, a brief discussion of this topic will be offered.

Typically, membrane research efforts focus upon the determination of the permeability and selectivity of candidate polymers without explicit consideration of the solubility and mobility terms comprising the permeability (11-13). This approach is reasonably effective for screening available polymers for a particular application but not optimum for providing guidelines to improve membrane performance by scientific alteration of the polymer structure. Moreover, it may lead one to an overly pessimistic view of the selectivity and permeability properties achievable as a result of polymer structural variations. As an adjunct to this typical approach, correlations of the penetrant diffusion coefficients and solubilities with the physical and chemical natures of the polymers and penetrants will be discussed. These correlations rationalize the generally observed relationship between high selectivity and low permeability. They also provide a partial basis for understanding reports of several deviant cases in which high selectivity and permeability are observed for H_2/CH_4 and CO_2/CH_4 systems. It is these deviant cases that may lead the way to a new generation of more productive and selective membranes.

Background and Theory

One-dimensional diffusion through a flat membrane will be treated in the following discussion. The effects of membrane asymmetry will be neglected since the process of permselection occurs in the thin dense layer of effective thickness, ℓ, at the membrane surface. In such a case, the expression for the local flux of a penetrant at any point in the dense layer can be written as shown in Equation 1 (14):

$$N = - D \frac{dC}{dx} \qquad (1)$$

where the diffusion coefficient, D, may be a function of local con-
centration, C, in the membrane. The diffusion coefficient may be
interpreted in terms of a preexponential factor, $D°$, and an expo-
nential term that depends upon the activation energy for the dif-
fusion process, E_D (14).

$$D = D° \exp[- E_D/RT]$$ (2)

To a first approximation, E_D is the average energy that must be
localized next to the penetrant to generate an opening large enough
to permit the molecule to execute a jump. If concentration depend-
ence of the diffusion coefficient exists, both $D°$ and E_D may be
functions of the amount of penetrant present. At low concentrations,
the activation energy should be related strongly to the minimum cross
section of the penetrant, since this defines the critical opening
size necessary for a jump to occur. The large effect on molecular
mobility caused by differences in penetrant size or shape is illus-
trated in Figure 1 for a typical rubbery and glassy polymer, respec·
tively. The larger nonspherical penetrants tend to approach a pla-
teau diffusivity because the cross-sectional area of the molecule as
well as its volume determine its ability to find a gap of sufficient
size to permit a jump. Presumably, nonspherical penetrants move in
a somewhat oriented fashion, and the individual jump lengths may be
only fractions of the total length of the molecule. Associated with
the more highly restrictive glassy environment comes a greater abili-
ty to perform size or shape discrimination between penetrants. This
difference between the glassy and rubbery state is illustrated clear-
ly by the much larger spread in diffusion coefficients in the glassy
polymer compared to the rubbery one. Recognition of the preceding
facts often leads to the generalization that low membrane permeabil-
ity is necessary for high selectivity. Although the two generally
correlate, there appear to be attractive exceptions to the rule that
are worthy of serious investigation (11,13).

The permeability of a membrane to a penetrant is defined by
Equation 3:

$$P = \frac{N \ell}{[p_2 - p_1]}$$ (3)

where p_2 and p_1 are the upstream and downstream pressures of the com-
ponent acting across the effective membrane thickness, ℓ. Clearly,
the permeability of the membrane is not only determined by the mobi-
lity of the penetrant discussed above but also by its solubility, be-
cause the higher the solubility difference across the membrane, the
higher will be the observed flux and permeability. The contributions
of the two factors can be seen clearly for the case where the down-
stream pressure, p_1, is negligible. Substituting Equation 1 into
Equation 3 and integrating leads to Equation 5:

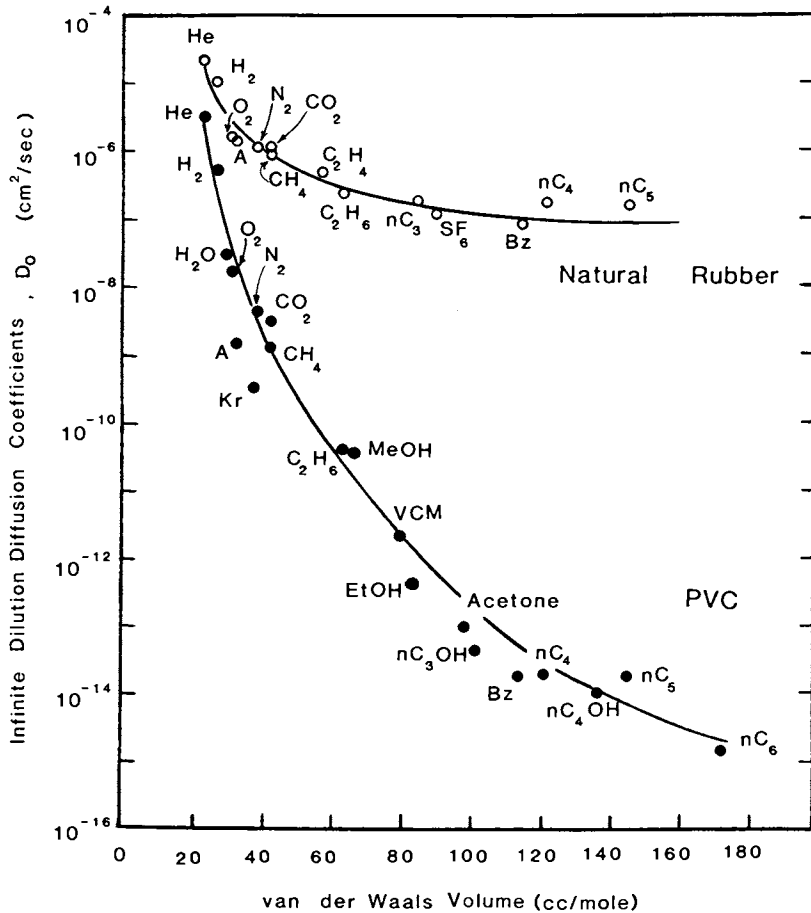$$P = - \left(D \frac{dC}{dx}\right)\left(\frac{\ell}{p_2}\right)$$ (4)

Figure 1. Diffusion coefficients for a variety of penetrants in natural rubber at 25 °C and rigid poly(vinyl chloride) at 30 °C. The van der Waals volumes are taken from The Handbook of Chemistry and Physics, 35th ed., 1953-54, page 21-24 to 21-26, CRC, Cleveland, Ohio.

so
$$\int_0^\ell \frac{P}{\ell} \, dx = \int_{0'}^{C_2} \left(\frac{D \, dC}{C_2}\right)\left(\frac{C_2}{P_2}\right) = \overline{D}\,\overline{S} \tag{5}$$

where $\overline{D} = \dfrac{\left(\displaystyle\int_0^{C_2} D \, dC\right)}{\left(\displaystyle\int_0^{C_2} dC\right)}$ defines an average measure of the penetrant's mobility in the membrane between the upstream concentration, C_2, and downstream concentration, $C_1 \approx 0$ ([14]). The parameter, $\overline{S} = C_2/p_2$, equal to the secant slope of the sorption isotherm evaluated at the upstream conditions, is a measure of the solubility of the penetrant in the membrane. The mobility factor in Equation 5 is kinetic in nature and largely determined by polymer-penetrant dynamics as discussed in the context of Equation 2. The solubility factor in Equation 5 is thermodynamic in nature and is determined by polymer–penetrant interactions and the amount of excess interchain gaps existing in the glassy polymer ([17]).

When the downstream pressure, p_1, is negligible compared to the upstream pressure, p_2, the separation factor, α_{AB}, defined by Equation 6 can be related to the ratio of the permeabilities of components A and B ([18]) as shown in Equation 7:

$$\alpha_{AB} = [y_A/y_B] \ [x_A/x_B] \tag{6}$$

$$\alpha_{AB}^* = P_A/P_B \tag{7}$$

where x_i's and y_i's are the local mole fractions of components A and B at the upstream and downstream membrane faces, respectively. The superscript $*$ in Equation 7 indicates that α^* is the so-called "ideal separation factor" which applies under the conditions described above. The ratio of the component permeabilities in such a case provides a useful measure of the intrinsic permselectivity of a membrane material for mixtures of A and B.

When the interaction between one penetrant and the polymer is not affected by the presence of another penetrant, the pure–component permeabilities of the two penetrants in the mixture can be used in Equation 7. For rubbery polymers at low penetrant partial pressures, this assumption of independent-permeation appears satisfactory ([19]-[20]). It does not, however, appear to hold in general for glassy polymer membranes ([12],[13],[21]-[25]). Moreover, it also has been shown that plasticization of both rubbery ([26]) and glassy ([27]) polymers can occur at higher penetrant activities.

Based on the recent study of the permeabilities of Kapton polyimide to CO_2/CH_4 mixtures ([21],[22]), it is expected that for systems which can be described by the generalized dual mode model ([17]), the permeability ratio of CO_2 over CH_4 in a mixture can be approximated to within about 20% by using the respective pure component permeabilities. Consequently, for the present general discussion, pure–component values will be used in Equation 7 in the following sections for discussing this important system.

Discussion

General Considerations. Representative CO_2 permeabilities for several glassy polymers at 35°C are plotted as a function of the upstream penetrant pressure in Figure 2 (8). Except for cellulose acetate, the permeabilities decrease monotonically with upstream pressure, consistent with the dual mode model predictions (17). The behavior of cellulose acetate will be addressed in a later section in terms of plasticization arguments. The ideal separation factors for CO_2/CH_4 at 20 atm, calculated using the pure-component permeabilities, are plotted in Figure 3 versus the solubility parameters of the various polymers. The solubility parameters of polymers (28-32) and the permeability data (5,6,33-35) were taken from a number of sources. A simple interpretation of Figure 3 might be that the higher intersegmental interactions associated with high solubility parameter polymers create a mobility selecting environment by making it more difficult to form a transient gap of sufficient size to pass a bulky, spherical CH_4 molecule compared to a streamlined, linear CO_2 molecule. As illustrated in later discussion of the separate mobility and solubility factors in Equation 5, this argument based solely on mobility selectivity appears to be oversimplified. Especially in the case of cellulose acetate, it will be shown that solubility considerations are of considerable importance.

Examination of Figures 2 and 3 supports the previous observation that low permeability and high selectivity are generally related. For example, the CO_2 permeability of poly(phenylene oxide) (PPO) is over twelve times higher than that of polysulfone, but its CO_2/CH_4 selectivity is less than half that of polysulfone. Kapton, on the other hand, is over twenty-five times less permeable to CO_2 than polysulfone, yet its CO_2/CH_4 selectivity is more than twice as high as that of polysulfone.

Such trends suggest that increases in permselectivity could be achieved by substituting a polar or hydrogen-bonding group on the phenylene ring of PPO to increase its cohesive energy density at the expense of its high CO_2 permeability. Alternatively, one could introduce irregularities into the Kapton backbone through the use of one or more comonomers along with the standard bis-4(aminophenyl ether) used as the diamine in Kapton production. Such modifications should inhibit packing and thereby lower the effective cohesive energy density. This "opening up" of the polymer structure would tend to markedly increase the CO_2 permeability but on the basis of Figure 3, may also reduce the selectivity. These concepts are derivative of those pioneered by H. Hoehn of DuPont in his work on the development of reverse osmosis membranes from aromatic polyamides (36).

Solubility and Diffusivity Considerations. The preceding general discussion has been largely conjectural in terms of the specific reasons for the relationship between variations in the cohesive energy density and variations in membrane selectivity and permeability. To pursue these issues in a more quantitative fashion, it is useful to consider the separate solubility and mobility contributions, D and S, for the various polymers shown in Figure 3.
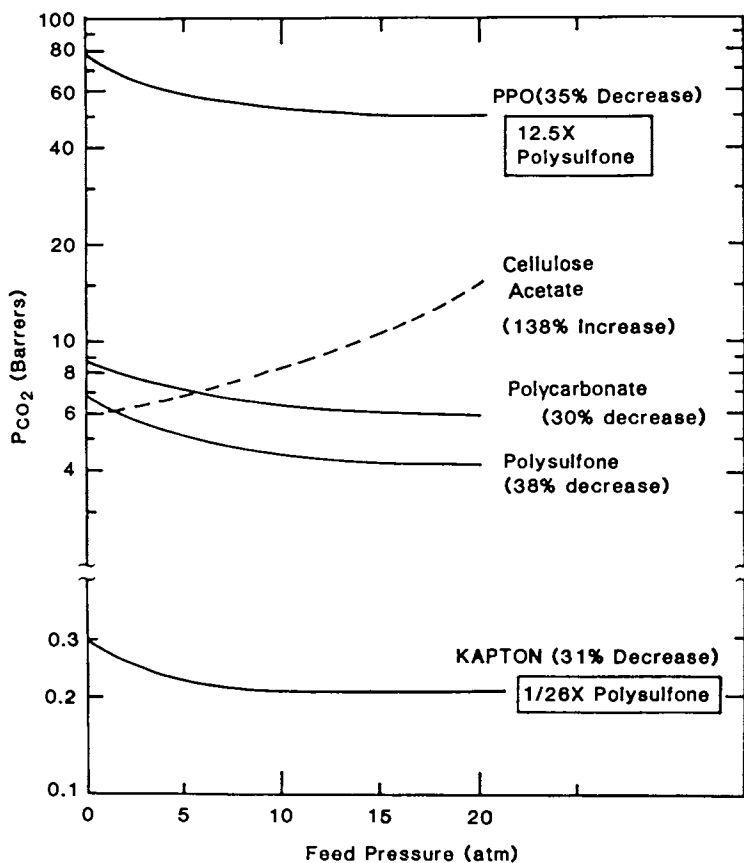
Figure 2.   Pressure dependence of CO_2 permeability in a variety of
glassy polymers at 35 °C.   The cellulose acetate data are
estimated from a number of sources including Ref. 5 and 6
and "The Science and Technology of Polymer Films", ed. by
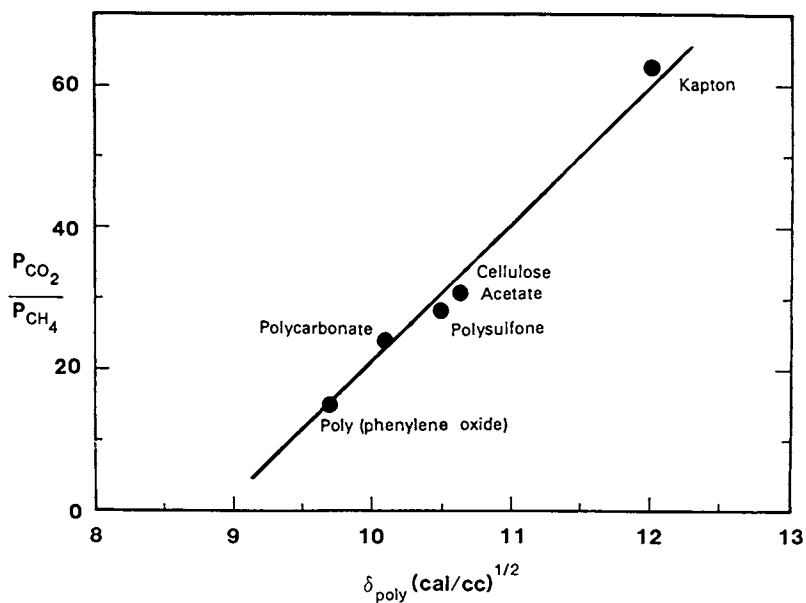O. J. Sweeting, Vol. II, Wiley Interscience, NY (1971).

Figure 3. Correlation between the solubility parameter of several
glassy polymers and the ideal separation factors for the
CO_2/CH_4 system calculated using the pure component per-
meabilities at 35 °C for a 20 atm upstream pressure of
each component.

    The sorption isotherms for most gases in glassy polymers tend to
have concave shapes like those shown in Figure 4. As a result, the
apparent solubility ($\overline{S} = C_2/p_2$) is a decreasing function of the up-
stream penetrant pressure. On the other hand, the diffusion coef-
ficients, $\overline{D}$, of gases in glassy polymers typically increase with
sorbed concentration even in the absence of plasticization (17).
Such increases are moderate for all of the materials in Figure 2 ex-
cept cellulose acetate and can be explained in terms of saturation
of excess volume in the polymer as concentration increases. Strong
plasticization, on the other hand, produces dramatic upswings in the
apparent mobility as appears to be the case with cellulose acetate.
The observed pressure dependence of the permeabilities shown in
Figure 2 are the net result of these two effects related to $\overline{D}$ and $\overline{S}$.
In the case of cellulose acetate, the sorption isotherm for CO_2 has
the same type of concave shape as shown in Figure 4, so a sharp in-
crease in $\overline{D}$ apparently overpowers the effect of the decreasing ap-
parent solubility coefficient. The reason for cellulose acetate's
greater tendency to be plasticized compared to the other polymers in
Figure 2 is currently not well understood. Since plasticization
tends to produce a more rubbery material, it is to be expected that
selectivity losses may attend the large upswing in CO_2 permeability,
but no published data are available to corroborate this suggestion.
    The apparent solubilities and average diffusivities, $\overline{S}$ and $\overline{D}$,
for CO_2 and CH_4 in a number of glassy polymers at 30°C and 20 atm are
shown in Table I. The values reported for cellulose acetate were
estimated from various sources in the literature (5,6,37). In the
case of cellulose acetate where CO_2 plasticization is apparently
significant, it was assumed that the CH_4 permeability in CO_2/CH_4
mixtures will increase by at least the same percentage as the CO_2
permeability. This assumption seems reasonable since the plasticized
matrix becomes more rubber-like and less discriminating for pene-
trants of different sizes and shapes (see Figure 1).
    According to Equation 7, the ratio of permeabilities is given
by Equation 8 after substitution from Equation 5 for components A
and B:

$$\alpha^*_{AB} = P_A/P_B = [\overline{S}_A/\overline{S}_B] \; [\overline{D}_A/\overline{D}_B] \tag{8}$$

Equation 8 demonstrates that the ideal separation factor can be sepa-
rated into a so-called "solubility selectivity", $[\overline{S}_A/\overline{S}_B]$, and a
"mobility selectivity", $[\overline{D}_A/\overline{D}_B]$. These two ratios are also reported
in Table I. Evidently, the contribution of the "mobility selectiv-
ity" is the dominant factor for all of the polymers considered ex-
cept cellulose acetate in which the opposite is observed. The CO_2
plasticization tendency of cellulose acetate may, in fact, be re-
lated to this polymer's apparent high "solubility selectivity".
Clearly, the available data do not justify more than a tentative sug-
gestion at this point that high "solubility selectivity" such as
that seen in cellulose acetate may be associated with a tendency to
be plasticized with a subsequent loss in glass-like selectivity.
More detailed sorption and diffusion measurements using a single
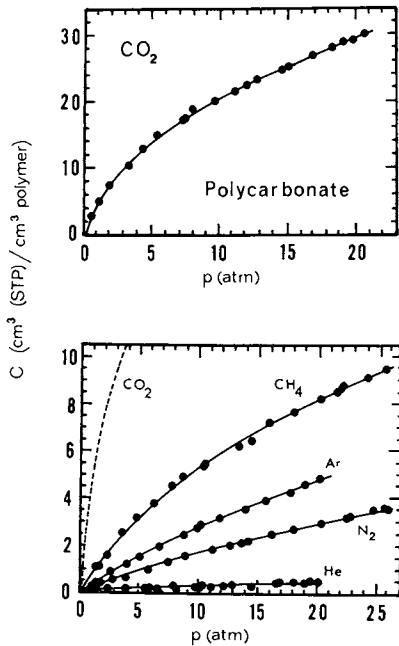
Figure 4.   Sorption isotherms for various gases in polycarbonate at
            35 °C.

Table I: Mobility and solubility contributions to the permeability
         and selectivity of typical glassy polymers at 35°C for a
         20 atm pressure of both components based on pure component
         parameters.

POLYMER	$\overline{D}_{CO_2}$ *	$\overline{S}_{CO_2}$ **	$\overline{D}_{CH_4}$ *	$\overline{S}_{CH_4}$ **	$\dfrac{\overline{P}_{CO_2}}{\overline{P}_{CH_4}}$	$\dfrac{\overline{D}_{CO_2}}{\overline{D}_{CH_4}}$	$\dfrac{\overline{S}_{CO_2}}{\overline{S}_{CH_4}}$
POLY(PHENYLENE OXIDE) (PPO)	2.2×10^{-7}	2.10	3.2×10^{-8}	0.95	15.1	6.88	2.2
POLYCARBONATE	3.2×10^{-8}	1.47	4.7×10^{-9}	0.41	24.4	6.81	3.6
CELLULOSE *** ACETATE	5.9×10^{-8}	2.05	1.4×10^{-8}	0.28	30.8	4.21	7.3
POLYSULFONE	2.3×10^{-8}	1.44	2.6×10^{-9}	0.45	28.3	8.85	3.2
KAPTON	1.0×10^{-9}	1.53	6.5×10^{-11}	0.37	63.6	15.38	4.1

  *$\overline{D}$ has units of $[cm^2/sec]$.
 **$\overline{S}$ has units of $[cc(STP)]/[cc \text{ of polymer- atm}]$.
***Estimated values as indicated in the caption of Figure 2.

well-characterized dense film sample for the cellulose acetate sys-
tem are needed to better understand the factors responsible for its
rather unusual behavior compared to the other polymers considered.
Understanding these principles may permit expansion of the ranks of
"solubility selective" materials for blending with more plasticiz-
ation resistant materials to enhance their solubility selectivity.

Poly(phenylene oxide) is an example of a material that might
benefit from such a blending approach if an appropriate miscible
"solubility selective" polymer could be discovered. As shown in
Figure 2 and Table I, PPO is highly permeable to CO_2 and has a re-
spectable mobility selectivity equal to 6.9 for the CO_2/CH_4 system.
The overall selectivity of PPO for this system is, however, rather
low due to the low solubility selectivity (the lowest in Table I).
If blending could raise the solubility selectivity from two to four
without a serious loss in CO_2 permeability, the resultant material
would be quite attractive as a membrane for CO_2/CH_4 separations.
No data are available for evaluating this latter possibility, al-
though it has been reported that both the solubility and perme-
ability of CO_2 in PPO are decreased when PPO is blended with poly-
styrene (35).

Apparent solubility coefficients $(\overline{S})$ evaluated at twenty at-
mospheres at 35°C for various penetrants in several glassy polymers
are shown in Figure 5 as functions of the critical temperatures of
the gases. The plot demonstrates the difficulty in achieving dra-
matic changes in solubility selectivity using a fairly large variety
of polymer types. The relative insensitivity of the solubility
ratios of different gases to changes in polymer types is due to the
fact that the gas solubility is strongly dependent upon the inherent
condensibility of the respective gases. Although the amount of un-
relaxed volume between chain segments and polymer-penetrant inter-
actions enters into the determination of $\overline{S}$, it is largely over-
shadowed by the condensibility of the gas which is related directly
to the critical temperature of the gas. Note that even in polymers
such as PPO with a large amount of unrelaxed intersegmental volume,
the sorption levels of all components tend to be high, so the ratios
are not changed much. One must, therefore, rely primarily upon dif-
ferences in polymer-penetrant interactions to yield the rather mode-
rate differences in solubility selectivity.

The range of solubility selectivities for the CO_2/CH_4 system,
for example, includes only the interval from 2.2 (for PPO) to 7.32
(for cellulose acetate). Although the solubility selectivity of
cellulose acetate is considerable, it is not large enough by itself
to be competitive without a substantial complementary factor of 4.2
contributed by its mobility selectivity (Table I). If this mobility
contribution is undermined by plasticization resulting from the inter-
actions that enhance the CO_2 solubility relative to that of CH_4, then
basing selectivity enhancement on solubility effects is somewhat
questionable. Certainly, more data are required on cellulose acetate
and any other polymers that can be discovered with high solubility
selectivities before such a negative conclusion is adopted. The use
of dopants in polymers to increase the solubility of one component
relative to others has been discussed by Heyd and McCandless (38).
If suitable nonmigrating additives can be found to provide sufficient-
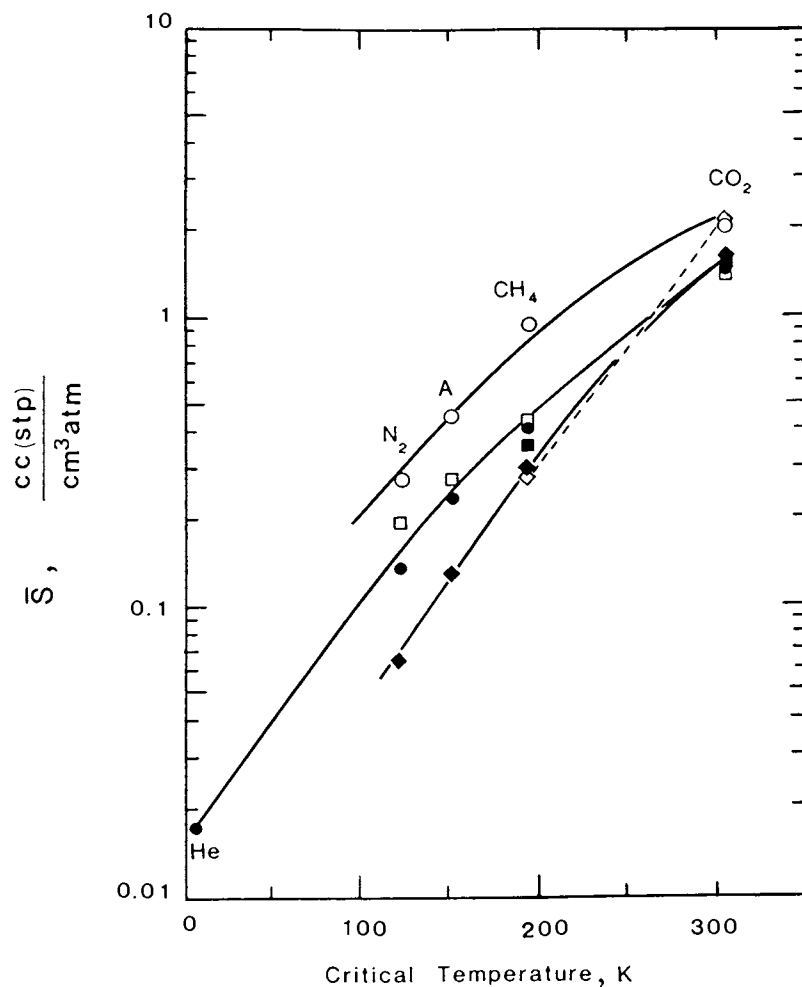ly high values of solubility selectivity, one could, in principle,

Figure 5.   Correlation of the apparent solubility at 20 atm and 35 °C with the critical temperatures of various penetrants in a number of glassy polymers: ● polycarbonate, ◯ poly(phenylene oxide), ☐ polysulfone, ■ Kapton, ◇ cellulose acetate, ◆ PMMA.

preclude the need to rely upon mobility regulating mechanisms to aid in the separation process. This is the basis for solvent extraction and liquid membrane systems. The problems and considerations in such cases are quite different from those in standard bulk polymer systems and will not be discussed here.

Manipulation of the structure of standard bulk polymers to alter their mobility selectivity can be guided somewhat by correlations such as those shown in Figures 6 and 7. Figure 6 shows a correlation of $\bar{D}$ for various penetrants in a number of different glassy polymers. The correlating variable, the kinetic diameter of the gas, is related to the zeolite window dimension that will just permit passage of the penetrant of interest (39). For molecules that are essentially spherical, such as methane, argon and helium, this dimension is similar to the Lennard-Jones diameter. For asymmetric molecules such as carbon dioxide and nitrogen, however, the kinetic diameter corresponds more closely to the minimum diameter of the molecule. This figure shows clearly the extremely strong effect on the penetrant mobility caused by small differences in minimum penetrant diameter. A difference of less than 1.5 Å distinguishes the kinetic diameters of helium and methane; however, there are almost three orders of magnitude difference in their mobility in polycarbonate. The spread in the various diffusivity values for a given penetrant in different polymers can be partially understood in terms of Figure 7. This figure shows the effects of variations in the specific volume of the polymer on the observed diffusion coefficients, $\bar{D}$. While this correlation is useful and intuitively satisfying, it undoubtedly oversimplifies the true differences in molecular-scale environments sampled by a penetrant as it moves through the polymers. The tendency for glassy polymers to exhibit local variations in the amount and distribution of molecular scale intersegmental gaps trapped during the quenching process from the rubbery state has been discussed in detail (17). Nevertheless, the correlation in Figure 7 is useful in depicting relative differences between extremes such as that represented by the highly open PPO environment and the rather compact Kapton environment. It is clear that the mobility selectivity is substantially higher for Kapton than for PPO. The ratios of the apparent diffusivities of CO_2 and CH_4 increase from 6.9 for PPO to 15.4 for Kapton; however, the permeability for CO_2 drops by more than two hundred fold in going from PPO to Kapton. Such a dramatic penalty in productivity certainly tends to confirm the general point of view that one cannot have both high selectivity and high productivity in the same membrane material.

Fortunately, encouraging exceptions to such a point of view can be found in the literature for both H_2/CH_4 and CO_2/CH_4 systems (11,13). These studies suggest the possibility of increasing the product permeability while maintaining or even increasing selectivity by proper design of the polymer molecular architecture. Examples of such exceptional polymers are given in Table II. Polymers A and B are generically classified as polyimides and were formed by condensation of 4,4'- hexafluoroisopropylidene diphthalic anhydride with 3,5-diaminobenzoic acid and with 1,5-diaminonaphthalene, respectively (13). Note that the high permselectivities of polymers A and B are consistent with correlations such as that in Figure 3, since polyimides typically exhibit high cohesive energies similar
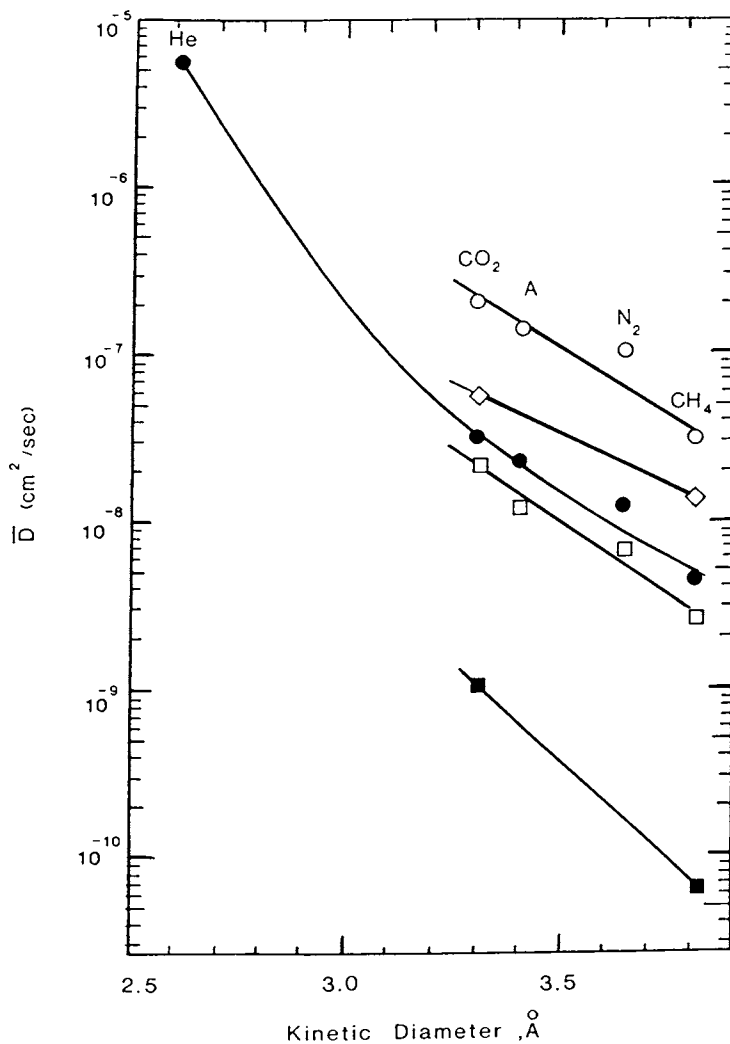
Figure 6. Correlation of the average diffusion coefficient, $\bar{D}$, and the kinetic diameters of several penetrants in a number of glassy polymers at 35 °C for an upstream penetrant pressure of 20 atm: ● polycarbonate, ○ poly(phenylene oxide), □ polysulfone, ■ Kapton, ◇ cellulose acetate.
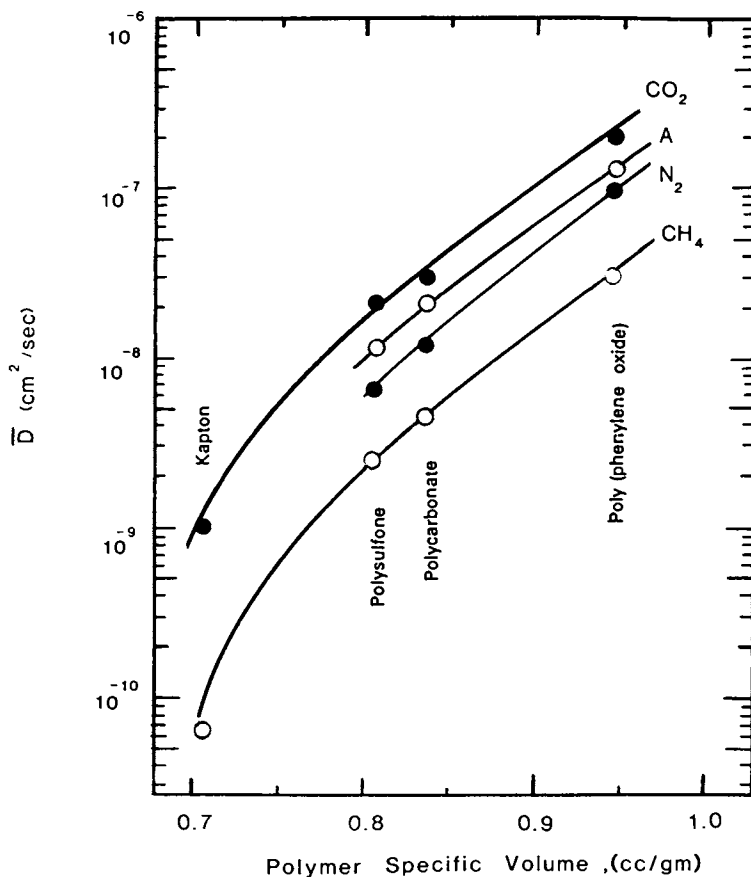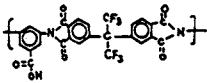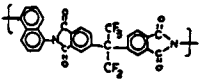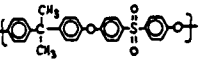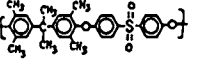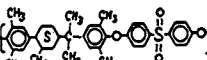
Figure 7. Correlation of the average diffusion coefficients of several penetrants with the specific volumes of the polymers for an upstream penetrant pressure of 20 atm at 35 °C.

Table II. Comparison of novel high flux, high selectivity poly-
           imides and polysulfones with standard polysulfone.

POLYMER	STRUCTURE	P_{H_2}	$\dfrac{P_{H_2}}{P_{CH_4}}$	P_{CO_2}	$\dfrac{P_{CO_2}}{P_{CH_4}}$
A		32	427	-	-
B		76	112	-	-
POLYSULFONE		12	78	4.4	28
C		-	-	21	68
D		-	-	65	24

to Kapton. Surprisingly, however, both polymers A and B exhibit
not only the expected high selectivities but also permeabilities
that are markedly higher than those of cellulose acetate or poly-
sulfone.
    A similarly encouraging exception to the general trend in selec-
tivity and productivity is found in the poly(aryl ether) family to
which the standard polysulfone material belongs. Polymers C and D
in Table II are also classified as polysulfones and are referred to
as poly(tetramethyl bis-A sulfone) and poly(tetramethyl bis-L sul-
fone), respectively (11). One would have overlooked this group of
materials if an oversimplified correlation such as that shown in
Figure 3 were the only guideline used in candidate selection. As
shown in Table II, polymers C and D are roughly five and fifteen
times respectively more permeable to CO_2 than standard polysulfone.
The CO_2/CH_4 selectivities of these two polymers are roughly 2.4 and
0.9 times respectively, that of standard polysulfone.
    In both the polyimides and the aryl ether cases, the backbones
are comprised of bulky structures that resist compact packing of
segments. The intersegmental separations in these rigid bulky poly-
mers may be large enough to permit relatively free movement of pene-
trants below a certain critical size. On the other hand, the sepa-
rations may be small enough and local chain motions restricted enough
to provide a substantial size- and shape-discriminating ability for
slightly less compact molecules. Although solubility and diffusiv-
ity data are not available for these materials, the above interpre-
tation appears to be reasonable. In the case of polymer D, the pre-
sence of the flexible cycloalkyl group presumably offsets the stif-
fening effect due to methylation and the selectivity is actually
slightly lower than that of standard polysulfone. Pilato et al (11)
suggested that densities of polymers C and D (1.15 and 1.10 g/cc,
respectively) compared to standard polysulfone (1.24 g/cc) results
in the higher permeabilities of these complex sulfones compared to
the standard material. Such a suggestion is clearly consistent with
the trends shown in Figure 7.
    The preceding observations suggest that a loosely packed glassy
polymer with sufficient cohesive energy and a rigid plasticization-
resistant backbone is conducive to both high flux and high selec-
tivity. Following this conclusion, even without synthesizing generi-
cally new polymers, relatively high permeabilities and selectivities
may be achievable by structural modifications of poly(aryl ethers)
polyimides, polyamides, polycarbonates, polyesters and polyurethanes.

Environmental Factors. Clearly, discovery of an extraordinarily per-
meable and selective material that can survive only weeks or months
in the required operating environment will be unacceptable. The
present brief discussion suggests approaches to consider in evaluat-
ing environmental challenges to a candidate material. Such tests
should be performed in parallel with detailed sorption and transport
measurements soon after a candidate material is found to have de-
sirable selectivity and permeability properties.
    Complex stress distributions can exist in quenched glassy poly-
mers and can make them subject to microscopic failure. This is es-
pecially true in the presence of thermal and penetrant level cycling
because surface layer expansion can induce substantial tensile

stresses. Under tensile stresses, many glassy polymers develop a
dense network of fine surface cracks or "crazes". Load bearing fi-
brils, composed of bundles of chains, and having void volumes in the
50% range (40), traverse the crazes. The basic sorption and trans-
port properties of such a material are drastically changed with es-
sentially complete loss of selectivity in the crazed region.
      A simple method for evaluating the stress cracking tendency of
materials by environmental agents can be used as a screening test.
The test sample is used in the form of a cantilevered beam loaded
with a weight as shown in Figure 8 (41). By exposing the sample to
a test environment containing various partial pressures of agents
such as CO_2, H_2S and H_2O, the potential for stress-cracking of the
polymer can be determined in a quantitative manner. Because the
stress in the bar varies from the maximum at the clamped end to zero
at the free end, a stress-cracking agent will cause cracking down to
the point where the stress is insufficient to produce a local fail-
ure of the secondary bonds between polymer segments. This test can
be performed as a function of temperature as well as composition to
identify operating conditions where potential problems can be anti-
cipated. The critical stress, S_c, is calculated from Equation 9
where F is the total force applied (clip plus weight), L is the dis-
tance along the bar between the free end and the stress crack closest
to it. The dimensions b and d are the width and thickness of the bar
in Figure 8.

$$S_c = \frac{6\ FL}{b\ d^2} \tag{9}$$

The surface crazes observed are typically on the order of a micron in
depth, so the entire sample bar thickness does not to be invaded for
the test to be useful. Even rather large molecules can penetrate to
the depth of a micron in a matter of hours or days, and smaller mole-
cules like CO_2 can do so in a matter of minutes or seconds.
      True chemical attack, as opposed to the above physical process
of crazing, can be predicted somewhat on the basis of known lability
of chain backbone groups. For example, it is known that ester link-
ages are particularly susceptible to hydrolytic attack. Imide groups
are, on the other hand, quite hydrolytically stable but are subject
to aggressive attack by Lewis bases. A combined infrared spectro-
scopic and gravimetric sorption study has been used to follow the
progressive attack of ammonia on the imide ring of Kapton (42).
The severity of the attack suggests that one should be cautious in
using materials such as the highly selective imides in Table II for
separations where Lewis bases are present.
      The focus of this paper and the multiplicity of environmental
hazards faced by a candidate membrane material make it impossible to
enumerate specifics in greater detail than that discussed above. If
strong stress-cracking tendencies are observed in the tests described
above (that is, low values of S_c observed), plasticization tendencies
may exist for the polymer-penetrant pair. In such a case, care
should be exercised to study the candidate material under conditions
that include the most demanding environment anticipated in actual
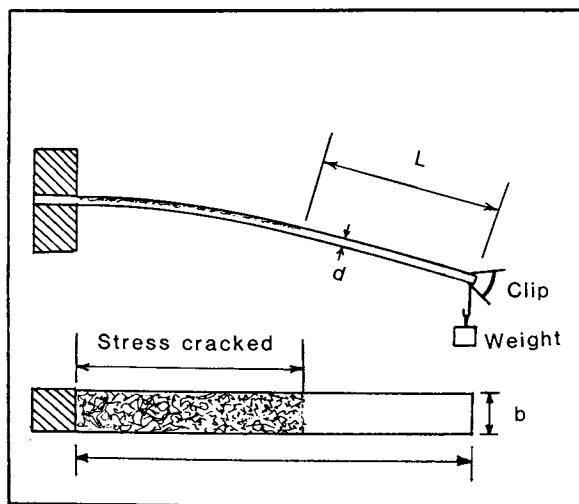use.

Figure 8.   Simple apparatus for evaluating stress cracking potential
of candidate membrane materials.

Conclusions

There appears to be reasons for cautious optimism concerning the possibility of developing more permeable and selective membranes in spite of the general inverse relationship between these two variables. Control of chain backbone rigidity and intersegmental packing density may provide a means of selectively permitting the passage of a relatively compact permeant molecule while substantially restricting the nonpermeant. Reliance on solubility selectivity to provide the major means of discriminating between gas penetrants in dense polymer films may be less promising. Cellulose acetate, the only material considered that is strongly selective for CO_2 compared to CH_4 on the basis of solubility, appears to exhibit a strong plasticizing response to increasing CO_2 pressures. Such an effect is expected to further reduce the mobility selectivity of cellulose acetate and thereby cause it to lose overall selectivity as CO_2 partial pressure increases. A similar trend may be observed for other glassy materials that rely strongly upon solubility as the principal basis for their selectivity, however, considerably more research is required before this tentative conclusion can be verified.

A correlative approach such as that shown in Figure 3 for the overall selectivity (or permeability) is useful in some senses but insufficient because it would have led one to overlook the extremely interesting family of poly(aryl ethers) which in some cases have both high selectivity and high permeabilities. A detailed analysis of the mobility and solubility contributions to the permeability and selectivity properties of an homologous series of candidate materials can be extremely valuable in membrane material selection. Such an approach permits one to assess the true cause of changes in the observed permeability and selectivity and can more effectively guide a systematic program to optimize membrane material transport properties.

Environmental sensitivity of candidate materials must be assessed under conditions of temperature, pressure and composition that simulate actual usage. Failure of a material in this context can severely limit the range of applicability of a membrane that otherwise has outstanding properties.

Acknowledgments

Literature Cited

1. Gardner, R. J.; Crane, R. A.; Hannan, J. F. CEP 1977, 73, 11, 76.
2. Bollinger, W. A.; MacLean, D. L.; Narayan, R. S. CEP 1982, 78, 10, 27.
3. Schell, W. J.; Houston, D. D. CEP 1982, 78, 10, 33 and Hydrocarbon Proces. 1982, 61, 9, 249.
4. Lane, V. O. Hydrocarbon Proces. 1983, 62, 8, 56.

5.   Mazur, W. H.; Chan, M. C. CEP 1982, 78, 10, 38.
6.   Coady, A. B.; Davis, J. A. CEP 1982, 78, 10, 45.
7.   Schendel, R. L.; Mariz, C. L.; Mak, J. Y. Hydrocarbon Proces.
     1983, 62, 8, 58.
8.   Koros, W. J. "Membrane-Based Gas Separations: Data Base and
     Models for Glassy Polymers", paper presented at Sunriver Mem-
     brane Conference, Sunriver, Oregon, September 1983.
9.   Koros, W. J. "Gas Separation Technology", International Membrane
     Technology Conference, Sydney, Australia, November 1983.
10. Cadotte, J. E.; King, R. S.; Majerle, R. J., Petersen, R. J.
     J. Macromol. Sci.-Chem. 1981, A15, 725.
11. Pilato, L.; Litz, L.; Hargitay, B.; Osborne, R. C.; Farnham,
     A.; Kawakami, J.; Fritze, P.; McGrath, J. Polym. Prepr., Am.
     Chem. Sci., Div. Polym. Chem. 1975, 16. 41.
12. McCandless, F. P. I&EC Process Des. Develop. 1972, 11, 470.
13. Pye, D. G.; Hoehn, H. H.; Panar, M. J. Appl. Polym. Sci. 1976,
     20, 287.
14. Crank, J. "The Mathematics of Diffusion", Clarendon, Oxford
     Press, 2nd Ed., 1975.
15. Van Amerongen, G. J. Rubber Chem. & Techn. 1964, 37, 1065.
16. Berens, A. R. J. Vinyl. Technol. 1979, 1, 38.
17. Chern, R. T.; Koros, W. J.; Sanders, E. S.; Chen, S. H.;
     Hopfenberg, H. B. ACS Symposium Series No. 233, Industrial Gas
     Separations, Whyte, T. E.; Yon, C. M.; Wagner, E. H. Eds; 1983;
     p. 47.
18. Stern, S. A.; Walawender, W. P. Separ. Sci. 1969, 4, 129.
19. Rogers, C. E. In "Physics and Chemistry of the Organic Solid
     State"; Fox, D.; Labes, M. M.; Weissberger, A. Eds.; Inter-
     science: New York 1965.
20. Yi-Yan, N.; Felder, R. M.; Koros, W. J. J. Appl. Polym. Sci.
     1980, 25, 1755.
21. Chern, R. T.; Koros, W. J.; Hopfenberg, H. B.; Stannett, V. T.
     J. Polym. Sci., Phys. Ed. in press.
22. Chern, R. T. Ph.D. Dissertation, North Carolina State Univer-
     sity, Raleigh, NC, 1983.
23. Chern, R. T.; Koros, W. J.; Hopfenberg, H. B.; Stannett, V. T.
     J. Polym. Sci.,Phys. Ed. 1983, 21, 753.
24. Chern, R. T.; Koros, W. J.; Sanders, E. S.; Yui, R. E.
     J. Membr. Sci. 1983, 15, 157.
25. Antonson, C. R.; Gardner, R. J.; King, C. F.; Ko, D. Y.
     Process Des. Develop. 1977, 16, 463.
26. Stern, S. A.; Mauze, G. R.; Frisch, H. L., J. Polym. Sci., Phys.
     Ed. 1983, 21, 1275.
27. Saxena, V.; Stern, S. A. J. Membr. Sci. 1982, 12, 65.
28. Hay, A. S.; Shenian, P.; Gowan, A. C.; Erhardt, P. F.; Haaf,
     W. R.; Therberge, J. E. In "Encyclopedia of Polymer Science and
     Technology"; Mark, H.; Gaylord, N. G.; Bikales, N. M. Eds.;
     Interscience, NY, 1964.
29. Schnell, H. "Chemistry and Physics of Polycarbonate", Inter-
     science, NY, 1964.
30. Johnson, R. N.; Farnham, A. G.; Clendinning, R. A.; Hale, W. F.;
     Merriam, C. N. J. Polym. Sci., 1967, A-1, 2375.
31. Lewis, O. G. "Physical Constants of Linear Homo-polymers",
     Springer-Verlag, NY, 1968.

32. Burrell, H. In "Polymer Handbook"; Bandrup, J.; Immergut, E. H. Eds.; John Wiley and Sons, NY, 1975.
33. Koros, W. J.; Chan, A. H.; Paul, D. R. J. Membr. Sci. 1977, 2, 165.
34. Erb, A. J.; Paul, D. R. J. Membr. Sci. 1981, 8, 11.
35. Morel, G.; Paul, D. R. J. Membr. Sci. 1982, 10, 273.
36. Hoehn, H.; Richter, J. W., US Patent Reissue, 1980, 30, 351.
37. Stern, S. A.; DeMerin̆o A. J. Polym. Sci., Phys. Ed. 1978, 16 735.
38. Heyd, R. L.; McCandless, F. P. J. Membr. Sci. 1977, 2, 375.
39. Breck, D. W. "Zeolite Molecular Sieves"; John Wiley and Sons, NY, 1974; p. 636.
40. Kambour, R. P. J. Polym. Sci. 1964, A2, 4159.
41. "Selecting Pastics for Chemical Resistance", Modern Plastics Encyclopedia, 1981-1982, p. 499.
42. Iler, L. R.; Laundon, R. C.; Koros, W. J. J. Appl. Polym. Sci. 1982, 27, 1163.

Selection and Evaluation of Membrane Materials for Liquid Separations

DOUGLAS R. LLOYD and TIMOTHY B. MELUCH

Department of Chemical Engineering, The University of Texas at Austin, Austin, TX 78712

Physicochemical interactions between permeating
molecules and the macromolecules which comprise the
membrane structure are considered. Dispersive, polar
and hydrogen-bonding interactions are used to
establish an index which can be useful in membrane
material selection. A number of material
characterization and evaluation procedures are
outlined.

The variety of materials from which membranes may be made is large
and ever increasing. Potential membrane materials include almost
every available homopolymer, copolymer and blend. It would be
convenient if the membrane material most suited for achieving a
desired separation could be selected prior to undertaking the often
difficult task of forming porous (1), integrally-skinned (2),
composite (3) or dynamic (4) membranes. Recognition of the fact
that membrane permeation is governed by both the chemical nature of
the membrane material and the physical structure of the membrane
facilitates the selection of an appropriate membrane material. The
objective of this paper is to present one possible approach to
membrane material selection for liquid separation applications. In
addition, methods for evaluating potential membrane materials are
discussed. A survey of membrane materials that have been utilized
for liquid separations is also included. Elsewhere in this volume
are comprehensive treatments of membrane materials for gas
separations (5), desalination (2,3,6) and biomedical applications
(7), as well as ion-exchange membranes (8). Thus, the discussions
of this chapter have been limited to the selection and evaluation
of membrane materials for the pressure-driven separation of
non-ionized liquid mixtures via reverse osmosis, ultrafiltration,
microfiltration and pervaporation. That is, only separations in
which electrostatic repulsion is not a factor are considered.
Evaluation and characterization of membranes are omitted and the
reader is referred to subsequent chapters in this volume (9,10) and
elsewhere (11).

The ability of a membrane to accomplish a desired separation
depends on the relative permeability of the membrane for the
solution components. The rate at which any compound permeates a
membrane depends upon two factors: an equilibrium effect
(partitioning of solution components between free solution and the
membrane phase) and a kinetic effect (for example, diffusion and
bulk flow). While it is true that the physical structure of the
membrane influences both of these phenomena, they must also be
considered in terms of the strength and nature (attraction or
aversion) of permeant-membrane physicochemical interactions. Strong
forces of attraction lead to increased solubility in the membrane
phase. However, if the attraction is too strong, permeation rates
may be decreased as the permeant is immobilized by the membrane
material. In the extreme, strong affinity may lead to swelling or
even dissolution of the membrane. On the other hand, strong
negative interactions (such as ionic repulsion) and steric effects
exclude the permeant from entering the membrane phase. For the
case discussed here, permeant-membrane interactions can be
considered in terms of physicochemical effects including dispersive
forces, polar interactions, hydrogen bonding and steric hindrance.
Because these effects are present over the complete range of
membrane porosity, an understanding of these physicochemical effects
and how they influence permeation will be beneficial in the
selection of membrane materials.

Physicochemical Considerations

In this section, the physicochemical effects mentioned above are
discussed in terms of how they influence permeation, how the
permeant and membrane material could be characterized in terms of
these effects and how these ideas can be used to assist in
membrane material selection.

Polar Forces. If a molecule is non-symmetric and contains atoms of
different electronegativities, a net separation of charge will
occur. The dipole moment, expressed in Debye units (1 Debye (D) =
1×10^{-18} esu cm), is a measure of the polar nature of the molecule;
increasing dipole moment indicates increasing polarity. Symmetric
molecules such as CH_4, CCl_4 and C_6H_6 have dipole moments which are
approximately zero and are known as non-polar molecules. Non-
symmetric molecules such as H_2O and HCl have permanent, non-zero
dipole moments in the range of 1 to 20 D.
     Polar forces between molecules in solution may arise from
either permanent dipoles or induced dipoles. When a molecule
possessing a permanent dipole comes into close association with a
non-polar molecule, a relatively weak (0.0001 kcal/mole) permanent
dipole-induced dipole interaction (Keesom force) arises. Close
association of two permanent dipoles produces a stronger (1 to 2
kcal/mole) dipole-dipole interaction or Debye force (12). In light
of the relative magnitudes of these interactive forces, the Keesom
forces and the extremely weak induced dipole-induced dipole
interactions will be omitted from further discussion.
     A number of empirical parameters have been used to quantify

the strength of polar forces between molecules. Originally developed for interactions between low molecular weight materials, these parameters can be classified as those assuming dissociation and those making no such assumption. For example, the polarity of a solute can be related to its degree of dissociation expressed in terms of pK_a. The Taft and Hammett numbers have also been developed (13,14) as a measure of the polar effect of a substituent group on reactivity. Other workers have used the dipole moment (15) or the polar component of the Hansen solubility parameter (16) as a measure of the polar character of a molecule.

Dispersive Forces. In the absence of permanent or induced dipoles, London dispersive forces (17) become important. Random fluctuations in the electron cloud produce a time-varying, temperature-independent intermolecular force of attraction termed the dispersive force. The magnitude of these dispersive forces (typically 0.1 to 2 kcal/mole) can be represented by a variety of cohesive parameters including the dispersive component of the Hansen solubility parameter (16).
     Typically dispersive forces are the dominating consideration when discussing hydrocarbon molecules. The dispersive character of a homologous series of hydrocarbons increases as the length of the aliphatic chain increases, is greater for a saturated hydrocarbon than for its unsaturated counterpart, and is greater for cyclic hydrocarbons than for their aliphatic counterparts. Polymers with long aliphatic hydrocarbon sections, such as poly(ethylene) and nylon-6 have strong dispersive character. It should be noted that the repeat unit of the polymer may have both a dispersive nature as well as a polar nature. For example, nylon-6 is dispersive due to the $-(CH_2)_5-$ segment and polar due to the -CO-NH- linkage. Similarly, copolymers may have polar segments as well as nonpolar segments. In either case, attraction due to dispersive forces between permeant and membrane material exists.

Hydrogen Bonding. The possibility of hydrogen bonding arises when the electron cloud of a hydrogen atom is pulled away from the nucleus by a strongly electronegative atom to which the hydrogen is covalently bonded. The hydrogen nucleus (a proton) is thus left exposed, allowing it to interact with a neighboring structure which contains lone pair electrons. The more electronegative the atom to which the hydrogen is covalently attached, the stronger the hydrogen bonding capability. The strength of hydrogen bonds are typically in the range of 2 to 10 kcal/mole. In general, atoms less electronegative than nitrogen do not cause hydrogen bonds of measurable strength. Therefore hydrocarbons, in addition to being free of polar effects, do not form hydrogen bonds. However, some compounds may have hydrogen bonding effects in addition to polar and dispersive forces.
     Because hydrogen bonds depend upon the coordination of the hydrogen nucleus with an electronegative atom, temperature variations have a strong influence on the strength and number of hydrogen bonds present in a system. A temperature increase tends to increase the random motion of molecules and so decrease the number of hydrogen bonds. Concentration also has a strong effect;

as the number of hydrogen bonding molecules in any system increases, the number of hydrogen bonds increases proportionally. Hydrogen bonds affect the dipole moment of the compounds in which they form. As a compound becomes more strongly hydrogen bonded, electron clouds shift and the dipole moment increases. Consequently, polar forces and hydrogen bonding are difficult to distinguish in systems in which they occur together.

   Hydrogen bonds have the potential of being stronger than either polar or dispersive forces and are of considerable importance in aqueous system.   They differ from the polar and dispersive interactions discussed above in that polar and dispersive effects are always intermolecular (forces between molecules) while hydrogen bonds can form intermolecularly and intramolecularly. Each of these two types of hydrogen bonds has a different effect upon permeation.   Intramolecular hydrogen bonds tend to form when a hydrogen atom is available for secondary bonding (that is, attached to an oxygen or nitrogen atom) in such a position that, by forming a hydrogen bond with another strongly electronegative atom within the same molecule, an unstrained ring structure is formed. Thus, intramolecular hydrogen bonding may slightly alter the effective size of permeant molecules. On the other hand, intermolecular hydrogen bonds may result in the formation of clusters of solute or solvent or in the coupling of solute and solvent. The formation of hydrogen bonded networks of molecules in solution may increase the effective size of the permeant thereby decreasing transport and, perhaps, increasing rejection due to steric effects.   If intermolecular hydrogen bonding between the membrane material and the species to be transported (for example, the solvent) is possible, then a layer of bound solvent molecules may be built up at the membrane surface. Because bound solvent typically has a decreased solvating capacity, the result is an increase in solute rejection. The effects of both inter- and intramolecular hydrogen bonding on physical properties have been tabulated previously (18).

   The concept of intermolecular hydrogen bonding leading to clustering was first introduced by Frank (19) and formalized by Zimm and Lundberg (20-22). Briefly, clustering is the association of molecules into a hydrogen bonded network. At equilibrium, individual molecules enter and leave clusters, which form and dissipate rapidly. The number of molecules within the average cluster at equilibrium is a function of temperature and the presence of foreign chemical species or functional groups, which may enhance or disrupt intermolecular hydrogen bonding. For purposes of the present discussion, clustering of solvent or solute near or within the membrane phase is of importance. To date, the majority of the work has dealt exclusively with clustering of the solvent water and how this is influenced by the presence of solutes (low molecular weight as well as macromolecular) and solid membrane materials. Typical findings are briefly summarized here; for further details see References 23, 24 and 25. Sites such as hydroxyl, carboxyl and peptide bonds in the membrane material have the ability to form hydrogen bonds or strong polar interactions with water, resulting in a decrease in the average cluster size. To have any effect on the structure of water, the active sites within the membrane material must be neither involved in strong

inter- or intrachain hydrogen bonding nor hidden within highly
ordered crystalline structures. When polymer-water interactions
are possible, the water may form a bound layer on the membrane. In
this case, the water-membrane interaction decreases the available
energy of hydration per water molecule in the bound layer. Thus,
the capacity of the water to dissolve solute may be reduced and
rejection increased. Providing that the water-membrane attraction
is not so strong as to completely immobilize the bound water,
transport of water is still possible. Conversely, the availability
and accessibility of dispersive, hydrophobic sites in the membrane
material will lead to increased water clustering. Water-membrane
interactions of this type, which are common in polyolefins, vinyl
plastics and elastomers such as silicone, result in a decreased
equilibrium water content but an increased mobility of water within
the membrane phase. Selection of an appropriate membrane material
to achieve aqueous separations should be based on consideration of
the potential for water-membrane interactions and the strength of
such interactions relative to intermolecular water-water hydrogen
bonds; that is, their impact on water clustering.

   Most attempts to quantify hydrogen bonding effects have
exploited the disturbance of normal infrared and Raman spectra
which occurs when hydrogen bonds are formed. Shifts in the O-H and
N-H stretching frequencies were reported by Gordy (26-28) and later
used (15) to aid in the prediction of the solubility of polymers in
various organic solvents. These shifts have been divided into two
components representing the proton donating (acidic) and proton
accepting (basic) tendencies of various molecules (29). One other
approach, that of relating the change in heat of vaporization to
hydrogen bonding strength resulted in the hydrogen bonding
component of the Hansen solubility parameter (16). The
determination of the polar and hydrogen bonding components of the
Hansen solubility parameter was originally a trial and error
procedure. Therefore, the definition of hydrogen bonding used for
this parameter is somewhat imprecise, and perhaps some more
ambiguous terms, such as "weak chemical bonds" or perhaps
"association bonds," might be better.

Steric Effects. When solution components A (solute, minor solution
component) and B (solvent, major solution component) are similar in
chemical nature, the separation mechanism becomes one of distinction
on the basis of effective molecular size. Even when A and B are
chemically dissimilar, steric factors play a significant role in
achieving separation if A is much larger than B (for example,
microfiltration and ultrafiltration involving aqueous solutions of
macromolecules). In addition, the effective size of the permeating
species relative to the size of the available transport corridor is
important over the complete spectrum of membrane porosity (dense,
finely porous, porous). When the permeant is larger than the
transport corridor, it is sterically prevented from entering the
membrane phase. When the permeant is smaller than the transport
corridor, partitioning and transport occur under the influence of
chemical interactions.

   A number of parameters have been developed to describe the
effective size of suspended or dissolved compounds (29-32). One

parameter, which has found extensive use in the membrane literature, is the molecular weight of the permeating species. However, sufficient evidence exists to indicate that molecular weight alone does not provide an adequate description of the effective size of the permeant. A parameter capable of representing the effective size of a permeating species must take into account both the size and shape of the molecule in solution. One possible effective size parameter, ψ_I, is the product of a characteristic molecular dimension and the ratio of molecular volume to molecular surface area ($\psi_I = d_c v/a$). The molecular volume, v, can be obtained from molar volume data available in the literature (33), estimated (34) or obtained experimentally (35). The molecular surface area, a, can be estimated from the chemical structure of the compound (36). The characteristic dimension, d_c, may be represented by the radius r_v of a sphere of volume equal to the molecular volume, the radius r_a of a sphere of surface area equal to that of the molecule, the root mean square radius r_{rms}, the kinetic radius r_k, the Stokes radius r_s or, for high molecular weight solutes, the radius of gyration r_g (37,38). Synthetic high molecular weight solutes typically show a distribution in size. Therefore, a mean radius r_m, must be used; where r_m may be the arithmetic, geometric or harmonic mean of one of the characteristic dimensions listed above. In addition, when dealing with synthetic macromolecules , a knowledge of the frequency distribution (Gaussian, logarithmic, log-normal, etc.) is necessary (39). The data listed in Table I indicate the sensitivity of v, a, and the various radii to changes in chemical structure. The data given in Table I can be used to calculate ψ_I in a number of ways. In fact, as pointed out elsewhere in this volume (5), r_k alone may be an adequate effective size parameter ψ_I without the need to multiply by v/a. The ability of each of these methods to represent the effective size of the permeant is still to be determined. Because the sizes being discussed here are beyond the level of accurate experimental measurement, the evaluation of these various size parameters can only be done through permeation experiments and by making statistical comparisons of the ability of each parameter to fit the permeation data.

The ability of a molecule to permeate a membrane is not only a function of the effective size of the permeant, but also is dependent upon the effective size ψ_M of the transport corridor within the membrane. Thus, the physical structure of the membrane must be considered, that is, the macrostructure (porosity, asymmetry, membrane thickness) and the microstructure (arrangement and mobility of the polymer chain segments, a factor which governs polymer chain packing). Information regarding the macrostructure of the membrane can be obtained through the use of electron microscopy (11), bubble point (40), fluid permeation (41) and porosimetry methods such as mercury intrusion (42). Microstructure can be investigated through the use of sorption and permeation measurements in conjunction with the free volume theory (43), low angle X-ray scattering, differential thermal analysis (44), differential scanning calorimetry (45), X-ray scattering and diffraction (46) and infrared absorption (47). Additional information regarding membrane structure can be gained by studying

Table I

Typical Permeant Size Parameters

Compound	Molecular Weight	v Volume Å^3	a Area Å^2	r_v Å	r_a Å	r_k Å	r_{rms} Å	r_s (H_2O) Å
Water	18	22.58	41.87	1.7534	1.8254	1.592	0.677	-
Methanol	32.04	35.38	58.27	2.0365	2.1534	2.235	1.197	2.467
Ethanol	46.07	52.13	80.25	2.3174	2.527	2.604	1.558	2.869
n-Propanol	60.09	68.90	101.92	2.5432	2.8479	2.604	1.854	3.116
Hexane	86.17	113.63	159.07	3.0047	3.5579	2.604	2.650	3.600
1-Hexanol	102.17	119.53	166.5	3.055	3.64	2.604	2.755	N.A.
1,6-Hexanediol	118.17	126.07	176.03	3.1106	3.7427	2.604	2.933	N.A.
1,2,6-Hexanetriol	134.17	131.03	181.60	3.1508	3.8015	2.926	2.920	N.A.
Cyclohexane	84.16	100.94	133.8	2.8884	3.263	3.351	2.020	3.502
Benzene	78.11	81.57	101.88	2.6904	2.8473	3.346	2.011	2.901
Phenol	94.11	89.14	111.95	2.7712	2.9847	3.346	2.304	3.620
Toluene	92.13	99.34	124.49	2.8731	3.1475	3.346	2.133	3.166

N.A. indicates not available

the structure of water within the membrane via sorption isotherms,
the calorimetric capacity of the water within the membrane, nuclear
magnetic resonance and infrared absorption (23,24).

The ability to determine the pore size and pore size
distribution for porous membranes has existed for a number of years
(11,40-42). Recent advances have permitted the determination of
pore size and distribution for finely porous ultrafiltration
membranes (9,10). Determination of ψ_M (the average cross-sectional
area of the transport corridor) for the skin layer of reverse
osmosis and tight ultrafiltration membranes as well as pervaporation
membranes at present remains a challenge, although advances are
being made in this direction (9,10,48-50).

While the macrostructure can be attributed to the membrane
formation procedures as discussed elsewhere in this volume
(1,2,51,52), microstructure (the packing of chains) is dependent
upon both the membrane formation procedure and the chemical nature
of the polymer. The microstructure of dense membranes as well as
the active layer of skinned membranes influences permeation through
steric effects. The microstructure of the solid portion of the
porous support matrix of skinned membranes has little influence on
permeation; however, it does influence the mechanical strength of
the membrane. Thus, a knowledge of how the chemical nature of the
macromolecule influences microstructure will be beneficial in
selecting a membrane material.

The microstructure of the membrane is determined by the
chemical nature of the membrane material as well as by the membrane
production variables. The mechanical strength of the polymer is
determined by the flexibility of the chain, the magnitude of
secondary valence forces of interchain attraction and the closeness
of chain packing. The size of the transport corridor within the
polymer is determined by the closeness of chain packing and, to
some extent, chain flexibility. Polymer chain flexibility is
enhanced by the presence of single bonds in the backbone and
restricted by the presence of ring structures and double bonds in
the backbone, by stereo-irregularity and by bulky pendant groups.
The magnitude of secondary intermolecular forces of attraction
between neighboring polymers is determined by the polarity and
frequency of functional groups within or attached to the polymer
chains. In general, mechanical strength or cohesive energy
increases as the polarity and frequency of the functional groups
increases. Because van der Waals intermolecular forces of
attraction fall off with the seventh power of interchain distance,
maximum interchain attraction requires that the functional groups
of adjacent chains be in registry and that the chains be packed as
closely as possible. Closeness of chain packing is enhanced by
chain flexibility and stereoregularity (iso- and syndiotactic)
while being restricted by bulky substituent or side groups. In the
limit of close packing, crystalline domains (crystallites) form.
While crystallites (or their polycrystalline aggregates referred to
as spherulites) may contribute favorably to mechanical strength,
they are detrimental to permeation. That is, ψ_M is so small and
the chains so immobilized or inflexible following crystal formation
as to preclude permeation. Consequently, for polymers in which
partial crystallization is possible, permeation can only take place

in the amorphous regions (disordered flexible chains located
between impermeable domains). When dealing with semi-crystalline
polymers (100 % crystallization is rarely possible), one must
optimize the microstructure for physical strength and the size of
the transport corridors within the amorphous region. Crystal
nucleation and growth occur during the evaporation stage of
solution casting and wet spinning of membranes and while in the
molten stage of extrusion and melt spinning of membranes. Thus,
percent crystallinity, the orientation of polymer chains and ψ_M in
the amorphous regions can be controlled to some extent during
membrane production (52).

     The size of the transport corridor ψ_M within the amorphous
region of semi-crystalline and purely amorphous, crystal-free
polymer films depends upon the nature (rubber versus glass) of the
amorphous polymer. All amorphous polymers undergo a rubber-glass
transition at a specific temperature known as the glass transition
temperature, T_g. At temperatures greater than T_g, the polymer is a
rubbery, viscous liquid with flexible chains. At temperatures
below T_g, the polymer is a relatively inflexible solid. Whether a
polymer is rubbery or glassy at a given temperature (that is, an
elastomer or a plastic), is a function of the chemical structure of
the polymer. Low interchain attraction forces indicate a rubber;
high interchain attraction forces indicate a glass. In addition,
factors that restrict segmental mobility within the backbone (such
as bulky side groups, main-chain ring structures and strong
intermolecular attraction forces) render the chain stiff, thereby
increasing T_g and increasing the crystal melting temperature. For
a given polymer, density decreases with increasing temperature,
undergoing a second order transition at T_g. For semi-crystalline
polymers, an additional first order transition occurs at the
crystal melting point. Logically, ψ_M is expected to follow the
opposite trend; that is, increasing with increasing temperature.
Unfortunately, isothermal compressibility also increases (that is,
compaction resistance decreases) with increasing temperature
(undergoing a sharp discontinuity at T_g).

     Thus, membrane material selection and membrane fabrication
procedures often represent a compromise designed to optimize
performance (particularly for reverse osmosis, RO, and
ultrafiltration, UF). Typically, RO and UF membranes are glassy
polymers under the conditions of application while microfiltration
membranes are often highly crystalline with either glassy or
rubbery amorphous regions. Pervaporation membranes, on the other
hand, may be rubbery or glassy. Caution should be taken when
making use of published tables of transition temperatures.
Invariably, the published transition temperatures represent values
for dry pure polymer. However, the corresponding T_g value for the
membrane material may be somewhat lower under actual operating
conditions. This decrease in T_g may occur if solution component B
(or A, if present in large concentration) is capable of acting as a
plasticizer. Plasticizers are typically poor, rather than good,
solvents for the polymer. They facilitate chain slippage
(increasing ψ_M and decreasing compaction resistance) and extend the
temperature range for segmental rotation to lower temperatures
(depressing T_g). In the event that the plasticizer converts the

membrane from a glass to a rubber, it may be necessary to cross-link
or reinforce the membrane with inert materials or by blending
polymers.

Summarizing the discussion of steric effects, it is evident
that the effective size of the permeating species, ψ_I, and the
effective size of the permeation corridor in the membrane, ψ_M, must
both be considered. ψ_I can be estimated based on the chemical
structure of the permeant and by accounting for clustering. ψ_M is
governed by the microstructure of pervaporation membranes and the
skin layer of reverse osmosis and tight ultrafiltration membranes.
However, ψ_M is governed by the macrostructure of porous
ultrafiltration and microfiltration membranes. When $\psi_I > \psi_M$,
component I is sterically prevented from entering the membrane
phase. In this case the selection of the membrane material is less
critical than is the membrane formation procedure which controls
the membrane structure. This situation arises when solution
components A and B differ in effective size by orders of magnitude,
and porous membranes may be used to reject A while passing B. When
$\psi_I < \psi_M$, partitioning of the permeant between free solution and the
membrane phase is possible. The extent to which partitioning
occurs is a function of the strength and nature of the chemical
interactions between the solution components A and B and the
membrane material M. The rate at which the subsequent transport
occurs is a function of the magnitude of the driving force, the
strength and nature of the chemical interactions as well as steric
hindrance. As the magnitude of the difference $\psi_M - \psi_I$ increases,
the significance of steric hindrance decreases and, on a relative
basis, that of the chemical interactions increases. When $\psi_I \ll \psi_M$,
steric factors have little influence on transport.

Summary of Physicochemical Parameters.   In the previous section
steric parameters ψ_I and ψ_M were introduced to describe the
effective size of solution components and the average size of the
transport corridor, respectively. A variety of quantities that
could be used to represent ψ_I were presented. However, similar
quantitative representation of the average transport corridor size
is not yet available. Quantification of ψ_M is especially difficult
for dense membranes and the skin layer of reverse osmosis membranes
in which the transport corridors are beyond the resolution
capabilities of modern instruments and may be dynamic in nature.
Therefore, any discussion of membrane material selection based on
steric considerations must be qualitative.

In pervaporation, reverse osmosis, ultrafiltration and to a
lesser extent microfiltration, both steric and chemical factors
influence permeation and separation. Thus, proper membrane
material selection is important. While the physical structure of
the membrane is in large part a function of membrane preparation
procedures, the chemical nature and, to some degree, the physical
properties of the membrane are dependent upon the chemical nature
of the membrane material. Thus, membrane material selection based
on the chemical nature of the polymer and the solution components
to be separated is feasible.

The dispersive, polar and hydrogen bonding forces of
attraction between permeant and membrane material influence both

the thermodynamics and the kinetics of membrane transport. Thus, the chemical nature of the membrane material, M, and the components A (solute) and B (solvent) of the solution to be separated must be considered. Selection of a membrane material capable of separating a specific A-B combination can be based on the rule that "like attracts like." For separation to be achieved A and B must be dissimilar in some physicochemical aspect. For the rejection of A and transport of B, the membrane material should have favorable interactions (attraction) with B while having unfavorable (aversion) or at least less favorable interactions with A. However, the B-M interaction should not be favorable to the extreme of causing excessive swelling of the membrane.

A variety of parameters used to describe the polar interactions, dispersive forces and hydrogen bonding of molecules have been introduced. All of these parameters represent forces of attraction and were originally derived for low molecular weight compounds. Because the interactions between two molecules can be the result of a combination of all or any of these three force types, it is most convenient to select one parameter or a set of related parameters capable of dealing with all three forces. The Hansen cohesive energy parameter or solubility parameter, δ, with its three components, δ_p, δ_d and δ_h (where $\delta^2 = \delta_d^2 + \delta_p^2 + \delta_h^2$) is a logical choice (16,53-57). This parameter has been successfully applied to small molecules and macromolecules (58-60). Furthermore, it is possible to determine experimentally the partial parameters for low molecular weight compounds (54,57) and to estimate them for both small molecules and macromolecules based on the chemical structure of the compound or repeat unit (57,59-62). Finally, Hansen's three component parameter may be expanded to distinguish between induction and orientation polar contributions as well as proton donor and proton acceptor contributions to hydrogen bonding (63-66). The resulting five component solubility parameter has proven useful in describing the solubility of drug molecules (67) and may eventually find use in membrane science when this level of sophistication is experimentally warranted.

The solubility parameter has found previous use in membrane science. Casting solution components and composition have been selected using the Hansen solubility parameters (68-71). The total Hansen solubility parameter, which is equivalent to the Hildebrand parameter (72), has been used to explain permeation and separation in reverse osmosis (73). Hansen's partial parameters have also been used to explain permeation and separation in pervaporation (61). The findings of these studies (61,73) plus those reported elsewhere in this volume (74) do lend credence to the use of δ_p, δ_d and δ_h for membrane material selection.

The more similar two chemical species, the greater their mutual solubility and the smaller the difference in their solubility parameters, Δ_{IM}, will be. Expanding Δ_{IM} to include all three components of the Hansen parameter gives (61)

$$\Delta_{IM} = [(\delta_{dI} - \delta_{dM})^2 + (\delta_{pI} - \delta_{pM})^2 + (\delta_{hI} - \delta_{hM})^2]^{\frac{1}{2}} \quad (1)$$

Membrane Material Selection

Equation 1 provides a basis for membrane material selection. More
precisely, the ratio Δ_{AM}/Δ_{BM} can be used as a measure of
preferential sorption and thus as a membrane material selection
index.   For example, if it is desired to transport component B
while rejecting component A, the membrane material should be
selected to maximize the ratio Δ_{AM}/Δ_{BM} by maximizing Δ_{AM} and,
within limits, by minimizing Δ_{BM}. This objective can be met by
selecting a membrane material for which B has a strong affinity and
for which A has a low affinity. In the event that the B-M
interactions are extremely favorable (that is, Δ_{BM} is approximately
zero), a decrease in structural strength and a loss of selectivity
will result. In the presence of such strong interactions, the
membrane can be stabilized via cross-linking, blending with or
grafting onto a relatively inert polymer or through the use of an
inert support matrix (where inert indicates large Δ_{AM} and Δ_{BM}).
     If the forces of attractions between A and M are stronger than
those between B and M (that is, Δ_{AM}/Δ_{BM}<1), the permeant A may be
immobilized within the membrane phase causing a decrease in the
effective size of the transport corridor. A decrease in corridor
size would lead to a decrease in the transport of both A and B. If
the concentration of A in the membrane phase is significant, it may
lead to swelling, a decrease in membrane integrity and an increase
in the flux of both A and B.
     Therefore, in selecting a membrane material for a particular
A-B separation, extremely strong interactions should be avoided.
Similarly, high interfacial concentrations of potentially
detrimental permeants must be avoided.
     If $\Delta_{AM} = \Delta_{BM}$, separation cannot be achieved on a strictly
chemical basis despite the fact that A and B may show significant
chemical differences (that is, large Δ_{AB}). In this case, the
separation becomes one of size distinction.
     The ratio Δ_{AM}/Δ_{BM} can be used to quantify the findings of
Sweeny and Rose (75). In summarizing their studies, in which
pervaporation was used to transport organic compounds and to
separate organic mixtures, the authors stated that permeation is
greatest when the chemical nature of the permeant and the membrane
are similar (small Δ_{IM}) while separation is greatest when the
solution components differ significantly in chemical nature (large
Δ_{AB}). Their results also show that the solution component
preferentially transported is that which is most like the membrane
material. As a further example, consider the separation of
cyclohexane and benzene via pervaporation. Assume that one must
select between dense films of polyethylene and polyisoprene to
achieve the desired separation. Based on calculated values of the
material selection index (see Table II), polyisoprene is the
material of choice. Experimental data taken from the literature
(76,77) and reported in Table II, verify this prediction: the
polyisoprene film produces a more highly purified benzene permeate
stream at a higher rate than does the polyethylene film. Notice
that for the system cyclohexane-benzene-polyethylene, Δ_{AM}/Δ_{BM} is
less than one, indicating that cyclohexane is attracted to the
membrane more strongly than is the benzene. Therefore, the

Table II

Material Selection Examples for Pervaporation

Component	δ	δ_d	δ_p	δ_h
		$(cal^{\frac{1}{2}} / cm^{3/2})$		
C=cyclohexane	8.20	8.2	0	0.1
B=benzene	9.06	9.0	0	1.0
oX=o-xylene	8.9	8.8	0.7	1.4
pX=p-xylene	8.8	8.7	0	1.3
PE=polyethylene	8.34	8.34	0	0
PIP=polyisoprene	10.05	10.05	0	0
CAB·171[i]	10.1	7.9	3.2	5.5
CAB·272[ii]	10.3	8.1	3.1	5.5

System	$\Delta_{AM} / \Delta_{BM}$	Selectivity	Permeability $(\mu m \cdot \ell / hr \cdot m^2)$	Ref.
C-B-PE[v]	0.14	1.63[iii]	6.88	76
C-B-PIP[v]	1.28	2.19[iii]	12.64	77
oX-pX-CAB·171[vi]	0.92	1.43[iv]	2.3[vii]	61
oX-pX-CAB·272[vi]	0.91	1.33[iv]	1.1[vii]	61

(i)   CAB·171 = $(CH_2)(CH)_5(O)_2(OH)_{0.25}(OCCH_3)_{2.04}(OCC_3H_7)_{0.71}$

(ii) CAB·272 = $(CH_2)(CH)_5(O)_2(OH)_{0.35}(OCCH_3)_{1.49}(OCC_3H_7)_{1.16}$
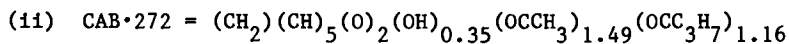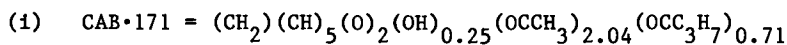
(iii) Selectivity = $(y_B/y_A)/(x_B/x_A)$, where x_I and y_I are the volume
              fractions of component I in the feed and the
              permeate

(iv) Separation Factor = as in (iii) except on a mass basis

(v)   Experimental Conditions: 25°C, 50:50 by mass feed solution

(vi) Experimental Conditions: 20°C, feed solution = 75 mass %
              p-xylene

(vii) flux reported in $cm^3/hr \cdot cm^2$

cyclohexane should be preferentially transported. However, the experimental data indicate that benzene is preferentially transported (that is, selectivity is greater than one). Evidently the strong cyclohexane-polyethylene attraction (Δ_{AM} = 0.17) results in the immobilization of cyclohexane within the polyethylene membrane. As suggested by Smolders and co-workers (61), similar arguments can be presented to justify the selection of the more polar CAB·171 rather than CAB·272 to maximize the separation of o- and p-xylene (see Table II). Once again in this case, the minor component (o-xylene) is preferentially attracted to the membrane material. However, because of the strength of this attraction, the transport of o-xylene is restricted and the membrane accomplishes a separation factor greater than one (that is, p-xylene is preferentially transported). The calculated Δ_{TM} values and the swelling studies (61) indicate that the p-xylene-CAB attraction is equal for CAB·171 and CAB·272 while the o-xylene is more strongly attracted to CAB·272 and thus more restricted in transport through CAB·272. Therefore, the CAB·171 membrane should have higher flux and a higher separation factor than does CAB·272: both predictions are experimentally confirmed.

It must be re-emphasized at this point that the solubility parameter and its use for quantifying physicochemical interactions is based on enthalpic considerations only; entropic considerations are neglected. Consequently, while the ideas outlined in this section provide a basis for membrane material selection (or at least for narrowing the number of possible choices), prediction of permeation and rejection remains elusive until the ability to predict effective transport corridor size ψ_M is more firmly established. At that time the differences $\psi_M - \psi_A$ and $\psi_M - \psi_B$ can be used in conjunction with Δ_{AM} and Δ_{BM} for membrane material selection. For example, the ratio Δ_{AM}/Δ_{BM} may be used to narrow the choice to a few possible materials. The final selection could be made from this reduced list of materials on the basis of optimizing $\psi_M - \psi_A$ and $\psi_M - \psi_B$ to achieve maximum transport of B and rejection of A.

Membrane Material Evaluation

Whether the approach outlined above is used to select *a priori* the membrane material or an approach based simply on polymer availability is used, it would be convenient to evaluate the material for its potential to accomplish the desired separation prior to forming a membrane. Once the membrane has been formed, it is difficult to distinguish the intrinsic properties of the polymer from the physical characteristics of the membrane such as porosity and asymmetry (that is, properties which are governed in large part by membrane formation procedures). In this section a number of techniques for evaluating the material in particulate form as well as in the form of a dense film are discussed. Recall that the membrane is to be used to separate a mixture of components A and B where B is the bulk or major solution component and that interaction between either solution component and the membrane material, M, may be influenced by the presence of the other solution component. Thus, it would be difficult to evaluate a

material's potential to achieve the A-B separation based on binary
A-M and B-M studies alone (a common practice in evaluating membrane
materials for gas separations (5)). In this section, discussions
are limited to evaluation studies involving binary B-M systems,
binary A-M systems (provided A is a liquid) and the ternary A-B-M
system.   Binary A-M in which A, like M, is a solid at room
temperature are not possible to study in a meaningful way. In the
event that the B-M or A-M interactions are sufficiently strong to
cause dissolution or excessive swelling of the polymer, the polymer
can be cross-linked.

Sorption Measurements. The strength and nature of the interactions
between the permeant and the membrane material will influence both
the equilibrium concentration of the permeant in the membrane phase
and the rate of permeant transport through the membrane. A common
method of determining the strength of the B-M and A-M interactions
is by measuring the sorption of permeant by the polymer in binary
system studies.   If the permeant is volatile, an accurate and
simple experimental procedure is available (78,79). Briefly, the
technique involves monitoring weight gained and lost by a
preweighed sample of polymer when subjected to changes in the vapor
content of the polymer's environment. Typically an electrobalance
chamber modified to permit control of the vapor pressure is used.
These studies may be carried out using the polymer in a particulate
form (78,79) or in the form of a dense film (80). Alternatively, a
dense polymer film may be weighed before and after soaking in
liquid permeant. These two alternative experimental techniques
provide data at different points in the permeant-polymer
concentration spectrum. The vapor studies represent exposure of
the polymer to dilute permeant. The immersion studies represent
exposure of the polymer to pure permeant. Values of diffusivities
and partition coefficients obtained by these alternative methods
can differ. The unsteady-state portion of these experiments can be
used to obtain a value of the diffusivity of the permeant in the
membrane material. The equilibrium concentration of permeant in
the membrane phase can be determined from the total weight gain at
steady state (78-80).   Large diffusivities, large equilibrium
concentrations or both indicate that B and M are chemically
similar. Because the objective of these binary system studies is
to investigate interaction between the permeant and the membrane
material, caution must be taken when using polymer films. The
sorption characteristics of the film are often influenced by the
film preparation procedures (2,81) and the results can be
misleading.
        The strength and nature of the interactions between the solute
and the membrane material will influence both the partitioning of
solute A between the free solution and the membrane phase as well
as the rate of transport of A through the membrane phase. The
equilibrium partitioning is typically represented by K_A, the ratio
of the concentration of A in the membrane phase to the concentration
of A in the free solution. The rate of transport is represented by
the diffusivity of A in the membrane phase, $D_{AB,M}$. The term
membrane phase is used to indicate the polymer plus sorbed solution
(the bulk of which is solvent B). Because diffusivities in liquids

are orders of magnitude greater than diffusivities in solids, for anything other than dense films permeation may be assumed to take place between, rather than within, regions of high polymer density. Thus, $D_{AB,M}$ differs from the diffusivity of A in the polymer as determined via the techniques outlined in the previous paragraph or by inverse gas chromatography (82). A number of experimental techniques for determining the equilibrium partitioning and the rate of transport are available. In one technique (80), a membrane film sample is soaked in an A-B solution containing the solute of interest at a known concentration. Once the film has equilibrated with the solute, the film is removed from the bath and any excess moisture is removed. The film sample may be analyzed for solute content or the sample may be placed in a bath of pure B and the amount of solute desorbed determined. Either method will yield the value of K_A. In addition, either the rate of absorption (83) or the rate of desorption (84) may be monitored to give $D_{AB,M}$ via equations developed by Crank and Park (85).

Alternative methods of determining K_A exist. In one method (86) particulate polymer is stirred in a closed container which contains a dilute A-B solution. The change in free solution solute concentration monitored over a period of time indicates the magnitude of the solute-polymer interaction and yields a value of K_A. The advantages of this method are the increased surface area presented by the particulate sample relative to the film and the removal of film preparation procedure dependence.

Chromatographic Methods. The forces that lead to the physicochemical interactions in membrane transport are present in other situations where the three components are in contact with one another; for example, liquid chromatography. The potential membrane material in particulate form or as polymer-coated beads may be packed into the chromatographic column to serve as the stationary phase. The solvent B is used as the carrier or mobile phase in the chromatographic study. The strength and nature of the A-M interactions in the presence of B is determined by injecting into the mobile phase a small amount of the solute A. The retention volume, V_A, (the volume of mobile phase that passes through the column to bring about the elution of A) is a measure of the strength of the A-M interaction. Solute-membrane attraction will delay elution, the length of the delay being dependent upon the strength of the interaction and thus the difference in solubility parameters. Similarly, A-M aversion forces will facilitate column transport and decrease retention volume. A series of experiments with fixed B and M can be used to indicate the potential that M has for rejecting various solutes. Conversely, a series of experiments with fixed A and B can be used to select the best membrane material for achieving the desired separation. In this case the objective is to maximize the difference between V_A and the retention volume of the mobile phase, V_B. When $V_A < V_B$, the polymer has a greater affinity for solvent B than for A; the membrane will preferentially sorb B while rejecting A. When $V_A > V_B$, the polymer has a greater affinity for A than for B. In this case, the separation of A and B by the transport of B and rejection of A by the membrane is difficult. The findings of these

experiments can be used to verify the predictions made based on the physicochemical arguments presented above.

<u>Permeation Studies</u>. Matsuura and co-workers have made use of liquid chromatography to estimate the extent of partitioning between free solution and the membrane phase (<u>48</u>,<u>87</u>-<u>89</u>), the magnitude of A-M and B-M interactions due to electrostatic repulsion and van der Waals attraction (<u>48</u>,<u>49</u>,<u>89</u>-<u>91</u>), the thickness of bound or interfacial water associated with the membrane (<u>87</u>-<u>89</u>), as well as the average size and size distribution of the transport corridor on the membrane surface (<u>92</u>-<u>94</u>).

Other methods for studying A-B-M interactions involve the use of dense film permeation (<u>95</u>). In one method, the film is mounted between two halves of a test cell. One compartment of the cell is filled with an A-B solution, the other compartment of the cell is filled with pure B. As the experiment proceeds the change in solute concentration of both solutions is monitored to indicate the solute transport under a concentration gradient. Using a modified version of this test apparatus, it is possible to conduct experiments in which the osmotic flow of B together with the flux of solute is measured. In addition to these direct osmosis techniques, pressure-driven studies using dense films may also be conducted. The disadvantages of the direct osmosis and the pressure-driven studies are numerous. The experiments only yield values for permeation; a transport model must be assumed and additional experiments (such as sorption studies) must be performed to resolve the permeation into its equilibrium and kinetic factors. The dense film must be uniform and free from defects. The applicability of the results of dense film studies to the actual transport in skinned membranes is questionable because the membranes are prepared via different procedures (<u>2</u>) and the influence of membrane formation on transport is well documented. An additional disadvantage of the studies involving permeation through dense films is the slow transport. The long experimental time required to collect sufficient sample can be detrimental if A or B are volatile and sufficient precautions are not taken to prevent losses.

<u>Membrane Materials: Past, Present and Future</u>

In light of the information presented above, it is interesting to look at the materials which have been studied for use as membranes. Summaries of recently investigated homopolymers, copolymers and blends for use as integrally-skinned (asymmetric) and nonintegrally-skinned (composite) membranes are presented in Tables III through VI. These lists are based in part on the survey published by Delyannis and Delyannis (<u>96</u>) and updated here through mid-1984 (<u>97</u>-<u>223</u>). While these lists are extensive, they could not possibly be exhaustive; much of the material development is shrouded in secrecy or disguised by the legal jargon of patents. In fact, it is virtually impossible to be specific about which members of these lists have attained commercial status; however, Table VII contains a partial list of materials and the processes in which they are utilized.

In general, membranes have been developed for aqueous

Table III

Selected Homopolymers Investigated for
Integrally-skinned Membranes

Polymer	Reference
Acrylic Derivatives	
Poly(acrylic acid)	97
Poly(acrylonitrile)	98,99
Poly(2-hydroxyethyl methacrylate)	100
Poly(methacrylic acid)	101
Poly(methacrylonitrile)	99
Aromatic Poly(amide) Polymers	
Nylon − 4	102
Nylon − 6	103
Nylon − 12	104
Poly(amide hydrazide)	105
Poly(p-phenylene terephthalamide)	106
Poly(piperazinamide)	107
Aromatic Poly(imide) Polymers	
Poly(amide imide)	108−110
Poly(benzimidazolone)	111−113
Poly(2,2'-(m-phenylene)-5,5'-bibenzimidazole)	114
Poly(ethylene) derivatives	
Poly(ethylene)	115,116
Poly(ethyleneimine)	117
Poly(ethylene terephthalate)	118
Poly(phenyl-p-(2,4-diaminophenoxy)ethylene)	119
Poly(tetrafluoroethylene)	120,121
Poly(vinyl alcohol membranes)	
Poly(vinyl acetate)	122,123
Poly(vinyl alcohol)	122−130
Poly(vinyl butyrate)	122

Table III (continued)

Polymer	Reference
Poly(vinyl) derivatives	
Poly(vinyl chloride)	131-135
Poly(vinyl fluoride)	136
Poly(vinyl formal)	137
Poly(vinylidene fluoride)	138-142
Poly(sulfone)	
Bisphenol-A-polysulfone	143-150
Bisphenol-S-polysulfone	151
Sulfonated hydroquinone polysulfone	152
Other	
Chitosan	153
Fluorinated resins	154,155
Poly(amic acid)	156
Poly(ether imine sulfone)	157
Poly(furfuryl alcohol)	158
Polyolefins	159
Poly(p-phenylene sulfide)	160
Poly(propene)	161
Poly(quinazolinone)	162,163
Poly(styrene sulfonate)	164
Poly(urea)	165
Poly(urethane)	166
Poly(γ-benzyl-L-glutamate)	167,168
Rayon	169,170
Sulfonated Poly(oxyphenylene)	171

Table IV

Selected Copolymers Investigated for
Integrally-Skinned Membranes

Copolymer	Reference
Acrylonitrile-Acrylamide	172
Acrylonitrile-Methyl Methacrylate	173
Acrylonitrile-Vinyl Acetate	174-176
Bisphenol-A-Polysulfone-Chlorohydrin	177
Butadiene-Methacrylic Acid	178
Butadiene- 2-, or 4-Vinylpyridine	178
Butadiene-Styrene	178
Styrene-Vinylpyridine	178
Ethylene-Vinyl Alcohol	179-181
Methacrylic Acid-Styrene	182
p-Aminobenzhydrazide-Terephthaloyl Chloride	183
Tetrafluoroethylene-Vinylidene Fluoride	184
4,4'-Sulfonyldianiline-Terephthaloyl Chloride	185
Vinyl Acetate-Vinylidene Fluoride	134
Vinylpyrrolidone-Ethyl Acrylate	186
Vinylpyrrolidone-Methyl Methacrylate	187,188
Vinylpyrrolidone-Vinyl Acetate	189
Polycarbonate-Polyether Block Copolymer	190,191

Graft Copolymer	
Acrylic Acid grafted to Nylon-6,6	192
Acrylic Acid grafted to Poly(vinyl alcohol)	193
Styrene grafted to Cellulose Acetate	194
4-Vinylpyridine grafted to Poly(tetrafluoroethylene)	195
2-, or 4-Vinylpyridine grafted to Poly[3,3-bis(chloromethyl)oxetane]	196

Table V

Selected Polymer Blends Investigated for
Integrally-Skinned Membranes

Polymer Blend Pair	Reference
Cellulose Acetate/ Poly(phenylene oxide dimethyl phosphonate)	197
Cellulose Acetate/Poly(styrene)	197
Cellulose Acetate/Poly(4-vinylpyridine)	198
Cellulose Diacetate/Cellulose Triacetate	199,200
Cellulose Nitrate/Poly(vinyl pyrrolidone)	201
Dimethylaminoethyl Methacrylate-Methyl Methacrylate copolymer/Poly(vinylidene fluoride)	202
Ethylene-Vinyl Alcohol copolymer/ Poly(styrene sulfonic acid)	203
Nylon-4/Nylon-6	204
Nylon-4/Nylon-6,6	204
Poly(acrylonitrile)/ Poly(2-hydroxyethyl methacrylate)	205
Poly(acrylonitrile)/Poly(vinyl tetrazole)	192
Poly(vinyl alcohol)/Poly(vinyl pyrrolidone)	192
Poly(ethylene)/Poly(styrene)	206
Poly(sulfone)/Poly(vinyl pyrrolidone)	197
Poly(vinyl acetate)/Poly(vinylidene fluoride)	207
Poly(vinylidene fluoride)/Poly(ethylene glycol)	208

Table VI

Selected Polymers and Blends Investigated for use as the Skin Layer
    of Nonintegrally-skinned (Composite and Dynamic) Membranes*

Polymer	Reference
Nylon-6,6	209,210
Poly(acrylic acid)	211
Poly(alkyleneimine)	212
Poly(amino styrene)	213
Poly(ethyleneimine)	214
Poly(furfuryl alcohol)	215,216
Poly(p-hydroxystyrene)	217
Poly(sulfone)	218-220
Poly(trishydroxyethyl urazole)	221
Poly(vinyl alcohol)	222
Poly(vinyl alcohol)/Poly(styrene sulfonic acid)	223

* for additional information and more detailed discussions of the
  polymers and blends used in these membranes consult the chapters
  by Cadotte (3) and Spencer (4) in this volume.

Table VII

Commercially Available Membranes for Specific Applications

Material	Process
Cellulose Acetate (CA)	Electrophoresis (EP), Microfiltration (MF), Ultrafiltration (UF), Reverse Osmosis (RO)
Cellulose Triacetate	MF, UF, RO
CA/Triacetate Blend	RO
Cellulose Esters (mixed)	MF
Cellulose Nitrate	MF
Cellulose (regenerated)	Dialysis (D), MF, UF
Gelatin	MF
Polyacrylonitrile (PAN)	UF
PAN-Polyvinylchloride Copolymer	MF, UF
PAN-Methallyl Sulfonate Copolymer	D
Polyamide (aromatic)	MF, UF, RO
Polyarylether Sulfone (polysulfone)	MF, UF
Polybenzimidazole (PBI)	RO
Polybenzimidiazolone (PBIL)	RO
Polycarbonate (track-etched)	MF
Polyester (track-etched)	MF
Polyimide	UF, RO
Polypropylene	MF
Polysodium styrene sulfonate-poly vinyl benzyl trimethyl ammonium chloride (polyelectrolyte complex)	UF
Polytetrafluoroethylene (PTFE)	MF

Table VII (continued)

Material	Process
Polyvinylchloride	MF
Polyvinylidenefluoride	UF
Metaphenylene-diamine + Trimesoyl chloride (i)	RO
Polyetheramine + Isophthaloyl chloride (i)	RO
Polyethleneimine + Isophthaloyl chloride (i)	RO
Polyethleneimine + Toluene diisocyanate (i)	RO
Polyacrylic acid + Hydrous zirconium oxide (ii)	UF, RO

(i) Skin layer of thin-film composite; see Reference 3.
(ii) Skin layer of dynamic membrane; see Reference 4.

separations and, in the case of reverse osmosis membranes, specifically for desalination. Therefore, materials for dense membranes, finely porous membranes, integrally-skinned membranes are well as the active layer of composite and dynamic membranes have been selected on the basis of having a hydrophilic/hydrophobic balance and a moderate ionic nature (high dielectric constant). Materials for more porous membranes have not been similarly restricted; hydrophobic as well as moderately hydrophilic materials have been used for microfiltration and dialysis membranes. In addition, thermal stability, resistance to degradation resulting from extremes in pH or biological attack and compaction resistance have been and continue to serve as valuable selection criteria as specific applications demand. These considerations have led to the use of rigid, synthetic materials with glass transition temperatures above application temperatures for RO and UF. More recently, the criteria of miscibility of copolymers and blends has been added to the list of desirable characteristics for membrane materials (74,224). Significant advances in the use of miscible copolymers and blends have come from research on pervaporation membranes (198,225), ultrafiltration membranes (201) and gas separation membranes. Expansion of the ideas presented above, as they apply to copolymer and polymer blend membranes, has been qualitatively expressed by Cabasso (225); however, a formal quantification of these ideas was not presented.

    In actual fact, the membrane material selection process is often not sophisticated. Merely the availability of a material capable of being formed into a dense or porous film or hollow fiber has stimulated membrane research efforts.

    Conversion of a membrane material or membrane from one developed for aqueous-inorganic salt separations to one for use in aqueous-organic or organic-organic separations often requires modifications such as copolymerization, polymer blending or radiation grafting onto the membrane surface. These approaches are often difficult, are not fully understood and are not always entirely successful.

Summary

In this paper an approach has been presented that will facilitate selection and evaluation of possible membrane materials. Having selected potential membrane materials for desired separations, steric considerations are taken into account in membrane preparation. This approach avoids starting with and subsequently modifying aqueous-separation membranes, allows a vast spectrum of polymers to be considered as potential membrane materials and focuses the selection process. A brief review of membrane material evaluation procedures have been discussed with emphasis on those techniques which do not require the fabrication of membranes. Finally, the survey of materials evaluated for possible membrane use indicates both the interest in this field and the need for appropriate material selection and evaluation procedures. The ideas presented here will continue to grow in value in the future as membranes are called upon to achieve more difficult separations in an energy efficient fashion.

Acknowledgments

Literature Cited

1. Hiatt, W. C.; Vitzthum, G. H.; Wagener, K. B.; Gerlach, K.;
    Josefiak, C. In "Materials Science of Synthetic Membranes";
    D. R. Lloyd, Ed.; American Chemical Society: Washington, D.C.,
    1985.
2. Kesting, R. E. *ibidem*.
3. Cadotte, J. *ibidem*.
4. Spencer, H. G. *ibidem*.
5. Chern, R. T.; Koros, W. J.; Hopfenberg, H. B.; Stannett, V. T.
    ibidem.
6. Hoehn, H. H. *ibidem*.
7. Ward, R. A.; Feldhoff, P. W.; Klein, E. *ibidem*.
8. Kyu, T. *ibidem*.
9. Zeman, L.; Tkacik, G. *ibidem*.
10. Smolders, C. A.; Vugteveen, E. *ibidem*.
11. Pusch, W.; Walch, A. J. Membr. Sci. 1982, 10, 325-360.
12. Moody, G. J.; Thomas, J.D.R. "Dipole Moments in Inorganic
    Chemistry"; Edward Arnold: London, 1971.
13. Taft, R. W. In "Steric Effects in Organic Chemistry"; M. S.
    Newman, Ed.; John Wiley and Sons, Inc.: New York, 1959;
    Chapter 13.
14. Hammett, L. P. Chem. Revs. 1935, 17, 125-136.
15. Crowley, J. D.; Teague, G. S.; Lowe, J. W. J. Paint Tech.
    1966, 38, 269-280.
16. Hansen, C. M. J. Paint Tech. 1967, 39, 104-117.
17. London, F. Trans. Faraday Soc. 1937, 33, 8-26.
18. Pimentel, G. C.; McClellan, A. L. "The Hydrogen Bond"; W. H.
    Freeman and Co.: San Francisco, 1960.
19. Frank, H.; Wen, W. Disc. Farady Soc. 1957, 24, 133-140.
20. Zimm, B. H. J. Chem. Phys. 1953, 21, 934-935.
21. Zimm, B. H.; Lundberg, J. L. J. Phys. Chem. 1956, 60,
    425-428.
22. Lundberg, J. L. J. Macromol. Sci. 1969, B3, 693-710.
23. Barrie, J. A. In "Diffusion in Polymers"; J. Crank and G. S.
    Park, Eds.; Academic Press: London, 1968; Chapter 8.

24. Jellinek, H.H.G., Ed. "Water Structure at the Water-Polymer Interface"; Plenum Press: New York, 1972.
25. Rowland, S. P., Ed. "Water in Polymers"; American Chemical Society: ACS Symposium Series No. 127: Washington, D.C., 1980.
26. Gordy, W. J. J. Chem. Phys. 1939, 7, 93-99.
27. Gordy, W. J. J. Chem. Phys. 1940, 8, 170-177.
28. Gordy, W. J. J. Chem. Phys. 1941, 9, 204-214.
29. Sourirajan, S.; Matsuura, T. In "Reverse Osmosis and Synthetic Membranes"; S. Sourirajan, Ed.; National Research Council of Canada Publications: Ottawa, Canada, 1977; Chapter 2.
30. Reid, R. C.; Prausnitz, J. M.; Sherwood, L. T. "The Properties of Gasses and Liquids", 3rd ed.; McGraw-Hill Book Co.: New York, 1975.
31. Fredenslund, A.; Gmehling, J.; Rasmussen, P. "Vapor-Liquid Equilibria Using UNIFAC"; Elsevier: Amsterdam, 1977.
32. Herdan, G. "Small Particle Statistics"; Elsevier: Amsterdam, 1953.
33. Handbook of Chemistry and Physics, 55 ed.; Weast, R. E., Ed. CRC Press: Cleveland, Ohio, 1974.
34. Fedors, R. F. Polym. Eng. Sci. 1974, 14, 147-154.
35. Field, P. E. "Physical Methods in Chemistry"; Virginia Polytechnic Institute and State University: Blacksburg, Va., 1979, pp. 38-41.
36. Pearlman, R. S. In "Physical Chemical Properties of Drugs"; S. H. Yalkowsky; A. A. Sinkula; S. C. Valvanti, Eds.; Marcel Dekker: New York, 1980.
37. Morawetz, H. "Macromolecules in Solution", 2nd ed.; Wiley-Interscience: New York, 1975, Chapter III.
38. Elias, H. G. "Macromolecules 1: Structure and Properties"; Plenum Press: New York, 1977, Chapter 4.
39. Edmundson, I. C. In "Advances in Pharmaceutical Sciences"; H. S. Bean; J. E. Carless; A. H. Beckett, Eds.; Academic Press: London, 1967.
40. Baruc, C. Amer. J. Med. Sci. 1894, 48, 451.
41. Lodge, J. P.; Pate, J. B.; Huitt, H. A. Amer. Ind. Hyg. Assoc. J. 1963, 24, 380-387.
42. Honold, E.; Skau, E. L. Science 1954, 120, 805-806.
43. Paul, D. R. Ber. Bunsenges. Phys. Chem. 1979, 83, 294-302.
44. Taniguchi, Y.; Horigome, S. J. Appl. Polym. Sci. 1975, 19, 2743-2748.
45. Kokta, B.; Luner, P.; Suen, R. In "Membranes From Cellulose and Cellulose Derivatives"; A. F. Turbak, Ed.; J. Appl. Polym. Sci., Appl. Polym. Symp. 1970, 13, 169-179.
46. Geil, P. H. In "Small Angle Scattering From Fibrous and Partially Ordered Systems"; R. H. Marchessault, Ed.; J. Polym. Sci. 1969, 28, 149-163.
47. Zundel, G. "Hydration and Intermolecular Interaction, Infrared Investigations with Polyelectrolyte Membranes"; Academic Press: New York, 1969.
48. Matsuura, T.; Taketani, Y.; Sourirajan, S. In "Synthetic Membranes II"; A. F. Turbak, Ed.; American Chemical Society: Washington, D.C., 1981; pp. 315-338.

49. Chan, K.; Matsuura, T.; Sourirajan, S. Ind. End. Chem. Prod. Res. Dev. 1982, 21, 605-612.
50. Chan, K.; Matsuura, T.; Rajan, K. J. Polym. Sci.: Polym. Lett. Ed. 1983, 21, 417-422.
51. Kamide, K.; Manabe, S. In "Materials Science of Synthetic Membranes"; D. R. Lloyd, Ed.; American Chemical Society: Washington, D.C., 1985.
52. Strathmann, H. ibidem.
53. Hansen, C. M. J. Paint Tech. 1967, 39, 505-510.
54. Hansen, C. M.; Skaarup, K. J. Paint Tech. 1967, 39, 511-514.
55. Hansen, C. M. Farbe Lack 1968, 14, 18-25.
56. Hansen, C. M. Ind. Eng. Chem. Prod. Res. Dev. 1969, 8, 1-11.
57. Hansen, C. M.; Beerbower, A. In "Encyclopedia of Chemical Technology: Suppl. Vol."; A. Standen, Ed.; Interscience: New York, 1971.
58. Burrell, H. In "Polymer Handbook"; J. Brandrup and E. M. Immergut, Eds.; Wiley-Interscience: New York, 1975; p. IV-337 - IV-359.
59. Van Krevelen, D. W. "Properties of Polymers, Their Estimation and Correlation with Chemical Structure"; Elsevier: Amsterdam, 1976.
60. Barton, A.F.M. "Handbook of Solubility Parameters and Other Cohesion Parameters"; CRC Press, Inc.: Boca Raton, Fl, 1983.
61. Mulder, M.H.V.; Kruitz, F.; Smolders, C. A. J. Membr. Sci. 1982, 11, 349-363.
62. Koenhen, D. M.; Smolders, C. A. J. Appl. Polym. Sci. 1975, 19, 1163-1179.
63. Keller, R. A.; Karger, B. L.; Snyder, L. R. In "Gas Chromatography"; R. Stock, Ed.; Inst. of Petrol.: London, 1971; pp. 125-140.
64. Karger, B. L.; Snyder, L. R.; Eon, C. J. Chromatog. 1976, 125, 71-88.
65. Snyder, L. R. Chemtech 1979, 9, 750-754.
66. Snyder, L. R. Chemtech 1980, 10, 188-193.
67. Martin, A.; Wu, P.; Adjei, A.; Beerbower, A.; Prausnitz, J. M. J. Pharm. Sci. 1981, 70, 1260-1264.
68. Klein, E.; Smith, J. K. In "Reverse Osmosis Membrane Research"; H. K. Lonsdale and H. E. Podall, Eds.; Plenum Press: New York, 1972; pp. 61-84.
69. Fredrich, C.; Driancourt, A.; Monnerie, L. Desalination 1981, 36, 39-62.
70. Chawla, A. S.; Chang, T.M.S. J. Appl. Polym. Sci. 1975, 19, 1723-1730.
71. Kinzer, K. E.; Lloyd, D. R.; Wightman, J. P.; McGrath, J. E. Desalination 1983, 46, 327-334.
72. Hildebrand, J.; Scott, R. "Solubility of Nonelectrolytes"; Dover Publications: New York, 1964.
73. Spencer, H. G.; Gaddis, J. L. Desalination 1979, 28, 117-124.
74. Krause, S. In "Materials Science of Synthetic Membranes"; D. R. Lloyd, Ed.; American Chemical Society: Washington, D.C., 1985.
75. Sweeny, R. F.; Rose, A. Ind. Eng. Chem. Prod. Res. Dev. 1965, 4, 248-251.

76. Huang, R.Y.M.; Lin, W.J.C. J. Appl. Polym. Sci. 1968, 12, 2615.
77. Kucharsli, M.; Stelnaszek, J. Int. Chem. Eng. 1967, 7, 618.
78. Berens, A. R. Polym. Prepr. 1974, 15, 203.
79. Berens, A. R. Angew. Makromol. Chem. 1975, 47, 97-110.
80. Lonsdale, H. K.; Croys, B. P.; Milstead, C. E. In "Permselective Membranes"; C. E. Rogers, Ed.; Marcel Dekker: New York, 1971.
81. Kesting, R. E. "Synthetic Polymeric Membranes"; McGraw-Hill Book Co: New York, 1971, Chapter 3.
82. Guillet, J. E. In "New Developments in Gas Chromatography"; J. H. Purnell, Ed.; Wiley-Interscience: New York, 1973; p. 187.
83. Lonsdale, H. K.; Merten, U.; Riley, R. L. J. Appl. Polym. Sci. 1965, 9, 1341-1362.
84. Frommer, M. A.; Murday, J. S.; Messalem, R. M. Eur. Polym. J. 1973, 9, 367-373.
85. Crank, J.; Park, G. S. In "Diffusion in Polymers"; J. Crank and G. S. Park, Ed.; Academic Press: London, 1968, p. 1-39.
86. Sourirajan, S.; Matsuura, T.; Hsieh, F. H.; Gildert, G. R. In "Ultrafiltration Membranes and Applications"; A. R. Cooper, Ed.; Plenum Press: New York, 1980; pp. 21-43.
87. Matsuura, T.; Taketani, Y.; Sourirajan, S. Desalination 1981, 38, 319-337.
88. Taketani, Y.; Matsuura, T.; Sourirajan, S. Sep. Sci. Technol. 1982, 17, 831-838.
89. Matsuura, T.; Taketani, Y.; Sourirajan, S. J. Coll. Interface Sci. 1983, 95, 10-22.
90. Taketani, Y.; Matsuura, T.; Sourirajan, S. J. Electrochem. Sci. 1982, 129, 1485-1492.
91. Farnand, B. A.; Talbot, F.D.F.; Matsuura, T.; Sourirajan, S. Ind. Eng. Chem. Proc. Des. Dev. 1983, 22, 179-187.
92. Matsuura, T.; Sourirajan, S. Proc. Int. Symp. Fresh Water Sea 1978, 6, 227-238.
93. Matsuura, T.; Sourirajan, S. Ind. Eng. Chem. Proc. Des. Dev. 1978, 17, 419-428.
94. Matsuura, T.; Sourirajan, S. J. Coll. Interface Sci. 1978, 66, 589-592.
95. Lonsdale, H. K.; Merten, U.; Riley, R. L.; Vos, K. D. "Reverse Osmosis for Water Desalination", Tech. Report 150, U.S.D.I.--OSW R&D, 1965.
96. Delyannis, A.; Delyannis, E.-E. Seawater and Desalting 1983, 3, 176-210.
97. Huang, R.Y.M.; Gao, C. J.; Kim, J. J. J. Appl. Polym. Sci. 1983, 28, 3063-3073.
98. Quemeneur, F.; et al. Entropie 1980, 16, 22-29.
99. Wrasidlo, W. J. Eur. Patent 36,315, 23 Sep., 1981.
100. Yoon, S. C.; Jhon, M. S. J. Appl. Polym. Sci. 1982, 27, 3133-3149.
101. Osada, Y.; et al. J. Polym. Sci.-Polym. Lett. Ed. 1982, 19, 303-308.
102. Huang, R.Y.M.; et al. J. Appl. Polym. Sci. 1981, 26, 1907-1918.

103. Haruvy, Y.; Rajbenbach, A. L. J. Appl. Polym. Sci. 1981, 26, 3065-3071.
104. Uragami, T.; Fujisawa, T.; Sugihara, M. Polym. Bull., Berlin 1981, 5, 195-200.
105. Yeager, H. L.; et al. Ind. Eng. Chem. Proc. Des. Dev. 1981, 20, 451-456.
106. Strathmann, H.; Zschocke, P. Ger. Patent 2,940,447, 9 April, 1981.
107. Parrini, P. Desalination 1983, 48(1), 67-78.
108. Iwama, A.; Kazuse, Y. J. Membr. Sci. 1982, 11, 297-309.
109. Nitto Electric Industrial Co. Ltd. Jap. Patent 83/14,903, 28 Jan., 1983.
110. Nitto Electric Industrial Co. Ltd. Jap. Patent 81/24,007, 7 Mar., 1981.
111. Murakam, H.; Igrashi, N. Ind. Eng. Chem. Prod. Res. Dev. 1981, 20, 501-508.
112. Davis, H. J.; et al. Report 1981, Order No. AD-A102173, Avail. NTIS. from Gov. Rep. Announce. Ind. (U.S.), 1981, 81, 5098.
113. Teijin Ltd. Jap. Patent 83/58,113, 6 April, 1983.
114. Kuder, J. E. J. Appl. Electrochem. 1981, 11, 413-416.
115. Matsuda, K.; Kohno, M.; Koi, Y. Ger. Patent 3,038,886, 30 April 1981.
116. Soehngen, J. W.; Chen, J. C. U.S. Patent Appl. 54,050, 2 July, 1979.
117. Riley, R. L. U.S. Patent 4,411,787, 25 Oct., 1983.
118. Strusovskaya, N. L.; Ageev, E. P.; Kagan, D. F. Vestn. Mosk. Univ., Ser. 2, Khim 1981, 22, 541-544.
119. Teijin Ltd. Jap. Patent Appl. 79/55,227, 8 May, 1979.
120. Sumitomo Elec. Ind. Ltd. Jap. Patent Appl. 72/100,038, 5 Oct., 1972.
121. DeMotte, R. Rec. Dev. Filter Media Their Appl., Proc. Int. Symp., 1980, 5.6.1-5.6.8.
122. Peter, S.; Stefan, R. ACS Symp. Ser. 1981, 154, 281-291.
123. Wafilin, B. V. Neth. Patent 80,03,026, 16 Dec., 1981.
124. Katz, M. G.; Wydeven, T. ACS Symp. Ser., 1981, 153, 383-398.
125. Tsuchihara, T.; et al. Maku 1981, 6, 355-359.
126. Chang, H. W. Desalination 1982, 42, 63-77.
127. Hayashi, S.; Hirai, T.; Hojo, N. Kobunshi Kako 1981, 30, 485-488.
128. Kuraray Co. Jap. Patent 81/8,442, 28 Jan., 1981.
129. Kuraray Co. Jap. Patent 82/78,908, 17 May, 1982.
130. Sueoka, A.; et al. U.S. Patent 4,279,752, 21 July, 1981.
131. Vasil'eva, A. A.; et al. Poluchenie i Primenenie Volokon so Spetsiffch. Svoistmami, Mytishchi, 1980, 26-31.
132. Nachinkin, I. G.; et al. Plast. Massy 1981, 6, 36-37.
133. Guseva, L. Ya.; et al. Plast. Massy 1981, 7, 56.
134. Buschatz, H.; et al. E. Ger. Patent 144,206, 8 Oct., 1980.
135. Agency of Indust. Sci. and Technol. Jap. Patent 81/105,706, 22 Aug. 1981.
136. Teijin Ltd. Jap. Patent 83/91,731, 31 May, 1983.
137. Kuraray Co. Jap. Patent 81/68,104, 8 June, 1981.
138. Vigo, F.; Capannelli, G.; et al. Desalination 1981, 36, 63-73.

139. Benzinger, W. D.; et al. NTIS Publ. PB81-203101, 1980.
140. Vigo, F.; Capannelli, G.; Uliana, S.; Munari, S. <u>Chim. Ind.,</u>
     <u>Milan</u> 1982, <u>64</u>, 74-79.
141. Liu, S. J.; Wang, J. R.; Liu, F. L. <u>Memb. Sep. Sci. Technol.</u>
     1981, <u>2</u>, 74-79.
142. Benzinger, W. D.; Robinson, D. N. Eur. Patent 40,670, 2 Dec.,
     1981.
143. Graefe, A. F.; Wong, D. NTIS Publ. PB81-115420, 1980.
144. Lloyd, D. R.; et al. <u>ACS Symp. Ser.</u> 1981, <u>153</u>, 327-350.
145. Han, S. J.; et al. <u>Huan Ching K'o Hsueh</u> 1980, <u>1</u>, 14-18.
146. Rose, J. B. <u>Res. Disc.</u> 1981, <u>210</u>, 367.
147. Benzinger, W. D.; Hinde, G. M.; Toal, M. G. Eur. Patent
     36,947, 7 Oct., 1981.
148. Kanegafuchi Chem. Ind. Co. Jap. Patent 82/71,606, 4 May, 1982.
149. Kuraray Co. Jap. Patent 82/35,906, 26 Feb., 1982.
150. Daicel Chem. Ind. Jap. Patent 82/94,309, 11 June, 1982.
151. Tsukasa, O.; Toshikazu, K. Eur. Pat. Appl. 37,185, 7 Oct.,
     1981.
152. Cinderey, M. B.; Rose, J. B. Eur. Pat. Appl. 29,633, 3 June,
     1981.
153. Yang, T.; Zall, R. R. <u>J. Food Sci.</u> 1984, <u>49</u>, 91-93.
154. Silva, R. H.; et al. U.S. Pat. Appl. 79,173, 26 Sep., 1979.
155. Bachot, J.; Grosbois, J. Ger. Pat. Appl. 33,262, 5 Aug., 1981.
156. TDK Electronics Co. Jap. Patent 82/12,801, 22 Jan., 1982.
157. Taketani, Y.; Kunst, B.; Matsuura, T.; Sourirajan, S. <u>Proc.</u>
     <u>Bioenergy R&D Seminar</u> 1981, 3rd, 145-149.
158. Toray Industries, Inc. Jap. Patent Appl. 79/95,086, 27 July,
     1979.
159. Evans Products Co. Jap. Patent 82/49,629, 23 March, 1982.
160. Dainippon Ink & Chem. Co. Jap. Patent 83/67,733, 22 April,
     1983.
161. Mitsubishi Rayon Co. Jap. Patent 81/76,208, 23 June, 1981.
162. Abe, M.; Ichinose, H.; Noda, Y. Fr. Patent 2,485,549, 31 Dec.,
     1981.
163. Abe, M.; Iwama, A.; Noda, H.; Ichinose, H. W. Ger. Patent
     3,038,012, 23 April, 1981.
164. Noordegraaf, D. A.; Smolders, C. A.; DeBoer, R.; Romijn, D. S.
     <u>Desalination</u> 1982, <u>41</u>, 249-261.
165. Joshi, S. V.; Rao, A. V. <u>J. Appl. Polym. Sci.</u> 1983, <u>28</u>,
     1457-1463.
166. Tetenbaum, M. T.; Case, B. C. U.S. Patent Appl. 106,571,
     26 Dec., 1979.
167. Kim, K. Y.; Lee, Y. M.; Ko, J. H. <u>Pollimo</u> 1980, <u>4</u>, 499-504.
168. Kim, K. Y.; Kim, H. J. <u>Pollimo</u> 1981, <u>5</u>, 372-380.
169. Mitsubishi Rayon Co. Ltd. Jap. Patent Appl. 78/38,909,
     3 April, 1978.
170. Gensrich, H. J.; et al. E. Ger. Patent 143,037, 30 July, 1980.
171. Sanderson, R. D.; Loubser, N. E. S. Afr. Patent 80/3,750,
     24 June, 1981.
172. Saltonstall, C. W.; Highley, W. S.; Kesting, R. E. <u>Research</u>
     <u>and Development Progress Report No. 150</u>, Office of Saline
     Water, U.S. Dept. of Interior, 1966.
173. Mitsubishi Rayon Co. Ltd. Jap. Patent 81/30,441, 1981.
174. Japan Exlan Co. Ltd. Jap. Patent 81/31,407, 30 March, 1981.

175. Agency of Ind. Sci. and Technol. Jap. Patent 81/123,408,
     28 Sep., 1981.
176. Linder, C.; et al. Ger. Patent 3,035,134, 9 April, 1981.
177. Daicel Chem. Ind. Jap. Patent 81/87,403, 16 July, 1981.
178. Yasuda, H.; Schindler, A. In "Reverse Osmosis Membrane
     Research", H. K. Lonsdale and H. E. Podall (Eds.); Plenum
     Press: New York, 1972; pp. 299-316.
179. Orofino, T. A. Research and Development Progress Report
     No. 549, Office of Saline Water, U.S. Dept. of Interior, 1970.
180. Kuraray Co. Ltd. Jap. Patent 81/149,438, 1981.
181. Nitto Electric Industrial Co. Ltd. Jap. Patents 81/139,824
     and 81/139,825, 26 Oct., 1981.
182. Iijima, T.; Komiyama, J.; Uemura, T.; Makino, Y. Kenkyu
     Hokoku - Asahi Garasu Kogyo Gijutsu Shoreikai 1979, 35,
     235-250.
183. Dvornic, S.; Obradovic, S. Naucno-Teh. Pregl. 1982, 32,
     14-23.
184. Madorskaya, L. Ya.; et al. USSR Patent 883,100, 23 Nov., 1981.
185. Miseyuk, A. V.; Kirillova, R. M.; Alfonchenko, O. V.; Dubyaga,
     V. P. Plast. Massy 1983, 57.
186. Lonsdale, H. K.; Merten, U.; Riley, R. L.; Vos, K. D.
     Research and Development Progress Report No. 167, Office of
     Saline Water, U.S. Dept. of Interior, 1966.
187. Rassulin Yu. A.; et al. Prikl. Biokhim. Mikrobiol. 1981, 17,
     238-240.
188. Khalilova, L. S.; et al. Tr. Mosk. Khim. Tekhnol. Inst. im.
     D. I. Mendeleeva 1979, 109, 106-109.
189. Lonsdale, H. K.; Merten, U.; Riley, R. L.; Vos, K. D.
     Research and Development Progress Report No. 150, Office of
     Saline Water, U.S. Dept. of Interior, 1965.
190. Behnke, J.; Pitowski, H. J. Ger. Patent 2,932,761, 26 Feb.,
     1981.
191. Gambro Inc. Jap. Patent 82/55,154, 1 April, 1982.
192. Beasley, J. K. Desalination 1977, 22, 181-189.
193. Shantora, V.; Huang, R.Y.M. J. Appl. Polym. Sci. 1981, 26,
     3223-3243.
194. Kimura-Yeh, F.; Hopfenberg, H. B.; Stannett, V. T. In
     "Reverse Osmosis Membrane Research", H. K. Lonsdale and H. E.
     Podall (Eds.); Plenum Press: New York, 1972; pp. 177-203.
195. Vigo, F.; Capannelli, G.; Munari, S. Desalination 1981, 37,
     313-324.
196. Bittencourt, E.; Stannett, V.; Williams, J. L.; Hopfenberg,
     H. B. J. Appl. Polym. Sci. 1981, 26, 879-888.
197. Cabasso, I. In "Ultrafiltration Membranes and Applications",
     A. R. Cooper (Ed.); Plenum Press: New York, 1980; pp. 57-78.
198. Aptel, P.; Cabasso, I. J. Appl. Polym. Sci. 1980, 25,
     1969-1989.
199. Cannon, C. U.S. Patent 3,497,072, 1970.
200. King, W. M.; Horenschemeyer, D. L.; Saltonstall, C. W. In
     "Reverse Osmosis Membrane Research", H. K. Lonsdale and H. E.
     Podall (Eds.); Plenum Press: New York, 1972; pp. 131-161.
201. Tamura, M.; Uragami, T.; Sugihara, M. Polymer 1981, 22,
     829-835.
202. Jakabhazy, S. Z. Eur. Patent Appl. 54,354, 1982.

203. Koyaman, K.; Nishimura, M.; Iitami, K.   Nippon Kagaku Kaishi
     1981, 2, 288-291.
204. Orofino, T. A.   Research and Development Progress Report
     No. 549, Office of Saline Water, U.S. Dept. of Interior, 1970.
205. Hirabayashi, Y.; Tai, H.; Takayama, S.; Ohtsuka, Y.   Kobunshu
     Ronbunshu 1981, 38, 175-181.
206. Yamamoto, S.; Ohnishi, S.; Kuwabara, S.   Kenkyu Hokoku - Sen'i
     Kobunshi Kenkyusho 1981, 129, 69-78.
207. Jakabhazy, S. Z.; Zeman, L. J.   U.S. Patent 4,248,913, 3 Feb.,
     1981.
208. Uragami, T.; Naito, Y.; Sugihara, M.   Polym. Bull. (Berlin)
     1981, 4, 617-622.
209. Csell, T. C.; Joffee, I. B.; Dogen, P. J.   Fr. Patent
     2,521,028, 12 Aug., 1983.
210. Shin-Kobe Electric Machinery Co.   Jap. Patent 81/152,850,
     26 Nov., 1981.
211. Wrasidlo, W. J.   Eur. Patent 56,512, 28 July, 1982.
212. Nippon Shokubai Kagaku Kogy Co.   Jap. Patent 81/139,105,
     30 Oct., 1981.
213. Teijin Ltd.   Jap. Patent 80/97,204, 24 July, 1980.
214. Nitto Electric Industrial Co.   Jap. Patent 82/27,101, 13 Feb.,
     1982.
215. Toray Industries   Jap. Patent 81/21,604, 28 Feb., 1981.
216. Toray Industries   Jap. Patent 81/21,605, 29 Feb., 1981.
217. Teijin Ltd.   Jap. Patent 80/147,105, 15 Nov., 1980.
218. Nitto Electric Industrial Co.   Jap. Patent 81/30,442,
     27 March, 1981.
219. Nitto Electric Industrial Co.   Jap. Patent 81/126,407, 3 Oct.,
     1981.
220. Kanegafuchi Chemical Industry Co.   Jap. Patent 81/133,007,
     17 Oct., 1981.
221. Elfert, K.   Eur. Patent Appl. 43,481, 13 Jan., 1982.
222. Linder, C.; Perry, M.; Kotraro, R.   Eur. Patent Appl.
     47,953, 24 March, 1982.
223. Koyama, K.; Okada, M.; Nishimura, M.   J. Appl. Polym. Sci.
     1982, 27, 2783-2789.
224. Hopfenberg, H. B.; Paul, D. R.   In "Polymer Blends"; D. R.
     Paul and S. Newman, Eds.; Academic Press: New York, 1978.
225. Cabasso, I.   Ind. Eng. Chem. Prod. Res. Dev. 1983, 22,
     313-319.

Aromatic Polyamide Membranes

H. H. HOEHN

Central Research and Development Department, E. I. du Pont de Nemours and Company, Experimental Station, Wilmington, DE 19898

Aromatic polyamide (aramid) membranes represent an important segment of the rapidly developing technology for the separation of components of aqueous solutions, gaseous mixtures and organic liquid mixtures. This paper highlights the historical aspects of polyamide membrane research in Du Pont from 1962 to 1984. Materials science aspects of this paper deal with the broad range of structures possible with aramid polymers and membranes. Structure-property relationships of aramid membranes are illustrated on four levels of structure: segmental composition of the polymer, steric relationships of the segmental structure, morphology of the asymmetric membranes and morphology of thin-film composites. Steric relationships for aromatic polyamides and polyimides for membranes intended for gas separations correlate well with flux/selectivity properties. The nature of asymmetry in aromatic polyamide membranes is discussed with reference to flux/selectivity properties of membranes for water desalination. Characteristics and performance of Du Pont's Permasep permeators which employ aramid membranes in the form of fine hollow fibers for desalination of brackish and sea water illustrate how the materials science studies of aromatic polyamide membranes have been applied to provide the basis of an important membrane business.

For a variety of reasons, a comprehensive review of the history, current developments and recent results in Du Pont research on aromatic polyamide membranes is not possible. In fact, this paper will be limited to Du Pont research and limited further to some key polyamides and derivatives that illustrate the relationship between structure-level and membrane properties.

Historical Development of Permasep Permeators

Membrane research and development started in Du Pont in 1962 and
culminated in the introduction of the first B-9 Permasep permeator
for desalination of brackish water by reverse osmosis (RO) in 1969.
The membrane in this B-9 Permasep module consisted of aramid hollow
fibers. In 1969, proponents of RO technology had ambitious dreams
and hopes. Today, RO is a major desalination process used worldwide
to provide potable water from brackish and seawater feeds.
Du Pont's membrane modules for RO are sold under the trademark
Permasep permeators. The RO business is a virtually autonomous
profit center that resides in the Polymer Products Department. The
growth and success of the Permasep products business is a direct
result of Du Pont's sustained research and development commitment to
polyamides, a commitment that dates back to the 1930's and the
classic polymer researches of Wallace H. Carothers. Since 1969,
improved and new Permasep permeators have been introduced six
times, as shown in Table I.

Table I. Permasep Permeator Developments

o 1969 Introduced first B-9 Permasep permeator for desalting
   brackish water.

o 1970 The B-9 Permasep permeator for desalting brackish
   feedwater offered greater productivity per unit than its
   predecessor.

o 1974 The 4-inch B-10 Permasep permeator made seawater
   desalting with reverse osmosis commercially attractive.

o 1977 The 8-inch B-10 Permasep permeator with four times the
   capacity of the 4-inch model reduced seawater RO system
   costs.

o 1980 Based on operating experience, guarantees offered for
   new Permasep permeator RO systems were extended from three
   to five years.

o 1981 Replacement bundles for large Permasep permeators
   reduced permeator replacement costs.

o 1983 Introduced new B-15 spiral-wound permeator based on
   aramid membranes from polyamides similar to those in B-9 and
   B-10 Permasep permeators.

Du Pont does not currently market Permasep permeators for gas
separations. They did, however, in the B-1 Permasep permeator,
introduce the first commercial, hollow fiber permeator for gas
separations. This permeator employed hollow fibers of polyethylene
terephthalate as the membrane. Later, permeators having aramid
hollow fiber membranes were field tested for hydrogen separations.
Du Pont is presently actively engaged in research for the develop-
ment of membrane technology for a wide variety of applications.

This brief historical summary of Permasep permeator develop-
ments introduces the subject of structure-property relationships for
membranes from aromatic polyamides and derivatives.

Structure-Property Relationships for Membranes

The development of the aramid membranes in Permasep permeators for
RO had its origins in membranes that were intended for gas
separations. Corporate approval for further research and commercial
development of the B-1 Permasep permeator for gas separations was
granted in 1964. At that time, our knowledge of membrane science
was limited. The decision to proceed with the separations venture
was based largely on the hopes of solving the productivity-economic
requirements for permeation separations through the use of membranes
comprising melt-spun hollow fibers. Technology for melt-spinning
hollow fibers with an outside diameter of less than 100 μM and a
wall thickness of less than 25 μM provided a potential solution to
the large membrane area requirements at a low cost. In addition to
the area advantage of hollow fiber membranes for permeators, the
large number of polymers Du Pont had available and the know-how to
make others for conversion to hollow fiber membranes were important
factors in the decision to proceed. Enthusiasm was sufficiently
high that hollow fiber membranes for water desalination were also
included in the venture.

Explorations with homogeneous membranes quickly showed that the
flux-selectivity requirements for water desalination membranes would
demand more than a simple melt-spun hollow fiber. In fact, it has
been necessary to work out structure-property relationships on all
levels of structure to bring RO membrane technology involving
aromatic polyamides to its current status.

In discussing the architecture and properties of aromatic
polyamide membranes, it is convenient to refer to four levels of
structure. Broadly speaking, these levels of structure are useful
for understanding the properties of any synthetic membrane,
irrespective of what type of polymer is used to make the membrane or
whether the membrane is intended for RO, gas separation or
ultrafiltration. The levels of structure as used in this paper are
defined in Table II.

Table II.   Structural Levels of Synthetic Membranes

o   Structure Level I - Segmental composition of the polymer.

o   Structure Level II - Steric relationships in the
    segmental structure.

o   Structure Level III - Morphology of asymmetric membranes.

o   Structure Level IV - Morphology of thin-film composite
    membranes.

Structure Level I refers to the segmental composition of the
polymer. It may be helpful to call Structure Level I the primary
structure because it affects all of the other levels of structure of
the membrane. Structure Level II, which can also be called the

secondary structure, refers to the steric relationships of the segmental units. Structure Level III (tertiary structure) concerns the morphology of asymmetric membranes. Structure Level IV (quaternary structure) is useful for characterizing thin-film composite membranes.

It is important to bear in mind that Structure Levels I and II are primarily properties of the polymer whereas levels III and IV are properties of the membrane. These definitions are arbitrary and additional levels of structure can be used to describe membrane properties. For example, it may be useful to have levels of structure relating to crystalline-noncrystalline properties, globular domains, pore character and orders of symmetry that can give rise to periodic structures, specific coil character and other important structural details.

Structure Level I. Structure Level I variations for aromatic polyamides are broad. The wide range of segmental structures possible with these polymers is what makes them so interesting for membrane science. The discussion of Structure Level I will be limited to some representative segmental units in polyamides, polyhydrazides and polyamide-hydrazides. Structures and abbreviations for some typical diamines that are condensed with mixtures of isophthaloyl chloride (I) and terephthaloyl chloride (T) to give the aromatic polyamides discussed in this paper are shown in Table III.

Table III.   Structures and Abbreviations of Diamines

H_2N—⬡—NH_2 (MPD) H_2N—⬡—NH_2 (PPD)

H_2NNH-CO—⬡—O-CH_2CH_2O—⬡—CO-$NHNH_2$ (OB(O)2(O)BO)

H_2NNH-CO—⬡—CO-$NHNH_2$ (OIO) H_2N—⬡—CO-$NHNH_2$ (1,3 BO)
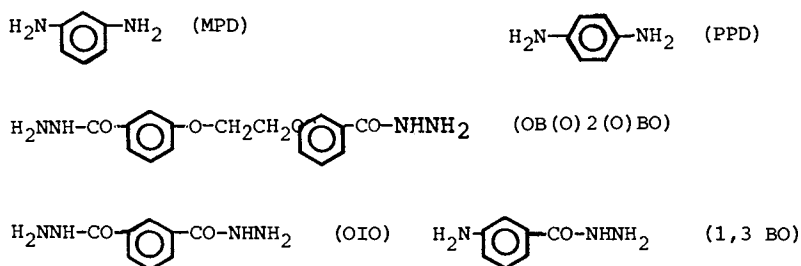
All that needs to be said about the synthesis of aromatic polyamides is that the condensations were usually carried out in N,N-dimethylacetamide (DMAC) or N-methyl pyrrolidone (NMP) with the appropriate diamine and phthaloyl chloride.

Major contributions to the synthesis of aromatic polyamides were made by Morgan, Kwolek and coworkers (1-6). G. N. Milford prepared the aromatic polyamide and J. W. Richter synthesized the polyhydrazides and polyamide-hydrazide discussed in this paper (7). Other investigators have also contributed extensively to the synthesis and characterization of aromatic polyamides; for example, Preston and coworkers at Monsanto (8-10). Important contributions to the polyamide synthesis literature have also been made by Australian, Canadian, European, Japanese and Russian scientists (11).

Structure Level II.   Structure Level II is in some ways the key
structural feature that determines whether a polyamide has any merit
for membrane applications. The importance of the steric relation-
ships in the segmental structure are readily illustrated with the
simplest aromatic polyamide one can make. For example, the homo-
polymers of p-phenylenediamine (PPD) or m-phenylenediamine (MPD)
condensed with either isophthaloyl chloride (I) or terephthaloyl
chloride (T) crystallize so readily that suitable casting solutions
of these polyamides cannot be made. On the other hand, mixed
monomers of MPD/PPD-I/T give copolyamides that are sufficiently
disordered to have good solubility in organic solvents. A space
filling model of the MPD-I/T segment shows relatively open character
and low symmetry compared to PPD-T or even MPD-I. The lower level
of segmental symmetry results in a more open membrane structure.

     The preference of the 1,3 orientation for the diamine used for
polyamide synthesis carries over to the OIO and 1,3 BO diamines used
for synthesis of polyhydrazides and polyamide-hydrazides,
respectively. One of the reasons that the 1,3 BO-I/T polyamide-
hydrazides give such good RO membranes is that the ring symmetry is
lowered a second time by having different amine groups in the 1,3
positions on the benzene ring. The effect of Structure Level II on
RO properties will be apparent when we discuss Structure Level III.

     The role of Structure Level II on membrane properties is not
limited to RO membranes. In fact, the secondary structure is
probably even more important in membranes that are intended for gas
separations. Patents exist for gas separation membranes where
Structure Level I is aromatic amide, aromatic ester and aromatic
imide combined with Structure Level II of a precisely defined type
(12, 13). For example, the repeating segmental unit (a) contains at
least one rigid divalent subunit; the two main chain single bonds
which extend from it are not colinear, (b) is sterically unable to
rotate 360° around one or more of the main chain single bonds, and
(c) more than 50% of the atoms in the main chain are members of an
aromatic ring. The polyimide designated 1,5 ND-6F illustrates these
structural requirements. This polyimide has the structure shown in
Table IV.

Table IV.   Steric Features of 1,5 ND-6F

Rigid subunit	Colinearity	Restricted bonds
1	N	A,B
2	N	B,C
3	N	C,D
4	N	D,A

The structural requirements in the Du Pont patents are shown in Table IV. The repeating unit contains 4 rigid subunits connected by noncolinear bonds (N), 4 bonds with restricted rotation; and 22/29 of the chain atoms are aromatic.

The polyimide is prepared from 1,5 naphthlene diamine (1,5 ND) and 3,3',4,4'diphenylhexafluoroisopropylidene tetracarboxylic acid dianhydride (6F). A polyamide acid is obtained initially and this is cyclized to give the polyimide. Because polyimides are derivatives of polyamides, polyimides are often included in reviews of aromatic polyamides. Another reason polyimides are included in this paper is that they illustrate the role of Structure Level II on gas transport properties in a straightforward manner.

The 1,5 ND-6F polyimide membrane was prepared by the following procedure. A casting solution was made by dissolving 20 wt% 1,5 ND-6F in DMAC and filtering the solution through a silver membrane with a nominal pore size of 8 μM. The degassed solution was cast on a Teflon -coated glass plate using a 25-mil doctor knife. The films were covered, dried at 100°C for 5 minutes with the cover vents closed and 10 minutes with the cover vents open. The films were then stripped from the plate and stored in air at room temperature. Control films were tested without further treatment; other films were heated at 200 to 340°C under a vacuum of 2 μM for 6 hours.

The permeation properties of 1,5 ND-6F membranes to pure hydrogen and pure methane are shown in Table V.

Table V. Permeability Properties of 1,5 ND-6F Polyimide Membranes

Post Treatment* Temperature(°C)	Thickness (mils)	Centibarrers (cB)		Selectivity (H_2/CH_4)
		H_2	CH_4	
Control	1.66	5,320	189	28
200	1.95	9,260	68	136
250	1.92	8,700	43	202
300	1.91	10,010	61	164
340	1.74	9,070	63	144

*6 hr. at 2 μM vacuum

$$cB = \frac{10^{-12} cm^3(STP) \cdot cm}{cm^2 \cdot sec \cdot cm\ Hg}$$

The unique feature of these results is that the hydrogen flux increased and the methane flux decreased when the 1,5 ND-6F homogeneous membranes were heat treated. Here is a case where post-treatment of the membrane has given increased flux for hydrogen with improved H_2/CH_4 selectivity at the same time. With most membranes, one gets increased flux only at the expense of lower selectivity. More conventional membranes also tend to lose considerable flux on annealing. Membranes of 1,5 ND-6F are thermodynamically stable after heat treatment.

The polyimide from 3,5 diaminobenzoic acid (3,5 DBA) and 6F has the structure shown in Table VI.

Table VI.   Steric Features of 3,5 DBA-6F

Rigid subunit	Colinearity	Restricted bonds
1	N	--
2	N	C
3	N	C,D
4	N	D

The repeating unit has 4 N subunits, 2 bonds with restricted rotation, 3 of the N subunits have at least one bond with restricted rotation, and 18/27 of the atoms in the chain are aromatic.

The 3,5 DBA-6F polyimide film permeated H_2 at 32 B (B=10^{-10} cm^3 (STP) $\cdot$ cm/ cm^2 $\cdot$ sec $\cdot$ cm Hg) and CH_4 at 0.075 B for a H_2/CH_4 selectivity of 427 at 114.7 psia and 30°C.

The polyimide from 3,3' diaminobenzanilide (3,3' DBAN) and 6F has the structure shown in Table VII.

Table VII.   Steric Features of 3,3' DBAN-6F

Rigid subunit	Colinearity	Restricted bonds
1	N	--
2	N	--
3	N	--
4	N	--
5	N	F
6	N	F, G
7	N	G

The repeating unit has 7 N subunits, 2 bonds with restricted rotation, 3 of the N subunits have at least one bond with restricted rotation, and 24/33 of the atoms in the chain are aromatic.

The heat treated film of 3,3' DBAN-6F permeated H_2 at 20 B and CH_4 at 0.025 B for a H_2/CH_4 selectivity of 800.

Structure Level II effects on gas permeability properties of the polyimides discussed in this paper are especially interesting when considered with regard to the role of solubility and diffusion parameters on permeability properties. From segmental shape considerations it is clear that the solubility and diffusion

properties are not independent of one another. Koros, Paul, Hopfenberg, Stannett and coworkers (14-17) have been pointing this out for some time.

Structure Level III. Although the permeability through a homogeneous membrane is strongly dependent on the primary and secondary polymer structures, the permeability coefficient as defined by Equation (1) is usually too low for commercial gas and RO separations.

$$P = \frac{Quantity \cdot Thickness}{Area \cdot Time \cdot Pressure} \text{ (Temperature specified)} \tag{1}$$

In order to achieve the desired flux levels in membranes, it is generally necessary to reduce the thickness of the diffusion layer to low levels. One way to do this is to cast the membrane with asymmetric morphology. This was done with the aromatic polyamide membranes intended for water desalination.

The permeation properties of homogeneous and asymmetric membranes of MPD-I/T (100-70/30) are shown in Table VIII.

Table VIII. Effect of Asymmetric Morphology on Polyamide RO Properties

Polyamide	Membrane	Flux (gal/ft^2·day)	Solute Rejection (%)
MPD-I/T (100-70/30)	Homogeneous	0.03	99.6
MPD-I/T (100-70/30)	Asymmetric	5.3	99.8

Conditions: 30°C, 3.5% NaCl feed, 1500 psi

The flux of 0.03 gfd for the homogeneous polyamide membrane was more than two orders of magnitude too low for commercial desalination. The flux was increased 175 fold with no decrease in salt rejection by casting the membrane with asymmetric morphology. Even higher fluxes, up to 3.5 times that observed for the asymmetric MPD-I/T (100-70/30) polyamide membrane, were obtained with asymmetric membranes cast from polyhydrazides and polyamide-hydrazides. Permeation properties for the three types of aromatic polyamides are shown in Table IX. The RO properties of this group of membranes illustrate the combined effects of Structure Levels I, II and III on membrane performance.

Table IX.   Permeation Properties of Asymmetric Polyamide Membranes

Polymer		Flux	Solute Rej.
Type	Composition	$(gal/ft^2 \cdot day)$	%
Polyamide	MPD-I/T (100-70/30)	5.3	99.8
Polyhydrazide	OB(O)2(O)BO/OIO-I/T (50/50-70/30)	13.2	99.3
Polyamide-hydrazide	1,3 BO/1,4 BO - I/T (83/17-70/30)	17.0	99.5

The asymmetric polyamide membranes were prepared using a casting solution consisting of 15 g polymer, 85 g DMAC and 35 wt % $LiNO_3$ (BOP) as the lyotropic salt. Salt concentrations in the casting solution are conveniently expressed as percent based on polymer (BOP). The doped polyamide solution was cast on a Pyrex® glass plate using a 25-mil doctor knife. The film was then partially dried to obtain a gel membrane of polymer/solvent/salt. The air side (skin side) was identified and the gel film immersed in ice water. After an hour in ice water, the membrane was transferred to distilled water and stored until it was tested.

In addition to DMAC, the solvents DMF, DMSO and NMP can be used for casting aromatic polyamide membranes. Lyotropic salts that give good polyamide membranes are those with lithium, calcium and magnesium as the cation and chloride, bromide, iodide, nitrate, thiocyanate and perchlorate as the anion.

The nature of asymmetry in aromatic polyamide membranes has been described by Panar, Hoehn and Hebert (18). Electron micrographs of freeze-cleaved aromatic polyamide membranes show considerable substructure as part of Structure Level III character. Details of the morphology are apparent in the various electron micrographs shown in this paper.

Figure 1 shows the top edge of cross-section of a polyamide-hydrazide asymmetric gel membrane. The surface shows a structure formed from a closely packed monolayer of polyamide-hydrazide micelles of about 400 to 600 Å diameter.

The substrate consists of similar spherical units or globular domains oriented with 75 to 100 Å voids between the spheres. In the skin or surface layer, these globular units are compressed and somewhat distorted so that few voids are seen. The important point is that the skin is a denser form of the same "micellar" structure that forms the bulk of the membrane.

Figure 2 shows a surface layer that broke off the substrate during fracture and adhered to the water "pot." The grainy surface in this micrograph is the fracture surface of water in the gel membrane.

Figure 3 shows a fracture surface of a dried polyamide-hydrazide gel membrane. Fusion of the micelles to give a typically homogeneous, bulk phase is clearly evident from this micrograph.
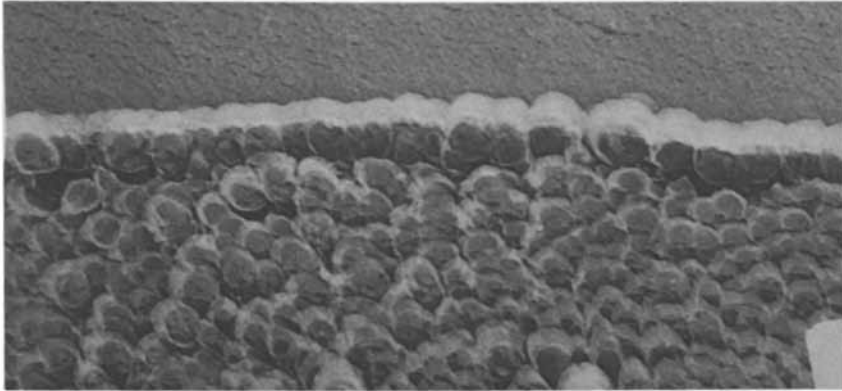
Figure 1. Top edge of cross section of a polyamide-hydrazide
           asymmetric gel membrane. Reproduced from Ref. 18.
           Copyright 1973 American Chemical Society.
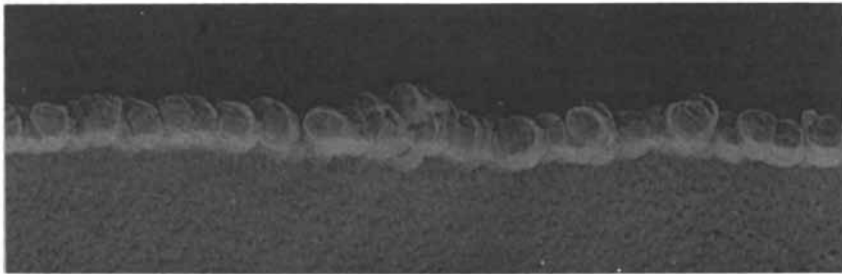
Figure 2. Surface skin of a polyamide-hydrazide membrane. Repro-
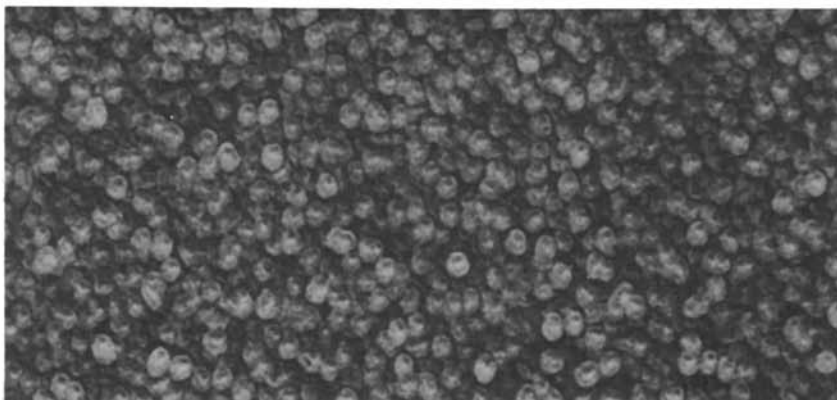   duced from Ref. 18. Copyright 1973 American Chemical
           Society.

The micellar structure of asymmetric membranes having a surface monolayer as the functional portion is seen with polyamides and also with cellulose acetate as shown in Figure 4 and 5.

Figure 4 is a micrograph of the skin structure of an asymmetric polyamide and Figure 5 is a micrograph of the skin structure of an asymmetric cellulose acetate membrane.

Figure 6 shows the skin structure of a polyamide-hydrazide that has been freeze-dried. Unlike the Figure 3 micrograph of an air-dried polyamide-hydrazide membrane that has a homogeneous appearance, the freeze-dried membrane shows a micellar structure.

Figure 7 shows that the casting solution has a micellar character similar to that of the membrane.

One can actually consider the trapped solution morphology as a functional definition of the asymmetric membranes. It should be emphasized that this viewpoint clearly differentiates asymmetric membranes that have shown the highest reverse osmosis fluxes from membranes with a thin dense layer of normal solid morphology.

Asymmetric membranes prepared by phase inversion are discussed in considerable detail by Kesting (19).

Structure Level IV. The membrane structure of composite membranes is designated Structure Level IV in this paper. Composite membranes usually consist of a thin film of polymer on a porous substrate and are generally referred to as "thin-film composite" membranes. The coating polymer and substrate polymer are generally different polymers selected for the unique properties that each polymer component imparts to the composite membrane.

The functional thin coating in composite membranes for water desalination is often a polyamide formed in-situ on the porous substrate by interfacial polymerization. Interfacial polymerization of polyamides is a polymerization technique that was pioneered by Du Pont (20).

Universal Oil Products (UOP) developed reverse osmosis equipment for demineralization of brackish and seawater using composite membranes with a polyamide as the functional coating. The UOP products carry a "TFC" registered trademark. Another good example of a thin-film composite membrane involving a thin film of polyamide as the functional coating is the FilmTec FT-30 membrane for RO (21).

Monsanto's Prism permeators for gas separation also employ composite membranes. Polyamide coatings are not used for the composite membrane in the Prism module. The Prism membrane consists of a coating of silicone rubber applied from an organic solvent on a porous polysulfone substrate. The Prism membrane is another good example of a composite membrane where Structure Level IV is used to obtain good membrane properties (22).

B-9 and B-10 Permasep Permeators

The membranes in Du Pont's B-9 and B-10 Permasep permeators consist of bundles of aramid hollow fibers. A drawing illustrating the construction of B-9 and B-10 modules is shown in Figure 8 (23, 24).

Specifications for B-9 and B-10 Permasep permeators are given in Du Pont's PEM (Permasep Engineering Manual) (23) and in Du Pont's Hollow Fiber Membranes (24). These references also
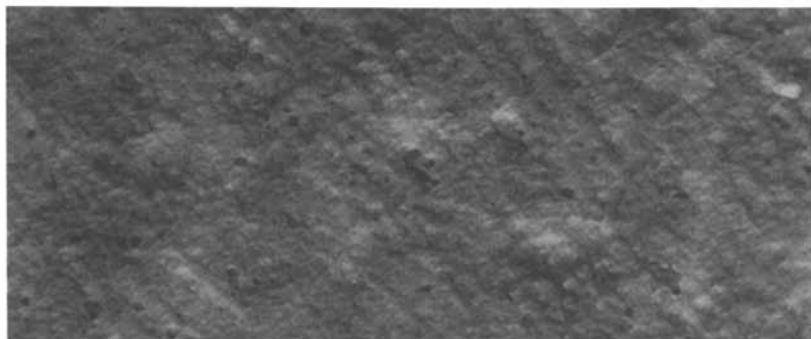
Figure 3.   Fracture surface of an air-dried polyamide-hydrazide
            membrane. Reproduced from Ref. 18. Copyright 1973
            American Chemical Society.
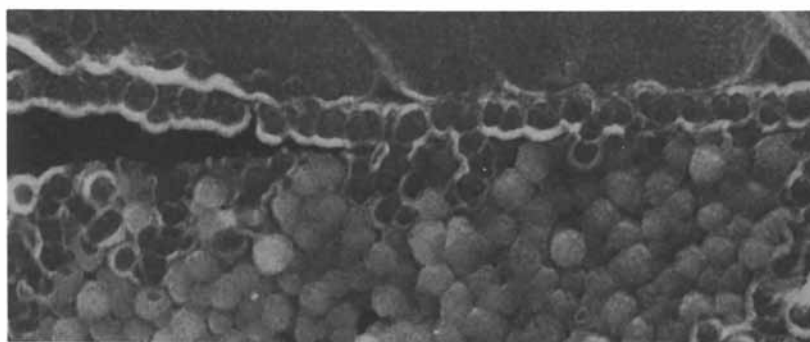
Figure 4.   Skin structure of a polyamide asymmetric membrane.
            Reproduced from Ref. 18. Copyright 1973 American
            Chemical Society.
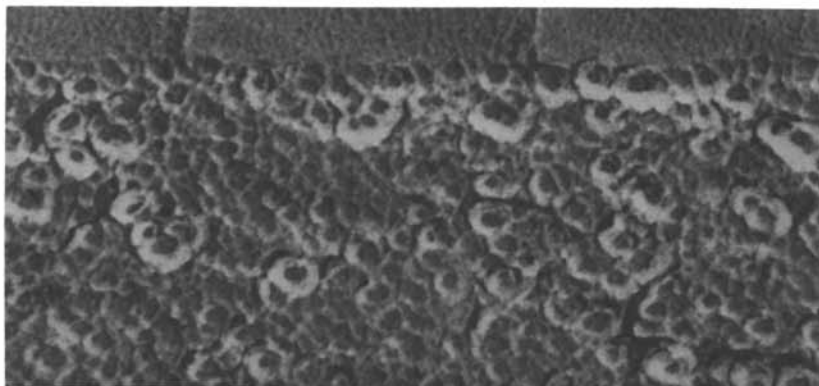
Figure 5. Skin structure of a cellulose acetate membrane. Reproduced from Ref. 18. Copyright 1973 American Chemical Society.
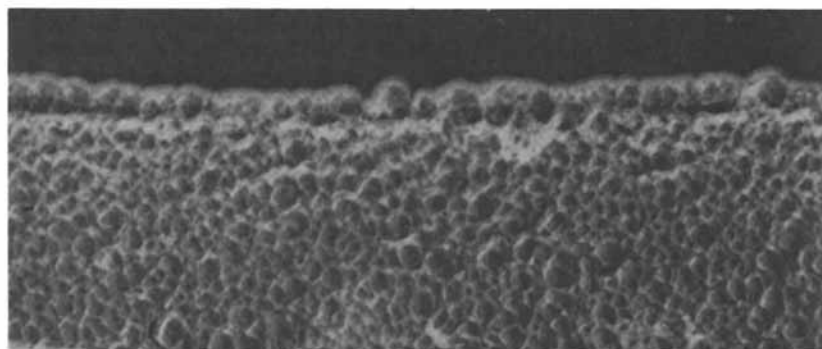
Figure 6. Skin structure of a freeze-dried polyamide-hydrazide membrane. Reproduced from Ref. 18. Copyright 1973 American Chemical Society.

Figure 7. Fracture surface of a casting solution of polyamide-
           hydrazide. Reproduced from Ref. 18. Copyright 1973
           American Chemical Society.
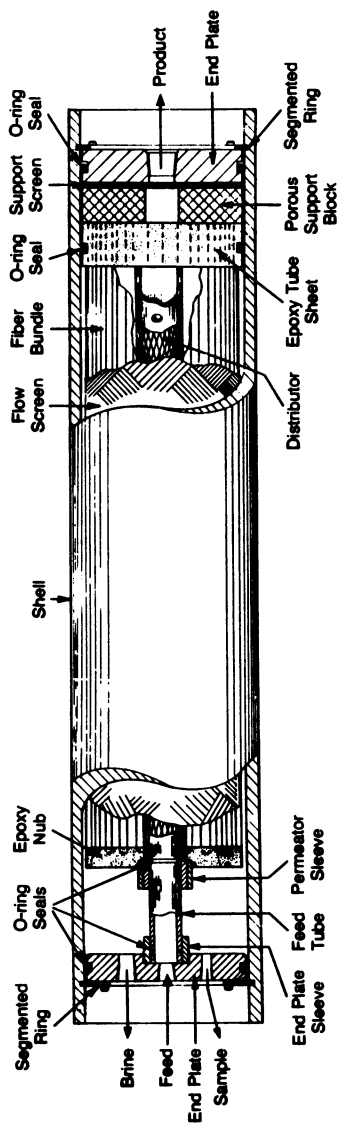
Figure 8. Schematic of Permasep Permeator.

discuss the desalination process, case histories and economics, desalination of brackish water, seawater desalting, pretreatment and applications other than desalination.

Microporous Membranes

The role of phase inversion processes in the production of micro-porous aromatic polyamide membranes is discussed by Strathmann (25).

Acknowledgments

The work described in this paper is the work of a large team in the Du Pont Company. Contributions of J. W. Richter, G. N. Milford, and M. Panar merit special mention. The author also wishes to acknowledge the helpful discussions with P. Blais, S. Sourirajan and T. Matsuura. Sourirajan's group at the Divison of Chemistry, National Research Council of Canada have published extensively on their studies with aromatic polyamide membranes (26-46). Others that the author wishes to acknowledge for their citations and discussions of material presented in this paper are: V. T. Stannett and H. B. Hopfenberg at North Carolina State University; W. J. Koros, D. R. Paul and D. R. Lloyd at the University of Texas at Austin; J. M. S. Henis at Monsanto, and H. K. Lonsdale at Bend Research (47).

Literature Cited

1. Morgan, P. W. "Condensation Polymers"; Wiley-Interscience: New York, 1965.
2. Morgan, P. W.; Kwolek, S. L. J. Polym. Sci. 1959, 40, 299.
3. Wittbecker, E. L.; Morgan, P. W. J. Polym. Sci. 1959, 40, 389.
4. Morgan, P. W.; Kwolek, S. L. J. Polym. Sci. 1962, 62, 33.
5. Morgan, P. W.; Kwolek, S. L. J. Polym. Sci. 1963, A1, 1147.
6. Hill, H. W.; Kwolek, S. L.; Morgan, P. W. U.S. Patent 3 006 899, 1961; Kwolek, S. L.; Morgan, P. W.; Sorenson, W. R. U.S. Patent 3 063 966, 1962; Kwolek, S. L.; Hill, H. W.; Sweeny, W. U.S. Patent 3 094 511, 1963. (All assigned to Du Pont.)
7. Richter, J. W.; Hoehn, H. H. U.S. Patent 3 567 632, assigned to Du Pont.
8. Preston, J.; Dobinson, F. J. Polym. Sci. 1964, B2, 1171.
9. Preston, J.; Dobinson, F. U.S. Patent 3 205 199, 1965; U.S. Patent 3 232 910; U.S. Patent 3 240 760. (All assigned to Monsanto.)
10. Preston, J.; Black, W. B. J. Polym. Sci. 1966, B4, 267.
11. Blais, P. In "Reverse Osmosis and Synthetic Membranes"; Sourirajan, S., Ed.; National Research Council: Ottawa, Canada, 1977, Chapter 9.
12. Hoehn, H. H.; Richter, J. W. U.S. Patent Re 30 351, assigned to Du Pont.
13. Hoehn, H. H. U.S. Patent 3 822 202, assigned to Du Pont.
14. Stannett, V. T.; Koros, W. J.; Paul, D. R.; Baker, R.; Lonsdale, H. Adv. in Poly. Sci. 1979, 32, 71.

15. Koros, W. J.; Chern, R. T.; Sanders, E. S.; Hopfenberg, H. B.
     Proc. of the Second GRI Gas Separation Workshop, Boulder, CO.
     1982, 189.
16. Chern, R. T.; Koros, W. J.; Hopfenberg, H. B.; Stannett, V. T.
     In "Materials Science of Synthetic Membranes"; Lloyd, D. R.,
     Ed.; American Chemical Society: Washington, D.C., 1985.
17. Koros, W. J.; Chern, R. T.; Stannett, V. T.; Hopfenberg, H. B.
     J. Poly. Sci.: Phys. Ed. 1981, 19, 1513.
18. Panar, M.; Hoehn, H. H.; Hebert, R. R. Macromolecules
     Sept.-Oct., 1973, 6, 777-79.
19. Kesting, R. E. In "Materials Science of Synthetic Membranes";
     Lloyd, D. R., Ed.; American Chemical Society: Washington,
     D.C., 1985.
20. Morgan, P. W. "Condensation Polymers: By Interfacial and
     Solution Methods"; Wiley-Interscience: New York, 1965.
21. Cadotte, J. E. In "Materials Science of Synthetic Membranes";
     Lloyd, D. R., Ed.; American Chemical Society: Washington,
     D.C., 1985.
22. Henis, J. M. S.; Tripodi, M. K. U.S. Patent 4 230 463,
     assigned to Monsanto.
23. Permasep Engineering Manual. E. I. du Pont de Nemours & Co.,
     Inc., Polymer Products Department, Permasep Products, Glasgow,
     DE 19898.
24. Caracciolo, V. P.; Rosenblatt, N. W.; Tomsic, V. J. In
     "Reverse Osmosis and Synthetic Membranes"; Sourirajan, S., Ed.;
     National Research Council: Ottawa, Canada, 1977; Chapter 16.
25. Strathmann, H. In "Materials Science of Synthetic Membranes";
     Lloyd, D. R., Ed.; American Chemical Society; Washington, D.C.,
     1985.
26. Matsuura, T.; Blais, P.; Dickson, J. M.; Sourirajan, S. J.
     Appl. Polym. Sci. 1974, 18, 3671.
27. Dickson, J. M.; Matsuura, T.; Blais, P; Sourirajan, S. J.
     Appl. Polym. Sci. 1975, 19, 801.
28. Matsuura, T.; Baxter, A. G.; Sourirajan, S. J. Food Science
     1975, 40, 1039.
29. Matsuura, T.; Dickson, J. M.; Sourirajan, S. Ind. Eng. Chem.
     Process Des. Dev. 1976, 15 (1) 149.
30. Dickson, J. M.; Matsuura, T.; Blais, P.; Sourirajan, S. J.
     Appl. Polym. Sci. 1976, 20, 1491.
31. Matsuura, T.; Blais, P.; Sourirajan, S. J. Appl. Polym. Sci.
     1976, 20, 1515.
32. Matsuura, T.; Sourirajan, S. AIChE Symposium Series 1976/77,
     74, (172) 196.
33. Matsuura, T.; Sourirajan, S. Proc. 6th Inter. Symposium, Fresh
     Water from the Sea 1978, 3, 227.
34. Matsuura, T.; Blais, P.; Pageau, L; Sourirajan, S. Ind. Eng.
     Chem. Process Des. Dev. 1977, 16, (4) 510.
35. Matsuura, T.; Sourirajan, S. Ind. Eng. Chem. Process Des. Dev.
     1978, 17, (4) 419.
36. Sourirajan, S.; Matsuura, T. Proc. EPA Textile Industry
     Technology Symposium, December 5-8, 1978, Williamsburg, VA.
37. Baxter, A. G.; Bednas, M. E.; Matsuura, T.; Sourirajan, S.
     Chem. Eng. Commun. 1980, 4, 471.
38. Tweddle, T. A.; Thayer, W. L.; Matsuura, T.; Hsieh, Fu-Hung;
     Sourirajan, S. Desalination 1980, 32, 181.

39. Matsuura, T.; Taketani, Y.; Sourirajan, S. Desalination 1981,
     38, 319.
40. Yeager, H. L.; Matsuura, T.; Sourirajan, S. Ind. Eng. Chem.
     Process Des. Dev. 1981, 20, (3), 451.
41. Chan, K.; Matsuura, T.; Sourirajan, S. Ind. Eng. Chem. Product
     Res. and Dev. 1982, 21 (4), 605.
42. Matsuura, T.; Taketani, Y.; Sourirajan, S. Proc. Fourth
     Bioenergy R&D Seminar, Mar. 29-31, 1982.
43. Taketani, Y.; Matsuura, T.; Sourirajan, S. Separation Science
     and Technology, 1982, 17 (6), 821.
44. Taketani, Y.; Matsuura, T. M.; Sourirajan, S. Desalination
     1983, 46, 455.
45. Chan, K.; Matsuura, T.; Rajan, K. J. Polym. Sci.: Polym.
     Letters Ed. 1983, 21, 417.
46. Tinghui, L.; Matsuura, T.; Sourirajan, S. Ind. Chem. Prod.
     Res. Dev. 1983, 22 (1), 77.
47. Lonsdale, H. K. J. Memb. Sci. 1982, 10, 81-181.

Membrane Materials for Therapeutic Applications in Medicine

RICHARD A. WARD, PAMELA W. FELDHOFF, and ELIAS KLEIN

Division of Nephrology, School of Medicine, University of Louisville, Louisville, KY 40292

The state of the art of membranes for therapeutic use in medicine is reviewed. Applications considered include hemodialysis, hemofiltration and plasmapheresis; however, membranes for gas exchange and controlled drug release are omitted. Membrane materials include cellulose, cellulose acetate, polyacrylonitrile, polymethylmethacrylate, polyethylene-co-vinylacetate, polysulfone, polycarbonate, polyethylene and polypropylene. Major problems requiring a solution if the growth of membrane-based therapies is to continue are discussed. These include: (1) improved control of transport-related properties, such as pore size distribution, so that separations more closely resemble their natural counterparts, and (2) increased understanding of blood-membrane interactions, leading to reduced membrane thrombogenicity and complement activation.

Synthetic membranes are being used increasingly in medicine to process blood for a variety of therapeutic purposes. Such procedures are characterized by extracorporeal circulation and mass transfer across a synthetic membrane in direct contact with blood. The most common of these procedures is hemodialysis, which is used for the treatment of acute or chronic renal failure and drug detoxification (1). Estimates indicate that more than 57,000 people with end-stage renal failure in the United States are currently sustained by this therapy (2). Other applications for these membranes include hemofiltration for fluid removal (3) and the treatment of renal failure (4), plasmapheresis for the treatment of a variety of hematologic and autoimmune diseases (5) and gas exchange for short-term pulmonary function replacement during cardiac by-pass surgery (6). In addition to blood processing applications, membranes are also used in pharmaceutics for the controlled release of drugs (7).

In blood processing applications, the therapeutic goal is achieved by separating one or more components from the patient's

blood. In some cases, this is coupled with adding factors depleted
by the disease or by the therapy. Mass transfer occurs across the
membrane by diffusion and/or convection in response to applied
concentration or pressure gradients. The ability of the various
procedures to meet their therapeutic goal is limited both by the
inherent mass transfer characteristics of the membrane and by
interactions between the membrane and blood. This paper reviews
the state of the art of synthetic membranes for therapeutic use in
medicine and identifies some of the major problems that require
solution if the growth of membrane-based therapies is to continue.
Both gas exchange membranes (6) and controlled drug release systems
(7) have been reviewed recently and are excluded from this paper.

Replacement of Renal Function. The natural prototype for membrane
devices used in the replacement of renal function is the nephron of
the kidney. The nephron consists of a negatively charged
ultrafilter, the glomerulus, followed by a series of selective
reabsorption units, the tubules. The glomerulus has a sharp
molecular weight cut-off; solutes with molecular radii less than
about 3.2 nm are passed, while those larger are rejected (Figure
1). Approximately 120 ml/min of ultrafiltrate is formed and enters
the tubules. Osmotic pumping, together with a series of selective
ion pumps, results in reabsorption of about 119 ml/min of the
ultrafiltrate, while concentrating waste products in the remaining
1 ml/min that becomes urine. The reabsorptive process conserves or
expells both water and electrolytes to continually maintain the
body's normal homeostasis.
     Two membrane-based therapies, hemodialysis and hemofiltration,
are used as substitutes for renal function. On comparing these
substitution therapies with the natural kidney, it should be
remembered that each therapy functions for four to six hours, three
times per week, in contrast to the continuous performance of their
natural counterpart. Hemodialysis and hemofiltration may also be
used to augment normal renal function in the cases of drug
detoxification and fluid removal, respectively.
     Unlike the nephron, hemodialysis relies on diffusion to remove
waste substances from the blood. A membrane is used to separate
blood from an essentially physiologic electrolyte solution, the
dialysate, which usually flows countercurrent to the blood. Small
molecular weight solutes diffuse through the membrane in response
to transmembrane concentration gradients. These solute fluxes are
selective only on the basis of molecular size, causing vital blood
solutes, such as amino acids, as well as waste metabolites to be
removed from the blood. In addition, the molecular weight cut-off
of most hemodialysis membranes shows little resemblance to that of
the glomerulus (Figure 1). Removal of many larger metabolic waste
products, such as hormone fragments, is negligible. Electrolytes,
such as sodium, potassium and chloride, are included in the
dialysate in concentrations designed to maintain their blood levels
in the normal range. Finally, water is removed by applying a
hydrostatic pressure gradient across the membrane.
     In contrast to hemodialysis, hemofiltration relies on
convective transport and thus is more analogous to nephron
function. Hydrostatic pressure is used to form about 80 to 100
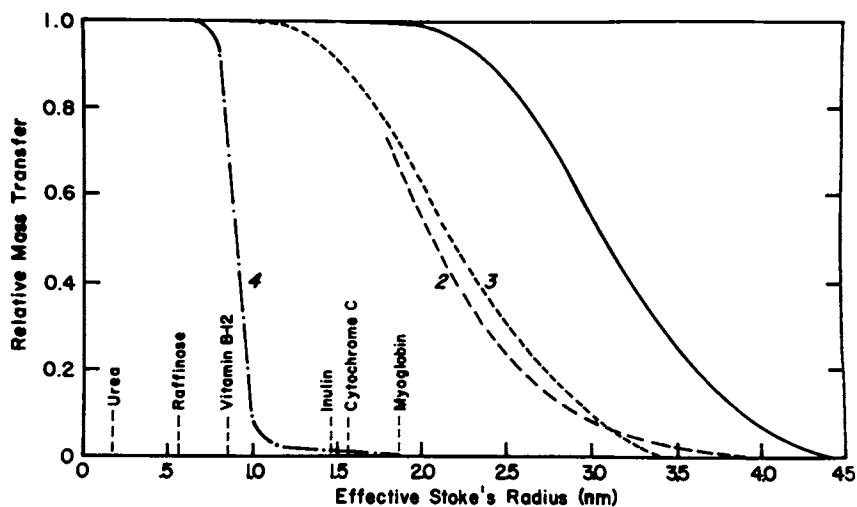
Figure 1: Relative permeability spectra for synthetic and natural membranes. Curves (1) and (2) represent the glomerular membrane for neutral and anionic solutes, respectively (8), curve (3) hemofiltration membranes (9), and curve (4) hemodialysis membranes (10). Reproduced with permission from Ref. 52. Copyright 1980 Kidney International.

ml/min of ultrafiltrate. Instead of utilizing a reabsortive step, the ultrafiltrate is discarded and a sterile, nonpyrogenic electrolyte solution infused intravenously to maintain fluid and electrolyte balance. Although the molecular weight cut-off of hemofilters is higher than that of hemodialyzers, it remains substantially less than that of the glomerulus (Figure 1). Solute removal is selective only on the basis of molecular weight; again, vital solutes are lost in the ultrafiltrate.

Plasmapheresis.   Unlike hemodialysis and hemofiltration, plasmapheresis does not seek to mimic a natural process. It is used therapeutically to nonspecifically remove soluble factors, such as immunoglobulins and immune complexes, from blood. A microporous membrane separates the blood cells from their plasma, the latter being discarded. Volume balance is maintained by the subsequent addition of a buffered electrolyte solution and albumin to the concentrated cell stream. Use of albumin or some plasma protein fraction in the replacement fluid is required to maintain oncotic pressure and prevent potentially catastrophic movement of fluid out of the patient's vascular space. This therapy would be more cost-effective if albumin could be separated from the discarded plasma stream. The recovered albumin could then be reinfused into the patient, significantly reducing the need for donor albumin. Although substantial effort has been expended, this goal remains elusive.
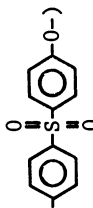
Membrane Materials

The structures and physical characteristics of the various membrane materials used in medical devices are summarized in Table I.

Cellulose. Cellulose is an enzymatically formed semicrystalline polymer consisting of sequential cellobiose (4-O-beta-D-gluco-pyranosyl-D-glycopyranose) units. To form semipermeable membranes, the insoluble polymer must first be dissolved or melted as a cellulose derivative. Esterification with acetic anhydride in the presence of small amounts of perchloric or sulphuric acid catalysts leads to soluble cellulose acetate (11). The acetylation is generally taken to completion (that is, degree of substitution (DS)=3.0). The resulting product is randomly hydrolized to the diacetate derivative (DS=2.5) which can be formed into membranes from organic solvents or melt extruded in the presence of plasticizers. To regenerate the insoluble cellulose form, the ester moieties of the formed membrane are removed by hydrolysis with mild alkali.
    Water soluble derivatives of cellulose have also been made through the formation of sodium cellulose xanthate (Cell-O-CS$_2$$^-Na^+$) (12) and copper amine complexes (that is, the cuprammonium process) (13). Both these derivatives require regeneration of the insoluble cellulose structure at the time of membrane formation. Strong salt and acid solutions are used to precipitate the soluble derivatives and simultaneously recover the cellulose structure. Residues of xanthate or cuprammonium salt decomposition must subsequently be washed out of the resulting membrane.

TABLE I: MEMBRANE MATERIALS AND CHARACTERISTICS

NAME	MONOMER	CO-MONOMER	SYMMETRY	WATER CONTENT	HYDRO-PHOBICITY	UTILIZATION
CELLULOSE		(4-0-β-D-glucopyranosyl-D-glycopyranose)	symmetric	high	–	hemodialysis
CELLULOSE ACETATE		(4-0-β-D-glucopyranosyl-D-glycopyranose-pentaacetyl)	asymmetric	medium	+	hemodialysis hemofiltration plasmapheresis
POLYACRYLONITRILE	(–C–C–) C≡N	(–C–C–) C–SO$_3^-$	symmetric	medium	++	hemofiltration hemodialysis
POLYMETHYLMETHACRYLATE	(–C–C–) CH$_3$, COOCH$_3$	—	?	low	+++	hemodialysis hemofiltration plasmapheresis
ETHYLENE/POLYVINYL ALCOHOL	(–C–C–)	(–C–C–) OH	symmetric	high	?	hemodialysis hemofiltration
POLYSULFONE	(–O–⬡–S(=O)$_2$–⬡–O–)	(–⬡–C(CH$_3$)$_2$–⬡–O–)	asymmetric	low	++++	hemofiltration
POLYCARBONATE	(–O–⬡–COO(CH$_2$CH$_2$O)$_n$OC–)	(–⬡–OCO–)	asymmetric	low	++	hemodialysis
POLYPROPYLENE	(–C–C–) CH$_3$	—	symmetric	low	++++	plasmapheresis

When cellulose membranes are first formed, they exhibit a high degree of swelling in water. There is an irreversible collapse of this hydrated structure following the initial drying of the gelled membrane, with further subsequent collapses of the gel structure after each wet/dry cycle. The observed swelling hysteresis following wet/dry cycles has been attributed to compaction of the fringe micellar structure of the cellulose crystallites. In terms of this model, the cellulose structure is in a quasi-equilibrium state with the water vapor of the surroundings. The extent of gel shrinkage is a function of the temperature, the rate of drying and plasticizer concentrations in the membrane. Generally, the cellulose membranes finally used for hemodialysis will contain 45 to 50 percent water when equilibrated with aqueous solutions. The permeability of cellulosic membranes, as well as other hydrogels, has been correlated with their hydration state (14). To maintain a high permeability during extended storage, cellulosic membranes are generally shipped containing 5 to 40 percent glycerin by weight of polymer. The low volatility polyol is not lost during storage and serves to maintain the expanded solvation state of the membrane.

The high equilibrium water content of cellulose classifies it as a hydrogel. However, in contrast to hydrogels formed from acrylic polymers, cellulose does not readily adsorb globular proteins. The permeability of hydrogels can be interpreted in terms of hydrodynamically equivalent pore dimensions. On such a basis, cellulose membranes used for hemodialysis have an average pore radius of 1.72 nm (15). Special preparations can be used to produce membranes with pore radii up to 4.92 nm (16). Solutes approaching the size of peptides (500 to 1000 daltons) permeate cellulosic membranes only slowly while larger proteins are totally excluded.

The processes used to prepare cellulosic membranes generally lead to homogenous cross-sectional structures. Cellulose prepared from xanthate derivatives may exhibit a 'cuticle' or skin structure; however, this asymmetry does not produce significant resistance to mass transfer. Most membranes currently used for hemodialysis are prepared via the cuprammonium process. These membranes do not form a skinned structure during coagulation/regeneration.

Cellulose Acetate. Cellulose acetate membranes used for hemodialysis or hemofiltration are generally prepared in hollow fiber form. A mixture of polymer and plasticizer is extruded at an elevated temperature, and the phase separated structure is established by cooling in a gas stream. Extrusion is followed by leaching of the plasticizer from the resulting porous structure. Cellulose acetate membranes can also be prepared by solution/coagulation processes but at much lower rates than by melt extrusion. Cellulose acetate (DS=2.5) contains approximately 16 percent water by weight of polymer when equilibrated with water. It presents a more hydrophobic surface than the parent cellulose and is not classified as a hydrogel. Proteins are more readily adsorbed than on the parent polymer. Comprehensive morphological data have not been published, but cellulose acetate hemodialysis

fibers are not thought to be asymmetric in structure. The average pore size is controllable to some extent by varying the percentage of nonsolvent or plasticizer in the extrusion formulation. Data on one cellulose acetate sample prepared by solution casting indicated a relatively large average pore radius with a low pore density (15).

Acrylic Polymers. Polyacrylonitrile (PAN) used for hemodialysis membranes is a copolymer generally containing less than 15 mole percent of an acrylic monomer and greater than 85 mole percent of acrylonitrile, because a polymer prepared solely from acrylonitrile is too intractable for processing. The comonomer may be allylsulfate (17) or methyl acrylate. The membranes are generally cast from solvent solutions (dimethylformamide, dimethylacetamide) into aqueous coagulation baths. After extensive washing to remove residual solvent and heat stabilization, the membranes are dried from a wash containing glycerol. The polyol serves to prevent collapse of the porous structure during storage. Polyacrylonitrile has a small equilibrium water content in the presence of aqueous solutions, depending on the comonomer type and concentration. It is not a hydrogel. Pore diameters of 2.52 nm have been reported in a widely available hemodialysis sheet membrane (15). Albumin and other globular proteins are readily adsorbed to the surfaces of PAN, causing alteration in effective pore diameter when the membranes are used in hemodialysis and hemofiltration.

Blends of isotactic and atactic polymethylmethacrylate (PMMA) in solution have been used to form semipermeable membranes, for both hemodialysis and hemofiltration. Details of the polymer properties are not available (18).

Polyethylene-co-vinylalcohol/polyethylene-co-vinylacetate (PVA) polymers have been fabricated into membranes for both hemodialysis and microfiltration. The fabrication procedure and physical properties of the finished membrane material have not been published. Both the PMMA and PVA membranes have been developed in Japan, where most of the application studies have been performed.

Polysulfone. Polysulfone homo- (19) and copolymers have been formed into hollow fiber membranes for hemofiltration by solution extrusion, followed by coagulation and washing. Equilibrium water absorption by these membranes varies between 0.85 and 2.1 percent. The water-equilibrated polymers are glassy at room temperature. Sieving properties of copolymer hemofilters prepared with a 2-phenyl-2-phenoxy propane segment have been characterized (9). The hydrophobicity of this polymer is reflected in a significantly altered rejection spectrum in the presence of protein when compared to saline solutions.

Polysulfone hollow fibers are usually asymmetric in cross-section, with either an internal skin (for use in blood filtration) or an external skin (for use in gas separation). The ability to form asymmetric structures with divergent permeabilities attributable to the skin and supporting structures makes glassy polymers, such as the polysulfones, attractive for use in the development of separation devices. In contrast to membranes having a uniform cross-section, these asymmetric structures permit much higher filtration rates with equivalent sieving spectra.

Polycarbonate.   Polycarbonate membranes are solvent cast from a
polymer prepared by the condensation of bisphenol A and a diol in
the   presence of phosgene (20). The mass transfer properties of
these membranes are competitive with cellulosic membranes of the
same thickness (15).   Polycarbonate membranes may have some
advantages in terms of biocompatibility, but insufficient clinical
trials have been reported to confirm this. Polycarbonate membranes
are easily degraded by alkaline solution, and although this does
not present a problem with hemodialysis per se, it does have an
impact on possible cleaning methods for hemodialyzer re-use.
Although polycarbonate can be heat-sealed to facilitate fabrication
of filter devices, the glycerin content required to maintain pore
integrity is high and interferes with some sealing procedures.

Polyolefins. Low density polyethylene and polypropylene have been
developed   as   sheet and hollow fiber microporous membranes,
respectively, for use in plasmapheresis.   Polyethylene is made
porous by stretching the annealed film (21), while polypropylene is
made   porous by coextruding hollow fibers with a leachable
plasticizer.   Neither membrane has been prepared with small pore
dimensions suitable for protein rejection.   These polyolefin
membranes are characterized by good chemical stability, but require
special surfactant treatments to make them wettable. Their low
deformation temperature precludes the use of steam sterilization.
Because they are extruded without the usual anti-oxidants and
stabilizers, their stability is lower than injection molding
formulations of the same polymer.

Membrane Performance

Mass Transfer Properties.   The particle size distribution of
interest in medical devices is extremely wide, ranging from urea
and electrolytes (<1 nm diameter) in hemodialysis to platelets and
red cells (3 to 8 μm diameter) in plasmapheresis. Between these
extremes, molecular size ranges can be defined that roughly
delineate filters suitable for hemodialysis and hemofiltration
(that is, impermeable to albumin), protein separation (that is,
albumin permeable, IgM impermeable) and microfiltration (that is,
retentive to platelets and red cells). The lower end of these size
distributions is indicated in Figure 1.
     As outlined earlier, hemodialysis and hemofiltration require
the removal of solutes smaller than albumin from blood. Solute
mass transfer rates across hemodialysis membranes cannot exceed the
diffusivity of the solute in water. Solute diffusivity decreases
with increasing molecular diameter (Stokes-Einstein relationship);
consequently, solute mass transfer rates for hemodialyzers
intrinsically decrease with increasing molecular size. In addition
to limitations imposed by diffusion in solution, mass transfer is
further limited by diffusion resistance in the membrane as well as
boundary layer effects resulting from laminar flow; both of these
effects are also functions of molecular size. The quantitation of
mass transfer in hemodialyzers has been reviewed extensively (22).

Hemofilters, which utilize convective transport, are not limited by diffusivity of the solute, but depend on solute rejection by the membrane. The rates of transfer of partially rejected solutes and of the solvent are also affected by boundary layer considerations in hemofilters (23). In Figure 1, the relative mass transfer rates of dialytic and convective devices are shown in comparison to the normal kidney. The decrease of dialyzer mass transfer rates at relatively low molecular sizes is a consequence of both the types of membrane available and the diffusive process, per se. Hemofilters can mimic glomerular sieving properties effectively, although they do not possess any of the instrinsic reabsorptive capacity of the tubules.

Mass transfer resistance in a dialyzer is the sum of three contributions: diffusion resistance on the blood and dialysate sides, respectively, and resistance within the membrane. Proper fluid channel design minimizes resistance external to the membrane to the extent possible within blood shear rate limitations; therefore, relative dialyzer performance becomes a function of membrane permeability. Solute permeability through the membrane decreases more rapidly with increasing molecular size than does solute diffusivity in solution. This is shown in Figure 2, where the ratio of membrane diffusivity to solution diffusivity is plotted against molecular weight for several dialysis membranes. For dialysis membranes of equal thickness, it has been universally observed that lower resistance to solute diffusion is accompanied by an increase in hydraulic permeability. This relationship does not extend to hemofiltration membranes; convective transfer is independent of solute diffusivity. Moreover, hemofiltration membranes are generally cast asymmetrically so that volume flux resistance and sieving are not always coupled in the same direction. There is no general relationship between the sieving spectrum of a hemofilter and its hydraulic permeability. Pore density and pore size distribution govern both the hydraulic permeability and solute sieving of hemofilters. These variables are functions of the membrane fabrication process rather than some intrinsic polymer property. For example, polysulfone hollow fibers are made both for hemofiltration (19) and as microporous supports for other membranes (25).

Adsorption of proteins in the pore structure of hydrophobic hemofiltration membranes alters their hydraulic permeability and their solute rejection spectrum. This is demonstrated in Figure 3 for filters containing either cellulose or polysulfone membranes. While there is no alteration in the rejection spectrum of the cellulosic filter following exposure to proteins, a marked 'tightening' of the pore distribution of the polysulfone membrane is evidenced by a change in the rejection spectrum. It should be noted that the interactions of plasma proteins with artificial surfaces are extremely complex and incompletely understood. The nature of protein deposition will be a function of many surface properties, including hydrophobicity and surface charge and will be further influenced by interactions between proteins of the coagulation, complement and kinin systems. Some of these factors are considered in the following sections and additional information can be obtained from some recent reviews (26,27).

Figure 2: Ratio of membrane to solution diffusivity as a function of solute molecular weight for: cellulose 150-PM (o), cellulose HDF-250 ($\triangle$), polycarbonate (x), and polyacrylonitrile ($\bullet$). See reference 24 for methodology.

Figure 3: Rejection spectra of cellulosic (A) and polysulphone (B) membranes in saline (o) and plasma (●). See reference 9 for methodology. Reproduced with permission from Ref. 9. Copyright 1984 International Society for Artificial Organs.

Interfacial effects are important not only in regard to protein exposure but also in determining the degree of utilization of the filter's pore size distribution. Polypropylene plasmapheresis membranes have a wide pore size distribution, with a maximum diameter of approximately 0.6 μm. The minimum diameter through which flow will occur is a function of transmembrane pressure and interfacial tension. The relationship between interfacial tension and the pressure required to permit flow of a wetting fluid through a pore of diameter, d, is given by the Young and Laplace equation (28):

$$\Delta P = \frac{4\gamma}{d}$$
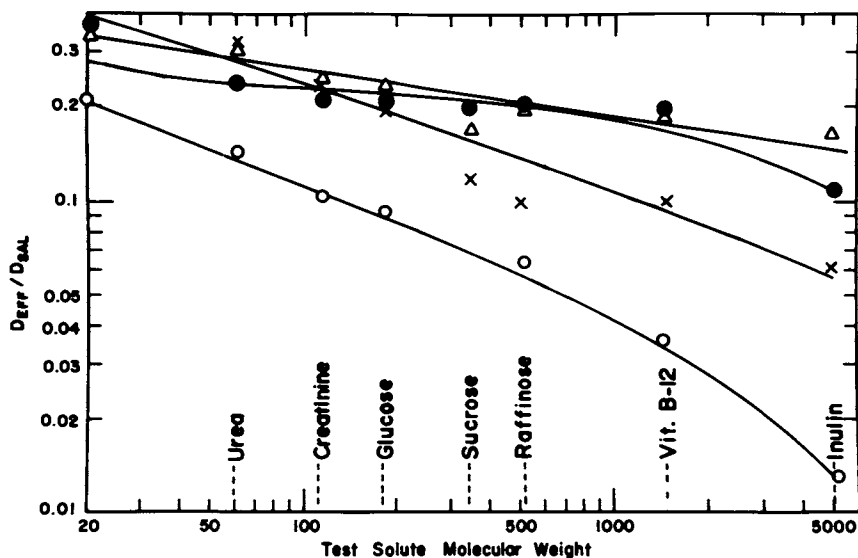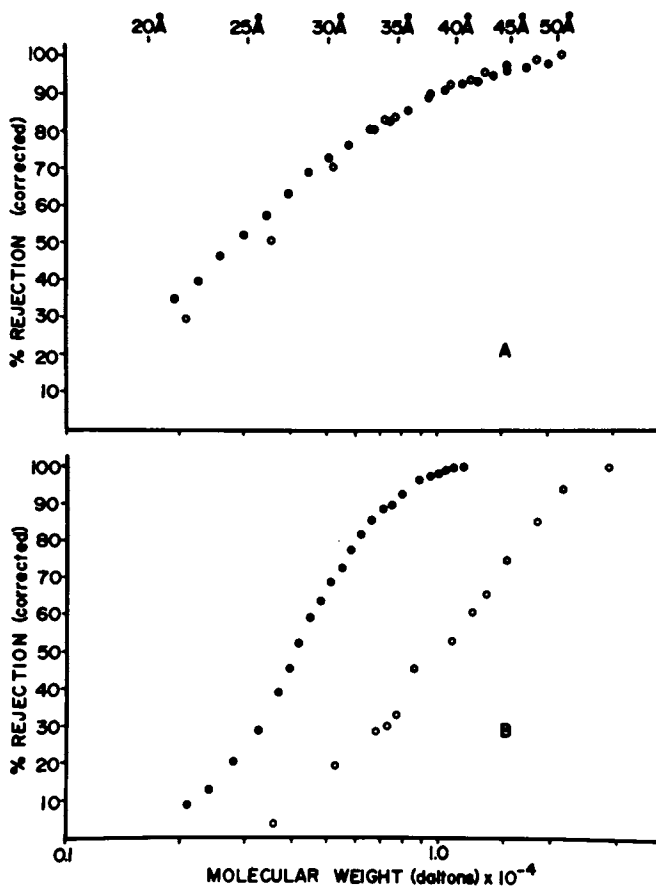
where ΔP is the pressure difference across the pore and γ is the gas-liquid surface tension of the wetting fluid. Surfactants are used to lower the surface tension between polyolefins and aqueous solutions so that applied pressures in clinical use can be less than 0.1 atm.

Biocompatibility - Thrombogenicity. Blood coagulation (thrombo-plastic activity) can be initiated in two ways, as shown in Figure 4. One mechanism, the extrinsic pathway, begins with the release of a lipoprotein, termed the tissue factor, from damaged tissue. In combination with an activated glycoprotein, Factor VIIa, the tissue factor initiates a series of reactions in which circulating proteins of little or no indigenous coagulant activity are converted to an active form. This series of reactions leads to the conversion of prothrombin to thrombin. The production of thrombin may also result from activation of the intrinsic pathway initiated by the interaction of a serine protease zymogen, Factor XII, with a negatively charged surface (27). The surface-bound Factor XII then undergoes proteolytic cleavage, leading to triggering of the intrinsic coagulation pathway. A platelet dependent mechanism for activation of Factor XII has also been identified. Ionized calcium is required for all but the initiating reactions, and most reactions probably also require the presence of phospholipid material. Thrombin is a proteolytic enzyme that converts fibrinogen, a 341000 dalton protein, into fibrin, a polymerizable protein oligomer. The polymerized fibrin strands serve as a framework upon which both platelet (white) and red cell (red) thrombi are formed. The coagulation mechanism is extremely complex; interactions occur between the intrinsic and extrinsic pathways, and feedback reactions serve to accelerate coagulation. In addition, a series of inhibitors to the various reactions counterbalance the procoagulants. These inhibitors are present in greater concentration and are slower acting than the procoagulants. The extrinsic pathway is activated by tissue injury and is not of major concern in the clinical use of membrane devices. The intrinsic pathway, however, is initiated by a multitude of factors, including interactions between serum proteins and exogenous materials. Hydrodynamic forces acting on platelets may also lead to the release of platelet factors that trigger the intrinsic pathway. Thus, the selection of membrane materials to minimize thrombogenesis cannot be fully separated from the design of devices to contain them because of this potential for shear forces to activate the clotting cascade.

The result of thromboplastic activity is clot formation. Functionally, clots deposit in regions of lowest shear and at narrow orifices, such as in the headers of hollow fiber devices, leading to loss of active transport area, increased resistance to flow, and blood loss by the patient. To avoid clotting, patients are given anticoagulant. The most commonly used anticoagulant is heparin (31), a complex mixture of glycosaminoglycans which interacts wth antithrombin III, an inhibitor of thrombin and Factor X activity, to accelerate its action. Recently, prostacyclin, a potent inhibitor of platelet function, has been used experimentally as an alternative to heparin in hemodialysis (32). Anticoagulation has also been achieved in plasmapheresis and, experimentally, in hemodialysis (33) by administration of citrate ions to complex free calcium, an important co-factor in the clotting cascade. All membrane devices, even those fabricated from the least thrombogenic materials known, require the use of anticoagulants. Further, even high doses of anticoagulants do not prevent clot formation with highly thrombogenic materials such as nylon.

The mechanisms through which interaction between plasma and a foreign surface lead to the initiation of clotting are not well defiзed. However, it is believed that the initiating process is adsorption of plasma proteins by the surface, leading to their morphological rearrangement. Because these structural changes require a source of energy, it is probable that they are proportional to the strength of the interacting forces between protein and surface. Thus, the presence of crystallites at the membrane surface, the availability of highly charged surface ions and multiple hydrophobic bonding sites all have been identified with thrombogenic surfaces (34). Hydrogels and elastomers well above their glass transition temperatures have been shown to be low in thromboplastic activity, while semicrystalline silica (used as filler in silicone rubbers) is thrombogenic (35). Attempts have been made to increase the thromboresistance of membrane materials by modifying their surface properties. Grafting of hydrogels (36), ionic binding of heparin (37) and slow release of adsorbed heparin complexes (38) have been studied. Most of these procedures have altered membrane transport properties and, therefore, have not found their way into general use.

Biocompatibility - Complement Activation. In a manner analogous to the clotting process, blood contains a series of proteins, the complement system, which responds to immunologic stimulae. Complement activation proceeds through two routes: 1) classical pathway activation results from the binding of C1 to IgG or IgM that has combined with an antigen, and 2) alternative pathway activation is produced by substances which adsorb C3b, such as endotoxin (Figure 5). These pathways converge at the point of activation of C3. Subsequently, a common pathway is followed, leading to formation of the membrane attack complex and cell lysis.

With regard to synthetic membrane surfaces, complement activation operates solely through the alternative pathway (40). The biological role of the alternative pathway is to act as a defense mechanism against endotoxin introduced into the circulation. Endotoxin is a lipopolysaccharide material and has
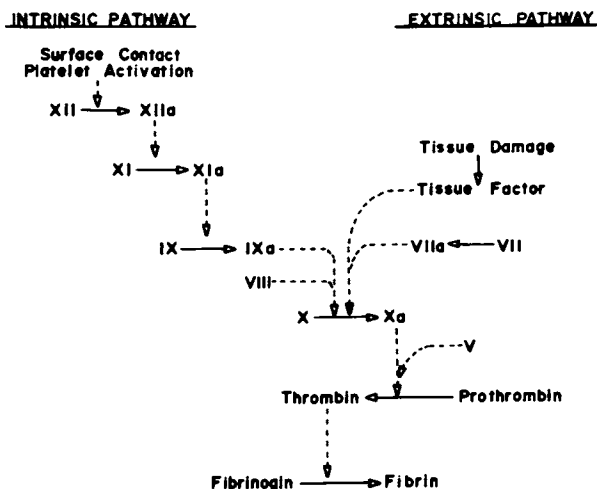
Figure 4: Simplified schematic representation of the blood coagulation system leading to the formation of fibrin. Further details are given in the text; for comprehensive reviews see references 29 and 30.
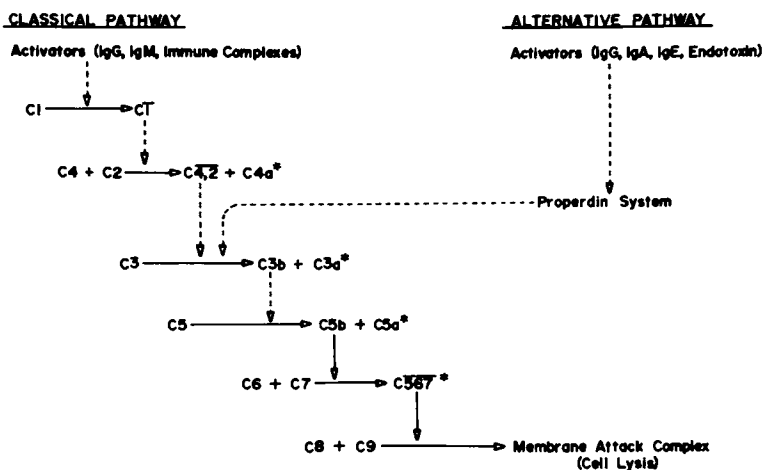
Figure 5: Simplified schematic representation of the complement system leading to the formation of the membrane attack complex. Components with vasoactive or chemotactic properties are indicated by *. For more details see reference 39.

many nucleophilic groups on its surface to which C3b may bind (41). Cellulose is a semicrystalline carbohydrate and, as such, expresses surface groups similar to those of endotoxin. This similarity may explain the significant differences in complement activation observed between cellulose and other membrane materials, such as polycarbonate, which express few nucleophilic groups on their surfaces (42).

One of the complement components, C3, continuously undergoes spontaneous hydrolysis to form two fragments, C3a and C3b; the latter is able to bind to the surface of a membrane. If the membrane surface is non-activating, negative regulatory proteins bind to C3b and convert it to an inactive form. However, if the surface is activating, positive regulatory proteins bind to C3b facilitating the deposition of additional C3b and concurrent rapid formation of C3a. Through a series of incomplete proteolytic reactions, the immobilized C3b cleaves C5, releasing a fragment, C5a, into the circulation. C5a is rapidly taken up by circulating neutrophils, causing their sequestration in the pulmonary vasculature and peripheral leukopenia (43). These phenomena, as shown in Figure 6, are transitory, suggesting that C3b binding sites on the membrane become saturated as exposure continues.

In addition to causing their pulmonary sequestration, C5a can induce release of oxygen radicals from neutrophils (45). Further, both C3a and C5a stimulate mast cells to release histamine. These substances can cause injury to the pulmonary endothelium, increased vascular permeability and smooth muscle contraction. Such processes have been associated with the severe anaphylactoid reactions reported to occur on rare occasions with the clinical use of membrane devices (46). A connection between complement activation and such reactions has been suggested but not proven. In addition, the sequelae of complement activation may produce the hypoxemia observed during hemodialysis (47) and the pulmonary hypertension described in an animal model of extracorporeal circulation (48).

Biocompatibility - Toxicity. Although none of the membrane materials currently in use (vide supra) is intrinsically toxic, manufacture of devices containing these membranes requires the use of a variety of solvents, lubricants, sterilants and plasticizers. Such chemicals may be toxic at high concentrations; however, their exact composition is often unknown, and frequently their toxicity has not been determined. Normal practice in determining toxicity is to quantify dose-response data on pure chemical agents, either in vitro or in an animal model (49). Because of the uncertainty of the composition and biological availability of these leachable membrane additives, the assessment of membrane toxicity must be made under conditions as close to its end use as possible. The nature of current toxicity tests does not preclude the possibility of finding unanticipated long-term toxic effects from chronic exposure, particularly when these are manifest in an indirect manner. For example, residual levels of ethylene oxide from sterilization, while not toxic per se, can induce the formation of antibodies which on subsequent exposure may lead to hypersensitivity reactions (50).
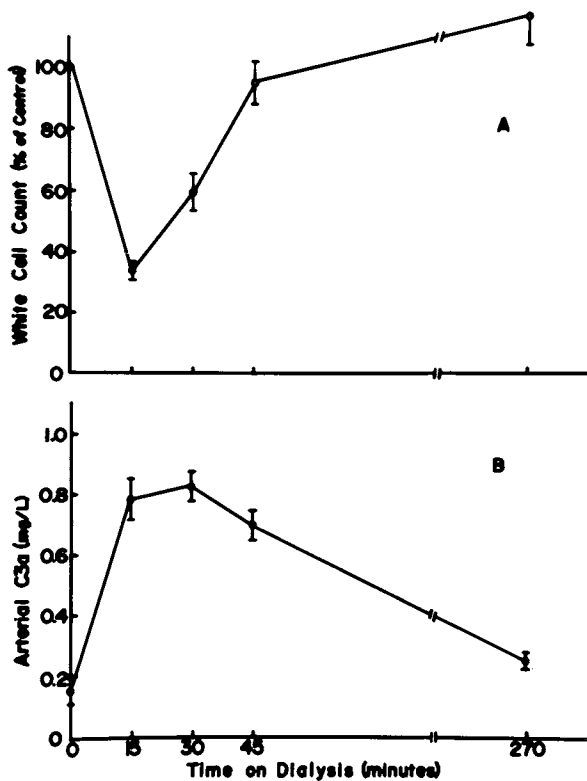
Figure 6: Total white cell count (A) and arterial C3a concentration (B) as a function of time on dialysis for a dialyzer containing cellulose membranes. Data are shown as mean ± SEM, n=14. See reference 44 for methodology.

Contaminants in cellulosic membranes include residual salts such as copper, oligomers of cellulose, glycerin and other humectants, and organic spinning aids. Salt concentrations are reduced to acceptable levels by extensive water washing, which may or may not reduce residual oligomer content. The glycols and organics that are added at extrusion or immediately afterward are generally selected to exhibit minimal toxicity so that residues will not pose problems. For example, isopropylmyristate, a pharmaceutical agent, is used as a spinning aid to maintain dimensions when cuprammonium cellulose hollow fibers are extruded. However, when cellulose fibers are prepared by hydrolysis of cellulose acetate, the plasticizer used, as well as the hydrolytic agent, must be removed by washing.

For solvent cast membranes, such as polysulfone, polycarbonate, polyacrylonitrile and polyethylene-co-vinylacetate, the major contaminants are oligomers and solvents. These are removed by extensive washing, generally to a level below 10 μg/ml. Many solvent cast membranes require the presence of a wetting agent to maintain pore integrity; glycerin is generally used for this purpose with polysulfone, polyacrylonitrile and polycarbonate membranes. Such additives must be removed at the point of use and, thus, should undergo the sterilization process without alteration.

Sterilization. Sterility is a necessary requirement for all membrane devices used clinically, and the sterilization procedure must not change the functional or biocompatible character of the device. Sterility, the condition of absolute absence of viable life forms, can be achieved by physical (heat, irradiation) or chemical means. Chemicals used to sterilize membrane devices may be either gaseous (ethylene oxide) or liquid (formaldehyde, peroxides, hypochlorite) in nature. The generally accepted conditions for achieving sterile devices are shown in Table II.

Table II: Sterilization Methods for Membrane Devices

Methods	Sterilization Conditions	Comments
Dry heat	140°–170° C for 180 – 60 minutes, respectively	Not suitable for thermoplastic membranes
Steam	15-30 psi for 3-15 minutes	Not suitable for thermoplastic membranes
Ionizing radiation	2.5 Mrad	Suitable for selected materials
Ethylene oxide	R.H. 40%, 55° C	Requires extensive degassing

Ethylene oxide (ETO) is the predominantly used sterilant in the United States for membrane devices destined for medical use. Conditions for its use have been well established to assure sterility (51), although some problems arise from the slow diffusion of the gas from thick sections of thermoplastics, such as the headers in hollow fiber devices. The majority of hemodialyzers are prepared with cellulosic membranes, which are partially

degraded by ionizing radiation. In Table III the clearances and ultrafiltration rates of two groups of identical dialyzers are shown, one sterilized by ethylene oxide and the other by gamma irradiation. While small solute mass transfer is unaffected, the data demonstrates that membrane degradation by gamma irradiation does reduce the hydraulic permeability of the membrane.

TABLE III: Mass Transfer and Hydraulic Permeability Data[†] for a Hemodialyzer Following Sterilization with Ethylene Oxide and Gamma Irradiation

	Sterilant	
	Ethylene Oxide (n=27)	Gamma Irradiation (n=14)
Mass Transfer Coefficient (hoA) ml/min		
Urea	283 ± 5	289 ± 6
Creatinine	183 ± 3	196 ± 6
Hydraulic Permeability (L$_p$A) ml/hr/mm Hg	2.20 ± 0.11	1.57 ± 0.04*

† Data obtained according to the methods outlined in reference (22).
* Significantly different from ethylene oxide sterilized, $p < 0.001$.

    Initially, formaldehyde was a common sterilant for devices containing cellulosic membranes, both on original manufacture and prior to reuse, as its use avoided drying the membranes. Once a cellulose membrane has been wet with water its hysteresis shrinkage property does not permit it to be dried without significant changes in transport properties (vide supra). However, when final washing to remove a sterilant is relegated to the clinical situation, a danger of incomplete wash-out exists. Manufacturers no longer use formaldehyde, having learned how to ship dry devices that were sterilized either by ethylene oxide or irradiation. Some new developments using peroxides for sterilization prior to re-use of devices have been announced recently, but long term results are not yet available.

    Steam sterilization of medical devices is used in Japan. It has the advantage of facilitating removal of water soluble residues left after membrane manufacturing, but requires that the device be shipped filled with water. Steam sterilization appears to alter the pore structure of hydrophobic membranes, despite the fact that their glass transition temperatures may be quite high, for example, the permeability of polysulfone membranes is altered above $70°C$.

Literature Cited

1. "Replacement of Renal Function by Dialysis"; Drukker, W.; Parsons, R.M.; Maher, J.F., Eds; Martinus Nijhoff: The Hague, 1978.
2. "End-Stage Renal Disease Program Medical Information System Facility Survey Tables"; Rept. No. HCFA 82-09000; U.S. Department of Health and Human Services, 1983.

3. Lauer, A.; Saccaggi, A.; Ronco, C.; Belledonne, M.; Glabman, S.; Bosch, J. <u>Ann. Intern. Med.</u> 1983, 99, 455-60.
4. "Hemofiltration"; Schaefer, K.; Koch, K.M.; Quellhorst, E.; von Herrath, D.; Eds.; CONTRIBUTIONS TO NEPHROLOGY Vol. 32, S. Karger: Basel, 1982.
5. "Plasmapheresis: Therapeutic Applications and New Techniques"; Nose, Y.; Malchesky, P.S.; Smith, J.W.; Krakauer, R.S., Eds.; Raven Press: New York, 1983.
6. "Physiological and Clinical Aspects of Oxygenator Design"; Dawids, S.G.; Engell, H.C., Eds; Elsevier: New York, 1976.
7. Urquhart, J. <u>Drugs</u> 1982, 23, 207-26.
8. Brenner, B.M.; Bohrer, M.P.; Baylis, C.; Deen, W.M. <u>Kidney Int.</u> 1977, 12, 229-37.
9. Feldhoff, P.; Klein, E.; Turnham, T. <u>Artif. Organs</u> 1984, 8, 186-92.
10. Klein, E.; Holland, F.F.; Donnaud, A.; Lebeouf, A.; Eberle, K. <u>J. Memb. Sci.</u> 1977, 2, 349-64.
11. Malm, C.J.; Hiatt, G.D. In "Cellulose"; Ott, E.; Spurlin, H.; Grafflin, M.; Eds.; Interscience: New York, 1954; pp. 763-809.
12. Cross, C.F.; Bevan, E.J.; Beadle, C. <u>Berichter der Deutchen Chem. Ges.</u> 1893, 26, 1090.
13. Browning, B.L.; Sell, L.O.; Abel, W. <u>TAPPI</u> 1954, 37, 273-83.
14. Yasuda, H.; Lamaze, C.E.; Ikenberry, L.D. <u>Makromol. Chem.</u> 1968, 118, 19-35.
15. Klein, E.; Holland, F.F.; Eberle, K. <u>J. Memb. Sci.</u> 1979, 5, 173-88.
16. Klein, E.; Holland, F.F.; Eberle, K. <u>Proc. Europ. Dial. Transpl. Assoc.</u> 1979, 16, 198-204.
17. Klein, E.; Smith, J.K.; Holland, F.F. "Rhone Poulenc Polyacrylonitrile Membrane - Laboratory Evaluation of Permeability, Physical and Mechanical Properties."; Rept. No. PB 225066/OSET; National Technical Information Service: Springfield, VA, 1977.
18. Kumitomo, T.; Lowrie, E.G.; Kumazawa, S.; O'Brien, M.; Lazarus, J.M.; Gottlieb, M.N.; Merrill, J.P. <u>Trans. Amer. Soc. Artif. Int. Organs</u> 1977, 23, 234-42.
19. Henderson, L.W.; Ford, C.; Colton, C.K. <u>Trans. Amer. Soc. Artif. Int. Organs</u> 1970, 16, 107-12.
20. Cantor, P.; Fisher, B.S. "Polycarbonate Membranes"; Rept. No. PB 213150A; National Technical Information Service: Springfield, VA, 1972.
21. Sarada, T.; Sawyer, L.C.; Ostler, M.I. <u>J. Memb. Sci.</u> 1983, 15, 97-113.
22. "Evaluation of Hemodialyzers and Dialysis Membranes"; Klein, E., Ed.; Publication No. (NIH) 77-1299; U.S. Department of Health, Education and Welfare, 1977.
23. Jaffrin, M.Y.; Butuille, Y.; Granger, A.; Vantard, G. <u>Trans. Amer. Soc. Artif. Int. Organs</u> 1978, 24, 448-53.
24. Klein, E.; Holland, F.; Lebeouf, A.; Donnaud, A.; Smith, J.K. <u>J. Memb. Sci.</u> 1976, 1, 371-96.
25. Klein, E.; Smith, J.K.; Morton, F.C. U.S. Patent 4 051 300, 1977.
26. Sundsmo, J.S.; Fair, D.S. <u>Clin. Physiol. Biochem.</u> 1983, 1, 225-84.

27. Colman, R.W. <u>J. Clin. Invest.</u> 1984, 73, 1249-53.
28. Adamson, A.W. "Physical Chemistry of Surfaces"; Wiley: New York, 3rd Ed., 1976; Chap. 1.
29. "Haemostasis: Biochemistry, Physiology, and Pathology"; Ogston, D.; Bennett, B., Eds; Wiley: London, 1977.
30. "Haemostasis and Thrombosis"; Bloom, A.L.; Thomas, D.P., Eds; Churchill Livingstone: Edinburgh, 1981.
31. Farrell, P.C.; Ward, R.A.; Schindhelm, K.; Gotch, F.A. <u>J. Lab. Clin. Med.</u> 1978, 92, 164-76.
32. Zusman, R.M.; Rubin, R.H.; Cato, A.E.; Cocchetto, D.M.; Crow, J.W.; Tolkoff-Rubin, N. <u>N. Engl. J. Med.</u> 1981, 304, 934-9.
33. Pinnick, R.V.; Wiegmann, T.B.; Diederich, D.A. <u>N. Engl. J. Med.</u> 1983, 308, 258-61.
34. Barenberg, S.A.; Anderson, J.M.; Mauritz, K.A. <u>J. Biomed. Mater. Res.</u> 1981, 15, 231-45.
35. Mason, R.G. <u>Biomat. Med. Dev. Artif. Organs</u> 1973, 1, 131-9.
36. Ratner, B.D.; Hoffman, A.S. In "Hydrogels for Medical and Related Applications"; Andrade, J.D., Ed.; ACS SYMPOSIUM SERIES NO. 31, American Chemical Society: Washington, D.C., 1976; pp. 1-36.
37. Grode, G.A.; Falb, R.D.; Crowley, J.P. <u>J. Biomed. Mater. Res. Symposium</u> 1972, No. 3, 77-84.
38. Holland, F.F.; Gidden, H.E.; Mason, R.G.; Klein, E. <u>asaio J.</u> 1978, 1, 24-36.
39. Cooper, N.R. In "Basic and Clinical Immunology"; Stites, D.P.; Stobo, J.D.; Fudenberg, H.H.; Wells, J.V., Eds.; Lange Medical: Los Altos, CA, 1982; pp. 124-35.
40. Craddock, P.R.; Fehr, J.; Dalmasso, A.P.; Brigham, K.L.; Jacob, H.S. <u>J. Clin. Invest.</u> 1977, 59, 879-88.
41. Law, S.K.; Lichtenberg, N.A.; Levine, R.P. <u>J. Immunol.</u> 1979, 123, 1388-94.
42. Aljama, P.; Bird, P.A.E.; Ward, M.K.; Feest, T.G.; Walker, W.; Tanboga, H.; Sussman, M.; Kerr, D.N.S. <u>Proc. Europ. Dial. Transpl. Assoc.</u> 1978, 15, 144-51.
43. Craddock, P.R.; Hammerschmidt, D.; White, J.G.; Dalmasso, A.P.; Jacob, H.S. <u>J. Clin. Invest.</u> 1977, 60, 260-4.
44. Ward, R.A.; Feldhoff, P.W.; Klein, E. <u>Artif. Organs</u> In Press
45. Sacks, T.; Moldow, C.F.; Craddock, P.R.; Bowers, T.K.; Jacob, H.S. <u>J. Clin. Invest.</u> 1978, 61, 1161-7.
46. Nicholls, A.J.; Platts, M.M. <u>Brit. Med. J.</u> 1982, 285, 1607-9.
47. De Backer, W.A.; Verpooten, G.A.; Borgonjon, D.J.; Vermeire, P.A.; Lins, R.P.; De Broe, M.E. <u>Kidney Int.</u> 1983, 23, 738-43.
48. Walker, J.F.; Lindsay, R.M.; Peters, S.D.; Sibbald, W.J.; Linton, A.L. <u>asaio J.</u> 1983, 6, 123-30.
49. "Guidelines for Blood-Material Interactions"; Mason, R.G., Ed.; Publication No. (NIH) 80-2185; U.S. Department of Health and Human Services, 1980.
50. Poothullil, J.; Shimizu, A.; Day, R.P.; Dolovich, J. <u>Ann. Intern. Med.</u> 1975, 82, 58-60.
51. "Guideline for Industrial Ethylene Oxide Sterilization of Medical Devices"; Association for the Advancement of Medical Instrumentation: Arlington, VA, 1981.
52. Klein, E.; Holland, F.F.; Eberle, K. <u>Kidney Int.</u> 1980, 18, Suppl. 10, S-20.

Selection of Supports for Immobilized Liquid Membranes

J. DOUGLAS WAY, RICHARD D. NOBLE, and BLAINE R. BATEMAN

Center for Chemical Engineering, National Bureau of Standards, Boulder, CO 80303

Criteria for immobilized liquid membrane (ILM) support selec-
tion can be divided into two categories: structural properties
and chemical properties. Structural properties include
geometry, support thickness, porosity, pore size distribution
and tortuosity. Chemical criteria consist of support surface
properties and reactivity of the polymer support toward fluids
in contact with it. The support thickness and tortuosity
determine the diffusional path length, which should be min-
imized. Porosity determines the volume of the liquid membrane
and therefore the quantity of carrier required. The mean pore
size determines the maximum pressure difference the liquid
membrane can support. The support must be chemically inert
toward all components in the feed phase, membrane phase, and
sweep or receiving phase.

High performance membranes can be made by immobilizing a liquid phase
containing a complexation agent (carrier) in a thin porous support.
By judicious choice of the membrane liquid, complexation agent and
support, immobilized liquid membranes (ILM) can have both high selec-
tivity and high permeant fluxes. Liquid membranes have the additional
advantage that diffusion coefficients in liquids are several orders
of magnitude larger than in polymeric membranes. Previously reported
ILM research in the literature includes purification and recovery
processes in both gas and liquid phases (1).   This variety of appli-
cations creates different requirements for supports for ILMs. This
paper discusses criteria which influence selection of ILM support
materials.

Background

Immobilized liquid membranes have traditionally been prepared using
commercially available materials such as ultrafiltration or reverse

osmosis membranes as supporting substrates. The pore structure of
the support is impregnated with the liquid containing the complexa-
tion agent. Little consideration has been given to the special
characteristics of these supports, primarily due to the lack of a
large market at present.

Many researchers have reported using filter paper as the support
during experimental investigations of both liquid and gas transport.
Cussler (2) studied ion transport using liquid films by supporting
the solvent and carrier in filter paper. The supported membrane was
mounted in a diaphragm cell. Cussler noted that the membranes fre-
quently leaked during extended experiments and that placing cellophane
on each surface of the filter paper reduced the leakage problem but
drastically reduced the flux. This latter effect was presumably due
to increased diffusional resistance of the membrane when the cello-
phane films were added. Reusch and Cussler (3) also used filter
paper as a support for studying the selectivity of cyclic polyethers
toward alkali metal cations in chloroform solutions. Louie (4)
studied CO transport through acetonitrile and benzonitrile solutions
containing an iron porphyrin carrier immobilized in filter paper.
Without humidification, the liquid would volatilize over time causing
the membrane to "dry out" and preventing the separation.

Some researchers have also used nitrocellulose filters as liquid
membrane supports. Mochizuki and Forster (5) used this material as a
support for hemoglobin solutions to study the facilitated transport
of O_2 and CO. Enns (6) used the same support for studying the facili-
tated transport of CO_2 using aqueous solutions of carbonic anhydrase.
Donaldson and Quinn (7) utilized both nitrocellulose filters and
cross-linked protein membranes as supports to investigate CO_2
facilitated transport using enzymatically active liquid membranes.

Porous cellulose acetate films have been used as liquid membrane
supports. Ward and Robb (8) used this material to support an aqueous
bicarbonate-carbonate solution for CO_2-O_2 separation. The researchers
noted that immobilizing the carbonate solution reduced the total flux
by a factor of 1.7 compared to a pure liquid film. Suchdeo and
Schultz (9) used a highly porous (85% porosity) cellulose acetate
membrane to support a liquid bicarbonate film in the investigation of
CO_2 facilitated transport. Hughes, Mahoney, and Steigelman (10)
reported the use of cellulose acetate hollow fiber membranes as
liquid membrane supports. This is the only reported pilot plant
scale application of supported liquid membranes to gas separation.
These membranes were commercially available for reverse osmosis
applications in water treatment. The membrane was used to support
Ag+ solutions for facilitated transport of olefins and operated up to
110 days. The investigators concluded that the asymmetric thin skin
was the controlling resistance limiting the mass transfer.

Baker et al. (11) used a microporous polypropylene film to sup-
port an organic solution containing a β-hydroxyoxime carrier for
coupled transport of copper from an aqueous solution. The liquid
membrane separated the copper feed solution from an acid strip solu-
tion. The flux of copper was coupled to the flux of hydrogen ions in
the opposite direction through an interfacial ion-exchange reaction.
Babcock et al. (12, 13) studied uranium transport across a tertiary
amine solution using microporous polypropylene as the support for the
amine solution. Bateman et al. (14) have reported on the facilitated
transport of nitric oxide using an organic solution of Fe(II) ion

supported in microporous polypropylene and track-etched polycarbonate films. They observed that humidification of the gas streams would be required if volatile solvents were used.

Matson, Herrick, and Ward (15) immobilized a 30 wt.% K_2CO_3 solution in a microporous cellulose acetate and polyether sulfone polymer membranes 25 to 75 μm in thickness and having 60 to 70% porosity. They reported that the surface tension forces held the liquid in the pores of the support even when a pressure difference of $2.07 \cdot 10^6$ N/m^2 was applied across the membrane. The membrane was used at a temperature from 363 to 403 K. To prevent evaporative loss of the liquid from the membrane, the relative humidity of the gases adjacent to the membrane was controlled in the range of 60 to 90%. Kimura, Matson, and Ward (16) discussed the immobilization of bicarbonate solutions for CO_2 and H_2S facilitated transport. They indicated that a major problem was maintaining the integrity of the supported liquid membrane when large pressure differences were imposed across the membrane.

Smith and Quinn (17) supported cuprous chloride solutions in a relatively inert, porous polyvinyl chloride filter which was 190 μm thick. They were studying CO facilitated transport.

Polymer membranes have also been used as a "sandwich". In this configuration, the liquid film is supported between two polymer membranes. Ward (18) used two silicone rubber membranes to contain a solution of ferrous ions in formamide. Ward noted that Bernard convection cells could be maintained if the complex were formed at the upper surface. Ward (19) used this same system and membrane configuration to study electrically-induced, facilitated gas transport. The silicone rubber membranes provided the mechanical support so the electrodes could be placed next to each liquid surface. Otto and Quinn (20) immobilized the liquid film in a horizontal layer between two polymer films. The polymer was described as an experimental silicone copolymer having high CO_2 permeability as well as excellent mechanical properties. They were studying CO_2 facilitated transport in bicarbonate solutions with and without carbonic anhydrase.

A recent approach has been to use ion-exchange membranes as a support for the carrier. This support has the advantage that the carrier cannot easily be forced out or washed out of the membrane since the carrier is retained by strong electrostatic forces. This approach could provide a longer useful operating life. Both anion and cation exchange membranes were used by Leblanc et al. (21) to prepare facilitated transport membranes selective for CO_2 and ethylene. Kajima et al. (22) also used an ion-exchange membrane for copper extraction.

Matson, Lopez, and Quinn (23) have written a recent review article on gas separations using synthetic membranes. They indicate that the membrane support for liquid films is chosen with a combination of thinness, inertness, high porosity, and small pore size in mind. They point out that additional support for the liquid film can be provided by using liquid-impervious barrier films as support backings; both non-wetting microporous films and dense membranes have served this purpose. Another technique to prevent solvent loss involves gelling the liquid membrane within the pores of the support by adding a few weight percent of a suitable polymer such as hydroxy-methyl cellulose or polyvinyl alcohol.

Criteria for ILM Support Selection

Criteria for ILM support selection can be divided into two cate-
gories: chemical properties and structural properties. Chemical
properties consist of support surface properties and the reactivity
of the polymer support toward fluids in contact with it. Structural
characteristics include porosity, pore size distribution, tortuosity,
support thickness and geometry.

Chemical Properties. The stability of an immobilized liquid membrane
is in part determined by the reactivity of the support toward the
species in contact with it. As shown in Figure 1, an ILM for liquid
phase separations has up to four different species in contact with
the support: the feed phase, the liquid membrane phase containing the
complexation agent, and the receiving phase. For example, an ILM for
coupled-transport of metal ions has four different species in contact
with the liquid membrane support: an aqueous feed phase, a
hydrocarbon membrane phase containing the solvent and ion-exchange
reagent, and an acidic receiving phase (11). A facilitated transport
membrane for acetic acid separation (24) would be in contact with
acidic feed phase and basic receiving phase. Consequently, the
support phase must be nonreactive toward all the species in contact
with it and must not be degraded physically or chemically by extended
contact.
      Chaiko and Osseo-Asare (25) studied the long-term structural
changes in microporous polypropylene films used as a support in a
coupled-transport liquid membrane for cobalt separation using scanning
electron microscopy and mercury porosimetry. They observed a decrease
in the pore volume of the polypropylene support after a 55 day contact
with a 0.2 kmol/m^3 solution of dinonylnapthalene sulfonic acid in
dodecane. Fresh, unimpregnated polypropylene films had a narrow pore
size distribution where 90% of the radii were between 0.01 μm and
0.062 μm. The pore size distribution for treated films was the same
at the larger pore sizes and the pore volume decreased sharply corres-
ponding to radii less than 0.003 μm. The authors concluded that
support degradation may occur under liquid membrane extraction condi-
tions due to swelling of the support which reduces the pore volume.
      Largman and Sifniades (26) observed qualitative changes in the
structure of a microporous polytetrafluoroethylene (PFTE) film used
as a support for a kerosene/beta-hydroxyoxime liquid membrane for Cu+
ion extraction. Structural differences were observed between un-
treated PFTE, kerosene impregnated films, and films kept in contact
with the kerosene solution for several days.
      Narebska and Wodski (27) measured swelling equilibria for
ion-exchange membranes as a function of temperature and electrolyte
concentration. They concluded that polyethylene - poly(styrene sul-
fonic acid) and poly(perfluorosulfonic acid) membranes were highly
swollen by aqueous solutions of sulfuric acid and that increasing
both temperature and electrolyte concentration decreased the degree
of swelling. LeBlanc (21) observed that gas transport rates through
carrier impregnated ion-exchange membranes were a function of humidity
and temperature. Consequently, further study of the chemical behavior
of the structure of ion-exchange membranes is necessary to success-
fully predict the performances of facilitated transport in ionomer
films.

For ILM applications, it is desirable for the liquid membrane to wet the support, such that the pore structure of the support would be completely filled with the liquid membrane. In situations where a liquid interacts with a surface and does not wet the surface, the angle a drop makes with the surface is called the contact angle (28). This is shown schematically in Figure 2. Materials should be chosen such that the contact angle between the liquid membrane phase and the support is zero or close to zero. In this case, the liquid is said to wet the solid. When the contact angle is 90 degrees or greater, the liquid is nonwetting. Thus, drops move around on the surface easily and liquid is unlikely to enter pores without application of external force. Zisman (29) observed that the cosine of the contact angle θ is usually proportional to the liquid surface tension. Linear extrapolation of the data in a plot of cosine contact angle versus liquid surface tension to zero contact angle yields a quantity Zisman has called the critical surface tension. He proposed critical surface tension to be a characteristic quantity of a given solid. Two common liquid membrane support materials, polytetrafluoroethylene and polypropylene, have critical surface tensions of 18 mN/m and 35 mN/m, respectively. Manufacturers often supply critical surface tensions for their porous films. Liquids with a surface tension, γ, less than the critical surface tension will probably wet the surface. Therefore, hydrocarbons will wet polypropylene, but water (γ = 72 mN/m) will not. Shafrin and Zisman (30) have summarized critical surface tension data for many materials and correlated the data such that critical surface tensions may be estimated from knowledge of the functional groups in the chemical structure of the surface.

Several methods for measurement of contact angle are summarized by Adamson (28). Neumann and Renzow (31) describe the Wilhelmy slide method which offers significantly higher precision than other techniques.

Structural Properties. Three geometries have been proposed for immobilized liquid membrane permeators: flat-sheet, spiral wound, and hollow fiber. Flat-sheet membranes have been used primarily in laboratory studies of solute transport. Spiral wound modules are prepared by winding a flat-sheet membrane with an interleaving spacer mesh around a distributor tube in a "jelly-roll" fashion. Spiral wound modules have wide commercial applications in polymeric membrane separations such as reverse osmosis due to the high surface area/volume ratio attainable with the geometry. The highest surface area/volume ratios are obtained with hollow fiber membranes. Spiral wound or hollow fiber modules are constructed, then the pore structure of the membrane elements is impregnated with the solvent containing the complexation agent. The use of hollow fiber membrane supports for pilot-scale liquid membrane permeators has been reported by Parkinson (32) and Hughes (10). Parkinson discussed a pilot scale uranium extraction process utilizing polysulfone hollow fibers. Hughes immobilized $AgNO_3$ solutions in cellulose acetate hollow fibers to prepare immobilized liquid membranes for ethylene and propylene transport.

The support thickness contributes to the mechanical strength and diffusional path length of an immobilized liquid membrane. The solute flux decreases monotonically with increasing diffusional path length

which is the product of the support thickness and the tortuosity of
the pores. To maximize the flux, the support thickness should be
minimized while maintaining adequate strength to withstand the trans-
membrane pressure required for a particular application.

The porosity of the support refers to the percentage of the
total volume which is void space. The porosity determines the total
volume of the liquid membrane which can be immobilized in the pore
volume. The volume of liquid membrane solvent and the carrier
solubility determine the maximum amount of carrier which can be
immobilized in the membrane. Increasing the amount of carrier in the
membrane will increase the solute fluxes. The strength of the
functional dependence of the solute flux on carrier concentration
will depend on whether the facilitated transport system is reaction
or diffusion limited. Consequently, a high porosity support is
desirable for liquid membrane applications.

The other support parameter determining the diffusional path
length is the tortuosity, which is a measure of the deviation of the
structure from cylindrical pores normal to the support surface.
Figure 3 is a schematic representation of a tortuous pore in a liquid
membrane support. Lee et al. ($\underline{33}$) define the tortuosity, τ, as the
following:

$$\tau = \frac{\text{mean path length}}{\text{membrane thickness}} \quad >1$$

The authors state that while the above definition is used widely,
other authors have defined tortuosity as $1/\tau$, τ^2, and $1/\tau^2$ as these
forms are frequently encountered in expressions for ionic conductivity
and mobility through tortuous membranes. Experimental measurement of
liquid membrane support tortuosity is described by Bateman et al.
($\underline{14}$). Support tortuosity should be minimized to reduce the diffu-
sional path length. However, many membrane preparation techniques,
such as casting, produce support materials with tortuous pores.

Operating Pressure Considerations

The mean pore size of a liquid membrane support determines the force
which holds the liquid membrane within the pore structure. The
Young-Laplace equation ($\underline{28}$) relates the force holding a liquid within
a cylindrical capillary to the contact angle, the surface tension,
and the radius of the pore:

$$\Delta P = \frac{2\gamma \cos\theta}{R}$$

where ΔP is the pressure difference across the liquid membrane inter-
face, γ is the surface tension, θ is the contact angle, and R is the
radius of the cylindrical pore. The pressure difference required to
dislodge the liquid membrane from the pore is inversely proportional
to the pore diameter. Thus, the mean pore size should be minimized
to increase the resistance of the immobilized liquid membrane to
transmembrane pressure differences.

FEED PHASE

Liquid membrane phase
containing solvent and
complexing agent

Porous Support

RECEIVING PHASE
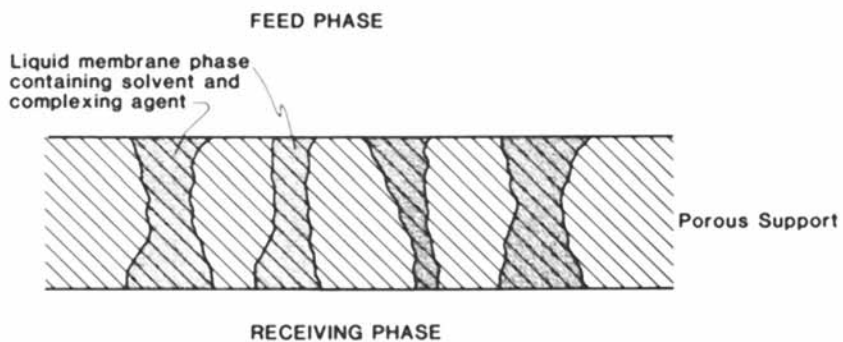
Figure 1. Cross Section of an Immobilized Liquid Membrane

Gas

Liquid

θ

Solid
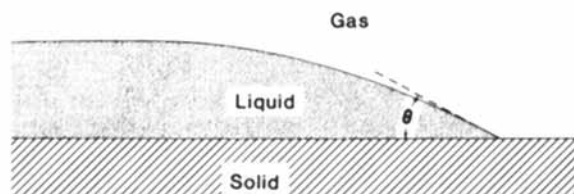
Figure 2. Cross Section of a Liquid Drop on a Surface With
Contact Angle θ

$\tau\ell$

ℓ
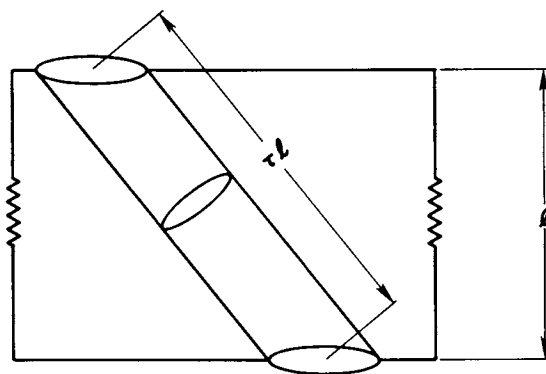
Figure 3. Schematic Diagram of a Tortuous Pore

Table I is a tabulation of the maximum pressure difference a supported liquid membrane could withstand for several solvent/support systems which have been described in the literature (11, 14, 16). The pressure differences in Table I were calculated assuming a small contact angle between the solvent and support (wetting system). Therefore, the calculated pressure differences represent maximum values. At a pore radius of 0.1 μm or less, the pressure differences become quite large which reduces the chance of solvent and carrier being forced out of the support during operation. At transmembrane pressures of up to $2.07 \cdot 10^6$ N/m², the burst strength of the thin, microporous support is a much more important factor to consider than loss of solvent from excessive differential pressure.

The pressure difference is directly proportional to the cosine of the contact angle. For a nonwetting fluid, θ approaches 90°, and ΔP approaches zero. The implication of immobilizing a nonwetting or poorly wetting fluid through solvent-exchange or other methods is that the immobilized liquid membrane would have little resistance to small transmembrane pressures.

Several investigators have demonstrated the feasibility of immobilized liquid membrane gas separations in applications where large pressure differences are encountered such as acid gas removal from synthetic natural gas. The immobilized liquid membranes prepared by Kimura et al. (16) using 100 μm cellulose acetate supports withstood CO_2 partial pressure differences of up to $6.89 \cdot 10^5$ N/m². Matson et al. (15) used microporous cellulose acetate and polyethersulfone films of 25-75 μm thickness to successfully immobilize potassium carbonate solutions for H_2S transport at pressure differences of up to $2.07 \cdot 10^6$ N/m². The ILMs were supported by macroporous non-wetting polymer films such as polypropylene and polytetrafluoroethylene to increase the resistance to high transmembrane pressures.

Kimura and Matson (16) described another approach to prevent high pressure differences from forcing the liquid membrane from the support. They created a hydrophobic-hydrophilic-hydrophobic support

Table I. Maximum Pressure Differences Required
to Displace a Liquid Membrane from a Porous Support

Solvent/Support	$\gamma\left(\dfrac{mN}{m}\right)$*	R(μm)	$\Delta P\left(\dfrac{N}{m^2}\right)$
Water/cellulose acetate	72.14	0.05	$2.88 \cdot 10^6$ (438.0 psia)
		0.1	$1.44 \cdot 10^6$ (219.0 psia)
		1.0	$1.44 \cdot 10^5$ (21.9 psia)
Formamide/surfactant-treated polypropylene	58.0	0.02	$1.45 \cdot 10^6$ (206.45 psia)
n-Decane/polypropylene	23.0	0.02	$5.75 \cdot 10^5$ (31.9 psia)

*Surface tension data from Reference 28.

composite. The aqueous liquid membrane was supported in a
hydrophilic cellulose acetate or polysulfone film. A microporous
hydrophobic film such as polytetrafluoroethylene was placed on both
sides of the liquid membrane. The aqueous liquid membrane was
retained in the hydrophilic support by capillary forces and by the
nonwetting character of the composite films.

Support Characterization

As new membranes are developed, methods for characterization of these
new materials are needed. Sarada et al. (34) describe techniques for
measuring the thickness of and characterizing the structure of thin
microporous polypropylene films commonly used as liquid membrane
supports. Methods for measuring pore size distribution, porosity,
and pore shape were reviewed. The authors employed transmission and
scanning electron microscopy to map the three-dimensional pore
structure of polypropylene films produced by stretching extended
polypropylene. Although Sarada et al. discuss only the application
of these characterization techniques to polypropylene membranes, the
methods could be extended to other microporous polymer films. Chaiko
and Osseo-Asare (25) describe the measurement of pore size
distributions for microporous polypropylene liquid membrane supports
using mercury intrusion porosimetry.

Conclusions

Selection of the ideal support for a liquid membrane requires careful
consideration of the characteristics of the particular separation
such as gas or liquid phase, pressure, temperature, and chemical
nature of the phases in contact with the membrane. However, a few
generalizations can be made. The ideal support should be thin (< 100
μm), have a high porosity (> 50%), have a mean pore size of less than
0.1 μm, have a narrow pore size distribution, and be available in
geometries that will produce permeators with a high surface area
/volume ratio.

Literature Cited

1. Way, J. D.; Noble, R. D.; Flynn, T. M.; Sloan, E. D. J. Membr.
    Sci. 1982, 12, 239.
2. Cussler, E. L. AIChE Jour. 1971, 17, 1300.
3. Reusch, C. F.; Cussler, E. L. AIChE Jour. 1973, 19, 736.
4. Louie, B., M. S. Thesis, University of Colorado, Boulder, 1983.
5. Mochizuki, J.; Forster, R. E. Science 1962, 138, 897.
6. Enns, T. Science 1983, 155, 44.
7. Donaldson, T. L.; Quinn, J. A. Chem. Eng. Sci. 1975, 30, 103.
8. Ward, W. J.; Robb, W. L. Science 1967, 156, 1481.
9. Suchdeo, S. R.; Schultz, J. S. Chem. Eng. Sci. 1974, 29, 13.
10. Hughes, R. D.; Steigelman, E. F.; Mahoney, J. A. AIChE Spring
    National Meeting, 1981, paper 1d.
11. Baker, R. W.; Tuttle, M. E.; Kelly, D. J.; Lonsdale, H. K. J.
    Mem. Sci. 1977, 2, 213.
12. Babcock, W. C.; Baker, R. W.; LaChapelle, E. D.; Smith, K. L. J.
    Mem. Sci. 1980, 7, 71.

13. Babcock, W. C.; Baker, R. W.; LaChapelle, E. D.; Smith, K. L.
    J. Mem. Sci. 1980, 7, 89.
14. Bateman, B. R.; Way, J. D.; Larson, K. M. Sep. Sci. Tech. 1984,
    19, 21.
15. Matson, S. L.; Herrick, C. S.; Ward, W. J. Ind. Eng. Chem.,
    Process Des. Dev. 1977, 16, 370.
16. Kimura, S. G.; Matson, S. L.; Ward, W. J. In "Recent
    Developments in Separation Science"; Li, N. N., Ed.;
    CRC Press: Cleveland, Ohio, 1979; Vol. 5, p. 11.
17. Smith, D. R.; Quinn, J. A. AIChE Jour. 1980, 26, 112.
18. Ward, W. J. AIChE Jour. 1970, 16, 405.
19. Ward, W. J. Nature 1970, 227, 162.
20. Otto, N. C.; Quinn, J. A. Chem. Eng. Sci. 1971, 26, 949.
21. LeBlanc, O. G.; Ward, W. J.; Matson, S. L.; Kimura, S. G.
    J. Mem. Sci. 1980, 6, 339.
22. Kajima, T.; Furusaki, S.; Takao, K.; Miyauchi, T. Can. J. Chem.
    Eng. 1982, 60, 642.
23. Matson, S. L.; Lopez, J.; Quinn, J. A. Chem. Eng. Sci. 1983, 38,
    4, 503.
24. Gregor, H. P.; Kuo, Y. Sep. Sci. Tech. 1983, 18, 421.
25. Chaiko, D. J.; Osseo-Asare, K. Sep. Sci. Tech. 1983, 17, 1659.
26. Largman, T.; Sifniades, S. Hydrometallurgy 1978, 3, 153.
27. Narebska, A.; Wodzki, R. Die Angewandte Makromolekulare Chemie
    1982, 107, 51.
28. Adamson, A. W. "Physical Chemistry of Surfaces"; John Wiley: New
    York, 1976.
29. Zisman, W. A. ADVANCES IN CHEMISTRY SERIES No. 43, American
    Chemical Society: Washington, D. C., 1964.
30. Shafrin, E. G.; Zisman, W. A. J. Phys. Chem. 1960, 64, 519.
31. Neumann, A. W.; Renzow, D. Z. Phys. Chem. 1969, 68, 11.
32. Parkinson, G. Chemical Engineering (August 22, 1983).
33. Lee, J. A.; Maskell, W. C.; Tye, F. L. In "Membrane Separation
    Processes"; Meares, P., Ed.; Elsevier: Amsterdam, 1976; p. 400.
34. Sarada, T.; Sawyer, L. C.; Oster, M. I. J. Memb. Sci. 1983, 15,
    97.

Phase Inversion Membranes

R. E. KESTING

SPMK, Inc., 4625 Green Tree Lane, Irvine, CA 92715

The science of membrane formation via phase inversion
and the technology of producing phase inversion
membranes are related in this paper. The discussion
begins by presenting the phase inversion mechanism and
continues by distinguishing and describing in detail
four membrane formation processes used to achieve phase
inversion. The structure of the resulting membranes
are discussed in terms of asymmetry or skinning and
anisotropy. Skinned membranes are classified as
integrally- and nonintegrally-skinned microgels and
ultragels. Finally, structural irregularities such as
wavemarks, macrovoids and blushing are discussed.

Phase inversion refers to the process by which a polymer solution
(in which the solvent system is the continuous phase) *inverts* into
a swollen three-dimensional macromolecular network or gel (where
the polymer is the continuous phase). As a thin film designed for
use as a barrier, such a gel constitutes a *phase inversion membrane*.

Mechanism of Phase Inversion

Phase inversion typically begins with a molecularly homogeneous,
single-phase solution (Sol 1) which undergoes a transition into a
heterogeneous, metastable solution of two interdispersed, liquid
phases (Sol 2) which subsequently form a gel (Sol 1 → Sol 2 → Gel).
Alternatively, Sol 2 may serve as the starting point for the
formation of the gel (Sol 2 → Gel). The dispersed phase of Sol 2
consists of spherical droplets or micelles which are coated with
polymer molecules. The composition in the interior of the micelles
and in the continuous phase differ from case to case depending upon
the particular variation of the phase inversion process. The
micellar structure which exists in the primary gel immediately
following gel formation differs only infinitesimally from that of
Sol 2 just prior to gelation. Therefore, Sol 2 is conceded
structural as well as temporal primacy over the gel (1). In fact

as well as in theory, the structure and function of the final phase
inversion membrane is primarily controlled by adjustments to Sol 2.
By comparison, post formation changes to the gel have only a
secondary impact on membrane structure.

The reader may find it helpful at this junction to consider the
phenomenological model originally developed by Cahn (2) to describe
two phase metal alloys and more recently used in conjunction with
polymer alloys. This model explains the appearance of isotropic,
interdispersed domains in terms of spinodal decomposition. This
may yield some insight into the reasons why "uphill" diffusion
(that is, diffusion against the concentration gradient) occurs in
phase inversion. The reader is also referred to the contribution
of Strathmann in the present volume (3).

Sol 2 is present either when one phase separates into two phases
or when two phases are prevented from recombining into a single
phase. It is expedient to entitle this factor *incompatibility*, and
to discuss the various phase inversion processes in terms of the
reasons for incompatibility. In the sections to follow four phase
inversion processes are discussed: a dry process, a wet process, a
thermal process and a polymer assisted phase inversion process.

The Dry Process

The *dry* or *complete evaporation* phase inversion process is the
oldest and easiest to understand. It can be illustrated by a
typical cellulose nitrate (CN) casting solution (see Table I).
This system can be used to exemplify the various macroscopically
observable stages involved in the formation of membranes by the dry
process:

(1) Loss of volatile solvents and the inversion of a clear
one-phase solution into a turbid, two-phase solution.
(Alternatively, the solution may be turbid and two-phase to begin
with.) Ease of processing and reproducibility are enhanced if the
solution begins with a Sol 1 or at least a Sol 2 which is somewhat
removed from the point of incipient gelation. In most cases, it is
desirable to formulate a clear single phase solution which does not
invert until some time after it has been cast.

(2) Gelation, which is marked by a decrease in the reflectivity
of the cast solution

(3) Contraction of the gel accompanied by *syneresis*. In the
case of skinless membranes, syneresis causes expelled liquid to
appear at the air/solution interface. If the membrane is cast on a
porous support, liquid may appear at both surfaces. In the
case of membranes which are skinned at the air/solution interface
only, syneresis occurs downward into the porous support. Where
no such support exists, syneresis does not occur at all. In such
a case, drying can be a slow process requiring the diffusion of
vapor rather than liquid through what may be a relatively
impervious skin layer

(4) *Capillary depletion*. Here the largely nonsolvent liquid
encompassed by the gel departs, leaving behind empty capillaries.
Frequently this results in the formation of snowflake patterns that
gradually fill in until the entire membrane becomes opaque. The
reason for this is light scattering by the micrometre-sized empty

Table I. Decrease in Casting-solution Weight and Thickness
with Drying Time

Evaporation time, min	Solution weight, g	Thickness of nascent membrane, μm
0	10.5	650
0.40	9.5	-
0.83	9.0	500
1.58	8.5	-
2.08	8.0	450
2.8	7.5	350*
4.0	7.0	300
5.16	6.5	280
6.67	6.0	250
8.25	5.5	220
10.50	5.0	200
13.16	4.0	170
20.33	3.5	155
24.16	3.0	150
31.0	2.5	135
35.5	2.0	-
43.0	1.75	125
47	1.50	-
54	1.25	115
74	1.25	115
130	0.99	-
900	0.82	100

*From this point on values refer to the thickness of the gel
exclusive of the layer of expelled liquid.

Evaporation at 21±1°C in a 62±2% relative humidity environment.

Original casting solution: 5% cellulose nitrate, 54.2% methyl
acetate, 23.7% ethyl alcohol, 12,3% butyl alcohol, 3.3% water
and 1.5% glycerol.

voids. On the other hand, those membranes which contain voids that
are less than 0.5 μM in diameter can be opalescent or clear. Subtle
differences in void size can sometimes be discerned from the
turbidities of the dry gels once they have been wet by water.

    (5) Loss of residual nonsolvent (final drying). Depending on
such factors as the volatility and concentration of residual liquids
in the membrane, the amount of membrane on the take-up roll and
storage temperature, final drying can require between two weeks and
six months. It is also possible to take up the membrane in an
essentially dry condition by passing it over heated rollers. In
either case, no membrane should be handled unless it is completely
dry. Otherwise it is subject to shrinkage and warpage while still
in a plasticized condition.

    In this process, final membrane thickness is only a fraction of
the as-cast thickness owing to solvent loss and the resultant
increase in the concentration of polymer per unit volume. However,
because of the inclusion of voids, the final membrane thickness is
substantially greater than the thickness of a dense membrane
containing an equivalent amount of polymer. The weight and
thickness as functions of evaporation time for a typical CN membrane
casting are shown in Table I.

    The sequence of events on the colloidal level corresponding to
the five macroscopically observable stages outlined above has been
deduced from the nature of the gel network in the finished membrane
(4,5) and from the ghosts of the *nascent membrane*; that is, the
frozen and lyophilized nonvolatile remnants of the *membrane in its
various formative phases* (6). The polyhedral cell structure of
the final membrane gel is considered to be an immobilized and
flattened version of the sol precursors which exists in the solution
immediately prior to the sol-gel transition. As the loss of
volatile solvent progresses, the solvent power of the solution
decreases; that is, its capability for retaining the polymer in a
homogeneous single phase Sol 1 solution is diminished. If only
polymer and solvent are present, then at least three situations are
possible:

    (1) Separation into two liquid phases may not occur prior to
gelation. This would be the case if polymer and solvent are
infinitely miscible. Even after gelation the solvent will continue
to act as a plasticizer. When combined with the effect of gravity,
this can lead to collapse and densification of the gel, ultimately
resulting in a dense film.

    (2) Phase separation may occur prior to gelation if there is
only limited polymer solubility in the solvent. However, even in
this case residual solvent can act as a plasticizer and a dense or
nearly dense (low porosity) film may result.

    (3) For those cases in which polymer-polymer interactions
are unusually strong; for example, in the evaporation of solutions
of Nylon 6,6 in 90% formic acid (7), gelation will occur with the
formation of strong virtual (perhaps crystalline) cross-links.
Such a gel can overcome the combined effects of plasticization and
gravity so that porosity is maintained throughout complete
evaporation. After phase inversion has occurred and prior to
gelation, the sol structure exhibits long range order. Virtually
any disruption of this order or *nucleation* in the sol by rapid

agitation or fine filtration will produce larger pores than would
have otherwise resulted.

Both the interior of the micelles and the continuous phase of a
two component system consist of polymer-poor regions. The micellar
wall consists of polymer-rich regions. In the cell wall, polymer-
polymer interactions predominate over polymer-solvent interactions.
Most dry process casting solutions, however, consist of three or
more components: polymer, volatile solvent and one or more
poreformers from the nonsolvent side of the *polymer-solvent
interaction spectrum*. The nonsolvent should be substantially less
volatile than the solvent. A practical rule of thumb is a 30 to
40°C minimum difference in boiling points between the two. Although
Sol 1 is homogeneous on the colloidal level, compatibility decreases
as evaporation proceeds. Eventually the solvent power of the
remaining solvent system is insufficient to maintain Sol 1, and
inversion into Sol 2 occurs. Most of the polymer molecules
distribute themselves around the micelles which have formed.
Relatively few polymer molecules (perhaps 0.5 percent) remain
dispersed in the liquid matrix. In this case, the interior of the
micelle consists of a liquid with a large concentration of the
nonsolvent components of the casting solution. The presence of
nonsolvent in the casting solution and/or strong polymer-polymer
interaction forces leads to phase inversion, gelation and the
maintenance of gel porosity in spite of forces which act to collapse
the gel. In other words, in the dry process incompatibility is an
internal characteristic of the system. Because solvent loss
continues after phase inversion, the spherical micelles approach
one another and eventual make contact in the initial phase of
gelation. As the gel network contracts, the micelles deform into
polyhedra and the polymer molecules diffuse into the walls of
neighboring micelles causing an intermingling of polymer molecules
at the interface. If the walls are sufficiently thin, contraction
causes a tearing of the walls which then retract and form the
hoselike skeleton which constitutes the gel network. This occurs
when a high initial concentration of components other than polymer
and solvent causes the formation of numerous micelles with a large
total surface area. A similar phenomenon occurs during the bursting
of soap bubbles (8) and the formation of open-celled polyurethane
foams. However, the micelles may be covered with such a thick
polymer coating that rupturing of cell walls is hindered or entirely
inhibited. In this case, either mixed open- and closed-cell or
entirely closed-cell structures result.

Consider the principal factors which determine the porosity
and pore size characteristics of dry process membranes:
(1) Polymer volume concentration in Sol 2 is inversely
proportional to gel porosity.
(2) The ratio of nonsolvent volume/polymer volume in Sol 2
is directly proportional to gel porosity.
(3) The difference in boiling points between solvent(s) and
nonsolvent(s) is proportional to porosity and pore size.
(4) The relative humidity of the evaporation environment is
proportional to porosity and pore size.
(5) The presence of more than one polymer with less than
perfect compatibility increases porosity.

(6) The presence of high molecular weight polymer tends to increase porosity because these polymers tend to be less compatible.

The effects of polymer and nonsolvent concentration upon cell structure, porosity and permeability are discussed next.

Because dry process solutions use nonsolvent poreformers, the polymer dissolving capacity of the solvent system is severely limited. In spite of this, the casting solution must be sufficiently viscous to permit handling during flat sheet and tubular casting or hollow fiber spinning. This dilemma is resolved by utilizing high molecular weight polymers which, although slightly less soluble than their low molecular weight counterparts, do contribute significantly to solution viscosity. However, most engineering plastics are available only in the low to intermediate molecular weight range because they are designed for melt processing applications such as injection moulding and extrusion. This can, and often does, limit the application of the dry process. Methods for circumventing this obstacle include the preparation of special grades of high molecular weight polymers (9), the utilization of viscosity enhancers such as a second polymer (10,11) or finely divided colloidal silica, and casting at low temperatures. In the absence of any nonsolvent poreformer or strong polymer-polymer interactions, phase inversion (Sol 1 → gel) does not take place and a dense, high-resistance membrane or film is formed. As a first approximation, such a structure consists of a single dense skin layer. With low concentrations of nonsolvent, membranes possessing closed cells, low porosity and substantial resistance to material transport are encountered. However, the thickness of the dense skin layer is substantially diminished. At intermediate concentrations of nonsolvent, a mixture of open and closed cells is formed. The dense skin layer has thinned considerably and a thin transition layer consisting of closed cells is discernible. Polymer density in this transition layer is intermediate between that of the dense skin layer and that of the porous, open-celled substructure which is found in the bulk of the membrane. Permeability is small but measurable at this point. At high concentrations of nonsolvent, a bilayered structure comprised of a thin skin and a porous, open-celled substructure is found. There is a break in the curve of permeability versus porosity at that concentration at which mixed open and closed cells give way to open cells. As the concentration of nonsolvent is increased beyond this point, skin thickness decreases and permeability increases. Eventually the skin becomes sufficiently thin that its integrity is breached in places and the porous substructure becomes visible. At extremely high nonsolvent concentrations, the dense skin layer is absent altogether and both surface and interior regions consist of open cells with tears in the walls. In this case, the porous surfaces characteristic of microfiltration membranes are encountered. As nonsolvent concentration is increased beyond this point, cell size, pore size and permeability continue to increase. Eventually the integrity of the porous substructure cannot be maintained. If structures with pore sizes greater than about 5 μM are desired, processes other than phase inversion are employed.

The relationship between Δ b.p. (nonsolvent boiling point –
solvent boiling point) of the two solvents acetone (b.p. 56°C) and
dioxolane (b.p. 75°C) and the level of a single nonsolvent
isobutanol (b.p. 110°C) required to produce equivalent skinned
membranes (as deduced from their equivalency in permeability and
permselectivity) is shown in Table II.
    Both solvent and nonsolvent evaporate simultaneously.
Therefore, if a critical solvent/nonsolvent ratio must be reached
before gelation occurs, a less volatile solvent will require a
higher initial concentration of a given nonsolvent to reach this
ratio at a given porosity than will a more volatile solvent.
Similarly, the concentration of nonsolvent in the casting solution
required to achieve a given porosity is inversely related to its
volatility.
    Bjerrum and Manegold (12) were among the first to observe the
influence of the atmosphere above the desolvating solution upon
membrane structure and function. A high concentration of solvent
vapor retards gelation, whereas high temperatures and high air
velocities will hasten it. *Skinning* is enhanced by high air flow
rates and high polymer concentration. Atmospheric moisture hastens
gelation and thus increases average pore size and permeability
(Table III). The inclusion of water in the casting solution has a
pronounced effect in those cases in which water plays a nonsolvent
role (Table IV). In hydrophobic sols, water acts both to hasten
gelation and to increase the size of voids in the gel structure.
This is attributable to two factors: first, a substantial degree
of incompatibility with the solvated polymer component of the
casting solution, and second, high surface tension. Both factors
act to cause water to separate from the remainder of the solution
in the form of comparatively large micelles which then result in
coarse microgels. The presence of a microgel structure in membranes
from moderately hydrophilic polymers such as cellulosics and
polyamides confers the important property of wet-dry reversibility
on these membranes (6). This occurs because the magnitude of the
capillary forces coming into play upon drying depends on the
internal surface area of the membrane which in turn depends on cell
size. Microgel membranes possess large (1 to 10 μM diameter) cells.
Therefore, such membranes have a relatively small internal surface
area and as a result will not lose porosity during drying.
Ultragel membranes, on the other hand, have small (1.5 to 0.5 μM
diameter) cells and consequently possess a larger internal surface
area. Ultragels are therefore more likely to lose porosity during
drying and less likely to be wet-dry reversible. In comparison to
the wet process, the dry process tends to use more dilute solutions
and less compatible poreformers (both of which promote the formation
of microgels). Therefore, the dry process is more likely to produce
microgels than is the wet process. However, there are many
exceptions to this rule and it is possible both to produce microgels
by a wet process and ultragels by a dry process.
    Because the principles which govern the dry process are now so
well understood and because the process itself is so amenable to
control, the dry process is considered by the present author as the
technique of choice whenever it can be applied.

Table II. Equivalent Nonsolvent Concentrations in Acetone- and Dioxolane-Solutions* for Dry-RO Blend Membranes of CA and the TMA Salt of CA 11-bromoundecanoate

Solvent	boiling point (°C)	Δ b.p. (b.p. nonsolvent - b.p. solvent) (°C)	Nonsolvent concentration (gIBA/formulation)	Permea-bility* (gfd)	Salt** Rejection (%)
Acetone	56	54	38	5.6	97.9
Dioxolane	75	35	54	5.5	97.8

* Total Polymer Conc. 10% W/V; Polymer Ratio 6/1 JLF-68CA/TMA salt of CA 11-bromoundecanoate (made from E-383-40 CA with 0.3D.S. quat); methanol, 10g/formulation

**0.5% NaCl feed @400 psi and 25±1°C

Table III. Effect of Relative Humidity upon
Permeability and Pore Size

Relative humidity at 20°C, %	Filtration time for 500 ml $H_2O/12.5$ cm^2 at 70 cm Hg, sec	Average pore diameter, nm
80	25-40	∿600
60	40-60	∿500
40	60-80	∿400

Reproduced with permission from Ref. 4. Copyright 1960.

Table IV. Influence of Casting-solution Water Concentration upon Pore Size and Permeability of Collodion Membranes

H_2O concentration in casting solution, %	Filtration time for 500 ml H_2O/12.5 cm^2 at 70 cm Hg, sec	Average pore diameter, nm	Casting-solution viscosity at 20°C, centipoises
3.3	40	600	2,011
0.4	800	30	1,813
0.0 (trace)	4,000	15	1,600

Reproduced with permission from Ref. 4. Copyright 1960.

The Wet Process

The *wet,* or *combined evaporation-diffusion, technique* is that
variation of the phase inversion process in which a viscous polymer
solution is either allowed to partially evaporate prior to immersion
in a nonsolvent gelation bath, or immersed directly into a
nonsolvent gelation bath. Upon immersion, any residual solvent or
poreformer is exchanged for nonsolvent.

   A wet process solution must be relatively viscous ($>\sim$10,000
centipoise) at the moment of immersion in the nonsolvent so that it
will retain integrity throughout gelation. When the solution is
too fluid, the primary gel will be subject to disruption by both
the weight of the nonsolvent and the currents coming into play
during immersion. The requirement for high viscosity and hence
high polymer concentration is, in most cases, inconsistent with the
attainment of high porosity via the inclusion of nonsolvent
poreformers. Therefore, when they are required, poreformers are
frequently chosen from the swelling agent--weak solvent side of the
polymer-solvent interaction spectrum. Moreover, the presence of
poreformers within the casting solution is not a requirement of
every wet process solution. In many instances, particularly when
nonvolatile solvents with a strong affinity for the nonsolvent
gelation medium are utilized, the phase inversion sequence Sol
1 → Sol 2 → gel is evoked by the simple act of immersion into
nonsolvent without prior evaporation. In such a case, the
nonsolvent bath represents an *external* source of incompatibility.
A two-component solution (polymer + solvent) becomes a three-
component solution (polymer + solvent + nonsolvent poreformer) as a
result of the diffusion of nonsolvent into, and solvent out of, the
nascent membrane gel.

   The effect of the nonsolvent gelation medium may be influenced
by the presence of certain components of the casting solution. For
example, lyotropic salt swelling agents from the Hofmeister series
cause aggregation of water molecules around the electrophilic
cations, thereby modifying the properties of a water gelation
medium (<u>13</u>). This interaction causes a change in the role of water
from that of a nonsolvent to that of a swelling agent (Table V).
Other polar nonsolvents such as aliphatic alcohols function in much
the same manner as water, except that their nonsolvent tendencies
are less pronounced.

   Increasing the concentration of the weak nonsolvent poreformer,
ethanol, in a casting solution containing CA and acetone increases
the porosity of the resultant membranes (Table VI). Because the
poreformer is a nonsolvent, solution compatibility decreases with
increasing ethanol concentration. As the concentration of ethanol
is increased, the solution approaches the point of incipient
gelation; that is, the perimeter of the solubility envelope.
Because a solution containing a high concentration of nonsolvent
can be presumed to be of the Sol 2 type and close to gelation,
immersion into a nonsolvent bath and subsequent gelation will be
accompanied by less gel concentration than would occur if the
solution were further removed from the perimeter of the solubility
envelope. The result is that the micelle diameter in Sol 2, as
well as the porosity and permeability of the final membrane,

Table V. Casting-solution Water-concentration Effects

Water concentration, g/formulation*	Swelling-agent concentration, g ZnCl$_2$/formulation*	Description of membrane	Wet thickness of unheated membrane, mm x 10^2	Gravimetric swelling ratio of unheated membrane, wet wt/dry wt	Rate of water transport, ml/(cm^2)(day)†		Salt retention, %
					Deionized water feed	0.6 M NaCl feed	
0	0	Brittle, opaque (microgel)	5.8	1.47	<1	-	-
5	0	Brittle, opaque (microgel)	6.4	1.77	<1	-	-
10	0	Brittle, opaque (microgel)	7.1	1.99	<1	-	-
15	0	Brittle, opaque (microgel)	8.0	2.35	<1	-	-
0	5	Clear (ultragel)	8.7	2.53	24	16	90.3
5	5	Opalescent (ultragel)	9.0	2.79	34	22.8	97.2
10	5	Opalescent (ultragel)	9.2	2.85	72	48	98.5
15	5	Opalescent, opaque (ultra-gel—microgel)	9.6	2.92	136	82	96.2

* Formulation: cellulose acetate, 22.2 g; acetone, 66.7g (doctor-blade gap 0.25 mm).
† Rate of water transport and salt retention at 102 atm pressure for heated membranes (86°C for 5 min.)

Reproduced with permission from Ref. 13. Copyright 1965.

Table VI.   Effect of Swelling Agent (Ethanol) on the Membrane Water Content

Membrane code no.	Mixed solvent		Calculated values of mixed solvents		Membrane water content wt-%
	Ethanol, mole-%	Acetone, mole-%	δ_p	δ_h	
CA-24	20	80	4.99	4.23	50.7
CA-23	30	70	4.93	4.69	50.3
CA-22	40	60	4.86	5.20	53.4
CA-25	46.6	53.4	4.83	5.47	61.2
CA-21	50	50	4.79	5.75	65.8

Reproduced with permission from Ref. 14.   Copyright 1975.

increase as the concentration of poreformer increases. This causes
greater opacity in the final membrane. It is worthy of note that
it is only the insufficient Δ b.p. of 23°C between acetone and
ethanol which prevents this solution from being a candidate for the
dry process. If methyl formate (b.p. 30°C) or propylene oxide
(b.p. 35°C) were used as the solvent in conjunction with the
poreformer ethanol, this solution could be used in either a wet or
dry process. If acetone was used as the solvent in conjunction
with poreformers propanol (b.p. 97°C) or isobutanol (b.p. 108°C)
the same would be true.

     The effect of the concentration of a solvent-type poreformer
such as formamide upon the properties of CA membranes are shown in
Table VII (15). By way of comparison, the use of this solution in
the dry process leads to the formation of a dense film. Because
both acetone and formamide are solvents, the loss of the more
volatile acetone leaves behind a high boiling solvent formamide,
which plasticizes the CA gel as it evaporates. The fact that
intrinsic viscosity, [η], increases and both solution and membrane
turbidity decrease with increasing formamide concentration suggests
that solvent power increases as well. Concurrent increases in
thickness, porosity and permeability are attributed to the strong
hydrogen bonding capacity of formamide and its strong affinity for
CA. After immersion in a water gelation bath, desolvation is slow
because the water can hydrogen bond with formamide. Thus, water's
role as a strong nonsolvent is lessened. The net result appears to
be that the Sol 2 → gel transition occurs at a reduced rate. During
this time the aggregating mass is more amenable to the infusion of
a higher concentration of nonsolvent than would otherwise be
possible.

     The gelation bath temperature also influences the structure and
function of RO membranes (Table VIII). Increasing temperature
hastens the onset of gelation and results in increased void size,
degree of swelling and permeability, as well as decreased
permselectivity.

     Increasing the evaporation (drying) time prior to immersion in
the nonsolvent medium causes a decrease in cell size and porosity
and hence a decrease in permeability (Table IX). As the solvent
concentration in the nonsolvent bath increases, permselectivity
first increases and then decreases owing to stresses imposed on the
skin layer and possibly to some swelling and rehardening of skin.

     The greater the affinity of the gelation medium for the casting
solution components, the more gradual will be the Sol 2 → gel
transition and the more porous will be the final membrane. For
example, since methanol has a greater affinity for CA than does
water, gelation of a CA solution in methanol will produce a membrane
of higher porosity. Immersion of a CA casting solution in a strong
nonsolvent such as water often leads to a skinned membrane.
Therefore, when a skinless membrane is desired, the casting solution
should be immersed in a nonsolvent solution containing some solvent.
Likewise, when a skinned membrane is available by any process, the
skin may often be removed by immersing it in a nonsolvent/solvent
solution. A closely related phenomenon known as *clearing* is
utilized to collapse opaque microporous electropheresis membranes
into clear dense films. Here the reserve of the dry casting process

Table VII. Properties of Sols and Gels from Acetone-Formamide Solutions of CA

Formamide Concentration (mol %)	SOL* PROPERTIES			GEL PROPERTIES		
	$[\eta]25°C$	Turbidity @546 μm $(\times10^2)$	Turbidity @546 μm $(\times10^{-1})$	Thickness (μm)	Wet wt / Dry wt	Water Flux** (cm/day)
0	0.895	1.6	38.7	36	1.71	no flow
10	0.942	0.9	33.2	43	2.10	no flow
20	0.948	0.6	-	46	3.01	26
30	0.963	0.5	20.7	74	3.44	128
40	-	0.45	7.8	86	3.90	384
50	-	0.45	1.4	94	4.40	1320

* 15g E-398-10 CA/100ml solution
**Distilled water feed @40.8 atm and 25°C

Reproduced with permission from Ref. 15. Copyright 1969.

Table VIII. Gelation-bath Temperature Effects*

Gelation-bath temperature °C	Membrane appearance	Intrinsic viscosity [η] of cellulose acetate in acetone-water (66.7:100)†	Wet thickness of unheated membrane, mm x 10²	Gravimetric swelling ratio of unheated membrane, wet wt/dry wt	Rate of water transport, ml/(cm²)(day)‡		Salt retention, %‡
					Deionized water feed	0.6 M NaCl feed	
0	Opalescent	0.985	9.2	2.85	84	50	98.6
10	Opaque	0.940	14.0	3.80	83	50	97.1
25	Opaque	0.05	22.8	5.80	90	58	90.1
40	Opaque	0.745	31.0	6.98	118	74	81.1

* Casting-solution composition: cellulose acetate, 22.2 g; acetone, 66.7 g; water 10.0 g; ZnCl$_3$, 5.0 g (doctor-blade gap 0.25 mm).

† Measured at the corresponding gelation-bath temperature.

‡ Rate of water transport and salt retention at 102 atm pressure for heated membranes (86°C for 5 min).

Reproduced with permission from Ref. 13. Copyright 1965.

Table IX. Drying-time Effects

Drying time, min†	Description of membrane	Wet thickness of unheated membrane, mm × 10²	Gravimetric swelling ratio of unheated membrane, wet wt/dry wt	Rate of water transport, ml/(cm²)(day)		Salt retention, %‡
				Deionized water feed	0.6 M NaCl feed	
1	Opaque-opalescent (microgel blending into ultragel)	13.9	2.88	116	72	98.0
3	Opalescent (ultragel)	12.2	2.98	84	50	98.6
5	Opalescent (ultragel)	10.2	2.65	86	54	98.8
10	Opalescent-clear (ultragel)	8.5	2.41	80	50	96.3
20	Clear (ultragel)	5.8	1.75	72	50	75.1
30	Clear (ultragel)	5.3	1.60	50	36	71.5

* Casting-solution composition cellulose acetate, 22.2 g; acetone, 66.7 g; water, 10.0 g; ZnCl₃, 5.0 g (doctor-blade gap 0.25 mm).

† Drying time – interval between casting at –11°C and immersion into gelation bath (0°C).

‡ Rate of water transport and salt retention at 102 atm pressure for heated membranes (86°C for 5 min).

is employed. Instead of utilizing a volatile solvent and a
nonvolatile nonsolvent to gradually decrease compatibility, a
volatile nonsolvent and a nonvolatile solvent are employed. The
affinity of the clearing solution for the membrane substance is
gradually increased as drying progresses and gravity slowly
collapses the softened but intact gel.

Immediately following the Sol 2 → gel transition in the dry
process, a primary gel structure is obtained. This gel is seldom
isolated because continued evaporation produces the completely
consolidated membrane, known as the secondary gel. The secondary
gel is ordinarily the only product of interest. However, this is
not usually the case for the wet process. After the viscous
solution has been gelled by immersion and the solvent system
removed, a stable primary gel is obtained. Such a membrane is
easily distinguished from the secondary gel which results after the
primary structure has been subjected to various postformation
treatments.

Casting-solution and environmental variables permit far greater
control over the ultimate structure and performance of phase
inversion membranes than does the modification of a primary gel
into a secondary gel by postformation treatments. Because the
properties of the primary gel determine to a large extent those of
its secondary counterpart, the former should be considered as more
fundamental and important in discussing the effects of fabrication
parameters such as casting-solution composition, upon performance.
Once a primary gel has been formed, it may be utilized as such
(particularly for low-pressure applications) or it may be subjected
to various physical and/or chemical treatments for conversion into
a more pressure-resistant secondary gel.

Physical modifications of primary gel structures can be used to
influence porosity (degree of swelling, void volume, water content,
etc.), pore size, permeability and permselectivity. The technique
utilized to produce porous membranes from dense films can be used
to effect an increase in porosity. In this variation of Brown's
(16) technique, an already porous primary gel is immersed in a
swelling medium. To fix the secondary gel in its more expanded
condition, the swelling medium is removed by exchange with a
nonsolvent (nonsolvent-swelling agent miscibility is essential) or
by simple evaporation. This technique adds another step to the
fabrication process and is complicated by the leaching of low
molecular-weight polymer from the primary gel. Therefore, it is
usually circumvented by reformulating the casting solution and
producing a primary gel with an initially higher void volume.
However, this process is frequently encountered as an undesired
factor in the permeation of certain organic solutes. These
organics interact with and swell the membrane, thereby altering
pore characteristics and permeability.

Of much greater practical importance are physical alterations
of the primary gel structure to effect decreases in porosity. The
most important means to this end are thermal annealing,
pressurization and solvent shrinking.

Annealing a porous membrane (particularly one which contains a
nonsolvent capable of functioning as a plasticizer) produces a
decrease in void volume and permeability and, because pore size is

generally decreased as well, an increase in permselectivity. The
reason for this can be seen on the molecular level where the
introduction of thermal energy causes translational motion of the
macromolecules. This results in polar groups on the same and/or
neighboring molecules approaching one another closely enough to
form dipole-dipole cross-links. These cross-links decrease chain
mobility and, in a nonsolvent medium, are irreversible; that is,
the nonsolvent is not able to solvate the polar groups so enjoined.
     Annealing has some continuous and some discontinuous effects.
A continuous effect is the decrease in water content and void volume
with increasing temperature. Water is lost from the primary gel
during annealing, both because of the formation of virtual cross-
links and because of the decrease in hydrogen bonding and cluster
size in the water itself. An example of a discontinuous effect is
the dramatic increase in permselectivity (salt rejection) observed
when cellulose acetate membranes are heated above the glass
transition temperature 68.6°C. In fact, not one but two
discontinuities are found on the permselectivity versus annealing
temperature curve for cellulose acetate desalination membranes.
The first indicates an increase and the second a decrease in
permselectivity. The increase, on the basis of the previously
cited structural interpretation, may be attributed to the attainment
of the critical interchain spacing or pore diameter. The decrease
may be related to a disruption in the uniformity of these spacings.
This nonuniformity is due to closer alignment of polymer chains in
some regions at the expense of strain-induced separation of polymer
chains in other regions.
     Whereas heating causes shrinkage in three dimensions, the
application of pressure causes shrinkage primarily in one dimension;
that is, in the plane perpendicular to the surface. Two stages may
be distinguished in the shrinkage of porous membranes under
pressure: (1) the rapid loss of void volume in the porous
substructure, which occurs at comparatively low pressures, and (2)
the slower, more gradual loss of void volume in the comparatively
dense skin layer. Inasmuch as the skin layer more closely
approaches the structure of the bulk polymer, it is to be expected
that significant compaction of this layer will require pressures in
excess of the compressive yield point.

The Thermal Process

One of the most significant recent developments in phase inversion
membrane technology is the invention of the thermal process by
Castro (17). The thermal process is applicable to a wide range of
polymers which, because of their poor solubility, are otherwise
inaccessible to the phase inverison approach. In essence, the
thermal process utilizes thermal energy and a latent solvent (that
is, a substance which is a solvent for the polymer only at elevated
temperatures) to produce a Sol 1 solution which upon cooling inverts
into a Sol 2 solution. Further cooling causes gelation. The
incompatibility which evokes Sol 2 is due to the loss of solvent
power by heat removal. The latent solvent may be either a liquid
or a solid at room temperature. If, however, a solid is employed,
it must be a liquid at the elevated temperature at which Sol 2

appears. Because the latent solvents are nonvolatile substances,
they must be removed from the final gel by extraction with a liquid
which is a solvent for the latent solvent and a nonsolvent for the
polymer.

The thermal process is perhaps the most universally applicable
of all the phase inversion processes because it can be utilized
over the widest range of both polar and nonpolar polymers. However,
its commercial use for membrane applications will probably be
restricted to polyolefins, particularly polypropylene. A large
number of the substances can function as latent solvents (Table X).
They usually consist of one or two hydrocarbon chains terminated by
a polar hydrophilic end group. Therefore, they exhibit surface
activity which may explain their ability to form the emulsion-like
Sol 2 micelles at elevated temperatures. One latent solvent which
is worthy of special mention because of its broad applicability is
N-Tallowdiethanolamine (TDEA).

The thermal process has a number of unique features:

(1) Spherical cells exist in the final gel matrix. Although
all phase inversion membranes possess spherical micelles in their
nascent Sol 2 condition, only the thermal process retains the
spherical micellular shape into the final open-cell gel
configuration. The diameters of the cells are between 1 and 10 μM
and the apertures or pores between them have diameters narrowly
distributed between 0.1 and 1 μM. The Sol 2 micelles of dry and
wet process membranes deform into polyhedra and flatten out by the
time they have been fully formed.

(2) Only the thermal process is capable of yielding isotropic
microporous structures in thick sections. Wet and dry processes
tend to become increasingly anisotropic as the thickness of the
membrane gel is increased. This unique property renders thermal
process gels ideally suitable for use in controlled release
applications. The gels can be cooled, ground up, extracted and
filled with volatile insect repellants, for example.

Table X.   Thermal Process Polymers and Latent Solvents

Polymer*	Latent Solvent(s)	Extrusion Temperature (°C)
LDPE	saturated long chain alcohols	–
HDPE	TDEA	250
PP	TDEA	210
PS	TDEA, dichlorobenzene	200
PVC	trans-stilbene	190
SBB	TDEA	195
EAA	TDEA	190
Noryl (PPO/PS)	TDEA	250
ABS	1-dodecanol	200
PMMA	1,4-butanediol, lauric acid	210
Nylon 11	sulfolane	198
PC	menthol	–

*Commonly employed abbreviations

Reproduced from Ref. 17.

If the solution is cooled slowly (8°C/min to 1350°C/min), Sol 2 micelles appear. If, however, cooling is too rapid (∿2,000°C/min), a continuous lace-like, noncellular polymer network is apparent in photomicrographs. This lace-like network is the frozen Sol 1 structure which, for kinetic reasons, is unable to assume the Sol 2 configuration before it becomes immobilized.

If the solution is cooled by casting on a chilled metal belt, the surface adjacent to the belt will be skinned whereas the surface adjacent to the air/solution interface will be skinless. This is just the opposite to that which usually occurs in wet and dry processes. The skin thickness is approximately equal to the thickness of a single cell wall and can either be integral (totally nonporous) or nonintegral (some porosity) depending on the particular processing conditions. The presence of an integral skin is desirable if the membrane is to be utilized for gas separations, reverse osmosis (RO), ultrafiltration (UF), etc. If, on the other hand, the skin is not desired it may be removed by allowing the membrane to be exposed briefly to a suitable solvent such as hexane in the case of polypropylene.

The latent solvent is removed from the membrane gel after the latter has attained sufficient strength to allow further processing. Typical leaching agents include volatile liquids such as isopropanol, methyl ethyl ketone, tetrahydrofuran, ethanol and heptane.

Further discussions of the thermal process are presented elsewhere in this volume (18).

The Polymer Assisted Phase Inversion (PAPI) Process

The polymer assisted phase inversion (PAPI) variation of the phase inversion process utilizes a solution consisting of a solvent and two physically compatible polymers to cast a dense film with a morphology known as an interpenetrating polymer network (IPN). After complete (dry PAPI) or partial (wet PAPI) solvent evaporation the IPN film is immersed in a liquid, usually water, which is a solvent for one of the polymers and a nonsolvent for the other. The insoluble network which remains after leaching is a skinless microporous PAPI process membrane. As originally conceived, the polymer which was leached was viewed as filling the role of a high molecular weight nonsolvent poreformer. As such it "assisted" the membrane polymer to assume the Sol 2 micellar structure prior to gelation. Physical compatibility, but not necessarily single T_g miscibility, is required for practical PAPI blends. Molecular compatibility presumably leads to Sol 1 structures which gel without assuming the necessary Sol 2 configuration. PAPI membranes are usually skinless and isotropic with a narrow pore size distribution of intermediate porosity (∿50%). Typically they have good to excellent mechanical properties. The choice of both membrane and leaching polymers for the PAPI process is governed by the empirical "rules" which apply to polymer blends (19).

A potential application for PAPI process membranes is microporous supports for thin film composites. ·This is particularly attractive when the thin film can be deposited prior to leaching the "assisting" polymer, thereby providing a dense impermeable

surface, ideal for coating. After a thin film of preformed or
in situ formed polymer has been deposited from solution and/or
cured, the support layer of the composite membrane can be made
porous by leaching.

Asymmetry and Anisotropy

Prior to 1960, only isotropic or slightly anisotropic phase
inversion membranes were known. Today there are two types of
inhomogeneity in depth which are of importance: *skinning* and
anisotropy.
     Skinning or asymmetry refers to a structure in which a thin
(0.1 to 0.25 μM) relatively dense skin layer is integrally bonded
in series with a thick ($\sim$100 μM) porous substructure. The skin
layer determines both the permeability and permselectivity of the
bilayer, whereas the porous substructure functions primarily as a
physical support for the skin. The first skinned membrane, the wet
process cellulose acetate type developed in 1960 by Loeb and
Sourirajan [20] for desalination by reverse osmosis, is universally
acknowledged as the instrument which heralded the advent of the
golden age of membranology. In this *integrally-skinned membrane*
the skin and substructure are composed of the same material.
Differences in density between the two layers are the result of
interfacial forces and the fact that solvent loss occurs more
rapidly from the air/solution and solution/nonsolvent bath
interfaces than from the solution interior. Certain aspects of the
skin layer remain a hotly debated issue. The earliest electron
microscopy studies failed to detect any specific details of the
microstructure. It was deduced that the skin was in an amorphous
glassy state, similar to that of a solvent cast bulk film. As we
shall see, this conclusion was only partly true. Schultz and
Asunmaa [21] discovered the presence of spherical micelles $\sim$200 Å
in diameter in the skin of cellulose acetate membranes which had
been etched with Argon ions. Similar micelles were subsequently
found by Kesting [6] in the skin of dry process membranes of
cellulose acetate. Panar, Hoehn and Hebert [22] then discovered
that the micellar morphology was quite general to skinned membranes
not only of cellulose acetate but of polyamide-hydrazides and
polyamides as well.
     Immediately below the skin layer of integrally-skinned
membranes is found a substrate [22] or transition [23] layer with a
density between that of the skin and that of the porous
substructure. This layer consists of micelles less closely packed
than those in the skin layer plus mixed open and closed cells. The
depth and structure of the transition layer in wet process membranes
are functions of the various fabrication parameters rather than
immutably fixed quantities. Although this layer is commonly found
in wet process membranes which employ concentrated polymer casting
solutions, it is encountered in dry process membranes which employ
more dilute casting solutions only under special conditions.
Trudelle and Nicolas [24] utilized light reflection, differential
refractometry and densitometry to find that the skin of integral
CA membranes had a water content of 38 percent by weight whereas
the substructure contained 61.8 percent. The water content

increased steadily from the surface inward, quite quickly in the
surface region and more slowly, but not negligibly, in the deeper
regions. The transition layer was estimated to have a thickness of
19 µM (out of a total membrane thickness of 140 µM). Significantly,
it was found that annealing the membrane resulted in increased
asymmetry. The water content was decreased to a greater extent in
the skin than in the substructure layer (Table XI).

The conclusion which can be drawn from the above studies is
that the skin layer in integrally-skinned reverse osmosis membranes
consists of a single layer of consolidated Sol 2 type micelles.
This structure differs in kind from that of a solvent-cast film
which results from the direct conversion of Sol 1 (a homogeneous
molecular dispersion of macromolecules) to the gel without the
intermediate step of Sol 2 micelle formation. Thus, supermolecular
structure of a specific nature is present in the skin layer of
integrally-skinned reverse osmosis membranes, which is not present
either in the specially prepared thin, dense films utilized by
Krishnamurthy and McIntye (25) to mimic the skin layer or in the
thick dense films utilized by Lonsdale (26) to determine the
"intrinsic" salt rejections of various RO membrane polymer
candidates. The ultrathin film X-ray studies of Krishnamurthy and
McIntyre (25) and the thick solvent cast film DSC studies of Morrow
and Sauer (27) were previously cited (28) as evidence for the
existence of crystallinity in the skin layer of integrally-skinned
membranes. However, from our present knowledge of the skin
structure, it now appears that these two studies were largely
irrelevant. They dealt with structures which were unrelated to
those of the skins in integrally-skinned membranes. Furthermore,
several additional facts argue against the necessary existence of
crystalline order in the skins of RO membranes:

(1) Interfacial thin film polycondensates, whose mode of
formation makes crystallinity highly improbable, are known to
function as excellent RO membranes.

(2) Richter and Hoehn (29) deliberately designed their
aromatic polyamides to be amorphous, and yet they are highly
permselective.

(3) The trimethyl ammonium salts of CA 11-bromoundecanoate
both by themselves and as blends with CA (30) result in integrally-
skinned membranes with the highest permselectivity in a series of
quaternized omega halo esters of various chain lengths. The
inclusion of C_{10} to C_{12} chains into cellulose (Table XII) (31) is
known to result in minimum T_m values and hence minimum
crystallinity. Therefore, it follows that crystallinity in the
skins of integrally-skinned membranes is not only unnecessary but
may actually be detrimental.

Because the skin is not crystalline, it is amorphous. It cannot
be a rubber so it must be a glass. However, the glassy state is a
nonequilibrium condition. Thus, a good deal of uncertainty
regarding the nature of this state and how it relates to RO membrane
performance remains.

It is not easy to accommodate both micellar skins and
interfacial thin films into a single structural model which is
consistent with the functional behavior of skins of RO membranes.
In view of the above, the "solution-diffusion" theory of

Table XI. Effect of Thermal Annealing upon the Indices of
Refraction and Water Contents of Skin and
Substructure Layers of Loeb-Sourirajan-type
Membranes

Membrane	Index of refraction of skin layer	Skin H_2O %	Index of refraction of substructure layer	Substructure H_2O, %
N.T.*	1.409	46	1.3799	63
T.†	1.420	38.6	1.3823	61.8

* Unheated membrane.
† Membrane heated at 80°C for 5 min.

Reproduced with permission from Ref. 24.

Table XII. Apparent melting temperature of various higher
aliphatic acid esters of wood prepared by the
TFAA or the chloride method[a]

Sample (acyl)	N (Carbon Atoms)	Melting temperature (°C)	
		TFAA	Chloride
Butyroyl	4	300	310
Valeroyl	5	235	305
Caproyl	6	250	260
Capryloyl	8	210	245
Capryl	10	205	290
Lauroyl	12	195	240
Myristoyl	14	200	–
Palmitoyl	18	195	295
Stearoyl	20	–	220

[a] Measured under a pressure of 3 kg/cm^2

Reproduced from Ref. 31. Copyright 1983 American Chemical Society.

demineralization by RO membranes should be critically reexamined.
Consider the following:

(1) The structures of the skins of integrally-skinned and thin
film composite membranes are known (6,21,22) to be different in
kind from those of the thick dense films of the type which are
utilized to determine "intrinsic" salt rejections.

(2) Matsuura and Sourirajan (32) have calculated that RO
membranes have pores with two different pore size distributions.

(3) Katoh and Suzuki (33) have developed an electron microscope
(EM) technique which enables them to establish the presence of
pores within integrally-skinned CA RO membranes.

(4) Panar, Hoehn and Hebert (22) have obtained EM evidence
that imperfections in the form of incompletely fused micelles exist
in the skins of internally-skinned membranes. It seems probable
that these gaps represent the larger of the two pore size
distributions calculated in Reference 32 and seen in Reference 33.

(5) Mathematical treatments (34) of various models suggest
that pore defects combined with predictions from solution-diffusion
theory yield the best agreement between theory and experiment.

With these thoughts in mind, it is time to restrict RO
performance predictions using the solution-diffusion model to some
specially prepared, defect-free, dense films. Such films are
unrelated to any functional membrane of either the integrally-
skinned or the thin film composite type.

Perhaps because much attention has centered on reverse osmosis
membranes, the fine pores present in their skins were observed
prior to the discovery of the functionally larger pores of
ultrafiltration (UF) membranes. Recently, pores of $\sim$30 Å have been
observed by Zeman (35) in the skins of UF membranes. Their density,
uniformity and diameters leave no doubt that these are actually the
pores which function during UF. Our ability to actually "see" the
intermicellar defect pores (the population of larger size pores) in
the skins of RO membranes extends to the 10 Å range. Therefore, it
is reasonable to expect that at some point we shall be able to
extend this ability to the population of smaller sized pores, whose
existence is predicted by Sourirajan's pore theory (36).

The list of polymer membrane materials is virtually endless
insofar as possible chemical varieties are concerned (37). However,
the number of fundamental physical structures into which they may
be formed is much more limited. For present purposes, a distinction
is made between skinned and skinless membranes. However, in view
of the substantial and growing evidence cited above for the
existence of pores in RO and UF membranes, even this is done with
trepidation. Further subdivision results in three types of skinned
membrane: *integrally-skinned ultragels, integrally-skinned
microgels* and *nonintegrally-skinned microgels* (that is, thin film
composite membranes). Such skinned membranes are utilized in gas
separations, reverse osmosis and ultrafiltration.

On the other hand, two types of skinless membranes are
discernible for use in microfiltration and related applications:
isotropic (actually, slightly anisotropic) microgels and highly
anisotriopic microgels. The former are the conventional
microfiltration membranes of commerce. Both surfaces of the
conventional membrane are similar in appearance and the cross-

section reveals only a slight degree of anisotropy with little difference in pore and cell size from one surface to the other. In contrast, a considerable difference is apparent between the pore sizes at opposite surfaces of the highly anisotropic microgel. SEM photomicrographs reveal a *degree of anisotropy*, DA, (that is, a difference in pore size from one surface to the other) of approximately five (38). The cross-section indicates the presence of two integral layers, the thicker of which contains the coarser cells.

A simple but graphic illustration of the morphology of anisotropy is also afforded by a wick test. In this procedure, a hollow-point pen is brought into contact with either surface of a microfiltration membrane. Circular ink stains of unequal diameter then appear on the opposite side of the filter. Photomicrographs of the cross-sections of the stained membranes indicate wicking patterns attributable to differences in capillarity. A low degree of anisotropy leads to minimal wicking. An intermediate degree of anisotropy leads to modest wicking. A high degree of anisotropy leads to maximum wicking. In the last of these, an integral bilayer is indicated; one layer consisting of fine cells (in which capillarity is quite pronounced) and the other of much coarser cells.

This gradiation of pore sizes from one surface to the other confers upon the filtration capacity of a prefilter-filter combination these upon integral bilayers and accounts for their significantly higher dirt-holding capacity. Because the fine-pored layer of highly anisotropic membranes is only a fraction of the overall membrane thickness, its cells and pores are deliberately made smaller than those of a similarly rated isotropic membrane filter. For example, a 0.2 μM rated highly anisotropic membrane may have pores in its fine layer of ∿0.15 or even 0.1 μm and pores in its coarse layer as large as 10 μM. In the latter case DA equals 100.

Highly anisotropic membranes are produced by manipulation of casting solution parameters such as solvent volatility and environmental factors such as temperature and relative humidity. These variables influence the kinetics of phase inversion, gelation, syneresis and capillary depletion. The surface of the membrane which constitutes the air/solution interface during its nascent phases becomes the fine-pored side of the finished membrane. During filtration, however, it is the coarse-pored side of the membrane which is positioned to face the feed solution. When this is done, the throughput of the highly anisotropic membrane is much greater than that of the conventional isotropic type. The throughput is greatly diminished, however, when the fine-pored surface faces the feed, although it is still roughly equivalent to that for the coarser-pored surface of the conventional membrane.

Composite Membranes

The combination of two or more membranes in series results in a composite membrane. The permeability constant P for a composite membrane may be expressed (39)

$$\frac{1}{P} = \sum_{1}^{n} \frac{x_i}{\ell} \frac{1}{P_i}$$

When P = overall permeability constant

    n = number of layers of membrane, each of thickness x

    ℓ = total thickness of the composite structure

    The permeability constant of the composite membrane is therefore represented by the harmonic average of the permeability constants of the individual layers, the respective weights being x_i/ℓ, the ratio of layer thickness to the total. Although composite membranes include layers of dense films or even liquid layers in series with films, in this discussion the term is being limited to those series in which at least one of the members is a phase inversion membrane of either the integrally-skinned or skinless variety.
    In the case of a composite membrane consisting of a skinless porous substrate and a dense film, permeability and permselectivity may be determined solely by the resistance of the denser film. Different membrane polymers may therefore be employed for the thin barrier layer and the thick support structure. This permits a combination of properties which are not available in a single material. Such membranes were initially developed for desalination by reverse osmosis where they are known as thin- or ultrathin-film composites or nonintegrally-skinned membranes. A second type of composite membrane is utilized for gas separations. It is a composite consisting of an integrally-skinned or asymmetric membrane coated by a second, more permeable skin which is used to fill skin defects. The inventors of the latter have entitled their device a *resistance model* membrane, but the present author prefers the term *coated integrally-skinned composites.*
    Thin film composites all utilize a pre-existing porous membrane as a support onto which a thin barrier layer film is deposited. The porous support layer is a skinless microgel with approximately 0.1 µM pores and, in most cases, consists of polysulfone.
    The porous support layer can be combined with the thin film to form the thin film composite membrane in a variety of ways:
    (1) A dilute solution of a preformed polymer can be separately cast onto water, preferably from a surface active spreading solvent such as cyclohexanone. The thin film is then laminated onto a porous support layer. This approach was originally developed by Carnell and Cassidy (40) and was first utilized by Cadotte and Francis in 1964 to coat microporous CA membranes. Petersen also utilized this approach to cast thin films of ethyl cellulose perfluorobutyrate which were then laminated to Celgard[®] and Tyvek[®] supports for use as blood oxygenation membranes (41).
    (2) Either a preformed polymer or a prepolymer solution can be applied by dip coating, wicking or some other transfer procedure directly onto the porous support where it is subsequently dried or cured. This procedure avoids the difficulty of handling thin films. It has the disadvantage that only solutions which do not interact

with the porous support may be utilized in the application of the
barrier layer. This is, of course, not a disadvantage if, as is
frequently the case, the coating can be applied from an aqueous
solution. This approach was first utilized in the application of
an aqueous solution of polyethyleneimine (PEI) and the subsequent
reaction with tolylenediisocyanate (TDI) in hexane to yield the
cross-linked polyurea constituting the North Star NS-100 membrane.
When PEI or an ethoxylated derivative of PEI were coated and reacted
with a hexane solution of isophthaloyl chloride, the resultant thin
film was a polyamide (NS-101 or PA-300). The reaction of furfuryl
alcohol with sulfuric acid resulted in a sulfonated polyfuran known
as NS-200. Recently, interest in coating and subsequent cross-
linking of a water-soluble sulfonated polysulfone has been revived.
     (3) *Plasma polymerization* involves the buildup of a dense
layer from the deposition of monomers produced in an RF plasma
(42). Such monomers are unrelated to those encountered in free
radical polymerization. Hydrophilic coatings can sometimes be
produced from materials which, prior to their conversion to a
plasma, were hydrophobic and *vice versa*. No commercial use is
being made of this approach at present.
     (4) *Interfacial polycondensation* of reactive monomers on the
surface of the porous support can also be used. The basic
interfacial polycondensation technique is known (43) to have a
number of unusual but desirable features among which the lack of
strict requirements for monomer purity and reagent stoichiometry
are perhaps the most outstanding. Cadotte (44) applied this
concept to the preparation of the commercially successful Film Tec
FT-30 desalination membrane. A polysulfone support is coated with
an aqueous solution containing at least 0.01% of m-phenylene
diamine. The coated membrane is then brought into contact with a
hexane solution containing trimesoylchloride. Reaction is swift
and terminates when the completed interfacial thin film inhibits
further reaction. Only slightly more than two of every three
carboxylic acid chloride groups condense so that the lightly
cross-linked final membrane polymer closely approximates the
formula:

$$\left[HN - \bigcirc - NHOC - \bigcirc_{COOH} - CO \right]_n$$
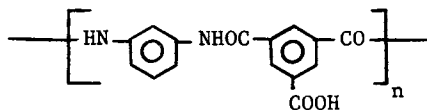
The high permeability of the FT-30 membrane is attributable to
the presence of the hydrophilic carboxyl groups. SEM
photomicrographs of the cross-section show that the barrier layer
is itself composed of several layers of varying density for a
total depth of approximately 0.25 μM. This thickness adds
physical strength in the form of flexibility and abrasion
resistance which earlier and thinner thin film barrier layers did
not possess. The fact that none of the thin film composites,
including FT-30, exhibits any appreciable resistance to oxidative
degradation by chlorine is believed to be coincidental with the
chemical characteristics of the particular thin films which have
thus far been investigated rather than with the nature of thin film

composites *per se.* The *cross-linked polyether* membrane (45) for example is so subject to degradation even by dissolved oxygen, that the feed must be continuously dosed with sodium bisulfite. On the other hand, thin film composites consisting of cross-linked thin films of sulfonated polysulfone are expected to be chlorine-resistant.

The finer the particles in a mixture the more difficult it is to obtain an appreciable difference in the rates at which they permeate a membrane. Thus, separation of bacteria from a suspension is routinely achieved with log reduction values (LRVs) =

$$\log_{10} \frac{\text{colony forming units (CFUs) in feed}}{\text{CFUs in product}}$$

of between 7 and 11 whereas the salt reduction factors (SRFs) =

$$\frac{(\text{salt concentration in feed})}{(\text{salt concentration in product})}$$

of 100 or less; that is, LRVs of 2, are the norm for desalination. In the case of many gas separations, even lower separation factors are observed. Furthermore, because the fluidity of gases is so high, the gas permeation rate of unseparated gas mixtures through porous imperfections in the skin layer of an integrally-skinned membrane can be so great as to overwhelm, by dilution of separated gas with unseparated gas mixture, the effects of whatever separation was achieved. Thus even CA/CTA blend membranes which are capable of SRFs of 100 in a desalination application, frequently encounter difficulty when utilized—after suitable drying—as gas separation membranes. Henis and Tripoldi (46) noticed this effect while investigating integrally skinned hollow fiber membranes of polysulfone and circumvented the problem by applying a coat of silicone-polymerized *in situ* to effectively seal any imperfections in the skinned polysulfone membrane against a high flow rate of unseparated feed gas mixture. This approach should be applicable to virtually any skinned membrane. The sealing polymer coat itself need not be capable of separating gaseous mixtures so long as it is sufficiently permeable as not to significantly reduce the permeability of gases through the separating membrane while sufficiently impermeable to act as a barrier to the bulk flow of unseparated gases.

Structural Irregularities

A partial list of commonly encountered structural irregularities in phase inversion membranes includes: irregular gelation, wavemarks, macrovoids and blushing.

Irregular gelation can take many forms. Streaks or draglines may appear at the top side of the membranes; that is, the surface which constitutes the air/solution interface during the nascent phases of membrane formation. If a solution is close to the point of incipient gelation when it passes under the casting knife and is first exposed to air, virtually any imperfection, such as a scratch

on the blade surface, can serve to nucleate a gel particle. This particle can adhere to the blade and cause the formation of streaks when additional gel particles are nucleated in the solution passing under the original site. Such premature gelation is prevented by the elimination of nucleation sites, for example, by polishing the casting blade and by postponing gelation until the solution is a safe distance downstream from the casting blade. The latter is usually accomplished by the installation of a *quiet zone* immediately downstream from the hopper. An impermeable plate, a few centimetres in length, is positioned close to the surface of the casting solution to maintain the concentration of solvent vapor sufficiently high to prevent gelation until the solution has passed beneath the plate. Another type of irregular gelation is visible as subsurface imperfections which are most easily seen during light box inspection. Although such subsurface gel particles are often only a cosmetic defect, they can be at times more serious and do represent a potential locus of failure, for example, when roll stock is convoluted for inclusion in pleated cartridges. Such subsurface gels are usually traceable to inadequate filtration of the casting solution. Good manufacturing practice requires that a casting solution be constantly recirculated through a filter after mixing. It then receives a final filtration just prior to being fed into the casting hopper. Any particle, however minute, represents a potential nucleation site for random gelation. This can sometimes be seen in the form of irregular snowflake patterns during capillary depletion. Ordinarily, snowflake patterns appear in an even line in the transverse direction across the entire width of the membrane. If they appear on one side earlier than on the other, the membrane is thinner in that area. If snowflakes suddenly appear randomly, this may indicate a thin spot or even a pinhole. Both defects are apparent during light box inspection.

As the name implies, *wavemarks* are encountered only in wet process membranes. The casting solution enters the nonsolvent bath at which point a skin is formed. Interfacial tension causes the gelation medium to adhere to the leading edge of the membrane. Continued motion of the nascent membrane into the nonsolvent medium causes the medium to break away and establish another leading edge. Wavemarks represent a thickening of the membrane at the crest of the wave and, depending on factors such as casting solution fluidity, can achieve varying amplitudes at the crests. The problem is overcome by adjusting the angle of entry of the casting solution into the nonsolvent bath.

Large (10 to 100 μM in the longest dimension) subsurface voids, teardropped, spherical, ellipsoidal or finger-like in shape are known as *macrovoids*. They represent at the very least, weak spots within the gel matrix, and at worst, that is when located near the high pressure surface of the membrane in pressure-driven applications, areas of potential rupture. In the past, when means for their elimination were unavailable, a virtue was made of them. It was even suggested that finger-like cavities were desirable in that they represented volume elements of low resistance which contributed to overall permeability. In fact, such cavities are never advantageous and should be avoided whenever possible. There are two basic reasons for the appearance of macrovoids. An

examination of SEM photomicrographs of membrane cross-section
usually permits the responsible cause to be established. When the
walls of the cavity are made up of open cells identical to the
structure of the undisturbed gel matrix, then the cavity is the
result of a trapped pocket of solvent vapor which has accumulated
in a subsurface domain faster than it can diffuse out. If the
surrounding matrix gels before the solvent vapor can depart, then a
skinless cavity wall remains. The presence of a high concentration
of solvent prevents the skinning of the cavity walls. Such voids
can be eliminated by minimizing the buildup of solvent vapor by
lowering solution viscosity and/or by lowering the environmental
temperatures.

        Another cause of similar voids is the physical entrapment of
air bubbles owing to leaks in the hopper area or to too rapid an
influx of casting solution into the hopper. When the cavity walls
are skinned, this is a clear indication that nonsolvent intrusion
from the gelation bath has taken place. Such intrusions can occur
irregularly when certain voids close to the surface rupture for any
reason prior to the gelation of the matrix surrounding the void.
Thus a given membrane can contain voids with skinned as well as
skinless interior surfaces. The finger-like cavities, on the other
hand, appear on a regular basis with predominantly skinned interior
surfaces. Cabasso has shown that no permeation of product takes
place through these cavities which represent useless dead space
(22). They appear to be due to skinning of somewhat too fluid
solutions followed by *osmotic shock* to the formed skin. The skin
subsequently ruptures, permitting the rapid intrusion of nonsolvent
into the still fluid substructure. Gelation eventually takes place
in the matrix surrounding the finger-like intrusions of water. The
surface pores, which result from the rupture of the skin are the
reason why such UF membranes are unable to quantitatively remove
bacteria whereas nominally coarser microfiltration membranes can.
They can be avoided, or at least minimized, by the addition of
solvent to the gelation medium to lessen the osmotic shock and by
utilizing more viscous casting solutions.

        The presence of a fine white powder on one or both surfaces of
a polymer film or membrane following wet or dry casting is known as
blushing. Microscopical examination shows that the powder consists
of spherical particles characteristic of polymer lattices. The
presence of these particles is, or can be, deleterious because the
potential exists for their inadvertent sloughing off and adding to
the product stream, the purification of which was the principal
reason for utilizing a supposedly integral membrane in the first
place. These particles consist of the most soluble polymer
components within the casting solution. They are the constituents
remaining in solution the longest, which means that they are soluble
in the solvent system even after it has become depleted of most of
the more volatile true solvent. Furthermore, it is likely that
they consist of lower molecular weight fractions because they are
more soluble than higher molecular weights.

        Water is, in most instances, a strong nonsolvent; making it a
causative factor in the occurrence of blushing. After phase
inversion and gelation but prior to capillary depletion, the
membrane gel is still filled with the less volatile nonsolvent

components of the casting solution. Only residual amounts of true
solvent remain. Therefore, any polymer remaining in solution is in
a metastable state. The presence of water, either in the solution
or in the atmosphere, acts to precipitate the remaining polymer.
Blushing can appear at either or both surfaces. When it appears on
the surface exposed to air during drying, it is the result of
poreformer (nonsolvent) liquid which has been expelled through this
surface in the gel contraction known as *syneresis*. The expelled
liquid contains the last traces of polymer in solution. Their
precipitation, as latex particles at this point, depends on relative
humidity and the composition of the syneresed liquid. The presence
of blushing on the bottom surface, on the other hand, depends on
the composition of the liquid which is still within the gel near
the bottom surface.

    There are several ways to prevent or minimize blushing:

    (1) Addition of a high-boiling (retarder) solvent to the mix.
This is the approach taken for polymer films. It must be utilized
judiciously with membranes because it can lead to loss of porosity.
The presence of a solvent as the last liquid component to leave the
scene prevents precipitation.

    (2) Elimination of water from the casting solution and/or
reduction of relative humidity.

    (3) Employment of poreformers such as 1-butanol which carry
the water with them as they evaporate.

Literature Cited

1. Kesting, R. E. In "Cellulose and Cellulose Derivatives, Part
    V"; Bikales, N.; Segal, L., Eds.; Wiley-Interscience: New
    York, 1971; Chap. XIX.
2. Cahn, J. J. Chem. Phys. 1963, 42, 93.
3. Strathmann, H. In "Materials Science of Synthetic Membranes";
    Lloyd, D. R., Ed.; American Chemical Society: Washington,
    D.C., 1985.
4. Maier, K.; Scheuermann, E. Kolloid Z. 1960, 171, 122.
5. Helmeke, J.-G. Kolloid Z. 1954, 135, 29.
6. Kesting, R. E. J. Appl. Polym. Sci. 1973, 17, 1771.
7. Kesting, R. E.; Cunningham, L.; Morrison, M.; Ditter, J.
    J. Parenteral Drug Assoc. 1983, May/June, 98.
8. Scheludko, A. Kolloid Z. 1957, 155, 39.
9. Kesting, R. E. U.S. Patent 3 945 926.
10. Cabasso, I. In "Ultrafiltration Membranes and Applications";
    Cooper, A., Ed.; Plenum Press: New York, 1980.
11. Kesting, R. E. U.S. Patent 3 957 651.
12. Bjerrum, N.; Manegold, E. Kolloid Z. 1927, 42, 97.
13. Kesting, R. E.; Barsh, M.; Vincent, A. J. Appl. Polym. Sci.
    1965, 9, 1873.
14. Chawla, A. S.; Chang, T.M.S. J. Appl. Polym. Sci. 1975, 19,
    1723.
15. Kesting, R. E.; Manefee, A. Kolloid Z. & Z. Polym. 1969,
    230(2), 341.
16. Brown, W. Biochem. J. 1915, 9, 591.
17. Castro, A. U.S. Patent 4 247 498.

18. Hiatt, W. C.; Vitzthum, G. H.; Wagener, K. B.; Gerlach, K.; Josefiak, C. In "Materials Science of Synthetic Membranes"; Lloyd, D. R., Ed.; American Chemical Society: Washington, D.C., 1985.

19. Paul, D. R.; Newman, S., Eds. "Polymer Blends, Vol. I and II"; Academic Press: New York, 1978.

20. Loeb, S.; Sourirajan, S. U.S. Patent 3 133 132.

21. Schultz, R.; Asunmaa, S. Recent Prog. Surface Sci. 1970, 3, 291.

22. Panar, M.; Hoehn, H.; Hebert, R. Macromol. 1973, 6, 777.

23. Gittens, G.; Hitchcock, P.; Wakely, G. Desalination 1973, 2, 315.

24. Trudelle, Y.; Nicolas, L. Presented at Paris Membrane Symposium; December, 1966.

25. Krishnamurthy, S.; McIntrye, D. In "Reverse Osmosis Membrane Research"; Lonsdale, H. K.; Podall, H., Eds.; Plenum Press: New York, 1972.

26. Lonsdale, H. K. In "Industrial Processing with Membranes"; Lacey, R.; Loeb, S., Eds.; Wiley-Interscience: New York, 1972.

27. Morrow, L.; Sauer, J. Rpt. to OSW on Grant 14-01-0001-2130; 1969.

28. Kesting, R. E. "Synthetic Polymeric Membranes"; McGraw-Hill: New York, 1971.

29. Richter, J.; Hoehn, H. H. U.S. Patent 3 567 732.

30. Kesting, R. E.; Newman, J.; Nam, K.; Ditter, J. Desalination 1983, 46, 343.

31. Shiraishi, N. Chem. Tech. 1983, June, 366.

32. Chan, K.; Tinghui, L.; Matsuura, T.; Sourirajan, S. I&EC Prod. Res. & Dev. 1984, 23, 116-125, 124-133.

33. Katoh, M.; Suzuki, S. In "Synthetic Membranes"; Turbak, A. F., Ed.; ACS Symp. Series No. 153, American Chemical Society: Washington, D.C., 1981.

34. Applegate, L.; Antonson, C. In "Reverse Osmosis Membrane Research"; Lonsdale, H. K.; Podall, H., Eds.; Plenum Press: New York, 1972.

35. Zeman, L. In "Materials Science of Synthetic Membranes"; Lloyd, D. R., Ed.; American Chemical Society: Washington, D.C., 1985.

36. Sourirajan, S. I&EC Fund. 1963, 2, 51.

37. Lloyd, D. R.; Meluch, T.B. In "Materials Science of Synthetic Membranes"; Lloyd, D. R., Ed.; American Chemical Society, 1985.

38. Kesting, R. E.; Murray, S.; Newman, J.; Jackson, K. Pharm. Tech. 1982, 5(5), 52.

39. Bhargawa, R.; Rogers, C.; Stannett, V. T.; Szwarc, M. Tappi 1957, 40, 564.

40. Carnell, P.; Cassidy, H. J. Polym. Sci. 1961, 55, 233.

41. Petersen, R. U.S. Patent 4 210 529.

42. Yasuda, H. In "Reverse Osmosis and Synthetic Membranes"; Sourirajan, S., Ed.; NRCC Press: Ottawa, 1977.

43. Morgan, P. "Condensation Polymers"; Interscience: New York, 1965.

44. Cadotte, J. U.S. Patent 4 277 344; In "Materials Science of
     Synthetic Membranes"; Lloyd, D. R., Ed.; American Chemical
     Society: Washington, D.C., 1985.
45. Kuritara, K. U.S. Patent 4 366 062.
46. Henis, J.; Tripoldi, M. U.S. Patent 4 230 463; <u>J. Memb. Sci.</u>
     1981, <u>8</u>, 233; <u>Science</u> 1983, <u>220</u>, 11.

Production of Microporous Media by Phase Inversion Processes

H. STRATHMANN

Fraunhofer-Gesellschaft IGB, Nobelstrasse 12, 7000 Stuttgart 80, Federal Republic of Germany

The majority of todays membranes used in microfiltration, dialysis or ultrafiltration and reverse osmosis are prepared from a homogeneous polymer solution by a technique referred to as phase inversion. Phase inversion can be achieved by solvent evaporation, non-solvent precipitation and thermal gelation. Phase separation processes can not only be applied to a large number of polymers but also to glasses and metal alloys and the proper selection of the various process parameters leads to different membranes with defined structures and mass transport properties. In this paper the fundamentals of membrane preparation by phase inversion processes and the effect of different preparation parameters on membrane structures and transport properties are discussed, and problems utilizing phase inversion techniques for a large scale production of membranes are specified.

In recent years, microporous media such as microfiltration, ultrafiltration or reverse osmosis membranes have gained considerable technical and economical significance in mass separation processes. The membranes used today in the various separation processes differ considerably in their structure, their function and in the way they are produced (1). Preparation procedures for the different membrane types are described in patents and publications in detailed recipes, which are deeply rooted in empiricism. Superficially the preparation technique of a microporous polyethylene tube made by extrusion seems to have nothing in common with the preparation of an asymmetric skin-type reverse osmosis membrane made by the precipitation technique described by Loeb and Sourirajan (2). A more detailed analysis, however, indicates that the formation of both membrane types is determined by the same basic mechanism and governed by a process referred to by Kesting (3) as phase inversion. In fact, basically all polymeric ultrafiltration and reverse osmosis membranes and the majority of the microfiltration membranes, no matter how different their structures and their mass transport properties may be, are made by the phase inversion process. This process involves the conversion of liquid homogeneous polymer solutions of two or more components into a two-phase system with a solid, polymer-rich phase forming the rigid membrane structure and a liquid, polymer-poor phase forming the

membrane pores. Phase separation can be achieved with any polymer mixture, which forms, under certain conditions of temperature and composition, a homogeneous solution and separates at a different temperature or composition into two phases. To obtain a microporous medium such as a membrane requires both phases to be coherent. If only the solid phase is coherent and the liquid phase incoherent, a closed-cell foam structure will be obtained. If the solid phase is incoherent, a polymer powder will be obtained instead of a rigid structure.

The phase separation in polymeric systems is determined by thermodynamic and kinetic parameters, such as the chemical potentials and diffusivities of the individual components and the Gibb's free energy of mixing of the entire system. Identification and description of the phase separation process is the key to understanding the membrane formation mechanism, a necessity for optimizing membrane properties and structures.

Fundamentals of Phase Separation

Three different techniques are used for the preparation of state of the art synthetic polymeric membranes by phase inversion: 1. thermogelation of a two or more component mixture, 2. evaporation of a volatile solvent from a two or more component mixture and 3. addition of a nonsolvent to a homogeneous polymer solution. All three procedures may result in symmetric microporous structures or in asymmetric structures with a more or less dense skin at one or both surfaces suitable for reverse osmosis, ultrafiltration or microfiltration. The only thermodynamic presumption for all three preparation procedures is that the free energy of mixing of the polymer system under certain conditions of temperature and composition is negative; that is, the system must have a miscibility gap over a defined concentration and temperature range (4).

Thermogelation of a Two-Component Mixture.

The simplest procedure for obtaining a microporous system is the thermogelation of a two component mixture. At a specific temperature, the mixture forms a homogeneous solution for all compositions but at a lower temperature shows a miscibility gap over a wide range of compositions. This behaviour is illustrated schematically in Figure 1, which shows a phase diagram of a two component mixture of a polymer and a solvent as a function of temperature.

The points P and S represent the pure components polymer and solvent respectively, and points on the line P-S describe mixtures of these two components. If a homogeneous mixture of the composition X_p at a temperature T_1, as indicated by the point A in Figure 1, is cooled to the temperature T_2, as indicated by point B, it will separate into two different phases, the compositions of which are indicated by the points B' and B''. The point B' represents the polymer-rich solid phase and the point B'' the solvent rich, polymer poor liquid phase. The lines B'-B and B''-B represent the ratio of the amounts of the two phases in the mixture; that is, the overall porosity of the obtained microporous system.

Evaporation of a Volatile Solvent From a Three-Component Polymer Solution.

This method was one of the earliest used in making microporous membranes (5) and has subsequently been applied by Kesting for making reverse osmosis membranes in his dry or complete evaporation process (6). This process consists of a three-compound mixture: a polymer , a volatile solvent and a third component, which by itself is a nonsolvent for the polymer. This
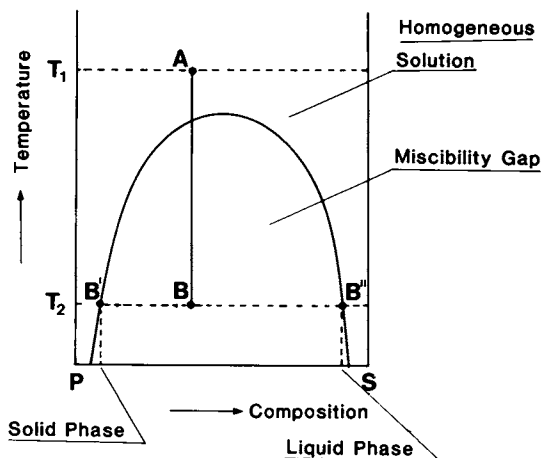
Figure 1.   Schematic diagram showing the formation of a microporous mem-
brane by thermal gelation of a polymer solution exhibiting a
miscibility gap at certain conditions of temperature and com-
position.

three-component mixture is completely miscible over a certain composition range and contains a miscibility gap over another composition range as indicated in Figure 2, which presents an isothermic phase diagram of the three components. The corners of the triangle represent the pure components. Boundary lines between any two corners represent mixtures of two components, and any point within the triangle represents a mixture of all three components. Within a certain compositionally defined range of thermodynamic states, all three components are completely miscible, whereas in a different range – the miscibility gap – the system decomposes into two distinct phases. If the volatile solvent is completely evaporated from a homogeneous mixture of 10 % polymer, 60 % solvent and 30 % nonsolvent, as indicated by point A in Figure 2, the composition of the mixture will change from that represented by point A to that represented by point B. At point B the system consists of only two components: polymer and nonsolvent. Since this point is situated within the miscibility gap, the system is separated into two phases: a polymer-rich phase indicated by point B' forming the rigid structure, and the phase B" forming the liquid filled pores of the membrane.

Addition of a Nonsolvent to a Homogeneous Polymer Solution. This technique is widely used today for the preparation of symmetric microfiltration membranes as well as for manufacturing asymmetric "skin-type" ultrafiltration or reverse osmosis membranes (7). The preparation procedure can again be rationalized with the aid of a three-component isothermic phase diagram shown schematically in Figure 3.

The phase diagram of the three-component mixture shows a miscibility gap over a large range of compositions. If a nonsolvent is added to a homogeneous solution consisting of polymer and solvent, as indicated by the point A on the solvent-polymer line, and if the solvent is removed from the mixture at about the same rate as the nonsolvent enters, the composition of the mixture will change following the line A - B. At point C, the composition of the system will reach the miscibility gap and two separate phases will begin to form: a polymer-rich phase represented by the upper boundary of the miscibility gap and a polymer-poor phase represented by the lower boundary of the miscibility gap. At a certain composition of the three-component mixtures, the polymer concentration in the polymer-rich phase will be high enough to be considered as solid. This composition is represented by point D in Figure 3. At this point the membrane structure is more or less determined. Further exchange of solvent and nonsolvent will lead to the final formation of the membrane, the porosity of which is determined by point B, which represents the mixture of the solid polymer-rich phase and the liquid phase which is virtually free of polymer and solvent as represented by points B' and B" respectively.

The thermodynamic description of the formation of microporous systems by means of the phase diagrams, as illustrated in Figures 1 to 3, is based on the assumption of thermodynamic equilibrium. It predicts under what conditions of temperature and composition a system will separate into two phases and the ratio of the two phases in the heterogeneous mixture. As related to the membrane formation procedure, the thermodynamic description predicts the overall porosity that will be obtained at specified states. However, no information is provided about the pore sizes, which are determined by the spatial distribution of the two phases. Equilibrium thermodynamics is not able to offer any explanation about structural variations within the membrane cross-section; that is, whether the membrane has a symmetric or asymmetric structure or a dense skin at the surface. These
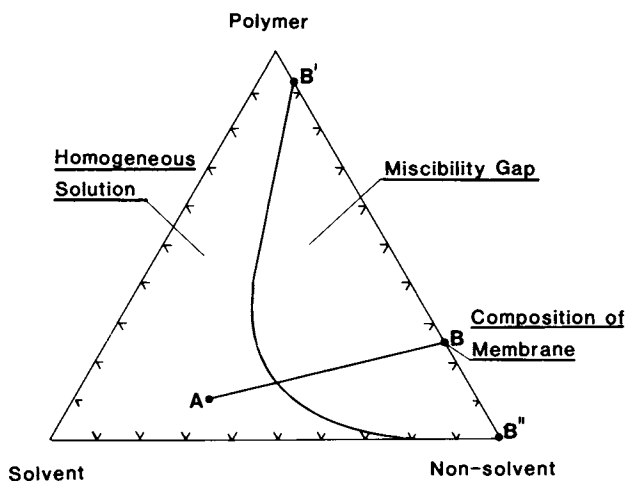
Figure 2. Schematic diagram showing the formation of a microporous membrane by evaporation of a solvent from a three-component polymer mixture exhibiting a miscibility gap at certain conditions of temperature and composition.
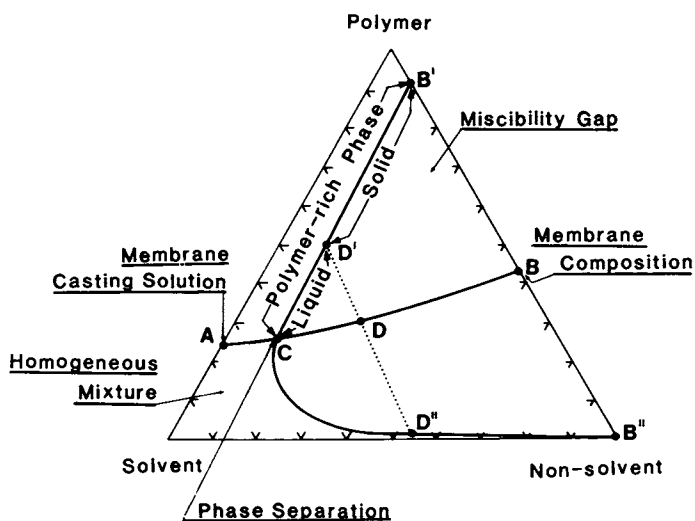
Figure 3. Schematic diagram showing the formation of a microporous membrane by addition of a non-solvent to a homogeneous polymer solution.

parameters are determined by kinetic effects, which depend on system properties such as the diffusivities of the various components in the mixture, the viscosity of the solution and the chemical potential gradients which act as driving forces for diffusion of the various components in the mixture. Because these parameters change continuously during the phase separation, which constitutes the actual membrane formation process, no transient states of equilibrium will be achieved. Especially in polymer systems, frozen states will often be obtained that are far from equilibrium and that can be stable for long time periods, on the order of years. The chemical potential and diffusivities of the various components in the system, and their dependencies on composition, temperature, viscosity, etc., are difficult to determine by independent experiments and therefore are not readily available. This makes a quantitative description of the membrane formation mechanism nearly impossible. A qualitative description, however, which allows rationalization of the membrane formation and correlation of the various preparation parameters with membrane structures and properties, is possible.

Experimental Procedures

The experimental procedures described in this paper are mainly concentrated on the preparation of membranes from various polymer-solvent systems by precipitation in a nonsolvent, generally water. The membranes are then characterized in terms of their transport properties and structures. Furthermore, the three-component phase diagrams are determined for various polymer-solvent-precipitant systems.

The Preparation of Phase Inversion Membranes. The preparation of phase inversion membranes is described in detail in the literature (7 - 9).

Description of Relevant Preparation Parameters. In the preparation procedure of phase inversion membranes several significant parameters determining the structure and properties of the membrane can be identified:

1. The polymer and its concentration in the casting solution
2. The solvent or solvent system
3. The precipitant or precipitant system
4. The precipitation temperature

In addition to these parameters several other procedures may affect the properties of the membrane, for example, an annealing step by which a membrane may be shrunk due to heat treatment or an evaporation step during which part of the solvent or solvents are evaporated from the surface of the film prior to precipitation.

Polymers, Solvents, Precipitants and Procedures Used in the Membrane Preparation Process. The majority of the membranes discussed in this paper are prepared from three different polymers; that is, cellulose acetate E-393-3 manufactured by Eastman Chemical Corporation, polysulfone PS 1700 made by Union Carbide and an aromatic polyamide Nomex made by DuPont. Dimethylsulfoxide (DMSO), dimethylacetamide (DMAc), dimethyformamide (DMF), n-methylpyrrolidone (NMP) and acetone served as solvents for the preparation of the casting solutions. Several additives such as benzene, tetrahydrofuran (THF), formamide and lithium chloride were used in the casting solution. Water, methanol, glycerole, formic acid and mixtures of these components were used as precipitants. The precipitation of membranes

was carried out at temperatures varying from $-30°$ to $+ 35°C$. The polymer concentration in the casting solution was varied between 5 and 25 wt % polymer. In some cases an evaporation step or a post treatment procedure in form of a heat treatment or chemical treatment was also part of the membrane preparation processes (10).

Characterization of the Membranes in Terms of Structure and Transport Properties. The membranes are generally characterized in terms of their mass transport properties, that is their transmembrane fluxes and molecular weight cut-off, by filtration tests using hydrostatic pressure differences between 5 and 100 bar. The membrane structures are studied by scanning electron micrographs.

Determination of the Three-Component Phase Diagrams. The phase diagrams of four different polymer-solvent-precipitant mixtures were determined using the cloud point method and analysing the two phases obtained during the phase separation. The process is described in detail elsewhere (10).

Rate of Polymer Precipitation During Membrane Formation. The rate of precipitation of the polymer during the membrane formation process was determined by precipitating films of different thickness and by an optical microscope using a technique described in the literature (11).

Experimental Results and Discussion

General Observations. In this part of the paper several general observations concerning membrane structures, filtration properties and preparation procedures are described.

The Membrane Structure. Using scanning electron microscope techniques, four different rather typical structures shown in Figures 4a to d can be observed with phase inversion membranes. Photograph a) shows a cross-section of a microfiltration membrane prepared from a cellulose nitrate solution by precipitation with water vapor in a humidity controlled environment. The membrane shows a "sponge"-like structure with no skin on the bottom or top surface. Photograph b) shows a cross-section of a typical ultrafiltration membrane prepared from a polyamide solution and precipitated in water by immersing the polymer solution into a water bath. The membrane shows a "finger"-type structure with a dense skin at the surface and large pores penetrating the entire membrane cross-section. The pores increase in diameter from the top to the bottom side. Photograph c) shows the cross-section of a typical reverse osmosis membrane prepared from a polyamide solution and precipitated in water by immersing the polymer solution into a water bath. The membrane shows a sponge-type structure with a dense skin at the surface and a porous structure underneath with increasing pore diameter from the top to the bottom side of the membrane. The only differences in the preparation procedures of the membranes shown in photographs b) and c) are the polymer concentration and the precipitation temperature. Photograph d) shows the cross-section of a reverse osmosis membrane prepared from a polyamide solution and precipitated in a water-solvent mixture. The membrane shows a sponge-type structure with a dense skin at the surface and a porous structure underneath with a relative uniform pore size distribution over the entire cross-section. Membranes with this type of structure can usually be dried without changing their mass-transport properties.
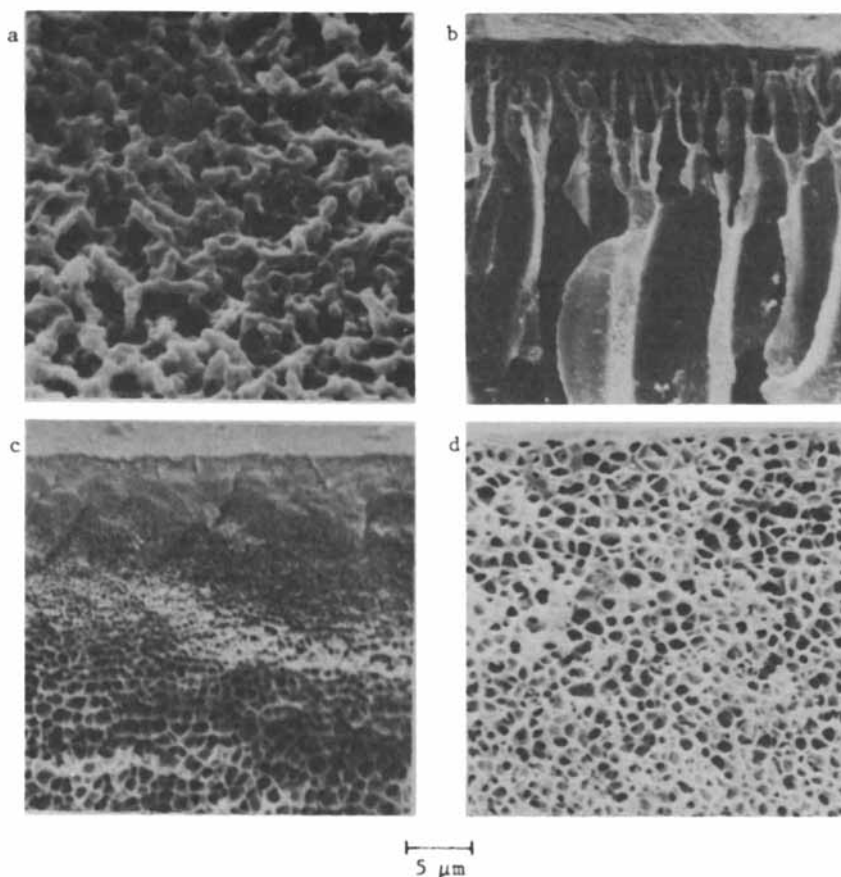
Figure 4. Scanning electron micrographs of membrane cross-sections with typical structures:

a) symmetric microporous membrane without a skin

b) asymmetric membrane with a "finger"-type structure and a dense skin at the surface

c) asymmetric membrane with "sponge"-type structure, a dense skin at the surface and a porous substructure with increasing pore diameters from the top to the bottom side of the membrane

d) asymmetric membrane with a "sponge"-type structure, a dense skin at the surface and a porous structure with uniform pore size distribution over the entire cross-section.

<u>The Polymer, Polymer Concentration and the Membrane Structure.</u>   The
scanning electron micrographs of Figures 5a to c show the cross-sections
of three membranes with nearly identical structures and ultrafiltration
properties listed in Table I prepared from three different polymers; that is
cellulose acetate, polyamide and polysulfone, by precipitation in a water
bath. The scanning electron micrographs of Figures 6a to c show the
cross-sections of membranes made from one polymer-solvent system; that
is polyamide in DMAC, with different polymer concentrations. These mem-
branes show completely different structures and filtration properties which
are listed in Table II. The results of Figures 5 and 6 indicate that the same
type of membrane can be prepared from various polymers and that from
one polymer various types of membranes can be made.

Table I.   Filtration properties and porosities of membranes prepared from
           different polymer-solvent systems by precipitation in water

Polymer	Filtration rate[*] (cm/s)	Rejection[+] (%)		Membrane porosity (%)
		γ-globulin	bov.albumin	
Cellulose acetate in DMAc	3.5×10^{-3}	99	98	80
Polyamide in DMSO	2.1×10^{-3}	97	72	82
Polysulfone in DMF	1.9×10^{-3}	96	80	83

* The filtration rates were determined with DI-water at 2 bar and room
  temperature
+ The rejections were determined at 2 bar and room temperature with
  solution of 1 % γ-globulin and bov. albumin

Table II.   Filtration properties and porosities of membranes prepared from
            a polyamide-DMAc-water system

Polymer-concentration	Precipitant	Porosity (%)	Filtration rate[*] (cm/s)	Rejection[+]	Structure
10 % polyamide in DMAc	water vapor	89	2×10^{-1} at 2 bar	0 % for Dextran 100	symmetric "sponge"-type
10 % polyamide in DMAc	water	79	1.8×10^{-3} at 2 bar	88 % for bov.albumin	asymmetric "finger"-type
22 % polyamide in DMAc	water	71	8×10^{-5} at 100 bar	99 % for $MgSO_4$	asymmetric "sponge"-type

* The filtration properties were determined with deionized water and solu-
  tions of 1 % solids at room temperature
+ The molecular weight of Dextran 100 was approximately 2 million Dalton
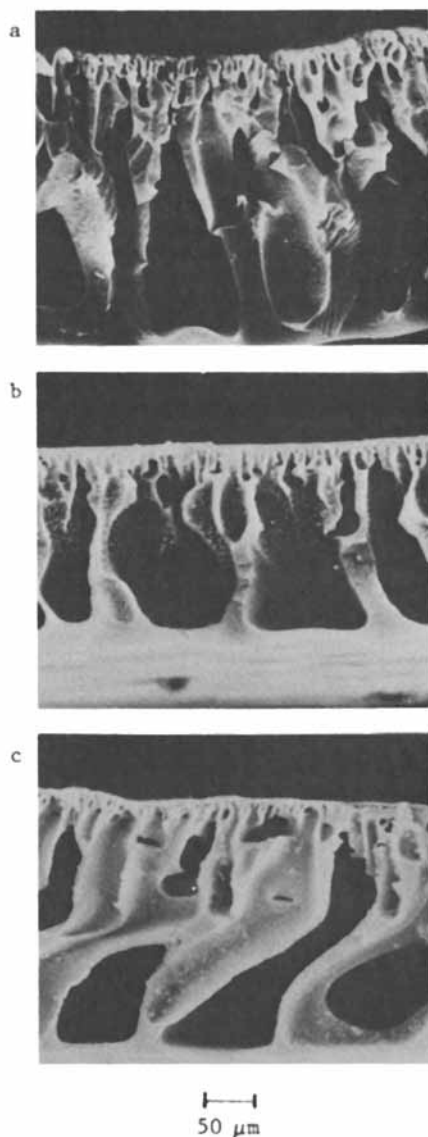
Figure 5.   Scanning electron micrographs of membrane cross-sections pre-
pared from three different polymer-solvent systems by precipita-
tion in water:

a) 12 % cellulose acetate in DMAc
b) 12 % polyamide in DMSO
c) 12 % polysulfone in DMF.

18 μm
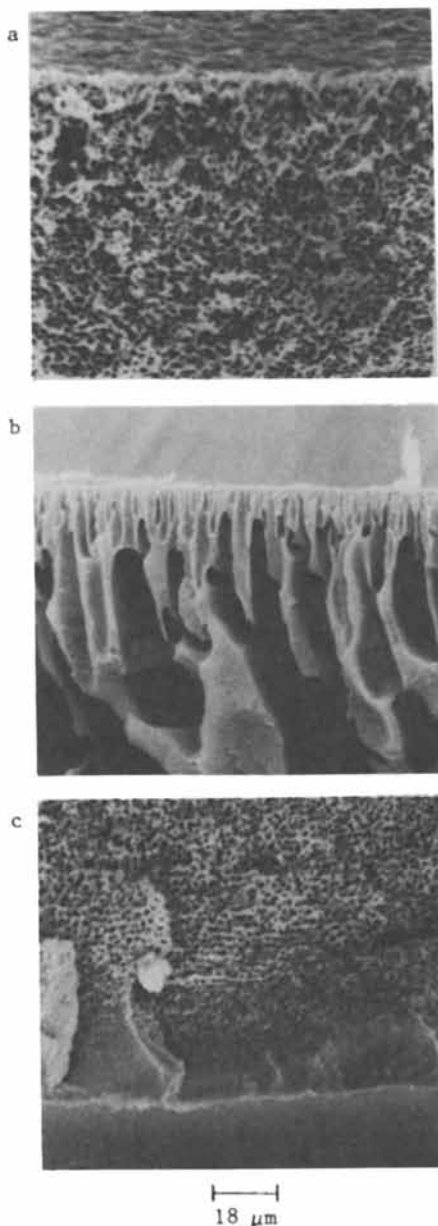
Figure 6.   Scanning electron micrographs of membrane cross-sections pre-
pared from polyamide solutions of different concentration and
by different precipitation procedures:
a) 10 % polyamide in DMAc precipitated by water vapor
b) 10 % polyamide in DMAc precipitated in a water bath
c) 22 % polyamide in DMAc precipitated in a water bath.

Precipitation Rate and Membrane Structure. Characteristic membrane
structures can generally be correlated with the rate of precipitation of the
polymer solution. Figure 7 shows two series of photographs taken during the
precipitation process under an optical microscope. The magnification and
the time interval at which the photographs were taken is the same in both
cases. The rate of precipitation slows down as the precipitation front moves
further into the casting solution. The photographs also show that the
finger-type structure precipitates much faster than the sponge-type structure.
There are various simple means by which the rate of precipitation can be
altered. An increase in the polymer concentration of the casting solution
generally results in an decrease in the precipitation rate and a transition
from a finger-type structure to a sponge-type structure. Figure 8 shows the
structure of membranes prepared from a polyamide-NMP casting solution
of various polymer concentrations by precipitation in water at room tempera-
ture. In Table III the precipitation rates and the filtration properties of
these membranes are summarized. The same effect can be achieved using
different fluids as precipitants as indicated in Figure 9 and Table IV where
the structures and precipitation rates of different membranes prepared from
a solution of 15 % polyamide in DMAc by precipitation in different fluids
are shown. Going from formic acid to glycerin in the precipitation bath,
the rate of precipitation decreases drastically and the structure changes
from a finger- to sponge-type structure. Various solvents or solvent mixtures
may lead to the same result as indicated in Figure 10 and Table V where
the structures, precipitation rates and filtration properties of membranes
prepared from a solution of polyamide in DMAc and DMAc-benzene mixtures
are shown. In all cases, fast precipitation leads to a finger-type structure
and slow precipitation generally results in a sponge-type structure.

Table III. Rates of precipitation and filtration properties of membranes
            prepared from polyamide-NMP solution of various polyamide con-
            centrations by precipitation in water at room temperature

| Polymer-concentration (%) | Rejection[+] | | | Filtration rate (cm/s x 10^4) | Porosity (vol.%) | Precipitation rate (s) |
	$MgSO_4$	Cytochrome C	bov. albumin			
5 x	0	0	10	56	91	32
10 x	0	43	84	32	85	40
15 x	8	92	100	9	81	52
18 xx	75	100	100	18	79	83
20 xx	90	100	100	4	77	142
22 xx	98	100	100	1,6	76	212

+ The rejection was determined with solutions of 1 % solids
x) applied pressure 5 bar
xx) applied pressure 100 bar

Specific Experimental Results and Their Discussion. In this part some
specific test results, which are rather helpful in rationalizing the formation
mechanism of phase inversion membranes, will be described and discussed.

The Ternary Phase Diagram. The ternary phase diagrams of various poly-
mer-solvent-precipitant systems have been determined. The results shown in
Figure 11 indicate that the phase diagrams determined for the systems
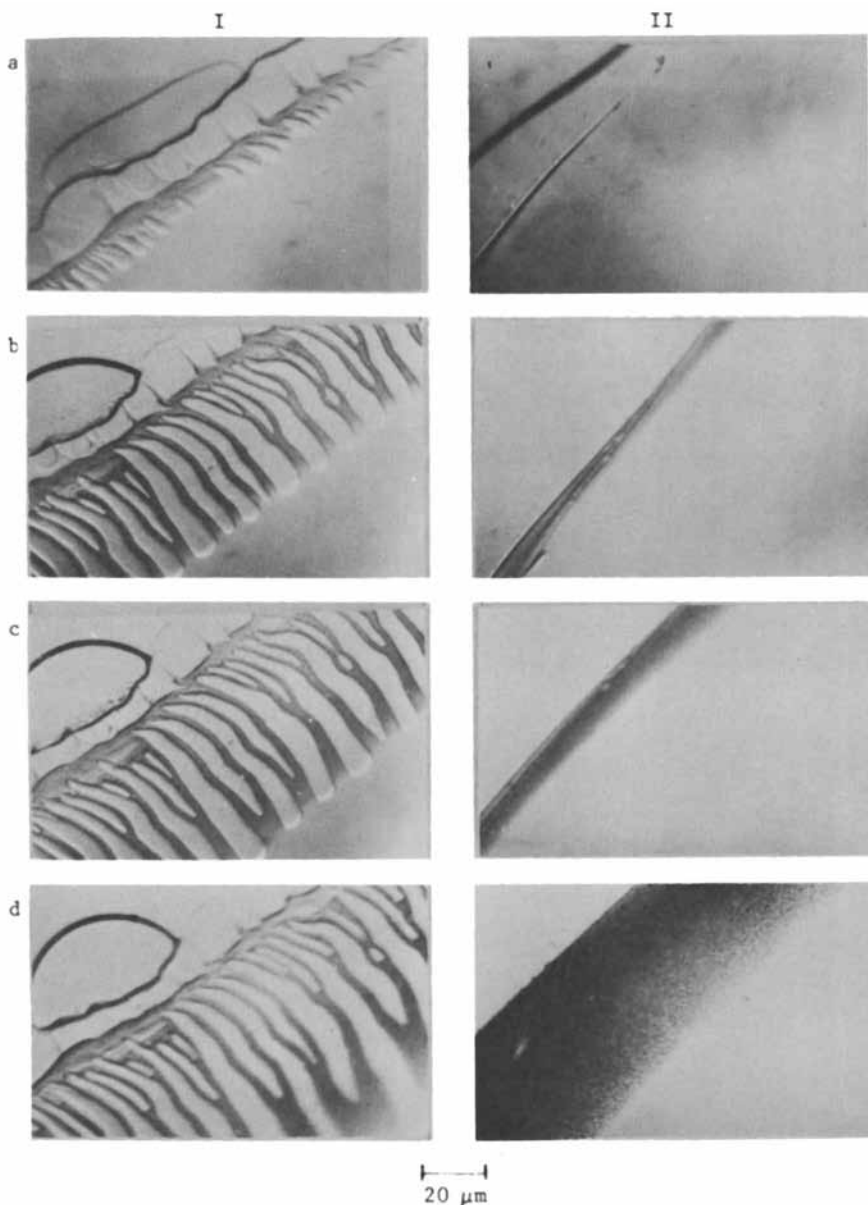
Figure 7.   Photo-micrographs of the casting solution/precipitant interphase at (a) the beginning of the precipitation and after (b) 12 sec., (c) 24 sec. and (d) 5 min. Series I giving a "finger"-type structure and series II giving a "sponge"-type structure.
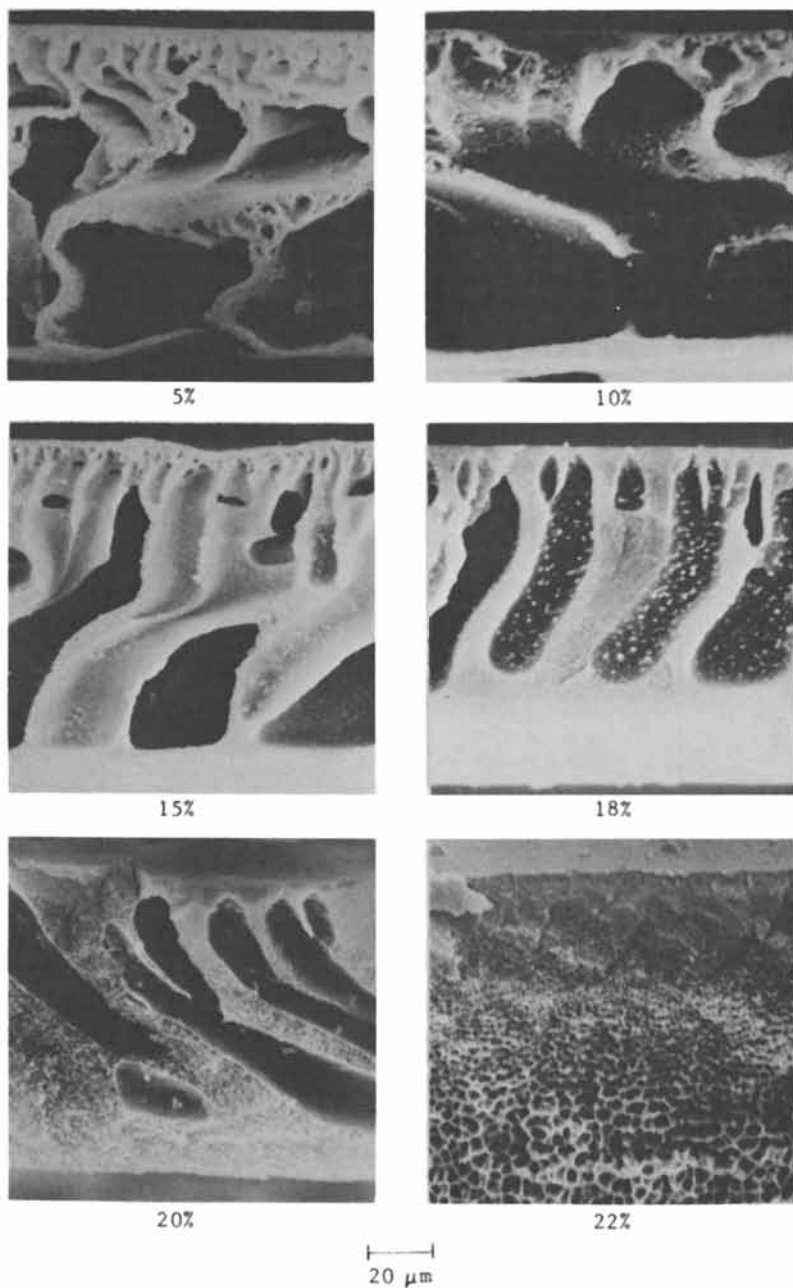
Figure 8.   Scanning electron micrographs of membrane cross-sections prepared from various polyamide concentrations in NMP by precipitation in water at room temperature.

formic acid

methanol

water

acetone

acetic anhydride

glycerol

|—————————|
50 μm
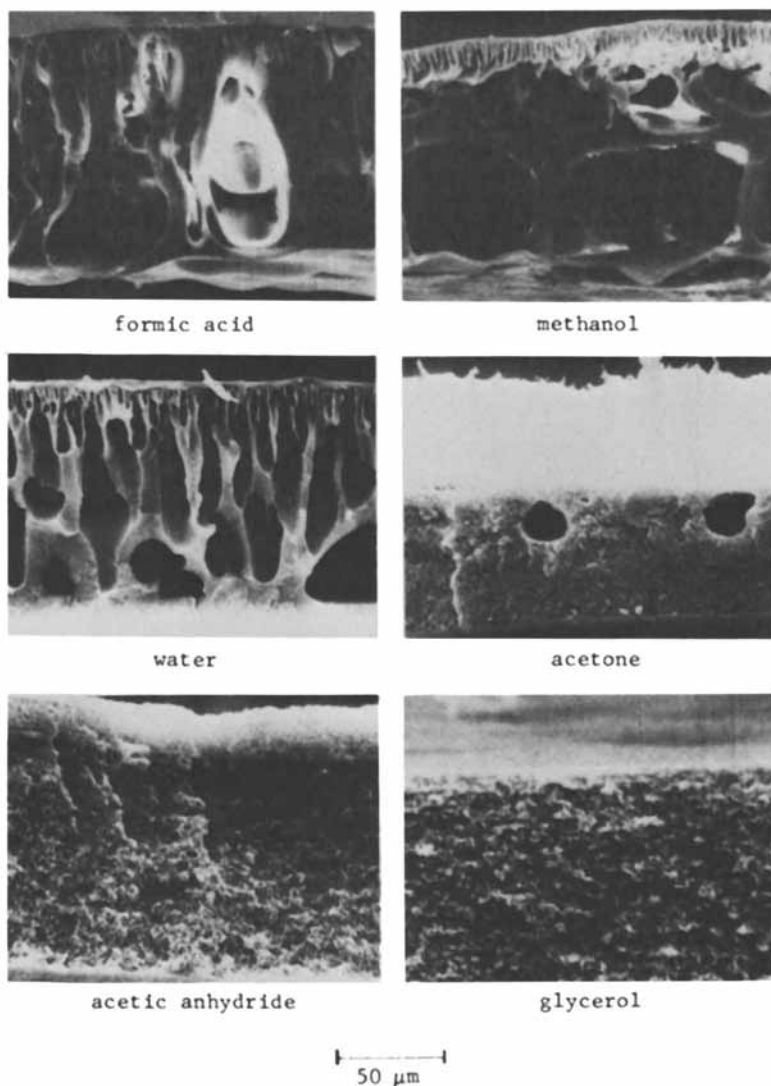
Figure 9.   Scanning electron micrographs of membrane cross sections prepared from a casting solution of 15 % polyamide in DMAc precipitated at room temperature in various precipitation media.
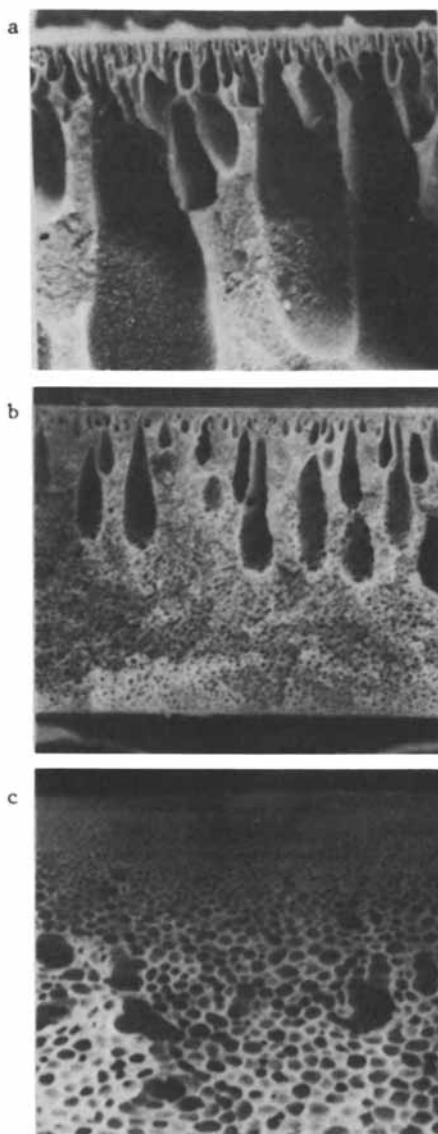
Figure 10.   Scanning electron micrographs of membrane cross-sections pre-
pared from a solution of 15 % polyamide in a) DMAc b) 75 %
DMAc and 25 % benzene and c) 60 % DMAc and 40 % benzene
by precipitation in water at room temperature.

Table IV. Rates of precipitation and structures of membranes prepared from a casting solution of 15 % polyamide in DMAc by precipitation in different media

Precipitant	Rate of precipitation (sec)	Membrane structure
Formic acid	32	"finger"-type structure
Methanol	39	" " "
Water	50	" " "
Acetone	110	"sponge"-type structure
Acetic anhydride	234	" " "
Glycerol	667	" " "

Table V. Precipitation rate and filtration properties of membranes prepared from a solution of 15 % polyamide in DMAc or DMAc-benzene mixtures by precipitation in water at room temperature

Solvent	Precipitation rate (s)	Filtration rate[x] $(cm/s \times 10^4)$	Rejection[xx] (%)
DMAc	50	18	5
75 % DMAc 25 % benzene	180	13	53
60 % DMAc 40 % benzene	340	28	76

x The filtration rate was determined with deionized water at 5 bar applied pressure

xx The rejection was determined with a solution of 1 % bacitracin in DI-water
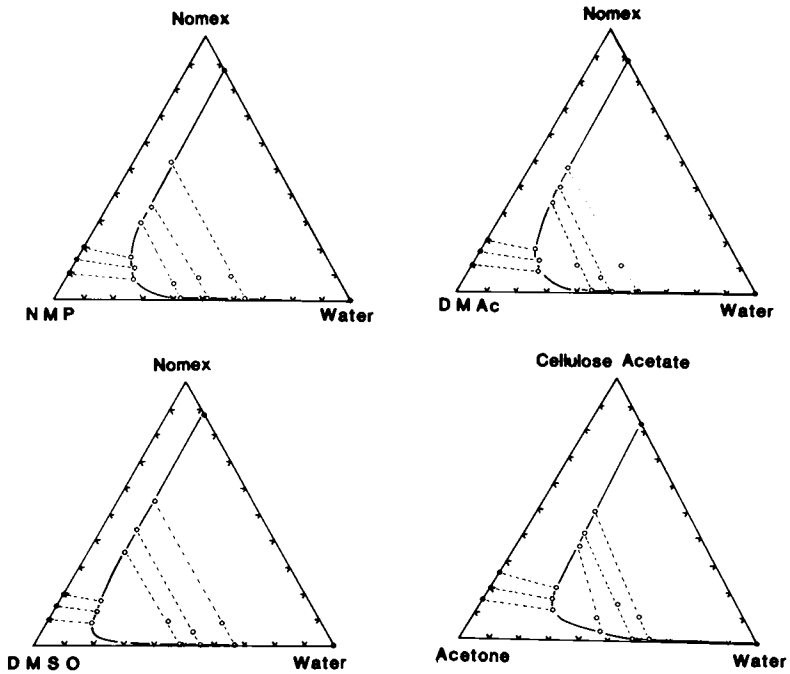
Figure 11. Three-component phase diagram at 25 °C at the systems polyamide-NMP-water, polyamide-DMAC-water, polyamide-DMSO-water, and cellulose acetate-acetone-water.

a) polyamide-NMP-water, b) polyamide-DMAc-water, c) polyamide-DMSO-water and d) cellulose acetate-acetone-water look similar to the phase diagram shown schematically in Figure 3. However, as indicated during the discussion of the membrane formation, the phase diagram is the description of an equilibrium state. It reflects the conditions under which a multi-component mixture is either stable as a homogeneous phase or decays into two separate phases. In macromolecular systems, however, equilibrium is frequently never reached and the phase separation is largely governed by kinetic parameters, which are rather difficult to determine for systems with more than two components. For simplicity, the basic thermodynamic and kinetic relations of the phase separation process are first discussed briefly for a binary system. These relationships, however, are also valid for multi-compound systems and can therefore be applied to rationalize the membrane formation mechanism.

Thermodynamic Description of a Binary System With Limited Miscibility. The thermodynamic state of a system with limited miscibility can be described in terms of the free energy of mixing. At constant pressure and temperature, three different states can be distinguished:

1.   A stable state with a homogeneous solution in a single phase, which is thermodynamically determined by (4, 12):

$$\Delta G > 0 \quad \text{and} \quad \left(\frac{\delta \mu_i}{\delta X_i}\right)_{P,T} > 0 \ . \tag{1}$$

2.   An unstable state where the homogeneous solution separates spontaneously into two phases in equilibrium. This state, which is always located within the miscibility gap, is thermodynamically determined by:

$$\Delta G < 0 \quad \text{and} \quad \left(\frac{\delta \mu_i}{\delta X_i}\right)_{P,T} < 0 \ . \tag{2}$$

3.   An equilibrium state given by the phase-boundary composition and thermodynamically determined by:

$$\Delta G = 0 \quad \text{and} \quad \left(\frac{\delta \mu_i}{\delta X_i}\right)_{P,T} = 0 \ . \tag{3}$$

Here, ΔG is the free enthalpy of mixing, μ_i is the chemical potential of component i, and X_i is its mole fraction.

Kinetic Description of a Binary System With Limited Miscibility. The kinetic interpretation of a system with limited miscibility can be expressed in terms of the diffusion coefficient D of the system. At constant pressure and temperature, again three different states can be distinguished (4):

(1)   A stable state with the homogenous solution in one phase which is kinetically determined by:

$$D > 0. \tag{4}$$

(2)   An unstable state, where the homogeneous solution decays spontaneously into two different phases. This state is determined by:

$$D < 0. \tag{5}$$

(3)   An equilibrium state given by the phase-boundary composition. Here the diffusion coefficient becomes zero.

$$D = 0. \tag{6}$$

The physical significance of these three states becomes clear when one realizes that the diffusion coefficient is defined by Fick's law in terms of a concentration gradient as the driving force. However, the actual driving force for the flux of a component is not the gradient in its concentration but the gradient in its chemical potential. It is possible to produce situations where the gradients in concentration and chemical potential are of different sign. In this case the diffusion coefficient defined by Fick's law will be negative.

The diffusion coefficient can be related to the chemical potential driving force by:

$$D_i = B_i \left(\frac{\delta \mu_i}{\delta X_i} \right)_{P,T} = 0 \ . \tag{7}$$

Here D_i is the diffusion coefficient of component i, μ_i is its chemical potential and X_i its mole fraction. B_i is a mobility term, which is always positive. Introducing the chemical potential of a nonideal solution, which is given by:

$$\mu_i = \mu_i^o + RT \ln X_i + RT \ln f_i^s \ . \tag{8}$$

into Equation (7) leads to:

$$D_i = \frac{B_i RT}{X_i} \left(1 + \frac{\delta \ln f_i^s}{\delta \ln X_i} \right) \ . \tag{9}$$

Here μ_i^o is a standard potential, f_i is an activity coefficient referring to the pure phase, R is the gas constant and T is the absolute temperature. The last term in Equation (9) determines whether the diffusion coefficient is positive, negative or zero according to these three possibilities:

$$\frac{\delta \ln f_i^s}{\delta \ln X_i} > -1 \ , \ < -1 \ , \ \text{or} \ = 1 \ . \tag{10}$$

A solution of the differential relation (10) leads to:

$$f_i^s = \frac{1}{X_i^n} \tag{11}$$

where n is $0 < n < 1$ for the stable state, $n > 1$ for the unstable state, and $n = 1$ for the equilibrium state.

Equations (8) to (11) indicate that, if for any reason the activity coefficient of a component i in a binary solution is raised to the extent that the product $f_i X_i$ becomes larger than unity, phase separation will occur and the component i will flow from an area of lower concentration into an area of higher concentration. Thus the flux of the component i is against the concentration gradient but i follows the chemical potential gradient.

In summary:

(1)   The driving force for any mass flux is not the concentration gradient
      but the gradient in the chemical potential.
(2)   In phase separation processes, the components are transported against
      their concentration gradient because the activity coefficient is increased
      to such an extent that the product of f_iX_i is larger than unity.

      The activity coefficient of a component can be changed for example
by changing the temperature or the composition of the mixture. A typical
example is the so-called "salting-out" effect, where the activity of the salt
in an aqueous solution is raised by adding an organic solvent to such an
extent that the salt precipitates from the solution.

Consequences of the Basic Relations of Phase Separation For the Preparation
of Microporous Membranes.   Most of the structural differences of phase
inversion membranes can be rationalized by the basic thermodynamic and
kinetic relations of phase separation.

The Precipitation Process.   Before discussing the details of the formation
of symmetic or asymmetric finger- or sponge-type membrane structures it
is useful to describe the concentration profiles of the casting solution
components through the precipitating membrane. Figure 12 shows the con-
centration profiles of polymer, solvent and precipitant at some intermediate
time during the precipitation of a polymer film cast on a glass plate. This
figure shows the composition of the casting solution at the point of pre-
cipitation (C), the point of solidification (D) and the final membrane com-
position (B) taken from the precipitation pathway in Figure 3.
      During precipitation the casting solution can be divided into three
layers. Traveling from the glass plate towards the precipitation bath these
layers are:
      (1) The casting solution layer: This is the layer closest to the glass
plate, and has a composition similar to the original casting solution A. Little
solvent has diffused out, and little precipitant has diffused into the layer.
      (2)   The fluid polymer layer: This layer lies between the point of
precipitation on one side and the point of solidification on the other side.
In this layer the casting solution divides into a polymer-rich and a polymer-
poor phase. The composition of the components in both phases are shown
in Figure 12. Assuming the phases are in equilibrium, their compositions
can be related by the tie lines in the phase diagram, Figure 3. At the point
of precipitation, the precipitated polymer contains a high solvent concentra-
tion and a low precipitant concentration; it is therefore quite fluid. The
polymer nearest the precipitation bath has been precipitated longer, has lost
solvent and gained precipitant; its viscosity is therefore higher. Thus, the
viscosity of the precipitated polymer climbs from the point of precipitation
C until it becomes almost a solid at the point of gelation, D. During this
time bulk movement of the precipitated polymer takes place to form the
matrix of the final membrane.
      (3)   The solid polymer layer: In this layer, the solid, polymer-rich
phase undergoes continuous desolvation, and the system composition changes
from D to B. It is the shrinkage or syneresis of the solid polymer accompany-
ing this composition change that produces stresses in the polymer. Because
the polymer is solid, these stresses cannot be as easily relieved by bulk
movement of polymer as in the fluid polymer layer. Instead, the polymer
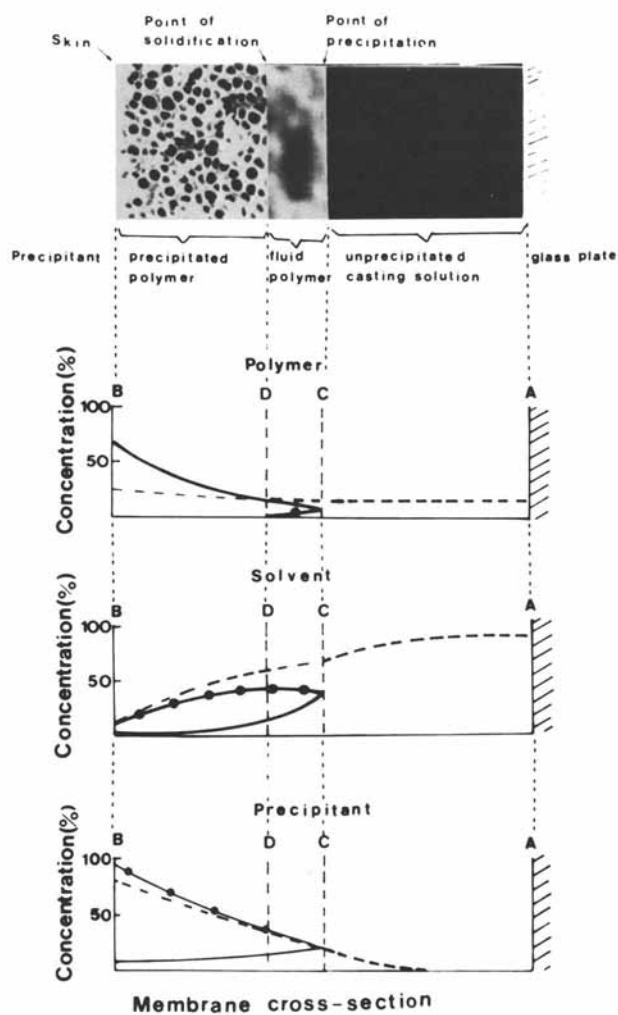
Figure 12. Schematic diagram of the concentration profiles of polymer,
solvent, and precipitant through a precipitating membrane.

---- total concentration

—— concentration in the polymer-rich phase

—•— concentration in the polymer-poor phase.

structure either slowly undergoes creep to relieve the stress, or, if the stress builds up too rapidly to be dissipated by creep, the polymer matrix breaks in weak spots.

Two different techniques have been employed for the precipitation of membranes from a polymer casting solution. In the first method, the precipitant is introduced from the vapor phase. In this case the precipitation is slow, and a more or less homogeneous structure is obtained without a dense skin on the top or bottom side of the polymer film. This structure can be understood when the concentration profiles of the polymer, the precipitant and the solvent during the precipitation process are considered. The significant feature in the vapor-phase precipitation process is the fact that the rate-limiting step for precipitant transport into the cast polymer solution is the slow diffusion in the vapor phase adjacent to the film surface. This leads to uniform and flat concentration profiles in the film. The concentration profiles of the precipitant at various times in the polymer film are shown schematically in Figure 13.

Because of the flat concentration profiles, the solution precipitates at virtually the same time over the entire film cross section, and no macroscopic gradients of activity or concentration of the polymer are obtained over the film cross-section. On a microscopic scale, however, because of thermal molecular motions, there are areas of higher and lower polymer concentration, which act as nucleation centers for polymer precipitation. These microscopic areas of higher polymer concentration are randomly distributed throughout the cast polymer film. Therefore, a randomly distributed polymer structure is obtained during precipitation. This structure is also shown in Figure 13 in the form of a scanning electron microscope picture of the cross section of a symmetric membrane obtained with a vapor phase precipitant.

In the second membrane preparation procedure the precipitant is added to the casting solution by immersing the cast polymer film in a bath of the precipitation fluid. In this case the precipitation is rapid, and a skinned membrane structure is obtained. This structure, and especially the skin formation, can again be understood by considering the concentration profiles of the polymer, the solvent and the precipitant during the precipitation process. These profiles over the cross-section of the cast polymer film are shown schematically in Figure 14. The most important feature in immersion precipitation are the steep concentration and activity gradients of all components obtained at the polymer solution - precipitation medium interface. Because of the activity gradients, the transport of the polymer at the interface is no longer random, but definitely directed into the casting solution.

When the cast polymer film is immersed into the precipitation bath, solvent leaves and precipitant enters the film. At the film surface the concentration of the precipitant soon reaches a value resulting in phase separation. In the interior, however, the polymer concentration is still far below the limiting concentration for phase separation. Phase separation therefore occurs initially at the surface of the film, where due to the very steep gradient of the polymer chemical potential on a macroscopic scale, there is a net movement of the polymer perpendicular to the surface. This leads to an increase of the polymer concentration in the surface layer. It is the concentrated surface layer which forms the skin of the membrane. This skin also serves to hinder further precipitant flux into and solvent out of the casting solution. The skin thus becomes the rate-limiting barrier for precipitant transport into the casting solution, and the concentration profiles in the casting solution interior become less steep. Thus, once the precipitated
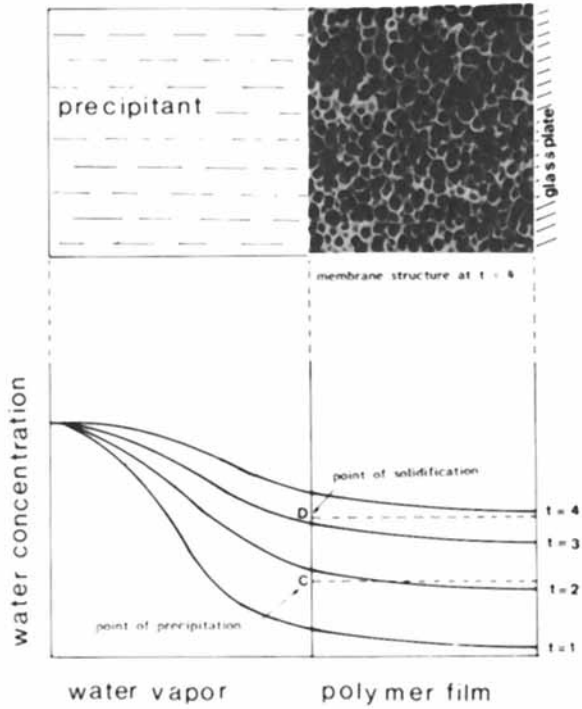
Figure 13. Concentration profiles of the precipitant in the casting solution at various times during the formation of a symmetric structured membrane.
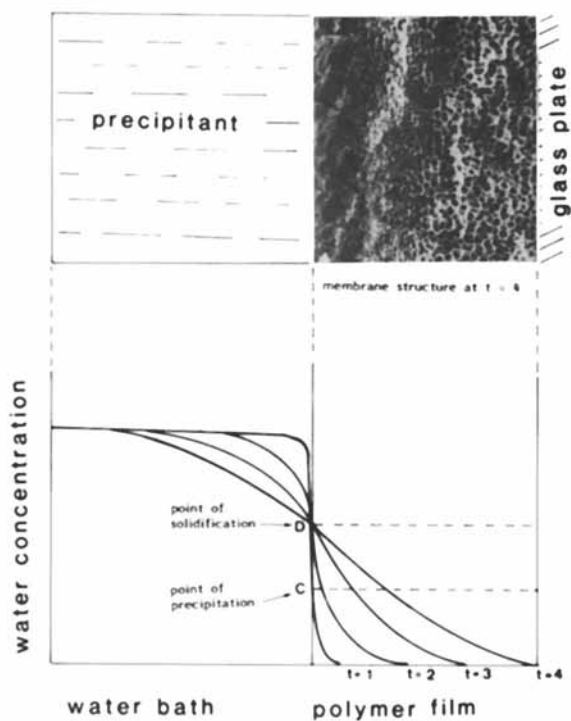
Figure 14   Concentration profiles of the precipitant in the casting solution at various times during the formation of an asymmetric skin type membrane.

skin is formed, the same situation in the sublayer is obtained as in a membrane precipitated from the vapor phase, and a structure with randomly distributed pores is formed.

Skin Type Membranes With "Sponge"- and "Finger"-Like Structures.   In skin-type membranes two characteristic structures shown in Figure 4 are obtained. One is a sponge-like structure and the other is a finger-like substructure underneath the skin.

The formation of the sponge-structured membranes can be easily rationalized utilizing the description of the precipitation process given above. With finger-structured membranes the formation process is more complex and cannot entirely be described by the thermodynamic and kinetic arguments of phase separation processes.

Other phenomena such as syneresis, shrinkage and stress relaxation in the precipitated polymer also play an important role. The formation of finger-structured membranes is conveniently divided into two steps: the initiation and the propagation of fingers. The formation of the skin is identical with that of the sponge-structured membranes. However, as the result of syneresis, shrinkage stress in the solid polymer skin cannot be relieved by creep relaxation of the polymer and the homogeneous layer ruptures. The points at which the skin has been fractured form the initiation points for the growth of the fingers. Once a finger has been initiated, shrinkage of the polymer causes it to propagate by draining the freshly percipitated polymer at the bottom of the finger to the side of the finger. This is schematically shown in Figure 15 which shows the growth of a "finger" at various times. Within a finger the exchange of solvent and precipitant is much faster than through the unfractured skin, and the precipitation front moves much faster within a finger than in the casting solution bypassed between fingers. This solution is protected from immediate exposure to the precipitant by a layer of precipitated polymer. Precipitation therefore occurs much slower and a sponge-like structure is formed between the fingers. Typical finger-like structure membranes almost always have a bottom skin. This bottom skin may be caused by the adhesion of the casting solution to the glass plate, preventing the last polymer fluid at the bottom of the finger from moving to the sides of the finger. This fluid polymer thus solidifies in place sealing off the finger.

Uniform and Graded Pore Structure of Skin-Type Membranes.   In sponge-structured, skin type membranes, it is assumed that the diffusion of the precipitant through the skin is the rate-limiting step leading to a more or less flat concentration profile of the precipitant in the casting solution just beneath the skin. Depending on the resistance of the skin to the flux of precipitant, the concentration profile may vary from a completely flat one (virtually no concentration gradient over the cross-section of the cast polymer film) to a concentration profile showing an initially steep gradient at the beginning of precipitation which decreases as precipitation proceeds through the polymer film. This is indicated in Figure 16 where the concentration profiles of the precipitant during the precipitation of a graded pore (a) and a uniform pore (b) sponge-structured membrane is shown. A uniform pore structure is obtained when the concentration profiles are flat (b), and the time that the system needs to move from the point of precipitation to the point of solidification (points C and D in the Figure 6), is about the same over the entire film cross-section. A graded pore distribution is obtained when the time between precipitation and solidification of the polymer increases with increasing distance from the skin.
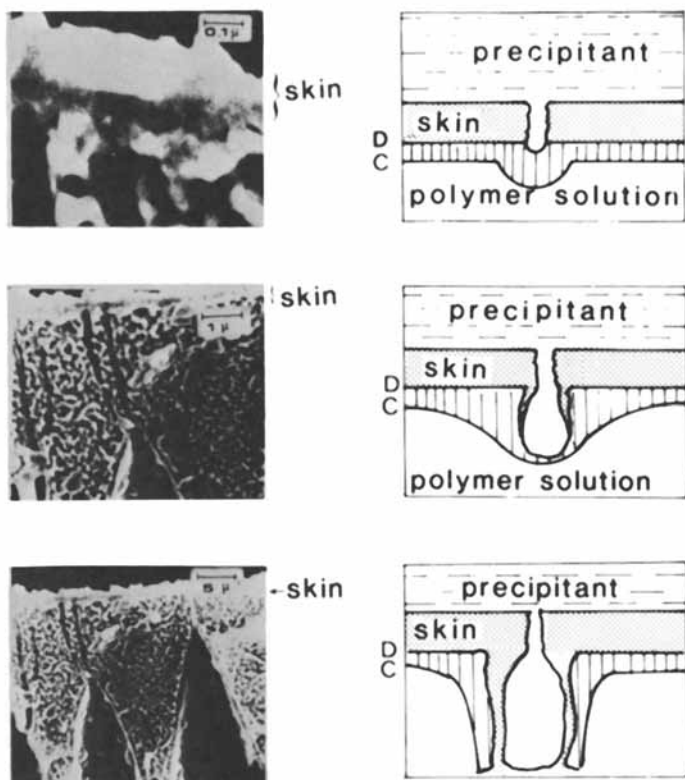
Figure 15. Schematic diagram of finger formation at various times during precipitation.
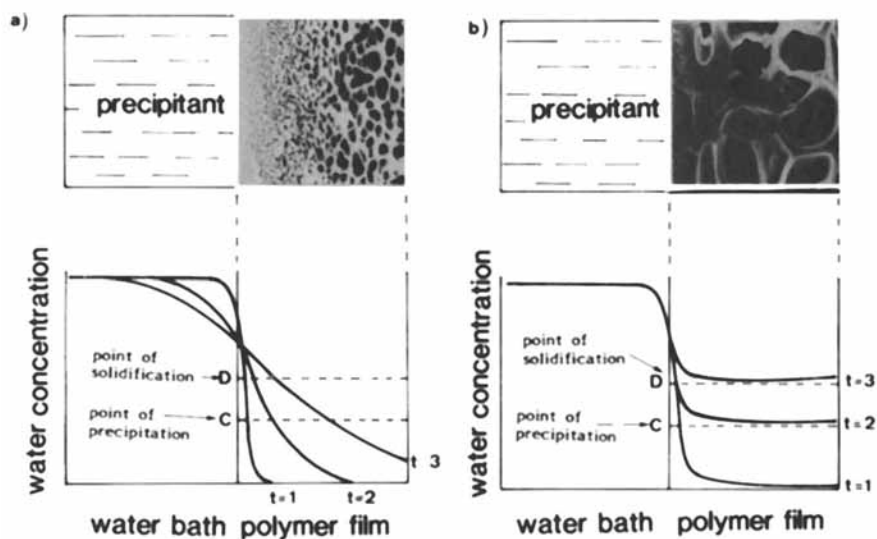
Figure 16.   Concentration profiles of precipitant in the casting solution at various times during precipitation of membranes with (a) graded and (b) uniform pore substructures.

Different Preparation Parameters and Their Effect on Membrane Structure and Performance

The mechanism for the formation of symmetric or asymmetric microporous membranes outlined above allows many of the variables of the membrane preparation procedures to be rationalized.

The Selection of the Polymer-Solvent-Precipitant System.

The precipitant and the solvent used in membrane preparation determine both the activity coefficient of the polymer in the solvent-precipitant mixture and the concentration of polymer at the point of precipitation and solidification. Unfortunately, values for the activity coefficients of the polymer, the solvent or the precipitant, and the dependence of these activity coefficients on the composition, are generally not available, and are difficult to obtain experimentally. A quantitative treatment of the membrane precipitation process is therefore not possible. However, the polymer-solvent interaction can be approximately expressed in terms of the disparity of the solubility parameter of polymer and solvent. The smaller the solubility parameter disparity of solvent and polymer, the better is the compatibility of solvent and polymer, the more time it takes to remove the solvent from the polymer structure and the slower is the precipitation of the polymer. Therefore, when all other parameters are kept constant, the tendency for change from a sponge to a finger structure membrane increases with decreasing compatibility of solvent and polymer. The compatibility of polymer and precipitant can also be expressed in terms of the solubility parameter disparity. The greater this disparity is, the less compatible will be the polymer and the precipitant, the greater will be the activity coefficient of the polymer in the solvent-precipitant mixture and the faster will be the precipitation. The tendency to change from a sponge to a finger structure will increase with decreasing compatibility of polymer and precipitant. This has been demonstrated in results published elsewhere (13).

The solvent-precipitant interaction is apparently a particularly important parameter. One measure of this interaction is the heat of mixing a solvent and precipitant. Systems which have a large heat of mixing show high precipitation rates and a tendency to form finger-structured membranes (14).

The effect of additives to the casting solution or precipitant on the membrane structure can also be explained by changes of the activity coefficients of the polymer, the solvent or the precipitant. These activities on the precipitant such as salts, sugars, glycerin, etc. reduce the rate of precipitation and clearly favor a more densesponge structure. The same additives in the casting solution generally increase the rate of precipitation and therefore favor a finger structure, while other additives in the casting solution, such as benzene, reduce the rate of precipitation and therefore favor a sponge structure.

The Effect of the Polymer Concentration in the Casting Solution on the Membrane Structure.

A low polymer concentration in the casting solution tends to precipitate in a finger structure, while high polymer concentrations tend to form sponge-structured membranes. The effect of polymer concentration on membrane structures can be explained by the initiation and propagation of fingers. Higher polymer concentration in the casting solution produces a higher polymer concentration at the point of precipitation, which

will thus tend to increases the strength of the surface layer of polymer first precipitated, and tend to prevent initiation fingers. The increasing viscosity of the casting solution has the same effect.

Pre- and Post-Precipitation Procedures. Pre- and post-precipitation procedures such as a partial evaporation of the casting solution prior to the precipitation or an anealing of the precipitated polymer film. Both have a significant effect on the structure and filtration properties of the final membrane. During the evaporation step, the polymer concentration in the surface layer of the cast film is increased. When solvent mixtures (such as acetone-formamide for the preparation cellulose acetate membranes) are used, the evaporation procedure may also change the ratio of the two solvents in the casting solution at the membrane surface, thus affecting the structure and transport properties of the final membrane rather drastically. The post-precipitation annealing step generally leads to a rearrangement of the polymer chains, which by the rapid precipitation procedure are often in a metastable state far from equilibrium. In an annealing process the membrane usually shrinks and changes its transport properties (15). The same effect, however, can be achieved by a chemical treatment at room temperature using a plasticizer.

Although most aspects of the formation of asymmetric skin type membranes can satisfactorily be rationalized by applying the basic thermodynamic and kinetic laws of phase separation processes, there are other parameters, such as surface tension (16), polymer relaxation (17), solvent loss by evaporation (18), etc., which are not directly related to the phase separation process, but nevertheless will have a strong effect on the membrane structure and properties.

In this paper the discussion was concentrated mainly on the phase separation in polymer solutions due to the change of the composition of the mixture. The basic relations are also valid for phase separations induced by temperature changes, that is thermal gelation and can be applied to glass and metal alloys as well as to polymers.

Literature Cited

1. Lonsdale, H. K., J. Membr. Sci. 1982, 10, 81.
2. Kesting, R. E. "Synthetic Polymeric Membranes"; McGraw-Hill: New York, 1971.
3. Loeb, S.; Sourirajan, S. Adv. Chem. Serv. 1962, 38, 117.
4. Haase, R. "Thermodynamik der Mischphasen"; Springer Verlag: Berlin, 1956.
5. Zsigmondy, R.; Carius, C. Chem. Ber. 1927, 60 B, 1047.
6. Kesting, R. E. J. Appl. Polym. Sci. 1973, 17, 1771.
7. Strathmann, H. "Trennung von Molekularen Mischungen mit Hilfe Synthetischer Membranen"; Steinkopff: Darmstadt 1979.
8. Loeb, S. In "Desalination by Reverse Osmosis"; Merten, U., Ed.; M.I.T. Press: Cambridge, Mass., 1966.
9. Manjikian, S. Ind. Eng. Chem. Prod. Res. Develop. 1967, 6, 23.
10. Strathmann, H. Habilitationsschrift, Universität Tübingen, 1981.
11. Frommer, M. A.; Matz, R.; Rosenthal, U. Ind. Eng. Chem. Prod. Res. Develop. 1971, 10, 193.
12. Stauff, J. "Kolloidchemie"; Springer Verlag: Berlin, 1960.
13. So, M. T.; Eirich, F. R.; Baker, R. W.; Strathmann, H. Polymer Letters 1973, 11, 201.

14.   Strathmann, H.; Kock, K.   Desalination 1977, 21, 241.
15.   Strathmann, H.; Scheible, P.; Baker, R. W.   J. Appl. Polym. Sci. 1971,
       15, 811.
16.   Tanny, G. B.   J. Appl. Polym. Sci. 1974, 18, 2149.
17.   Koenhen, D. M.; Mulder, M. H. V.; Smolders, C. A.   J. Appl. Polym.
       Sci. 1977, 21, 199.
18.   Anderson, J. E.; Ullman, R.   J. Appl. Phys. 1973, 44, 4303.

Role of Microphase Separation Phenomena in the Formation of Porous Polymeric Membranes

KENJI KAMIDE and SEI-ICHI MANABE

Textile Research Laboratory, Asahi Chemical Industry Co. Ltd., Hacchonawate 11-7, Takatsuki City, Osaka, Japan

A theoretical approach to the formation of porous polymeric membranes is demonstrated through the phase separation phenomena of polymer solutions. If the initial polymer concentration is smaller than the critical solution concentration, the polymer-rich phase separates as small particles (primary particles) between 10 nm and 30 nm in diameter. The primary particles amalgamate into larger secondary particles with diameters of 50 nm to 300 nm. The secondary particles subsequently coagulate to form pores. A theory for the growth process of primary particles into secondary particles is presented assuming that particles can grow only via collisions with primary particles. The theory predicts that the phase ratio in the micro-phase separation and the size of the secondary particles determine membrane pore characteristics.

For many years polymeric membranes have been utilized widely for material separation without detailed characterization of the pore size and the pore size distribution. Most of the commercially available membranes are prepared by either a dry or a wet phase-inversion process. These membranes are formed by the phase separation of multicomponent polymer-solvent systems, the underlying principle being phase separation of the polymer solution.

Many scientific papers (1) on membranes are primarily concerned with phenomenological correlations between the preparation of the membrane and its performance, including fluid permeability and permselectivity to solutes. The performance of the membrane is principally governed by its pore characteristics in a complicated manner (2). These pore characteristics in turn are influenced by the molecular characteristics of the polymer and the preparative method (3,4,5).

In 1977 Kamide, Manabe and co-workers (3) demonstrated, for solvent-cast cellulose diacetate membranes, the effect of

preparative conditions on pore characteristics such as the average
pore size and the porosity of the membrane. In their study, a
cellulose diacetate membrane was prepared by casting a solution of
cellulose diacetate/acetone/methanol/cyclohexanol/$CaCl_2 \cdot 2H_2O$. For
a given composition of the casting solution, both the mean pore
size and the porosity, Pr, are determined unambiguously, provided
that all other conditions are kept constant.

      Although the phase separation of the casting solution has been
known by many investigators to be a necessary process in membrane
formation (3-7), no one has successfully quantitatively described
the role of phase separation in the pore forming process in
connection with the pore characteristics of the resultant membrane.

Theoretical Background

The phase separation phenomena are schematically represented in
Figure 1. At thermodynamic equilibrium, the chemical potential of
each component, $\Delta\mu_i$, in both the polymer-rich (II) and the polymer-
lean (I) phases should be the same (that is, $\Delta\mu_i^I = \Delta\mu_i^{II}$). Since
1968, the thermodynamics of phase equilibrium of quasibinary (that
is, polydisperse polymer-single solvent) and quasiternary
(polydisperse polymer-solvent(1)-solvent(2)) systems at constant
temperature and pressure has been studied by Kamide et al. (8-10).
At present the detailed phase separation characteristics, including
the partition coefficient, σ', the phase volume ratio, R, the
polymer volume fraction in both phases, and the molecular weight
distribution of the polymers in the phases can be calculated for a
given polymer/solvent or two solvent system. The volume fraction
of polymer-lean phase, L, can be obtained from R by using the
relation $L = R/(1 + R)$.

      The solvent casting procedure is considered here as the most
common procedure causing phase separation in the pore forming
process. Any modifications, such as using phase separation
phenomena other than solvent casting, are considered to not change
the pore formation mechanism. This paper considers the case of
evaporation of solvent to originate phase separation as shown in
Figure 1. Immediately after the polymer solution is cast on the
plane surface, a volatile solvent component near the surface of the
solution begins to evaporate, resulting in a significant
concentration gradient perpendicular to the solution surface. Then
the solution becomes turbid, indicating the occurrence of a phase
separation by the relative decrease in good, volatile solvent. In
place of the vaporization of solvent in the membrane-forming process also causes phase separation to occur
within a plane.

      The phase separation initiated at the surface proceeds to the
inner region of the solution with the lapse of time. The phase
separation is considered to occur simultaneously throughout a
hypothetical plane in the solution parallel to the surface. In
other words, the polymer membrane cast from solution is a laminate
of extremely thin membranes.

      According to our previous paper (3), micro-phase separation in
the hypothetical plane proceeds through the creation of a small
particle having a diameter of less than 50 nm. The growth of this

particle into a large particle with a diameter of more than 200 nm
and the amalgamation of the large particles result in the formation
of a noncircular pore. According to the criteria proposed by Cahn
(11), the nucleation of a particle and its growth indicate that the
phase separation occurs by a nucleation mechanism rather than by
the spinodal-type phase separation. Nucleation of particles and
voids, depending on solution concentration was qualitatively
proposed by Kuehnen et al. (12).

Appearance of the Primary Particle due to Phase Separation and
Growth into the Secondary Particle. Figure 2 shows a schematic
representation of the mechanism of pore forming in the solvent
casting process. Depending on the initial polymer concentration,
$v_p°$, the polymer-rich phase or the polymer-lean phase separates
initially from the solution. If $v_p°$ is smaller than the critical
solution concentration, $v_c°$, the polymer-rich phase separates as a
small particle, whose size, defined by its radius S_1, may be almost
equal to or slightly larger than the critical radius, S_c, of the
phase separation. Hereafter we call this particle the "primary
particle" (see Figure 2). As shown in a later section, primary
particles have diameters, $2S_1$, of around 20 to 30 nm in the cases
of cellulose cuprammonium solution/acetone and cellulose acetate/
acetone systems. These particles grow into secondary particles
with radii of S_2.

When the density of the primary particle, the polymer weight
fraction of this particle and the molecular weight of a polymer are
given by ρ_s, C and M, respectively, the number of polymer molecules
in this particle, N_p, can be calculated by using Equation 1.

$$N_p = (\rho_s C/M)(4\pi S_1^3/3) N_A \qquad (1)$$

where N_A is Avogadro's number. Setting values of ρ_s of 1.3 g/ml, C
of 0.4, M of 1×10^5 and S_1 of 10 nm in Equation 1, we get $N_p = 40$.

Assume the shape of the nucleus to be spherical with a radius
of S. The free energy of nucleus formation, $\Delta\phi$, is related to the
Gibbs free energy change Δf per unit volume, Δf, accompanied by
phase separation (under constant pressure and temperature T), and
the intersurface energy per unit area, σ, at the surface of the
nuclei in the form;

$$\Delta\phi = (4/3)\pi S^2 \sigma - (4/3)\pi S^3 \Delta f \qquad (2)$$

The radius of critical nuclei, S_c, is derived by applying the
condition of $\partial\Delta\phi/\partial S = 0$ to yield

$$S_c = (2/3)\sigma /\Delta f \qquad (3)$$

The necessary condition for the stable existence of the primary
particle is $\Delta\phi \leq 0$ and then we obtain

$$S_1 \geq \sigma/\Delta f \qquad (4)$$
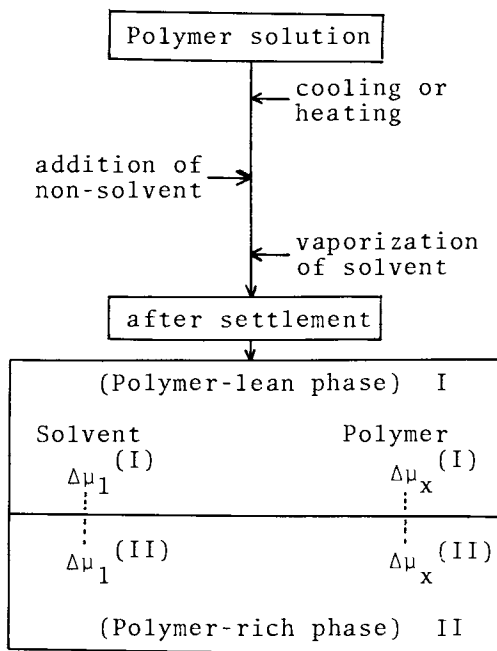
Figure 1. Phase separation phenomena.
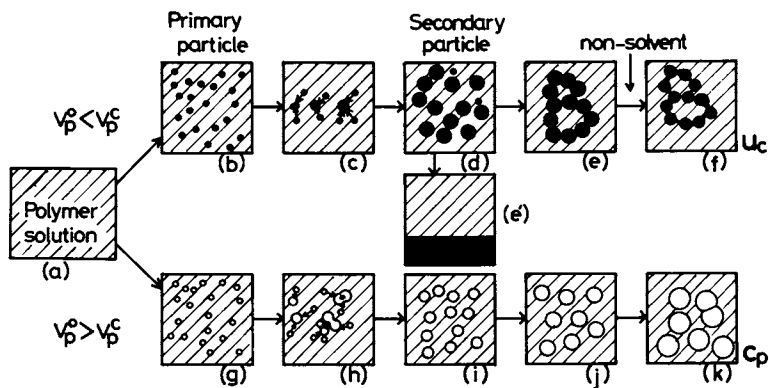
Figure 2. Schematic representation of the formation of pores in the casting process.

If the distribution function of the particle radius changes continuously with time, it can be regarded that the particles grow only through collisions with primary particles. We assume that all primary particles have the same radius (S_1). The rate at which primary particles of radius S_1 are generated per unit volume of the original solution at time t is defined by $M(S_1,t)$. The number of growing particles whose radii range between S and S + dS at time t in the unit volume is expressed as $L(S,t)dS$. The quantity $M(S_1,t)$ is assumed to be proportional to the number of the primary particles generated per unit volume of original solution during the interval from time t to infinity (that is, $\int_t \dot{M}(S_1,t)dt$) and to the nucleation rate of nuclei of the primary particles, $k_n\exp(-\Delta\phi^*/kT)$. Here, k_n is the rate constant of the nucleation and $\Delta\phi^*$ is the activation energy of the nucleation. $\Delta\phi^*$ can be calculated by Equation 5, which was derived by substituting Equation 3 into Equation 2 under the condition of $S = S_c$.

$$\Delta\phi^* = (16/81)\pi(\sigma^3/\Delta f^2) \qquad (5)$$

Then we obtain the integration equation of $\dot{M}(S_1,t)$

$$\dot{M}(S_1,t) = k_1\exp(-\Delta\phi^*/kT) \int_t^\infty \dot{M}(S_1,t)dt \qquad (6)$$

where k_1 is the proportionality constant that is given by the product of k_n and the growth rate of the critical nuclei to the primary particles.

Figure 3 is a schematic representation of the amalgamation of the primary particles to the secondary particle. The growth rate of a radius of the growing particle, dS/dt, is proportional to the probability of the collision between the particle in question and primary particles and to the number of primary particles per unit volume of the original solution. It is also proportional to the diffusional velocities of a primary particle and the growing particle and to the reciprocal of the surface area of the growing particle, $1/\pi S^2$. This collision probability may be proportional to the maximum sectional area of the growing particle, πS^2.

The number of primary particles per unit volume of original solution at time t equals the difference between the number of particles generated during the time interval t = 0 to t = t and the number of the particles consumed in making the growing particles whose radii range between S_1 and infinity. Consequently, the number of primary particles is $[\int_0^t \dot{M}(S_1,t)dt - (1/S_1^3)\int_{S_1}^\infty S^3 L(S,t)dS]$.

The Stokes equation gives the friction constant of a rigid sphere with radius S as $6\eta_o S$ (where η_o is the viscosity coefficient of the liquid surrounding the sphere). The diffusional velocity of a sphere is proportional to the inverse of the friction constant. The inverse of the viscosity coefficient of the original solution, $1/\eta_o$, is expressed by $k_d\exp(-\Delta F_d^*/kT)$ (where k_d is a constant

independent of temperature, and ΔF_d* is the apparent activation energy). Then the diffusional velocity of a primary particle may be given by $[(k_2/S_1)\exp(-\Delta F_d*/kT)]$ and that of the growing particle by $(k_2/S)\exp(-\Delta F_d*/kT)$ with $k_2 = k_d/6$.

We define the probability of amalgamation, P_a, as the ratio of the number of primary particles which amalgamate after collision with a growing particle to the total number of primary particles which collide with the growing particle. The decrease in surface area that accompanies amalgamation is approximated by $4\pi S_1^2 [1 - (2/3)(S_1/S)]$ in the case of $S \gg S_1$. The probability of amalgamation, P_a, may increase with a decrease in the surface area. Thus P_a can be evaluated by using the Boltzmann distribution as

$$P_a = \frac{\exp[4\pi S_1^2 \sigma\{1 - (2/3)(S_1/S)\}/3kT]}{1 + \exp[4\pi S_1^2 \sigma\{1 - (2/3)(S_1/S)\}/3kT]} \tag{7}$$

Therefore, dS/dT can be given in the form,

$$dS/dt = k_c(\pi S^2)[\int_0^t \dot{M}(S_1,t)dt - (1/S_1^3)\int_{S_1}^\infty S^3 L(S,t)dS](k_2^2/S_1 S)$$

$$\exp(-2\Delta F_d*/kT)(1/\pi S^2)P_a$$

$$= [\int_0^t \dot{M}(S_1,t)dt - (1/S_1^3)\int_{S_1}^\infty S^3 L(S,t)dS](Zk_c k_2^2/S_1)$$

$$\exp(-2\Delta F_d*/kT) \tag{8}$$

$$L(S,t)dS = P_a \dot{M}(S_1,t)dt \tag{9}$$

$$\text{with } Z = P_a/S \tag{10}$$

where k_c is a proportional constant independent of time, temperature and composition of the solution. Z is a constant which depends on S_1 and S, but is nearly independent of S because of the positive S dependence of P_a (see Equation 7).

By solving simultaneously Equations 6, 8 and 9, we can get $L(S,t)$. Because it is difficult to solve these equations analytically, a numerical method is used.

The slow rate of transition from stage (b) to stage (d) in Figure 2 is an indispensable condition in the solvent-cast process of ultrafiltration membrane technology. Stage (d) is a kind of micro-phase separation, which is apparently metastable. The transitions (b) to (c) and (c) to (d) are governed by the mobility and the surface free energy of the particle.

Pore Size Distribution of the Membrane Formed by Micro-phase
Separation. Consider a hypothetical plane parallel to the surface
of the cast solution. Assume that the secondary particles are
placed on this plane in a two-dimensional lattice of hexagonal
close packing (see Figure 4). The lattice coordination number is
6. Let the number of the secondary particles (referred to as
polymer particles) per unit area be represented by $N_o(1 - L)$.
Here, N_o is the total number of particles and is equal to $1/(\pi S_2^2)$.
L is the volume fraction of polymer-lean phase and is equal to $R/(1 + R)$. Assume that "hypothetical" particles of the polymer-lean
phase (in the case of $v_o > v^c$) have the same radii of S_2 as the
polymer particles. Obviously, the polymer-lean "hypothetical"
particles build a pore. They are hereafter referred to simply as
"pore particles." Let the number of pore particles per unit area
be represented by $N_o L$, and the number of pores or "cells" (which is
equal to the number of the aggregates of pore particles) be N. The
area of a "cell" is the sum of the area of pore particles and of
the effective area of the polymer particles surrounding a pore.
The latter is defined as the area of the polymer particles divided
by n, when the polymer particle contributes to building n pores.
Figure 5 is an example of a cell which is composed of four pore
particles and ten polymer particles. These polymer particles are
composed of one polymer particle of n = 1, five polymer particles
of n = 2 and four polymer particles of n = 3. Thus the area of the
cell in Figure 5 is given by $4\pi S_2^2 + [1 + 5(1/2) + 4(1/3)]\pi S_2^2$ (=
$(10/3)\pi S_2^2$).

The number of cells per unit area equals the pore density, N.
Note that the size of the cell is not constant, and that the number
of the polymer particles and pore particles are $N_o(1 - L)$ and
$N_o R$, respectively. The number of ways, $_{N_o L, N_o(1-L)}\Omega_N$, of
partitioning the $N_o L$ pore particles and the $N_o(1-L)$ polymer
particles into the N cells is given by

$$_{N_o L, N_o(1-L)}\Omega_N = [N_o + N - 1]!/[(N - 1)!(N_o L)!\{(N_o(1 - L)\}!]$$

(11)

By using the same procedure used to derive Equation 11, the
number of ways, $_{N_o L-x, N_o(1-L)-f(x)}\Omega_{N-1}$, of partitioning $N_o L - x$
pore particles and $N_o(1 - L)-f(x)$ polymer particles into N - 1
of the cells is given by

$$_{N_o L-x, N_o(1-L)-f(x)}\Omega_{N-1} = [N_o + N - 2 - x - f(x)]!/[(N - 2)!$$

$$(N_o L - x)!\{N_o L(1 - x) - f(x)\}!]$$ (12)

Here, f(x) is the number of polymer particles necessary to
isolate x pore particles.

The probability, q(x), that a given cell contains x pore
particles (in the case of Figure 5, x = 4) is expressed by
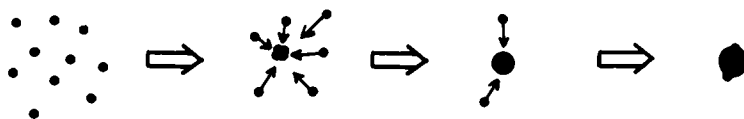
Figure 3. Amalgamation of the primary particles to the secondary
           particle.
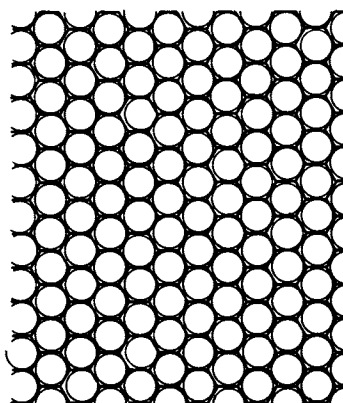
Figure 4. Two-dimensional hexagonal lattice for representing the
           packing of secondary particles on the hypothetical plane.
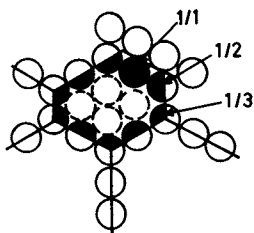
Figure 5. A cell in the membrane:
           circle with broken line = pore particle; circle with full
           line = polymer particle; shadowed area indicates the part
           composing a cell.

$$q(x) = \sum_{f(x)=(min)}^{max} \frac{{}_{N_oL-x,N_o(1-L)-f(x)}\Omega_{N-1} {}^{[x-1+f(x)]!}}{{}_{N_oL,N_o(1-L)}\Omega_N (x-1)!f(x)!} \tag{13}$$

where (max) stands for the upper limit of $f(x)$ and (min) the lower limit. The geometrical limitation of the packing number of particle gives $2x + 4$ to (max) and $3 + (5 + 4x)^2$ to (min) (see Figure 6). After some calculation of Equation 12 under the conditions of $N_o > N \gg 1$, and $(N_o + N) \gg (x + f(x))$, we obtain finally

$$q(x) = \frac{{}_{N_oL-x}\Omega_{N-1}}{{}_{N_oL}\Omega_N} \sum_{f(x)=(min)}^{(max)} (1-L)^{f(x)} \frac{[(x-1)+f(x)]!}{(x-1)!f(x)!} \tag{14}$$

where $\quad {}_{N_oL-x}\Omega_{N-1} = \dfrac{(N_oL - x + N - 2)!}{(N-2)!(N_oL - x)!} \tag{15}$

and $\quad {}_{N_oL}\Omega_N = \dfrac{(N_oL + N - 1)!}{(N-1)!(N_oL)!} \tag{16}$

We define the probability $P(x)$ that a cell contains x pore particles under the condition that N cells are constructed with $(1 - L)N_o$ polymer particles independent of x. Then, we obtain $P(x)$

$$P(x) = {}_{N_oL-x}\Omega_{N-1}/{}_{N_oL}\Omega_N \tag{17}$$

It should be noted that $P(x)$ is normalized for the range $x = 0$ to $x = \infty$. When we employ the following approximation,

$$\sum_{f(x)=(min)}^{(max)} (1-L)^{f(x)} \frac{[(x-1)+f(x)]!}{(x-1)!f(x)!} = 1 \tag{18}$$

$q(x)$ reduces to $P(x)$.

Under the condition of $N \gg 1$ and $N_oL \gg x$, which are acceptable for the membranes obtained by the micro-phase separation method, Equation 17 reduces to

$$P(x) = [N/(N_oL + N)][N_oL/(N_oL + N)]^x \tag{19}$$

The average number, $\bar{x}$, of pore particles contained within a cell is

$$\bar{x} = LX = L(N_o/N) \tag{20}$$

where $\quad X = N_o/N$

Equation 19 can be rewritten with the aid of Equation 20 as

$$P(x) = [1/(1 + \bar{x})][\bar{x}/(1 + \bar{x})]^x \tag{21}$$

The necessary condition for forming a two-dimensional pore is that the pore in question be fully surrounded by polymer particles. When a polymer particle is shared by n pores (see Figure 5), we define k as the reciprocal average of n.

Table I shows the probability, $_mP_n$, that a given polymer particle is shared by n pores (that is, n cells) and is surrounded in part by m pore particles. The maximum n is 3 for hexagonal packing. The summation of m under the fixed value of n gives the probability that a polymer particle is shared with n pores, P_n. Thus

$$P_n = \sum_{m=1}^{4} {}_mP_n$$

The value of $\bar{k}$ is given by

$$\bar{k} = \sum_{n=1}^{3} (1/n)P_n \Big/ \sum_{n=1}^{3} P_n \tag{23}$$

Substituting the values of $_mP_n$ given in Table I into Equation 22, we can express P_1, P_2 and P_3 in terms of L.

$$P_1 = 6[L(1 - L)^5 + L^2(1 - L)^4 + L^3(1 - L)^3 + L^4(1 - L)^2]$$

$$P_2 = 9L^2(1 - L)^4 + 12L^3(1 - L)^3 + 9L^4(1 - L)^2 \tag{24}$$

$$P_3 = 2L^3(1 - L)^3$$

$\bar{k}$ is determined by the volume fraction of polymer-lean phase L. Because a pore must be closely surrounded by polymer particles, the boundary condition that the summation of polymer particles composing pores is less than the total number of polymer particles per unit area should be satisfied. When a pore grows circularly, as shown in Figure 6a, this boundary condition is given by

$$\sum_{x=0}^{N_oL} [3 + (5 + 4x)^{\frac{1}{2}}]P(x)\bar{k} \leq (1 - L) \tag{25}$$

When a pore grows linearly, as shown in Figure 6b, the boundary condition is

Table 1   Probability that a given polymer particle is
shared with n pores and is surrounded by m pore
particles $P_{m\,n}$

	n = 1	2	3
m = 1	$6P_r(1 - P_r)^5$	0	0
2	$6P_r^2(1 - P_r)^4$	$(_6C_2 - 6)P_r^2(1 - P_r)^4$	0
3	$6P_r^3(1 - P_r)^3$	$(_6C_2 - 6)P_r^3(1 - P_r)^3$	$2P_r^3(1 - P_r)^3$
4	$6P_r^4(1 - P_r)^2$	$(_6C_4 - 6)P_r^4(1 - P_r)^2$	0
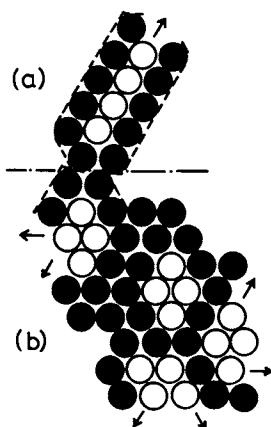
Figure 6.   Schematic representation of pore growth (x = 4):
arrows indicate the direction of pore growth; (a) one
dimensional growth (linearly growing pore), (b) two
dimensional growth (circularly growing pore).

$$[7/(1 + XL) + 6/(1 + XL)[XL/(1 + XL)] + 8/(1 + XL)[XL/(1 + XL)]^2$$

$$+ 1/(1 + XL) \sum_{x=3}^{N_oL} (1.5x + 5)[XL/(1 + XL)]^x \ \bar{k} \leq (1 - L) \qquad (26)$$

Assume that L and S_2 are predetermined. Then, $\bar{k}$ is calculated by Equations 23 and 24 and N_o is determined from S_2 as $1/\pi S_2^2$. By solving either Equation 25 or 26, we obtain X. By putting the value of L and X thus obtained into Equation 20, N and x can be calculated. Accordingly, P(x) can be evaluated from Equation 21.

The wet, coagulated membrane gel is usually dipped into a nonsolvent bath. Desolvation followed by partial replacement with nonsolvent and shrinkage of the gel occur. After being dipped, the membrane is dried. The volume fraction polymer concentration in the polymer-rich phase is given as V. The unit volume of a polymer particle decreases to $V(\rho_s/\rho_p)$ after drying. Here, ρ_s and ρ_p are the densities of the polymer-rich phase and of polymer, respectively. The radius of the polymer particle S_2 changes to S_2' $(=S_2(V\rho_s/\rho_p)^{1/3})$ by drying.

The pore radius r of the membrane after drying is

$$r = r_w + [1 - (V\rho_s/\rho_p)^{1/3}]S_2 \qquad (27)$$

where r_w is the pore radius before drying and is approximated by $x^{1/2}S_2$. Therefore, we obtain

$$r = [x^{1/2} + 1 - (V\rho_s/\rho_p)^{1/3}]S_2 \qquad (28)$$

The porosity, Pr, is approximated as

$$Pr = N \ [\bar{x}^{-1/2} + 1 - (V\rho_s/\rho_p)^{1/3}]^2 S_2^2 \qquad (29)$$

Figure 7 shows the change in pore size during drying treatment in the case of x = 3. Note that we assume no two-dimensional shrinkage of the membrane during drying and that even if no pore particle exists (that is, x=0), a small, but not negligible, clearance remains as an inscribed circle of contacted polymer particles, resulting in a pore. By using V, ρ_s, ρ_p and S_2 data, x can be readily transformed into r through Equation 28.

The probability P(x) can be easily transformed into the pore size distribution function N(r) of the membrane with the aid of the following approximation in which x is assumed to be continuous

$$NP(x)dx \doteq N(r)dr \qquad (30)$$

with

$$N = \int_0^\infty N(r) \ dr \qquad (31)$$

Combining Equations 21, 27 and 30, we obtain

$$\log N(r) = \log 2N/[S_2^{\ 2}(1 + \bar{x})] + \log[r - \{1 - (V\rho_s/\rho_p)^{1/3}\}S_2\ ]$$

$$+ [r/S_2 - 1 + (V\rho_s/\rho_p)^{1/3}]^2 \log[\bar{x}/(1 + \bar{x})] \qquad (32)$$

In actual cases, the radii of the secondary particles, S_2, are not uniform (that is, S_2 is not constant), and an approximate equation (Equation 18) is not always acceptable. Consequently, the theoretical value of $N(r)$ given by Equation 32 shows a somewhat sharper distribution than that of an actual case. Equation 32 reveals that i-th order mean pore radius $\bar{r}_i$, defined by

$$r_i = \int_0^\infty r^i N(r)dr / \int_0^\infty r^{i-1}N(r)dr \qquad (33)$$

decreases as both S_2 and L decrease.

The theory presented here for the formation of porous polymeric membranes will also be applicable to the formation of dense membranes. In the latter membrane formation, the solution at stage (b) in Figure 2 (or at most between stages (b) and (c)) is dipped into a nonsolvent bath and rapid coagulation and gelation occur. If this is true, the theory predicts the existence of heteogeneity on order of some tens of nanometres, even in the dense polymer membrane.

Experiments

Membrane Preparation. Cuprammonium cellulose solutions with cellulose concentrations ranging from 3 wt% to 10 wt% were cast on a flat glass plate. The cast solution was kept in an atmosphere of a binary gas mixture of saturated acetone and nitrogen at 25°C. Alternatively, the solution was immersed immediately into the coagulation solution of acetone/ammonia/ water (30/1/69 by weight) at 25°C. After a given time, the cast solution was transferred into liquid nitrogen and then evaporated under a vacuum of 10^{-7} mm Hg at -110°C. The dried sample was fractured using a knife, shadowed by platinum vapor and then replicated by carbon under a vacuum of 10^{-7} mm Hg at -110°C. The sample thus prepared was immersed into a 2% aqueous solution of sulfuric acid in order to remove the cellulosic membrane.

Cellulose diacetate (combined acetic acid content of 54.1%) membranes with various mean pore radii were prepared from solutions of cellulose diacetate/acetone/methanol/cyclohexanol/ $CaCl_2 \cdot 2H_2O$. The solution was cast on the glass plate and acetone was evaporated following the method previously described (3).

Measurement. Transmission and scanning electron photomicrographs were taken using two types of electron microscopes (model HU-11C manufactured by Hitachi Co. Ltd. and model JSM-U3 by JEOL in Japan). The detailed method for analyzing pore characteristics by applying stereology will be given elsewhere (13).

Results and Discussion

Observation of Primary Particles. Figure 8 shows two examples of
the primary particles observed in a cuprammonium cellulose
solution. In Figure 8a, the primary particles that were nucleated
in the casting solution have diameters of about 20 nm. The
particle size distribution is rather sharp. As shown in Figure 8b,
primary particles were also observed when the solution was immersed
in a liquid composed of nonsolvents. These are dispersed from the
interfacial surface between the casting solution and immersing
liquid. The particle size is about 20 nm in diameter.

   Primary particles were also observed in the dry cellulosic
membrane as shown in Figure 9, indicating insufficient amalgamation
because of the short time duration after collisions of a primary
particle. Primary particles were also observed in the cellulose
acetate membrane after drying (3).

Observation of Growing Particles. Figure 10 shows growing particles
obtained at an intermediate stage (stage (c) of Figure 2) for a
cellulose cuprammonium solution. The particle radii are in the
range 50 to 200 nm. The diameter of the growing particle increases
through collisions with primary particles. Figures 10 and 11
illustrate these collisions and evidence of insufficient
amalgamation at the time of observation.

Observation of Secondary Particles. The growing particles quickly
amalgamate into large particles. Ultimately, the growth rate of
the growing particle approaches zero, resulting in the formation of
secondary particles. Figure 12 shows examples of the secondary
particles observed with electron microscopy. The size of the
secondary particles (radius of S_2) depends on the preparative
conditions, including the polymer volume fraction and the polymer-
solvent interactions. Under the given preparative conditions, the
secondary particle size is surprisingly uniform as seen in Figure
12.

   Some typical mean radii of the secondary particles $\bar{S}_2$ of
commercially available (F, T, S, G and M in Figure 13) and
laboratory-scale (L_1, L_2 and L_3) cellulose acetate and cellulose
membranes are shown in Figure 13. Here, $\bar{S}_2$ was calculated from the
radii of particles of the dry membranes, $\bar{S}_2'$. The $\bar{S}_2$ values in
Figure 13 range from 0.5 to 1.0 μm.

Numerical Calculation Based on Equations 6, 8 and 9. Figure 14
shows the change in the radius distribution of growing particles,
L(S,t), with time t after micro-phase separation. Note that the
weight fraction polymer concentration in in the primary particle,
V, gives the integration constant which appears when integrating
Equation 6. The values of k_1, $k_c k_2^2/S_1$, S_1, $\exp[-(2F_d^* + \Delta\phi^*)/kT]$,
V and Z are assumed to be 1.0 sec^{-1}, 5.0×10^{-6} cm/sec, 2×10^{-6} cm,
0.1, 0.4 and 0.25, respectively. There are two peaks in the L(S,t)
vs. S curve whose locations closely correspond to the radii of the
primary particle and that of the secondary particle. The existence
of these two peaks explains the reason why the primary and
secondary particles can frequently be observed experimentally. The

x = 0

(dry)

x = 3
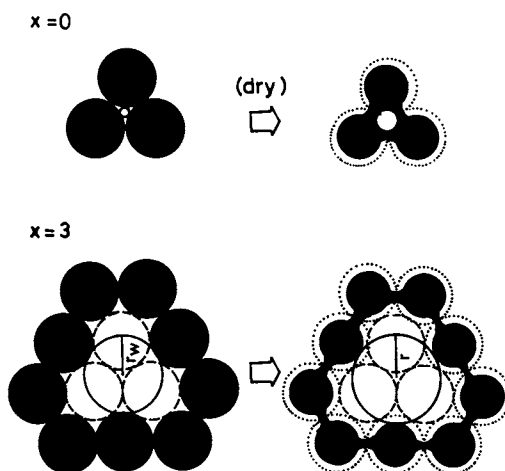
Figure 7.   Change in pore size during drying treatment.
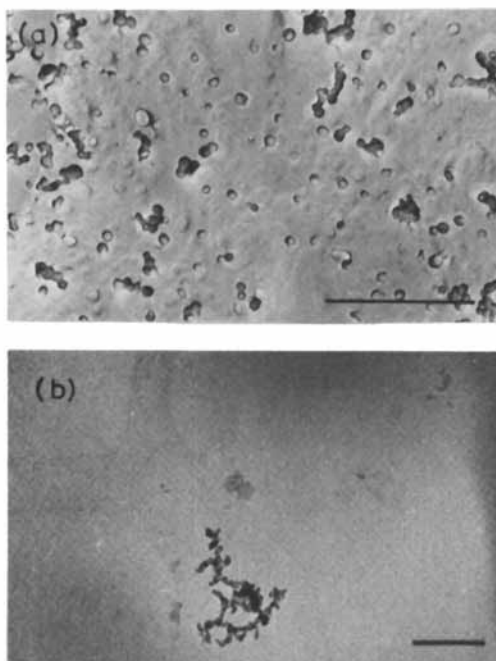
Figure 8.   Electron microphotographs of the primary particles in
cuprammonium cellulose solution:
scale bar stands for 500 nm in length; (a) primary parti-
cles in the casting solution, (b) primary particles in
the immersing liquid.

500 nm
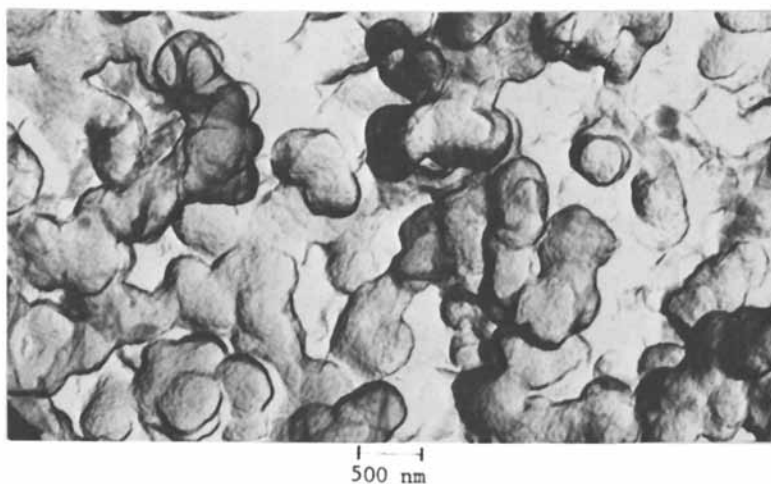
Figure 9. Electron microphotograph of the dry regenerated cellulose
           membrane prepared through micro-phase separation method:
           primary particles are observed in a secondary particle
           with a diameter of ca. 300 nm.
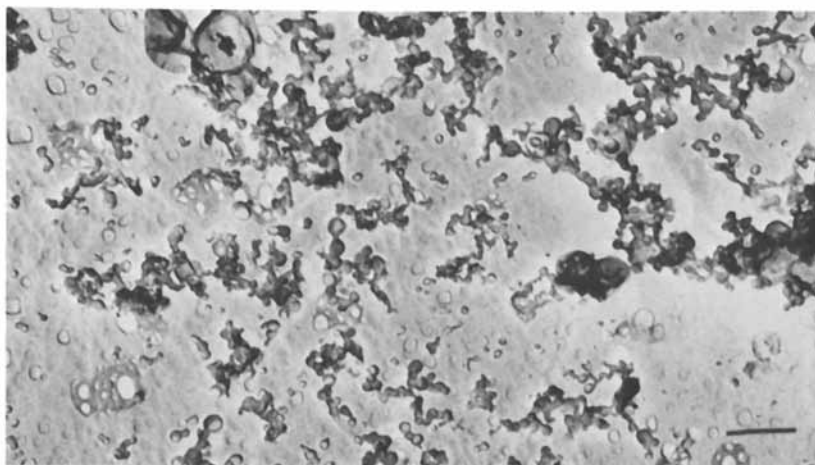
Figure 10. Electron microphotograph of the particles at intermediate
            stage in cuprammonium cellulose solution:
            scale bar stands for 500 nm in length.
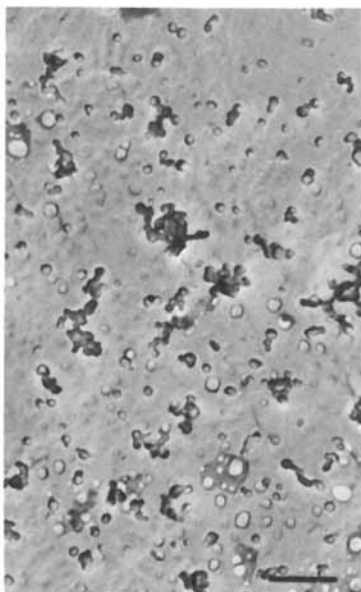
Figure 11.   Electron microphotograph of the growing particles in
             sufficient amalgamation state:
             scale bar stands for 500 nm in length.
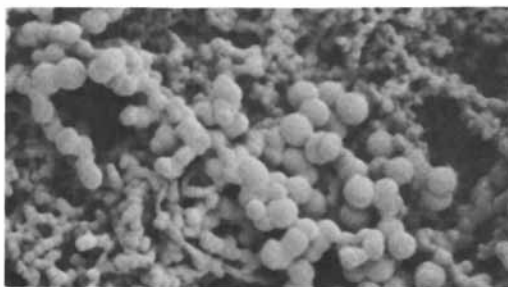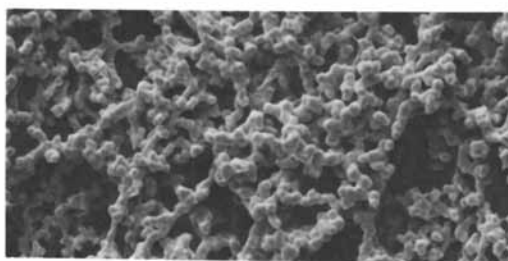
Figure 12.   Scanning electron microphotographs of generated cellulose
             membranes.

two peaks exist in all the theoretical curves of $L(S,t)$ vs. S calculated by chosing the values of t between 20 and 250 sec, k_1 between 1.0 and 10 , $k_c k_2/S_1$ between 5×10^{-6} and 1×10^{-5} cm/sec, S_1 between 2×10^{-6} and 5×10^{-5} cm, $\exp[-(2F_d* + \Delta\phi*)/kT]$ of 0.1, C between 0.1 and 0.8 and z between 0.001 and 1.0. The particle radii of the secondary particles scatter narrowly in all cases examined. With an increase in t, the mean particle radius increases. The mean radius of the growing particle is defined by

$$\bar{S}(t) = [\int_0^\infty S^2 L(S,t)dS / \int_0^\infty L(S,t)dS]^{1/2} \qquad (34)$$

By putting the value of $L(S,t)$, calculated numerically on the basis of Equations 6, 8 and 9, into Equation 34, $\bar{S}(t)$ can be evaluated as it is shown in Figure 15. The values of k_1, $\exp[-(2F_d* + \Delta\phi*)/kT]$ and S_1 are the same as those employed in the case of Figure 14. Two cases of $k_c k_2/S_1 = 1\times10^{-5}$ cm/sec, $Z = 0.01$ and $k_c k_2/S_1 = 5\times10^{-6}$ cm/sec, $Z = 0.25$ are shown in this figure. The growth rate of the particles rapidly approaches zero, due to a remarkable decrease in the number density of primary particles surrounding the growing particles, as depicted in Figure 15. We denote this asymptotic particle as the secondary particle. The radius of the secondary particle, S_2, is mainly governed by Z; that is, the greater Z is, the smaller S_2 is.

Figure 16 shows the dependence of $\bar{S}(100)$ on the parameter Z relating to the amalgamation probability after the collision of primary particles and the growing particle ($S_1 = 20$ nm, $k_1 = 1.0$ sec^{-1}, $k_c k_2/S_1 = 1.0\times10^{-5}$ cm/sec, $\exp[-(2F_d* + \Delta\phi*)/kT] = 0.1$, V = 0.4, $t = 100$ sec). The value of $\bar{S}(100)$, which is nearly equal to the radius of a secondary particle S_2, decreases abruptly with increasing Z, approaching the asymptotic value of 20 nm.

Figure 17 shows the relationship between $\bar{S}(100)$ ($=S_2$) and S_1 ($k_1 = 1.0$ sec^{-1}, $k_c k_2/S_1 = 1\times10^{-5}$ cm/sec, $\exp[-(2F_d* + \Delta\phi*)/kT] = 0.1$, $Z = 0.01$). A high correlation was observed between $\bar{S}(100)$ and S_1, and is expressed as $\bar{S}(100) = (10S_1)^{0.8}$ in Figure 17.

The value of $\bar{S}(100)$ also changes according to the polymer concentration V in the polymer-rich phase (in this case, primary particle), the rate constant k_1 related to the creation of the primary particle and the constant $k_c k_2/S_1$ related to the growth rate of the growing particle. Figure 18 shows the V dependence of $\bar{S}(100)$ ($S_1 = 20$ nm, $k_1 = 1.0$ sec^{-1}, $k_c k_2/S_1 = 1.0\times10^{-5}$ cm/sec, $\exp[-(2\Delta F_d* + \Delta\phi*)/kT] = 0.1$, $t = 100$ sec, $Z = 0.01$ are adopted in Figure 18(a)), the k_1 dependence of $S(100)$ ($S_1 = 20$ nm, $k_c k_2/S_1 = 1.0\times10^{-5}$ cm/sec, $\exp[-(2F_d* + \Delta\phi*)/kT] = 0.1$, V = 0.4, $t = 100$ sec, $Z = 0.01$ in Figure 18(b)), and the $k_c k_2/S_1$ dependence of $\bar{S}(100)$ ($S_1 = 20$ nm, $k_1 = 1.0$ sec^{-1}, $\exp[-(2F_d* + \Delta\phi*)/kT] = 0.1$, V = 0.4, $Z = 0.25$, $t = 100$ sec, in Figure 18(c)). $\bar{S}(100)$ increases with increasing V, and $k_c k_2/S_1$ and with decreasing k_1.

Pore Size Distribution of Membrane Prepared Through Micro-phase Separation Methods. In Equation 32, V and ρ_s are determined from
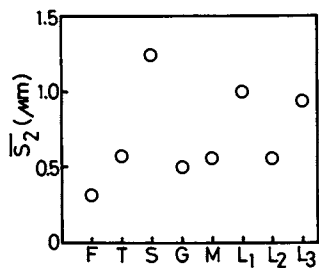
Figure 13. $\overline{S}_2$ of various cellulose acetate and regenerated membrane.
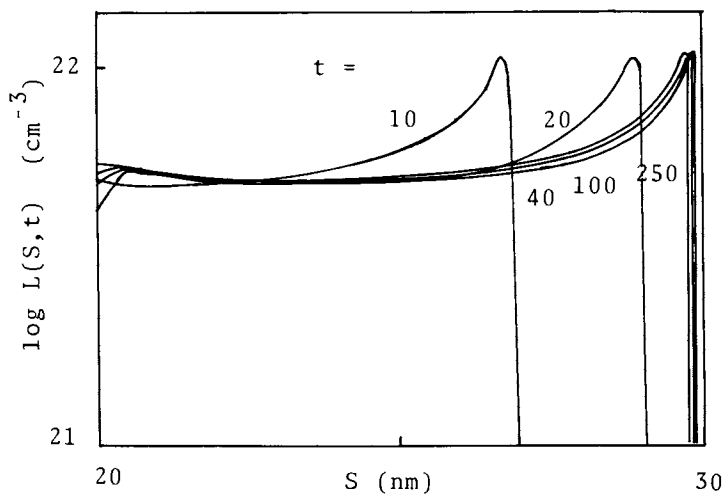
Figure 14. Change in the theoretical radius distribution function of
            the growing particles L(S,t) with time t:
            the numbers in this figure indicate t in seconds.
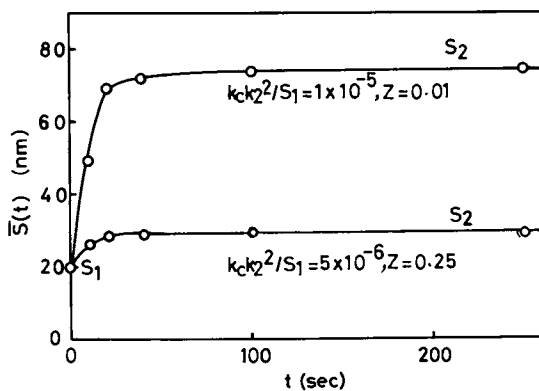
Figure 15. Theoretical $\overline{S}(t)$ vs. t curves.
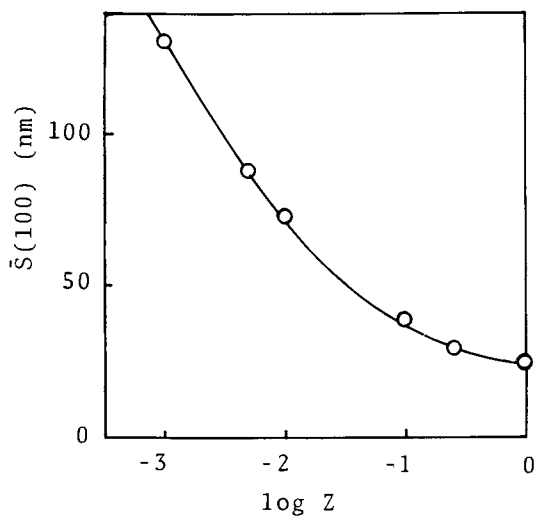
Figure 16.   Theoretical $\overline{S}(100)$ vs. log Z curve.
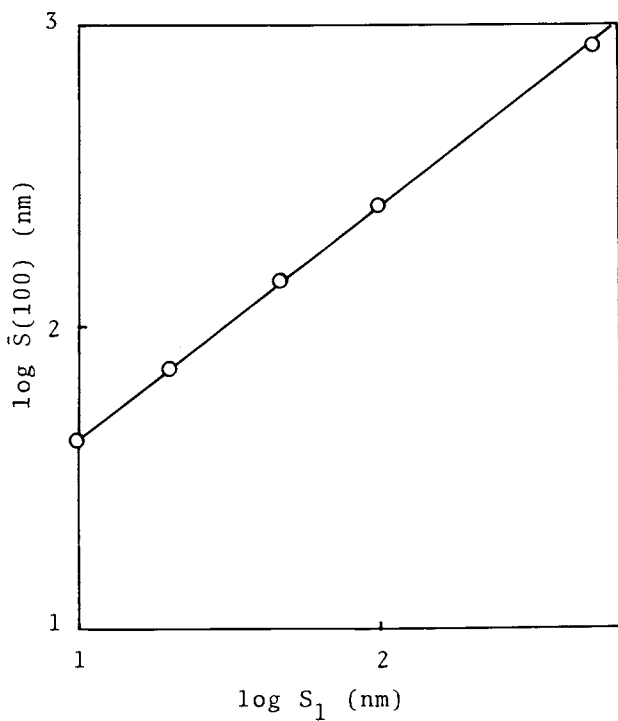
Figure 17. S_1 dependence of $\overline{S}(100)$.
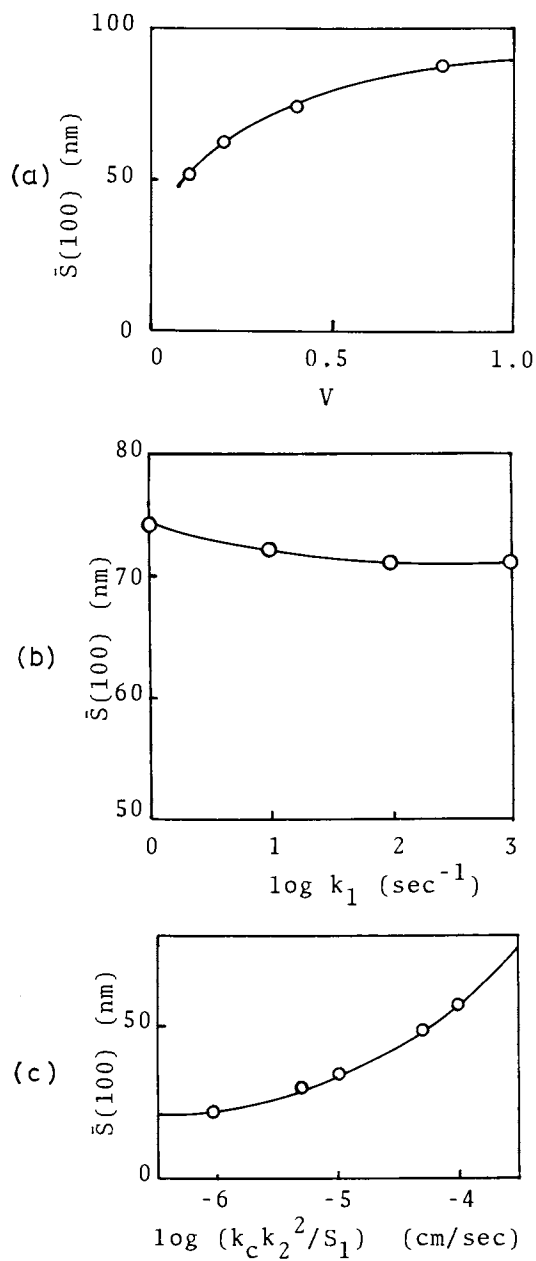
Figure 18. Dependence of $\bar{S}(100)$ on V, k_1, and $k_c k_2^2/S_1$.

the phase equilibrium experiment, and ρ_p is a constant inherent to the polymer species adopted. When the values of S_2 and L are set in advance, X can becalculated (consequently $\bar{x}$ by Equation 20) by using Equations 19, 23, 24 and 25 for the case of the circularly growing pore or Equations 19, 23, 24 and 26, for the case of a linearly growing pore. Then the pore size distribution function N(r) can be calculated using Equation 32. In numerical calculation of Equation 32, $\bar{k}$ should be determined in advance from Equations 23 and 24.

Figure 19 shows the theoretical relations between $\bar{k}$ and L, calculated according to Equations 23 and 24. In a relatively large L region, $\bar{k}$ is nearly constant (= 0.7).

Assuming that the radii of the secondary particles S_2 are uniform, N(r) can be calculated unambiguously if Pr, V, ρ_s and ρ_p are known. The N(r) vs. r curves thus obtained are shown in Figure 20(a) (V = 0.4, ρ_s = 1.1 g/ml, ρ_p = 1.5 g/ml). When S_2 increases under the constant value of Pr = 0.231 , the N(r) vs. r curve shifts to the larger r value, thus expanding its width. Various N(r) vs. r curves obtained for different S_2 and constant Pr can be reduced to a master curve if $N(r)S_2{}^3$ is plotted against r/S_2 (Figure 20(b)). Equation 32 can be rearranged into

$$\log N(r)S_2 \;\; = \log 2 - \log(1 - \bar{x}) + \log[\,(r/S_2) - 1 + (V\rho_s/\rho_p)^{1/3}\,]$$

$$+ \,[r/S_2 - 1 + (V\rho_s/\rho_p)^{1/3}]^2 \log \{\bar{x}/(1 + \bar{x})\} \qquad (35)$$

Equation 35 indicates that $N(r)S_2{}^3$ is a function of r/S_2 for the given combination of Pr, V, ρ_s and ρ_p. When $N_0 > 10^5$, numerical calculations show that $\bar{x}$ is practically independent of N_0 and N, and is mainly governed by L (and accordingly Pr) (see Equation 25. Consequently, the $N(r)S_2{}^3$ vs. r/S_2 curve is independent of S_2, and this curve is hereafter referred to as the "reduced curve." Figure 21 shows the reduced curves as a function of Pr. With an increase in Pr, the $N(r)S_2{}^3$ vs. r/S_2 curve becomes broader. The peak value of the curves decreases and the peak location shifts to the larger r/S_2 side. The value of $\bar{r}_1$ is given by $[\bar{x}^{1/2} + 1 - (V\rho_s/\rho_p)^{1/3}]S_2$ derived from Equation 28. As $\bar{r}_1$ and other kinds of mean pore radii increase, the pore size distribution unavoidably becomes broader with an increase in Pr.

Figure 22 shows the pore size distribution N(r), evaluated by electron microscopy (13), of regenerated cellulose membranes. Although this N(r) is determined under the assumption that spherical pores disperse into three-dimensional space in the membrane, the shape of the N(r) vs. r curve is similar to those of the cylindrical shaped pore (two-dimensional membrane). Still, the absolute value of N(r) is different, depending on the pore shape. The distribution curve becomes broader with an increase in mean pore radius. The slope of the N(r) vs. r curve in the range of r larger than peak location of N(r) is smaller than that in the range of smaller r. These experimental results agree qualitatively with the theoretical expectations shown in Figures 20 and 21. The validity of Equation 32 is confirmed by quantitatively comparing the theoretical N(r) with the observed one.
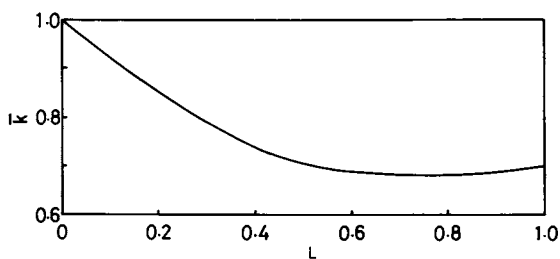
Figure 19. Theoretical $\bar{k}$ value as a function of L.
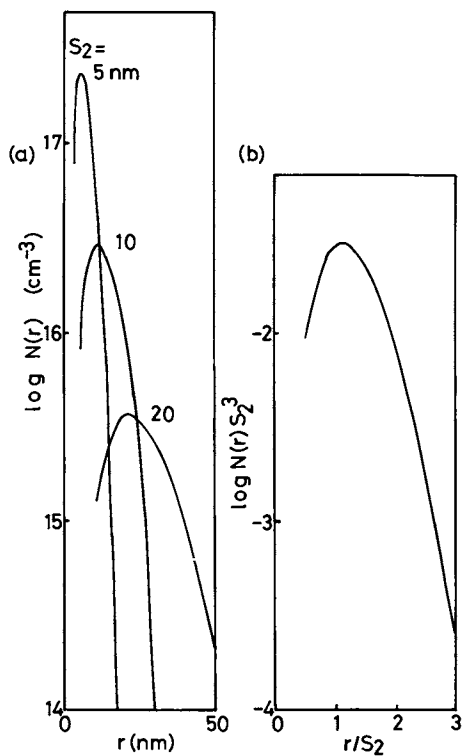
Figure 20. Theoretical $N(r) - r$ curves (a) and $N(r)S_2{}^3 - r/S_2$ curve (b).
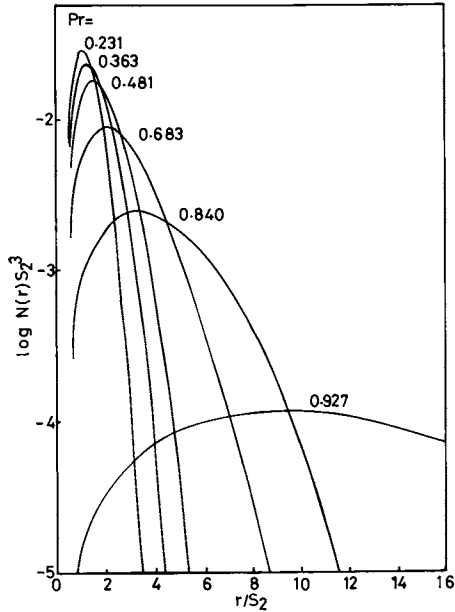
Figure 21.   Change in $N(r)S_2^3$ vs. r/S_2 curves with Pr:
the numbers in this figure denote Pr value.
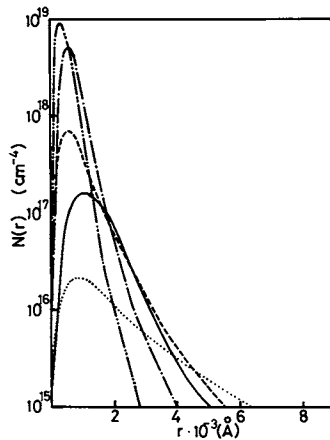
Figure 22.   Pore size distribution $N(r)$ estimated by electron micro-
scopy for regenerated cellulose membranes with different
mean pore radius (12).

The pore size distribution $N(r)$, experimentally determined for the regenerated cellulose membrane prepared through the micro-phase separation method, is compared with the theoretical $N(r)$ in Figure 23. The solid line is the experimental curve, estimated by electron microscopy on the basis of a cylindrical pore model. The broken line is the theoretical curve calculated from the experimental S_2 and Pr ($S_2 = 0.177$ μm and Pr $= 0.206$) using Equation 32 . For this membrane, we can calculate N_0 directly from the experimental S_2, using the relation $N_0 = 1/(\pi S_2^2)$ and X from the experimental Pr using the Equation 25. Here, L is calculated from the relation given by

$$L = (1 - \rho_p/\rho_s) + \rho_p Pr/\rho_s \qquad (36)$$

By putting N_0, X and L into Equation 20, we obtain $\bar{x} = 0.57$, N $= 1.75 \times 10^8$ number/cm^2 ($\rho_p = 1.5$ g/ml, $\rho_s = 1.1$ g/ml). The latter value is in excellent agreement with the experimentally evaluated pore density of 1.70×10^8 number/cm^2. The agreement between the theoretical and experimental values of $N(r)$ is fairly good.

We can conclude the following from an inspection of Figures 20, 21 and 22. Equation 32 gives an accurate pore size distribution function for the porous polymeric membrane prepared by the microphase separation method. The mean radius increases and the pore size distribution broadens with S_2 and Pr. The reduced pore distribution $N(r)S_2^3$ vs. r/S_2 curve is independent of S_2 but dependent on Pr. The effect of Pr on $N(r)$ is more remarkable than that of S_2. The reduced pore size distribution curves widen with an increase in Pr.

Relationship Between Pore Density, N, and Porosity, Pr. Equations 25 (in the case of the circularly growing pore), 20, and 35 relate the pore density and porosity. The theoretical relations between N and porosity Pr thus obtained are shown in Figure 24 with the value of S_2 as a parameter. Evidently, N decreases monotonical with an increase in Pr. Open circles, closed circles and rectangles in the figure indicate experimental data points for regenerated cellulose. Here, the radii of the secondary particles S_2 are calculated from the particles observed in the dry membranes S_2' by Equation 37.

$$S_2 = S_2'(\rho_p/V\rho_s)^{1/3} \qquad (37)$$

The theory is in reasonably good agreement with the experimental results.

Relationship Between Mean Pore Radius, $\bar{r}_1$, and Porosity, Pr.

The first order mean pore radius $\bar{r}_1$ is easily calculated from the value of $\bar{x}$ by the relation

$$\bar{r}_1 = [\bar{x}^{-1/2} + 1 - (V\rho_s/\rho_p)^{1/3}]S_2 \qquad (38)$$
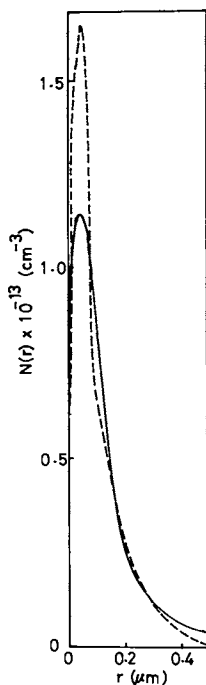
Figure 23. $N(r)$ of a regenerated cellulose membrane (12):
full line = experimental value; broken line = theoretical
value.
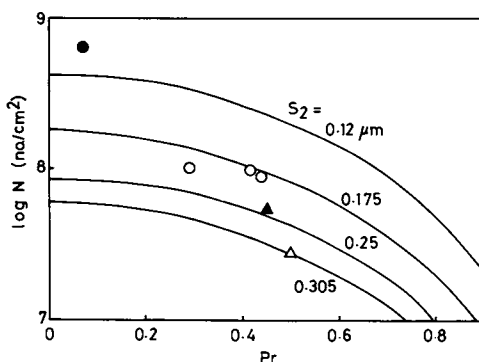
Figure 24. Theoretical relations between pore density N and Pr and
observed values of the combination of N and Pr for the
regenerated cellulose membranes with radius S_2 values:
$\bullet$, S_2 = 0.08 - 0.15 μm (observed value); O, S_2 =
0.15 - 0.20 μm (observed); $\blacktriangle$, S_2 = 0.15 - 1.25 μm
(observed); $\triangle$, S_2 = 0.27 μm (observed); full line =
theoretical curve; the numbers in this figure indicate
S_2 value in μm employed in numerical calculations.

If both S_2 and $(V\rho_s/\rho_p)^{1/3}$ are constant, irrespective of Pr, the plot of $\bar{r}_1/S_2$ vs. Pr affords a universal relation, which holds for any membrane prepared by the micro-phase separation method because $\bar{x}$ is a single-valued function of Pr only as indicated by Equations 35 and 25 (or 26). If $\bar{r}_1/\bar{r}_{1(Pr=0.5)}$ is employed in place of $\bar{r}_1/S_2$ (where $\bar{r}_{1(Pr=0.5)}$ is r_1 at Pr = 0.5), Equation 38 transforms into

$$\bar{r}_1/\bar{r}_{1(Pr=0.5)} = [\bar{x}^{1/2} + 1 - (V\rho_s/\rho_p)^{1/3}]/[\bar{x}^{1/2} + 1 - (V\rho_s/\rho_p)^{1/3}]$$

$$(Pr=0.5) \qquad (39)$$

The ratio $\bar{r}_1/\bar{r}_{1(Pr=0.5)}$ can readily be calculated from Equation 39 for a given combination of V, ρ_s and ρ_p. Figure 25 shows relations between Pr and $\bar{r}_1/\bar{r}_{1(Pr=0.5)}$ for a linearly growing pore (broken line) and two-dimensionally growing pore (solid line). For the former, a small change in $\bar{r}_1/\bar{r}_{1(Pr=0.5)}$ causes a drastic increase in Pr.

In Figure 26 the validity of the theoretical relations in Figure 25 is confirmed with actual experiments on the regenerated cellulose membrane. In the figure the value of $\bar{r}_{1(Pr=0.5)}$ corresponding to S_2 = 0.4 μm (that is, 1.2×10^{-4}) is taken as ordinate. The theoretical curve (solid line) is obtained by assuming a circularly growing pore with V = 0.4, ρ_s = 1.1 g/ml and ρ_p = 1.5 g/ml. The experimental data points are represented by various symbols whose meanings are the same as those used in Figure 24. The theoretical curves fit the data points well when the observed value of S_2 coincides with the S_2 value adopted in the calculation of the theoretical curve. This indicates the reliability of Equation 39.

Relationship Between Phase Separation Characteristics and Pore
Characteristics. Theoretical and experimental studies on phase separation show that as the initial polymer concentration v_p^o decreases, the volume ratio of the polymer-lean phase to the polymer-rich phase R (that is, L = R/(1 + R)) increases. Accordingly Pr increases and V increase. The increase in L is accompanied by an increase in the mean pore radius $\bar{r}_1$, porosity Pr and the width of the pore size distribution. An increase in V gives rise to an increase in the radius of the secondary particle S_2, resulting in a larger $\bar{r}_1$ value and smaller N value. Therefore, it is theoretically expected that the membrane with a larger mean pore radius can be prepared from a solution of lower polymer concentration. This is confirmed experimentally (see Figure 22).

Figure 27 shows the theoretical curve between R and v_p^o for a quasiternary system, in which the quasibinary solution with v_p^o was phase-separated with the addition of a nonsolvent. 14/15 (by weight) of the original polymer dissolved in the starting binary solution was precipitated (14).

When v_p^o is larger than v_p^c, the polymer-lean phase is separated as shown in Figure 2. Since this phase has low viscosity, the particles of the polymer-lean phase rapidly become larger by amalgamation. This process seems to obey the same mechanism as that of the growth of the primary particle to the
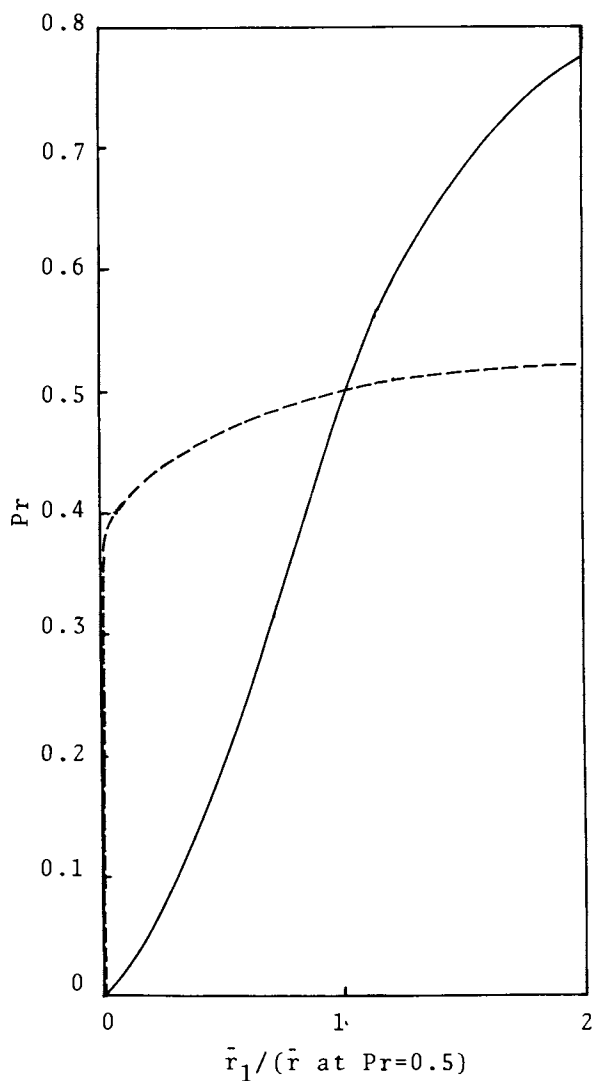
Figure 25.   Theoretical Pr vs. $\bar{r}_1/\bar{r}_{1(Pr=0.5)}$ curves:
full line = circularly growing pore; broken line =
linearly growing pore.
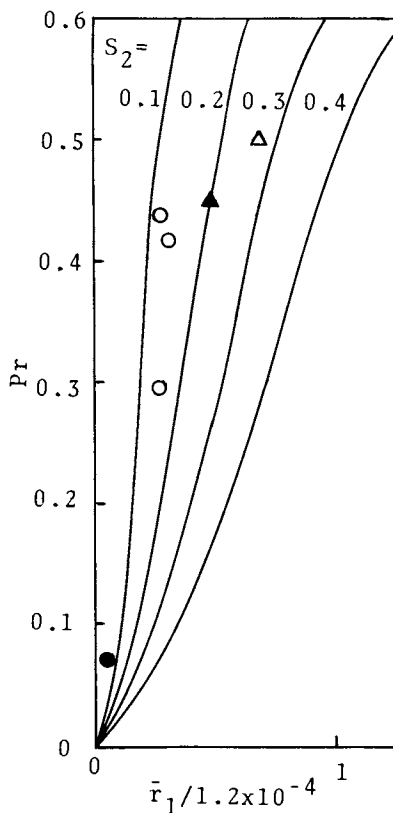
Figure 26.   Comparison between theoretical and experimental Pr values
as a function of $\bar{r}_1$:
full line = theoretical value under the fixed S_2 value;
the numbers in this figure indicate S_2 value in μm.
Various marks stand for the experimental data points
and the meanings of the marks are the same as those in
Figure 24.
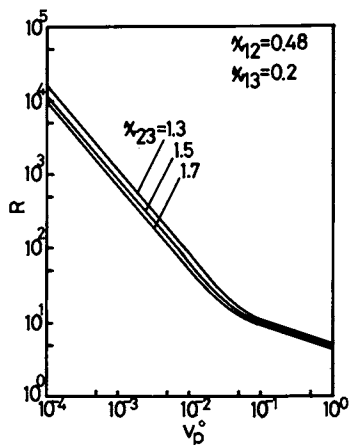
Figure 27. Relationship between the phase ratio R and $v_p^{\,o}$ for
            quasi-ternary system (14).
            Polymer: X_w (weight average degree of polymerization) =
            300, Schulz-Zimm type molecular weight distribution,
            X_w/X_n = 2 (X_n; number average degree of polymerization),
            χ_{12}, χ_{23}, χ_{13}; polymer(3)/solvent(1)/solvent(2) inter-
            action parameter.

secondary particle. Sometimes the remaining polymer-rich phase is observed to be just like the isolated particles. The aggregated polymer-lean phase particles are themselves circular, smooth pores. Even in this case, stage (j) in Figure 2 should be stable in order to prepare the microporous membrane. Figure 2 strongly suggests that uncircular pores will be obtained from relatively dilute solution and circular pores will be found from concentrated solution, although the upper critical solution temperature of the multicomponent systems is difficult to determine experimentally. Figure 28 shows typical electron photomicrographs of two kinds of porous membranes.

Another factor which governs pore characteristics is S_2, which changes slightly with the polymer concentration in the polymer-rich phase, as demonstrated in Figure 18. Both the radius of the primary particle, S_1, and the probability of the amalgamation Pa (that is, Z) are dominant variables. As S_1 satisfies the condition given by Equation 4 and Pa is given by Equation 7, the intersurface energy σ and the free energy change according with phase separation Δf control S_2. That is, when σ increases, S_1 becomes larger, resulting in a large S_2. When Δf decreases (that is, the deviation from the thermal equilibrium becomes small), S_1 and also S_2 increase.
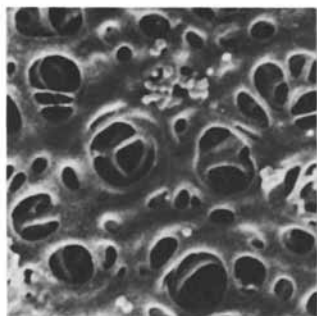
CP pore of acetate membrane
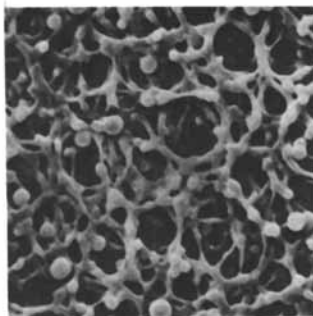
UP pore of acetate membrane
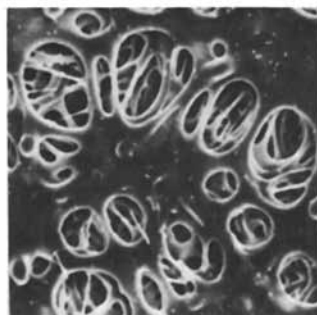
CP pore of regenerated cellulose membrane
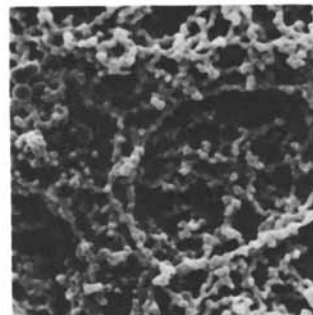
UP pore of regenerated cellulose membrane

Figure 28.   Electron scanning microphotographs of cellulose acetate and regenerated cellulose membrane.

Acknowledgment

    We would like to thank Dr. Douglas R. Lloyd for his contributions, his fruitful discussions, and help in preparing this manuscript.

Literature Cited

1. For example, Stannett, V. T.; Koros, W. J.; Paul, D. R.; Lonsdale, H. K.; Baker, R. W. Adv. Poly. Sci. 1979, 32, 69.
2. Kamide, K.; Manabe, S. In "Ultrafiltration Membranes and Applications"; Cooper, A. R., Ed.; Plenum Press: New York, 1980, p. 173; and also Polymer J. 1981, 13, 459.
3. Kamide, K.; Manabe, S.; Matsui, T.; Sakamoto, T.; Kajita, S. Kobunshi Ronbunshu 1977, 34, 205.
4. Kesting, R. E.; Manefee, A. Kolloid Z. 1969, 230, 241.
5. Pusch, W.; Walch, A. J. Membrane Sci. 1982, 10, 325.
6. Smolders, C. A. In "Ultrafiltration Membranes and Applications"; Cooper, A. R., Ed.; Plenum Press: New York, 1980, p. 161.
7. Strathmann, H.; Schble, P.; Baker, R. W. J. Appl. Polymer Sci. 1971, 15, 811.
8. Kamide, K. In "Fractionation of Synthetic Polymers"; Tung L. H., Ed.; Marcel Dekker, Inc: New York, 1977, p. 103.
9. Kamide, K.; Abe, T.; Miyazaki, Y. Polymer J. 1982, 14, 355.
10. Kamide, K.; Matsuda, S.; Miyazaki, Y. Polymer Preprints, Japan 1983, 32, 669.
11. Cahn, J. W. J. Chem. Phys. 1965, 42, 93.
12. Kuehnen, D. M.; Mulder, M.H.V.; Smolder, C. A. J. Appl. Polymer Sci. 1977, 21, 202.
13. Kamide, K.; Manabe, S.; Shigemoto, Y. to be published.
14. Kamide, K.; Matsuda, S. to be published.

Microporous Membranes via Upper Critical Temperature Phase Separation

W. C. HIATT[1], G. H. VITZTHUM[1], K. B. WAGENER[1,3], K. GERLACH[2], and C. JOSEFIAK[2]

[1]Membrana Research Department, Akzona Inc., American Enka Research, Enka, NC 28728
[2]AKZO Research Institute, Obernburg, Federal Republic of Germany

Flat stock microporous membranes can be made using a
variety of polymer types by dissolving the polymer in
a solvent at an elevated temperature, followed by
casting this solution on a temperature controlled flat
surface, provided that the system, polymer/solvent,
shows a miscibility gap. Extraction of the solvent,
called "pore former", is done with low molecular
weight alcohols. Decidedly different pore structures
can result depending upon, among other factors,
polymer concentration and rate of solution cooling.
Pore dimensions can be varied widely. The pore
structures have been well characterized, and these
data are presented.

The literature describes numerous manufacturing methods for syn-
thetic membranes. A recent review by Pusch and Walch (1) considers
membranes from a number of techniques for manufacturing membranes
and discusses applications ranging from microfiltration to desali-
nation to gas separation. In this paper, a thermal phase-separation
technique of preparing membranes is presented. The method is a
development of an invention described in US Patent 4,247,498 by
Anthony J. Castro (2). This technique is similar in many respects
to the classical phase-inversion methods; however, the additional
consideration of thermal solubility characteristics of the poly-
mer/solvent pair offers new possibilities to membrane production.
W. Henne, M. Pelger, K. Gerlach, and J. Tretzel (3) described the
same process of dissolving polypropylene in an amine for producing
microporous hollow fibers to be used in plasmapheresis.
    The development of solvent resistant commercial microporous
membranes via thermal phase separation began with an unexpected
laboratory discovery. The early workers were searching for a way to
make a concentrate of an anti-static agent in polypropylene that

[3]Current address: Department of Chemistry, University of Florida, Gainesville, FL 32611.

would be easier to handle. In doing so, they discovered that a
single-phase solution could be formed at high temperatures, but,
that as the solution cooled, a two-phase system developed. Thermal
phase separation had occurred. The resulting structure of the
polymer matrix appeared to be dependent on a number of controllable
process variables including polymer concentration, solution tempera-
ture, and cooling rate. Of these, the most significant variable for
controlling membrane structure is the cooling rate. This discovery
of thermal phase separation led to commercialization in two main
areas: controlled release and microfiltration. Flat stock, hollow
fiber, and hollow-tube membranes are all produced commercially using
this technology.

      This paper covers several aspects of the membrane manufacturing
process, membrane structural characteristics, and current applica-
tions. In addition, this paper briefly discusses applications of
the manufacturing process to two polymers and a variety of solvents.

Phase Separation in Membrane Formation

Broens, Altena, and Smolders (4) describe the theoretical consid-
erations for phase separation from concentrated polymer solutions by
chemically induced means. The authors discuss three separate
phenomena: liquid-liquid phase separation, crystallization of the
polymer, and gelation. They also address phase separation for some
classical polymer/solvent/non-solvent systems; specifically, systems
using cellulose acetate, polysulfone, polyacrylonitrile or polydi-
methylphenyleneoxide are considered. In their discussions, exten-
sive use is made of ternary phase diagrams similar to that schemat--
ically represented in Figure 1. Key features are the equilibrium
phase curve or binodal, the spinodal, the stable one-phase region,
the metastable region between binodal and spinodal, and the instable
two-phase region. A more detailed discussion of such ternary
diagrams is presented by Strathmann (5).

      Broens, et al, describe two types of liquid-liquid phase
separation: nucleation followed by growth and spinodal decomposi-
tion. The nucleation and growth process is initiated by a small
amount of nonsolvent entering the homogeneous polymer solution which
causes the localized concentration to move from the single-phase
region across the binodal curve. A nucleus is formed which contains
almost no polymer. This nucleus grows, and the polymer-rich regions
surround the polymer-poor regions, ultimately resulting in a cellu-
lar structure.

      In the metastable region between the binodal and spinodal
curves, phase separation has to occur by the mechanism of nucleation
and growth. In this region, the one-phase-state is indeed stable
against small concentration fluctuations but unstable against
separation into two phases of more different concentrations. Phase
transformations in one-component systems like condensation, evapora-
tion or solidification as well as the crystallization of solutes
from solvents occur by the nucleation and growth mechanism. The
well known phenomena of oversaturation and hindered-phase transfor-
mation can be explained by discussing the nucleation as an equili-
brium reaction with the creation of the "critical nucleus" (6, 7).
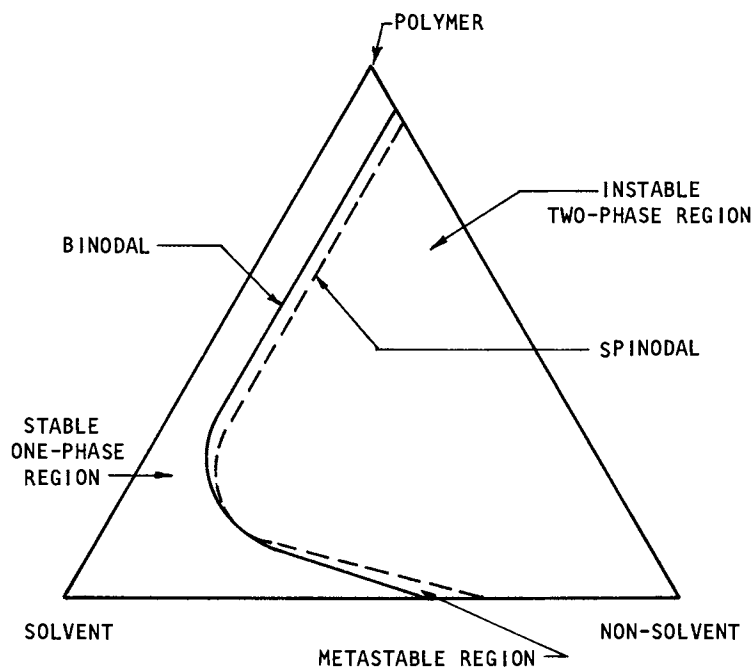
Figure 1. Classical Binodal/Spinodal Phase Diagram for Polymer/Solvent/
Non-Solvent System

In low molecular weight systems, no hindrance of phase separation during liquid-liquid-demixing could occur by the spinodal mechanism.

Spinodal decomposition is the second mechanism of liquid-liquid phase separation. Here, the solution spontaneously separates into interconnected regions of high and low polymer concentration with intertwined networks. The authors report that for chemically induced systems (polymer/solvent/nonsolvent), the nucleation and growth kinetics are much too rapid to permit spinodal decomposition.

It is possible that the mechanism of the upper critical temperature phase-separation process is different from classical liquid-liquid phase separation as described by Broens, et al (4). Classical phase separation is induced by nonsolvent diffusing into the homogeneous polymer solution, thus inducing local composition changes and causing a shift from the one-phase to the two-phase area of the phase diagram. Diffusion through a polymer solution is relatively slow compared with the nucleation and growth kinetics which predominate in the metastable region of the phase diagram. In the upper critical temperature phase-separation process, the spinodal curve can be rapidly passed since liquid-liquid phase separation is induced by thermal rather than chemical means.

Two major types of structure can occur, designated Type I and Type II, whereby the primary determining factor in the development of these two structures is the rate of cooling. At relatively low cooling rates, the Type I structure results as shown in Figure 2. Type I materials are characterized by a polymeric matrix of interconnecting pores or passageways with pores ranging in size from 10 micrometers to approximately 0.02 micrometers. Type II structure develops at higher cooling rates (Figure 3) and has a lacy appearance. Both of these structures are characterized by a high specific surface area, 90 m^2/g, which is almost independent of solvent concentration. The void volume is approximately equal to the solvent-volume fraction in the solution. The Type I structure is believed to be the result of binodal decomposition by the nucleation and growth phenomena resulting from relatively low cooling rates, whereas Type II structure is a product of relatively high cooling rates and is thought to be the product of true spinodal decomposition. This difference is important because the nucleation and growth structure (Type I) is characterized by the membranes having extremely low air or liquid flows due primarily to the relatively small passageways between the open cells.

The polymer/solvent combination polypropylene/N,N-bis-(2-hydroxyethyl) tallow amine has received the most attention in these investigations. The amine and polypropylene form a complete solution at temperatures above the melting point of the polypropylene. Upon cooling, the mixture undergoes a complete phase separation on a microscopic level wherein each of the two phases is essentially free of the other component. The solid phase is all polypropylene, and the liquid phase is all amine; thus, the amine solvent can subsequently be extracted leaving a microporous structure.

As mentioned, the classical description of a polymer/solvent system uses a ternary diagram with a nonsolvent as the third component. This representation is valid at a constant temperature. In the case of thermally induced phase separation, this description is
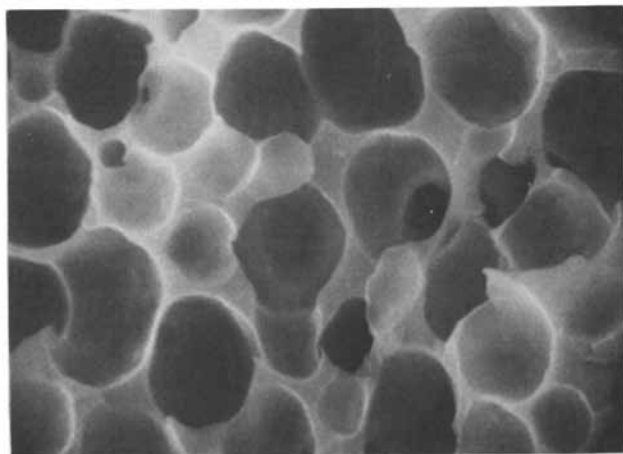
Figure 2. Type I "Open Cell"Structure of Polypropylene Formed at Low Cooling Rates (2400X)
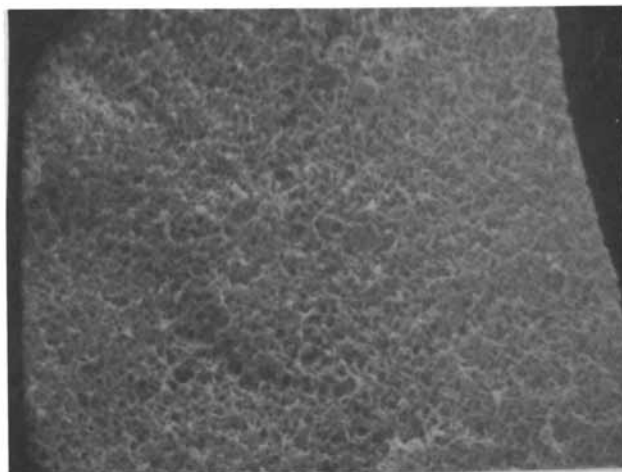
Figure 3. Type II "Lacy" Structure of Polypropylene Formed at High Cooling Rates (2000X)

expanded to include a temperature axis of the diagram. Thus, a
family of curves can be developed to describe a system. In practice
it is most useful to maintain a constant nonsolvent concentration,
often zero; so controlling solution concentration, temperature, and
cooling rate becomes the means of achieving the desired structure
and properties. Figure 4 shows a representation of these concepts.

Membrane Properties

Membrane preparation consists of three major steps: solution
preparation, membrane formation or casting, and aftertreatment.
Solution preparation can be either batch or continuous. Uniformity
of feed materials as well as process conditions are extremely
critical. The process can be described further using the simple flow
sheet as shown in Figure 5. The solvent is added to a large jac-
keted vessel and heated to the needed temperature, then polymer is
added slowly and the mixture is agitated under a nitrogen blanket
until solution is achieved. The solution is filtered and then cast
onto a water-cooled roll (known as the chill roll). The membrane is
taken up and trimmed on conventional film-winding equipment, fol-
lowed by extraction and inspection. A number of solvents, such as
methanol, ethanol, isopropanol, and methylene chloride, are suitable
for extraction, which is accomplished in a straightforward multi-
station fashion. Inspection consists of using a laser device
capable of detecting and marking the location of pinholes, thin
spots, dirty areas, etc.
     From the foregoing description, it becomes apparent that
several aspects of this process (8) are important (Table I).
The ratio of the weight of amine to the weight of polypropylene is
critical, as further reduction in the amount of polypropylene
results in a membrane with poor mechanical properties, such as a low
burst strength (measured as burst pressure). If the amount of
polypropylene is increased too much, the result may be unacceptably
low air and/or water flow rates.
     As mentioned above, the cooling rate of the solution of amine
and polypropylene is critical inasmuch as it affects the structure
type and the maximum pore size of the membranes. A rapid cooling
rate generally produces a small pore size, and a slower cooling rate
results in a larger pore size. As the cooling rate is related to
the length of time it takes the solution to solidify after the phase
separation has occurred, the primary tool in controlling the cooling
rate is the temperature of the chill roll. However, if the
temperature of the chill roll is too low, the result will be a
substantial formation of skin on the membrane side in contact with
the chill roll surface. A skin is simply a region within the
membrane which has an apparent polymer density different from that
of the remainder of the membrane.
     If the chill roll temperature is too warm, proper solidifica-
tion may not occur in time to remove a solidified sheet from the
chill roll on a continuous basis. Also, as stated, a warm chill
roll will result in a slower cooling rate and a possibly too large
pore diameter.
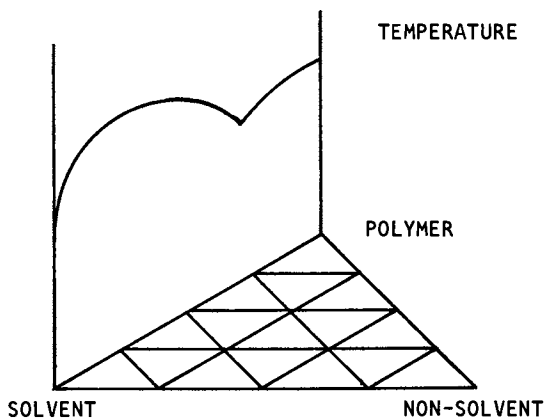
Figure 4. Representation of the Thermal Phase-Separation Process Diagram
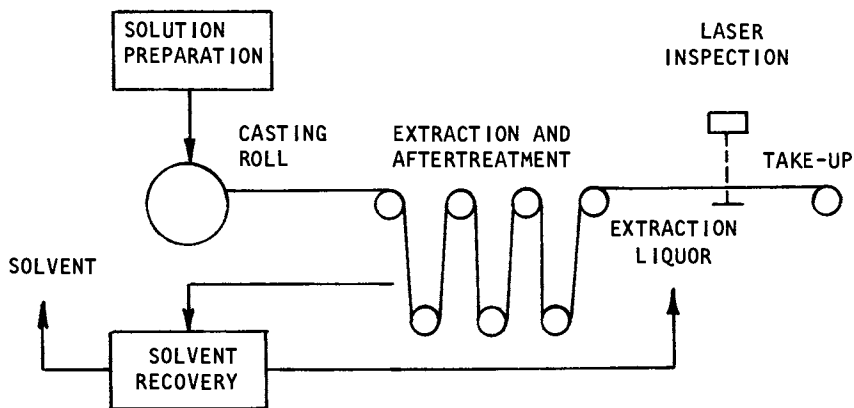
Figure 5. Simplified Process Flowsheet

Table I. Processing Conditions and Properties of Microporous ACCUREL Polypropylene Membranes

Solution Composition Amine/Polypropylene in Percent	Chill Roll Temperature in °C	Thickness in Micrometers	Maximum Pore Size[1] in Micrometers	Burst Pressure[2] kPa (psi)	Air Flow[3] at L/min cm² @ 69 kPa (10 psi)
79/21	60	140	0.46	77 (11.2)	0.96
79/21	65	140	0.58	-	1.86
79/21	78	190	0.77	-	1.64
75/25	75	168	0.54	129 (18.8)	1.16
70/30	60	86	0.27	101 (14.7)	0.87
70/30	62	165	0.35	154 (22.4)	0.51
70/30	70	173	0.37	162 (23.6)	0.51
70/30	70	81	0.34	83 (12.0)	1.10

[1] Determined by the bubble point method (8) (adapted from ASTM Method F361).
[2] Determined by measuring the maximum air pressure (8) when the membrane bursts
[3] See (8).

The thickness of the membrane, of course, affects the flow rate properties of the membrane: the thicker the membrane, the lower the flow rate. However, a thin membrane can have poor mechanical properties such as a low burst strength.

Microporous Polypropylene Membranes

The products of the thermal phase-separation membranes form a wide range of styles and configurations. Three pore sizes are currently in commercial production in polypropylene flat stock, rated at 0.45, 0.2, and 0.1 micrometers, having maximum pore sizes of about 1.0, 0.55, and 0.3 micrometers, respectively. The last two are particularly attractive for depyrogenation work which has been described by J. R. Robinson, et al (9). A similar membrane-manufacturing process is also used for making hollow fibers and tubes which are especially useful in cross-flow applications (10) and plasmapheresis (3).

Polypropylene membranes of this type can be used where the chemical resistance of polypropylene and tight control of pore size are needed. These polypropylene membranes, known as ACCUREL, are more chemically resistant than the remaining polypropylene filter cartridge components due to a proprietary process used during membrane manufacture and have replaced poly(tetrafluoroethylene) membranes in many applications.

Though polypropylene membranes do have many applications, a need also exists for microporous membranes that have a higher degree of chemical and heat resistance than polypropylene while still retaining the high flow rates and good selectivity of these membranes. Microporous membranes of polymers such as polytetrafluoroethylene (PTFE) are available. However, such membranes have typically been made by sintering processes, and the resulting membranes have lacked the good uniformity and flow rates needed in microfiltration applications.

Microporous Polyvinylidene Fluoride Membranes

Polyvinylidene fluoride (PVDF) possesses many desirable properties as a polymer. For example, it has a reasonably high melting point and good temperature resistance. It is highly resistant to oxidation and to the effects of gamma radiation. Due to its crystalline nature, it offers a satisfactory degree of solvent resistance. Its oxidation resistance makes these membranes reusable by cleaning them with aqueous sodium or calcium hypochlorite or hydrogen peroxide. Also, PVDF membranes typically possess superior ageing resistance as well as good resistance to abrasion. For these reasons, it is desirable to have microporous PVDF membranes which also possess suitable properties for filtration applications.

Several methods for producing microporous PVDF membranes are disclosed in the patent literature. U.S. Patent No. 3,642,668 (11) discloses a method for making a microporous membrane from polyvinylidene fluoride by heating and dissolving the polymer in dimethylsulfoxide or dimethylacetamide. The solution is cooled, coated onto a glass plate using a doctor blade, immersed in methanol, and finally air dried. Thus, a chemically induced phase-

separation process is utilized. U.S. Patent No. 3,518,332 (12)
discloses a method for making microporous polymer sheet material
from PVDF. In this process a mixture is formed of particles of the
polymer, a leachable particulate metallic salt, and a paraffin wax.
A sheet is formed from the mixture, the wax removed with a solvent,
and the sheet heated to sinter the PVDF particles. Subsequently,
the metallic salt pore-former is removed with a leaching solvent.
Japanese Patent No. 51-6268 (13) discloses a method for making
porous structures of PVDF with a closely controlled solution (or
gel) process with cyclohexanone. Solutions (or gels) of ten to
thirty percent polymer are cast at elevated temperatures during a
non-equilibrium state. The patent states that when the solution is
prepared by heating, the viscosity of the system increases with
time, reaches a maximum value, and then gradually decreases until an
equilibrium value is reached. It is critical that the casting takes
place during this period of descending viscosity. The patent states
that upon drying, a gel results, from which the cyclohexanone can be
removed by evaporation or extraction. None of the membranes made by
these processes have found substantial commercial success, and the
need for a suitable PVDF microporous membrane continues to exist.
     Microporous membranes of PVDF-containing polymers can be made
using the upper critical temperature phase-separation technique.
Either a homopolymer of vinylidene fluoride or a copolymer of
vinylidene fluoride with copolymerizable monomers, such as vinyl
fluoride, tetrafluoroethylene, or trifluoroethylene chloride have
been found useful. Typically the copolymerizable content will be
less than about 15% by weight. Compatible solvents which are useful
in this process include cyclohexanone, butyrolactone, propylene
carbonate, and carbitol acetate. These liquids are known to be
latent solvents for polyvinylidene fluoride, latent solvents being
defined as liquids which do not dissolve or substantially swell the
polymer at room temperature. Other compounds which are known as
being latent solvents for PVDF include butyl acetate, diacetone
alcohol, diisobutyl ketone, tetraethyl urea, isophorone, triethyl
phosphate, and dimethyl phthalate. Tetramethyl urea is also
believed to be a latent solvent.
     PVDF is a typical example for polymers with relatively low
molecular weights, resulting in relatively low viscosities of
polymer solutions needed for membrane production. Because of the
lower viscosities of these polymer solutions, phase separation
occurs faster than in the higher molecular weight polypropylene
solutions. For a given cooling rate predetermined by the process,
the solvents used for PVDF have to show a small temperature range
between liquid-liquid demixing and solidification of the polymer
phase. Choosing different solvents usually means choosing different
temperature gaps between the beginning of phase separation and
solidification. The final membrane structure is essentially deter-
mined when the solidification temperature is passed during cooling.
This solidification temperature is easily determined experimentally.
To achieve comparable structures and pore sizes with the high
molecular weight polypropylene, solvents must be chosen which
provide a remarkably broader temperature range between phase sepa-
ration and solidification. Because the final membrane properties,

especially air and water flows, are strongly dependent on polymer
concentration (flows decrease with increasing polymer concen-
tration), the viscosity of the PVDF solutions cannot be "corrected"
by increasing the PVDF concentration.

Depending upon the concentration of the polymer in solution and
upon how quickly the solution is cooled, one of two membrane struc-
tures may be formed, each being clearly distinct from the Type I and
Type II structures found for polypropylene (14).

Table II.   Experimental Data for Forming Polyvinylidene Fluoride
Microporous Membranes

Solvent	Polymer Concentration (%)	Temperatures (°C) Solution/Casting Roll	Structure Type
Cyclohexanone	20 to 40	185/RT	III
Butyrolactone	30 to 50	164/RT	III
Propylene Carbonate	20 to 40	165/RT	III
Carbitol Acetate	10 to 50	180/19-60	III & IV

Type III (Figures 6 and 7) membrane consists of a relatively tight
skin supporting spheres of polymer, whereas Type IV (Figures 8 and
9) contains "leaves" of polymer stacked upon a more open skin.
Depending upon the cooling conditions and the polymer concentration,
the same membrane can show a transition between Type III and Type IV
structures within its cross-section (Figures 10 and 11). Typical
membrane properties are found in Table III.

Table III.   Membrane Properties for Two Types of PVDF Membranes

Property	Type III	Type IV
Maximum Pore Size, Micrometers	0.2 - 0.5	1.0 - 2.0
Water Flow Rate, mL/min cm^2 @ 69 kPa (10 psi)	0.2 - 0.7	20 - 50

Structure Type III, although quite intriguing in its appearance, has
little to offer in terms of being a membrane because of the tight
skin that exists on the surface. Flow properties are too low to be
useful. However, the presence of so many spheres on the surface
lends to the suggestion that fine powders could be generated from
the membrane, powders that might be useful in controlled release
applications.

Type III structures are created at higher polymer concen-
trations and with slower cooling rates; experimental conditions
which promote nucleation and thus growth of polymer in the solid
state from solution. Using carbitol acetate as the solvent, Type
III structures could be generated either by using a polymer concen-
tration minimum of 30% or by maintaining the chill-roll temperature
above 40°C. Variations in skin thickness were present when changing
the casting roll temperature with an apparent increase in thickness
occurring when lowering the temperature.
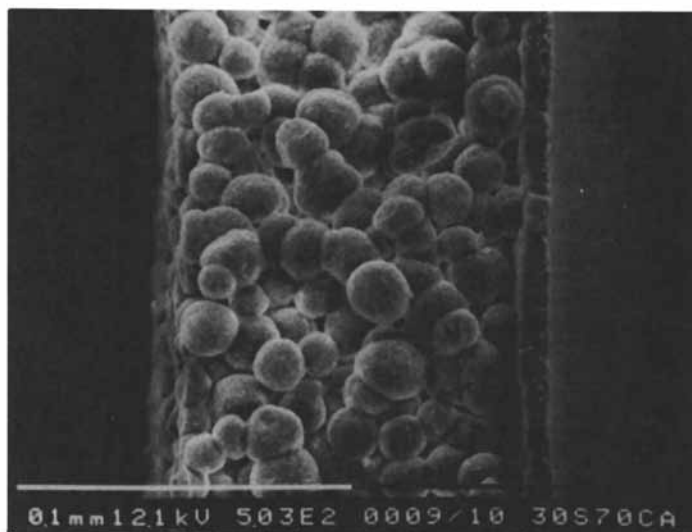
Figure 6. Type III Structure of Polyvinylidene Fluoride Membrane Formed
           at Low Cooling Rates and Higher Polymer Concentrations (503X)
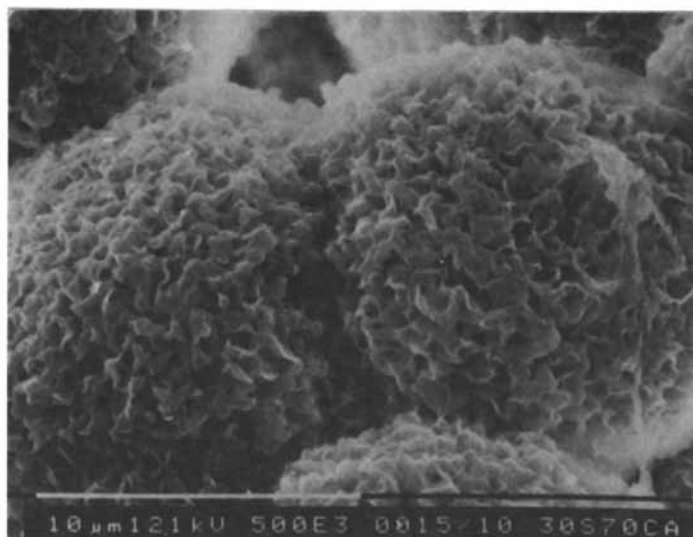
Figure 7. Type III Structure of Polyvinylidene Fluoride Membrane at
           Higher Magnification (5,000X; compare Figure 6)
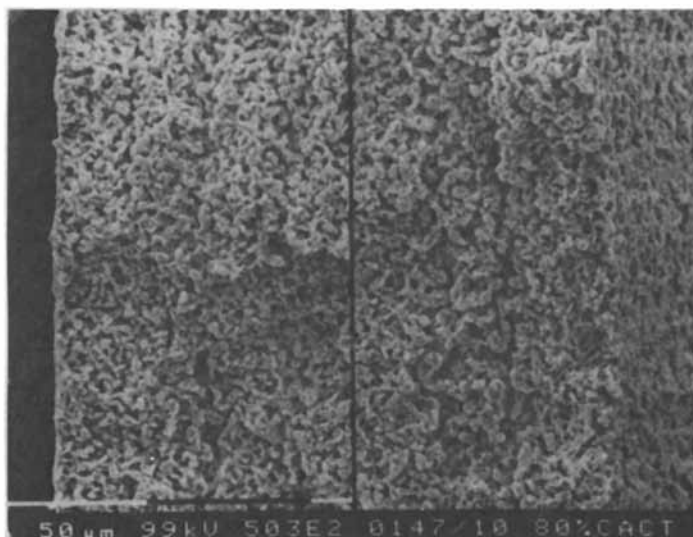
Figure 8.   Type IV Structure of Polyvinylidene Fluoride Membrane Formed
at Higher Cooling Rate and Low Polymer Concentration (Split
Image Photograph to Show Both Edges; 503X)
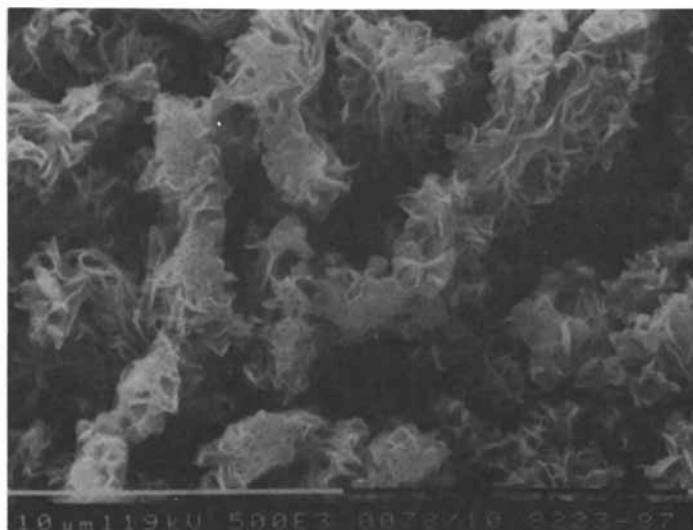
Figure 9.   Type IV Structure of Polyvinylidene Fluoride Membrane at
Higher Magnification (5,000X; compare Figure 8)
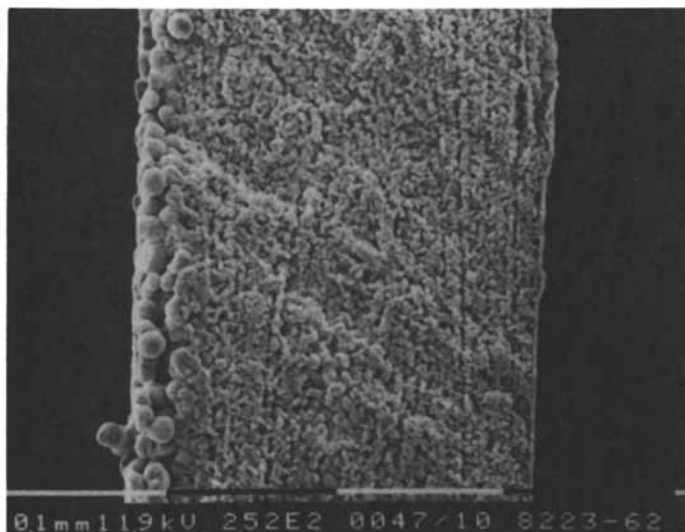
Figure 10. Transition Between Type III (Spherical) and Type IV (Leaf-
Like) Structure of Polyvinylidene Fluoride (252X)
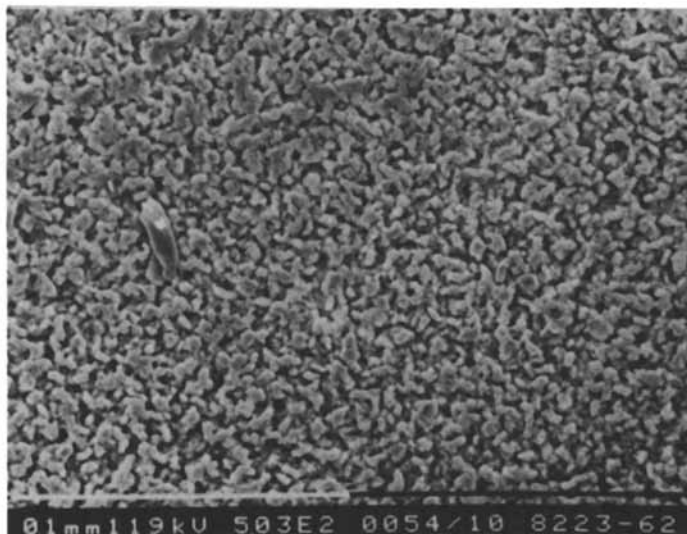
Figure 11. SEM Picture of Skin of Polyvinylidene Membrane Shown in
Figure 10 (503X; Right Side)

Type IV structures were formed from carbitol acetate solutions by maintaining a cold chill roll (less than 35 °C) and keeping the polymer concentration below 30 weight %.

This process is demonstrated in the following example. A homogeneous solution of 20 weight % PVDF and 80 weight % carbitol acetate is prepared in a resin kettle at 150°C in a dry atmosphere. This solution can be formed into a microporous embodiment simply by allowing it to cool. Microporous membranes can be made by feeding the solution into a heated casting box. (Membranes can also be made by using a heated doctor blade and glass plate arrangement.) The solution is then cast onto a roll maintained at room temperature. The membrane can be removed from the roll and has sufficient mechanical strength for all needed handling. The membrane is extracted with isopropyl alcohol and has the following properties:

Bubble Point (IPA)	43 kPa (6.3 psi)
Maximum Pore Size	1.4 micrometers
Water Flow	30.4 mL/min cm^2 @ 69 kPa (10 psi)
Air Flow	2.5 L/min cm^2 @ 69 kPa (10 psi)

Summary

The exploration of the thermal phase-separation process has added a new dimension to the science of microporous membranes. New and useful products can be made from a large spectrum of polymers ranging from hydrophobic polymers, like polypropylene or PVDF, to hydrophilic ones, like nylon which we have not touched upon in this article.

Acknowledgments

Literature Cited

1. Pusch, W.; Walch A. Angew. Chem. Int. Ed. Engl. 1982, 21, 660-685.
2. Castro, A. J. US Patent 4,247,498, 1981.
3. Henne, W.; Pelger, M.; Gerlach, K; and Tretzel, J. in "Plasma Separation and Plasma Fractionation," M. J. Lysaght and H. J. Gurland, Eds;, S. Karger AG: Basel, 1983; pp. 164-179.
4. Broens, L.; Altena, F. W.; Smolders, C. A. Desalination, 1980, 32, 33-45.
5. Strathmann, H. in "Material Science of Synthetic Membranes", D. R. Lloyd, Ed.; American Chemical Society: Washington, DC.
6. Volmer, M., "Kinetik der Phasenbildung," Steinkopff: Dresden und Leipzig 1939.
7. Zettlemayer, A. C., (Ed.); "Nucleation," M. Decker, New York 1969.

8.   Davis, M. A.; Vitzthum, G. H.   US Patent Application.
9.   Robinson, J. R.; Barnes, T.; Genovesi, C.; O'Dell, M.;
     Takacs, J.   "Task Force Report on Depyrogenation," Parenteral
     Drug Association, No. 1982, Chap. 6.
10. Klein, W.   Filtration & Separation, March/April 1982, 130.
     Schneider, K. and Klein W.   Desalination, 1982, 41, 263-275.
11. Bailey, J. L.; McCune, R. F.   US Patent 3,642,668, 1972.
12. Sklarchuk, J. C.; Kobie, W. F.   US Patent 3,518,332, 1970.
13. Murayama, Nahiro; et al.   Japanese Patent 51-6268, 1976.
14. Coggins, M. D.; Vitzthum, G. H.; Wagener, K. B.   US Patent
     Application.

Asymmetric Membranes for Gas Separations

HEINZ FINKEN[1]

Department of Chemical Engineering, The University of Texas at Austin, Austin, TX 78712

Recent membrane developments for gaseous mixture separations are compared to the development of reverse osmosis membranes for water desalination. The goals of these developments have been the search for ideal permselective polymeric materials, techniques for producing ultrathin membrane layers free of imperfections and transforming gelled reverse osmosis membranes into solid gas permeation membranes. A novel approach to meeting the basic requirements of high permselectivity is attempted by altering the physical polymer structure within the membrane prior to application for gas separation. The influence of these physical interactions on membrane properties is presented.

The development of membranes for gas separations has been closely linked to that for water desalination. Therefore, a short review of the history of reverse osmosis membranes is first given, followed by a presentation of the milestones leading to today's commercial, asymmetric membranes for gas separations.

Membrane Development for Water Desalination

The era of economically viable membrane development which began in the late 1950's and continues to this date, may be divided into two time periods: the first generation of integral-asymmetric, cellulosic membranes (1959 to 1970) and the second generation of asymmetric, non-cellulosic membranes (1971 to 1984).

[1] Current address: Institut fuer Chemie, GKSS Forschungszentrum, Geesthacht GmbH, Max-Planck-Strasse, D-2504 Geesthacht, Federal Republic of Germany

<u>Cellulosic Membranes</u>. In the first period, summarized in Table I, cellulose acetate (CA) was discovered as a highly selective material by Reid and co-workers (<u>1</u>) who found high salt rejections, but unfortunately low permeate water fluxes (40 L/m^{2}d) through their membranes. In 1960, Loeb obtained widely scattered results during permeation measurements of CA ultrafiltration membranes manufactured by the German company Schleicher & Schuell. This was first attributed to sealing problems, but later found to depend on the side of the membrane which was exposed to the feed water (<u>2</u>). He interpreted this behavior to be due to the asymmetric structure of the membranes, which was confirmed later by scanning electron miscroscopy. Loeb and Sourirajan (<u>3</u>) were successful in developing a procedure for preparing asymmetric membranes. They invented a solvent-casting/water-precipitating method. The membranes consisted of a 0.1 to 1.0 micron-thin skin layer and an integrally-bound, 100 to 200 micron-thick supporting layer. The skin layer was non-porous and so thin that dissolved salts were rejected almost completely, and water was allowed to permeate through it with fluxes 10 times greater than those of symmetric membranes (400 L/m^{2}d). The sponge-like, microporous sublayer had mechanical stability which allowed for high pressure operation and produced high permeate fluxes and recoveries.

The decade following this invention was devoted to improvements of the transport properties and simplifications of the preparation procedures. As CA membranes did not meet the salt rejection requirements necessary for one-stage seawater desalination, a search for more favorable materials started. In 1965, Merten and co-workers (<u>4</u>) prepared a double-layer CA membrane by solvent-casting on a water surface and laminating the ultrathin film on a microporous supporting membrane. A salt rejection for seawater of 99.8% was achieved. This type of membrane is now called a "thin-film composite membrane." The same preparation technique was used some years later by Cadotte and co-workers (<u>5</u>) to make 500 Å thin layers of cellulose acetate of varying acetyl content. A cellulose diacetate membrane with an acetyl content of 39.8% yielded a permeate flux of more than 650 L/m^{2}d with a salt rejection of 94%, whereas a cellulose triacetate membrane with an acetyl content of 43.2% exhibited a lower permeate flux of 200 L/m^{2}d at a higher salt rejection of 99%. All these membranes were only suitable for one-stage brackish-water desalination.

A breakthrough for seawater desalination occurred in 1970 with the findings of Cannon, Saltonstall and co-workers (<u>6,7</u>) that a blend of cellulose diacetate and triacetate resulted in membranes showing better permselectivities than those prepared from the single components. Blend membranes with an average acetyl content of 41.5% gave initial permeate water fluxes of 530 L/m^{2}d and salt rejection of 99.6% when tested with 3.5% NaCl-solutes at 25°C and 105 bar.

<u>Non-cellulosic Membranes</u>. Despite an intensive search for more favorable membrane polymers, cellulose acetate remained the best material for reverse osmosis until 1969 when the first B-9 permeator for brackish water desalination was introduced by Du Pont. Richter and Hoehn (<u>8</u>) invented aromatic polyamide asymmetric hollow-fiber

Table I: Milestones in membrane development for water desalination

Year	Inventor	Invention	Main Improvement
1959	Reid et al. (1)	selection of cellulose acetate (CA)	low water flux (40 L/m^{2}d) at a salt rejection of 96%
1960	Loeb and Sourirajan (3)	integral-asymmetric CA membranes	increased water flux (400 L/m^{2}d) and salt rejection (98.6%)
1965	Merten et al. (4)	thin-film composite (TFC) membranes of CA	high salt rejection (99.86%)
1970	Cadotte et al. (5)	thin-film composite CTA membranes	high salt rejection (99%) at medium water flux (200 L/m^{2}d)
1970	Cannon and Saltonstall (6,7)	integral-asymmetric CA blend membranes	higher water flux (500 L/m^{2}d) at high salt rejection (99.6%)
1969	Richter and Hoehn (8)	aromatic polyamide hollow-fibers	low-cost module system with high salt rejection
1977	Cadotte et al. (9,10)	interfacial-polymerization TFC membranes	extremely high water flux (800 L/m^{2}d) at high salt rejection (99.5%)

membranes for this module. Although this moderately hydrophilic, rather stiff-chain polymer showed an intrinsically lower water permeation (70 L/m²d) than cellulose acetate, it became competitive because of the low-cost self-supporting fiber technology and its high packing density. A hollow fiber module can reach packing densities up to 9200 m²/m³ compared to a spiral-wound module equipped with flat sheet membranes with only 660 m²/m³. The comparison of these systems is more realistic on the basis of their water flux densities: a value of 680 m³/d/m³ is calculated for a hollow-fiber and 230 m³/d/m³ for a spiral-wound module system.

In 1977, Cadotte and co-workers (9) combined the technique of thin-film composites with interfacial polymerization. This new method extended the range of possible membrane polymers to water-soluble compounds like polyethyleneimine which were stabilized after casting by cross-linking with, for example, toluene diisocyanate. The intrinsically high water permeability of these hydrophilic polymers along with the technique of making 500 Å thin, selective layers free of imperfections revealed a membrane with a permeate flux of 800 L/m²d at a salt rejection of 99.5% (North Star, NS 100).

Aside from these decisive milestones in the development of reverse osmosis membranes, further advances have been achieved which are important in terms of reproducibility, availability, flux improvements (more than 1100 L/m²d at 99.5% have been achieved to date), mechanical stability and chemical resistance. The inventions are listed here in chronological order. Their appropriate treatment would require a special discussion outside the realm of this paper:

        1966 - CTA hollow-fiber system (Dow) (10);
        1975 - flux-stabilized CA blend membranes (GKSS, M 97 TVZ)
               (11);
        1976 - thin-film composite membranes of cross-linked
               polyetheramide (UOP, PA 300) (12);
        1977 - polybenzimidazolone, thin-film composite membranes
               (Teijin) (13);
             - thin-film composite membranes of cross-linked
               polyether/urea (UOP, RC 100) (14);
        1980 - thin-film composite membranes of cross-linked polyether
               (Toray, PEC 1000) (15);
             - thin-film composite membranes of modified, cross-linked
               aromatic polyamide (Film Tec, FT 30) (16).

The Development of Asymmetric Membranes for Gas Separations

Cellulosic Membranes. The first asymmetric membrane for gas separation appeared in 1970 (Table II), and it was not surprising that this membrane was a modified CA membrane of the Loeb-Sourirajan type (17). Gelled CA membranes for water desalination must be stored wet in order to maintain their permeation performance. However, in gas permeation, wet, plasticized membranes tend to lose their properties with time due to plastic creep of the soft material under pressure and due to slow drying during which the microporous sublayer may collapse and thus increase the thickness of the dense skin-layer. Gantzel and Merten (17) dried CA membranes with an acetyl-content of 39.4% by quick-freezing and vacuum sublimation at

Table II: Milestones in membrane development for gas separation

Year	Inventor	Invention	Main Improvement
1970	Gantzel and Merten (17)	freeze-dried, asymmetric CA membranes	high N_2 permeation rate of 3.1×10^{-6} [1] at a He/N_2 selectivity of 34
1975	Schell (20)	solvent-dried, asymmetric CA blend membranes	higher N_2 permeation rate of 4.8×10^{-6} [1] at a He/N_2 selectivity of 68
1976	Ward et al. (31)	TFC membranes made of silicone/polycarbonate block copolymers	extremely high N_2 permeation rate of 8.6×10^{-2} [1] at a low O_2/N_2 selectivity of 2.3
1979	Henis and Tripodi (34)	asymmetric polysulfone hollow fibers coated with silicone rubber	high H_2/CO selectivity of 33 with a low-cost module system

1) $\bar{P}/\ell$, $cm^3(STP)/cm^2\text{-s-cmHg}$; to obtain $m^3(STP)/m^2\text{-s-MPa}$ multiply by 7.501.

$-10°C$. They obtained nitrogen permeation rates (permeability, $\bar{P}$, per unit thickness, ℓ) of 3.1×10^{-6} cm^3(STP)/cm^2-s-cmHg with a variable-volume/constant-pressure method at 22°C and a separation factor for He/N$_2$ of 34. The higher separation factor of 97 observed with a fully dense, symmetric membrane sample of identical chemical composition was explained by the presence of defects in the skin-layer of the asymmetric membrane.

Four years later, Stern and co-workers (18) investigated commercial desalination CA membranes with an acetyl-content of 40.8%. The membranes were dried by a simple method developed by Vos and Burris (19): first soaking them in an aqueous solution containing surfactants to reduce the water-polymer surface tensions, and then air-drying them. The nitrogen permeation rate of such a membrane was 4.7×10^{-7} cm^3(STP)/cm^2-s-cmHg at 30°C measured with the time-lag method which is a constant-volume/variable-pressure method with a downstream pressure of almost zero. Although this value indicates lower transport properties, the authors could demonstrate that the permeation of permanent gases through CA membranes can be described accurately by a solution/diffusion mechanism.

The same idea of drying membranes with solutions of decreasing surface tension was applied by Schell (20) to integral-asymmetric CA blend membranes. The membranes were prepared through a sequence of successive solvent exchange steps followed by air-drying. A typical permeation rate for nitrogen is 4.8×10^{-6} cm^3(STP)/cm^2-s-cmHg at 25°C. This value is better than that observed for CA membranes by Gantzel and Merten (17). The He/N$_2$ separation factor of 68 is twice that observed for a CA membrane. However, the higher intrinsic value of 97 for a dense, symmetric cellulose diacetate film could not be reached. Nevertheless, a high separation factor of 68 for an asymmetric CA blend membrane proves that its skin-layer must be dense and free of imperfections. The decreased hydroxyl content of the CA blend compared with the cellulose diacetate homopolymer diminishes the intermolecular hydrogen bonding of the polymer chains and leads to an increase of polymer segments mobility and to an easing of diffusion of penetrating gas molecules. These considerations explain the higher permeabilities for both helium and nitrogen gases through CA blend membranes at the expense of lowered selectivity.

CA blend membranes for gas separation are commercially available from Envirogenics Systems Co. (El Monte, CA), Separex Corp. (Anaheim, CA) and Grace Membrane Systems (Houston, TX), and are applied in spiral-wound modules for the separations of acidic gaseous components from natural gas, for the recovery of carbon dioxide in enhanced oil recovery processes for gas dehydration or the separation of hydrogen from carbon monoxide (21-23).

Non-cellulosic Membranes. While the development of CA gas permeation membranes can be directly attributed to the development of water desalination membranes, the invention of modified silicone membranes and polysulfone membranes was more influenced by the extension of knowledge of transport, sorption and diffusion of gases in polymers (24-27). In principle, rubbery polymers exhibit the highest gas permeabilities at the lowest selectivities, and,

unfortunately, they have a strong tendency to distend under higher
pressure differences. To solve this problem of mechanical instabil-
ity, Ward and co-workers (28-30) pioneered in 1976 the use of block
copolymers for gas permeation membranes. They combined the high
gas permeability of rubbery polymers like silicone with the
function of glassy polymers like polycarbonate which act as cross-
links between the rubbery segments, because glassy chain segments
tend to aggregate in rigid, microscopic domains. To increase the
throughput, they tried to decrease the membrane thickness (31) by
using a method known in biological membrane research as the
Langmuir-Blodgett technique. This method is used to build mono-
molecular layers of film-forming substances at water-air interfaces.
A schematic of a Langmuir trough is depicted in Figure 1. The film
formation at the air-water interface is accomplished by adding
drops of dilute film-forming solutions to the water surface or by
allowing the solution to flow down evenly onto a plastic block
installed a few millimeters above the water surface. If the film-
forming agent has surface activity, the solution spreads spontan-
eously on the water surface. Amphiphilic molecules with a hydro-
phobic, lyophilic paraffin tail and a hydrophilic, polar headgroup
best meet the requirements for film-forming materials. Polymers
that do not spread spontaneously can, nevertheless, be readily
adsorbed interfacially from solution in a volatile, water-immiscible
solvent like hexane, cyclohexane, benzene, dimethylformamide,
dimethylsulfoxide or their mixtures. The structure of the film can
be made dense by decreasing surface area. This is achieved by
moving the plastic block, which is partially immersed in the water,
toward the existing film. A typical surface-pressure/surface-area
isotherm, along with simplified structures of monolayers, is given
in Figure 2. The surface pressure, or the difference between the
surface tensions of the solute and solvent, changes through a series
of steps from a gas to a fluid and finally to a solid state when
the film is compressed (32,33).

Ward and co-workers adapted this technique to the preparation
of ultrathin silicone/polycarbonate membranes and advanced it by
spreading the dilute solution first on a limited water surface
between two plastic blocks and then moving the blocks apart. This
method spreads the polymer solution continuously, reducing the
thickness of the film. A nitrogen permeability rate of 8.6×10^{-2}
$cm^3(STP)/cm^2$-s-cmHg and an O_2/N_2 selectivity of 2.3 are reported
for a 1000 Å thin film.

Applications under investigation for this type of membrane are
the production of oxygen-enriched air for industrial combustion and
biological degradation processes or the production of nitrogen-
enriched air with less than 9% oxygen to inert fuel tank spaces and
vent lines of aircraft. A portable oxygen-enricher is commercially
available from Oxygen Enrichment Co. (Schenectady, NY) for respir-
atory disease oxygen therapy.

The latest major innovation, and also economically the most
successful breakthrough, was achieved by Henis and Tripodi (34-38)
with their invention of the resistance model (RM) fiber membranes
in late 1979. In agreement with the history of reverse osmosis
membrane development, they selected a high-strength, glassy polymer
as membrane material, such as polysulfone with a glass transition
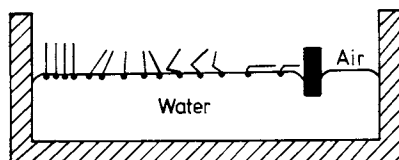
Figure 1. Principles of a Langmuir trough
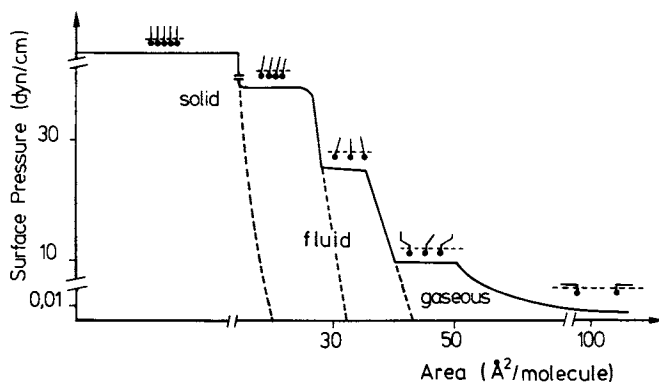
Figure 2. Typical surface pressure/area isotherm

temperature of 180°C. The intrinsic hydrogen permeability of polysulfone is 1.2×10^{-9} cm^3(STP)-cm/cm^2-s-cmHg and its selectivity for the system hydrogen/carbon monoxide is 40.0. Compared to silicone with a value of 5.2×10^{-8} cm^3(STP)-cm/cm^2-s-cmHg, the hydrogen permeation through polysulfone is lower by a factor of 43.3. But this disadvantage is more than compensated for by the ability to form polysulfone hollow fibers with a great volume-to-surface ratio, a technology that cannot be used for the rather soft rubbery polymers like silicone. In addition, the hydrogen/carbon monoxide selectivity for silicone is only 2.1 for silicone. In contrast, cellulose acetate shows a selectivity for the same gas pair of 46.3 and its hydrogen permeability is 5.0×10^{-10} cm^3(STP)-cm/cm^2-s-cmHg. Therefore, its transport behavior is similar to that of polysulfone which seems to be not surprising, since the glass transition of cellulose acetate is in the same temperature range of 180 to 185°C like polysulfone. A serious problem which Henis and Tripodi had to overcome was the production of reproducible hollow fibers free of imperfections. In contrast to reverse osmosis, skin layer fine pores with diameters larger than those of the penetrant gas molecules effect a viscous or pore flow through the membranes, which reduces drastically their separation capabilities. This is because the gas viscosities and gas diffusion coefficients are several orders of magnitudes lower and higher, respectively, than those of liquid solutions and solutes. From an engineering point of view, the higher diffusion coefficient of gas is advantageous, since the phenomena of concentration polarization on the upstream side of the membrane can be neglected, which allows a simplification of the module design. Whereas the surface porosity is difficult to prevent in flat-sheet membrane technology, it is much more vexing in hollow-fiber technology. In addition to the two concomitant requirements of very thin and defect-free skin-layers of integral-asymmetric membranes, the porosity of the supporting sublayer must be optimized simultaneously to prevent its collapse when subjected to high pressures and to minimize its resistance to gas flow. Therefore, Henis and Tripodi separated the problem of surface porosity from the actual preparation of the polysulfone fibers by vacuum coating a thin layer of silicone rubber inside the fiber bores.

A schematic view of the cross-section of an RM hollow-fiber and the electrical circuit analog is presented in Figure 3. In effect, the silicone is sucked into the pores and fills them. The total flow resistance R_t can be considered analogous to an electrical circuit consisting of four resistances installed in a series-parallel configuration. A gas must first pass through the coating layer (R_1), then either through the pores filled with coating material (R_2) or through the skin-layer of the fiber (R_3), and finally through the porous sublayer (R_4) to the fiber bores. The total resistance is given by

$$R_t = R_1 + \frac{1}{\dfrac{1}{R_2} + \dfrac{1}{R_3}} + R_4 \quad .$$

Because silicone rubber is a highly permeable polymer, the gas

transport through the underlying less permeable, glassy skin-layer of polysulfone is expected to be influenced only slightly by the coating-layer. This is verified in Table III where the resistances to permeate gas flows for the different parts of RM fibers have been calculated with the assumption of a membrane area of 1 m^2. On the basis of intrinsic permeabilities (36), the calculation reveals the lowest flow resistances for the coated silicone layer. Compared to this, the flow resistance of the polysulfone skin-layer to hydrogen is higher by a factor of 4.4, and resistance to carbon monoxide is higher by a factor of 84. The greatest resistances to the permeating flow are created by the pores filled with silicone. Their values are 4 to 5 orders of magnitude higher than the other resistances.

With the rational assumption of negligible resistance to flow offered by the porous sublayer and with the result that the pore resistance is much greater than the skin-layer resistance, the relation for the total resistance simplifies to

$$R_t = R_1 + R_3 .$$

According to Table III, the contribution of the silicone layer to the flow of the less permeable carbon monoxide is only 1.2% and can be neglected, but it does contribute remarkably to the flow of the more permeable hydrogen by approximately 20%. Correspondingly, the H_2/CO separation factor of the selective polysulfone skin-layer is reduced by 20% from 40 to 33, because the ideal separation factor is by definition the ratio of the permeability rates or - vice versa - the reciprocal of the ratio of the flow resistances. With this invention, Henis and Tripodi discovered a simple and ingenious solution to the problem of surface porosity. They found a limiting value for the surface porosity. If it exceeds the value of 10^{-4}, the selectivity of the fiber is destroyed almost completely (36).

The RM hollow-fibers are employed in the PRISM separators of Monsanto (St. Louis, MO) which have been successfully tested since 1979 in more than 40 industrial plants in the chemical and refinery field. They are being used for the recovery of hydrogen from waste-gases and purge-streams that contain varying amounts of N_2, Ar, CO, CO_2, C_1 to C_6 paraffins, and C_6 to C_8 aromatics.

The Influence of the Physical Structure of Integral-asymmetric CA Blend Membranes on Carbon Dioxide/Methane Separation

After the 1982 decision by the GKSS Research Center (a national laboratory in Geesthacht, Federal Republic of Germany) to shift the research and development activities in the field of membrane technology from seawater desalination to selective permeation for gas separation, several commercial RO membranes were first investigated for their utilization in gas separation by determination of their gas permeability rates. The permeation apparatus designed for a constant-pressure/variable-volume method is depicted in Figure 4. The flow test unit with an effective membrane area of 35.26 cm^2 is supplied with either a pure gas or a gas mixture from gas cylinders. The upstream gas pressure is adjusted by a pressure regulator and monitored by a precision manometer, while the

Table III: Resistances to H_2 and CO flows through RM hollow fibers
              made of silicone-coated polysulfone

Fiber part	Resistance ($s-cmHg/cm^3$) to	
	H_2	CO
silicone layer (R_1)	0.19	0.40
pores filled with silicone (R_2)	1.00×10^4	1.75×10^7
polysulfone skin-layer (R_3)	0.83	33.35
total fiber resistance	1.03	33.75

Note: It was assumed that area A_1 = 1 m^2; A_2 = A_1; A_3/A_2 = 1.9 x
10^{-6}; thickness ℓ_1 = 1 x 10^{-6} m; and ℓ_2 = ℓ_3 = 1 x 10^{-7} m;
and that the intrinsic permeabilities in cm^3(STP)–cm/cm^2–s–cmHg
were as follows [36]:

gas	silicone	polysulfone
H_2	5.2×10^{-8}	1.2×10^{-9}
CO	2.5×10^{-8}	3.0×10^{-11}

RM hollow fiber   Electrical circuit analog

$$R_t = R_1 + \cfrac{1}{\frac{1}{R_2} + \frac{1}{R_3}} + R_4$$
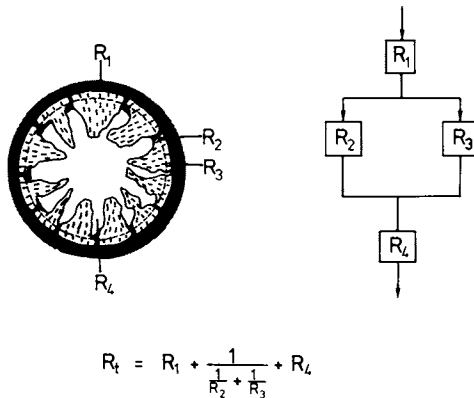
Figure 3.   Cross-section of a resistance-model hollow-fiber and electrical circuit analog
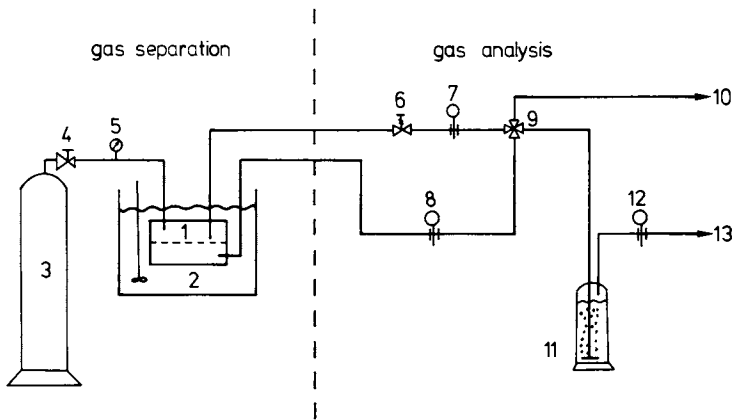
Figure 4.   Diagram of the permeation apparatus (1=flow test unit; 2=thermostated water bath; 3=gas cylinder; 4=pressure regulator; 5=pressure gauge; 6=back-pressure valve; 7,8=flowmeters; 9=four-way valve; 10=to gas chromatograph; 11=absorption column; 12=flowmeter; 13=vent line)

downstream pressure is equivalent to the atmospheric pressure. The
temperature is controlled by placing the test unit in a thermostated
water bath. The flow of the retentate is regulated by a back-
pressure valve. Permeate and retentate flows are measured, at
ambient pressure and temperature, by water or soap-bubble displace-
ment in graduated glass cylinders or burettes. Gas mixtures are
analyzed by gas chromatography or absorption techniques.

   The permeability rates of the commercial RO membranes for
helium, oxygen and carbon dioxide along with the ideal separation
factors for helium/nitrogen, nitrogen/oxygen and carbon dioxide/
methane are recorded in Table IV. The data were determined with
pure gases at a temperature of 25°C and at an upstream pressure of
40 bar. The readings were taken after the system had reached
steady-state conditions. The permeation experiments with different
gases were carried out in the following sequence: helium, oxygen,
nitrogen, methane and carbon dioxide. In general, the commercial
RO membranes had high permeability rates at low selectivities. As
the selectivities did not approach the intrinsic values of the
polymers, it was concluded that the selective skin or composite
layers were not free of pores and imperfections. One type of
composite membrane (UOP, RC 100) could not be investigated, because
the composite layer was so brittle that it tore when assembled in
the test unit. These results demonstrate that RO membranes do not
have the capability to separate gases. There is one remarkable
exception: the CA blend membranes showed a high selectivity of
41.8 for He/N_2 at a considerable permeability rate.

   The prospective gas separation properties of CA blend membranes
for carbon dioxide and methane are also outlined in Table V where
some literature data are summarized. This table shows again that
glassy polymers with a rigid back-bone and, hence, a high glass
transition temperature, such as polyimide, have the highest selec-
tivity for CO_2/CH_4 of 65.0, and that rubbery polymers, such as
dimethylsilicone, have the highest carbon dioxide permeability rate
of 1.08×10^{-4} $cm^3(STP)/cm^2$-s-cmHg. While the separation capability
of silicone is 19 times lower than that for polyimide, its permea-
tion rate for carbon dioxide is 13,500 times higher. The transport
properties of cellulose acetate are situated between these two
polymers: their selectivity is ten times higher than silicone, and
two times lower than polyimide, whereas their permeability rate is
32 times higher than polyimide and 420 times lower than silicone.
It may be also interpreted from the data of Table V that the gas
separation properties of CA films are almost independent on their
degree of substitution. This is inconsistent with the fact that
the glass transition temperature strongly depends on the hydroxyl
content of the cellulose acetate polymers. With the loss of
hydrogen bonding interactions, the glass transition drops from
185°C for a cellulose diacetate (d.s.=2.45) to 114°C for a cellu-
lose triacetate (d.s.=2.86). There are two reasons which suggest
that the CO_2 permeabilities of cellulose triacetate should be
higher than those of cellulose diacetate: the CO_2 sorption is
supposed to increase with the degree of acetylation due to favorable
electrostatic interaction between the dipoles of the carbonyl
groups of the ester and the polar carbon dioxide molecules. The
CO_2 diffusion should be eased by the lack of polymer-polymer inter-

Table IV: Pure gas permeability rates of commercial reverse osmosis membranes at 25°C and 40 bar

Membrane polymer	Manufacturer	Permeability Rate [1]			Ideal Separation Factor		
		He	O_2	CO_2	He/N_2	N_2/O_2	CO_2/CH_4
integral-asymmetric membranes							
cellulose acetate	Hydranautics	1389	-	-	2.9	-	-
CA blend	Envirogenics	1828	146	1292	41.8	0.3	4.2
thin-film composite membranes							
polyetherurea	U O P	tore apart, when assembled in test unit					
unknown (RO 98)	Osmonics	6542	-	19,001	3.1	-	9.0 [2]
polyamide (FT 30)	FilmTec	13,962	5811	5080	1.6	1.6	0.6 [2]
polyethyleneimine	Nitto	1681	-	-	1.8	-	-
polyurethane	Nitto	0.37	-	-	-	-	-

1) in 10^{-7} cm^3(STP)/cm^2-s-cmHg; to obtain m^3(STP)/m^2-s-MPa multiply by 7.501

2) for CO_2/N_2

Table V: Cellulose acetate in comparison to other polymers

Polymer	T_g [1]	$\bar{P}/\ell(CO_2)$ [2]	α^* [3] CO_2-CH_4	Reference
symmetric membranes [4]				
PI	400	0.08	65.0	[42,43]
CA	185	3.20	34.9	[20]
CA/CTA	170 [5]	2.24	34.9	[20]
CTA	155	2.28	33.5	[43]
Silicone	-117	1080.00	3.4	[44]
asymmetric membranes				
CA/CTA	170	1610.00	26.0	[20]

1) glass transition temperature T_g in °C

2) permeability rate $\bar{P}/\ell$ in 10^{-7} $cm^3(STP)/cm^2$-s-cmHg; to obtain $m^3(STP)/m^2$-s-MPa multiply by 7.501

3) ideal separation factor α^* for the gases carbon dioxide and methane

4) with a film thickness of 25 μm

5) estimated

actions. Verification of this hypothesis is currently under investigation.

The most important requirements of high selectivity and high permeability for the more permeable CO_2 gas seem to be met by the asymmetric CA blend membranes. They exhibit the permeability rates of rubbery materials and the selectivities of a glassy polymer with an intermediate high glass transition temperature.

These first results and suggestions stimulated further investigations of CA blend membranes for gas separation. At a given chemical composition of the CA blend, that is at a ratio of cellulose diacetate to triacetate of 1:1, and at a given phase inversion process for asymmetric membranes which is described in detail elsewhere (39-41), different kinds of membranes could be prepared by applying various post-treatment methods, such as annealing, freeze-drying and solvent-drying. As mentioned above, gas separation membranes should be in an unplasticized, solid state to maintain their separation properties over a long period of time. Therefore, the gel membranes swollen in water must be transferred to a dry, solid state.

Freeze-drying. To improve the CA blend membranes for gas separation, attempts were made to freeze-dry the membranes. Normally, the process of freeze-drying is applied to biological substances which are susceptible to structural damages and to loss of properties. It is the preferred method to pretreat sensitive specimens for investigation by scanning electron microscopy. The drying of wet membrane samples is similarly aimed at the maintenance of their asymmetric structure. The microporous sublayer with its high water content is particularly susceptible to collapse during the drying process and thus to enhance the thickness of the skin-layer. As the crystal size of the frozen water favorably decreases with increasing rate of cooling, the wet membranes were first shock-frozen at the nitrogen melting point. By this means, ice crystal growth during the phase transition, which would cause volume expansion and damage to the membrane structure, was almost prevented. The vitreous ice was then allowed to sublimate under vacuum. The temperature during sublimation influenced the rate of gas permeation (Figure 5), which was measured with pure gases at the test conditions of 25°C and 40 bar. The CO_2 rate increases from 1.85×10^{-4} to 2.40×10^{-3} $cm^3(STP)/cm^2$-s-cmHg with an increase in the sublimation temperature from -100°C to -40°C. The corresponding rates for helium, nitrogen and methane are reduced by 76, 91 and 91%, respectively, with the same 60°C increase in sublimation temperature. The plot of the permeability ratios for the system CO_2/CH_4 and He/N_2 in dependence of sublimation temperature (Figure 6) shows that the He/N_2 selectivity is almost not affected by the temperature of sublimation, but that the CO_2/CH_4 selectivity exponentially increases to values above 100 with increasing sublimation temperature. This effect of sublimation temperature on the physical structure of the membrane has not yet been investigated by independent methods like scanning electron microscopy. But the results of these permeation measurements may be interpreted in terms of a solution-diffusion model which was first introduced to describe the transport behavior through reverse
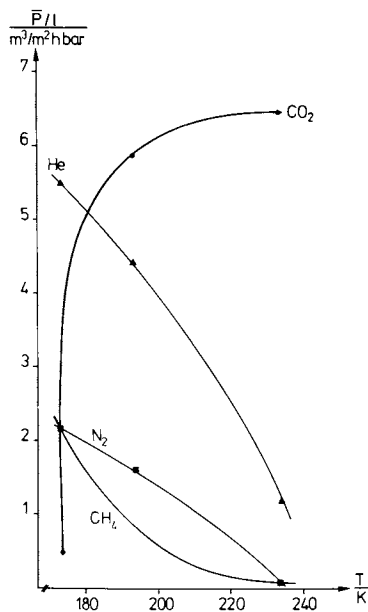
Figure 5. Permeability rate, $\bar{P}/l$, as a function of sublimation temperature, T, during the freeze-drying of CA blend membranes (pure gases, 25°C, 40 bar; to obtain $cm^3(STP)/cm^2$-s-cmHg multiply by 3.69×10^{-4})
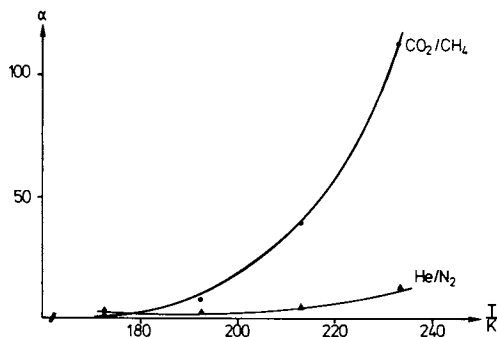
Figure 6. Ideal separation factor, α, as a function of sublimation temperature, T, during the freeze-drying of CA blend membranes (pure gases, 25°C, 40 bar)

osmosis membranes. In contrast to liquid-solute separations, where
the extremely low solubility of salts in the membrane excludes them
almost completely from transport through membranes, the diffusivity
term in gas-gas separations mainly contributes to the overall
permeations of permanent gases through glassy polymers. Exceptions
from this general rule occur only with those penetrating gas
molecules which strongly interact with the polymer. In this case,
the solubility may predominate the diffusivity.

As described above, the main problem in freeze-drying of
asymmetric membranes is the prevention of ice crystal growth during
the very short period of initial shock-freezing. But this may also
hold true for the long period of time of actual freeze-drying,
during which the ice inside the membrane must sublimate to water
vapor molecules and then diffuse to the membrane surface. At the
same time, the countercurrent effect of crystal growth may take
place, which is faster the higher the sublimation temperature is.
By this, the sponge-like structure of the supporting layer may
be partly damaged and compacted when pressurized. The effective
thickness of the selective barrier layer will, in turn, grow and
hence the permeation rate will decrease with increasing sublimation
temperature as shown for helium, nitrogen and methane (Figure 5).
The reduction in diffusion rate should also apply for CO_2.
Therefore, the observed increase in CO_2 permeation can only be
explained by an overproportional enhancement in CO_2 solubility,
which is the dominant factor for the permeation because of strong
interactions between CO_2 and cellulose acetate. It is clear from
the "dual-mode sorption" model that the solubility depends on the
nature of the polymer and penetrating gas and on the number and
size of pre-existing holes in the polymer. Only the latter can be
influenced by the freeze-drying process, and it is evident that the
number of pre-existing holes which can be filled with CO_2 should be
increased in the membranes prepared at higher sublimation
temperatures.

A comparison of gas transport rates of freeze-dried CA blend
membranes with those treated by simple air-drying shows that
freeze-drying produces membranes with CO_2/CH_4 selectivities higher
by a factor of 27 (see Table VI). The CO_2 permeation is faster and
reaches a value of 239.4 x 10^{-5} $cm^3(STP)/cm^2$-s-cmHg. However, the
selectivities for smaller penetrants such as He/N_2 are reduced by a
factor of 3.2.

The reason for the significant alterations of gas transport
with varying post-treatment procedures is not yet well understood.
The risk of damaging the selective skin-layers is increased when
membranes are dried in an uncontrollable and higher rate at ambient
conditions. Whereas the low selectivity of CO_2/CH_4 for air-dried
membranes supports this opinion, the high He/N_2 selectivity does
not.

Annealing. The final properties of Loeb-Sourirajan type CA
membranes are created by annealing the membranes in hot water at
temperatures between 70 and 100°C. In effect, salt rejection
increases at the expense of permeate water flux with increasing
temperature. Two mechanisms may be discussed to explain this

behavior. First, the active skin layer may either shrink, thereby
reducing its thickness but enhancing its density, or the skin-layer
may be thickened by partial conversion of the adjacent, microporous
sublayer into the dense skin layer. Secondly, the enhanced mobility
of the CA polymer segments during annealing may cause intra-
molecular or intermolecular hydrogen bonds to change to more favor-
able, exothermic interactions leading to a higher degree of polymer
crystallinity. More crystalline domains generally reduce sorption
and also represent barriers to diffusion.

The effect of wet annealing on gas permeation of CA blend
membranes is demonstrated in Figure 7. The wet membranes were
immersed in a hot water bath at temperatures of 90, 95 and 100°C
for 15 minutes, quenched to ambient temperature, soaked in ethanol
and air-dried. The permeability rates of He and N_2 of 11.0×10^{-5}
and 1.2×10^{-5} cm^3(STP)/cm^2-s-cmHg were not affected by this
procedure. The same is true for carbon dioxide with 6.3×10^{-4}
cm^3(STP)/cm^2-s-cmHg up to 90°C. But above this temperature, the
CO_2 permeation grows rapidly by 185% from 90 to 100°C. At 100°C,
the permeability ratio of the CO_2/N_2 system is 140 with a CO_2
permeability rate of 1.8×10^{-3} cm^3(STP)/cm^2-s-cmHg (see Table VI).
Compared to freeze-drying, the annealed membranes show permeability
rates for helium and carbon dioxide lowered by 75 and 25%,
respectively. The ideal separation factor for CO_2/CH_4 is, however,
increased by 28%. The observed constant permeability rates for
helium and nitrogen indicate that the first of the two above
proposed effects of annealing does not hold since changes in thick-
ness or density of the active layer would cause a direct response
in permeation. Only in the rare case that an increased density is
exactly compensated for by a decreased thickness would the permea-
tion be kept constant. The increase in CO_2 permeation, however,
may be explained satisfactorily by the second mechanism; that is,
by configurational changes of polymer interaction due to heat
treatment of the CA polymer plasticized by water. The steep
increase above 95°C indicates that second-order transitions combined
with a more randomly distributed order of the polymer can take
place. As transition temperatures are generally depressed by
plasticization, it is not surprising that this wet transition
temperature is somewhat lower than those observed for dry, unplasti-
cized polymers. The glass transition of dry, solid cellulose
diacetate and triacetate are in the range 180 to 190°C and in the
range 150 to 160°C , respectively, depending on hydroxyl content,
because the enhanced acetyl-content lowers the hydrogen-bonding
interaction between the polymer chains. Moreover, four second-order
transitions are reported for cellulose diacetate at temperatures of
15, 40 to 60, 70 to 90 and 114 to 120°C, and two are described for
cellulose triacetate at temperatures of 30 to 46 and 105 to 120°C
(45). Therefore, the transport of CO_2 through CA blend membranes
may be changed when annealed at 100°C which is above the glass-
transition temperature of wet CA blend polymers. The exponential
permeability increase of CO_2 may be attributed to the second-order
transitions described above leading to a higher solubility of CO_2
in cellulose acetate and a stronger plasticization at elevated CO_2
pressures.

Solvent-drying. After annealing at 100°C, the absorbed water inside
the membranes was removed by a proprietary procedure. Its effect
on gas permeation is given in Table VI. No effect is observed on
the helium and carbon dioxide permeability rates. But the permea-
bility rates of nitrogen and methane are considerably lowered so
that the separations of both systems, helium/nitrogen and carbon
dioxide/methane, are enhanced. With a value of 44.1 for helium/
nitrogen, the ideal separation factor of the external reference
membrane is slightly exceeded, whereas the separation factor for
CO_2/CH_4 of more than 2500 is improved by a factor of 600.
     It is evident that the permeability rates of gases similar in
size and shape like nitrogen and methane depend on the actual state
of the polymers. The transformation of gelled polymers to solids
by the drying procedure may change their state in such a manner
that the polymer density increases and the "free volume" decreases
resulting in lowered permeability rates. Exceptions from this
general rule apply only for molecules such as helium which are very
small and carbon dioxide which are able to plasticize the CA
polymers.

The Influence of Temperature and Pressure on the Transport Properties of CA Blend Membranes

Temperature. The outstanding transport behavior of the carbon
dioxide/cellulose acetate blend system was again experienced when
the test conditions were changed. The temperatures of the thermo-
stated water bath was set between 18 and 50°C, while the upstream
pressure of the pure gas was kept constant at 40 bar. As depicted
in an Arrhenius plot of logarithmic permeabilities versus reciprocal
temperatures in Figure 8, the permeations of He, N_2 and CH_4 were
accelerated by increasing temperatures, and the CO_2 permeation was
slowed down. Consequently, the He/N_2 separation is almost indepen-
dent of temperature as shown in Figure 9 whereas the CO_2/CH_4
separation declines steeply from 2500 to 500. It is a matter of
fact that the solubility of a given gas in polymers generally
decreases with increasing temperature while its diffusivity
increases. In cases where the permeability of gases through
polymer films increases with temperature, such as depicted in
Figure 8 for He, N_2 and CH_4, it is clear that the diffusivity is
the dominant factor for permeation. In those cases where the gas
permeability decreases with temperature, it may be concluded that
the solubility term mainly influences permeation. A reduction of
the CO_2 permeability by 71% is calculated for CA blend membranes
from Figure 8 where the temperature raises from 20 to 60°C.
Comparison to the temperature-dependence of solubilities for low-
molecular-weight analogs confirms this behavior. For the same
temperature increase from 20 to 60°C, the solubilities of CO_2 in
water and acetone decline by 63 and 95%, respectively (46). Thus,
the solubility decrease is in the same order of magnitude or even
higher which compensates for the enhanced diffusivity at higher
temperatures.

Pressure. Experiments with variable pressures were conducted with
pure gases at a constant temperature of 25°C. Pressures between 10
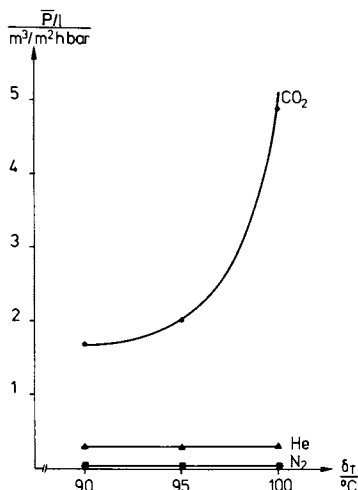
Figure 7. Gas permeability rate, $\bar{P}/\ell$, as a function of annealing temperature, δ_T, of asymmetric CA blend membranes (pure gases, 25°C, 40 bar; to obtain $cm^3(STP)/cm^2$-s-cmHg multiply by 3.69×10^{-4})
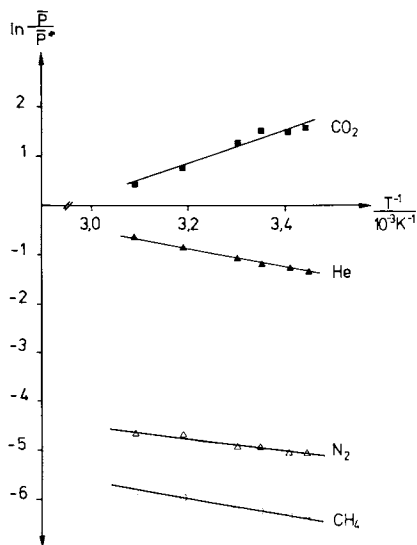
Figure 8. Temperature-dependence of permeability rate of asymmetric CA blend membranes (pure gases, 40 bar, $P^{\neq} \equiv$ 1 $m^3(STP)/ m^2$-h-bar, to obtain $cm^3(STP)/cm^2$-s-cmHg multiply by 3.69×10^{-4})
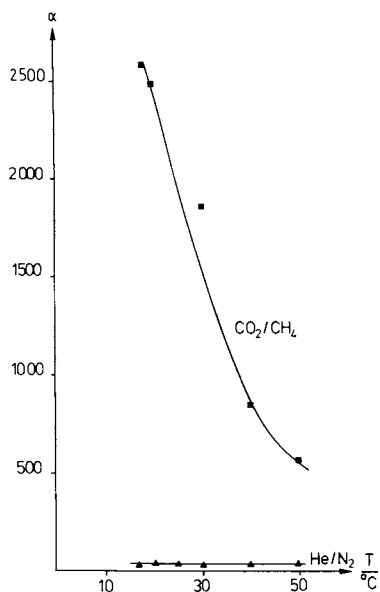
Figure 9. Temperature-dependence of ideal separation factor, α, of asymmetric CA blend membranes at 40 bar.

and 80 bar were set for the gases He, N_2 and CH_4, and between 10 and 40 bar for CO_2. Semi-logarithmic plots of permeability rates versus applied upstream pressure are presented in Figure 10. The He permeation is pressure-independent, but the permeations of the three other gases increase with pressure. Again, the steep slope of CO_2 is unique and will be discussed in detail. Due to these facts, the ideal separation factor for CO_2/CH_4 increases more than proportionally and that for He/N_2 decreases linearly with increasing pressure (Figure 11).

The unique behavior of cellulose acetate was supported recently by Koros (42). He found that of all glassy polymers investigated, cellulose acetate had the highest solubility selectivity, defined as the ratio of the solubilities of two gases CO_2 and CH_4. Its extremely high solubility value of 8.9 measured at 35°C and 20 atm exceeds the values of the other polymers listed below by factors of 2.5 to 4.0. Along with the mobility selectivities which were defined as the ratio of the diffusion coefficients of two gases in the polymer, Koros predicted that the CO_2 permeabilities for cellulose acetate should increase by 138% if the pressure increases from zero to 20 atm. The CO_2 permeabilities of all the other glassy polymers: PPO, PS, PC, polysulfone and polyimide were found to decrease by 30 to 35% with pressure. By extrapolating the CO_2 curve of Figure 10 to zero pressure, a value of 17.5×10^{-5} $cm^3(STP)/cm^2$-s-cmHg is obtained. Compared to the value of 42.6×10^{-5} $cm^3(STP)/cm^2$-s-cmHg at 20 bar an increase by 143% is calculated. This experimental finding verifies the above mentioned prediction.

The extreme sorption of carbon dioxide in cellulose acetate causes a strong plasticization of the polymer at elevated pressures. By this effect, CO_2 shows the highest permeability rates of all permanent gases investigated. Further investigations with gas mixtures containing carbon dioxide will demonstrate how the permeability of the less soluble and less permeable methane in the gas mixture is increased by the CO_2 plasticization. It is clear that, furthermore, the ideal separation factor given in this paper will be reduced to more realistic values which, when measured in the gas mixtures at zero recovery, will not exceed the permeability ratio calculated by extrapolating the permeability-pressure plots to zero pressure. An upper limit of about 300 is computed for the CO_2/CH_4 system from Figure 10 for zero pressure which is ten times higher than that derived by Koros (47).

Conclusions and Recommendations

The history of the membrane developments for reverse osmosis and gas permeation shows that because of inherent differences, it is not possible to simply apply the techniques and materials from one separation technology to the other. The success of the resistance-model hollow-fiber technology which is based on the glassy-fiber technology invented for reverse osmosis, demonstrates the necessity to search for advanced techniques to prepare more selective membranes free of imperfections, rather than to look for new, unavailable materials.

The interfacial-polymerization technology for the preparation of ultra-thin composite membranes with its self-sealing capability
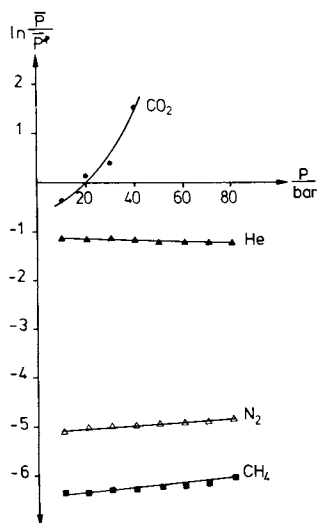
Figure 10. Pressure-dependence of permeability rate of asymmetric CA blend membranes (pure gases 25°C, P^+ ≡ $m^3(STP)/m^2$-h-bar; to obtain $cm^3(STP)/cm^2$-s-cmHg multiply by 3.69 x 10^{-4})
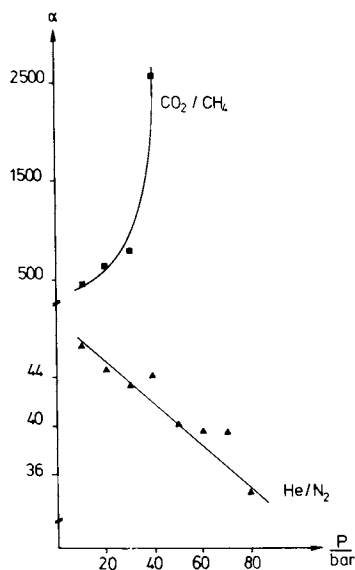
Figure 11. Pressure-dependence of ideal separation factor, α, of asymmetric CA blend membranes at 25°C

seems to be one promising way to overcome the problem of surface porosity.

Further approaches to meet the requirement of high selectivity may include the blending of glassy and rubbery polymers, the chemical alteration of the dense skin-layer of integral-asymmetric membranes and morphological variations of dense polymer films by proper post-treatment--as exemplified in this paper for CA blend membranes.

Acknowledgments

Literature Cited

1. Reid, C. E.; Breton, E. S. J. Appl. Polym. Sci. 1959, 1, 133.
2. Loeb, S. In "Synthetic Membranes"; Turbak, A. F., Ed.; ACS Symp. Ser., No. 153: Washington, D.C., 1981.
3. Loeb, S.; Sourirajan, S. Adv. Chem. Ser. 1962, 38, 117.
4. Riley, R. L.; Lonsdale, H. K.; Lyons, C. R.; Merten, U. J. Appl. Polym. Sci. 1967, 11, 2143.
5. Rozelle, L. T.; Cadotte, J. E.; McClure, D. J. In "Membranes from Cellulose and Cellulose Derivatives"; Turbak, A. F., Ed.; Interscience Publishers: New York, 1970.
6. King, W. M.; Cantor, P. A.; Schoellenbach, L. W.; Cannon, C. R. In "Membranes from Cellulose and Cellulose Derivatives"; Turbak, A. F., Ed.; ibidem.
7. King, W. M.; Hoernschemeyer, D. L.; Saltonstall, C. W. In "Reverse Osmosis Membrane Research"; Lonsdale, H. K. and Podall, H. E., Eds.; Plenum Press: New York, 1972.
8. Richter, J. W.; Hoehn, H. H. U.S. Pat. 3,567,632; March 2, 1971.
9. Rozelle, L. T.; Cadotte, J. E.; Cobian, K. E.; Kopp, C. V. In "Reverse Osmosis and Synthetic Membranes"; Sourirajan, S., Ed.; National Research Council of Canada: Ottawa, 1977; Chapter 12.
10. Mahon, H. I. U.S. Pat. 3,228,876; Jan. 1966.
11. Boeddeker, K. W.; Wenzlaff, A. Ger. Pat. 2,820,265 (1980).
12. Riley, R. L.; Fox, R. L.; Lyons, C. R.; Milstead, C. E.; Seroy, W. M.; Tagami, M. Desalination 1976, 19, 113.
13. Goldsmith, R. L.; Wechsler, B. A.; Hara, S.; Mori, K.; Taketani, Y. Desalination 1977, 22, 311.
14. Pusch, W.; Riley, R. L. Desalination 1977, 22, 191.
15. Kurihara, M.; Kanamaru, N.; Harumiya, N.; Yoshimura, Y.; Hagiwara, S. Desalination 1980, 32, 13.
16. Cadotte, J. E.; Petersen, R. J.; Larson, R. E.; Erickson, E. E. Desalination 1980, 32, 25.
17. Gantzel, P. K.; Merten, U. I&EC Proc. Des. Dev. 1970, 9, 331.
18. Stern, S. A.; Sen, S. K.; Rao, A. K. J. Macromol. Sci. - Phys., B 1974, 10, 507.
19. Vos, K. D.; Burris, F. O. I&EC Prod. Res. Dev. 1969, 8, 84.

20. Schell, W. J. ACS Div. Fuel Chem., Preprints 1975, 20, 253.
21. Schell, W. J.; Houston, C. D. U.S. Pat. 4,134,742, 1979;
    Hydrocarbon Processing 1982, Sept., 249.
22. Coady, A. B.; Davis, J. A. CEP 1982, Oct., 44.
23. Schell, W. J.; Houston, C. D. ACS Symp. Ser. 223, Washington,
    D.C., 1983.
24. Stannett, V. T.; Koros, W. J.; Paul, D. R.; Lonsdale, H. K.;
    Baker, R. W. Adv. Polym. Sci. 1979, 32, 69.
25. Cabasso, I. In "Encyclopedia of Chemical Technology";
    Wiley-Interscience: New York, 1980; Vol. 12.
26. Stern, S. A.; Frisch, H. L. Ann. Rev. Mater. Sci. 1981, 11,
    523.
27. Matson, S. L.; Lopez, J.; Quinn, J. A. Chem. Eng. Sci. 1983,
    38, 503.
28. Browall, W. R. U.S. Pat. 4,156,597, 1977.
29. Kimura, S. G.; Lavigne, R. G.; Browall, W. R. U.S. Pat.
    4,132,824, 1979; U.S. Pat. 4,192,842, 1980.
30. Ward, W. J., III U.S. Pat. 4,279,855, 1981.
31. Ward, W. J., III; Browall, W. R.; Salemme, R. M. J. Membr.
    Sci. 1976, 1, 99.
32. Gaines, G. L. "Insoluble Monolayers at Liquid-Gas Interfaces";
    Interscience: New York 1966.
33. Fendler, J. H. "Membrane Mimetic Chemistry"; Wiley-
    Interscience: New York, 1982.
34. Henis, J.M.S.; Tripodi, M. K. U.S. Pat. 4,230,433, 1980.
35. --- Sep. Sci. Techn. 1980, 15, 1059.
36. --- J. Membr. Sci. 1981, 8, 233.
37. --- Polym. Sci. Techn. 1982, 16, 75.
38. --- Science 1983, 220, 11.
39. FInken, H. Desalination 1983, 48, 207.
40. --- Desalination 1983, 48, 235.
41. --- I&EC Prod. Res. Dev. 1984, 23, 112.
42. Koros, W. J. "Membrane-based Gas Separations"; paper presented
    at the conference Membrane Technology in the 1980's; Sunriver,
    Oregon, Sept. 1983.
43. Ellig, D. L.; Althouse, J. B.; McCandless, F. P. J. Membr.
    Sci. 1980, 6, 259.
44. Kimura, S. G.; Walmet, G. E. Sep. Sci. Techn. 1980, 15, 1115.
45. Stern, S. A.; DeMeringo, A. H. J. Polym. Sci.: Polym. Phys.
    Ed. 1978, 16, 735.
46. Stephen, H.; Stephen, T. "Solubilities of Inorganic and
    Organic Compounds"; Pergamon Press: New York, 1963.
47. Chern, R. T.; Koros, W. J.; Hopfenberg, H. B.; Stannett, V. T.
    In "Materials Science of Synthetic Membranes"; Lloyd, D. R.,
    Ed.; American Chemical Society: Washington, D.C., 1985.

Evolution of Composite Reverse Osmosis Membranes

JOHN E. CADOTTE

FilmTec Corporation, Minneapolis, MN 55435

    The development of composite reverse osmosis membranes
    is reviewed with emphasis on those types that have sur-
    vived the selection for commercial development.

A composite reverse osmosis membrane is composed of a thin, dense
polymer skin (barrier layer) formed over a microporous support film.
Such membranes are direct descendants of the Loeb-Sourirajan membrane
developed in 1960 (1). In the early sixties it was shown that the
Loeb-Sourirajan cellulose acetate membrane was asymmetric, having a
thin dense layer about 200 nm (2000 Angstroms) thick over a micro-
porous film (2). Thus, knowing this, it was logical to attempt to
form the dense surface layer separately from the porous body as a
way to form equivalent or improved composite membranes. The distinc-
tion of composite membranes versus asymmetric membranes rests with
the mode of formation. Asymmetric membranes result from casting a
single polymer solution in one step that produces a microporous film
with a thin, dense layer over one surface. Composite membranes, on
the other hand, are formed in two steps--casting of the microporous
support first, followed by deposition of the barrier layer on the
surface of this microporous support layer. The advantage gained by
using the "composite" approach is that each material used for the
microporous support film and for the barrier layer can be optimized
separately to provide improved membrane performance.
    A schematic diagram of a typical commercial composite membrane
is presented in Figure 1. The microporous polysulfone support film
is cast on a woven or nonwoven backing material, usually made from
polyester fibers. The polysulfone support is approximately 50 μm
(two mils) in thickness. About half of this thickness sits above
the polyester backing material, and about half of it is embedded in
the fibrous carrier web. The thickness of the applied barrier layer
may range from 20 to over 500 nm, depending upon the composition of
the barrier layer.
    The methods that have been used to form composite membranes may
be grouped into the four general types listed in Table I.
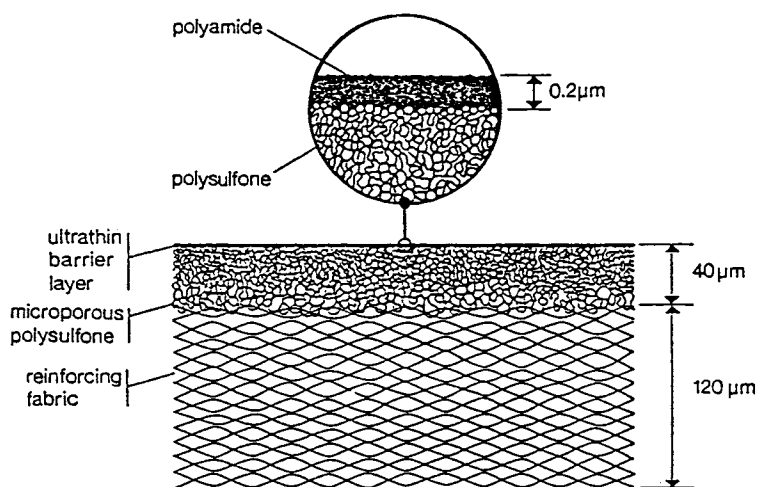
Figure 1.   Schematic representation of the structure of FT-30
            thin-film composite membrane.

Table I. General Methods for Forming Composite Membranes (3)

A. Casting of the barrier layer separately followed by lamination
    to the support film.
B. Dip-coating of the support film in a polymer solution and drying,
    or in a reactive monomer or prepolymer solution followed by
    curing with heat or radiation.
C. Gas-phase deposition of the barrier layer from a glow discharge
    plasma.
D. Interfacial polymerization of reactive monomers on the surface
    of the support film.

Barrier layers have been applied by all of the above methods on
microporous support film with a fibrous backing (as illustrated in
Figure 1), or on microporous hollow fibers. Normally, except for
Method C in Table I (gas-phase deposition), the support film is used
in the wet "as cast" condition for applying the reagents to form
the barrier layer. The final step of preparation, drying of the
membrane, frequently aids in bonding the barrier layer to the support
film.

Methods B, C and D in Table I use in situ formation methods in
contrast to Method A where the barrier layer is preformed. The in
situ methods are generally more practical for machine production of
composite membrane.

Separate Casting of the Barrier Layer

The first composite reverse osmosis membrane reported in the techni-
cal literature was developed by Peter Francis of North Star Research
Institute in 1964 (4). This membrane was formed by float-casting an
ultrathin film of cellulose acetate (CA) upon a water surface, re-
moving the membrane from the water surface by lamination onto a
pre-formed microporous support film and drying to bond the membrane
to the support. This float-casting procedure has since been de-
scribed in the technical literature for both flat sheet and tubular
membranes (5, 6, 7).

The initial microporous support films used in the work were
made from cellulose acetate by a modification of the Loeb-Sourirajan
procedure. Later work showed that several types of the membrane
filters manufactured by Millipore Corporation and Gelman Sciences,
Inc., performed as well and allowed higher flux. A continued search
for a more compression-resistant support film led to the development
of polycarbonate, polyphenylene oxide and polysulfone microporous
films in 1966 to 1967 (8). Of these, microporous polysulfone film
proved to have the best properties. The polysulfone support was
made by casting a liquid layer of a 12.5 to 15 percent solution of
Union Carbide Udel P3500 polysulfone in dimethylformamide onto a
glass plate at 4 to 7 mils (100-175 μm) thickness, then coagulating
the film in water.

The cellulose acetate, normally a medium viscosity type having
39 to 40 percent acetyl content, was dissolved at 5 to 10 percent
solids in a solvent with slight water solubility such as cyclohex-

anone. Flowing of this solution onto a water surface with mechanical
drawing produced thin membranes that floated on the water surface.
The thickness of the membranes could be controlled in a range of 20
to 500 nm. Optical interference colors of the ultrathin membrane
served as a guide for estimating thickness; actual measurements were
made by interferometric or gravimetric methods. Ultrathin films
could be cast on a water surface from many other commercial polymers
for preparation of composite membranes. However, only those formed
from cellulosic or related polysaccharide esters exhibited adequate
flux for use in reverse osmosis.

Similar composite membranes were developed by the team of
Merten, Riley and Lonsdale at about the same time (9, 10, 11). Their
ultrathin cellulose acetate films were formed by carefully controlled
withdrawal of a glass plate from a dilute acetone solution of cellu-
lose acetate. Film thickness was accurately controlled by the rate
of withdrawal of the glass plate. Immersion of the dried plate in
water released the thin film which was then mounted on a pre-formed
microporous support film.

These types of cellulose acetate composite membranes are of
historical interest only. During the period when this research was
done the composite membranes made using very thin cellulose acetate
barrier layers (under 100 nm) looked attractive for their high flux
properties. However, later optimization of the asymmetric cellulose
acetate membrane process improved flux and, in general, outdistanced
composite CA types for practical, low cost membrane manufacture.

Dip Coating Methods

It might appear that the most logical approach for preparation of
composite membranes would be a dip-coating method (Example B in
Table I). A pre-formed microporous support would be dipped or other-
wise coated in some manner with a polymer solution and dried. Addi-
tional variations of the method might include incorporation of cross-
linking agents in the polymer solution or the use of reactive mono-
mers in place of the polymer. The monomer compositions applied on
the support film could be cured with heat or ultraviolet radiation
to form the composite membrane. In spite of this apparent versatil-
ity for the dip-coating process, few membranes of commercial interest
have been developed. The main obstacle in this method appears to be
the filling of pores in the surface of the support to produce low
flux. This pore-sealing problem has usually been overcome in some
manner in the more effective dip-coated membranes.

One of the earliest membranes formed by dip-coating was reported
by Lonsdale and Riley (11, 12). The surface of a cellulose acetate-
cellulose nitrate (CA/CN) microporous film was first coated with an
aqueous polyacrylic acid solution. This formed a protective layer
on the CA/CN film to confer resistance to the subsequent solvent
coating operation. A coating of cellulose triacetate in chloroform
was then applied and dried. The membranes exhibited salt rejections
as high as 99 percent.

Two types of composite reverse osmosis membranes, formed by the
dip-coating approach, are known to be of commercial interest at the
present time and are discussed below. One type consists of membranes
made on a microporous support film by acid-catalyzed condensation of

furfuryl alcohol or its mixtures with 1,3,5-tris(hydroxyethyl)cyanur-
ic acid. The other type consists of membranes formed on a micro-
porous support film by heat-curing of a sulfonated polysulfone resin
layer deposited from aqueous or alcoholic solutions.

Furfuryl Alcohol Condensation Reactions. A membrane designated
"NS-200" was first discovered by the author at North Star Research
Institute during 1972. This membrane was made by dip-coating a
polysulfone support film in a 2:2:1 solution of furfuryl alcohol:
sulfuric acid:Carbowax 20M in 80:20 water:isopropanol (13-15). The
excess coating solution was allowed to drain off. Oven drying at
125 to 140°C produced a black composite membrane having a sulfonated
polyfurane barrier layer. The most outstanding property of the
NS-200 membrane was its high salt rejection. Tests of laboratory-
formed membranes in synthetic seawater at 1000 psi (6895 kPascals)
frequently produced salt rejections greater than 99.9 percent at
20 gfd (33 L/sq m/hr) flux. Attempts to decrease the thickness of
the barrier layer of NS-200 membranes by applying a thinner coating
resulted in a large loss in membrane flux. This suggests that the
membrane was somewhat asymmetric with a dense surface skin and a
higher flux type of structure underneath in the pores of the support
film. The surface of the highly catalyzed furfuryl alcohol solution
coating probably undergoes slight evaporation before the onset of the
rapid polymerization to produce a surface skin.
     From the beginning of its development, problems with the long
term stability of the NS-200 membrane were observed. A gradual in-
crease in water flux occurred, accompanied by a corresponding de-
crease in salt rejection. Three factors may have been involved:
(a) a tendency toward irreversible swelling in monovalent salt
solutions due to hydration of the sulfonic acid groups, (b) chemical
linkages that were unstable to hydrolysis (sulfate ester linkages
have been suggested as a potential weak link) and (c) a sensitivity
to oxidation. The chemical heterogeneity of the sulfonated poly-
furane resin made the instability problems difficult to resolve. Its
swelling behavior was decreased by increasing the oven temperatures
during the heat-cure step to give a tighter, apparently more cross-
linked, membrane. Also, the swelling behavior could be limited by
ionic cross-linking via periodic treatment with polyvalent metal ions
such as barium. Further studies by other groups (16, 17) did not
resolve the long term instability problems of NS-200 membranes.
     A recent patent granted to Kurihara and co-workers of Toray
Industries describes membranes formed by acid-catalyzed condensation
reactions of a variety of reactive monomers on polysulfone support
films under conditions similar to those used for NS-200 membranes
(18). The data (Example 2 in the patent) show that 1,3,5-tris
(hydroxyethyl)isocyanuric acid (THEIC), when polymerized at 150°C
on a polysulfone support film, produced a membrane exhibiting 96.7
percent salt rejection with a flux of 0.49 gfd (0.82 L/sq m/hr) when
tested toward 0.25 percent NaCl at 568 psi (3916 kPascals) and 25°C.
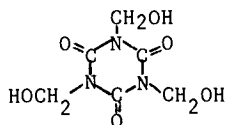
1,3,5-tris(hydroxyethyl)isocyanuric acid
(THEIC)

A number of co-reactants, including polyalcohols and polycarboxylic
acids, did not increase the membrane flux significantly. However,
when the reaction was carried out using one part THEIC to two parts
furfuryl alcohol and tested under the same conditions the flux in-
creased to 12.3 gfd (20.5 L/sq m/hr) with 99.9 percent salt rejection
(Example 40 in the patent). An interesting property of this type of
membrane made from the 1:2 THEIC:furfuryl alcohol composition was its
high rejection of organic solutes. For example, rejections of ethan-
ol and phenol by NS-200 membrane reported by Cadotte et al were 65 and
83 percent respectively (19). The corresponding rejections of ethanol
and phenol reported by Harumiya et al for the 1:2 THEIC:furfuryl
alcohol membrane was 97 and 99 percent (20). In this combination
of reactants to form the composite membrane, the THEIC component
contributes toward high rejection of organic solutes and the furfuryl
alcohol component contributes high flux and salt rejection properties.
    The PEC-1000 membrane of Toray Industries, Inc., has been des-
cribed by Kurihara et al (21). This membrane was characterized as a
thin-film composite type made by an acid catalyzed polymerization on
the surface. Membrane performance reported for seawater tests was
99.9 percent TDS rejection at fluxes of 5.0 to 7.4 gfd (8.3 to 12.3
L/sq m/hr) when tested with 3.5 percent synthetic seawater at 800 psi
(5516 kPascals). The membrane was stable in 1500-hour tests in spiral-
wrap elements and exhibited stability in a temperature range of 25 to
55°C and in a pH range from 1 to 13. High organic rejections were
reported for the PEC-1000 membrane; rejection of dimethylformamide
from a 10 percent solution was 95 percent and similar tests with
dimethylsulfoxide showed 96 percent rejection. The composition and
conditions for preparation of PEC-1000 membrane is not disclosed in
Reference 21. Apparently it is a dip-cast membrane related to com-
positions described by Kurihara, Watanaba and Inoue in Reference 18.

Sulfonated Polysulfone Membranes. A membrane of this composition,
made by the dip-coating process, is of interest because of its high
degree of chlorine resistance. The membrane was made by dip-coating
of polysulfone supports (flat sheets or hollow fibers) in a water or
water-alcohol solution of sulfonated polysulfone, drying and heat-
curing. The use of sulfonated aromatic polymers for reverse osmosis
membranes began in the late 1960's with the work of Plummer, Kimura
and LaConte of General Electric (22). Polyphenylene oxide was sul-
fonated using chlorosulfonic acid in chloroform, and asymmetric
membranes were cast from a chloroform/methanol solvent. Later a
Rhone-Poulenc patent described the preparation of asymmetric sul-
fonated polysulfone membranes (23). The degree of sulfonation was
limited so that the product would be water-insoluble. The asym-
metric membrane was cast from a dimethylformamide solution. Cadotte,
Steuck and Petersen at Midwest Research Institute in 1976 developed
a composite sulfonated polysulfone membrane (24). Polysulfone was
sulfonated to a degree to produce water solubility. This material in
water or water-alcohol solutions was used for dip-coating of poly-
sulfone support films. Oven drying of the coated support film at
100 to 140°C caused the formation of sulfone cross-links, that
served to immobilize the sulfonated polysulfone barrier layer.
Alternatively the addition of polyalcohols or polyphenols to the
solution could be used to produce sulfonate ester cross-links.

Generally, the salt rejections observed for these membranes in sea-
water reverse osmosis tests did not exceed 80 percent. This process
was applied at Albany International to form composite membranes on
hollow polysulfone fibers (25). Salt rejections on the hollow fiber
membranes were above 98 percent at an average flux of about 1.5 gfd
(2.5 L/sq m/hr) in a 12 000-hour test using 30 000 ppm seawater at
1000 psi. In other 5000-hour tests using 3500 ppm brackish water at
400 psi with addition of 100 ppm chlorine at pH 8 flux and salt re-
jection remained constant at 1 gfd and 98 percent respectively
(Figures 8 and 12 in Reference 25 a).

Gas Phase Deposition of the Barrier Layer

Plasma polymerization to form a barrier layer over a dry microporous
support film was reported in 1970 by Buck and Davan (26) and in 1973
by Yasuda and Lamaze (27) and by Hollahan and Wydeven (28). The
plasma reactions are quite heterogenious, not only involving poly-
merization, but depolymerization and modification of functional
groups. Yasuda and Marsh showed that interaction of the plasma with
the polymer of the support film also played a part in formation of
the barrier layer (29).
     In addition to the usual vinyl monomers, most organic compounds
having adequate vapor pressure could be used to deposit a barrier
layer on porous supports. Additional copolymers could be formed by
inclusion of nitrogen in the reactant gases. The supports used in-
cluded Millipore filters, porous polysulfone films and porous glass
tubes. Examples were presented of plasma formed membranes with 99
percent salt rejection, 38 gfd flux (63.3 L/sq m/hr) and low flux
decline in seawater tests. A recent report by Heffernan et al
describes gas phase deposition of membranes on hollow fibers (30).
     A membrane designated "Solrox" made by Sumitomo Chemical Company
is closely related to the above plasma polymerized composite mem-
branes. A 1980 report by T. Sano described the Sumitomo process (31).
A support film was cast from a polyacrylonitrile copolymer contain-
ing at least 40 mole percent acrylonitrile. The support film was
dried and exposed to a helium or hydrogen plasma to form a tight
cross-linked surface skin on the porous polyacrylonitrile support
film. Data in a U.S. Patent issued in 1979 to Sano et al showed
that the unmodified support film had a water flux of 87 gfd (145 L/
sq m/hr) at 142 psi (10 kg/sq cm). After the plasma treatment a
reverse osmosis test using 0.55 percent NaCl at 710 psi (4895 kPa)
showed 10.5 gfd (17.5 L/sq m/hr) flux at 98.3 percent salt rejection
(32). This membrane appears to fall between a conventional asym-
metric membrane and a composite membrane. If the surface skin is
only cross-linked, one might call it a modified asymmetric membrane.
However, if the surface skin is substantially modified chemically
to make it distinct from the bulk of the membrane it could be con-
sidered as a composite type.

Interfacial Polymerization of the Barrier Layer

Interfacial reactions to produce thin polymer films date back to the
early work of Wallace Carothers starting in 1929. Synthetic polya-
mides for producing nylon fibers were formed by long, carefully

controlled high-temperature condensation reactions. By the early
1940's, research was being done to produce the same type of linear
high polymers in low-temperature condensation reactions. The low-
temperature reactions were divided into two types: (a) a solution
polycondensation in which equimolar amounts of a diamine and diacid
chloride plus tertiary amine were dissolved in an inert solvent, and
(b) an interfacial polycondensation in which the diamine was dis-
solved in water and the diacid chloride in a non-water miscible
solvent. Upon contact of the two solutions, a polyamide membrane
was formed at the interface. The interfacial method has been of
wide general interest although its commercial use has not been ex-
tensive. The interfacial methods are applicable to production of a
wide variety of polyamides, polysulfonamides, polyurethanes and
polyesters. Reactions involved in both the solution polycondensation
methods and interfacial polycondensations were reviewed in a book by
P.W. Morgan published in 1965 (33).

The use of interfacially formed thin films for membrane separa-
tions was, therefore, obvious. Reference to such membranes in
Morgan's book characterizes them as retentive to dyes but permeable
to salts. Early attempts to use interfacially formed membranes at
the North Star Research Laboratories in the late 1960's tended to
confirm the low salt retention described by Morgan. In these early
attempts to prepare composite membranes polysulfone support films
were saturated in solutions of various diamines, acid acceptors and
surfactants. After draining, the films were contacted with hexane
solutions of various diacyl chlorides. In this initial work, salt
rejections of these membranes were generally too low for practical
use in seawater or brackish water applications. Similarly poor re-
sults were described in a patent by Scala and co-workers, dating to
that era, wherein interfacial condensation membranes were produced
(34).

Polymeric Amine Reactants: NS-100. In 1970 a different approach was
tried that produced an immediate and significant improvement in
membrane properties. A polysulfone support film was saturated in a
water solution of a polymeric amine (0.5 to 1.0 percent solution of
polyethylenimine) which was reacted with tolylene diisocyanate or
isophthaloyl chloride (0.1 to 1.0 percent in hexane). The membrane
was dried in a 110°C oven (35). This process gave salt rejections
in seawater tests in excess of 99 percent. Polyethylenimine, a con-
venient, commercially available water-soluble polyamine, contains a
high concentration of amine groups for high reactivity with the iso-
cyanate and acyl chloride reactants. The amine groups (one per each
two carbon atoms) are in a percent ratio of 30:40:30 primary:second-
ary:tertiary (36). The molecular weight of the more effective grades
of polyethylenimine was in a range of 10 000 to over 60 000 . Models
of this highly branched polymer indicate that it is spheroidal in
nature (36).

Two types of reactions involved in the preparation of NS-100
membranes are illustrated in Figure 2. The structural representa-
tion of polyethylenimine (PEI) is simplified to show only the re-
active primary and secondary amine groups. In the first step the
amine groups react rapidly with isophthaloyl chloride at the inter-
face to produce a polyamide surface skin, while amine groups below
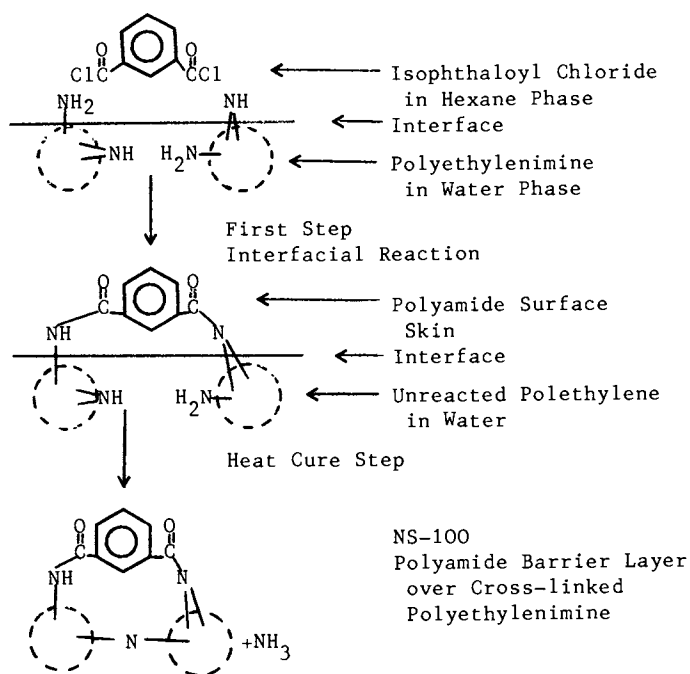
Figure 2.   Reactions involved in NS-100 membrane formation.

the interface remain unreacted. In the second step (drying and heat-
curing at 110°C) internal cross-linking of polyethylenimine takes
place with the elimination of ammonia between adjacent amine groups.
These reactions produce a membrane that has three distinct zones of
decreasing porosity: (1) the polysulfone support film, (b) a thin,
cross-linked polyethylenimine zone extending into the pores of the
support film and (c) the dense polyamide (or polyurea) surface skin
which acts as the high retention barrier.

     It is noteworthy that simple heat-curing of a polyethylenimine
coating on the microporous polysulfone, omitting the interfacial
reaction step, produced a cross-linked polyethylenimine membrane
that gave 70 percent salt rejection at 55 gfd (91.7 L/sq m/hr) flux
in the seawater test. Also, if a fully formed NS-100 membrane was
dried at 75°C rather than heat-cured at 110°C, salt rejection fell
to 96 percent. The evidence suggests that the polyamide surface
skin is very thin and that the cross-linked polyethylenimine under-
layer is needed for additional support. Morgan presented evidence
proving that interfacial polyamide reactions occurred primarily on
the solvent side of the interface; that is, the amine reactant mi-
grated across the interface into the organic phase in order for
reaction to occur. Since the bulky, hydrophilic polyethylenimine
macromolecule has essentially no solubility in the hexane phase in
the NS-100 reaction, the resulting dense surface skin is extremely
thin. The cross-linked polyethylenimine gel zone under this very
thin barrier layer is believed to be necessary for high salt rejec-
tion.

Other Polymeric Amine Reactants. Although the NS-100 membrane
showed high salt rejection capability, it had some limitations: (a)
the flux, 18 gfd in seawater tests at 1500 psi, might be increased,
(b) the sensitivity of NS-100 to chlorine led to attempts to modify
the amine structure to increase its oxidation resistance and (c) sur-
face brittleness of NS-100 due to its highly cross-linked structure
gave problems in mechanical processing of the membrane. This latter
problem could be overcome to a degree by over-coating the membrane
with a polyvinyl alcohol protective layer. These limitations, which
appeared in efforts to scale up NS-100 into commercial production,
led to experimentation on a wide variety of polyamines and acyl
chloride or isocyanate reactants.

     Riley and co-workers developed a series of membranes into commer-
cial production using a polyetheramine in place of polyethylenimine
(37). The polyetheramine, also called polyepiamine, is an adduct
of polyepichlorohydrin with ethylenediamine. It functioned similarly
to polyethylenimine in NS-100, except it exhibited an increased flux
and an incremental increase in chlorine resistance. The first of
this series of membranes, designated PA-300, was subsequently used
in the 3.2 mgd desalination plant at Jeddah, Saudi Arabia (38). The
PA-300 membrane is formed from polyetheramine and isophthaloyl
chloride. A closely-related membrane, designated RC-100, is be-
lieved to be the tolylene diisocyanate analog of PA-300.

     A recent patent granted to Toray Industries, Inc., described
the use of a similar amine polymer in composite membranes (39).
Polyepiiodohydrin was reacted with 4-(aminomethyl)piperazine to
form the reactive amine polymer. This polymer, 3 parts, plus 1 part

4-(aminomethyl)piperazine or related monomers was coated on a poly-
sulfone support film and reacted interfacially with isophthaloyl
chloride. The addition of the monomer reactant was beneficial in
attaining a minimum salt rejection of 99.5 percent in seawater
reverse osmosis tests.

Many additional polyamines have been proposed to replace poly-
ethylenimine in the NS-100 membrane type. Some of these polymers
have only secondary amine groups in the chemical structure, and
would presumably not undergo internal cross-linking by elimination
of ammonia, which occurs in polyethylenimine. Notable among these
latter reports are two U.S. patents issued to Kawaguchi et al of
Teijin in 1981 and 1982. The first of these patents (40) describes
a variety of reactive linear polymers containing anhydride, acyl
chloride or sulfonyl chloride groups, that were reacted with an ex-
cess of polyfunctional amines to produce water-soluble polymers con-
taining reactive primary or secondary amine groups. These polymers
were reacted interfacially on polysulfone support films with aromatic
di- or tri-acyl chlorides or sulfonyl chlorides to form composite
membranes. For example, a polyamine produced from the reaction of
tri-ethylenetetramine with a maleic anhydride-methyl acrylate co-
polymer was coated onto a polysulfone support. After interfacial
reaction using a mixture of isophthaloyl chloride and trimesoyl
chloride (1,3,5-benzene tricarbonyl chloride), the membrane was
dried at 115 to 120°C (Example 1 in the patent). Tested with 0.5
percent sodium chloride solution at 25°C and 600 psi (4137 kPa)
the membranes exhibited a flux after 200 hours of 59 gfd (98 L/sq m/
hr) and salt rejection of 96.8 percent.

The second patent of Kawaguchi et al (41) describes a number of
composite, interfacially-formed membranes that are amphoteric; that
is, they have both cationic and anionic functionality. This contri-
butes a degree of specificity to the membrane. A large proportion
of an ionic solute such as sodium chloride will pass through the
membrane while noncharged solutes such as sucrose are retained to a
high degree. Several synthetic routes were given for the prepara-
tion of various membranes. The approach utilized polymeric amines
having both reactive and non-reactive amine groups. The reactive
amine groups provided cationic sites in the membrane. Tri- or
tetrafunctional acyl chlorides were used in the solvent phase for
the interfacial reaction. Hydrolysis of a portion of the acyl groups
of these reagents provided the anionic sites in the membrane. The
membranes formed in these reactions were tested using feed solutions
containing one percent sodium chloride and three percent sucrose.
Several of the examples cited in the patent allowed more than 80
percent of the sodium chloride to pass through the membrane while
rejecting more than 97 percent of the sucrose.

One approach used by Kawaguchi et al for preparation of the
amphoteric membrane was the use of polyethylenimine having part of
the amine groups neutralized with hydrochloric acid. The inter-
facial reactants were trimesoyl chloride (TMC), 3-chlorosulfonyl
isophthaloyl chloride (SPC) and pyromellitic acid chloride (PMC).

TMC   SPC   PMC
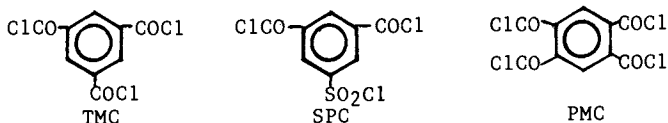
The neutralized amine groups did not react with the acyl chloride
reagents in the interfacial reaction step and did not undergo con-
densation reactions during the heat cure step of membrane formation.
A loosely cross-linked membrane was formed that was very hydrophilic
due to the high concentration of residual amine and carboxyl groups.
     Another approach used for deactivating part of the amine groups
of polyethylenimine was to use a partial quaternization of polyethyl-
enimine with ethyl iodide. The membranes formed were similar in
properties to those made by the partial polyethylenimine neutraliza-
tion. Still another type of amine polymer was prepared by free
radical polymerization of a mixture of diallylamine hydrochloride,
dimethyl diallyl ammonium chloride and sulfur dioxide. This polymer
in the free base form for interfacial reaction had reactive secondary
amine groups and non-reactive quaternary amine groups:
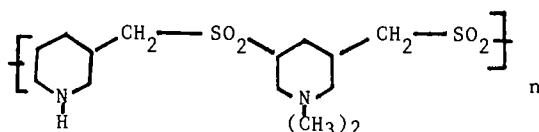
The membranes formed were similar in properties to the modified
polyethylenimine types.

Monomeric Amine Reactants: NS-300. For several years it was thought
that a polymeric amine was needed to span the pores in the support
film surface to obtain high salt rejection in the interfacial thin-
film composite membrane. However, a 1975 research report by the
North Star Division of Midwest Research Institute (42) showed that
a monomeric amine, piperazine, in interfacial reactions with isoph-
thaloyl chloride gave salt rejections of 90 to 96 percent in seawater
tests. The improved membrane performance had been achieved through
optimization of the interfacial reaction, concentration of reactants,
acid acceptors and surfactants. Credali et al had previously pre-
pared asymmetric membranes from pre-formed polypiperazineamides and
reported them to be chlorine resistant (43). Therefore, poly(piper-
azine isophthalamide) interfacial membranes had been made with the
objective of forming a chlorine resistant membrane. Because piper-
azine is a di-secondary amine, it was thought at that time that the
piperazine polyamides, having no amidic hydrogen atoms, would resist
chlorine oxidation. Actually, these membranes were found to be more
chlorine-resistant than NS-100, but not to the degree that they could
be used with continuous chlorination of the feedwater. Because of
their lower flux and salt rejection properties as compared with
NS-100, the piperazine-isophthalamide membranes were never developed
further, but modification of this reaction proved to be of consider-
able interest. Part or all of the isophthaloyl chloride was replaced
with the trifunctional acyl chloride, trimesoyl chloride (44). The
interfacial reaction of trimesoyl chloride with piperazine is be-
lieved to produce primarily the linear polyamide, with only moderate
cross-linking:
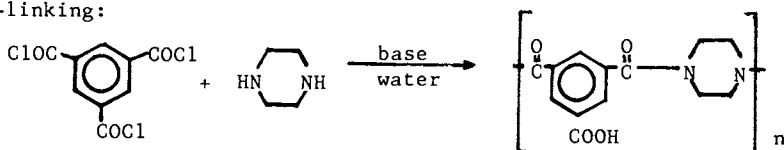
Perhaps through the introduction of free carboxylic acid groups, a
much higher flux membrane was formed. This membrane, which was
named NS-300, exhibited particularly high retention of salts having
polyvalent anions.
     Salt rejections by the NS-300 membrane toward synthetic sea-
water improved as the isophthalamide content of the barrier layer
increased. Surprisingly, membrane flux peaked rather than simply
declining as a function of increasing isophthalamide content. This
is illustrated by the data in Table II. Maximum water permeability
characteristics were found at an approximate copolymer ratio of 67
percent isophthalic and 33 percent trimesic groups. The differences
in the magnesium sulfate versus sodium chloride rejection appear to
be due to the anionically charged nature of the membrane barrier
layer, which is rich in carboxylate groups.

Table II.   Effect of the Isophthaloyl:Trimesoyl Chloride Ratio on
          the Performance of NS-300 Membranes in Reverse Osmosis Tests

| Acid Chloride Ratio* | | Reverse Osmosis Test Results | | | |
| | | 0.5% Magnesium Sulfate – 200 psig | | 3.5% Synthetic Seawater-1500 psig | |
Trimesoyl	Isophthaloyl	Flux (gfd–L/sq m/hr)	Salt Rej. (percent)	Flux (gfd–L/sq m/hr)	Salt Rej. (percent)
100	0	26 (43)	99.3	80 (133)	68
75	25	31 (52)	99.3	96 (160)	64
33	67	77 (128)	99.9	94 (157)	65
25	75	58 (97)	99.6	73 (121)	78
10	90	18 (30)	99.9	33 (55)	96
0	100	4 (6.7)	99.0	20 (33)	98

   * Aqueous phase contained 1% piperazine, 1% trisodium phosphate,
     0.5% dodecyl sodium sulfate; hexane phase contained 1% (w/v)
     of acyl chlorides.

     Table III illustrated this phenomenon, wherein a single test
specimen (made with the piperazine trimesamide homopolymer) was
sequentially exposed to feed solutions of sodium chloride, magnesium
chloride, sodium sulfate and magnesium sulfate. The chloride salts
were both poorly retained while retention of the sulfate salts was
excellent. Thus, salt retention in the carboxylate-rich NS-300
membrane was controlled by the anion size and charge. This membrane
could not distinguish between the univalent sodium ion and the diva-
lent magnesium ion, which is the opposite of the behavior observed
for asymmetric cellulose acetate membranes. Salt passage through
the NS-300 membrane may be described as anion-controlled.

Table III.   Effect of Cation and Anion Valence on Salt
             Rejection Properties of NS-300 Membranes

Solute	Flux (gfd)	(L/sq m/hr)	Salt Rejection (percent)
NaCl	42	(70)	50
$MgCl_2$	32	(53)	46
Na_2SO_4	41	(68)	97.8
$MgSO_4$	32	(53)	97.9

Reverse osmosis test conditions:
0.5% salt concentration, 200 psi (1380 kPa),
25°C, poly(piperazine trimesamide) membrane.

Attempts to scale up the NS-300 membrane preparation from the laboratory scale to continuous machine production led to a high degree of variability in membrane properties (45). The difference was attributed in part to the variability of machine-made polysulfone support film. Properties of the machine-made polysulfone supports differed from the laboratory cast support films. One of the major factors affecting this difference was that the machine-made support film was cast on a nonwoven polyester backing material which can vary in properties. Thus, the machine support film, which was quite adequate for NS-100 type membranes using polymeric amine reactants, still remained a limitation for the monomeric amine reaction of NS-300.

An approach to overcome this problem was replacement of piperazine in the NS-300 reaction with piperazine-terminated oligomers. Piperazine oligomers had been investigated in an earlier program (44). They were made by the reaction of excess piperazine with di- or triacyl chlorides in an inert solvent such as 1,2-dichloroethane, dichloromethane or t-butanol. The resulting amine-terminated polyamide oligomer had low solubility in the solvent system and precipitated. This served to limit the degree of polymerization of the oligomer. Even so, a portion of the products was insoluble in water and was filtered out during preparation of the aqueous oligomeric amine solution for the interfacial reaction step.

Table IV lists the best performance data obtained for piperazine oligomer membranes interfacially reacted with isophthaloyl chloride. The objective of these tests was to achieve single-pass seawater desalination membranes. As such, the presence of free carboxylate groups was avoided; use was made of the trimesoyl chloride or alternate triacyl halides in the oligomer formation step, and diacyl chlorides in the interfacial reaction step. A few samples of seawater desalination membranes were obtained. Best results were seen for piperazine-cyanurate pre-polymers interfacially cross-linked by isophthaloyl chloride, but fluxes were low in view of the operating test pressure of 1500 psi (10 342 kPascal). Also, individual membrane results with piperazine oligomers were equally as erratic as those experienced for piperazine directly. The only notable advantage of the piperazine oligomer approach was the ability to incorporate

cyanurate rings into the membrane structure. Cyanuric chloride was too prone to hydrolysis to provide good interfacial membranes with piperazine otherwise.

Table IV. Membranes Formed Using Piperazine Oligomers and Isoph-
thaloyl Chloride

Reactant used to prepare		Reverse Osmosis Test Data (a)		
Piperazine Oligomer	Acid Acceptor	Flux		Salt Rej.
		(gfd)	(L/sq·m/hr)	(%)
trimesoyl chloride	NaOH	13	(22)	99.0
trimesoyl chloride	triethylamine	58	(97)	93.8
cyanuric chloride	NaOH	14	(23)	99.2
cyanuric chloride	triethylamine	24	(40)	98.0
phosphorus oxychloride	N,N'-dimethyl-piperazine	45	(75)	93.9
1:1 trimesoyl: isophthaloyl chloride	triethylamine	34	(57)	92.4
cyanuric chloride (b)	NaOH	9	(15)	99.0

(a) Twenty to 24 hour tests, 1500 psi (10 342 kPascal) 25°C, 3.5% synthetic seawater
(b) Reacted wtih a 6:1 molar ratio of piperazine:morpholine

In conclusion, some of the high salt rejection properties found with interfacial polypiperazineamide membranes in the laboratory could not be attained by a machine-made membrane. However, the machine-formed membrane may still find applications where high rejection of monovalent salts is not required but where high flux and rejection of larger solutes are useful. A limited effort to replace piperazine in the reaction with piperazine-terminated oligomers did not appear to resolve the membrane reproducability problem. Recent studies made on the use of piperazine terminated oligomers in composite membrane preparation were reported by R. Sudak et al at Membrane Systems, Inc. (46) and by J.F. Wolfe et al at Stanford Research Institute (47).

Monomeric Amine Reactants: FT-30. In 1978 the FT-30 membrane was developed at FilmTec Corporation (48). The FT-30 membrane was produced by the interfacial reaction of aromatic diamines in the aqueous phase with triacyl chlorides in the solvent phase (49). As with the piperazine reactions described in the preceding paragraphs, reactions of diamines with a triacyl chloride such as trimesoyl chloride can lead to two types of side reactions in addition to the linear chain formation. These reactions are either hydrolysis of the third acyl chloride group of trimesoyl chloride to a carboxylic acid or to reaction with another diamine molecule to produce chain branching or cross-linking. Again, it is likely that both of these reactions occur, and for FT-30 it is believed on the basis of ESCA studies that the ratio of branching to carboxyl group formation is approximately 1:1 (50). For example, the following equation shows the reaction between m-phenylene diamine and trimesoyl chloride to produce a

polyamide having branching sites and free carboxyl groups:
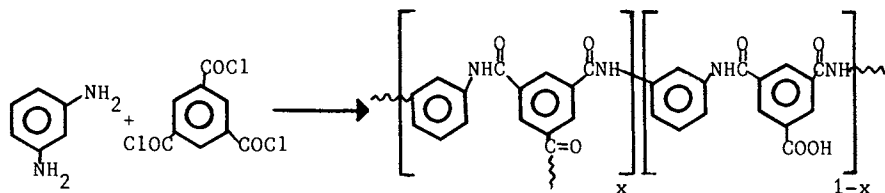
The free carboxylic acid content of the membrane has not been ana-
lyzed but there is a sufficient amount to produce a mild anionic
charge at neutral or alkaline pH levels. The membrane absorbs
cationic dyes and the effect of cationic surfactants added to the
feedwater is readily observed as a loss in flux.
     It can be seen from the above equation that branching and cross-
linking should produce a three-dimensional polymer network. The
membrane is insoluble in all solvents, including concentrated sulfur-
ic acid, which is an indication of cross-linking. The physical
properties of the FT-30 barrier layer are, however, not entirely
consistent with a highly cross-linked structure. A free-floating
membrane barrier layer, formed at a water-solvent interface from the
above reactants in the absence of polysulfone, is flexible. No
brittleness or lack of ductility is evident when the FT-30 membrane
is handled dry or when stressed while wet and under high pressure in
reverse osmosis tests at up to 1500 psi (10 342 kPascal). While the
actual conformation of the FT-30 barrier layer has not been definite-
ly established, it appears certain that a degree of cross-linking
is essential to obtain maximum membrane performance. Substitution
of difunctional acyl chlorides in the reaction produced membranes
with poor reverse osmosis properties. Also, pre-hydrolysis of one
acyl chloride group of trimesoyl chloride before the interfacial
reaction produced a membrane with only 60 to 85 percent salt rejec-
tion. Similar reverse osmosis test results were seen when trimel-
litic anhydride acyl chloride (TAC) was used as the reactant. This
reagent reacts difunctionally with aromatic diamines to give a
carboxylated polymer without cross-linking:

TAC
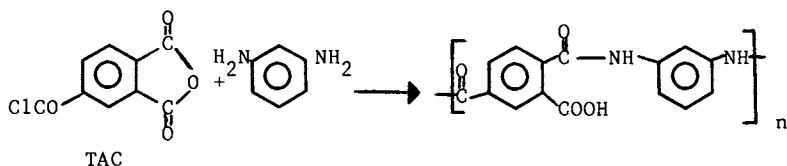
Reaction Mechanism. Electron micrographs of the face of FT-30
membrane show an unusual appearance. Unlike other interfacially
formed membranes such as the NS-100 which appear smooth and feature-
less in electron micrographs, the FT-30 has a rough surface with
protuberances coming out of the plane of the membrane (Figure 3).
This appearance of FT-30 seems to be related to the mechanism of the
interfacial reaction. As stated previously, Morgan presented evi-
dence that the reaction takes place primarily on the solvent side of
the interface; that is, the amine migrates from the water phase to
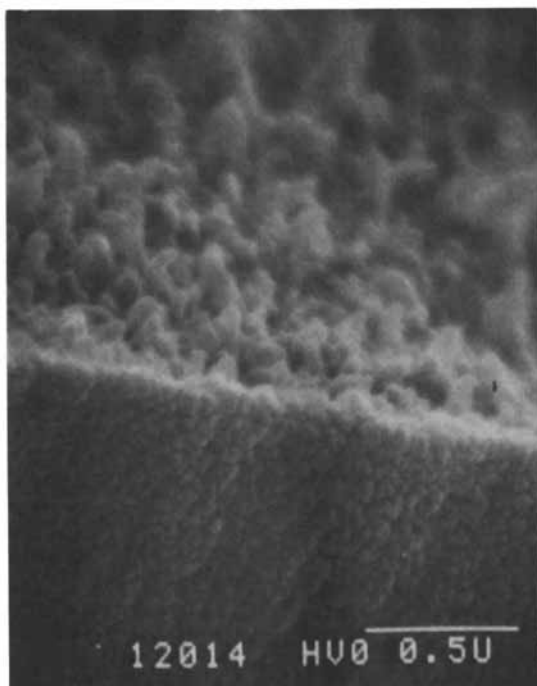
Figure 3. Electron micrograph showing surface and fractured edge of FT-30 membrane.

react with the acyl chloride in the solvent phase (33). Hydrogen
chloride liberated in the reaction is neutralized by excess amine.
The hydrochloride salts, being more water-soluble, then migrate to
the water phase. In this proposed mechanism one must assume that
the initial contact between the solvent and aqueous phases produces
a porous polyamide network at the solvent interface. Then the
amine continues to diffuse into the solvent phase wherever there is
an unclosed gap, eventually producing a continuous polymer barrier
between the two phases. Electron micrographs of the back surface of
the barrier layer pulled loose from the support film surface show a
highly porous structure which tends to confirm the amine-migration
mechanism. The barrier layer requires less than a minute to form,
and there is no further reaction of the reagents or change in mem-
brane properties upon longer contact of the two phases. Its thick-
ness is approximately 2500 Angstroms.

Properties of FT-30. The properties of FT-30 membranes have been
reviewed in several publications. Therefore, only the salient fea-
tures that relate to the chemistry of the barrier layer will be
considered here. Reverse osmosis performance of FT-30 under sea-
water and brackish water test conditions was described by Cadotte
et al (48) and by Larson et al (51). In commercially produced
spiral-wound elements the FT-30 membrane typically gives 99.0 to
99.2 percent salt rejection at 24 gfd (40 L/sq m/hr) flux in sea-
water reverse osmosis tests with 3.5 percent synthetic seawater at
800 psi (5516 kPascal) and 25°C.
    The aromatic polyamide structure of the FT-30 barrier layer
contributes a high degree of compression resistance and chemical
resistance. The membrane can be sterilized in boiling water with
no effect on its properties. Initial studies on the effect of feed-
water temperature were short term (2 hour) tests using synthetic
seawater in a temperature range of 20 to 60°C (48). A linear in-
crease of flux with temperature was observed which was reversible
upon cooling. However, later studies made using hot sucrose solu-
tions at up to 85°C and 800 psi showed a definite membrane compaction
phenomenon at 60 to 85°C (52). The losses in membrane flux were in
the range of 30 to 60 percent, depending upon the severity of the
temperature-pressure combination. In that these membrane compaction
effects are mostly offset by an increase in water diffusivity with
increasing temperature (hence, increased membrane flux), high-
temperature operation with this membrane remains technically and
economically feasible.
    A recommended pH range for FT-30 spiral-wound elements was set
at 3 to 11 for feedwaters at ambient temperatures. The membrane will
tolerate a much wider range of pH for limited periods, and strong
mineral acids such as phosphoric or nitric acids can be used for
cleaning. Also, dilute solutions of strong bases such as sodium
hydroxide or trisodium phosphate can be used with anionic surfac-
tants for cleaning at high pH.
    Chlorine resistance tests on FT-30 membranes, whether static-
jar storage tests or dynamic tests with chlorine added to the feed-
water showed a much lower rate of oxidation compared to other poly-
amide membranes such as the NS-100. A peculiar property of the
FT-30 membrane in regard to chlorine attack was that the rate of
oxidation was lowest in an acid pH range of 5 to 6 and higher in the

alkaline pH range. This pH effect on chlorine oxidation of FT-30 membrane was opposite of that normally observed with other membranes, because the hypochlorous acid at pH 5 to 6 would have a higher oxidation potential than sodium hypochlorite in the alkaline pH range. This has been observed both at FilmTec and by Glater and co-workers (53). Because of the low rate of oxidation of FT-30 membrane by chlorine it can tolerate an accidental exposure to chlorine. Shock chlorinations, if used with care, are possible, but not generally recommended.

Other Interfacial Reactions. Composite membranes can be made using reagents in place of the polyamines; that is, reagents having two or more alcohol, phenol or thiol groups. The barrier layers formed would be polyester or polythioester types. In comparison with the polyamide types described above, these reagents have a slower reaction rate in the membrane preparation. Also, the resulting membranes have always exhibited lower flux than the corresponding polyamides in studies to date, and furthermore would not be as resistant to alkaline hydrolysis. An example of such membranes is described in a recent Japanese patent application by Toray Industries (54). A polysulfone support film was saturated in a water solution containing hydroquinone, polyvinyl alcohol and sodium lauryl sulfate (1.5:0.2: 0.1 percent by weight). After an interfacial reaction with trimesoyl chloride the membrane was dried at 120°C. Following application of a protective polyvinyl alcohol coating, reverse osmosis tests with 3.5 percent sodium chloride showed 99.75 percent salt rejection at a flux of 5.15 gfd(8.6 L/sq m/hr).

Conclusions

Since the early 1970's rapid progress has been made in the commercial development of composite reverse osmosis membranes. Of the four general methods used for preparing composite membranes, the method using interfacial reactions has surpassed the others. However, none of the four methods has been ruled out if it can produce the desired membrane properties. Composite membranes have reached a relatively high level in regard to flux, salt rejection and stability. Naturally any improvements in these properties, as well as improved yields, are still desirable. Also, there are needs for membranes having specific separation abilities for solutes up to a few hundred in molecular weight. The need for membranes resistant to specific solvents or chemicals, particularly chlorine, remains an important objective. Additional problem areas that need further attention are compaction in feedwaters above 60°C and membrane fouling. The versatility inherent in composite membrane processes may contribute to the solution of these problems.

Literature Cited

1. Loeb, S; Sourirajan, S. Advan. Chem. Ser., 1962. 38, 117.
2. Riley, R.L.; Gardner, J.O.; and Merten, V. Science, 143, 801, 1964.
3. Cadotte, J.E. and Petersen, R.J. In ACS Symposium Series No. 153, "Synthetic Membranes: Volume I Desalination", Albin F. Turbak Ed., 1981.

4. Francis, P.S. "Fabrication and Evaluation of New Ultrathin Re-
     verse Osmosis Membranes", National Technical Information Service,
     Springfield, VA, Report No. PB-177083, 1966.
5. Forester, R.H. and Francis, P.S. U.S. Patent 3,551,244.
6. Rozelle, L.T.; Cadotte, J.E.; Senachal, A.J.; King, W.L.; and
     Nelson, B.R. In "Reverse Osmosis Membrane Research", Lonsdale,
     H.K.; and Podall, H.E., ed.; Plenum Publishing Co., New York,
     p. 305.
7. Petersen, R.J. and Rozelle, L.T. Trans. Amer. Soc. Artif. Int.
     Organs, 21, 242, 1975.
8. Rozelle, L.T.; Cadotte, J.E.; Corneliussen, R.D.; Erickson, E.E.
     "Development of New Reverse Osmosis Membranes for Desalination",
     NTIS Report No. PB-206329, 1967.
9. Merten, V.; Lonsdale, H.K.; Riley, R.L.; and Vos, K.D. "Reverse
     Osmosis for Water Desalination", Office of Saline Water Report
     No. 208, 1966.
10. Riley, R.L.; Lonsdale, H.K.; Lyons, C.R.; and Merten, V. J. Appl.
     Pol. Sci., 11, 2143, 1967.
11. Lonsdale, H.K.; Riley, R.L.; Lyons, C.R.; and Carosella, O.P., Jr.
     In "Membrane Processes in Industry and Biomedicine", Bier, M.,
     ed., Plenum Press, New York, 1971, p. 101.
12. Riley, R.L.; Lonsdale, H.K.; La Grange, L.D.; and Lyons, C.R.
     "Development of Ultrathin Membranes", Office of Saline Water,
     Report No. 386, 1969.
13. Cadotte, J.E. U.S. Patent 3,926,798, 1975.
14. Cadotte, J.E.; Kopp, C.V.; Cobian, K.E.; and Rozelle, L.T.
     "In Situ-Formed Condensation Polymers for Reverse Osmosis Mem-
     branes, Second Phase" NTIS Report No. PB 234198, 1974.
15. Cadotte, J.E.; Cobian, K.E.; Forester, R.H.; and Petersen, R.J.
     "In Situ-Formed Condensation Polymers for Reverse Osmosis
     Membranes" NTIS Report No. PB 248670, 1975.
16. Graefe, A.F. "Development of a Composite Reverse Osmosis Mem-
     brane for Single Pass Seawater Desalting" NTIS Report No. PB-80
     124852
17. Schiffer, D.K.; Davis, R.B.; Coplan, M.J. "Development of
     Composite Hollow Fiber Reverse Osmosis Membranes" NTIS Report
     No. 80-213044, 1979.
18. Kurihara, M.; Watanaba, T.; Inoue, T. U.S. Patent 4,366,062,
     1982.
19. Cadotte, J.E.; Cobian, K.E.; Forester, R.H.; and Petersen, R.J.
     "Continued Evaluation of In Situ-Formed Condensation Polymers
     for Reverse Osmosis Membranes" NTIS Report No. PB 253193, 1976.
20. Harumiya, N.; Kurihara, M.; Nakagawa, Y.; Kanamuru, N.; Watnabe,
     T.; Uemura, T. Japan PCT Int. Appl. 8100, 217, 1981, Chem.
     Abstr. 95:633959.
21. Kurihara, M.; Kanamaru, N.; Harumuja, K.; Yoshimura, K.; and
     Hagiwara, S. Desalination, 32, 13, 1980.
22. Plummer, C.W.; Kimura, G.; and LaConti, A.B. "Development of
     Sulfonated Polyphenylene Oxide Membranes for Reverse Osmosis",
     OSW Report No. 551, U.S. Government Printing Office, 1970.
23. Bourganel, J. U.S. Patent 4,026,977, 1977.
24. Cadotte, J.E.; Steuck, M.J.; and Petersen, R.J. "Research on
     In Situ-Formed Condensation Polymer for Reverse Osmosis Mem-
     branes", NTIS Report No. PB-288387, 1977.

25. a.) Schiffer, D.K. and Coplan, M.J. "Development of Hollow
          Fiber Reverse Osmosis Membranes", Final Report to OWRT,
          NTIS Report No. PB 81-167215, 1981.
     b.) Davis, R.B.; Schiffer, D.K.; and Kramer C.E. "Hollow
          Fiber Reverse Osmosis Composite Membranes; Process and
          Properties", ACS Symposium Series 153, Synthetic Membranes,
          Vol 1 ACS, Washington D.C. 367, 1981.
26. Buck, K.R. and Davan, V.K. Br. Polym. J. 2, 238, 1970.
27. Yasuda, H. and Lamaze, C.E. J. Appl. Polym. Sci., 17, 201, 1973.
28. Hollahan, J.R. and Wydeven, T. Science, 179, 500, 1973.
29. Yasuda, H. and Marsh, H.C. J. Appl. Polym. Sci. 20, 543, 1976.
30. Heffernan, P.J.; Yanaglhara, K.; Matsugawa, Y.; Hennecke, E.E.;
     Helmuth, E.W. and Yasuda, H. Ind. Eng. Chem. Prod. Res. Dev.,
     23, 153, 1984.
31. Sano, T. Chemical Economy and Engineering Review, 12, 22, 1980.
32. Sano T.; Takatoshi, S.; Masao, S. and Ichiki, M. U.S. Patent
     4,147,745, 1979.
33. Morgan, P.W. "Condensation Polymers by Interfacial and Solution
     Methods", Interscience Publishers, 1965.
34. Scala, L.C.; Ciliberti, D.F.; and Berg, D. U.S. Patent 3,744,
     642; 1973.
35. Rozelle, L.T.; Cadotte, J.E.; Cobian, K.E.; and Kopp, C.V., Jr.
     "Nonpolysaccharide Membranes for Reverse Osmosis: NS-100 Mem-
     branes for Reverse Osmosis and Synthetic Membranes", S. Sourira-
     jan, ed., National Research Council Canada, Ottawa, Canada,
     1977, p. 249.
36. Technical Literature "Corcat Polymers" CAS No. 9002-98-6 from
     Cordova Chemical Co.
37. Riley, R.L.; Fox, R.L.; Lyons, C.R.; Milstead, C.E.; Seroy, N.W.
     and Tagoni, M. Desalination, 19, 113, 1976.
38. Al-Gholaikah, A.; El Ramly, N.; Janyoon, I.; and Seaton, R.
     Desalination, 27, 215, 1978.
39. Kurihara, M.; Uemura, K.; and Okada, K. U.S. Patent No.
     4,387,024, 1983.
40. Kawaguchi, T.; Taketani, Y.; Sasaki, N.; Minematsu, H.;
     Hayashi, Y.; and Hara, S. U.S. Patent No. 4,302,336, 1981.
41. Kawaguchi, T.; Minematsu, H.; Hayashi, Y.; Hara, S.; and
     Veda, F. U.S. Patent No. 4,360,434, 1982.
42. Cadotte, J.E.; Cobian, K.E.; Forester, R.H. and Petersen, R.J.
     "Continued Evaluation of In Situ-Formed Condensation Polymers
     for Reverse Osmosis Membranes", NTIS Report No. PB 253193,
     1976.
43. Credali, L.; Chiolle, A.; and Parinni, P. Desalination,
     14, 137, 1974, and Parrini, P. Desalination 48, 67, 1983.
44. Cadotte, J.E.; Steuck, M.J. and Petersen, R.J. "Research on
     In Situ-Formed Condensation Polymers for Reverse Osmosis Mem-
     branes", NTIS Report No. PB 288287, 1978.
45. Petersen, R.J.; Cadotte, J.E.; Forester, R.H. and Buettner, J.M.
     "Development of Novel Polypiperazineamide Membranes in Spiral
     Wound Modules", Contract No. 14-34-0001-8547 to Office of
     Water Research and Technology, 1979.
46. Sudak, R.G.; Chirrick, J.M.; Fox, R.L.; McKee, W.E.; Bott, J.M.
     and Tomaschke, J.E. "Development of Chlorine Resistant Membrane
     Asymetric Polyimide Membrane and Porous Substrates", NTIS Report
     PB 81-142242.

47. Wolfe, J.F.; Jones, R.S.; Sybert, P.D. "Novel polymers for Reverse Osmosis Membranes", NTIS Report No. PB 83-173237, 1983.
48. Cadotte, J.E.: Petersen, R.J.; Larson, R.E. and Erickson, E.E. Desalination, 32, 25, 1980.
49. Cadotte, J.E. U.S. Patent 4,277,344; 1981.
50. Unpublished data, J-Y. Koo, FilmTec Corporation.
51. Larson, R.E.; Cadotte, J.E. and Petersen, R.J. Desalination, 38, 473, 1981.
52. Petersen, R.J.; Thorpe, J.N.; Cadotte, J.E.; Koo, J-Y "Temperature Resistant Elements for Reverse Osmosis Treatment of Hot Process Waters", Cooperative Agreement No. DE-FCO7-82ID12423 with U.S. Department of Energy, Industrial Programs, Washington, D.C. 20240.
53. Glater, J.; McCutchan, J.W.; McCroy, S.B. and Zachariah, M.R. Synthetic Membranes, Volume 1 – Desalination, Turbak, A.F., ed.; ACS Symposium Series 153, 1981, p. 171.
54. Japan PCT Int. Appl. 83 89910, 1983, Chem. Abstr. 99, 141281Y.

Dependence of Dynamic Membrane Performance on Formation Materials and Procedures

H. GARTH SPENCER

Department of Chemistry, Clemson University, Clemson, SC 29631

Dynamic membranes originated in the research at the Oak Ridge National Laboratory in the 1960's. Development has produced commercial ultrafiltration and hyperfiltration membranes for industrial separation applications. Research continues in several laboratories to improve the selectivity and productivity of the membranes and to tailor them for specific applications. The development of dynamic membranes and current research is reviewed briefly. Research on polyelectrolyte blend membranes is described in detail as a representative method for tailoring dynamic membranes.

Dynamic membranes are formed on microporous supports under appropriate pressure and cross-flow conditions by deposition of solute components contained in a feed solution. The formation steps are: (a) selection and conditioning of a porous support; (b) deposition of a filter aid, when needed; (c) deposition of a colloid to form the ultrafilter; (d) deposition of one or more polymers to produce the hyperfilter; and (e) post-formation treatments to enhance selected properties.

The properties of dynamic membranes can be influenced at each step in the formation by altering the materials and procedures. Hence, dynamic membranes are expecially suited for tailoring to optimize a membrane's performance in a specific application, and a variety of experimental and commercial membranes have been formed. In many cases it is possible to remove the membrane by chemical means, recondition the porous support, and reform either the same type or a different type of dynamic membrane at the application site. This feature gives each module a long operating life.

Successful applications of dynamic membranes in a number of industrial separation processes, membrane stability at high temperature and over a broad pH range, and membrane reformation capability on durable substrates have attracted a significant research and development effort. Much of the research has been directed toward

production of predictable, reproducible, and highly stable mem-
branes; attainment of low cost per unit of feed processed; and ex-
pansion of the family of dynamic membranes to improve performance
and meet additional application needs.

     This paper reviews some recent developments in dynamic membrane
research, describes properties and applications of commercial mem-
branes, and reports properties of dynamic polyblend membranes.

Formation of Dynamic Membranes

The poineering research and subsequent development of useful dyna-
mic membranes was accomplished by Johnson and co-workers at the Oak
Ridge National Laboratory. This very extensive research has been
reported in a series of reports and in numerous publications and
patents. Papers of special interest are: the detailed report of
the initial process for forming dynamic membranes with attractive
hyperfiltration properties by Marcinkowsky, et al. (1), an early
review of the research properties by Johnson (2), and a subsequent
review of hyperfiltration models and the development of hyperfiltra-
tion membranes by Dresner and Johnson (3). These reviews cite the
major references related to the formation, theory, properties, and
applications of dynamic membranes.

     Two useful membranes developed by the group at the Oak Ridge
National Laboratory have dominated the application of dynamic mem-
branes: the hydrous zirconium oxide ultrafilter and the hydrous
zirconium oxide-poly(acrylic acid) hyperfilter. The technology of
formation and utilization of zirconium oxide-poly(acrylic acid)
dynamic membranes has been described in detail by Thomas (4). The
effects of molecular weight of the poly(acrylic acid), pore dia-
meter of the porous support, formation cross-flow velocity, forma-
tion pressure, and pH of poly(acrylic acid) solution during initial
deposition of the polyacid on the hyperfiltration performance are
described and discussed.

Commercial Developments

Commercial dynamic ultrafiltration membranes are produced by the
Gaston County Dyeing Machine Co. and by CARRE, Inc. The former
uses porous carbon tubes and the latter porous metal tubes as the
membrane substrate and containment material. The ultrafiltration
properties of the CARRE, Inc. ZOSS ultrafilter, hydrous zirconium
oxide on porous stainless steel tubes, are provided in Table I as
an example of a dynamic ultrafiltration membrane.

     CARRE, Inc. also produces a series of dynamic hyperfiltration
membranes on porous metal tubes. The major product is the ZOPA
hyperfilter: hydrous zirconium oxide-poly(acrylic acid) on porous
stainless steel tubes. The hyperfiltration properties of the ZOPA
membranes are also listed in Table I. The most attractive proper-
ties of the ZOPA membrane are durability at temperatures of at
least 100°C, high membrane permeability, and reformation capability.
The hydrous zirconium oxide-poly(acrylic acid) membranes provide
modest rejection of simple electrolytes. Although the membrane
permeability is high compared to most cast reverse osmosis /hyper-

Table I. CARRE, Inc. Membrane Specifications

	Ultrafiltration ZOSS	Hyperfiltration ZOPA
Flow geometry	Tubular	Tubular
Membrane support	Stainless steel (316L)	Stainless steel (316L)
Membrane material	Zirconium oxide	Zirconium oxide polyacrylate
Method of Replacement	In place chemical solution	In place chemical solution
Prefiltration requirement	40 mesh screen	40 mesh screen
Pressure limitation	Greater than 1000 psig	Greater than 1000 psig
Temperature limitation	Greater than $100^{o}C$ ($212^{o}F$)	Greater than $100^{o}C$ ($212^{o}F$)
pH range	2 - 13	4 - 10
Permeability* with test solution at $100^{o}F$ (gfd/psi)	0.05 to 0.4	0.05 to 0.07
At $200^{o}F$	0.4 to 1.2	0.2 to 0.3
Salt rejection*	5 to 20%	80 to 90%

*Test solution 1000 mg/L of $NaNO_3$ in water.

filtration membranes, the rejection of simple electrolytes is sig-
nificantly lower. Hence, ZOPA membranes are not usually suitable
for desalination and other applications requiring very high rejec-
tion of simple electrolytes. However, they provide very high rejec-
tion of electrolytes with larger cations or anions, such as dyes and
ionic surfactants. Fouling in the presence of calcium and magnes-
ium ions may also limit this application in some cases. Modest
rejections of low molecular weight molecular solutes are also at-
tained with the hydrous zirconium oxide-poly(acrylic acid) membranes.

Additional types of hyperfiltration membranes produced by
CARRE, Inc. include polyblend membranes prepared by the deposition
of pairs of polymers that form miscible blends (5). High rejection
of molecular solute species in the molecular weight range above
about 80 is obtainable with these dynamic polyblend membranes.
Their properties will be described in a later section.

The largest ZOSS and ZOPA systems currently in operation are
used in the textile industry for recycling wash water in dyeing
processes and for renovating caustic solutions (6, 7). Systems are
also being used for oil-water separation, nuclear industry applica-
tions, and food processing.

Recent Developments

A significant advance in the preparation of dynamic membranes was
realized when the technology for depositing the membranes on porous
stainless steel tubes was developed by Gaddis and Brandon (8). The
replacement of porous carbon and ceramic materials by sintered por-
ous metal as a membrane support has facilitated manufacture of large
single-pass membrane systems, significantly reduced tube breakage,
and permitted high pressure operation.

Tanny (9) has prepared ultrafilters by depositing hydrous zir-
conium oxide on pliable porous materials in a fluted configuration,
providing a large membrane area in a small volume suitable for low
pressure ultrafiltration.

Wang (10) has prepared and characterized cross-linked poly-
(vinyl alcohol) dynamic membranes on porous ceramic tubes. The
post-formation cross-linking with a solution containing oxalic acid,
boric acid, and $KCr(SO_4)_2$ produced membranes with good stability
in both acidic and basic solutions.

Several research groups have investigated applications and
properties of dynamic ultrafilters and hyperfilters. Groves and
co-workers (11) have extensively investigated the use of dynamic
membranes and others for a variety of applications in textile pro-
cessing, such a renovation of dye process wash water, wool scouring,
and textile size recovery. Trauter and co-workers (12, 13) have
also investigated the application of dynamic zirconium oxide ultra-
filters for textile size recovery. Fuls (14), at the Council for
Scientific and Industrial Research, S.A., is investigating indus-
trial applications of dynamic ultrafilters and hyperfilters and also
the effects of altering preparation methods. Gaddis and Spencer
(6, 8, 15) have investigated the use of dynamic hyperfiltration mem-
branes for rejecting pollutants in textile dyeing process waste-
water, for treatment of dye manufacture wastewater, and for recycl-
ing shower water in spacecraft.

Dynamic Polyblend Hyperfiltration Membranes

Several types of dynamic polyblend membranes have been formed on stainless steel supports at CARRE, Inc. Investigations at Clemson University have been concerned with a preliminary determination of some of the properties of these potentially useful membranes (5). The formation procedures and hyperfiltration properties of one type of polyelectrolyte blend membrane are described here in detail.

   Preliminary work. Extensive literature exists on polyelecto-lytes in solution and in cross-linked states as ion-exchange beads and membranes (16). However, research on polyelectrolyte blend membranes has been limited. Michaels and co-workers (17 - 21) developed homogeneous cast membranes using strong acid-strong base pairs of polyelectrolytes suitable for a variety of applications but not for desalination. Kaneko and co-workers (22 - 24) prepared homogeneous molded membranes from blends of oppositely-charged polyelectrolytes for ultrafiltraiton and dialysis. Dresner and Johnson (3) formed and tested a few polyblend membranes dynamically formed by the simultaneous deposition of pairs of oppositely-charged polyelectrolytes on a porous substrate. However, development of these membranes was not pursued.

   Experimental. The complementary polyelectrolytes used in the membrane formation were poly(acrylic acid) (Acrysol, Rohm and Haas) and a high molecular weight weak base polyelectrolyte containing secondary and tertiary amine groups. A hydrous zirconium oxide membrane on stainless steel (a ZOSS membrane produced by CARRE, Inc.) was used as a substrate. The tubular module was 1.27 cm (0.50 in.) in diameter and 4.09×10^{-2} m^2 (0.44 ft^2) in membrane area. The solutes used in the characterization tests were reagent grade $NaNO_3$ and Na_2SO_4, and food grade fructose and sucrose. The characterization solutions were 2 g/L for the salts and 2% (w/v) for the sugars.

   The polyelectrolytes were deposited in sequence from aqueous solutions at room temperature under normal operating cross flow and applied pressure conditions (7). Characterization consisted of determinations of membrane permeability (flux to pressure ratio, J/p) and solute rejections (r) over a broad range of pH. Experiments were carried out at temperatures between 30 and $70^{\circ}C$, pressures up to 6.9 MPa (1,000 psig), and cross flow velocities of 1 to 2 m/s. Electrolyte rejections were determined by measuring the conductivity of the feed and permeate solutions. The concentrations of the sugar solutions were measured with a refractometer.

   Membrane Properties. The effects of each formation step on the hyperfiltration properties of a representative polyelectrolyte blend membrane and the characterization properties of the completed membrane are provided in Table II. The membrane permeability (J/p) has been corrected to $50^{\circ}C$, and indicated by $(J/p)_0$, using the equation

$$(J/p)_0 = (J/p)\exp\left[2500(1/T - 1/323)\right] .$$

The deposition of the poly(acrylic acid) converts the ZOSS ultra-filter to a hyperfiltration membrane exhibiting a simple electrolyte

rejection of greater than 0.85. Subsequent deposition of the poly-
base typically reduces the rejection of simple electrolytes, espe-
cially in the pH range 6 to 8, and reduces the membrane permeability
significantly. The extent of the reduction of the membrane perme-
ability can be controlled within limits by altering the deposition
procedure. The type of polybase, concentration and pH of deposition
affect the membrane permeability (5).

   Assuming that the electrolyte rejection by the membrane is
determined primarily by electrolyte exclusion, rules for this
phenomemon can be invoked to determine the sign of the net fixed
charge. For a positive net fixed charge, the rejection of $NaNO_3$
should exceed Na_2SO_4, while the opposite order should occur when
the net fixed charge is negative. In terms of this model, the mem-
brane described in Table II has a positive net fixed charge at pH 4,
where only a small fraction of the poly(acrylic acid) is dissocia-
ted. At pH 7, where both the weak base and the weak acid polyelec-
trolytes are primarily in their ionic forms, the rejections of
Na_2SO_4 and $NaNO_3$ are not significantly different. A study of re-
jection of electrolytes of different charge type as a function of
pH provides information about the relative amounts of the two poly-
electrolytes in the active region of the membrane. The model shows
that the minimum in the curve of the rejection of $NaNO_3$ is an indi-
cator of the isoelectric point of the membrane. See Table III for
comparison of the sign of the fixed charge as a function of pH for
a ZOPA membrane, a polyblend membrane with an excess of weak-acid
polyelectrolyte and a polyblend membrane with an excess of weak-
base polyelectrolyte.

Table II. Hyperfiltration Properties of a Dynamic Polyelectrolyte
           Membrane and its Precursors

Membrane Form	Solute	Temp. ($^{\circ}$C)	pH	Rej.	(J/p) (gfd/psi)
ZOSS	$NaNO_3$	38	3.9	0.05	0.42
Polyacid added	$NaNO_3$	34	6.9	0.86	0.18
Polybase added	Fructose	68	3.8	0.95	0.04
	Fructose	69	7.1	0.95	0.02
	$NaNO_3$	71	7.2	0.80	0.02
	$NaNO_3$	72	3.8	0.83	0.03
	Sucrose	65	3.8	0.97	0.04
	Sucrose	70	6.9	0.97	0.02
	Na_2SO_4	71	7.0	0.85	0.02
	Na_2SO_4	72	3.9	0.66	0.03

p = 5.5 MPa (800 psi)
(Reproduced with permission from Ref. 5. Copyright 1984, Elsevier)

   Attainment of high sugar rejection at high temperature was the
motivaiton for investigating polyblend membranes. It is not dif-
ficult to obtain fructose rejections greater than 0.95 with the

polyblend membranes, while fructose rejections greater than 0.4 are rarely obtained with ZOPA membranes. The penalty for this improved rejection of small hydrophilic non-electrolytes, represented by fructose and sucrose, is a reduction in both the membrane permeability and the rejection of simple electrolytes near the isoelectric point of the membrane. The membrane permeability for those membranes with fructose rejection greater than 0.95 is in the range 0.02 to 0.05 gfd/psi. The passage $(s = 1 - r)$ of fructose is directly related to membrane permeability in polyelectrolyte blend membranes, with $s = 1.7$ $(J/p)_0$ (5), and not specifically related to any single alteration in the formation procedures or materials. The passage of sucrose is about one-third the passage of fructose.

The rejection of $NaNO_3$ has been determined as a function of the feed solution concentration (c). Graphs of log s vs. log c are linear for ZOSS, ZOPA, and polyelectrolyte blend membranes. The slopes are near unity for ZOSS membranes (2), in the range 0.3 − 0.5 for ZOPA membranes (2), and 0.1 to 0.3 for polyelectrolyte blend membranes. The theoretical value of the slope for an ion

Table III. Dependence of the Sign of the Fixed Charge of a ZOPA and Dynamic Polyblend Membrane on pH

Membrane	pH	r($NaNO_3$)	r(Na_2SO_4)	Sign of Fixed Charge
ZOPA	4.0	0.60	0.59	*
(Weak acid	7.0	0.68	0.88	−
Polyelectrolyte)				
Polyblend	3.8	0.80	0.65	+
(excess weak-	6.0	0.68	0.82	−
acid poly-	8.0	0.62	0.87	−
electrolyte)				
Polyblend	3.9	0.82	0.55	+
(excess weak-base	7.2	0.82	0.77	+
polyelectrolyte)				

*Inconclusive difference in rejections. ZOPA membranes normally become positive at low pH.

exclusion mechanism with the ratio of mean ionic activity coefficients for the electrolyte in the membrane and in the feed solution equal to one is unity (2). Reduction of the slope is realized by the conversion of a ZOSS ultrafilter to a ZOPA hyperfilter and again by conversion to the polyelectrolyte blend membrane.

The polyelectrolyte membranes exhibit hyperfiltration properties distinctly different from ZOPA membranes and should find use in different applications. They retain their hyperfiltration properties at temperatures as high as 100°C and they appear to be stable in many application environments.

Concluding Remarks

Dynamic membranes formed on porous metal tubes are commercially available and are being used in several industrial separation processes. The _in situ_ formation procedures coupled with a permanent porous support provide the capability of reformation and tailoring of the membranes to obtain attractive performance characteristics in a variety of challengine operating environments; including high temperature and extremes in pH. The general procedure of forming polyblend membranes is but one example the tailoring process. There is potential for greater use of dynamic membranes in selected industrial environments. The major technical challenge is to extend the variety of formation procedures and materials to obtain improved membrane characteristics for selected applications. The number of laboratories involved in the research on dynamic membranes has increased significantly during the past ten years steming from the pioneering work at the Oak Ridge National Laboratory.

Acknowledgment

Literature Cited

1.   Marcinkowsky, A. E.; Kraus, K. A.; Phillips, H. O.: Johnson, J. S., Jr.; Shor, A. J. J. Am. Chem. Soc. 1966, 88, 5744.
2.   Johnson, J. S., Jr. In "Reverse Osmosis Membrane Research"; Lonsdale, H. K.; Pondall, H. E., Eds.; Plenum: New York, 1972; pp. 379-404.
3.   Dresner, L.; Johnson, J. S., Jr. In "Principles of Desalination"; Spiegler, K. S., Ed.; Academic: New York, 1980; Part B, Second Ed., pp. 401-450.
4.   Thomas, D. G. In "Reverse Osmosis and Synthetic Membranes"; Sourirajan, S., Ed.; National Research Council Canada: Ottawa, 1977; pp. 295-312.
5.   Spencer, H. G.; Todd, D. K.; McClellan, D. B. Desalination 1984, 49, 193.
6.   Brandon, C. A.; Jernigan, D. A.; Gaddis, J. L.; Spencer, H. G. Desalination 1981, 39, 301.
7.   Brandon, C. A.; Gaddis, J. L.; Spencer, H. G. In "Synthetic Membranes"; Turbak, A. F., Ed.; ACS Symposium Series No. 154, American Chemical Society: Washington, DC, 1981; Vol. II, pp. 435-453.
8.   "Dynamic Hyperfiltration Membrane for High Temperature Spacecraft Wash Water Recycle," National Aeronautics and Space Agency, 1978.
9.   Tanny, G. "Recent Progress in the Theory and Applications of Dynamically Fromed Membranes," presented at the 5th Seminar on Membrane Separation Technology, Clemson University, Clemson, SC, 1980.
10. Wang, Y.; et al. Desalination 1983, 46, 335.

11. Buckley, C. A.; Townsend, R. B.; Groves, G. R. Water Sci. Technol. 1982, 14, 705, and unpublished data.
12. Trauter, J.; Egbers, G. TPI, Text. Prax. Int. 1983, 38, 599.
13. Trauter, J. TPI, Text. Prax. Int. 1983, 38, 690.
14. Fuls, P. F., personal communication.
15. Gaddis, J. L.; Spencer, H. G. Symp. Proc: Text. Industry Technol. 1978, pp. 115–123.
16. Helfferich, F. "Ion Exchange"; McGraw-Hill: New York, 1962.
17. Michaels, A. S.; Miekka, R. G. J. Phys. Chem. 1961, 65, 1765.
18. Michaels, A. S.; Mir, L.; Schneider, N. S. J. Phys. Chem. 1965, 69, 1447.
19. Michaels, A. S.; Falkenstein, G. L.; Schneider, N. S. J. Phys. Chem. 1965, 69, 1465.
20. Michaels, A. S. Ind. Eng. Chem. 1965, 57, 32.
21. Michaels, A. S. U. S. Patents 3 419 430, 1968; 3 419 431, 1968; 3 467 604, 1969.
22. Kaneko, S.; Tagawa, K.; Negoro, J.; Miwa, M.; Tsuchida, E. Japanese Patent 74 10 232, 1974; Chem. Abstr. 1974, 81, 14466.
23. Kaneko, S.; Tagawa, K.; Miwa, M.; Negoro, J.; Tsuchida, E. Japanese Patent 74 10 233, 1974; Chem. Abstr. 1974, 81, 14467.
24. Miwa, M.; Tagawa, K.; Kaneko, S.; Negoro, J.; Tsuchida, E. Japanese Patent 74 15 735, 1974; Chem. Abstr. 1974, 81, 137 322.

14

Hollow Fiber Membrane Research

Morphology, Pervaporation, Gas Separation, and Durability Problems

ISRAEL CABASSO

The Polymer Research Institute, State University of New York, CESF, Syracuse, NY 13210

The rapid development of hollow fiber membrane technology frequently
has outpaced the advance of scientific fundamentals. Thus, a re-
visit to this membrane technology helps to unveil the cause of some
outstanding problems and contributes to the improvement of existing
processes and products. This paper describes four major topics that
are currently being studied in our laboratories: 1) The evolvement
of morphology in a nascent wet-spun hollow fiber. 2) Separation of
gas mixtures through double-layer composite membranes (1). 3)
Stress induced crystallization in cellulose ester, reverse osmosis,
hollow fiber membranes (2). 4) The separation of aqueous alcohol
mixtures through ion-exchange hollow fibers. Each of these topics
is a subject of doctoral thesis and, therefore, only some points of
immediate interest will be emphasized here.

Method to Trace the Evolvement of Morphology in a Dry-Jet Wet Spinning Process

The dry-jet wet spinning process is commonly used in hollow fiber
technology. This spinning method can be employed to obtain almost
every known membrane morphology and is described in several publica-
tions (3, 4). In general, a spinning dope composed of a certain
polymer dissolved with additives in a water miscible solvent is spun
through a tube in an orifice spinneret into water. The polymer
coagulates and the solvents, along with the additives, are even-
tually extracted through the nascent fiber walls. A method of
spinning polysulfone hollow fibers with varied characteristics has
been described elsewhere (4). This spinning method is based on the
ability of polyvinylpyrrolidone (PVP) to form a homogeneous blend
with polysulfone and the fact that PVP is a water soluble polymer.
Thus, ternary spinning dopes of polysulfone/PVP/dimethylacetamide
(DMA) were dry-jet wet-spun to produce asymmetric hollow fiber
membranes for applications such as reverse osmosis, ultrafiltration,
hemofiltration and gas separations. In the present study, the fact
that PVP is a high molecular weight additive with a much lower

mobility than the solvent was exploited. Therefore, segments of the nascent fiber can be severed and removed from the spinning line and directed to a subambient chamber without damage, virtually stopping the coagulation process. Unlike the casting of flat sheet membranes, the spun fiber has to establish considerable mechanical integrity in a short period of time, < 2 seconds; therefore, dope solutions that contain high fractions of polymers, up to 50 wt.%, are often used. In the present study the dope composition contained 15 wt.% PVP (molecular weight 15,000), 28 wt.% polysulfone (Udell 3500) and DMF. This composition was spun into a water bath at 25°C to produce the fiber structure shown in Figure 1; that is, macrovoid-free porous hollow fibers with an external porous skin.

The nascent fiber was sampled and sectioned at several points in the manufacturing process: the spot at which the spinning solution enters the coagulation bath; the bottom of the bath (75 cm depth), where the highly swollen plasticized fiber travels through two guides; and at the collecting spool (see Reference 3, Figure 7). The sections were quickly removed from the bath and placed in a cold dry chamber, 2°C or less, where stiffness was achieved by bringing the highly solvent-plasticized fiber near its glass transition temperature. Note that the T_g of polysulfone is ~ 180°C and that the T_g of the PVP is ~ 160°C. Considerable depression in these T_gs prevail when the fiber segments contain large amounts of solvent. Therefore, the morphology of the nascent fiber may be altered if it is kept at temperatures above it's depressed T_g. Subtle damage in the morphology of the substructure can occur during the spinning procedure due to defective equipment. Analysis of such a case, as well as the formation of porous structures, are shown in the scanning electron micrographs (SEM) below. The sample fibers prepared for the SEM were freeze dried to remove the solvent, fractured under liquid nitrogen and subsequently sputtered with gold. To avoid alteration of the delicate sample, the sputtering time (usually 2 minutes) was cut to fractions of 10 to 20 seconds, with "cooling" intervals of 40 seconds each.

Figure 1 shows an asymmetric macrovoid-free polysulfone hollow fiber, spun with the bore off-center, a method that previously (5) proved to be helpful in detecting the origin of irregularities in the substructure of such fibers. Figure 2 shows part of a cross-section of the fiber. Two parallel defects, "trails," stretching along the fiber are denoted with arrows in the micrograph. Sections of the fiber severed in the spinning line, between the coagulation bath guides, show that substantial damage occurred at the fiber's surface as a result of excessive friction of the nascent fiber with the first guide, Figure 3. The alignment of the guides was subsequently corrected to yield defect-free hollow fibers.

Sections of the fiber (Figure 4) severed at the bottom of the coagulation bath, 75 cm below the spinneret, after less than a one second coagulation period, provide insight to the first stages of the phase inversion. Non-uniform rather large closed cells are formed as a result of solvent depletion and phase separation. Most of the PVP (75%) is still in the fiber in the final stage. The result is the delicate uniform structure shown in Figures 1 and 2, where the PVP and the solvent are completely depleted.
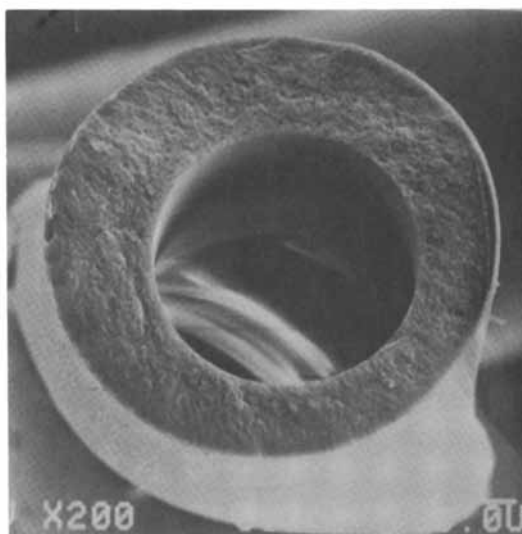
Figure 1:   Asymmetric macrovoid-free polysulfone hollow fiber [The
            fiber was spun with bore off-center to detect irregulari-
            ties in the substructure (5)].
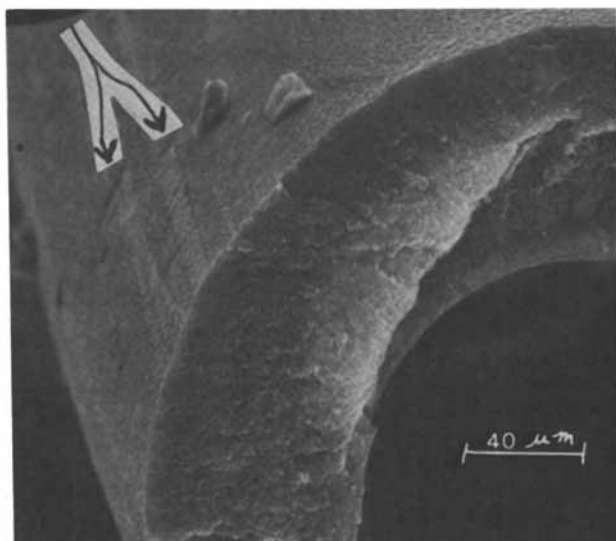
Figure 2:   Cross-section of asymmetric polysulfone hollow fiber.
            Two parallel "trails" stretched along the fiber skin are
            the result of damage in the surface substructure (see
            Figure 3).
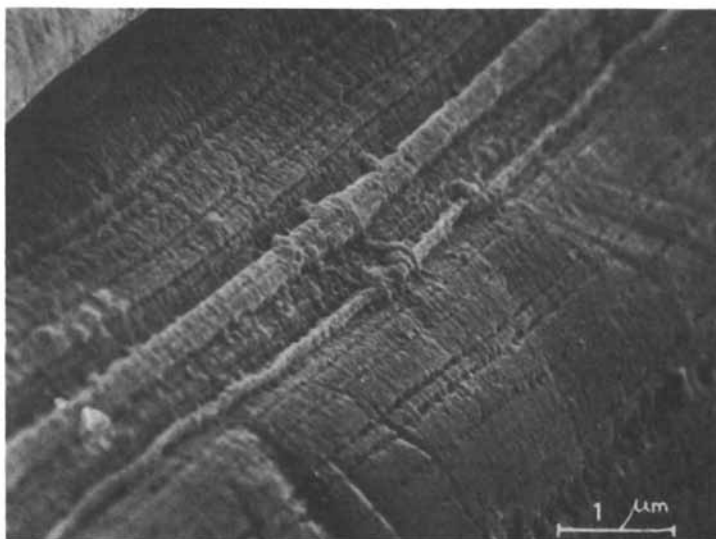
Figure 3:   Surface view of the fiber severed after the run through a
            guide in the coagulation bath. The apparent damage is a
            result of excessive friction of the nascent fiber with
            the guide, (and is shown in Figure 2 as two stipes on the
            fiber surface).
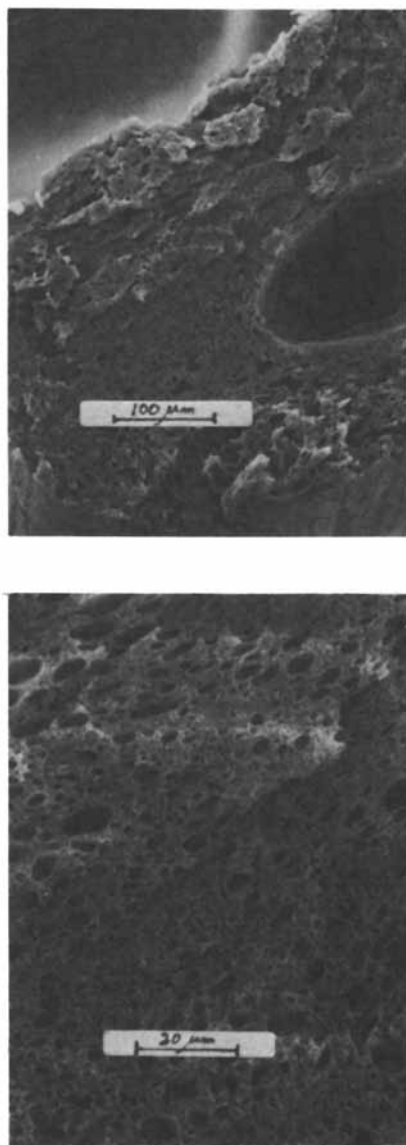
Figure 4: Cross-section of nascent fiber after 1 second coagulation period. (The fiber was severed 15 cm under the spinneret in the coagulation bath).

Double-Layered Membranes for Gas Separation

The introduction of the Prism separator by the Monsanto Company has
been a major breakthrough regarding the practicality of membrane
technology for gas separation processes. The Prism separator em-
ployees an asymmetric hollow fiber membrane whose skin is the
separating entity (same as in asymmetric membranes for reverse
osmosis). To eliminate the possibility of gas feed mixture flow
through the skin's imperfections (in this regard gas separation
processes are much more vulnerable than liquid separations) the
Prism membranes are coated with ultrathin layers of rubbery polymers
which plug all imperfections. This ultrathin coating is prepared
from a highly permeable polymer such as silicone rubber.
     The concept of the Prism membranes is similar to that of
reverse osmosis asymmetric membranes and differs substantially from
the principles that led to the successful development of thin layer
composite membranes for reverse osmosis. In the latter, a thin
layer consisting of two principal zones (6) is deposited on a highly
porous substrate. The first zone is the separating layer which
faces the feed liquid. The second zone is a gutter-layer (inter-
mediate layer) which channels the permeate into the substrate pores;
thus making use of the entire surface area of the membrane (without
the gutter zone the practical surface area will approach the cumula-
tive value of the substrate's pores surface area, which commonly
ranges between 1% and 14% of the total membrane area). The princi-
pal advantages of the thin film composite are as follows: 1) There
is no need to spin or cast a complex, defect-free asymmetric struc-
ture from the polymer which displays the desired separation charac-
teristics. In fact, many polymers cannot be cast and spun to yield
this structure. 2) Numerous "exotic" and expensive polymers can be
feasibly employed as an ultrathin separating layer, because the
quantity of polymer that is required in the deposition of such a
layer (~ 1 μ m) is marginal when compared to that of the porous
supporting material. For the latter, in most instances, poly-
sulfone, polypropylene, or glass porous supports (100 to 200 μ m
thickness) can be adequately employed.
     Unlike the thin film composite membranes that have been
successfully employed in reverse osmosis (for example, NS-100 and
PA-300) and which are composed of polysulfone porous supports coated
with thin film polyamide layers (6), the double-layer composite
membranes, that have been constructed in our laboratories (see
Figure 5), consist of two different polymers deposited on a highly
porous glassy polymer (for example, polysulfone). The top layer is
the separating entity, usually a glassy polymer, such as poly (2,6
dimethyl-1,4-phenylene oxide), PPO, while the second layer is a
highly permeable rubbery polymer, such as poly(dimethyl siloxane),
which serves as a "sink" and a gutter entity for the permeate which
is channelled to surface pores of the support. As shown in Figure
5, the double layer can be as thin as 1 μ m and the separating layer
can be easily deposited to display a thickness of 0.2 μ m or less.
The membrane performance depends upon the relationship between the
thicknesses of the sublayers, the porosity of the substrate and the
fraction of imperfections in the separating layers. Quantitative
correlations among these components will be reported elsewhere (1).
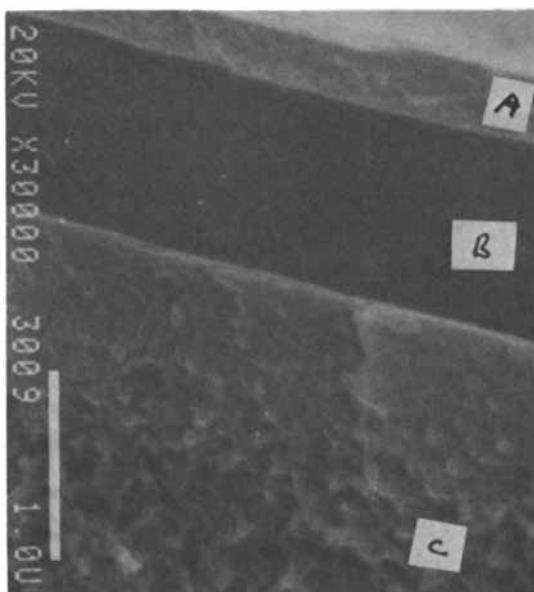
Figure 5: Cross-section of double-layered composite membrane: the top layer, A, is a dense poly(1,6-dimethyl-1,4-phenylene oxide), the intermediate layer, B, is made of poly(dimethyl siloxane) and the support, C, is a porous 150 m polysulfone support. The membrane displays a separation factor of 4.1 toward an O_2/N_2 air mixture and overall oxygen permeability of 65 x 10^{-10} cm^3 versus $cm/cm^2 \cdot$ seconds $\cdot$ cm Hg.

Nevertheless, it is apparent that minor damage to the separating
layers will not cause a total collapse of the membrane performance.
Severe damage to the separating layer (> 2% surface defects) will
reduce the separation ability of the membrane to that of the inter-
mediate layer. Therefore we have further modified this layer (1) to
yield better separation and to increase it's inertness. As such, if
the top layer is damaged, the intermediate layer can be recoated and
the membrane's initial performance restored, even in the module.
The separation of oxygen and nitrogen is displayed in Figure 6. The
curves show the enrichment of oxygen plotted versus applied operat-
ing pressure for three composite membranes made of: poly(dimethyl
siloxane), PDMS, modified PDMS (1) and a double-layer thin film
composite membrane composed of PPO coated on the modified PDMS
layer. The membrane's permeability to oxygen is close to (actually,
slightly higher than) that of a dense, isotropic PPO membrane, thus
indicating that the entire surface area of the membrane is utilized,
despite the fact that the effective surface area of the porous
polysulfone support in this instance is not more than 20%.

X-Ray Diffraction Studies on Reverse Osmosis Hollow Fiber Membranes

Some of the best polymer materials for use as reverse osmosis mem-
branes are semi-crystalline polymers; that is, materials that con-
sist of amorphous and crystalline regions. The nonpermeable
crystalline domains are thermodynamically the more stable of the two
regions. Therefore, the permeability of polymer membranes depends
upon the volume fraction of the amorphous regions. However, poly-
mers that easily crystallize display an inherent disadvantage; that
is, even if the membrane processing method minimizes the crystalline
fraction, the membrane's amorphous regions will still have a
tendency to crystallize in the solid state over a long period of
time. This time period will be shortened if enhancement of polymer
chain mobility prevails as a result of operating conditions, such as
plasticization by the permeate combined with exposure to stress.
The possibility of stress-induced crystallization in semicrystalline
hollow fiber membranes should be a major concern. Most melt and wet
spun hollow fibers develop longitudinal orientation associated with
the extensive draw of the nascent fiber during the spinning process.
The fast coagulation of the spun fiber does not permit establishment
of thermodynamic equilibrium of the "frozen" fiber matrix. Relaxa-
tion can perhaps be achieved by annealing the membrane at tempera-
tures near T_g. Annealing above this temperature often leads to
rapid crystallization, thus defeating the purpose of obtaining high
flux membranes via reduced crystallization. Such is the case for
example with cellulose triacetate, CTA. Hollow fibers of this
polymer are melt spun with certain additives which reduce the
spinning temperature far below the melting point range of pure CTA
(292 to 314°C) (3). The hot spun thread emerging from the spinneret
is quenched in a water bath or is allowed to cool quickly below T_g.
Thus, the polymer, which in slow precipitation from solution yields
~90% crystallinity, if spun as described would yield down to ~10%
crystalline domain only. Of course, this led to the development of
effective CTA hollow fiber membrane permeators, such as Dow Chemi-
cal's DOWEX RO-20K. However, some severe fouling problems (that is,
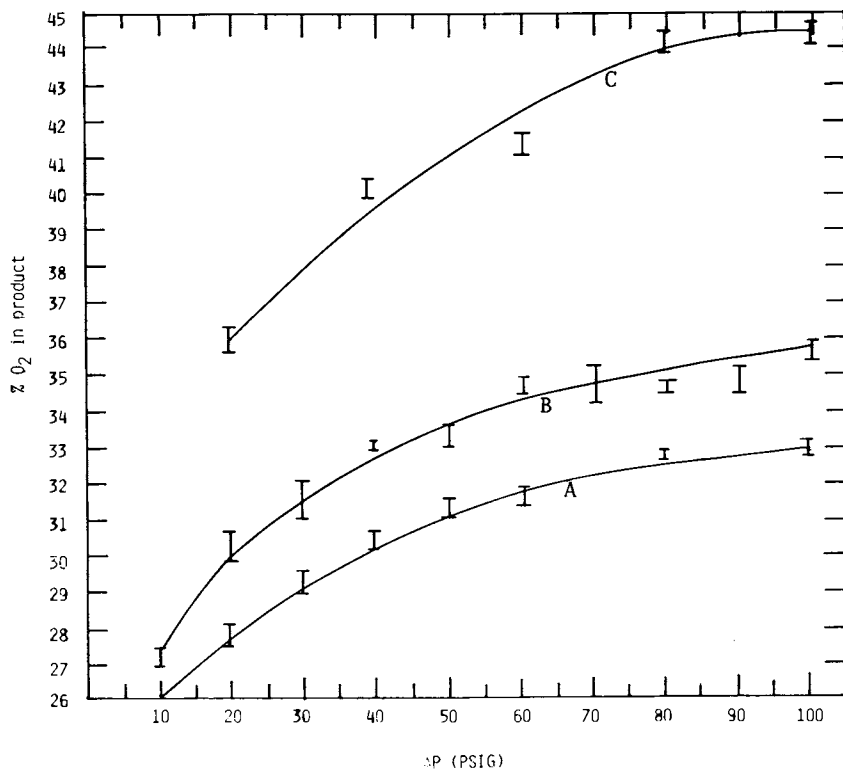
Figure 6: Oxygen enrichment curves versus pressure. (Feed mixture: air at 23°C). Composite membranes: A. PDMS B. Modified PDMS C. Double-layered PPO and PDMS modified.

decline in productivity) of the CTA hollow fiber membrane drew our
attention to the durability problems of semicrystalline hollow
fibers, especially to those made of cellulose esters. The fibers in
the permeators are exposed to stress, pressure and permeate plas-
ticization and they are indeed targeted for fouling problems as a
result of stress-induced crystallization. Some examples of an ex-
tensive program that deals with the identification, via X-ray dif-
fraction analysis, of progressive crystallization of hollow fibers
are discussed below.

X-Ray Diffraction Analysis. Three materials were examined by X-ray
diffraction techniques for crystallinity: a melt-spun CTA hollow
fiber for sea water desalination by reverse osmosis, a dry-jet wet-
spun cellulose acetate hollow fiber, and an ethyl cellulose hollow
fiber (spun in our laboratory). The fibers were inspected before
and after exposure to different degrees of longitudinal stress. All
X-ray data was collected on bundles of fibers. Bundles were placed
in 1.0 mm I.D. X-ray grade thin glass capillaries or mounted dry on
punch card holes for irradiation. For samples to be examined in
liquid media, the capillaries were sealed with 5-minute cure epoxy.
All samples were irradiated with Cu K radiation (1.542 A wavelength)
from a Norelco 1 KV generator. Diffraction patterns were collected
on flat packs of Ilford type G industrial X-ray film or Kodak DEF-5
X-ray film in an evacuated pinhole camera. To keep relative inten-
sities of diffraction spots approximately equal, exposures were 24
to 25 hours for unstressed and lightly stressed samples, and 12 to
14 hours for highly stressed samples.
        Samples examined were: 1) Cellulose triacetate hollow fibers,
CTAHF, as spun, in distilled water; 2) CTAHF stretched for eight
days in water with a 3.57 gram weight (22 psi stress), in distilled
water; 3) CTAHF air dried for two weeks, in an unsealed capillary;
4) CTAHF stretched for two weeks in water with a 15.77 gram weight
(100 psi stress) in distilled water.

Results and Discussion. Since the melt spinning of the fibers
approximate (with some qualifications) a solution process, it is
assumed that any observed crystallinity will be in the regions of
CTA II lattice. The CTA II crystalline lattice possesses an anti-
parallel packing of polymer chains due to the chain fold mechanism
of crystal growth from solution (7). For comparison purposes Figure
7 shows the diffraction pattern from a small bundle of CTA II
fibers. In this measurement, the camera film to sample distance for
the CTA II was roughly the same as for the cellulose triacetate
hollow fiber CTAHF. These d-spacings, which were calculated but are
not reported here, compare well to those from a calibrated sample
(7). Figure 8 shows the diffraction pattern for the as-spun and
water-stored CTAHF. The two concentric rings indicate that some
crystallinity is present in the sample, but no orientation with
respect to the fiber macrostructure is seen. The d-spacings of the
rings correlate well with the d-spacing of the strongest CTA II
reflections. The only problem in the comparison occurs at the inner
edge of the inner-most ring (highest d-spacing) where a substantial
amount of amorphous scattering obscures the exact edge of the ring.
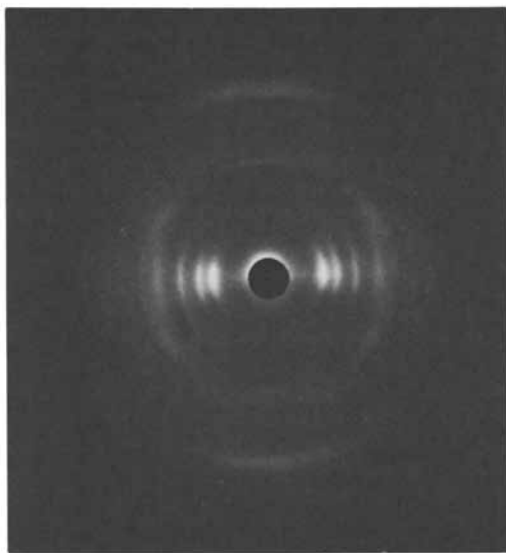
Figure 7: Diffraction pattern of CTA II fiber bundle.
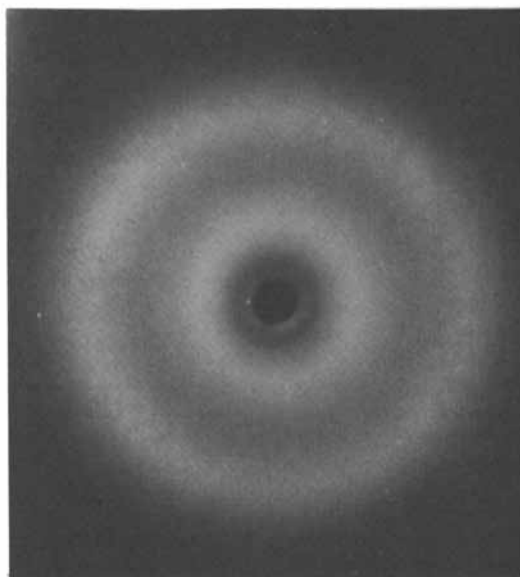
Figure 8: Diffractogram of as-spun and water-stored CTA hollow fiber (for reverse osmosis).

The diffraction pattern of the lightly stretched in water (22 psi for 8 days) CTAHF is shown in Figure 9. From the generally weaker intensity and specifically from the weaker and narrowed inner ring, it can be deduced that the crystallinity is less in this sample than in the original (Figure 8). The relatively unaffected outer ring is probably due to the meridional reflection (in comparison, the CTA II data indicates a long spacing along the chain axis). The observed reduction of crystallinity is contrary to the expected chain and crystallite orientation with respect to the fiber axis, which normally results from fiber stretching.

Figure 10 shows the dry diffraction pattern of the CTAHF. The sample was air dried at ambient temperature with no applied stress. Discrete reflections appear along the equatorial line underneath the general ring pattern. The appearance of discrete reflections is expected, as the removal of water from the matrix would allow the polymer chains to collapse into more ordered regions. Most notably, there appears to be better orientation of crystallites with the fiber axis in comparison to the original sample.

The diffraction pattern of the highly stretched in water CTAHF is shown in Figure 11 (calculated fiber stress on this sample is 100 psi). From the increased intensity of both rings it appears that the overall crystallinity is higher, but there still does not seem to have been much orientation of the crystallites in the fiber direction. The relative intensity of the two rings is the same as occurs in the original sample, with the inner ring much stronger than the outer, rather than as in the lightly stretched sample where the inner ring is diffused. An interesting feature about this diffractogram is a broad link-sausage-like intensity pattern around the outer diffracted ring. This regular pattern indicates the presence of some order in the sample. Closer inspection of Figures 9 and 11 reveal the sausage-like pattern is also present in the outer rings of the plain water stretched sample and the original sample patterns, but is less distinct. The fibers shown in Figures 9 and 11 do exhibit, upon drying, orientation which is similar to that shown in Figure 10, but with much higher intensity.

In addition to the CTA hollow fibers, diffraction patterns from dry-jet wet-spun cellulose acetate and ethyl cellulose fibers were also collected. The diffraction measurement was conducted with bundles of two fibers in the case of cellulose acetate (CA) and a single fiber for ethyl cellulose (EC), because of the large fiber size and wall thickness. The diffraction measurement for these two samples was conducted on dry fibers. Figure 12 shows the diffraction pattern from the CA sample. Though this pattern also exhibits two concentric rings as with the CTAHF, only the inner rings have the same d-spacing. With this sample the second ring d-spacing corresponds to the weaker equatorial and second layer reflections of CTA II; the strong third layer meridional reflection is gone. It appears as if crystallinity in this sample is only slightly less than in the CTAHF sample, but most notably crystallite orientation with the fiber axis is considerably less. Figure 13 shows the EC diffraction pattern. Here we see three diffraction rings, which are much sharper and accompanied by less amorphous scattering than in the other hollow fibers. This suggests that crystallinity is much higher in this sample, perhaps as much as 40%,

Figure 9: Diffractogram of CTAHF shown in Figure 8 after exposure to 22 psi stress for 8 days.

Figure 10: The diffraction pattern of CTAHF, shown in Figure 8, after drying (without stress). Orientation in the fiber is clearly seen.
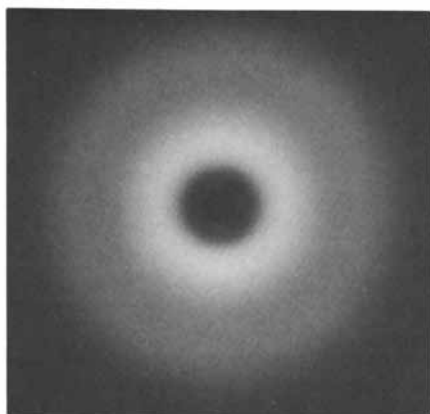
Figure 11: Diffractogram of the fiber shown in Figure 8 after ex-
posure to 100 psi stress for a period of two weeks.
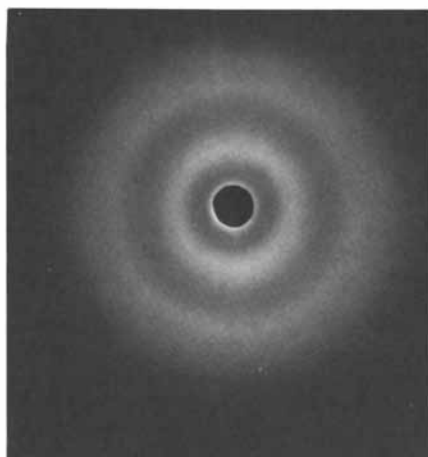
Figure 12: Diffractogram of dried cellulose acetate hollow fiber
membrane.

but again the continuous rings indicate little, if any, crystallite
orientation along the fiber axis.

Interim Conclusions. The X-ray study on the CTA hollow fibers was
undertaken to see if gross morphological changes prevail under
working conditions that include stress and considerable pressure.
The diffraction patterns of wet CTAHF demonstrate that morphological
changes in the polymer and its water clusters do exist. The col-
lapse of the microstructure of the melt-spun hollow fiber upon
drying follows a "memory pattern" and orientation is displayed. It
is most surprising that the dry-jet wet-spun fiber do not store any
recollection of the spinning orientation (draw) which is substan-
tially high (these fibers were spun with a draw ration of 7:1).

Separation of Aqueous Alcohol Solutions Through Ion-Exchange Hollow Fiber Membranes

The separation of organic liquid mixtures through ion-exchange mem-
branes was recently reported from our laboratories (8). It was
shown that the nature of the counter-ion in such membranes affects
substantially the membrane permeability and selectivity. Thus, new
concepts for the separation of organic liquid mixtures have been
conceived, the principal of which is that for each ion-exchange
membrane a myriad of variations can be easily formed, just by ex-
changing and replacing the counter-ion when needed. The interaction
of the counter-ion with the permeate determines, to a large extent,
the membrane's transport properties. This concept has been demon-
strated in our laboratories as an effective tool for the separation
of alcohols from their aqueous solutions. Some results of this on-
going study are delineated below.

Experimental. The hollow fiber membranes used for this study were
Nafion 811, which is a copolymer of polysulfonyl fluoride vinyl
ether and polytetrafluoroethylene, and sulfonated and/or quaternated
derivatives of polyethylene (kindly supplied by Dr. E. Korngold from
Ben Gurion University in Israel). The aqueous alcohol solutions
studied thus far are those of methanol, ethanol and 2-propanol. The
separations were accomplished via the pervaporation process as
described in Reference 9. Counter ions were replaced in the hollow
fiber by soaking the permeator for twenty four hours in 1 molar
solutions of the pertinent ions. For example, experiments were
conducted with Na^+ as a counter ion. When this set of experiments
was finished, the sodium was exchanged by Li^+ etc. Each data point
shown in Figure 14 consists of 6 to 10 measurements taken over a
time period of 8 hours. Re-runs with the various counter ions
proved that the intrinsic properties of the membrane remain un-
changed and the permeability measurements are reproducible.

Results and Discussion. Figure 14 demonstrates the principal of
separation through ion-exchange membranes, where the counter-
ion/permeate interactions determine the mass transport properties of
the system. In this set of experiments, the feed mixture was an
azeotropic composition of 2-propanol and water (88.5/11.5 wt.%). A
Nafion hollow fiber permeator was used in pervaporation mode. The
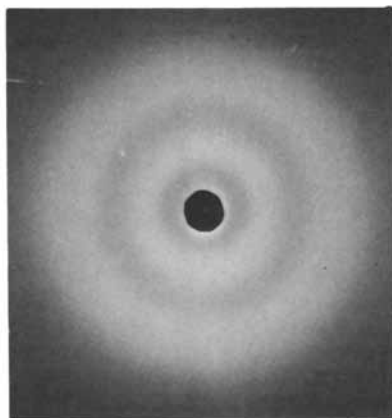
Figure 13: Diffractogram of dried ethyl cellulose hollow fiber mem-
          brane.
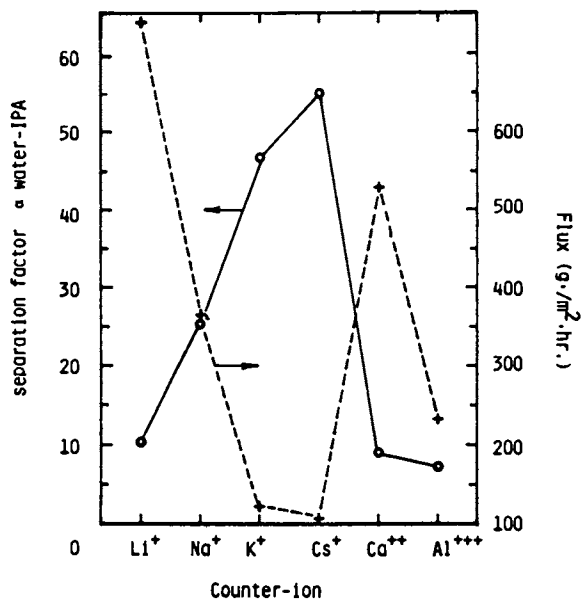
Figure 14: The effect of counter-ion on flux and separation factor
          of a Nafion hollow fiber.
          Feed composition: 2-propanol/water = 88.5/11.5
          Feed temperature: 19°C

permeator was charged with different counter ions, resulting in substantial differences in the mass transport properties of the unit. The mono-valent ion series follows the expected trend; that is, the higher the hydration number of the ion, the higher the flux. The hydrated Li^+ ion swells the fiber much more than the Cs^+ ion (Figure 15), which exhibits a rather weak association with the water shell around it. The fact that the 2-propanol hydration power is much lower than the water molecule also contributes to the rather high selectivity; that is, the membrane is not swollen enough to allow the 2-propanol "to slip by" the ionic conducting channels, and the hydration power of this alcohol is too small to compete with the water for interactions with large cesium or even potassium ions. Thus, the rates at which the separation factor increases and permeation decreases with the change in counters ions are large indeed. As for the multi-valent ions, the Ca^{2+} is a strongly hydrated ion, but it also cross-links the conducting channels and even more so is the Al^{3+}. Thus, a substantial decrease in the flux, without significant change in the separation factor, is shown for the series Li^+, Ca^{2+}, Al^{3+}. These patterns, shown in Figure 14 for the azeotropic composition, remain the same if the feed composition is reversed, as shown in Table I (for 5.2 wt.% in the feed mixture).

Table I. The Effect of Different Counter Ions on Separation Factor
and Flux of Nafion 811 Hollow Fiber (Feed[*] Composition:
Water/Isopropyl Alcohol: 12/88 wt.%)

No.	Counter Ion	Permeate Composition Water	IPA	Separation Factor	Flux $(g /m^2 hr)$	$(ml /m^2 hr)$
1	Li^+	57.4	42.6	10.2	742	816.4
2	Na^+	76.6	23.4	25.1	364	383.9
3	K^+	86.2	13.8	46.7	124	128.0
4	Cs^+	87.5	12.5	54.9	107	110.3
5	Ca^{++}	56.0	44.0	9.3	531	586.9
6	Al^{+++}	50.0	50.0	7.3	232	260.4

[*] Feed temperature: 29.0°C

Separation Factor $= (X_W/X_I)^P/(X_W/X_I)^F$

where X indicates weight fraction, subscripts I and W represent isopropanol and water and superscripts P and F represent permeate and feed.
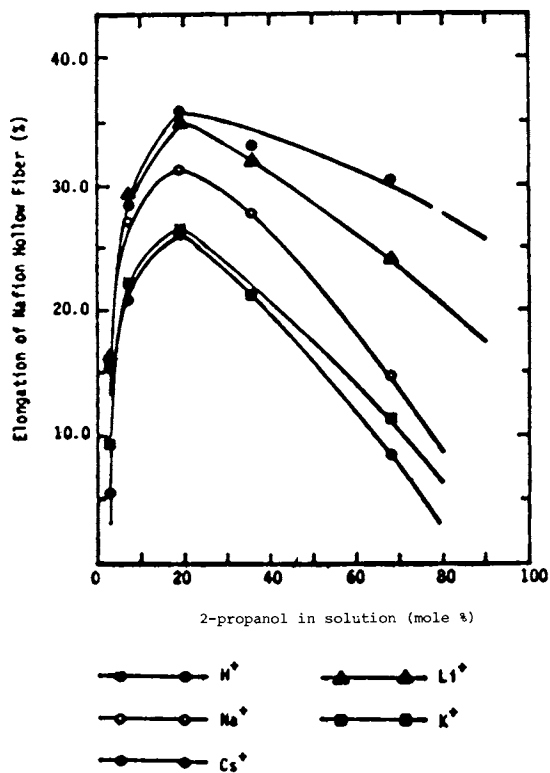
Figure 15: The elongation of a Nafion hollow fiber with different
counter ions versus 2-propanol concentration (in its
aqueous solution).

The swelling of the fiber in it's different counter-ion varia-
tions is in accord with the mass transport data. The maxima around
20 mole % 2-propanol in the feed mixture indicates the presence of
synergism related to hydrophilic/hydrophobic contributions. The
later results from the isopropyl sites of the alcohol and suggests
solubility of the 2-propanol in the amorphous non-ionic regions of
the membrane.

The various modifications of the polyethylene ion-exchange
hollow fiber membranes also proved that here we have a workable
concept. From this family of special interest membranes, results
were obtained for anion-exchange hollow fiber membranes. Separation
factors of 83, 18 and 3.5 were obtained for feed mixtures of 2-
propanol, ethanol and methanol, respectively (each feed mixture was
composed of 20 wt.% alcohol and the separation was conducted at
23°C).

Interim Conclusion. The use of ion-exchange membranes for the
separation of aqueous organic mixtures is a novel solution for many
difficult separations. It provides a vast number of possibilities
based on rather few membrane matrices. Quantitative analysis of
this transport phenomenon is to be discussed elsewhere (9).

Literature Cited

1. Lundy, K. "Separation of Gas Mixtures via Multi-Layered Com-
   posite Membrane" MS Thesis, Chem. Dept., State Univ. of N.Y.
   ESF Syracuse, N.Y. (1984).
2. Gardiner, E. "Cellulose Ester Blends, Ultrathin Deposits and
   Membranes" part of Ph.D. Thesis, Chem. Dept., State Univ. of
   N.Y. ESF Syracuse (1984).
3. Cabasso, I. "Hollow Fiber Membranes" In Kirk-Othmer Encycl. of
   Chem. Tech.; Grayson, M. and Eckroth, D., Eds.; John Wiley &
   Sons, Inc.: New York, 1980, 12, 492.
4. Cabasso, I.; Klein, E.; Smith, J.K. J. Appl. Polym. Sci.,
   1976, 20, 2377.
5. Ibid 1977, 21, 165.
6. Cabasso, I. In "Synthetic Membranes, Volume I," Turbak, A. F.,
   Ed.; ACS Symposium Series No. 153, 1981.
7. Roche, E.; Chanzy, H.; Boudelle, H.; Marchessault, R. M.;
   Sundararajan, P. Macromolecules, 1978, 11, 86.
8. Cabasso, I. Ind. Eng. Chem. Prod. Res. Dev. 1983, 22, 313.
9. Cabasso, I.; Liu, Z.; Korngold, E., to be published.

New Characterization Methods for Asymmetric Ultrafiltration Membranes

C. A. SMOLDERS and E. VUGTEVEEN

Twente University of Technology, Department of Chemical Technology, P.O. Box 217, 7500 AE Enschede, The Netherlands

Three new methods to characterize the pore structure and pore size distribution in the top layer of asymmetric membranes have been developed or refined in our laboratory during the past few years: *a)* the gas adsorption/desorption method, *b)* thermoporometry and *c)* selective permeation (fractional rejection).
Pore size distributions are determined from the hysteresis loop in gas adsorption/desorption isotherms and from calorimetric measurements by the shift in the melting (or freezing) peak for a phase transition of water inside the pores. The determination of the fractional rejection properties is done by permeation experiments of a macromolecular solute with a broad molecular weight distribution (MWD). The MWD of permeate and feed are compared and translated into a fractional rejection curve. The comparison of results obtained from these three independent methods for some characteristic membranes gives an indication of the strength and weakness of each of the methods studied.

The use of ultrafiltration (UF) membranes for the separation of dissolved molecules of different size and nature has seen an increased interest in recent years. Depending on their pore size, membranes can be used in a variety of fields, such as removal of particulates from air, filtration of colloidal suspensions, treatment of product streams in the food and beverage industry, recovery of useful material from coating or dyeing baths in the automobile and textile industries and treatment of industrial waste waters (1,2). UF membranes also serve as supports for ultrathin reverse osmosis (composite) membranes.
      Asymmetric ultrafiltration membranes consist of a thin, dense top layer (the skin), which is responsible for the selective rejection of solute molecules, and a more open, porous substructure that does not affect the membrane performance negatively.
      The most important characteristics of these membranes are the

thickness of the top layer (hydrodynamic resistance) and the pore structure (mean pore size and pore size distribution) of the skin. In order to develop and subsequently use the most appropriate membrane for a certain application, one has to determine the features just mentioned above, using independent characterization methods. Amongst these are:
- pure water flux and/or gas permeability (3,4);
- the critical air pressure (the bubble pressure) method (5);
- electron microscopy (3,6-8);
- molecular weight cut-off measurements.

However, only a few methods can be used to characterize the pores in the skin of the membrane. Although none of the techniques mentioned can give a complete description of the skin structure, a reasonable impression can be obtained by a combination of techniques.

In our laboratory three new methods have been developed or refined during the past few years and will be described below. These methods are:
a)   the gas adsorption/desorption method (9);
b)   thermoporometry (10);
c)   selective permeation (fractional rejection) (11).

The gas adsorption/desorption. The determination of pore size and pore size distribution from gas adsorption/desorption isotherms is known from other types of adsorbents: a hysteresis loop occurs between the adsorption and desorption curves when a full isotherm is measured. This has been explained as being due to capillary condensation in the pores of the adsorbent. As the pressure is reduced, the adsorbate does not evaporate as readily from the capillaries as it does from a flat surface due to a lowering of the vapour pressure over the concave meniscus formed by the condensed vapour in the pores. The lowering of the vapour pressure (p) for a cylindrical capillary of radius r_k is given by the Kelvin equation:

$$RT \ln \frac{p}{p_o} = \frac{-2\gamma V_L}{r_k} \cos \Theta \qquad (1)$$

Here p_o is the saturated vapour pressure of the system at temperature $T[K]$, γ and V_L are the surface tension and the molar volume of the adsorbate in liquid form, R is the molar gas constant and Θ the angle of contact between the liquid and the walls of the pore. For nitrogen adsorption/desorption at liquid nitrogen temperature (77 K) it leads to:

$$r_k = \frac{-4.1}{10^{\log(p/p_o)}} \qquad (2)$$

The pore radius (r_p) can be calculated by

$$r_p = r_k + t \qquad (3)$$

in which t is the thickness of the adsorbed layer of vapour in the pores. All experiments were carried out with a Carlo Erba Sorptomatic, model 1800. The method of Barrett, Joyner and Halenda (12) which was

refined in 1964 by Dollimore and Heal (13) was used to calculate the pore sizes from the isotherms. A complete description of the method will be given by Bodzek *et al.* (9).

The method has already been employed for polymeric membranes by several authors (14-16). Although there are some limitations for using this technique, for example, cylindrical pores are assumed and the membranes have to be dried without damaging the pore structure before the measurements can start, results were obtained for UF membranes made from different polymeric materials (Cellulose Acetate (CA), Poly-2,6-dimethyl-1,4-Phenylene Oxide (PPO) and some other non cellulosic materials).

Excellent results have been obtained for PPO membranes. In Figure 1 complete adsorption/desorption isotherms are given for PPO membranes, made from casting solutions containing 9% and 10% polymer (by weight). From the hysteresis loop the cumulative pore volume and the pore size distribution are calculated, and these are shown in Figure 2. From the differential pore volume versus pore radius graph it can be seen that pores with about 2 nm radius are present in both membranes. Furthermore, increasing the polymer concentration in the casting solution leads to higher pore volume. The abrupt change in the desorption branch of PPO membranes (Figure 1) indicates a narrow pore size distribution in contrast to the desorption isotherms of CA, Polysulfone (PSf) and Polyacrylonitrile (PAN) membranes, which will be shown in one of our future papers (9). There we will discuss our experimental results in more detail.

Thermoporometry. This method is based on the observation that the equilibrium conditions of solid, liquid and gaseous phases of a highly dispersed pure substance are determined by the curvature of the interface(s) (10,17). In the case of a liquid (in this work, pure water) contained in a porous material (the membrane), the solid-liquid interface curvature depends closely on the size of the pores. The solidification temperature therefore is different in each pore of the material. The solidification thermogram can be 'translated' into a pore size distribution of the membrane with the help of the equations derived by Brun (17). For cylindrical pores, with water inside the pores, it leads to the following equations:

$$\text{during solidification: } r_{p,s} = \frac{-64.67}{\Delta T} + 0.57 \tag{4}$$

$$\text{and during melting} : r_{p,m} = \frac{-32.33}{\Delta T} + 0.68 \tag{5}$$

In these equations r_p is the pore radius [nm] and ΔT is the extent of undercooling [K].

All the calorimetric experiments were performed by cooling the samples with maximal speed (320 K/min) to 210 K and subsequently heating (after equilibrium was reached). So Equation 5 was used for calculating the pore radii. A Perkin Elmer differential scanning calorimeter, model DSC II, was used. With this apparatus, pore radii from 2 to 20 nm can be determined. About 50 mg of membrane material (including water) was used for each experiment and a heating rate of 1.25 K/min gave reproducible results.

After a thermogram was obtained, it was analyzed with the help
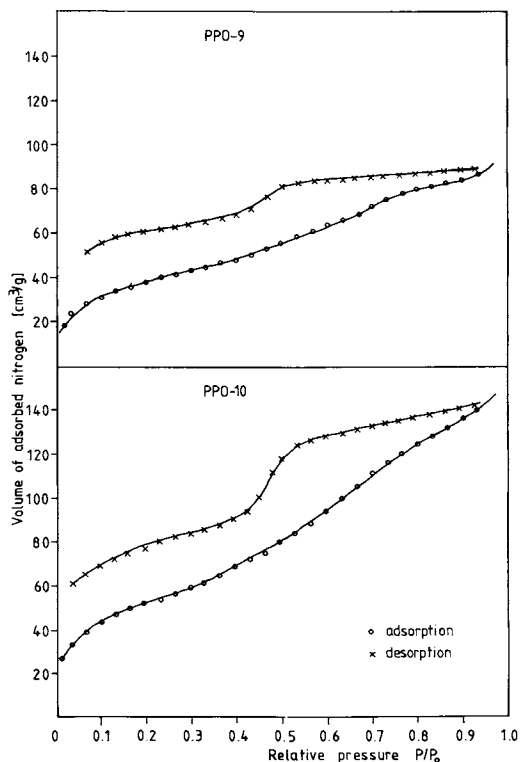
Figure 1.   Nitrogen adsorption and desorption isotherms for poly-
            phenylene oxide (PPO) membranes.   (PPO-9 and PPO-10
            indicate the polymer concentration (wt. %) in the cast-
            ing solution).
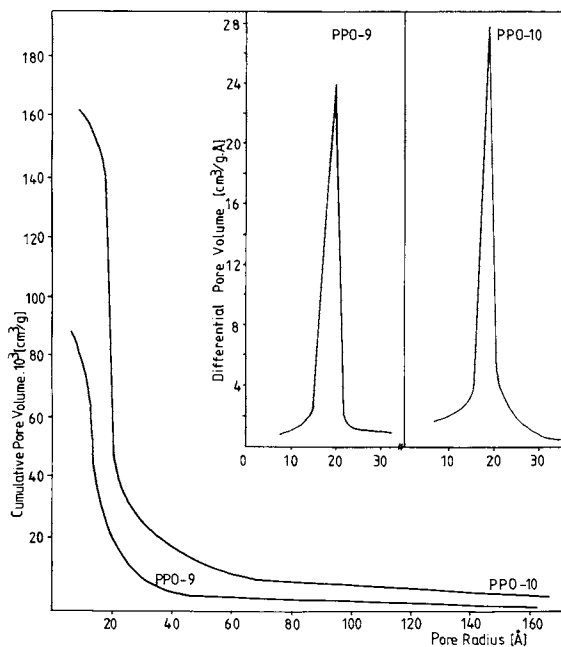
Figure 2. Cumulative pore volume and pore size distribution for PPO membranes, calculated from gas adsorption/desorption isotherms.

of a computer program in order to obtain the cumulative pore volume
vs. pore radius in integral or in differential form. More detailed in-
formation will be given in the near future by Vugteveen *et al.* (10).
    Several membrane materials were analysed (for example PPO and
PSf). In Figure 3 the cumulative pore volume (V_{cum}) and pore size
distribution (dV/dr_p) are given for some PPO membranes (casting solu-
tion 10% polymer by weight). In this figure the values 0.15 and 0.20
refer to the casting thickness (mm). The dependency of the pore volume
on the casting thickness is obvious. Assuming all the measured pores
are in the skin layer and assuming the porosity (ε) being constant, an
increase in pore volume means that the skin becomes thicker. Similar
results were found by Broens *et al.* (16) by means of the gas adsorp-
tion/desorption method. Furthermore, one can see from this figure that
the shape of the differential pore size distribution (dV/dr_p) does not
change significantly: most pores were between 1.5 and 4 nm in size,
and the mean pore radius remains practically constant. Therefore, we
may conclude that PPO membranes have a narrow pore size distribution.
    Experiments with UF membranes made of polysulfone (P3500, Union
Carbide) leads to a quite different thermogram as shown in Figure 4.
In this figure two thermograms are given, one for PSf and one for PPO.
The thermogram of the PSf membrane does not return to the baseline.
Hence no distinction can be made between the pores in the skind and
pores in the supporting layer. It is assumed that pores below the skin
of PSf membranes gradually increase in size and are cone-shaped.

Selective permeation. In order to come to a more precise characteriza-
tion of the rejection properties of an UF membrane we developed a meth-
od (11) in which the molecular weight distribution (MWD) of macromole-
cules present in the permeate is compared tp the one present in the
feed. For these experiments a macromolecular solute is used with a
broad MWD; For example Polyethylene Glycol (PEG) 100 000 or mixtures
of various PEGs. Comparing the MWD of the feed with the MWD of the
permeate, the fractional rejection (R_{M_i}) is defined as follows:

$$R_{M_i} = \frac{w_{M_i,feed} - w_{M_i,permeate}(1-R_{overall})}{w_{M_i,feed}} \qquad (6)$$

in which w_{M_i} is the weight fraction of a certain molecular weight M_i.
Equation 6 can be derived from:

$$R_{M_i} = \frac{C_{M_i,f} - C_{M_i,p}}{C_{M_i,f}} \qquad (7)$$

in combination with $C_{M_i} = C.w_{M_i}$ and $R_{overall} = 1 - \frac{C_p}{C_f}$, where C_{M_i} is the

concentration of macromolecules with molecular weight M_i, and C is the
total initial concentration of the macromolecular solute.
    The samples of permeate and feed were analysed using the high
performance liquid chromatographic/low-angle laser light scattering
(HPLC/LALLS) method. The columns used were TSK (Toyo Soda) G4000PW and
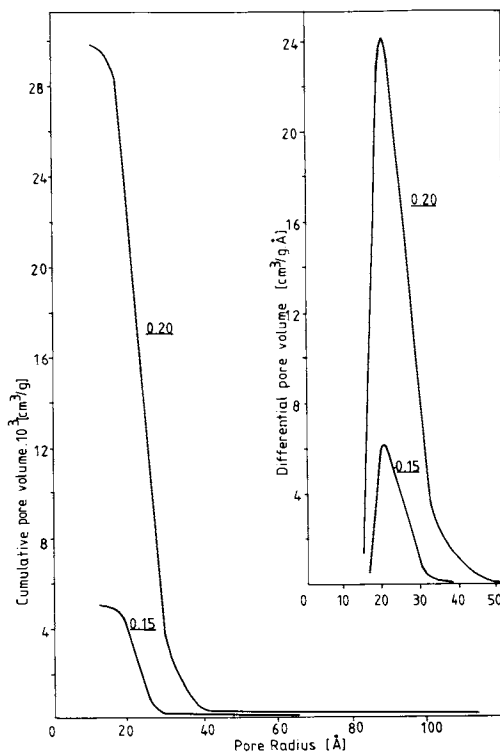
Figure 3.   Cumulative pore volume and pore size distribution for
PPO membranes, calculated from the thermograms.   (The
numbers 0.15 and 0.20 indicate the casting thickness
(nm) during preparation of the membranes).
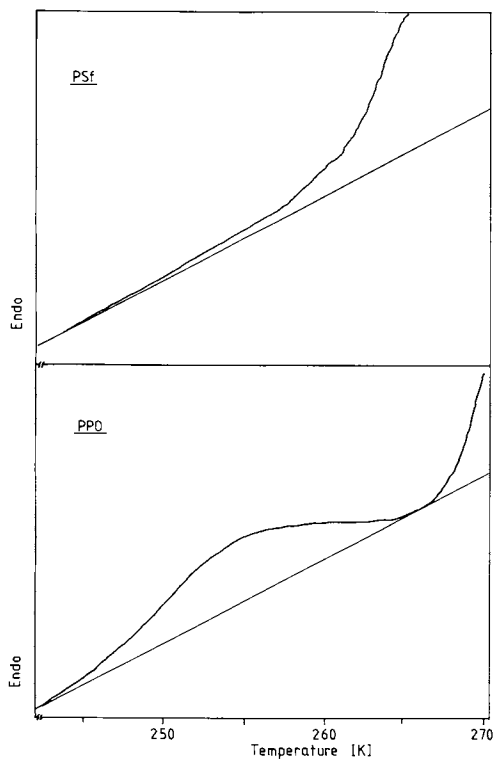
Figure 4.   Thermograms for a polysulfone (PSf) and a PPO membrane.

G3000PW (in series), detection took place with a differencial refractometer (Brice Phoenic, λ = 633 nm) and the LALLS apparatus KMX-6 of Chromatix, according to the method described by McConnell (18).

Most experiments were performed at laboratory temperature using an Amicon low pressure cell model 401S with an effective membrane area of 37.4 cm². An operating pressure of 0.3 MPa was used. The initial feed concentration was 1000 ppm. More details can be found in one of our future papers by Vugteveen *et al.* (11).

A comparison of the fractional rejection ($\overline{R_{M_i}}$) with the 'classical' cut-off curve, which can be seen in the upper part of Figure 5
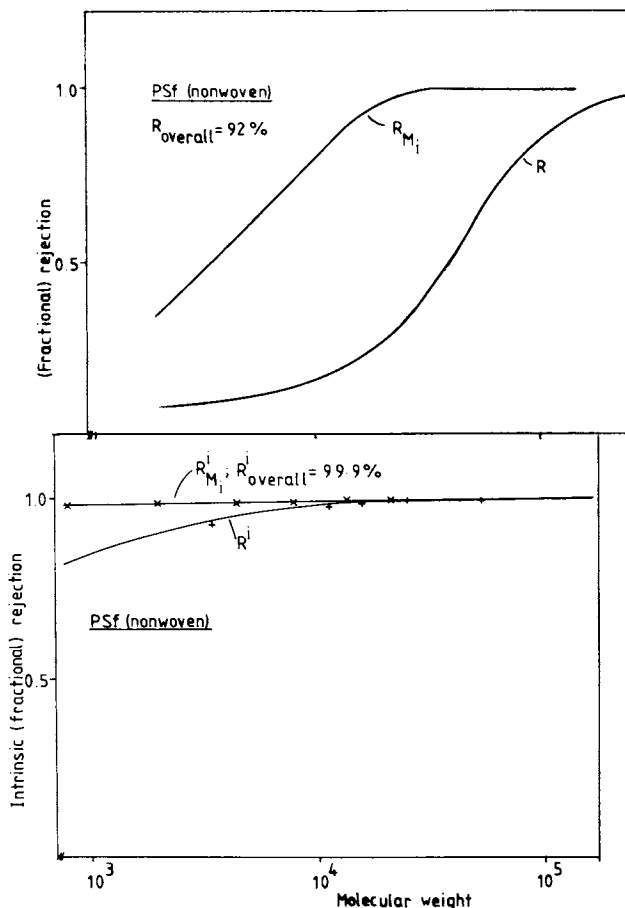
Figure 5. (Intrinsic) fractional rejection (R_{M_i}) and (intrinsic) classical rejection (R) curves for a PSf membrane, using PEG 100 000 as solute.

for a PSf membrane, seems to show that the 'cut-off' value is reached
at lower molecular weight. The magnitude of difference can be ex-
plained by the fact that until now, no correction has been made for
the influence of the concentration polarization phenomenon. Taking
this into account, a quite different curve is obtained (lower part of
Figure 5). However, in this case, the operating conditions lead to a
high concentration polarization at the membrane interface.
    Another point of interest is that the fractional rejection curve,
like the 'classical' cut-off curve, also depends on the type of macro-
molecular solute used as is shown in the upper part of Figure 6. The
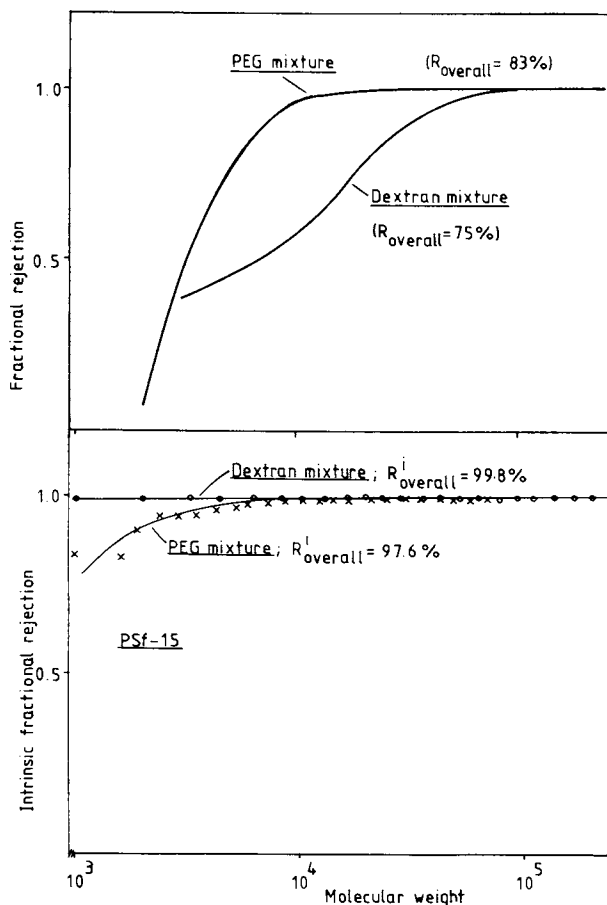
Figure 6. (Intrinsic) fractional rejection curves for a PSf
           membrane based on different kinds of macromolecular
           solutes.

PEG mixture consists of equal parts (by weight) of PEG with the following molecular weights: 3000, 6000, 10 000, 20 000, 40 000 and 100 000 at a total concentration of 0.1%. The dextran solution of equal parts of Dextran T10 and T500 with molecular weight of 10 000 and 500 000 respectively, also at a total concentration of 0.1%. However, also in this case the operating conditions are not well chosen as can be seen in the lower part of Figure 6. In future work (11) we will show experiments in which the influence of concentration polarization is not so overwhelming.

Together, fractional rejection curve (R_{M_i}) and traditional cut off curve will give more information on the rejection characteristics of ultrafiltration membranes.

Acknowledgments

Legend of symbols

C	=	total (initial) concentration of macromolecular solute [g cm^{-3}]
C_{M_i}	=	concentration of macromolecules with molecular weight M_i [g cm^{-3}]
p	=	vapour pressure of the system at temperature T (K)
p_o	=	saturated vapour pressure of the system at temperature T (K)
R	=	gas constant, 8.313 [J mol^1 K^{-1}]
R_{M_i}	=	fractional rejection of a certain molecular weight M_i
$R_{overall}$	=	'overall' rejection of a macromolecular solute
r_k	=	radius of the cylindrical capillary [nm]
r_p	=	pore radius [nm]
T	=	temperature [K]
ΔT	=	extent of undercooling [K]
t	=	thickness of the adsorbed layer of vapour in the pores [nm]
V_L	=	molar volume of the adsorbate [cm^3 mol^{-1}]
w_{M_i}	=	weight fraction of a certain molecular weight M_i
γ	=	surface tension of the adsorbate [dyne cm^{-1}]
Θ	=	angle of contact between the liquid and the walls of the pore [^{o}]

Subscripts

M_i	=	molecular weight (M) fraction i
f	=	feed
p	=	permeate

Literature Cited

1. Michaels, A.S. Chem. Eng. Progr. 1968, 64, 45.
2. Porter, M.C.; Michaels, A.S. Chemical Technology 1971, 1, 56; 1971, 1, 248; 1971, 1, 440; 1971, 1, 663; 1972, 2, 56.
3. Kesting, R.E. In "Synthetic Polymer Membranes", McGraw-Hill Inc., New York, 1971.
4. Yasuda, H.; Tsai, J.T. J. Appl. Polym. Sci. 1974, 18, 805.
5. Jacobs, S. Filtr. Separ. 1972, 9, 525.
6. Riley, R.L.; Gardner, J.O.; Merten, U. Desalination 1966, 1, 30.
7. Riley, R.L.; Gardner, J.O.; Merten, U. Science 1964, 143, 801.
8. Merin, U.; Cheryan, M. J. Appl. Polym. Sci. 1980. 25, 2139.
9. Bodzek, M.; Vugteveen, E.; Heskamp, H.; Noordegraaf, D.; Smolders, C.A. submitted to J. Membrane Sci.
10. Vugteveen, E.; te Hennepe, H.J.C.; Bargeman, D.; Smolders, C.A. submitted to J. Membrane Sci.
11. Vugteveen, E.; Bargeman, D.; Smolders, C.A.; to be submitted to J. Membrane Sci.
12. Barrett, E.P.; Joyner, L.G.; Halenda, P.P. J. Amer. Chem. Soc. 1951, 73, 373.
13. Dallimore, D.; Heal, G.R. J. Appl. Chem. 1964, 14, 109.
14. Ohya, H.; Imura, Y.; Moriyama, T.; Kitaoka, M. J. Appl. Pol. Sci. 1974, 18, 1855.
15. Ohya, H.; Konuma, J.; Negishi, Y. J. Appl. Pol. Sci 1977, 21, 2515.
16. Broens, L.; Bargeman, D.; Smolders, C.A. Proc. 6th Int. Symp. Fresh Water from the Sea 1978, Vol. 3, 165.
17. Brun, M.; Lallemand, A.; Quinson, J.F.; Eyraud, Ch. Thermochimica Acta 1977, 21, 59.
18. McConnell, M.L. American Laboratory 1978, May.

Pore Volume Distribution in Ultrafiltration Membranes

LEOS ZEMAN and GABRIEL TKACIK

Millipore Corporation, Bedford, MA 01730

Three polysulfone asymmetric ultrafiltration membranes having
distinctly different ultrafiltration properties were charac-
terized by high-resolution scanning electron microscopy (SEM),
nitrogen sorption/desorption isotherms as well as by water
permeability and polydisperse solute rejection measurements.
Even for the most retentive membranes, the surface pores were
visualized by SEM. Frequency distribution of pore radii was
approximated adequately by a log-normal distribution function.
Tentative prediction of solute rejections was made from these
results and compared with measured rejection curves for poly-
disperse dextrans. The agreement obtained was satisfactory.
Pore radii calculated from sorption/desorption isotherms by
two different methods were substantially larger than those sug-
gested by SEM of the membrane surfaces. A hypothesis can be
made that the isotherms reflect primarily pore volume distri-
butions in the subsurface (matrix) region of the asymmetric
structures.

Pore structures of typical polymeric ultrafiltration membranes,
produced by so called "phase inversion methods," consist of inter-
connected, irregular, three-dimensional networks of pores, inter-
stices and voids in their skin layers.

An investigator in this area typically has precise information
on composition of casting solutions and other physicochemical
factors affecting membrane formation. Functional measurements of
transport in terms of convective permeability, selectivity or dif-
fusive permeability are usually also available. However, without
proper techniques for quantitative description of membrane pore
structures, and their shape and size distributions, membrane de-
velopment efforts remain largely empirical.

Several attempts to characterize quantitatively pore struc-
tures in ultrafiltration membranes have been described in the
literature. Preusser(1) analyzed surface porosities of Amicon mem-
branes, using a carbon replica technique and a high-resolution
transmission electron microscopy (TEM). A similar approach was

used later by Fane, Fell and Waters(2). The replica approach pro-
vides only indirect visualizations of membrane surfaces. Also, it
is often very difficult to distinguish between real surface features
and artifacts. Until several years ago, the resolution of scanning
electron microscopy (SEM) was not sufficiently powerful to provide
direct visualization of surface-contained pores. A new generation
of SEM instruments with ultra high resolution (20-50Å) is, however,
becoming available. The analysis can now be assisted by powerful
computer-linked image analyzers.

Broens, Bargeman and Smolders(3) reported on the use of nitro-
gen sorption/desorption method for studying pore volume distributions
in ultrafiltration membranes. The pore volume distributions were
calculated for a cylindrical capillary model. More recent results
from the same laboratory are published in this volume(4). In our
view, applicability of cylindrical pore models for asymmetric mem-
branes should be verified, rather than assumed. This can be done,
for example, by analysis of both branches of the sorption isotherm.
For a reasonable model choice, the two pore volume distributions
should be in substantial agreement.

The method of thermoporometry, developed by Brun, Lallemand,
Quinson and Eyraud(5), represents another method applicable, at
least in principle, to characterization of pore volume in ultrafil-
tration membranes (4,6). However, for asymmetric membranes, pore
volumes explored by thermoporometry may not be the volumes associ-
ated with membrane skins and "functional" pores.

Some authors (7,8) have used measured parameters of solute and
solvent transport for calculation of membrane pore size distribu-
tions. Difficulties associated with this approach are of both ex-
perimental and theoretical nature. The experiments need to be
carried out under conditions that minimize or eliminate effects of
boundary phenomena (polarization) and of solute adsorption (fouling)
on the measured coefficients. This is rarely done. An even more
serious obstacle in this approach is the absence of quantitative
and valid relations between measured transport parameters and the
size parameters of a "representative pore."

It is therefore highly desirable to develop more quantitative
methods for characterization of pore structures. The results of
recent investigations, including ultrafiltration (water flux and
rejection of a polydisperse solute), high-resolution SEM and nitro-
gen sorption/desorption analysis, are described below.

Materials
Polysulfone membranes A, B and C had been prepared by machine-
casting polymer solutions on a spun-bonded polyethylene substrate
with subsequent immersion in a coagulation bath. Typical ultra-
filtration membrane morphologies were visualized by SEM: high degree
of structure asymmetry, the presence of large voids (finger-like
cavities) and a globular (nodular) substructure beneath the skin.
Diameters of nodules in the skin regions were typically about 1000Å
for all three membranes.

The Dextran polymers used were Pharmacia Dextran T fractions
T10 (lot No. 16026), T40 (lot No. 21945), T70 (lot No. 23155) and
T500 (lot No. 19073). Size-exclusion chromatography columns were
calibrated with these fractions. Molecular weight distributions
of these lots were determined by Pharmacia.

Experimental

Ultrafiltration experiments were performed with an Amicon 8050 cell
at 25°C using a stirrer speed of approximately 700 rpm. Water
fluxes (hydraulic conductivities) were measured at Δp = 1 psi;
dextran rejection was measured for feed solutions containing 0.2%
T40, 0.2% T10 and 0.1% T500 (see Materials) under conditions of low
concentration polarization. Transmembrane fluxes of dextran sol-
utions were of the order of 0.2×10^{-3} cm/s at Δp = 1 psi. Feeds
and permeates were analyzed by size-exclusion chromatography as
described in Reference 9, and the chromatographs were used to cal-
culate the rejection curves (Figure 1).

    Scanning electron microscopy of membrane samples was performed
by International Scientific Instruments, Santa Clara, California
(courtesy of Dr. R. Buchanan). The micrographs were obtained with
a DS130 scanning electron microscope, 5kV accelerating voltage, 0°
tilt angle and 90,100X magnification. Samples were thinly coated
with gold and no other non-routine sample treatment was used.

    Nitrogen sorption/desorption isotherms of membrane samples
(carefully dried at room temperature) were obtained by Micrometrics
Instrument Corp., Norcross, Georgia. About 1.5g of each membrane
samples was used for measurements of BET surface areas, 21 point
sorption and 22 point desorption isotherms. The instrument used
was DigiSorb 2500 with fully automated control. The most signifi-
cant experimental error introduced was from saturation pressure
variation of about + 1.5 mm Hg (that is, about 0.2% error in
relative pressure).

    After careful removal of the polyethylene backing, membrane
thickness was measured by an accurately calibrated micrometer. The
overall density of each membrane was determined by weighing on an
analytical balance accurate to + 0.1 mg.

Results

Ultrafiltration, Thickness, Density

Membranes were characterized by water flux measurements, ultrafil-
tration of a polydisperse dextran as well as thickness and overall
density measurements. Data are summarized in Table I.

<div align="center">Table I. Membrane Properties</div>

Membrane	A	B	C
Hydraulic Conductivity (cm^2 s/g)	1.60×10^{-9}	4.19×10^{-9}	4.13×10^{-9}
Water Flux (GFD/psi)	2.3	6.1	6.0
Rejection of dextran with r_s= 50Å	0.90	0.60	0.44
Thickness (cm)(without) support)	0.007	0.009	0.009
Density (g/cm^3)	0.370	0.215	0.238
Porosity % (calculated from density)	0.730	0.843	0.826

$$\text{Porosity} = 1 - \frac{\text{Membrane Density}}{\text{Polymer Density}}$$

$$\text{Polymer Density} = 1.370 \ g/cm^3$$

Dextran rejection curves for membranes A, B and C are plotted in Figure 1.

SEM of Surface Pores

SEM photomicrographs were obtained as described above. Rough pore size analysis was performed on 3X photographic magnifications of original micrographs by inscribing circles in dark areas on the membrane surface (putative pores) and counting frequencies for each size class. For all three membranes, data points fitted well on log-normal distribution curves (Figure 2). Each curve can be described by the values of mean radius (r_m) and standard deviation (σ) (Table II).

Table II. Pore Size Analysis by SEM

Membrane			
Mean pore radius, r_m(Å)	21.3	40.4	41.0
Standard deviation (log-normal), σ	0.62	0.56	0.74
Number of pores/cm^2	3.94×10^{10}	3.44×10^{10}	1.49×10^{10}
Area analyzed (cm^2)	4.37×10^{-9}	1.58×10^{-8}	1.23×10^{-8}

Nitrogen Sorption/Desorption

Nitrogen sorption/desorption isotherms of membranes A, B and C exhibit narrow hysteresis loops in regions close to saturation points (Figures 3a,b,c). The experimental points on both branches of the three isotherms were fitted by an analytical function. In each case, correlation coefficients were greater than 0.9995. This allowed not only averaging of experimental data, but also simplified numerical procedures of isotherm analysis. Analysis was performed only in the regions for which experimental points were available.

Since the early work of Wheeler (10), there has been a continuous effort to extract information on adsorbent pore size distribution from gas sorption isotherms. The most crucial step is a selection of a proper pore shape model. Cylindrical (11) and parallel plate (12) pore models have been used most often.

For membrane samples in the present study, pore volume distribution analysis was carried out with a cylindrical model (11), and a model-independent approach of Brunauer et al. (13).

   a) Cylindrical pore model
      This model imposed several restrictions (14). Pore volume distributions ($\Delta V / \Delta r$ vs. r) were calculated using the procedure of Barett et al. (11). The multilayer thickness of nitrogen adsorbate was calculated using Halsey's equation (15) with values for monolayer thickness (3.54Å) and Halsey's exponent (1/3) recommended by Dollimore and Heal (16). Pore volume distributions (Figures 4a and b) are plotted only for those regions in which radii are determinable with errors of less than 10%.

   b) Model-independent approach
      Brunauer, Mikhail and Bodor (13) developed a method of pore structure analysis which employs a hydraulic radius, r_h, as a measure of pore size. This radius is defined as $r_h = V/S$ where V is the volume of a group of pore "cores" with the wall surface area S. The "core" refers to the empty
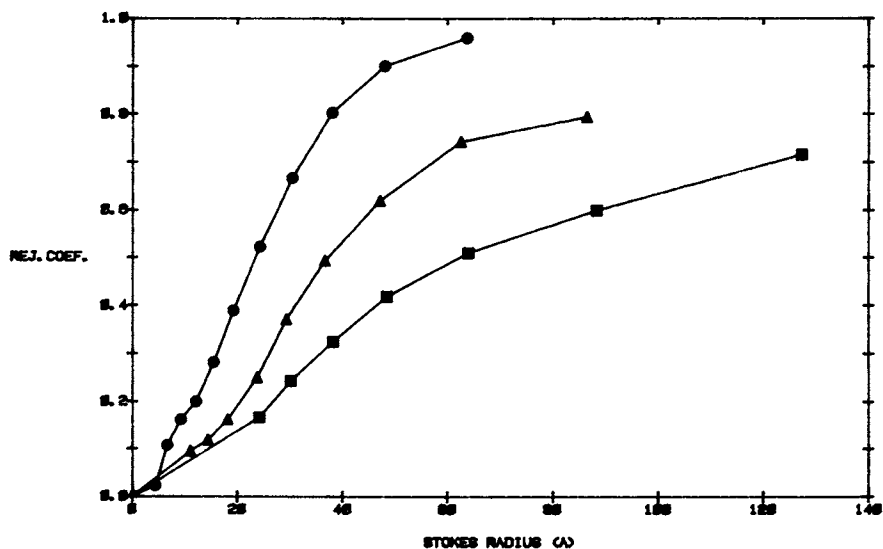
Figure 1.   Rejection coefficients vs. Stokes radii for a poly-
            disperse dextran feed.   Membranes: A(-●-), B(-▲-),
            C(-■-).
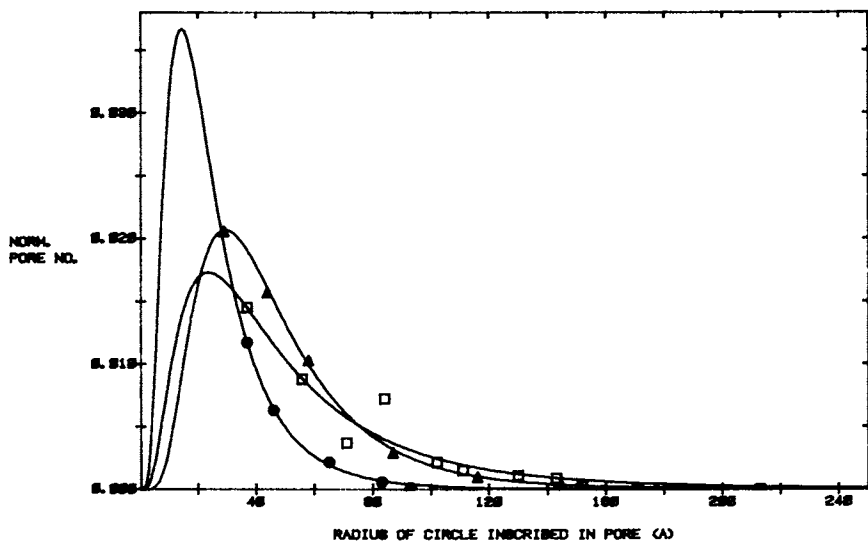
Figure 2.   Normalized distributions of pore size from SEM for
            membranes A(●), B(▲), C(□) and the fitted log-normal
            distribution curves (solid lines).
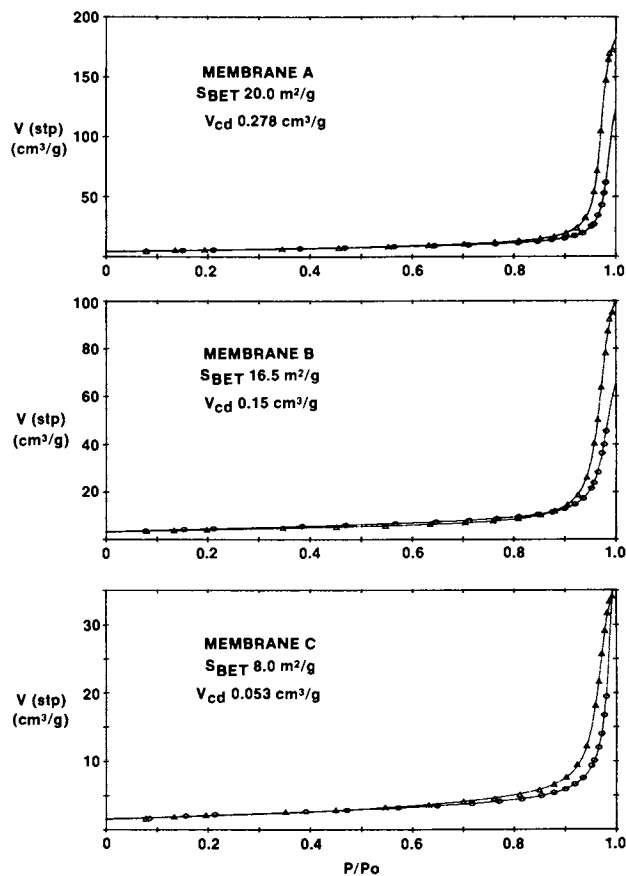
Figure 3. Nitrogen adsorption (O) and desorption (△) isotherms of membranes A, B and C. Solid lines represent the best fit of an analytical function.
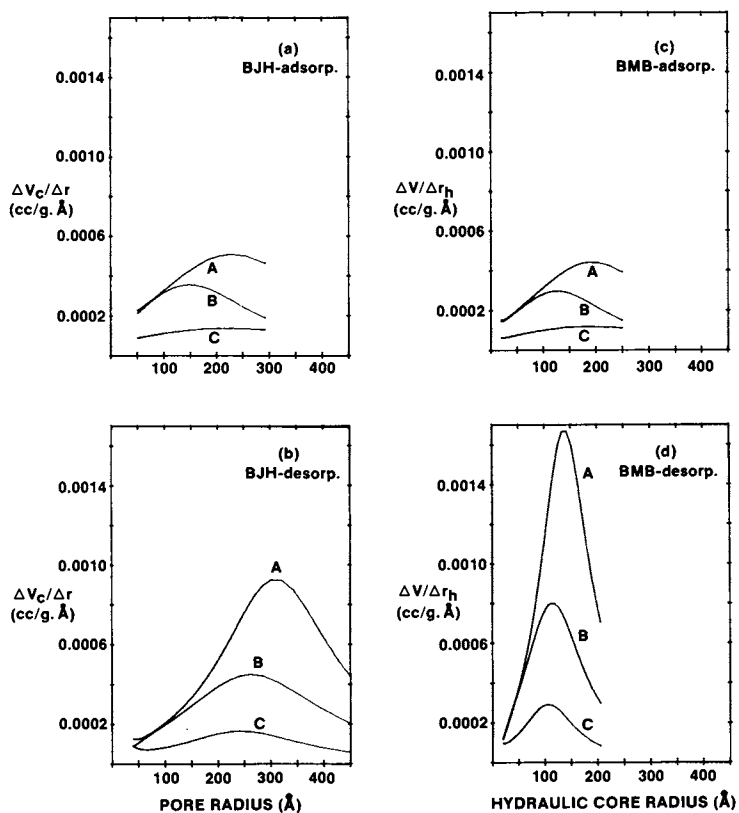
Figure 4.   Pore volume distributions calculated for membranes
A, B and C according to a cylindrical model (11):
4a - adsorption, 4b - desorption, and according to
the method of Brunauer et al. (13), 4c - adsorption,
4d - desorption.

part of a pore that contains an adsorbed film on its walls.
Quantities V and S are thermodynamically defined in terms
of the "core" of the pore and do not include contributions
from reversible multilayer adsorption. This leads to a
need for minor corrections in the calculated core volume
distributions. The curves calculated for the membrane sam-
ples (Figures 4b and c) were all corrected for the multi-
layer adsorption effects.

Theoretical analysis of gas sorption/desorption on a bed of packed spheres

Scanning electron micrographs of the membrane samples suggested
that the active layers of these membranes were comprised of spher-
ical agglomerates (nodules) with diameters around 1000Å(0.1 micron).
    Aristov et al. (17) developed a method for calculating sorption/
desorption isotherms for beds of regularly-packed uniform spheres.
In these beds, pore size is determined by the number of nearest
neighbors (coordination number) n, the sphere radius r, and the type
of packing geometry. Two radii characterize the pore size: one for
the "throat" and one for the "cavity" of the pore (18). Isotherms
have been calculated similar to those of Reference (9), for poly-
sulfone (density 1.370 g/cm^3) spheres for values of n = 4,6,8,10
(tetrahedral, primitive cubical, body-centered cubical, body-
centered tetragonal geometries, respectively). Nitrogen vapor at
-195.6°C was assumed and the adsorbed layer thickness was calculated
with Halsey's equation (15) as in the cylindrical pore model. Cal-
culated isotherms are plotted in Figure 5.

Discussion

Curves in Figure 1 show substantial differences in dextran rejection
by the three membranes. An increase in a rejection-controlling mean
pore size in the order A<B<C is suggested. After curve-fitting and
computation of the first derivative, the rejection curves were re-
plotted in a different form (Figure 6a). Comparison with the in-
formation presented in Figures 2 and 4 allowed the following inter-
pretation. The range of radii of rejected solutes seem to be com-
mensurate with the pore radius range measured by high-resolution
SEM but not with the one measured by the nitrogen sorption/
desorption method. The possible relation between Figures 6a and 2
was explored by using equations for the steric rejection theory
(19, Equations 4, 16b) for converting the curves of Figure 2 into
predicted rejection curves (Figure 6b). The agreement between
Figures 6a and 6b is rather remarkable. However, several words of
caution are justified. The equations used (19) are valid only for
straight cylindrical pores. Sorption/desorption results (Figures
3,4) suggest that larger pores within the membrane structure are
probably non-cylindrical. No reliable information is yet available
for shapes of surface-contained pores in ultrafiltration membranes
(similar to membranes A, B, C) and it is therefore uncertain
whether the use of the cylindrical model (Figure 6b) was a justi-
fiable approximation. Some uncertainties may also derive from pos-
sible artifacts generated in sample preparation for electron micro-
scopy (drying, metal coating, and so forth). We did not try to
correct for such effects.
    In nitrogen sorption/desorption experiments, BET areas and
total pore volumes rank clearly in the order A>B>C (Figures 3a,b,c).
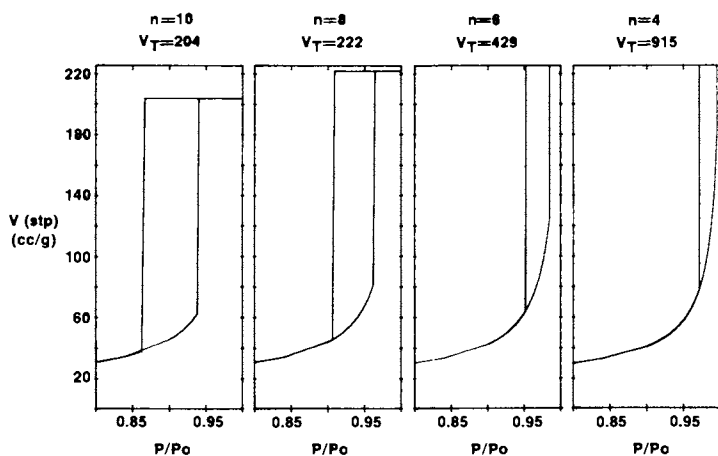
Figure 5. Hysteresis regions of nitrogen adsorption and desorption
           isotherms calculated for regular packings of spheres
           with uniform radii of 500 Å. Total pore volume, V_T,
           given for each packing.
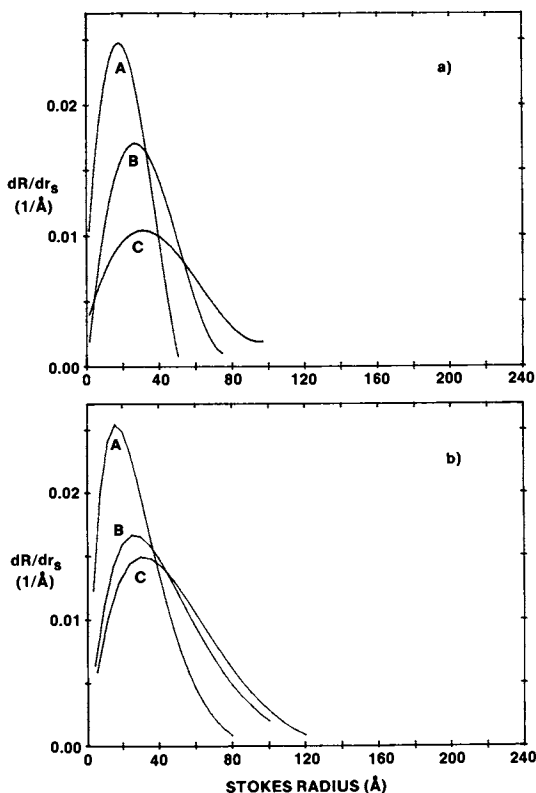
Figure 6. a) Derivatives of experimental rejection curves.
Values of dR/dr were calculated from smoothed re-
jection data in Figure 1 for membranes A, B and C.
b) Derivatives of theoretical rejection curves.
Log-normal pore size distributions from SEM (Figure 2)
and equations of the steric rejection theory (19)
were used.

For all three membranes, narrow hysteresis was observed in regions
close to $p/p_o = 1$. The cylindrical pore model (11) analysis yielded
different pore volume distribution curves from adsorption and de-
sorption (Figures 4a,b). Curve maxima for desorption are located
at higher r values than for adsorption. This is a physically un-
realistic result, suggesting lack of applicability of the cylindri-
cal pore model. Analysis with the model-independent method of
Brunauer et al. (13) yielded desorption curve maxima at lower r_h
values than for the corresponding adsorption curves. There is no
reason to expect identical curves in this case – the difference is
a direct consequence of sorption hysteresis. Desorption-controlling
pores are still considerably larger than surface pores visualized
by SEM, especially if we consider the fact that hydraulic radii are
smaller than geometric radii ($r = 2r_h+t$ for a cylinder; $r = 3r_h+t$
for a sphere).

It is likely, therefore, that pores analyzed by the nitrogen
sorption/desorption method are interstices in the subsurface strata.
In the membranes presented here, these strata consisted of agglom-
erated spherical nodules. It is worth noting that curve maxima in
Figures 4b,d are in the unexpected order A>B>C.

Theoretical isotherms calculated for regularly packed spheres
look encouraging. In spite of simplifying assumptions, we obtained
a qualitative agreement with experimental isotherms, mainly narrow
sorption hysteresis in the regions close to $p/p_o = 1$. Total pore
volumes depend strongly on the choice of n (coordination number).
More detailed analysis, allowing for polydispersity of both r and
n, is required for quantitative interpretation of isotherms.

Methods of quantitative characterization of porous membrane
structures have been explored. It is believed that knowledge ob-
tained through these and similar methods will lead to a better
understanding of both membrane formation and membrane function
processes.

Legend of Symbols

n   coordination number of packed spheres
p   pressure (mm Hg)
p_o saturation pressure (mm Hg)
r   radius of a sphere or a cylinder (Å)
r_h hydraulic radius of a pore core (Å)
r_m mean pore size (Å)
r_s Stokes radius of a solute (Å)
R   rejection coefficient
S   wall surface area of cores (cm^2/g)
t   thickness of adsorbed layer (Å)
V   volume of pore cores (cm^3/g)
V_c volume of cylindrical pores (cm^3/g)
V_{cd} cumulative desorption volume (as volume of liquid N_2 at 77.4K,
     cm^3/g).
V_T total pore volume of regular packing spheres (as volume of N_2
     at STP, cm^3/g).
σ   standard deviation of log-normal distribution

Literature Cited

1. Preusser, H.J. Kolloid Z. u. Z. Polymere 1972, 250, 133–141.
2. Fane, A.G.; Fell, C.J.D.; Waters, A.G. J. Membrane Sci.
    1981, 9, 245–262.
3. Broens, L.; Bargeman, D.; Smolders, C.A. Proc. 6th Int. Symp.
    Fresh Water from the Sea, 1978, 3, 165–171.
4. Smolders, C.A.; Vugteveen, E. In "Materials Science of
    Synthetic Membranes"; Lloyd, D.R., Ed.; American Chemical
    Society: Washington, D.C., 1985.
5. Brun, M.; Lallemand, A.; Quinson, J.F.; Eyraud, C.
    Thermochimica Acta 1977, 21, 59–88.
6. Desbrieres, J.; Rinaudo, M.; Brun, M.; Quinson, J.F. J. Chem.
    Phys. 1981, 78, 2, 187–191.
7. Schwarz, H.H.; Bossin, E.; Fanter, D. J. Membrane Sci. 1982,
    12, 101.
8. Chan, K.; Matsuura, T.; Sourirajan, S. Ind. Eng. Chem. Prod.
    Res. Dev. 1982, 21, 605.
9. Zeman, L.; Wales, M. Sep. Sci. and Technol. 1981, 16, 275–290.
10. Wheeler, A. Advan. Catalysis 1951, 3, 250.
11. Barrett, E.R.; Joyner, L.G.; Halenda, P.P. J. Am. Chem. Soc.
    1951, 73, 373.
12. Innes, W.B. Anal. Chem. 1957, 29, 1069.
13. Brunauer, S.; Mikhail, R.Sh.; Bodor, E.E. J. Colloid Interface
    Sci. 1967, 24, 451–563.
14. Faas, G.S., Master's Thesis, Georgia Institute of Technology,
    Atlanta, 1981.
15. Halsey, G. J. Chem. Phys. 1948, 16, 931–937.
16. Dollimore, D.; Heal, G.R. J. Colloid Interface Sci. 1970, 33,
    508–519.
17. Aristov, B.G.; Karnaukhov, A.P.; Kiselev, A.V. Russ. J. Phys.
    Chem. 1962, 36, 1159–1164.
18. Kruyer, S. Trans. Faraday Soc. 1958, 54, 1758.
19. Zeman, L.; Wales, M. In "Synthetic Membranes, Vol. II";
    Turbak, A.F., Ed.; ACS SYMPOSIUM SERIES No. 154, American
    Chemical Society: Washington, D.C., 1981; p. 411.

Partial Solubility Parameter Characterization of Interpenetrating Microphase Membranes

SONJA KRAUSE

Department of Chemistry, Rensselaer Polytechnic Institute, Troy, NY 12181

Ion exchange membranes and the dense layer of reverse osmosis membranes act as if they were composed of two interpenetrating microphases. One of these microphases consists of the ionic groups and/or the principal H-bonding groups (-OH, -NH$_2$, or > NH) of the membrane polymer with sufficient water to make a continuous pore-like phase. The other microphase consists of the remaining hydrophobic (principally hydrocarbon, ester and carbonyl) portions of the membrane polymer. On the one hand, water, ions, and the principal H-bonding groups, if any, of the organic molecules which go through these membranes are assumed to travel through the aqueous microphases. On the other hand, small organic molecules without major H-bonding groups and the hydrophobic portions of the other molecules are assumed to be transported through the hydrophobic microphases. It is proposed that solubility parameters calculated for only the hydrophobic portions of the membrane polymers and the hydrophobic portions of the small molecules of interest can be used to determine which small molecules can be sorbed by a particular membrane and, in some cases, be preferentially transported across the membrane. Some experimental data in the literature are examined using these ideas.

Both reverse osmosis and ion exchange membranes may be used to separate ions from water, and both types of membranes can also be used to separate organic solutes from water. Depending on the membrane used, some organic solutes remain mainly on the *feed* side of the membrane, while others are preferentially transported through the membrane; i.e., the concentration of solute on the *permeate* side of the membrane becomes greater than that on the *feed* side. Since it is generally assumed that transport of these organic solutes correlates with preferential sorption of the solute by the membrane, a simple method for predicting such preferential sorption would be useful. A rather complex, semi-empirical method for making such

predictions has been developed by Sourirajan and coworkers (1). It
nevertheless seems desirable to develop a simpler, less empirical
method to calculate preferential sorption and, if possible, distri-
bution coefficients for organic solutes between a membrane and an
aqueous solution.

The Interpenetrating Microphase Model

To develop such a method, a physical model for the "active" portion
of the membrane of interest is necessary. Membrane models that have
been developed previously for various purposes have been reviewed
elsewhere (see for example References 2 and 3). A slightly different
model is being proposed in this paper; this model is based on a
number of experimental observations on polymers and polymeric mem-
branes, some of which are summarized below:
    1. The dense layer of reverse osmosis membranes transports
water as if through pores, but no pores are observed in electron
micrographs of the dried membranes. This implies either that the
pores are too small to be observed by electron microscopy or that
they only exist in the presence of water, not in the dried polymer.
    2. Ion exchange membranes also transport water as if through
pores, but no pores have been observed directly.
    3. Although most reverse osmosis membranes are not cross-
linked, they do not dissolve in water; nevertheless, they absorb
about 10-15 wt. % water. Ion exchange membranes are usually cross-
linked and absorb similar amounts of water.
    4. Cylindrical structures of finite thickness were consistent
with the small angle light scattering (SALS) data obtained on hy-
drated poly(2-hydroxyethyl methacrylate), a polymer similar to those
used for reverse osmosis membranes (4).
    5. The properties of poly(methacrylic acid) show that consid-
erable association of the α-methyl groups occurs in aqueous solu-
tions of this polymer (5). This association is often referred to as
a hydrophobic interaction. Some properties of other polymers, such
as the polycondensate between L-lysine and 1,3-benzenedisulfonyl
chloride (6), are also attributed to hydrophobic interactions be-
tween parts of the polymer chains.
    These five sets of observations, plus knowledge of the phenome-
non of microphase separation in block copolymers leads to a model of
reverse osmosis or ion exchange membranes in which the hydrophobic
portions of the polymer chains have come together to form one more
or less continuous microphase, while the hydrophilic portions of the
polymer chains (ionic groups, -OH groups, $-NH_2$ or $>$ NH groups) have
"dissolved" in a small amount of water to form another more or less
continuous microphase when the membrane is swollen in water. The
hydrophilic groups, in most cases, probably form clusters but not
continuous microphases in the dried membranes.
    Such ionic clusters have been studied in ionomers such as
Nafion poly(perfluoropropylene oxide sulfonic acid) membranes;
clusters in ionomers have been reviewed recently by Mauritz and
Hopfinger (7). These reviewers also quote a model for hydrated
Nafion proposed by T. D. Gierke at the October, 1977, meeting of the
Electrochemical Society, Atlanta, Georgia, in which aqueous spher-
ical microphases $\sim$ 40 Å in diameter are connected by short, $\sim$ 10 Å

diameter corridors to form a continuous aqueous microphase. Gierke apparently observed small angle X-ray scattering patterns of Nafion which were consistent with 40 Å diameter spherical clusters, but the 10 Å corridors were conjectured rather than observed.

There is sufficient evidence for interpenetrating microphases in water-swollen, water-transporting membranes to use this as a working model for the membranes. Using this model, one may assume that water and ions transported through such a membrane travel through the aqueous microphases in which the ionic and hydrophilic groups intrinsic to the membrane polymer are also embedded. Molecules containing no major hydrophilic groups may then travel through the hydrophobic microphases if they travel through the membrane at all. These microphases are much smaller (of the order of 10 Å to 30 Å) than the phases found in immiscible polymer blends, semicrystalline polymers, or block copolymers. Models used to explain sorption or permeability in these larger phases (8) may not necessarily be extended without change to the much smaller (molecular diameter) microphases postulated here for reverse osmosis and ion exchange membranes.

To understand the sorption of small organic molecules containing no major hydrophilic groups by a reverse osmosis or ion exchange membrane, and thus the transport of these molecules through the membrane, it is necessary to consider the interaction of the hydrophobic molecule with only the hydrophobic portion of the membrane polymer. It is also useful to consider the interaction of small molecules containing hydrophilic groups as well as hydrophobic groups with the membranes and their transport through the membranes. It is likely that such molecules interact with both types of microphases within the membrane and move through the membrane more or less at the "interface" between microphases.

The concept of such an "interface" is hazy since the diameter of any of the microphases is probably very small, most likely below 30 Å. A "phase" with such dimension is a small system in the sense of Hill (9) and the fluctuations of its properties from their averages are large. With this *caveat* it is still possible to consider the average properties of these microphases and to assume that a small molecule with a hydrophilic and a hydrophobic part is situated, on the average, with its hydrophilic portion in the aqueous microphase and its hydrophobic portion in the hydrophobic microphase of the membrane polymer.

The Hildebrand Solubility Parameter

In the above considerations, the hydrophobic portions of both the membrane polymer and the small molecules that enter the membrane are expected to interact in the hydrophobic microphases in the membrane. It therefore becomes useful to find a numerical measure of the miscibility of these hydrophobic portions of molecules. In the case of complete molecules, both small and polymeric, the solubility parameter concept has been useful in the past. This concept is related to the enthalpy change which occurs on mixing in regular solution theory as developed by Hildebrand and coworkers (10) and as used for polymer solution theory by Flory (11). The Hildebrand solubility parameter is a measure of the attraction between molecules of the same kind, including dispersion forces, polar forces, and hydrogen bonding

interactions. In general, the closer the values of the Hildebrand
solubility parameters of two molecules, the more soluble in each
other they are expected to be. Because of entropy considerations,
the exact degree of proximity needed between the solubility para-
meters of two molecules in order to expect miscibility is greater
between a polymer and a small molecule than between two small
molecules.

The Hildebrand solubility parameter concept has worked well for
molecules that contain no major H-bonding groups, but many exceptions
to the predictions occur when major H-bonding groups are present,
even in only one of the molecules being considered. For this reason,
Hansen (12) developed the so-called three-dimensional solubility
parameter in which the contributions of dispersion forces, polar
forces, and H-bonding are considered as separate contributions to the
solubility parameter. Bagley (13) developed a two-dimensional sol-
ubility parameter in which the H-bonding contribution is considered
separately from the other two contributions which are lumped
together. One-, two- and three-dimensional solubility parameters
have been useful to membrane scientists and engineers (14-20) and
have fewer exceptions to their predictions than the simple
Hildebrand solubility parameter.

The solubility parameters of insoluble polymers are often deter-
mined by swelling the polymer in a series of solvents with different
solubility parameter values. Maximum swelling of the polymer then
occurs in those solvents whose solubility parameters are closest to
that of the polymer. It is interesting to note that swelling data
for Nafion, when interpreted in this way, indicate the presence of
two solubility maxima; that is, this ionomeric polymer acts as if it
had two different solubility parameters (21). This seems reasonable
for a polymer that is composed of two different phases; neither
solubility maximum, however, is very close to the solubility param-
eter of water.

The Partial Solubility Parameter of the Hydrophobic Portion of a Molecule

The simplest criterion for a theoretical calculation of the misci-
bility of the hydrophobic portions of small molecules with the
hydrophobic microphase of a membrane polymer appears to be a partial
solubility parameter; that is, calculation of the solubility param-
eter of only the hydrophobic portions of the molecules. This can be
done using a group contribution approach in which each group (for
example, a CH_3-group) in the molecule contributes a certain attrac-
tive force and a certain volume to the molecule. In this way, a
solubility parameter may be estimated for either a portion of a
molecule or for a whole molecule.

The solubility parameter of the hydrophobic molecule or portion
of a molecule, δ_{HP}, may be calculated using the relationship

$$\delta_{HP} = \frac{\Sigma F_i}{\Sigma V_i} \qquad (1)$$

where the F_i are group contributions to the molar attraction constant of the molecule and the V_i represent group contributions to the molar volume of a rubbery polymer or of a small molecule containing that group. Alternatively, δ_{HP} can be estimated by using the relationship

$$\delta_{HP} = \left(\frac{\Sigma U_i}{\Sigma V_i}\right)^{1/2} \qquad (2)$$

where the U_i are molar group contributions to the cohesive energy of the polymer or small molecule. Some investigators have tabulated F_i, while others use the U_i. Tabulations of F_i, U_i, and V_i that have been made by a variety of investigators have been shown and discussed by Van Krevelen and Hoftyzer (22) and by Barton (16), Van Krevelen and Hoftyzer (22) have made the most recent tabulation of F_i and V_i, while Fedors' (23) compilation of U_i with accompanying V_i includes values for the largest number of molecular groups. The two sets of tables give rather different values for the δ_{HP} of molecules and parts of molecules as will be seen below. This means that both sets of parameters will have to be evaluated against experimental data. Van Krevelen and Hoftyzer's values give values for solubility parameters numerically similar to those obtained from the F_i values from the revised Small's Table (24) or Hoy's Table (25). Note that References 24 and 25 give no values for V_i. Ordinarily, when calculations are made for complete molecules or polymer repeat units, the molar volume of the liquid or rubbery polymer can be used in the calculations instead of ΣV_i. This molar volume is easily calculated from the densities and molecular weights. In calculations of δ_{HP} for a portion of a molecule, however, group contributions to V_i are necessary. In some proprietary publications, Hoy (26) has calculated group contributions to V_i for polymers at their glass transition temperatures.

Table I gives the values of F_i and V_i used in this work in connection with Equation 1, and Table II gives the values of U_i and V_i used in this work in connection with Equation 2.

Comparison with Experimental Data

It should be expected that calculated values of δ_{HP} correlate better with equilibrium properties of the membranes in aqueous solution than with transport properties. One of the few such equilibrium measurements that have been published is by Anderson et al (27). Their measured partition coefficients (K), diffusion coefficients (D), and reverse osmosis rejection (R) of the organic solutes are shown in Table III for cellulose acetate membranes. Their data for cellulose acetate butyrate was similar and is not shown here. Aqueous solutions of the organic solutes, usually at concentrations of about 10^{-4}g 1^{-1}, were used in the measurement of partition coefficients by UV absorption. In Table III,

Table I. Group Molar Attraction Constant, F_i, and Molar
Volume Group Contributions V_i, of Rubbery Amorphous
Polymers and Small Molecules at 25°C According to
Van Krevelen (16,22)

Group	F_i $J^{1/2} cm^{3/2} mol^{-1}$	V_i $cm^3 mol^{-1}$
$-CH_3$	420	22.8
$-CH_2-$	280	16.45
$-CH<$	140	9.85
$>C<$	0	4.75
$-CH(CH_3)-$	560	32.65
$-C(CH_3)_2-$	840	50.35
$-CH=CH-$	444	27.75
$>C=CH$	304	20.0
$-C(CH_3)=CH-$	724	42.8
phenyl	1517	64.65
p-phenylene	1377	61.4
$-F$	164	10.0
$-Cl$	471	18.4
$-O-$	256	8.5
$-COO-$	512	24.6 (21.0 acrylic)
$-S-$	460	15.0
$-Br$	695*	25.3**
$-NO_2$	900*	12.9[†]
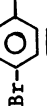
*From Reference 24.
**From Reference 26.
[†]Estimated from Chapter 6, Table 9 of Reference 16.

Table II. Group Contributions to the Cohesive Energy, U_i and
and Molar Volume Group Contributions, V_i, at 25°C
according to Fedors ([23])

Group	U_i kJ mol^{-1}	V_i cm^3 mol^{-1}
$-CH_3$	4.71	33.5
$-CH_2-$	4.94	16.1
$-CH<$	3.43	-1.0
$>C<$	1.47	-19.2
$H_2C=$	4.31	28.5
$-CH=$	4.31	13.5
$>C=$	4.31	-5.5
$HC\equiv$	3.85	27.4
$-C\equiv$	7.07	6.5
phenyl	31.9	71.4
phenylene (o,m,p)	31.9	52.4
phenyl(trisubstituted)	31.9	33.4
pheny(tetrasubstituted)	31.9	14.4
ring closure (5 or more atoms)	1.05	16
ring closure (3 or 4 atoms)	3.14	18
conjugation in ring (per double bond)	1.67	-2.2
halogen attached to C atom with double bond	20% of halogen U_i	—
$-F$	4.19	18.0
$-F$ (disubstituted)	3.56	20.0
$-F$ (trisubstituted)	2.30	22.0
$-CF_2-$ (in perfluoro compound)	4.27	23.0
$-CF_3$ (in perfluoro compound)	4.27	57.5
$-Cl$	11.55	24.0
$-Cl$ (disubstituted)	9.63	26.0
$-CL$ (trisubstituted)	7.53	27.3
$-Br$	15.49	30.0
$-OH$	29.8	10.0
$-O-$	3.35	3.8
$-CHO$	21.4	22.3
$-CO-$	17.4	10.8
$-CO_2-$	18.0	18.0
$-CO_3-$	17.6	22.0
$-NH_2$	12.6	19.2
$-NH-$	8.4	4.5
$-N<$	4.2	-9.0
$-N=$	11.7	5.0
$-NO_2$ (aliphatic)	29.3	24.0
$-NO_2$ (aromatic)	15.36	32.0
$-S-$	14.15	12

Table III. Partition Coefficients, Diffusion Coefficients, Reverse Osmosis Rejection at 68 atm, and δ_{HP} for Organic Solutes in Cellulose Acetate Membranes

Molecule	Calculated as	$K^{\dagger}$ at pH 5.6	$D \times 10^{10}$ $cm^2 sec^{-1}$	$R^{\dagger}$	δ_{HP}(Eq. 1) $J^{1/2} cm^{-3/2}$	δ_{HP}(Eq. 2) $J^{1/2} cm^{-3/2}$
Acetone	$(CH_3)_2CO$	0.3±0.1	300	+0.17	20.3*	18.6
Pyridine	[ring N]	0.7	75	–	21.9*	21.9
						18.1
Nitromethane	CH_3NO_2 CH_3-	2.1±0.5	150	–0.06	26.0*	24.3
					18.4	11.9
Hydroquinone	Phenylene HO–	3.5±0.2	–	–	22.4	24.7
					22.9	31.4
Aniline	Phenyl	20±2	20	+0.04	23.5	21.1
Phenol	Phenyl	37±1	10	–0.09	23.5*	21.1
Nitrobenzene	Nitrobenzene	54±4	8.0	–	20.5*	21.4
3,5-Di(Carbethoxy)phenol	$OOCC_2H_2$ $OOCC_2H_5$	129±12	1.8	–	20.0	24.3
p-Bromophenol	Br–	165±2	3.8	–	21.9	24.0(23.2)**
2,4-Dichlorophenol	Cl– Cl	332±7	1.5	–0.33	23.6	26.0(22.3)**

* Taken from Reference 24.
† Taken from Reference 27.
**Calculated by using only 80% of the U_i listed for the halogen; this halogen is not really attached to a C atom with a double bond but this idea was used in the calculation.

$$K = \frac{(\text{final wt. of solute in membrane})}{(\text{wt. of membrane})} \div$$

$$\frac{(\text{final wt. of solute in solution})}{(\text{wt. of solution})} \tag{4}$$

and
$$R = 1 - \frac{(\text{concentration of solute in product water})}{(\text{concentration of solute in feed water})} \tag{5}$$

Of the solutes used, acetone and pyridine are infinitely soluble in water at room temperature, nitromethane and phenol are somewhat soluble, and the others are only slightly soluble. Like many others, Anderson et al (27) noticed that solubility of organic solutes in the membrane seemed to be inversely correlated with their water solubility. They also noted that diffusivity in the membrane seemed inversely correlated with the partition coefficient.

The δ_{HP} values for the different organic solutes were calculated for several different portions of the molecules in some cases. The nitrogen in pyridine, for example, is a major hydrogen-bonding group and should not be considered in δ_{HP}, but the calculated value for the portion of the conjugated ring without the nitrogen can best be described as approximate. Since nitromethane is relatively water-soluble, its $-NO_2$ group may, at least in part, be more attracted to the aqueous than to the nonaqueous microphase in the membrane. In hydroquinone, it is difficult to decide which part of the molecule is attracted to the hydrophobic membrane microphase. It may be only a part of the phenylene ring which is attracted, in which case both calculations are erroneous. If the three solutes for which several calculations were made are disregarded, then the partition coefficients correlate well with the δ_{HP} values calculated using Equation 2 and Table II; the K values and these δ_{HP} values increase together. The alternate, double-starred values of δ_{HP} shown for the last two solutes in Table III were calculated assuming that the halogens were attached to a doubly bonded carbon instead of a singly bonded carbon. It is difficult to decide which calculation is the more reasonable. Using these starred values, the distribution coefficient is greatest when $\delta_{HP} = 22.3 \ J^{1/2} \ cm^{-3/2}$. This is close to the value $\delta_{HP} = 23.4 \ J^{1/2} \ cm^{-3/2}$ calculated using Equation 2 for the membrane, assumed to be cellulose diacetate with the $-OH$ group in the aqueous microphase. Values of δ_{HP} calculated using Equation 1 and Table I do not appear to correlate well with values of the partition coefficients, especially since δ_{HP} calculated in this way for cellulose diacetate without the $-OH$ group is 18.9, lower than the values calculated for any of the organic solutes used. It is thus too early to state whether the δ_{HP} concept will correlate well with partition coefficients, although these calculations make it seem that Equation 2 and Table II will be useful. Additional partition coefficient data on many organic solutes and on chemically different membranes would be helpful. One may hope to develop these ideas further so that partition coefficients may eventually be predicted for new membrane-solute pairs.

Table III shows that reverse osmosis solute rejection was only imperfectly correlated with partition coefficients, as might be expected for a transport process that must involve non-thermodynamic

as well as thermodynamic factors. Thus, for the moment, no δ_{HP} cal-
culations will be shown in connection with reverse osmosis rejection
data alone. Such calculations have been made in light of the reverse
osmosis rejection data of Sourirajan (1), Fang and Chian (28,29) and
Dickson and Lloyd (30); these calculations also showed only an im-
perfect correlation with the rejection data.

There are many reasons why δ_{HP} values may not predict even parti-
tion coefficients perfectly. Some of these reasons are:

1. The hydrophobic membrane microphase is so small that it may
not conform to the expected bulk density of this microphase. In ad-
dition, cross-links that are part of the hydrophobic microphase will
distort its density. This means that the membrane polymer's hydro-
phobic groups will not occupy the expected volumes, thus changing the
δ_{HP} of this microphase.

2. The hydrophobic portion of a hydrogen-bonding molecule such
as glycerol may be smaller than the hydrophobic portion of the mem-
brane polymer molecule. If only a portion of the membrane polymer
repeat group is next to the aqueous phase, the hydrophobic portion
of the small molecule may be in contact with only that portion of the
membrane polymer. This could happen, for example, when the membrane
polymer is polystyrene sulfonate, where the phenylene groups to which
the sulfonate is attached are constrained to be next to the aqueous
phase. In that case, perhaps when considering interaction with mol-
ecules like glycerol, the δ_{HP} of the phenylene groups alone would be
more relevant than the δ_{HP} in which the polymer backbone groups are
included.

3. It is not always clear, as in the case of nitromethane
(Table III), whether a particular group in a molecule will be pri-
marily in the hydrophobic or in the aqueous microphase of the mem-
brane polymer.

The swelling data for Nafion in various organic solvents (21),
referred to earlier, are thermodynamic data, but they were obtained
in the absence of water, so that the interpenetrating microphase net-
work as postulated in this paper did not exist. Nevertheless, some
calculations of δ_{HP} for both the membrane polymer and for the organic
solvents were made. Table IV shows the portions of the molecules
used in the calculations, the calculated values of δ_{HP} according to
both Equation 1 and Equation 2, the values of the total solubility
parameters, δ_T, of the molecules as used in Reference 21, and the
percent increase in weight during swelling as found in Reference 21.
Maximum swelling of both NAFION membranes tested occurred at
$\delta_{HP} = 17.4 \pm 0.5$ $J^{1/2}$ $cm^{-3/2}$ when Equation 1 was used, and at
$\delta_{HP} = 15.8 \pm 0.2$ $J^{1/2}$ $cm^{-3/2}$ when Equation 2 was used. Yeo (21)
found two swelling maxima, corresponding to $\delta_T = 19.6 \pm 0.4$ and
34 ± 6 $J^{1/2}$ $cm^{-3/2}$. The hydrophobic repeat groups in Nafion,
$-OCF_2CF(CF_3)-$ and $-OCF_2CF<$, have δ_{HP} (Eq. 1) = 15.0 and
15.6 $J^{1/2}$ $cm^{-3/2}$, respectively, and δ_{HP} (Eq. 2) = 14.5 and
22.8 $J^{1/2}$ $cm^{-3/2}$, respectively, with both membrane 1100 and 1200
having $\delta_{HP} = 15.0$ using either Equation 1 or 2. Equations 1 and 2
give very different values for most of the solvent δ_{HP}'s;
again, as in the case of the partition coefficients, Equation 2 seems
to work better, in the sense that the maximum swelling
δ_{HP} = (Eq. 2) = 15.8 ± 0.2 $J^{1/2}$ $cm^{-3/2}$ is close to the

Table IV. Values of δ_{HP} and δ_T of Molecules used to Swell Nafion (21) and the Percent Swelling Obtained

Molecule	Calculated as	δ_{HP}(Eq. 1) $J^{1/2} cm^{-3/2}$	δ_{HP}(Eq. 2) $J^{1/2} cm^{-3/2}$	δ_T(21) $J^{1/2} cm^{-3/2}$	% increase in wt. Membrane	
					1100[a]	1200[a]
Glycerol	CH_2CHCH_2	16.4	20.7	33.7	56	40
Cyclohexanol	$(CH_2)_5CH-$	16.7	17.5	23.3	—	64
Ethylene Glycol	$-CH_2CH_2-$	17.0	16.4	29.8	66	44
2-Ethyl hexanol	$CH_3(CH_2)_3CH(C_2H_5)CH_2-$	17.3	16.0	19.4	—	77
n-Amyl alcohol	$CH_3(CH_2)_4-$	17.4	15.8	22.3	73	59
n-Butanol	$CH_3(CH_2)_3-$	17.5	15.5	23.3	74	65
1-Propanol	$CH_3(CH_2)_2-$	17.6	14.9	24.3	55	40
2-Propanol	$(CH_3)_2CH-$	17.7	14.0	23.5	58	50
Ethanol	CH_3CH_2-	17.8	13.9	26.0	50	32
Diethylamine	CH_3CH_2-	17.8	13.9	16.4	21	40
Triethylamine	CH_3CH_2-	17.8	13.9	15.1	22	24
Methanol	CH_3-	18.4	11.9	29.6	54	37

[a] Equivalent weight per sulfonate group

δ_{HP} (Eq. 2) = 15.0 $J^{1/2}$ $cm^{-3/2}$ of the membrane polymer. Again, as in the case of δ_{HP} (Eq. 2) which included the starred values in Table III of the cellulose acetate membrane used for the partition coefficient data discussed above, the δ_{HP} (Eq. 2) of the membrane polymer is about 1 $J^{1/2}$ $cm^{-3/2}$ less than the δ_{HP} (Eq. 2) of the organic solvent that gives maximum swelling.

Conclusions

An interpenetrating microphase model of reverse osmosis and ion exchange membranes has led to the idea of calculating the solubility parameter of only the hydrophobic portions of both the membrane polymer and of small organic solute molecules that may interact with and swell the hydrophobic membrane polymer microphases. This partial solubility parameter, δ_{HP}, may be calculated in several ways. A comparison of calculated values of δ_{HP} for some solvents and membrane polymers for which partition coefficients or equilibrium swelling data appear in the literature indicates that one of these methods of calculating δ_{HP} may prove to be useful in predicting such equilibrium data and, probably in connection with additional assumptions, in predicting preferential sorption.

Acknowledgments

Literature Cited

1. Sourirajan, S. Am. Chem. Soc. Symp. Ser. 1981, 153, 11-62.
2. Dresner, L.; Johnson, J. S. Jr. In "Principles of Desalination," Second Ed., Part B; Spiegler, K. S.; Laird, A. D. K.; Academic Press, New York; 1980, 401-560.
3. Kesting, R. E. "Synthetic Polymer Membranes"; McGraw-Hill, New York; 1971.
4. Prins, W. In "Polym. Networks, Struct. Mech. Props." Proc. ACS Symposium, 1970; 323-339.
5. Eliassaf, J. Polym. Letters 1965, 3, 767-769.
6. Fenyo, J-C.; Beaumais, J.; Selegny, E. J. Polym. Sci. Polym. Chem. Ed. 1974, 12, 2659-2670.
7. Mauritz, K. A.; Hopfinger, A. J. Modern Aspects Electrochem. 1982, 14, 425-508.
8. Hopfenberg, H. B.; Paul, D. R. In "Polymer Blends"; Paul, D. R.; Newman, S., Eds.; Academic: New York, 1978; Vol I, 445-489.
9. Hill, T. L. "Thermodynamics of Small Systems" Part I and Part II, W. A. Benjamin: New York, Part I, 1963; Part II, 1964.
10. A relatively recent discussion appears in Hildebrand, J. H.; Prausnitz, J. M.; Scott, R. L. "Regular and Related Solutions. The Solubility of Gases Liquids, and Solids"; Van Nostrand, Reinhold: New York, 1970.

11.   Flory, P. J. "Principles of Polymer Chemistry" Cornell Univ.
      Press: Ithaca, N.Y.; 1953. (The concept of solubility param-
      eters is not explicitly referred to in this book, but the con-
      comitant regular solution concept is employed.)
12.   Hansen, C. M. "The Three Dimensional Solubility Parameter and
      Solvent Diffusion Coefficient. Their Importance in Surface
      Coating Formulation" Danish Technical Press: Copenhagen; 1967.
13.   Bagley, E. B.; Scigliano, J. M. "Polymer Solutions" In Dack,
      R. J., Ed.; "Solutions and Solubilities" Part 2, Vol. 8 of
      Weissberger, A., Ed.; "Techniques of Chemistry"
      Wiley-Interscience: New York; 1976, 437-485.
14.   Klein, E.; Smith, J. K. In "Reverse Osmosis and Membrane
      Research"; Lonsdale, H. K.; Podall, H. E.; Eds.; Plenum Press:
      New York; 1972, 61-84.
15.   Chawla, A. S.,; Chang, T. M. S. J. Appl. Polym. Sci. 1975, 19,
      1723-1730.
16.   Barton, A. F. M. "CRC Handbook of Solubility Parameters and
      Other Cohesion Parameters"; CRC Press: Boca Raton, Florida;
      1983.
17.   Spencer, H. G.; Gaddis, J. L. Desalination 1979, 117-124.
18.   Lloyd, D. R.; Meluch, T. B. In "Material Science of Synthetic
      Membranes"; Lloyd, D. R., Ed.; American Chemical Society:
      Washington, D.C., 1985.
19.   Cabasso, I. Ind. Eng. Chem. Prod. Res. Dev. 1983, 22, 313-319.
20.   Shen, T. C.; Cabasso, I. In "Macromolecular Solutions";
      Seymour, R. B. and Stahl, G. A., Eds.; Pergamon: New York, 1982;
      108-119.
21.   Yeo, R. S. Am. Chem. Soc. Symp. Ser. 1982, 180, 65-77.
22.   Van Krevelen, D. W.; Hoftyzer, P. J. "Properties of Polymers.
      Their Estimation and Correlation with Chemical Structure",
      Second Ed.; Elsevier, Amsterdam; 1976.
23.   Fedors, R. F. Polym. Eng. Sci. 1974, 14, 147-154.
24.   Burrell, H. In "Polymer Handbook"; Second Ed.; Brandrup, J.;
      Immergut, E. H.; Eds. John Wiley & Sons: New York, 1975,
      IV 337-IV 359.
25.   Hoy, K. L. J. Paint Technol. 1970, 42, 76-118.
26.   Hoy, K. L. "Tables of Solubility Parameters"; Union Carbide
      Corporation, South Charleston, W.V.; 1975.
27.   Anderson, J. E.; Hoffman, S. J.; Peters, C. R. J. Phys. Chem.
      1972, 76, 4006-4011.
28.   Fang, H. H. P.; Chian, E. S. K. J. Appl. Polym. Sci. 1975, 19,
      1347-1358.
29.   Fang, H. H. P.; Chian, E. S. K. Env. Sci. Technol. 1976, 10,
      364-369.
30.   Dickson, J. M.; Lloyd, D. R. Am. Chem. Soc. Symp. Ser. 1981,
      154, 293-314.

Structure and Properties of Perfluorinated Ion-Exchange Membranes

THEIN KYU

Polymer Engineering Center, The University of Akron, Akron, OH 44325

This review paper presents the relationships between
structure and properties of perfluorinated ion-exchange
membranes. The state-of-the-art characterization
methods employed in the structural investigation of
ionic aggregates are reviewed. The techniques include
wide-angle x-ray diffraction (WAXD), small-angle x-ray
scattering (SAXS), small-angle neutron scattering
(SANS), light scattering (LS), electron microscopy
(EM), nuclear magnetic resonance (NMR), Mossbauer and
Fourier transform infrared spectroscopy (FTIR). The
effects of water absorption on the domain structure of
the ionic species are discussed. Stress relaxation
studies under various environments such as vacuum,
water, methanol and electrolyte solutions are de-
scribed. The relaxation mechanisms of the precursor,
acid and salt forms of the perfluorinated membranes
are examined by means of dynamic mechanical, dielectric
and NMR studies. The influence of various parameters
such as the effect of neutralization, the kind of
counterion and the crystallinity on the viscoelastic
properties is investigated.

The field of ionomers, that is polymeric materials containing
ionic groups, has undergone a remarkable growth in recent years.
This is evidenced by the amount of literature on ionomers and by the
appearance of two monographs devoted to the subject (1,2). Most of
the research effort on the ionomers has focused on only a small
number of materials, notably ethylenes (3-9), styrenes (10,11),
rubbers (12-16) and recently aromatic (17) and fluorocarbon-based
ionomers (18). The last material is known for its high water
permeability and cation permselectivity. Because of its unique
properties, it has been employed as an ion-exchange membrane in
chlor-alkali cell operations in electrochemical industries.
Perfluorinated ion-exchange membranes are the subject of the present
chapter.

Perfluorinated ion-exchange membranes are derived from co-polymers of tetrafluoroethylene (TFE) and a perfluorovinyl ether terminated by a sulfonyl fluoride group. The precursor of the perfluorinated membrane has the form

$$- (CF_2CF_2)_n — CF_2CF —$$
$$(OCF_2CF \longrightarrow)_m OCF_2SO_2F$$
$$\qquad\qquad CF_3$$

where the value of m may be 1 and n depends on the equivalent weight of the membrane (19-21). The sulfonyl fluoride groups can be hydro-lyzed to yield Nafion polymers in the form of sulfonic acid or various metal sulfonates. The tetrafluoroethylene main chain is hydrophobic while the acid or salt pendent groups are highly hydro-philic and are permselective to ion transport (19-23). Another class of perfluorinated cation-exchange membrane has been produced by completely or partially replacing the sulfonic acid groups by carboxylic acid. These materials are the Flemion membrane products (Asahi Glass Co. Ltd.), Neosepta-F[R] Membranes (Tokuyama Soda Co. Ltd.) and the perfluorinated membranes produced by the Asahi Chemical Industry Company (18). Recently, carboxylate perfluorinated materials have been available from DuPont Company.

As is common with many ion containing polymers, the ionic ex-change sites of the perfluorinate membranes tend to aggregate or form clusters (24-30). The existence of phase-separated, ionic domain clusters in the Nafion membranes has been clearly demonstrated by small-angle x-ray (24,26,28) and neutron scattering (26,27). This evidence has been backed up by a wide variety of spectroscopic and other characterization techniques including infrared spectroscopy (31,32), nuclear magnetic resonance (33-35), Mossbauer spectroscopy (37-39), electron microscopy (25,29), and ion transport studies (19-23). Such ionic clustering not only exerts profound effects on the mechanical and ion transport properties of these polymers but also presents a second glass transition attributable to the ionic regions (in dynamic mechanical or stress relaxation) in addition to the usual T_g of the matrix polymer. This new transition generally appears at a higher temperature than the matrix T_g. In spite of bulky and long side-groups, the precursor and its acid or salt forms are not amorphous materials, but show significant levels of crystallinity (24,39). Recently, the crystal structure has been determined by wide-angle x-ray diffraction (39).

A sizable amount of literature (24-38) exists on various aspects of ionic structure and proposed models (29, 40-42), thus interested readers are refered to the original literature. This paper presents a brief review of the recent advances in the structure and properties of perfluorinate ion-exchange membranes.

Structure

Wide-Angle X-Ray Diffraction Studies. An interesting feature of the Nafion membranes is its ability to crystallize in spite of the long side-chain groups. The presence of crystallites in perfluorinated

membranes was first noted by Gierke in wide-angle x-ray diffraction
studies (24). The level of crystallinity strongly depends on the
equivalent weight, EW. As shown in Figure 1, the amount of crystal-
linity, by resolving the amorphous and crystalline peaks, is in the
range of 12 to 22 wt % for EW of 1100 to 1500. It was observed that
neutralization of the acid membrane reduces the crystallinity.

The unit cell and crystal structure of the precursor and its
sulfonic acid form of varying equivalent weight were investigated by
Starkweather (39). According to his study, the crystal structure
appears to be similar to that of poly(tetrafluoroethylene) PTFE. The
unit cell is hexagonal in structure having a lattice dimension of
approximately 5.8 Å for the a-axis and approximately 2.6 Å for the
c-axis. The positions of the (100), (101) and (002) reflections in
the fiber pattern were unchanged by hydrolysis. The lateral crystal-
lite size was estimated to be approximately 39 Å or about eight
polymer chains, which is greater than the average separation between
side groups.

Small-Angle Scattering Studies

Small-Angle X-Ray Scattering. Small-angle x-ray scattering (SAXS)
has been of central importance in the identification of the existence
of ionic domain structure in many ion containing polymers. Ionic
aggregation occurs as a result of phase separation between ionic
groups (called clusters) and the polymer matrix. Perfluorinate ion
exchange membranes are no exception. The SAXS studies of such
membranes reveal two distinct scattering maxima characteristic of
crystalline morphology and ionic domains. This observation was first
obtained by Gierke and co-workers (24,25) on the perfluorinated
sulfonic acid membrane as shown in Figure 2. The higher angle SAXS
peak, which has been attributed to ionic aggregates, is less pro-
nounced in the dry acid sample but is still discernible. This peak
becomes more distinct upon wetting and moves to smaller angles as a
result of the swelling of the ionic region. The estimated average
size of the ionic aggregates in dry state is approximately 40 to 50 Å
depending on the equivalent weight of the membrane. It is interest-
ing to note that the SAXS peak in the acid form of perfluorinated
membranes is unique; that is, it has not been observed in the acid
form of hydrocarbon-based ionomers (7,43).

The effects of equivalent weight and the type of counterions on
the SAXS maxima were further examined by the same investigators. As
shown in Figure 3, the scattering maximum peaks appearing at higher
scattering angles gradually move to lower angles and intensify with
decreasing equivalent weight. This result is expected because lower
equivalent weight samples contain more ionic groups, hence the size
of ionic domains will be larger. The increase in the SAXS invariant
may be attributed to the increase in the volume fraction of the ionic
regions. According to the theory of small angle scattering, equal
volume fractions of two-phase systems will reveal a maximum intensity.
Any continued increase of ionic volume fraction exceeding that of the
matrix polymer will lead to a reduction in scattered intensity.

The effect of different counterions on the SAXS profile is shown
in Figure 4. Little change in the position of the scattering maximum
is seen with changing cation. The scattered intensity increases as
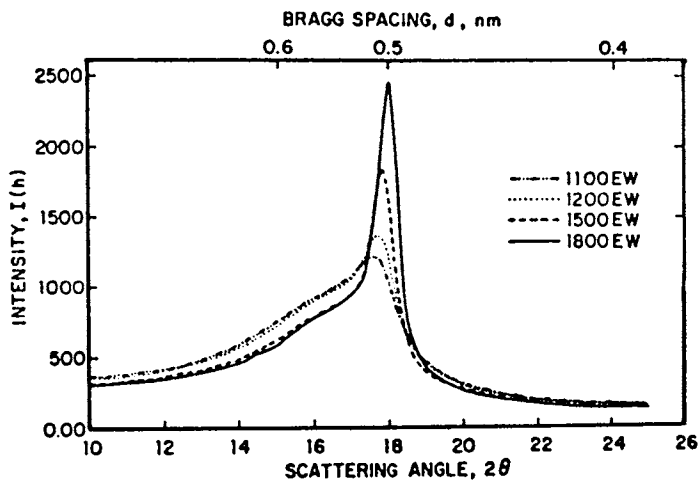
Figure 1. Wide-angle x-ray diffraction scans from precursor polymer with various equivalent weights. Reproduced with permission from Ref. 25. Copyright 1981 John Wiley & Sons, Inc.
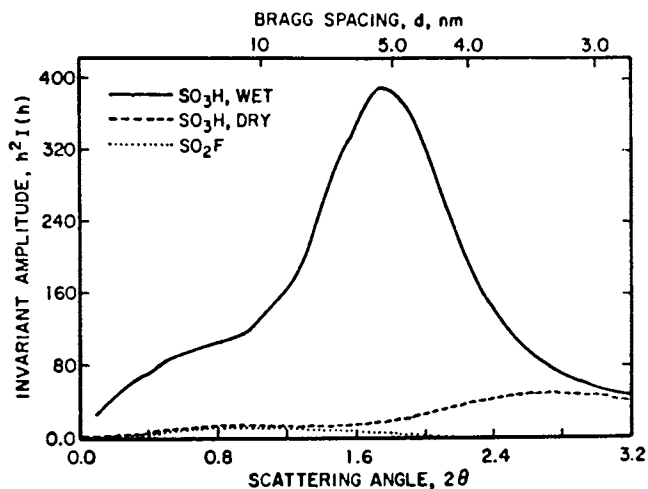
Figure 2. Small-angle x-ray scattering invariant versus scattering angle for 1100 equivalent weight precursor and its acid form showing the effect of hydration. Reproduced with permission from Ref. 25. Copyright 1981 John Wiley & Sons, Inc.
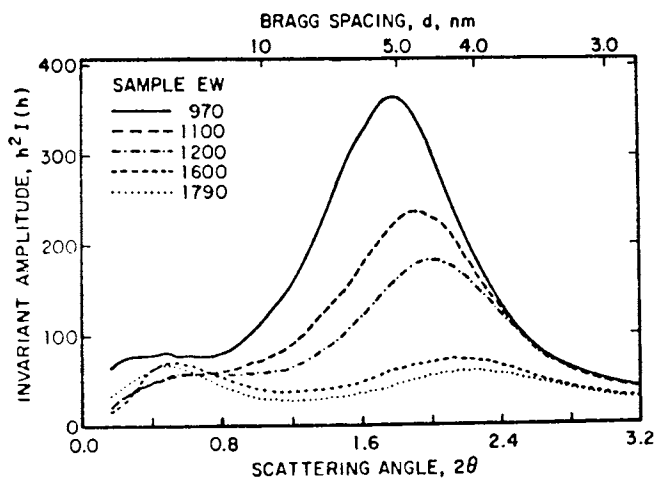
Figure 3.   Small-angle x-ray scattering scans of hydrolyzed Nafion-Na
with various equivalent weights. Samples are conditioned
by boiling in 0.2% NaOH for 1 h. Reproduced with permis-
sion from Ref. 25. Copyright 1981 John Wiley & Sons, Inc.
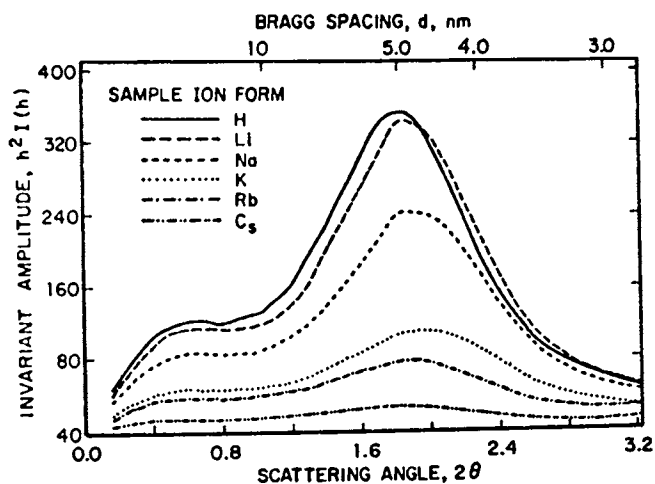
Figure 4.   Small-angle x-ray scattering scans of hydrolyzed Nafions
in various ion forms swollen with water. Samples are con-
ditioned by boiling 1 h in water. Reproduced with permis-
sion from Ref. 25. Copyright 1981 John Wiley & Sons, Inc.

the cation size decreases. This may be a consequence of either a change in absorption or a change in electron density contrast for x-ray scattering between the ionic clusters for heavier cations, which are also less hydrophilic (19,20). This observation parallels the effect of the level of water absorption of Nafion-Li as shown in Figure 3, in that the peak shifts to lower scattering angles with increasing water content. The scattered intensity increases concurrently. This may be explained by the increase in the electron density contrast of the hydrophilic ionic region and the matrix polymer.

Similar dual scattering maxima were also observed by Fujimura et al (28) on both carboxylate and sulfonate perfluorinated membranes . The higher angle scattering peak corresponding to ionic regions is not distinct in the case of carboxylic acid samples, but it becomes obvious with hydration. In a subsequent paper (29), they examined the deformation mechanism of ionic domains by SAXS. Two dimensional SAXS contour patterns are depicted in Figure 5. The pattern elongates in the direction perpendicular to the stretching direction and shows the movement of the peak to the equatorial region with increasing draw ratio, indicating that clusters become anisotropic in shape due to sample deformation. The microscopic deformation of clusters is smaller than the macroscopic deformation of the bulk sample. Their conclusion was that the deformation of the perfluorinate membranes is likely to be inhomogeneous.

<u>Small-Angle Neutron Scattering</u>. SANS arises due to the difference of coherent scattering length. A difference in the scattering length of 4×10^{10} cm^{-2} is generally needed to produce a reasonably good contrast. Values of coherent scattering length of CF_2 in amorphous, crystalline and side chain ionic group are 3.84×10^{10}, 4.45×10^{10} and $2.5 - 3.7 \times 10^{10}$ cm^{-2}, respectively. A larger contrast exists between the scattering lengths of the matrix chains and water. Hence, the SANS technique seems to be more sensetive to the aggregation of water molecules than to the ionic groups or the polymer structure.

A preliminary study of this kind was conducted by Roche, Pineri and coworkers (26,27) on the Nafion acid membrane with varying humidity or water content (Figure 6). A SANS maximum at low scattering angle reveals the Bragg spacing estimated to be 180 Å. This presumably corresponds to the first maximum of SAXS studies which is attributed to the long period of the crystal structure (25,28). The effect of hydration on the scattering profile can be seen from the movement of the SANS peak to lower angles and from the increase in intensity. The former may be associated with the swelling in the intercrystalline region, while the latter is attributed to the increase in the volume fraction of water.

The second SANS maximum appears at larger scattering angles. The Bragg spacing is approximately 40-50 Å. This peak is analogous to the second SAXS peak observed by Gierke (24) and others (28). It is believed to be associated with the ionic aggregation. The domain size tends to increase upon boiling in water. It seems that hydration takes place predominately in the hydrophilic ionic regions. Quasi-elastic neutron scattering studies of these membranes indicate that water molecules are freely transported, approaching the self-diffusion of bulk water (27).

Nf-SO₃Cs(IIOO)
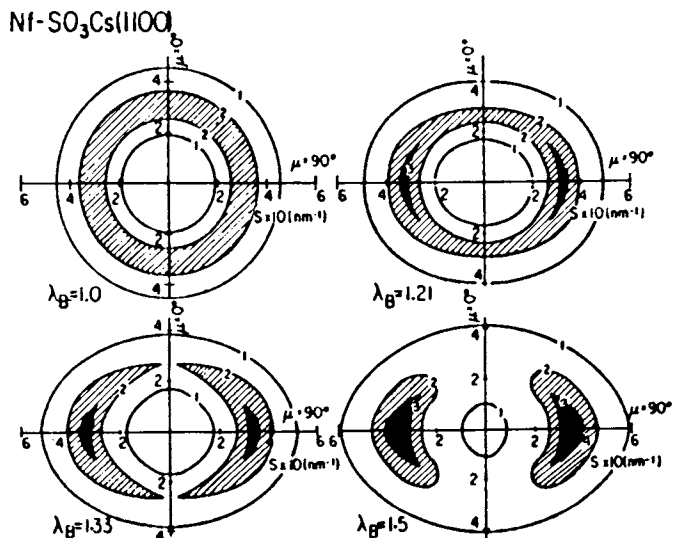
Figure 5. SAXS isointensity contour patterns from ionic region of Nafion-C as a function of draw ratio. The scattering direction is vertical. Reproduced from Ref. 29. Copyright 1982 American Chemical Society.
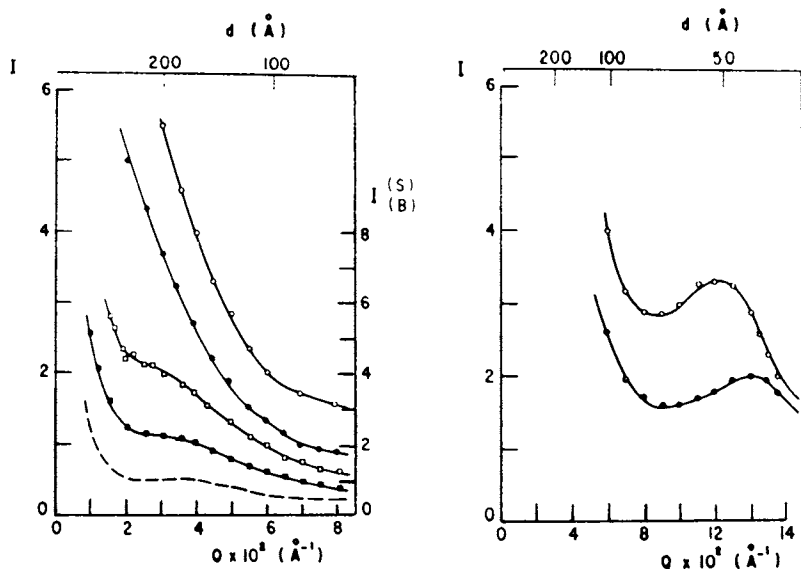
Figure 6. Small-angle neutron scattering scans from Nafion acid with various water contents, (a) low-angle SANS peak (Key: ---, dry; ■ , 50% R.H.; ☐ , 90% R.H.; ● , soaked; 0 , boiled) and (b) high-angle SANS peak (Key: ● , soaked 1 h; 0 , boiled 1 h). Reproduced with permission from Ref. 26. Copyright 1981 John Wiley & Sons, Inc.

Small-Angle Light Scattering. SALS has been used as a complementary
technique for the elucidation of the structure in perfluorinated
sulfonate and carboxylate materials (30). In general, the SALS
method is suitable for characterizing structural entities comparable
to or larger than the wavelength of light. Hashimoto et al (30)
observed a four-lobe clover pattern in the H_v scattering obtained
under cross-polarization (Figure 7). Such a scattering pattern is
characteristic of a spherulitic texture. The carboxylate membranes,
which reveal a pronounced interlamellar spacing in SAXS study, have
a higher degree of crystallinity than that of the sulfonate materials.
These carboxylates exhibit a well defined spherulitic scattering
pattern. In contrast, the sulfonates show a rather anisotropic
scattering attributed to residual local strain.

     The effect of water absorption on the H_v scattering of the
carboxylic and sulfonic acid and their Na salts was investigated by
the same authors (30). Interestingly the scattering pattern gets
larger upon water or ethanol swelling, suggesting that the scattering
entities become smaller. Considering the low level of crystallinity
in these membranes, it is conceivable that spherulites may not volume-
fill the whole system but rather are dispersed in the noncrystalline
matrix. The swelling would thus be inhomogeneous in that the degree
of swelling in the interspherulitic amorphous region would be dominant
over that within the spherulites (intraspherulite). This in-
homogeneous swelling may compress or destroy the peripheral (boundary)
regions of the spherulites, causing some reorganization of the
orientation correlation of the optically anisotropic scattering
elements of the spherulite. They noted that the change in the
spherulite size is reversible upon dehydration.

Spectroscopic Studies

Nuclear Magnetic Resonance (NMR). Alkali metal NMR is of interest
because it is a sensitive probe to monitor the immediate chemical
environment and the mobility of alkali metal ions in aqueous or non-
aqueous solvents. Sodium-23 NMR method (26.46 MH_z) was first employ-
ed by Komoroski and Mauritz (33) to study cation binding in a
perfluorinated sodium salt membrane (EW=1100) as a function of water
content and temperature. A profound chemical shift and an increase
in line width were observed with decreasing water content. These
effects reversed as temperature increased. It was interpreted that
as the amount of water or temperature is reduced, a larger fraction
of sodium ions is bound to the membrane at any given instant. This
causes the observed line width and the chemical shift to approach
the values for the completely bound species.

     In Figures 8 and 9 are shown plots of the line width and the
chemical shift respectively versus water content and the molar ratio
of H_2O/Na. The behavior of the two NMR parameters is quite similar.
The profound changes begin to occur in the range of three to five
water molecules per sodium ion. This behavior suggests the presence
of three to five water molecules in the first hydration sphere of Na^+
in Nafion sodium salt. Since sodium chemical shifts are sensitive to
only the immediate environment of the cation, the large change of
chemical shift would be a manifestation of the formation of contact
ion pairing. The ionic interaction between the bound anion and the
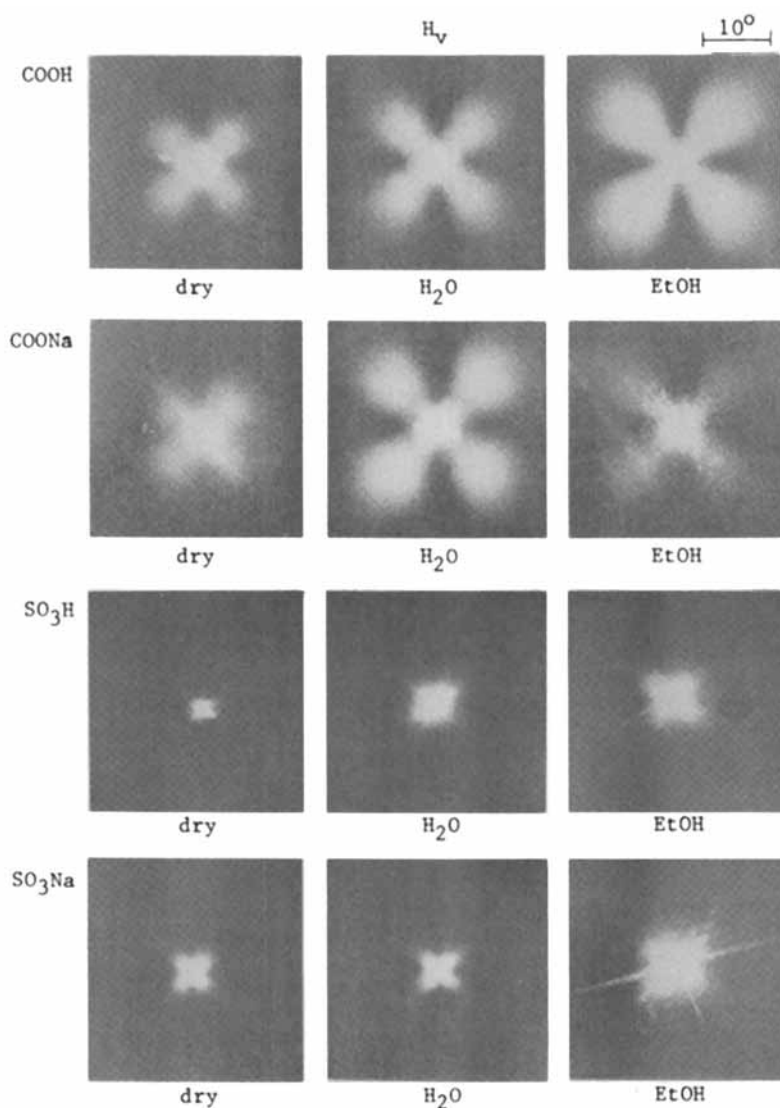
Figure 7.   Depolarized small-angle light scattering H_v patterns (under cross-polarization condition) from perfluorinate carboxylic and sulfuric acid membranes showing the effect of swelling in water and ethanol. Reproduced from Ref. 30. Copyright 1982 American Chemical Society.
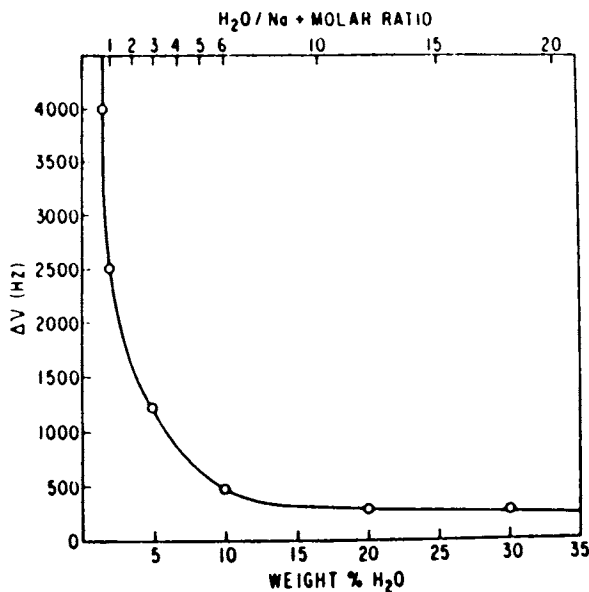
Figure 8. Plot of the sodium-23 NMR line width of Nafion-Na at 30 °C versus water content and the H_2O/Na molar ratio. Reproduced from Ref. 33. Copyright 1978 American Chemical Society.
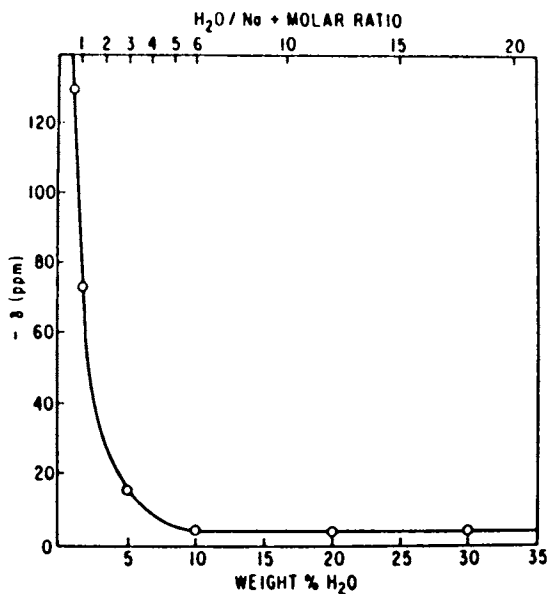
Figure 9. Plot of the sodium-23 NMR chemical shift of Nafion-Na at 30 °C versus water content and the H_2O/Na molar ratio. Reproduced from Ref. 33. Copyright 1978 American Chemical Society.

unbound cation must be strong in the dry state. The introduction of water into ionic regions will reduce the interaction and eventually will lead to the isolation of cation by water shielding. The profound water affinity will exert drastic changes in the mechanical and ion transport properties of Nafions as discussed below.

Mossbauer Spectroscopic Studies. Similar to alkali metal NMR, Mossbauer spectroscopic technique can selectively probe one isotope of a single chemical element, most commonly ^{57}Fe. Rodmacq and co-workers (36–38) have conducted Mossbauer studies of Nafion membranes by introducing iron into sulfonate ionic groups. This method is particularly useful in characterizing the immediate chemical environment, interactions of the counter cations with their surroundings and, to a lesser extent, the structure of ionic domains within the membrane. A feature common to the Mossbauer spectra of all Nafions is the disappearance of the Mossbauer absorption at approximately 225°K for Fe^{2+} and 245°K for Fe^{3+}. The temperature at which the absorption disappears is plotted against the water content of the membranes in the inset of Figure 10. The results indicate that the ferrous ions are fully hydrated when the water content exceeds 6 wt.%. They found that ferrous ions are located entirely in an aqueous phase of the membrane but were not directly incorporated in the fluoro-carbon matrix. This result is consistent with those of Na-NMR (33) and FTIR (31) studies.

In Figure 10, ln f is plotted as a function of temperature, where f is the recoilless fraction representing a nonvanishing probability for a resonant absorption process to take place. The plots follow the prediction of Debye's model (36) at low temperatures. Significant deviations are seen from characteristic temperatures at approximately 160°K. Deviations are greater as water content increases. In general, the temperature at which a break occurs in the ln f (T) curve may be identified with the glass transition of matrix backbone chains. It should be kept in mind that the Mossbauer result is inconclusive in assigning T_g, whether it is due to the ionic region or the matrix. This leads to an incorrect assignment in the original paper. This T_g, however, corresponds to the mechanical β relaxation process of Nafion salts, the origin of which will be discussed in a later section.

Fourier Transform Infrared Studies. While Na-23 NMR and Mossbauer spectroscopic methods have been extremely useful to monitor the mobility of cations in a perfluorinate ion-exchange membrane, FTIR spectroscopy is useful in examining the behavior of $—SO_3^-$ anions under similar conditions. Such a study was first carried out by Lowry and Mauritz (31) who measured the location and width of the peak corresponding to the $—SO_3^-$ symmetric stretching mode ($\bar{\nu}SO_3^-$) of the ionomer as a function of the degree of hydration and the type of counterion. It was observed that the symmetric stretching vibrational mode of the sulfonate group in Nafions is affected by changes in its local chemical environment; that is, the $\bar{\nu}SO_3^-$ peak shifts to higher frequency and broadens as the water content of the membrane decreases in Figure 11. The changes have been interpreted in terms of an increased interaction between the polyanion and the counterion as the shielding water is removed. The smaller Li^+ ion has both a stronger
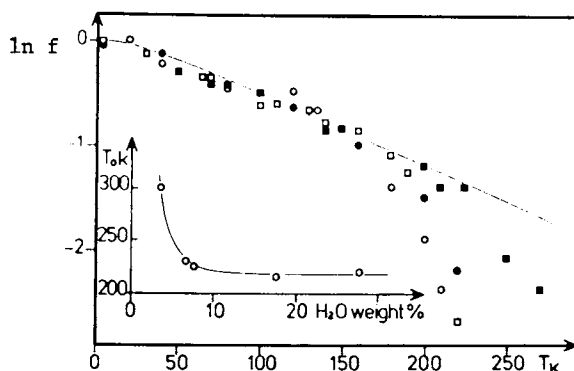
Figure 10. Plot of ln f as a function of temperature of Nafion Fe^{++}
            from Mossbauer studies (Key: ■   , 3.6% H_2O; ●, 6.6%
            H_2O; □   , 7.8% H_2O; 0, 17.5% H_2O. The solid line repre-
            sents the theoretical Inf curve with Θ_D = 140 K.) Repro-
            duced from Ref. 38. Copyright 1982 American Chemical
            Society.
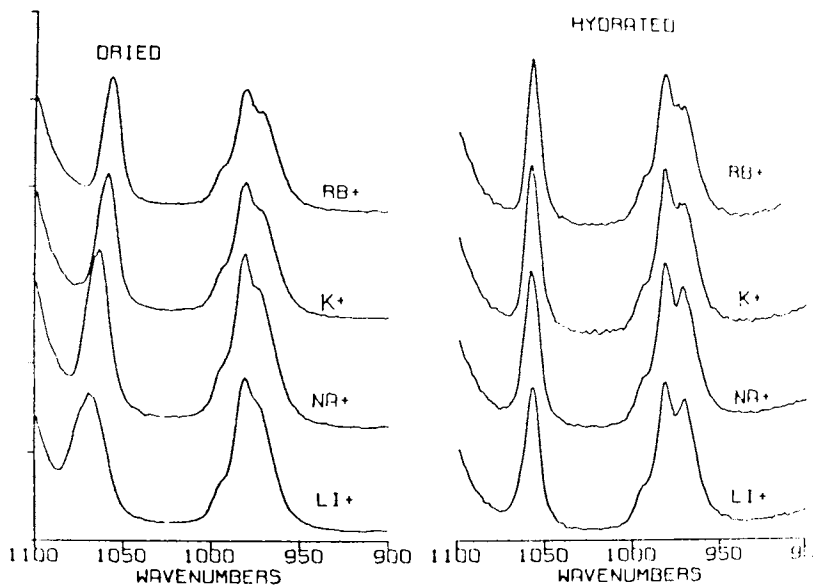
Figure 11. Infrared spectra of the —SO_3 symmetric stretch region
            from Nafion membranes in the Li^+, Na^+, K^+, and Rb^+ salt
            forms. Reproduced from Ref. 31. Copyright 1980 American
            Chemical Society.

electrostatic field at contact and a larger hydration sphere than the larger cations. This causes the largest shift for the Li^+ form upon ion pair formation. Lesser shifts are seen in the membrane containing sodium and potassium ions, and no shift is observed in the rubidium form.

To understand better the relationship between degree of hydration and $\bar{v}SO_3^-$, IR spectra were acquired as a function of water content in Nafion membranes as shown in Figure 12. The $\bar{v}SO_3^-$ peak remains fairly unchanged until the water content is below about six molecules per ion exchange site. This suggests that the shift is caused by short-range interactions; that is, formation of certain ion pairs. The pronounced broadening of the peak upon drying has been postulated to result from polarization within the sulfonate group which depends on various states of the hydration mediated disassociation equilibrium between unbound and bound ions.

A similar but more thorough examination was carried out by Falk on the geometry of ionic clusters and the interaction of water with the fluorocarbon environment using infrared spectroscopy (32). The difference of his approach from the previous IR study (31) is that instead of probing —SO_3^- anions, he focused on the behavior of H_2O and D_2O in perfluorinate ionomer. His infrared data confirmed that a minimum of about 5 water molecules are needed to complete the process of ion hydration.

Most of the small-angle scattering and spectroscopic studies suggest the presence of phase-separated ionic clusters embedded in the surrounding fluorocarbon matrix and explain the water plasticization of the ionic regions. Little is known about the interaction between water molecules and the fluorocarbon matrix. Falk observed evidence for the occurence of $O-H\cdots CF_2$ contacts from the occurence of some specific bands corresponding to the stretching region of the spectrum of HDO, H_2O and D_2O. According to Falk's model, the lone pairs of electrons on the water molecules within the clusters may interact either with a sodium ion or with an OH group of another water molecule. Similarly, the OH groups may interact either with an oxygen atom of an anion or with the oxygen atom of another water molecule. Because of electrostatic repulsion, the periphery of the cluster cannot be covered completely with — SO_3^- ions, so that some water molecules must find themselves in direct contact with the fluorocarbon phase. This explains the observation of $O-H\cdots CF_2$ contacts may also arise through the penetration of parts of the pendent side-chains into the hydrated cluster. This effect is observed through the changes of band shape of the 980 cm^{-1} band with the water content. Some effort has been made to estimate the size of the ionic domain at low water contents ($2H_2O/SO_3$ site), leading interestingly to a cluster size on the order of 12 Å. However, this estimation is model dependent and inadequate for greater levels of water content. The important conclusion here is that water molecules do interact with fluorocarbon matrix either directly or through penetration of the pendent side chains. This evidence is of crucial importance in the interpretation of the profound water sensitivity of both mechanical α and β relaxations as discussed below.

Electron Microscopic Studies.   Electron microscopy has been widely used as a means of identifying the ionic aggregate structures in many

ion containing polymers including perfluorinate ionomer membranes. A
typical micrograph of ion domain structure of a Nafion-Li membrane is
shown in Figure 13. The average size of the ionic inclusions are in
the order of 50 Å which is consistent with that obtained by small-
angle x-ray scattering studies. The interpretation of the EM micro-
graph of the ionic domains is by no means straightforward. Recently,
Handlin, Thomas and MacKnight (44), who studied the electron micro-
graphs of various hydrocarbon-based ion containing polymers, raise
serious questions whether or not the reported micrographs represent
the ionic domains. They did not, however, study perfluorinate ionomer
membranes. There is compelling evidence of the existence of ionic
aggregates in Nafion membranes as demonstrated by many spectroscopic
and radiation scattering techniques (24-38). Hence, the controversy
in the interpretation of EM micrographs should not influence the
conclusion that the perfluorinate ionomer membranes are indeed semi-
crystalline polymers in which ionic aggregates are phase separated
from the fluorocarbon matrix. We shall examine the effect of the
three-phase structure on the physical properties of these membranes
in a subsequent section.

Properties

Undervacuum Stress Relaxation Studies. The stress relaxation
behavior of the Nafion system presents some unusual characteristics.
The relaxation master curves of the precursor, as well as of Nafion
in its acid and salt forms, are very broad and are characterized by a
wide distribution of relaxation times. The individual stress relaxa-
tion curves and the master curves for the precursor (45), Nafion acid
and Nafion-K (46), are shown in Figures 14, 15 and 16 with the
reference temperatures indicated in the captions. Time-temperature
superposition of stress relaxation data appears to be valid in the
precursor and in the dry Nafion acid, at least over the time scale
of the experiments. In the case of Nafion-K, time-temperature super-
position is not valid, because it leads to a breakdown at low tempera-
tures, which is reestablished at high temperatures (above 180°C).
Similar behavior was also observed for a low molecular weight $(5x10^4)$
styrene ionomer. The addition of small amounts of water to the
Nafion acid can lead to a breakdown in the time-temperature super-
position. The influence of crystallinity and of strong ionic inter-
action will be discussed in the section on underwater stress relaxa-
tion studies.

The ten-second tensile moduli, $E(10 \text{ sec})$ of the precursor, the
Nafion acid and the Nafion-K salt are plotted versus temperature in
Figure 17. The primary relaxation temperature of the precursor rose
dramatically upon ionization. This dramatic rise in the glass
transition is undoubtedly related to the effects of ion aggregation
which will be discussed in detail in a subsequent section.

Underwater Stress Relaxation Studies. The underwater stress relaxa-
tion studies on Nafion perfluorinated ion-exchange membranes were first
conducted by Kyu and Eisenberg (47,48). The primary objective of
their studies was to elucidate the nature of ionic aggregation and
its effect on the primary relaxation (α process) in the materials by
introducing water into the ionic region. Due to the hydrophilic
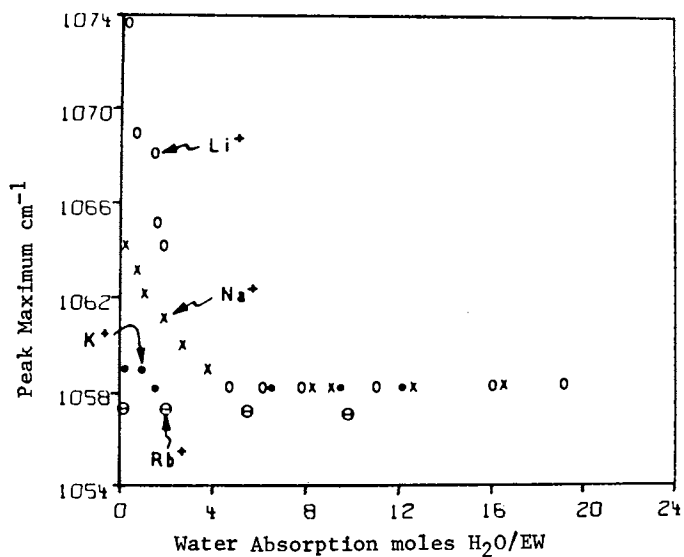
Figure 12. Plots of the —SO₃ symmetric stretch peak maxima as a function of the H_2O/SO_3 mole ratio for various salts of 1100 EW Nafion. Reproduced with permission from Ref. 32. Copyright 1983.
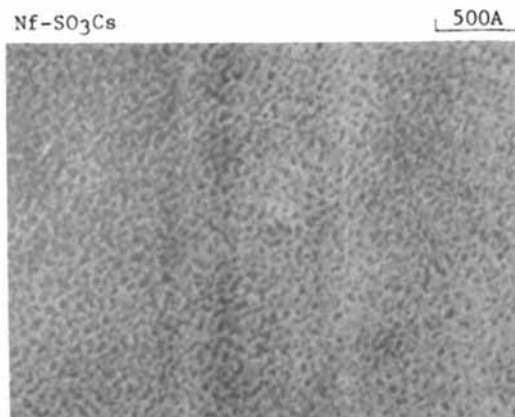
Figure 13. Typical transmission electron micrograph of an ultrathin section (about 60nm) of cesium sulfonate groups having 1100 EW. Reproduced from Ref. 28. Copyright 1981 American Chemical Society.
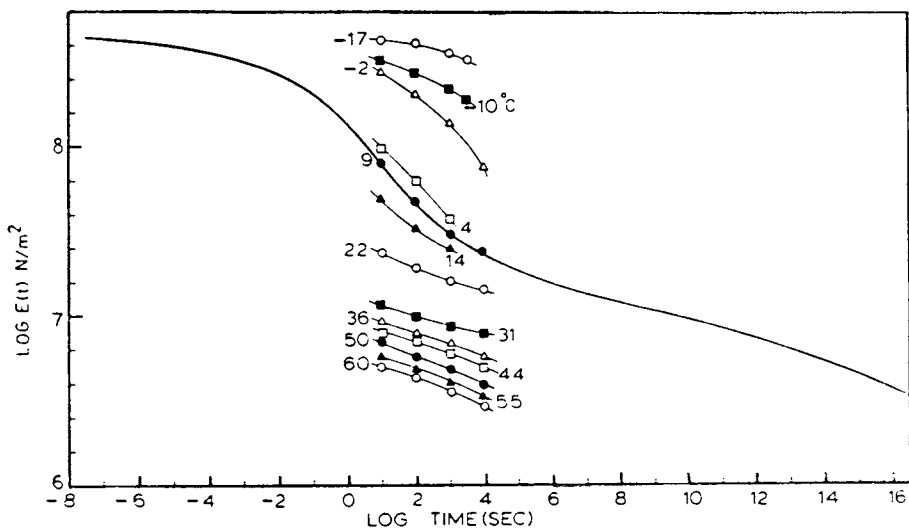
Figure 14. The individual stress relaxation curves and master curves
reduced to the reference temperature of 9 °C for the
precursor. Reproduced from Ref. 45. Copyright 1978
American Chemical Society.
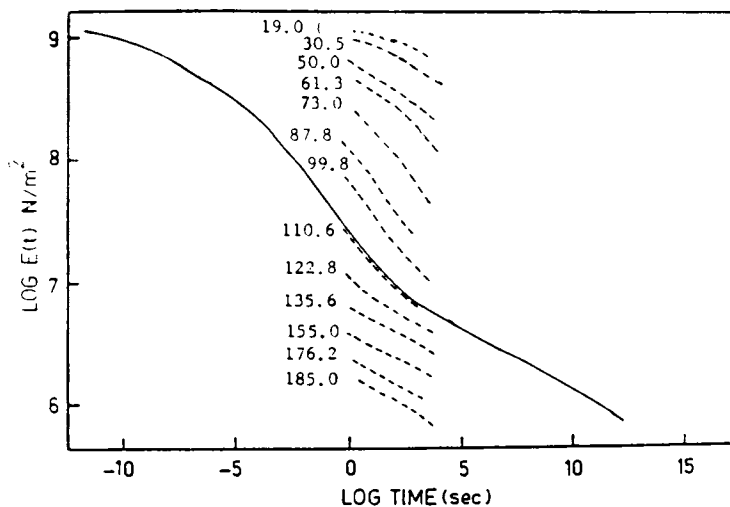
Figure 15. The individual stress relaxation curves and master curves
reduced to the reference temperature of 110 °C for Nafion
acid. Reproduced with permission from Ref. 46. Copy-
right 1977 John Wiley & Sons, Inc.
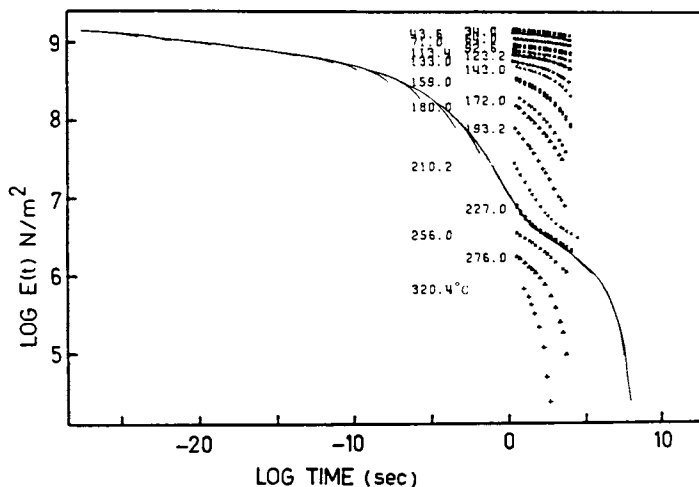
Figure 16. The individual stress relaxation curves and master curves reduced to the reference temperature of 227 °C for Nafion-K. Reproduced with permission from Ref. 46. Copyright 1977 John Wiley & Sons, Inc.
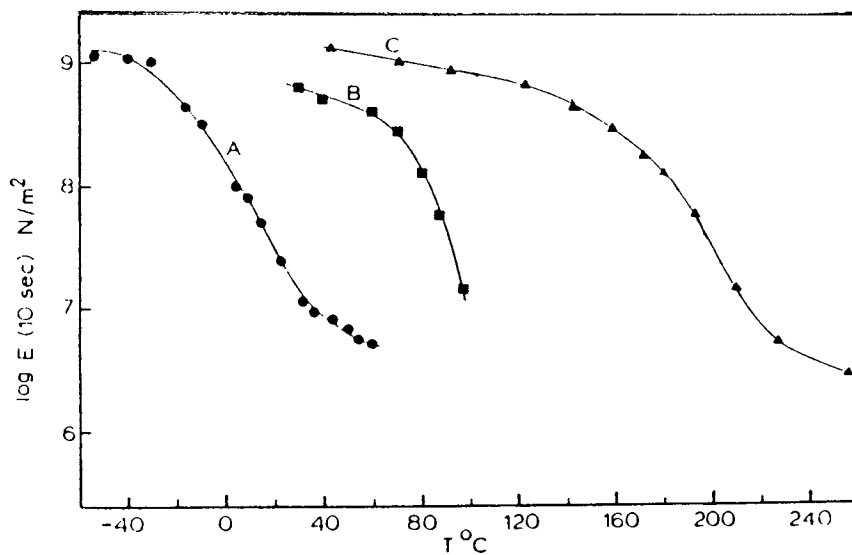
Figure 17. The comparison of E (10s) vs. temperature curves for the precursor, Nafion acid and Nafion-K; A. precursor; B. Nafion acid; and C. Nafion-K. Reproduced from Ref. 45. Copyright 1978 American Chemical Society.

nature of the ionic aggregates, water plasticization can be expected
to occur preferentially in the ionic regions, although, as discussed
above, it should also take place at the surface of the fluorocarbon
regions (18,32). The ionic contribution to the primary relaxation
process should therefore be drastically reduced by the introduction
of water into the Nafions.

   In the experiments, the specimen was stretched and held at a
constant length in a water environment. The decay of the stress on
the membrane was monitored as a function of time and temperature.
Typical results of the underwater stress relaxation studies of Nafion
acid (EW=1200) and its sodium and barium salts are displayed in
Figure 18. The degree of neutralization of the Na and Ba salt forms
are 90% and 77%, respectively. The relaxation behavior appears to be
similar for these three samples. The modulus values for Nafion-Na
are comparable to those of the corresponding divalent Ba salt at most
temperatures, while the moduli for the acid membrane are somewhat
lower as a result of higher water absorption. These values are one
order of magnitude lower than those in the dry state.

   These features are more evident in the comparison of time-
temperature superposed master curves for the three systems, reduced
to a reference temperature of 50°C by a combination of horizontal and
slight vertical shifts as shown in Figure 19. The master curves for
the monovalent Na and divalent Ba salts are almost identical. The
acid sample exhibits a similar relaxation behavior to those of the
corresponding monovalent and divalent salts except that the elastic
modulus is slightly lower for the acid, a feature which is probably
due to the difference in the degree of water absorption of the acid
and salt samples (19,49). As the swelling of Nafion acid in water is
greater than that of the salts, it is reasonable to expect the acid
form to have a lower modulus. As the superposition was only conduct-
ed in a limited part of the glass transition region, a detailed
consideration of the superposition procedure and the value of the
activation energy in not warranted. Only the shape and the magnitude
of the relaxation curves are significant.

   The most striking behavior of these underwater stress relaxation
studies is perhaps the great similarity of the superposed master
curves of the acid and the corresponding salts. In contrast, the
corresponding conventional stress relaxation curves in the dry state
are significantly different from one another as discussed above. The
phase-separated hydrophilic regions are expected to contain a sub-
stantial fraction of the ether side-chains, anchored in the ionic
domains by their end groups. In the dry state, the Coulombic inter-
actions within the ionic aggregates would be so strong that these
domains would serve as effective cross-links, reducing not only the
mobility of molecules within the domains but also controlling the
mobility of the fluorocarbon matrix through the anchored side-chians.
This would lead to an increase in the primary relaxation temperature
because of the close proximity of the ionic aggregates.

   When the samples are immersed in water, the ionic domains swell
due to their hydrophilic nature. According to Mauritz et al (31,33)
the direct interaction of the bound anion and the unbound cation
would be reduced upon hydration, the cation becoming highly mobile
with increasing degree of hydration. This suggests that the strength
of the ionic association as well as its effect on the glass transition
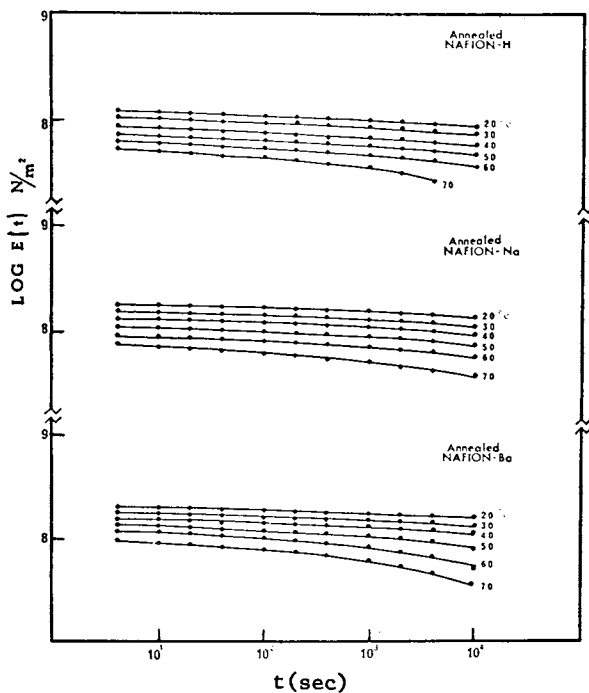
Figure 18. Typical underwater stress relaxation results at various temperatures for Nafion acid, Nafion-Na, and Nafion-Ba. Reproduced with permission from Ref. 47. Copyright 1984 John Wiley & Sons, Inc.
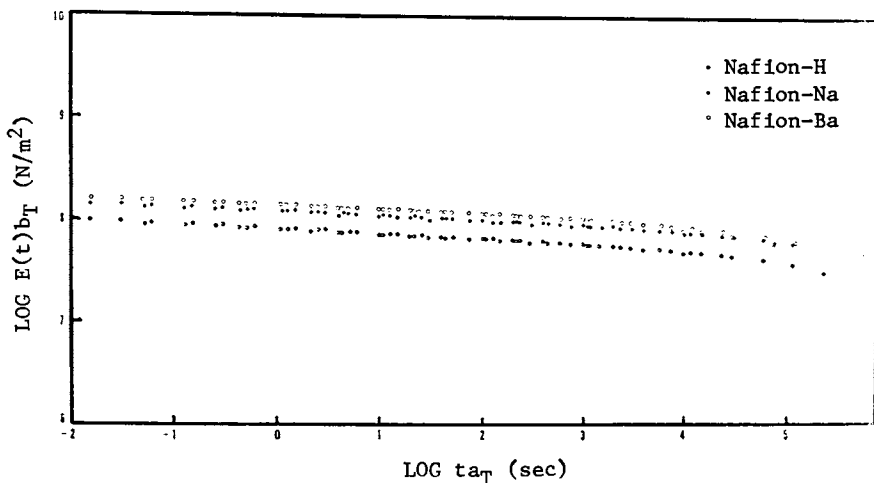
Figure 19. Time-temperature superposed master curves for Nafion-H, Nafion-Na, and Nafion-Ba reduced to a reference temperature of 50 °C. Reproduced with permission from Ref. 47. Copyright 1984 John Wiley & Sons, Inc.

of the matrix would be reduced by hydration. This is analogous to
the well explored ionic domain plasticization effect (50) in which
stress relaxation is accelarated in plasticized specimens relative to
dry samples. The resemblence of the underwater stress relaxation
curves for the three systems implies that the relaxation process may
be independent of the kind of counter cation in the underwater tests.
The counter cation may be isolated from the bound anion by water
shielding, resulting in a weakening of the interaction between the
cation and the anion. Hence the nature of the counterion would have
an insignificant effect on the mechanical relaxation in water
environment. It was concluded that the increase in the primary re-
laxation temperature upon neutralization of Nafion membranes in the
dry state is due mainly to the strong ionic interaction.

     Another factor which enhances the relaxation temperature of
Nafion membranes is the presence of crystals in the materials. An
amorphous Nafion-Na was prepared by quenching the melt (at 300°C)
into ice water (0°C). A comparison was made between the stress
relaxation behavior of the as-received, semicrystalline and quenched
amorphous Nafion-Na in the dry state and in the underwater condition
(Figure 20). As expected, the relaxation in the amorphous material
is faster than in the semicrystalline sample. It was concluded that
chain mobility is hindered both by the presence of crystalline
regions which immobilize backbone segments and by the ionic
aggregates. The underwater stress relaxation study alone is, however,
inconclusive in distinguishing whether the primary relaxation is due
to the glass transition of ionic region or due to the T_g of the
fluorocarbon matrix. This leads to the utilization of undermethanol
stress relaxation as discussed in the following section.

Undermethanol Stress Relaxation Studies. While water preferentially
plasticizes the ionic domains, methanol can possibly swell, at least to
some extent, both the ionic regions and the polymer matrix of the
Nafions via interaction with the side-chains (51). The undermethanol
stress relaxation was carried out by Kyu and Eisenberg (47) on both
semicrystalline and amorphous Nafion-Na in order to elucidate the
effect of additional swelling by methanol on the stress relaxation
behavior. The results are depicted in Figure 21 in comparison with
those from the underwater stress relaxation studies. It is seen that
the moduli of the specimens undermethanol are almost one order of
magnitude lower than those obtained with the water plasticization,
which is undoubtedly due to the higher degree of swelling of the
Nafion polymer in methanol. A striking observation is that, while
the modulus is substantially lower in the methanol-swollen samples,
the rate of stress relaxation is not necessarily faster. Similar
behavior is also noted for amorphous Nafion. This observation may be
accounted for as follows.

     When submerged in water, Nafion swells due to water preferen-
tially plasticizing the ionic domains, although some water molecules
would plasticize the interfacial region between the matrix and the
ionic domains. This type of plasticization can greatly accelerate
stress relaxation relative to that in the dry state. In the present
case, the excessive swelling in methanol, which yields a modulus
about one order of magnitude lower than that of the water-swollen
polymer, could be caused either by swelling of the interfacial
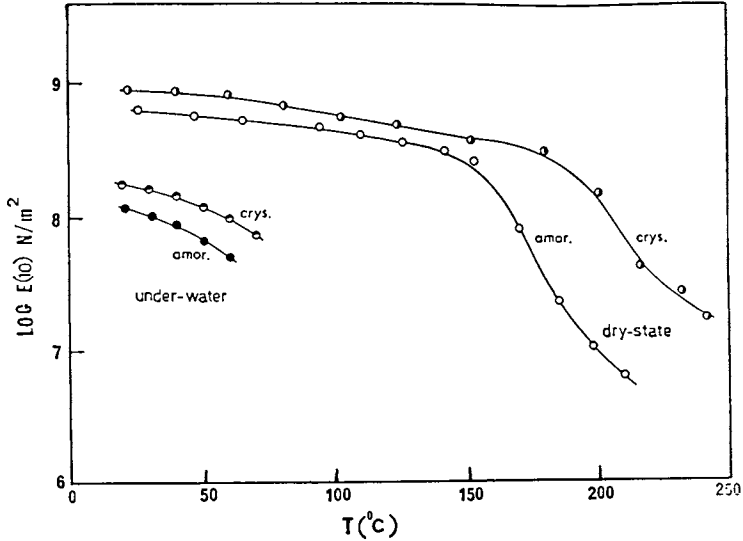
Figure 20. The comparison of E (10s) vs. temperature curves of the dry state and underwater stress relaxation studies for amorphous and semicrystalline Nafion-Na. Reproduced with permission from Ref. 47. Copyright 1984 John Wiley & Sons, Inc.
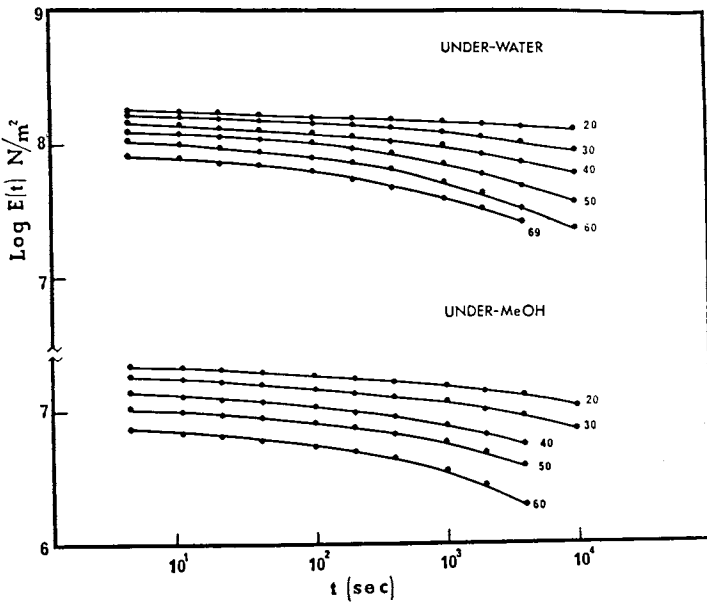
Figure 21. Undermethanol stress relaxation curves at various temperatures in comparison with those of underwater stress relaxation test of Nafion-Na. Reproduced with permission from Ref. 47. Copyright 1984 John Wiley & Sons, Inc.

regions or by increased swelling of the ionic domains (51). If such
increased swelling were to occur primarily in the ionic regions, one
would expect to observe a faster relaxation rate. Because the stress
relaxation is not necessarily faster in the undermethanol studies
than in the underwater studies, it is more likely that increased
swelling is occuring within the interfacial or the fluorocarbon
matrix region. Subsequently, it was concluded that the primary re-
laxation (α transition) region is probably associated with the glass
transition of the ionic regions.

Undersolution Stress Relaxation Studies. Kyu and Eisenberg (52) have
extended their studies further to the investigation of relaxation be-
havior under various catholyte and anolyte solutions with varying
concentrations. These measurements are useful to gain better insight
into membrane performance under severe environments such as strong
alkali solutions. Some preliminary results obtained under 0, 1, 6.25
and 12.5 M NaOH concentrations are shown in Figure 22. The stress
relaxation curves at a low level of concentration (1 M NaOH) are
similar to those of the underwater tests; that is, the values of
moduli are almost comparable, and the relaxation time remains un-
changed for the underwater and undersolution (1 M NaOH) conditions.
This observation is not surprising in view of the fact that excess
water is still present at such low levels of NaOH concentration; thus
little or no effect is expected to hinder the relaxation process.
     When the concentration reaches a level of 6.25 M NaOH, the
modulus of the Nafion membrane increases noticably while the rate of
relaxation appears to slow down. The increase of modulus values may
be attributed to the reduced swelling due to decreased water absorp-
tion of the membrane with increasing caustic concentration (53-55).
The latter observation may be due to the enhancement of the Coulombic
interaction between the bound anion and the sodium counterion within
ionic region (31, 33). Further increase in NaOH concentration to a
level 12.5 M accentuates the above tendency in that the modulus in-
creases remarkably, and the relaxation continues to slow down further.
It seems that the ionic interaction within the ionic regions is
enhanced at such high levels of caustic concentration due to reduced
water absorption. This in turn immobilizes the chains leading to de-
celeration of the relaxation process.
     The same authors continued to explore the undersolution stress
relaxation properties in various NaCl concentrations of 0, 1, 3.45
and 5.2 M. As shown in Figure 23, the relaxation patterns are
similar for different NaCl concentrations in the temperature range
investigated. Similar studies in Na_2SO_4 solutions also show no con-
centration dependence, and the relaxation curves are reminiscent of
those in NaCl solutions. It is interesting to note that while the
relaxation under NaOH solution slows down the increasing concentra-
tion, no appreciable changes are seen in the relaxation of Nafion
under various concentrations of NaCl and Na_2SO_4 solutions. The
reason for this observation is still unclear. Some anology, however,
exists in the Na^+ ion transport properties of Nafion (22,55).
     According to Burkhardt (22), the current efficiency of the
Nafion membrane exhibits unusual characteristics with respect to NaOH
concentration in the electrochemical experiment. Three distinct
regions exist in the plots of current efficiency versus caustic con-
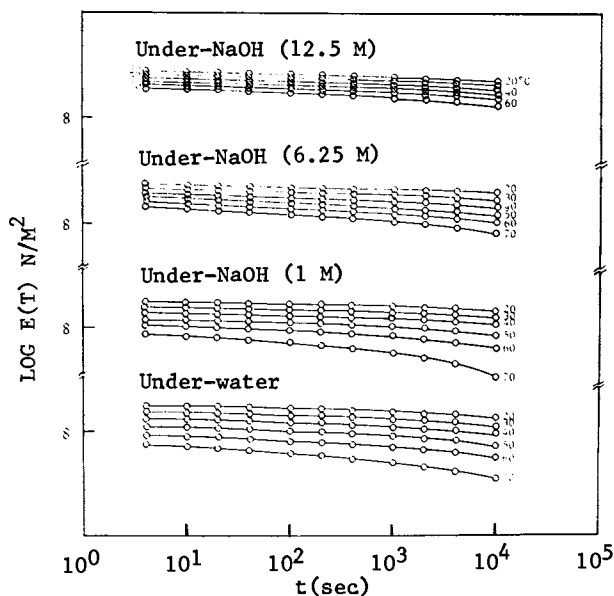
Figure 22.   Undersolution stress relaxation curves of Nafion–Na at various NaOH concentrations and various temperatures.
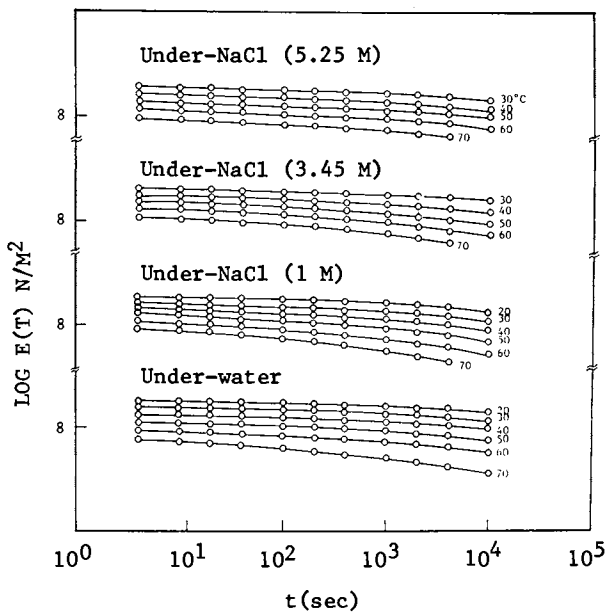
Figure 23.   Undersolution stress relaxation curves of Nafion–Na at various NaCl concentrations and various temperatures.

centration. At low concentrations of 1 to 5 M NaOH, the current
efficiency drops with increasing concentration. The current effi-
ciency then begins to increase, showing a maximum around 10 to 13 M
and decreases sharply at higher concentrations (above 13 M NaOH). On
the other hand, the current efficiency remains constant for all NaCl
concentrations. Their conclusion was that the catholyte NaOH con-
centration is more important than the anolyte NaCl concentration.
The effect of NaOH concentration on the ion transport and rheological
properties of the Nafion ion exchange membranes may be attributable
to some variation in the ionic domain structure in the presence of
NaOH. Therefore, it is extremely important to understand the ionic
domain structure under these conditions. The anomalous behavior of
Na^+ ion transport as a function of NaOH concentration is seen more
frequently in bilayer Nafion membranes in which one layer is treated
with diamine and also in perfluorinated carboxylic ion exchange mem-
branes. Several mechanisms have been proposed to explain their ion
transport results including water absorption, transport of hydroxide
ion tunneling, ion pairing mechanisms, etc. (54-56). As the ion
transport properties are beyond the scope of this review, no detailed
discussion will be presented.
    The bulging or permanent deformation of unreinforced Nafion ion
exchange membranes is often observed under conditions similar to
those employed in the electrochemical industry. This phenomenon was
considered to be associated with a rheological effect. This leads to
an investigation of stress relaxation of these ion exchange membranes
under conditions of current passage similar to those encountered in
the industrial application of these materials (57). A Nafion sample
of 1200 equivalent weight in the form of a cylindrical tube was
immersed in either a 6.25 or a 12.5 M NaOH solution between the co-
cylindrical cathode and anode. Stress relaxation measurements were
carried out with and without current passage (6 A of current applied
perpendicularly to the direction of applied stress) over the temper-
ature range from 30 to 70°C. As seen in Figure 24, the application
of current accelerates the stress relaxation, the effect being more
pronounced at elevated temperatures.

Dielectric Relaxation Studies. The dielectric properties of the pre-
cursor have been investigated by Hodge and Eisenberg (45) over a
frequency range of 10 to 10^5 Hz and a temperature range of -196 to
70°C. The temperature dependencies of the dielectric loss, ε'', at
the indicated frequencies, are shown in Figure 25. Three relaxation
peaks are evident and are labelled γ, β and α in order of increasing
temperature. Isothermal frequency spectra of the γ and β dielectric
relaxations are shown in the insets of Figure 25. The peak
frequencies of these γ, β and α relaxations are plotted against re-
ciprocal absolute temperature in Figure 26 in comparison with the
mechanical data (shown in a subsequent section). The apparent acti-
vation energies as estimated from the slopes are on the order of 73,
11.3 and 4.1 cal/mol for α, β and γ respectively. The β peak seems
to be a composite of two relaxation processes which are termed β' and
β'' in the original literature.
    Of the three labelled relaxations, the γ relaxation is by far
the most intense dielectrically. No comparable dielectric relaxation
is observed in Nafion acid or its salts (46). It was considered that
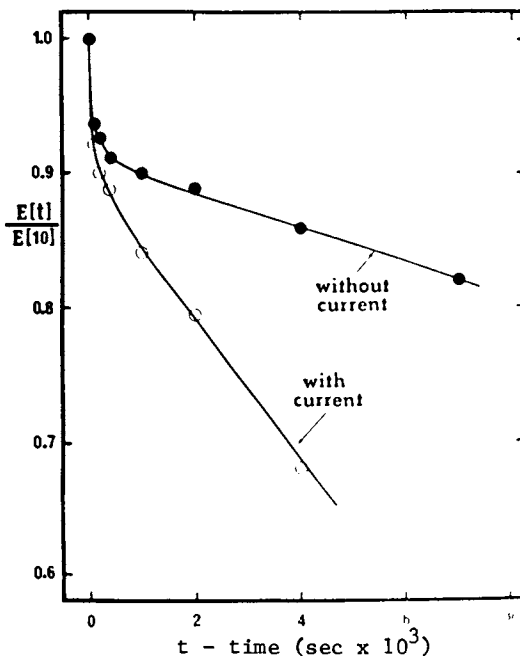
Figure 24. The ratio of modulus to 105 modulus for a Nafion tube
specimen immersed in 6.25 M NaOH at 30 °C with a 6A
current flowing and without current flowing across the
membrane. Reproduced with permission from Ref. 57.
Copyright 1983 John Wiley & Sons, Inc.
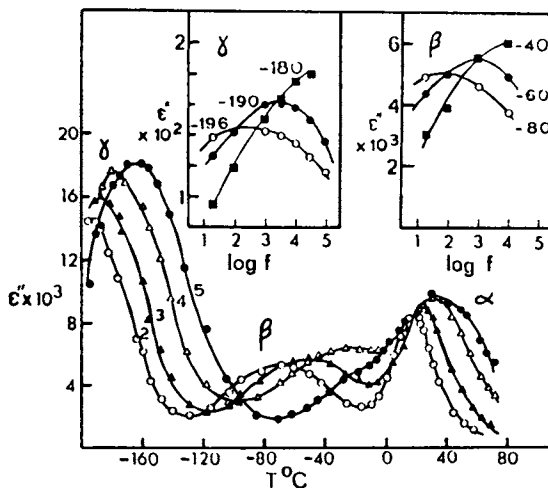
Figure 25. Temperature dependence of the dielectric loss at four
different frequencies indicated in logarithmic value.
Isothermal frequency spectra for the γ and β relaxations
are shown in the insets. Reproduced from Ref. 45.
Copyright 1978 American Chemical Society.

the γ dielectric process must be unique to the precursor. Because
—SO_2F group is the only chemical structure which is different from
that of the Nafion acid or its salts, the γ dielectric relaxation may
be associated with some kind of motion of the —SO_2F group. As will
be shown below, this dielectric γ relaxation corresponds to the
mechanical δ process of the precursor.

The composite β relaxations appearing around -80°C in the
dielectric loss spectrum of the precursor, that is β' and β'', are
identified with the motions of fluorocarbon backbone and ether side-
chains respectively. The higher temperature β'' process is dominant
in the dielectric spectrum as it originates from motions of the ether
side-chains.

The assignment of the origin of the α transition is relatively
straightforward. It is characterized by a high activation energy of
approximately 73 kcal/mol and corresponds to a large decrease in
mechanical modulus as shown below. The transition is therefore
unambiguously identified with the glass transition of the precursor.

Dynamic Mechanical Studies

The Precursor. The dynamic mechanical properties of the Nafion pre-
cursor (EW=1200) have been examined by Hodge and Eisenberg (45) and
more recently by Kyu and coworkers (58) using vibrating reed and
torsion pendulum methods. Figures 27 and 28 show the dynamic
mechanical results of the precursor obtained by the above methods
respectively. Four relaxation peaks with the revised nomenclature
(labelled α, β, γ and δ in descending order of temperature) are
evident over the temperature range from -195°C to 125°C. The tan δ
peak positions of the torsional pendulum are located 20° to 30°C
lower than those of the vibrating reed studies due primarily to the
difference in the oscillation frequency of the samples.

The lowest temperature δ peak appears at approximately -160°C in
the vibrating reed measurement whereas only the onset of δ relaxa-
tion can be seen near -180°C in the torsional pendulum test. As
discussed below, this peak is not present in the Nafion acid or in
its salt membranes in both mechanical and dielectric measurements.
The origin of this δ relaxation must be unique to the precursor,
perhaps associated with the motions of —SO_2F groups.

The G" (or E") and tan δ peaks occuring in the temperature range
from -20° to -120°C are extremely broad and skewed in both vibrating
reed and torsion pendulum experiments. These peaks are considered
to be the sum of two overlapping peaks—the β and γ relations. The
highest temperature α relaxation is seen around 5° to 20°C on the
tan δ curves; the drastic drop in G' (or E') and the sharpness of the
tan δ_G peak are characteristic of typical glass transition behavior
of a neutral amorphous polymer.

Nafion Salts. Figure 29 shows the relaxation behavior of the Nafion-
Na sample hydrolyzed from the precursor with the degree of 90% con-
version; G', G" and tan δ are plotted with respect to temperature.
Four distinct relaxation regions are evident, the peaks being
labelled α, β, β' and γ in order of decreasing temperature. The
curves are similar to those of Yeo and Eisenberg (46) with the
exception of the β' peak which appears at approximately -30°C in the
Nafion-Na.
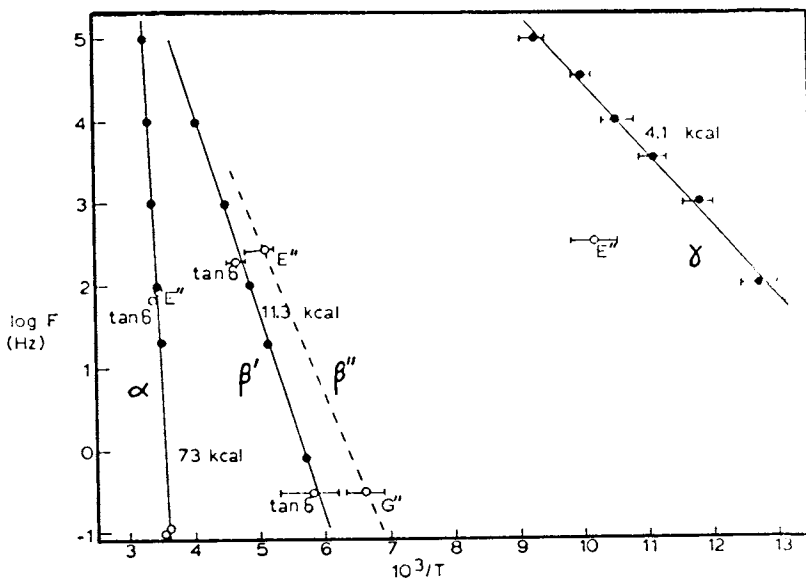
Figure 26. Plot of logarithmic peak frequency against reciprocal
absolute temperature for the four observed dielectric and
mechanical relaxations. Filled points represent dielec-
tric data whereas open circles are mechanical data.
Reproduced from Ref. 45. Copyright 1978 American Chemical
Society.
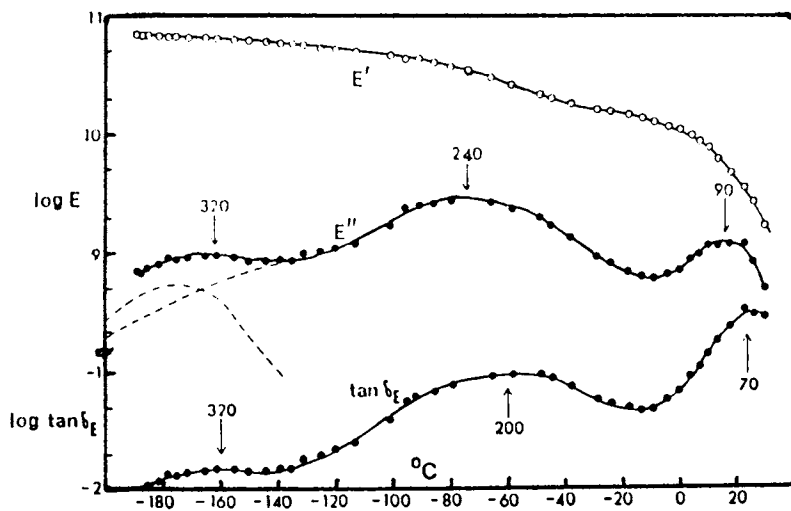
Figure 27. Temperature dependence of the mechanical tensile storage
modulus, loss modulus, and loss tangent the precursor
measured with a vibrating reed. The peak maximum fre-
quencies in Hz are indicated. Moduli are in dyn cm^{-2}.
Reproduced from Ref. 45. Copyright 1978 American
Chemical Society.
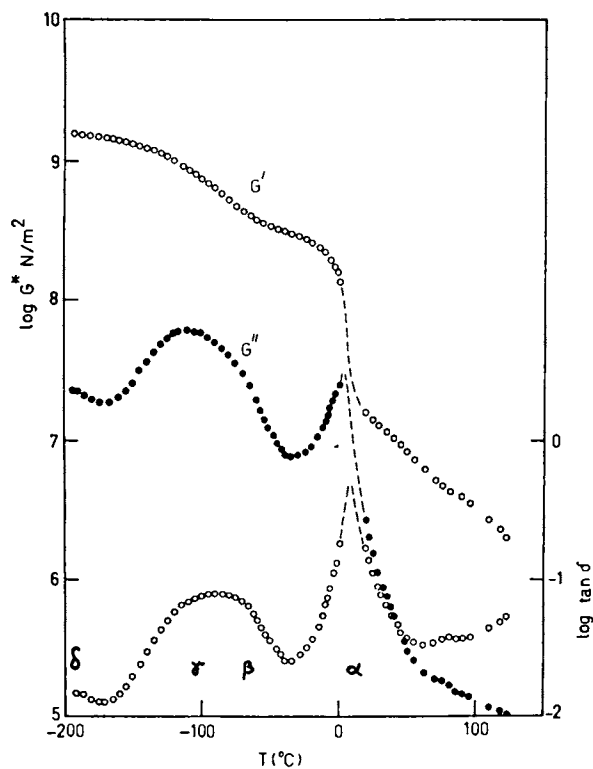
Figure 28.   Temperature dependence of the mechanical shear storage
              modulus, loss modulus, and loss tangent of the precursor
              measured with a torsion pendulum. The frequency being
              approximately 1 Hz at the γ region. Reproduced with
              permission from Ref. 58. Copyright 1983.

The lowest temperature δ peak which was detected as a tail in the spectrum of the precursor, has disappeared both in the G" and the tan δ_G curves of the 90% Nafion-Na. Also, this δ peak was not observed in the dielectric studies of the Nafion acid (46), strongly indicating that the peak may be a unique feature to the precursor which is not encountered in the ion containing Nafion materials. This relaxation was identified previously with the motion of —SO₂F groups.

In the γ region, G' decreased markedly with temperature, with the corresponding G" and tan δ_G plots indicating a peak centered around -100°C. The γ peak is more symmetrical and slightly higher in magnitude than that of the precursor, supporting the earlier suggestion that the peak which appears at approximately -100°C in the precursor could result from the overlapping of the β and γ relaxations. In addition, a minor β' peak, which is not present as a separate peak in the precursor, is seen at approximately -30°C in the highly ionized Nafion-Na sample.

The highest temperature α relaxation occurs at approximately 240°C. It is the peak of largest intensity in the tan δ_G curve, with the β peak appearing as a shoulder at approximately 140°C. This observation is consistent with the previous study by Yeo and Eisenberg (46), but the assignments of the origins of these peaks are reversed by Kyu et al (58). The reasons for this reversal will be discussed below.

Nafion Acid. The dynamic mechanical behavior of Nafion acid (EW=1365) was investigated by Yeo and Eisenberg by means of a torsion pendulum in a temperature range of -150°C to 250°C (46). A similar study on a Nafion acid of 1155 equivalent weight was performed by Kyu, Hashiyama and Eisenberg (58). A slight variation in the equivalent weight of the membrane does not appreciably affect the relaxation behavior. The temperature dependence of the storage shear modulus, G', and the loss tangent, tan δ, of the Nafion acid is shown in Figure 30. Three dispersion regions, labelled α, β and γ in descending order of temperature, are evident in the tan δ versus temperature curve. Of the three mechanical relaxations, the α peak shows the largest intensity. The β peak is located between the pronounced α and γ peaks.

The mechanical γ peak occurs at approximately -100°C at about 1Hz for the acid which corresponds to the γ peak found in PTFE (polytetrafluoroethylene) and the Nafion salts in the same temperature region. According to Yeo and Eisenberg (46), the γ peak position remains unaffected by the variations in counterion size and degree of neutralization.

The mechanical β peak in the dried acid occurs at approximately 20°C. The water sensitivity of the β peak position is remarkable (46). This β peak migrates to lower temperatures with increasing water concent and eventually merges with the γ peak. The depression of the β peak temperature with moisture content is also found in the dielectric measurement on the same Nafion acid. Similar behavior was observed for the salts, the decrease in temperature of β peak position with increasing water content being perhaps even more drastic.
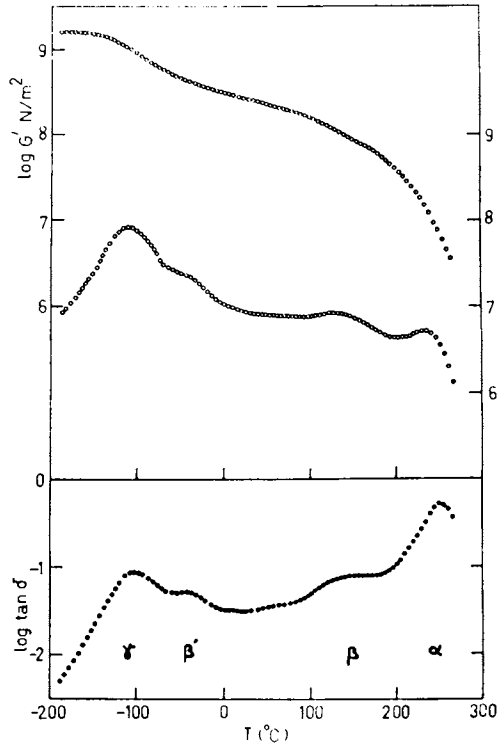
Figure 29.   Variations of G', G", and tan δ_G with temperature for
             Nafion-Na from a torsion pendulum. The frequency being
             1 Hz at the γ region. Reproduced with permission from
             Ref. 58. Copyright 1983.
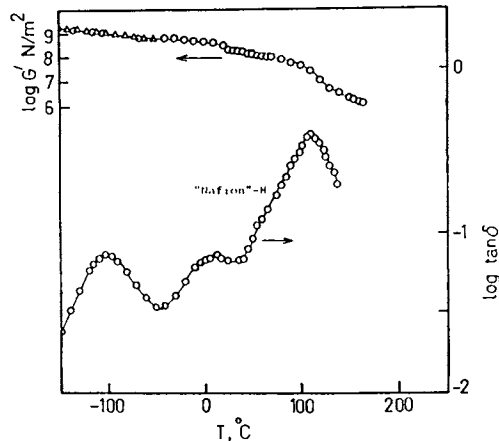
Figure 30.   Variations of G' and tan δ with temperature for Nafion
             acid. The frequency being approximately 1 Hz at the γ
             region. Reproduced from Ref. 30. Copyright 1982 American
             Chemical Society.

The α peak is located at approximately 110°C for the acid sample. Examination of moisture content on the α peak is ambiguous because samples loose water during the course of increasing temperature. Preliminary evidence from Yeo (59) is that the α peak is insensitive to moisture content. This leads originally to the suggestion that the α peak might be associated with the fluorocarbon matrix due to its hydrophobic nature while the β peak is attributed to the hydrophilic ionic domain due to its profound water sensitivity. However, a recent study (47), as mentioned above, presents evidence of a definite shift to lower temperature of the primary transitions of Nafion acid and its sodium salt upon immersion in water, relative to those obtained in the dry state. On the basis of this observation along with additional evidence from dynamic mechanical studies (58), Kyu and Eisenberg (48) reversed the original assignments of the α and β peaks. Recently, the water sensitivity of the α peak in partially neutralized perfluorinated carboxylic acid sample has been confirmed by Nakano and MacKnight (60) in the dynamic mechanical studies.

Another interesting feature is the qualitative similarity of the behavior of tan δ versus temperature of the Nafions to that of other ionomer systems (2, 61). In the hydrocarbon-based ionomers studied to date, two tan δ have been observed in the glass transition region. The one occurring at the lower temperature is generally identified with the matrix T_g while the one at the higher temperature, which usually has the greater magnitude, is attributed to the T_g of the ionic regions. As an example one may consider the studies of Rigdahl and Eisenberg (61), who investigated polystyrene sulfonated to varying extents and who showed that the 2 to 9 mole % samples exhibit the ionic T_g peak at higher temperatures and with a greater intensity than that of the styrene matrix. Many other examples exist (2). Because the Nafions are not an exceptional class of ionomer, the original assignments regarding the α and β peaks could be reversed. Further evidence in support of the reversal of assignments of α and β in Nafions were obtained by Kyu et al (58) and are presented in subsequent sections.

Effect of Counterions. The influence of the type of counterions of Nafion membranes on the dynamic mechanical properties of the materials was examined by Yeo and Eisenberg (46), comparing the results of Li^+, Na^+, K^+ and Cs^+ salts in Figure 31. In the high temperature α relaxation region, the position of the tan δ peaks for Na^+, K^+ and Cs^+ salt is, except for the Li^+ salt, in qualitative agreement with the $T_g \propto cq/a$ relation (where c stands for ion concentration, q for electrical charge and a for distance between centers of charge of anion and cation), which has been found operative in many ion containing polymers (2). The comparison of the α peak positions can be influenced by the degree of neutralization as well as by the degree of crystallinity. In addition to the above mentioned effects, it is conceivable that the effect of residual water, even at these high temperatures, may be responsible for the failure of the Li^+ ion to fit the relation. The effect of water on the position of the α peak could not be studied because the salts lose water at a rapid rate at elevated temperatures.

A comparison of the position of the β relaxation peaks for
various counterions was not performed due to the extreme water
sensitivity of the β peak. A slight presence of moisture can drasti-
cally affect the results. In the lowest temperature γ region, it was
found that the γ peak position is unaffected by variations in
counterion size and degree of neutralization as demonstrated in a
later section. However, magnitude of the tan δ peak in γ region is
inversely proportional to the counterion radius, except for the acid
for which it is anomalously low. Introduction of water into both the
acid and the salts does not appreciably affect the position of the γ
peak, at least at the low levels of water content investigated.

Because the effect of neutralization by monovalent cations on
the mechanical relaxations presents interesting features, it is also
of interest to explore the effect of divalent cations. A preliminary
study of this kind was conducted by Kyu and coworkers (58). Nafion
acid of 1155 EW was neutralized with an appropriate $BaCl_2$ solution to
prepare a Ba-salt sample. The torsion pendulum results in the form
of G', G" and tan δ versus temperature are depicted in Figure 32. A
peak is evident at approximately -90°C in the tan δ and G" curves.
Judging from the peak temperature, this γ relaxation is probably
caused by the same mechanism as in the acid and the monovalent salt
samples described before. The β peak occurs at approximately -20°C
and thus overlaps slightly with the γ peak. The observation of the
β region at such a low temperature may be due to the presence of
residual water which would reduce ionic interactions within the ionic
domains and in turn would enhance backbone mobility.

A clear drop in G' and the corresponding peak in G" are discern-
ible at about 275°C. This peak is possibly due to the crystal melt-
ing process, as it corresponds to the crystal melting temperature
found in the DSC (47) and in the WAXD studies (28) of the monovalent
Nafion salts. It is also conceivable that the glass transition
temperature of the material has been raised to that level, and that
the peak in this case may be due to two mechanisms; that is, crystal
melting and/or T_g of the ionic region. The α peak is not observed in
the tan δ plot, at least up to about 320°C. Comparing the tempera-
ture dependence of G' of the Ba-salt with those of monovalent cations.
This phenomenon is expected from the q/a effect on the T_g, which has
been found operative in many ion-containing polymers (2). This
feature supports the idea that the α peak is most likely attributed
to the glass transition of the ionic regions because it is hard to
understand the matrix T_g to be higher than the crystal melting
temperature. Hence, the assignment of the α and β peaks respectively
to the T_g of ionic region and that of the Nafion matrix seems more
reasonable.

Partially Ionized Nafion-Na. Partially ionized samples were prepared
by Kyu et al (58) by immersing the precursor samples in a 10% NaOH
solution at approximately 75°C for varying periods of time. The
precursor is a hydrophobic material, therefore NaOH diffusion must be
extremely slow initially with the conversion taking place primarily
at the surface of the sample. Once the outermost layer is converted
to the Nafion salt, the rate of water diffusion appears to be greatly
enhanced, allowing the conversion of the inner layers into ionic
Nafion material. The conversion is therefore expected to occur layer
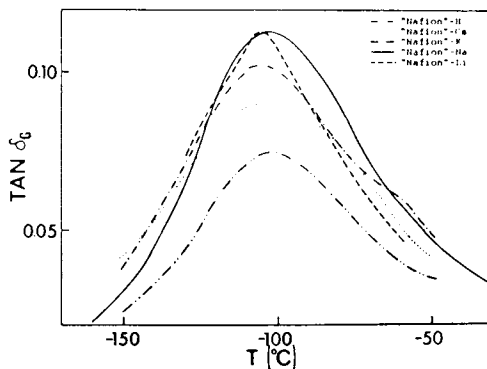
Figure 31. Mechanical loss tangent versus temperature for Nafion with various counterions in the γ relaxation region at approximately 1 Hz. Reproduced from Ref. 30. Copyright 1982 American Chemical Society.
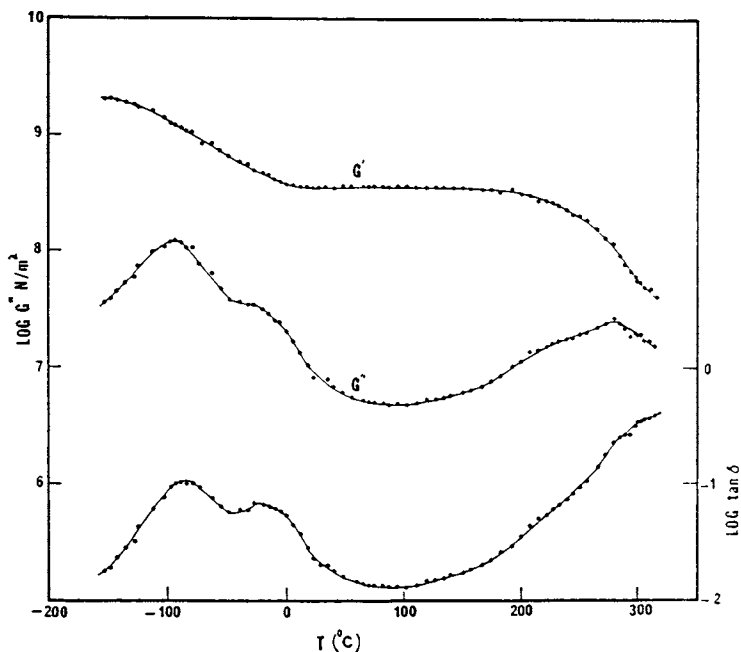
Figure 32. Variations of G', G", and tan δ with temperature for Nafion-Ba (EW = 1155 with 77% neutralization). The frequency being approximately 1 Hz at the γ region. Reproduced with permission from Ref. 58. Copyright 1983.

by layer producing a heterogeneous material with a "sandwich" struc-
ture, which is a composite of the Nafion salt (outer layer) and the
precursor (inner layer). The degree of conversion as estimated from
the weight change of the —SO$_2$F to —SO$_3$Na were about 10%, 34%, 56%,
79%, 86% and 90% neutralization.

The dynamic torsional pendulum results of these partially
ionized Nafion specimens are shown in Figure 33. The low temperature
δ relaxation of the precursor, previously observed in dielectric and
vibrating reed studies, was detected as an increase in the energy
dissipation over the temperature range around -185°C in the present
torsion pendulum experiments. The gradual disappearance of the δ
peak with increasing degree of conversion confirms that the relaxation
mechanism involved must be unique to the precursor; it may be associ-
ated with the motion of —SO$_2$F groups, as has been previously
suggested.

The peak present in the spectrum of the precursor at approxi-
mately -100°C is broad and skewed, which was considered due to the
overlapping of the γ and β peaks. Dielectric and mechanical studies
suggest that the relaxation mechanisms responsible for these two
peaks involve local —CF$_2$— backbone motions and ether side-chain
motions, respectively. For low degrees of conversion from the pre-
cursor to the Nafions, the shape and temperature position of this
peak are retained. However, materials with higher degrees of con-
version yield more symmetrical peaks in the temperature region
centered around -100°C, with an additional minor peak (β' of acid
form) appearing at approximately -30°C in the case of the two highest
conversion samples. This latter relaxation is not present as a
separate dispersion in the precursor. Because the height and
symmetry of this minor peak increase with increasing conversion, it
is reasonable that the overlapping γ and β peaks of the precursor are
split into two separate peaks with the introduction of a large number
of ionic groups into the polymer. As the β peak of the precursor has
been associated with the ether side-chain motion, the β' process of
the Nafion may be related to a kind of ether side-chain motion which
is influenced by Coulombic forces originating with the phase-
separated ionic domains.

In an earlier study of the Nafions by Yeo and Eisenberg (46),
this β' peak was not seen to the extent observed here in the dry
monovalent salts. Instead, a similar β peak was found in about the
same temperature region in hydrated Nafions, this peak migrating to
lower temperatures with increasing water content and eventually
merging with the γ peak. It is tempting to suggest that the β' peak
may be related to the water-plasticized β peak observed in the
previous Nafion acid samples. If this were the case, however, the
position of the β' should depend on the moisture content. Since
samples with a low degree of conversion contain fewer ionic sites
than those with higher conversions, there should be less residual
water in the former materials. Hence the peak would be expected at a
higher temperature for a specimen with a lower degree of conversion.
Because the β peak appears to move to higher temperatures with in-
creasing conversion, it is probably not related to the previously
observed water-plasticized β peak in Nafion-H.

The identification of the γ peak is relatively straightforward;
its temperature position in both the precursor and the Nafions is
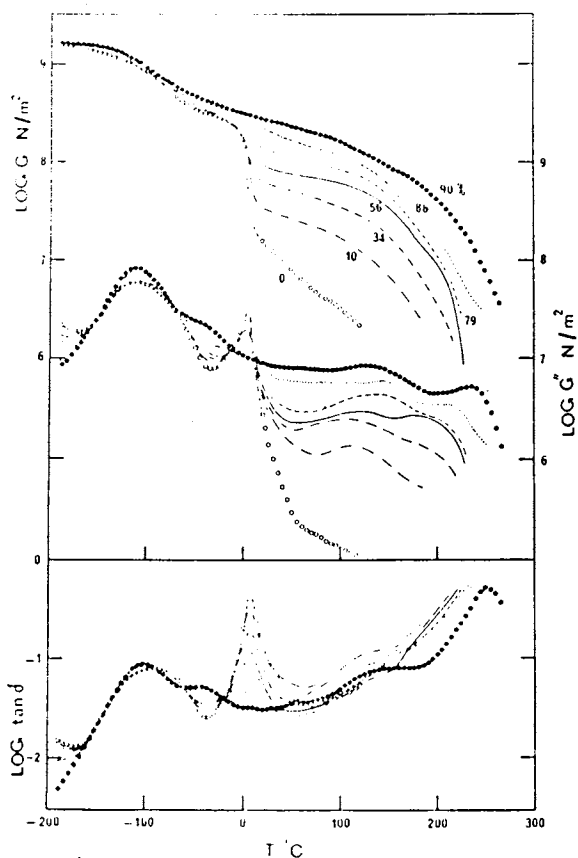
Figure 33. Variations of G', G", and tan δ with temperature for the precursor and particularly ionized Nafion-Na samples with varying degrees of neutralization %. The frequency being approximately 1 Hz at the γ region. Reproduced with permission from Ref. 58. Copyright 1983.

close to that observed for the relaxation in PTFE (62). The activa-
tion energy of the process as determined in dielectric studies is
also comparable to that observed in PTFE. Thus, the γ relaxation in
Nafion may have the same origin as the relaxation in PTFE where it is
attributed to local — CF_2— backbone motions.

In the glass transition or α region of the precursor, which
occurs at approximately 0°C, the magnitude of the G" and the tan δ_G
peaks decreases with increasing degree of conversion, the peak
temperature remaining constant. At higher temperatures, two peaks
(denoted β and α in ascending order of temperature) appear in the G"
curves of the partially ionized Nafion-Na samples, both peaks shift-
ing to higher temperature with increasing degree of ionization.
These motions reflect the strong ionic interactions within the
polymer. The mechanisms of the β and α are assigned to the glass
transitions of the fluorocarbon matrix and the ionic domain, respect-
ively.

Partially Neutralized Nafion-Cs. Dynamic mechanical studies of
partially neutralized Nafion-Cs from the Nafion acid was performed by
Kyu et al (58). The starting material used in their study was Nafion
acid of equivalent weight 1155. The acid samples were first boiled
in distilled water to ensure extensive swelling, and then immersed in
0.1 N CsOH solution for differing periods of time, which gave varying
degrees of neutralization of 39%, 50%, 76% and 90%. In contrast to
the partially ionized Nafion-Na samples prepared from the precursor,
the diffusion coefficient of the Cs^+ and H^+ ions in both Nafion acid
and its salts was high (18), resulting in a final sample containing
a homogeneous distribution of cations.

Figure 34 shows torsion pendulum results of Nafion-H and Nafion
Cs samples with various degrees of neutralization from −150° to
250°C. The Nafion acid (0% neutralization) reveals three distinct
peaks in the tan δ versus temperature curve, which are termed α, β
and γ in descending order of temperature.

The γ peak in the partially neutralized Nafion-Cs samples occurs
at approximately −90°C, regardless of the degree of neutralization of
the specimens, which is consistent with the results of partially
ionized Nafion-Na materials. The relaxation mechanism is likely the
same as that occurring in PTFE or in the precursor, where the peak
has been assigned to local —CF_2— backbone motions. In contrast to
its effect on the α and β peaks, the influence of the degree of
neutralization on the temperature position of the γ peak appears to
be extremely small. A small dispersion, corresponding to the β'
minor peak of highly ionized Nafion-Na., occurs at about the same
temperature in the case of highly ionized Nafion-Cs. The relaxation
mechanism here is probably the same as that of the β' peak.

Except for the 39% neutralization sample, the position of the β
peak shifts to higher temperatures with increasing degree of neutral-
ization, while the peak intensity decreases markedly. This behavior
is quite common in the hydrocarbon-based ionomers which generally
show two tan δ peaks in the glass transition region (2, 61), the
lower temperature peak showing a gradual movement to higher tempera-
tures with increasing ion content, accompaning a slight decrease in
magnitude. This peak is identified with the T_g of the matrix. In
the present case, this behavior is explainable on the basis that in-
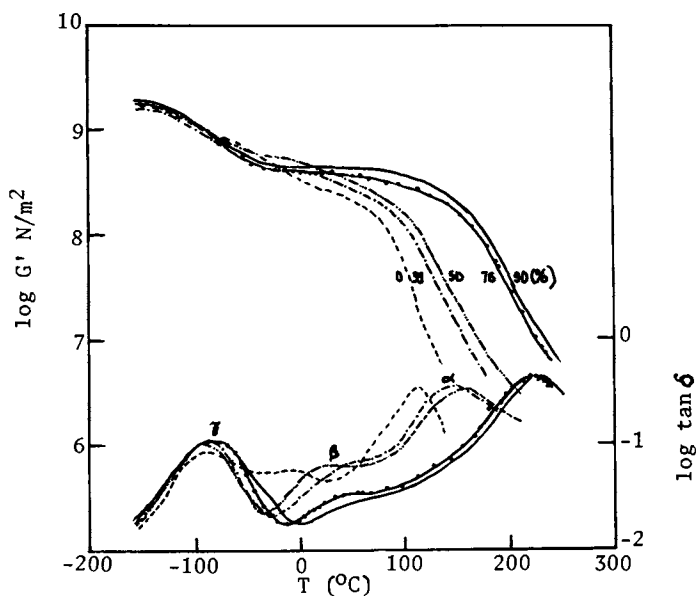
Figure 34.   Variations of G' and tan δ with temperature for Nafion-
Cs with varying degrees of neutralization.   The frequency
being approximately 1 Hz at the γ region.   Reproduced
with permission from Ref. 58.   Copyright 1983.

creased neutralization enhances the strength of the ionic inter-
actions in the material, thereby increasing the peak temperature
while depressing the relaxation intensity. If this β relaxation is
representing the T_g of the ionic region, one would not expect such a
decrease in the relaxation strength with increasing degree of
neutralization.

The tan δ peak position for the α relaxation, which corresponds
to a pronounced drop-off in G', moves dramatically to higher tempera-
tures with increasing degree of neutralization, accompanied by a
slight increase in the peak height. This feature is common to other
ionomer systems in which the higher temperature peak shifts markedly
to higher temperatures with increasing ion content. This higher
temperature peak may be identified with the T_g of the ionic region.

Summary

The structure of perfluorinate ion-exchange membranes is extremely
complex as revealed by various structural characterization and
spectroscopic techniques. The techniques employed by different
research groups probe different aspects of the structural features.
Because of their complexity as well as the different regimes to which
the individual methods address themselves, no single view of the
structure of these polymers has been agreed upon as yet. Wide-angle
x-ray diffraction in conjunction with small-angle x-ray scattering
indicates clearly that the perfluorinate ionomers are indeed semi-
crystalline polymers; the degree of crystallinity ranges up to a
level of 40%. In addition, two distinct noncrystalline regions are
present, the hydrophobic fluorocarbon phase and the hydrophilic
ionic regions. Small-angle x-ray scattering, which focuses on the
electron density contrast between regions of heavy metal atoms and
fluorocarbon matrix, is of particular importance in detecting hetero-
geneous regions. Small-angle neutron scattering, by contrast, is
sensetive to the presence of protons and has thus been used exten-
sively in the study of hydrated materials. The existence of the
phase segregated ionic regions is also confirmed by the SANS studies.

On the other hand, the spectroscopic techniques probe individual
ionic species which build up the ionic aggregates. These techniques
permit the investigation of the immediate chemical environments, the
mobility of cations and water-ions interactions. Metal nuclear
magnetic resonance and Mossbauer spectroscopy are sensitive probes of
counter cations and provide valuable information on the cations and
their environment. Infrared spectroscopy is complementary to the
above methods and addresses itself to the bound SO_3^- anions or water
and the interaction of water molecules with the various species with
which it is in contact. A common conclusion that is reached in the
above mentioned studies is that four or five water molecules are
needed to complete the hydration process. Reducing the level of
moisture content (which surrounds the ionic species) below four water
molecules per unit SO_3^- site enhances the Coulombic interaction
between the ionic species. This eventually leads to the formation
of ion pairs in the dry membranes. These ion pairs do not necessarily
disperse homogeneously in the fluorocarbon matrix but tend to form
aggregates, phase separated from the matrix materials as demonstrated
in the scattering studies.

These aggregates exert a profound effect on mechanical and ion transport properties. Occasionally, mechanical and transport studies provide indirect insight into the structural aspects of these materials. The dynamic mechanical and dielectric studies have demonstrated that the presence of ionic domains not only raise the glass transition of the matrix polymer but also reveal a new glass transition attributed to the ionic regions. The assignment of the origins of mechanical α and β relaxations in the Nafion acid and salt membranes is still subject to considerable debate. The original assignment of the α and β peaks in the Nafion acid or salts were to the T_gs for the matrix and ionic regions, respectively. This assignment was derived from the fact that the α peak of acid shows little or no movement with water content while the β peak shifts dramatically to low temperatures. The effect of water plasticization is extremely complex as the samples lose water near the α peak temperature. Recently newer evidence of the water sensitivity of the α relaxation was obtained by underwater stress relaxation studies (47) and dynamic mechanical studies of partially neutralized membranes(60). Moreover, the α relaxation peak of divalent salts (Nafion-Ba) is located at a higher temperature than the crystal melting temperature. This evidence strongly suggests that the α relaxation cannot be due to the glass transition of the fluorocarbon backbone. Consequently, the original assignment of α and β processes have been reversed (48, 58). The revised assignments of the two T_gs of the perfluorinate membranes would be in line with the behavior of hydrocarbon-based ionomers. The corresponding transitions are seen in the Mossbauer spectroscopy (37,38) and NMR relaxation studies (35). Their interpretations of these transitions are inconclusive as they are based on the original assignments of previous literature (46). Additional work is needed to clarify this controversy.

The identification of the γ and δ relaxations is generally agreed. The γ relaxation is assigned to the local motions of the fluorocarbon backbone chains while the δ relaxation is attributed to — SO_2F groups and is unique to the precursor materials.

Acknowledgment

Literature Cited

1. Holiday, L. "Ionic Polymers"; Holstead Press: Wiley, NY, 1975.
2. Eisenberg, A. and King, M. "Ion Containing Polymers"; Academic Press: New York, 1977.
3. Rees, R.W. and Vaughan, D.J. Am. Chem. Soc. Polym. Prepr. 1965, 6, 287 and ibid. 1975, 6, 296.
4. Ward, T.C. and Tobolsky, A.V. J. Appl. Polym. Sci. 1967, 11, 2403.
5. Otocka, E.P. and Kwei, T.K. Macromolecules 1968, 1, 244 and 401.
6. Otocka, E.P. and Kwei, T.K. Macromolecules 1969, 2, 110.
7. Longworth, R. and Vaughan, D.J. Am. Chem. Soc. Polym. Prepr. 1968, 9, 525.

8. MacKnight, W.J., McKenna, L.W. and Read, R.E. J. Appl. Phys.
    1967, 38, 4208.
9. MacKnight, W.J., Kajiyama, T. and McKenna, L.W. Polym Eng. Sci.
    1968, 8, 267.
10. Fitzgerald, W.E. and Nielsen, L.E. Proc. R. Soc. London Ser.
    1964, A282, 137.
11. Navratil, M. and Eisenberg, A. Macromolecules 1974, 7, 84.
12. Haplin, J.C. and Bueche, F. J. Polym. Sci. 1965, A3, 3935.
13. Otocka, E.P. and Eirich, F.R. J. Polym. Sci. 1968, A-2, 6, 921
    and 933.
14. Tobolsky, A.V., Lyons, P.F. and Hatta, N. Macromolecules, 1968,
    1, 515.
15. Pineri, M., Meyer, C.T., Levelut, A.M. and Lambert, M. J. Polym.
    Sci. Polym. Phys. Ed. 1974, 12, 115.
16. Meyer, C.T. and Pineri, M. Polymer 1976, 17, 382.
17. Rigdahl, M., Reinhardt, B.A., Harris, F.W. and Einsenberg, A.,
    Macromolecules 1981, 14, 833.
18. Eisenberg, A. and Yeager, H.L. "Perfluorinated Ionomer Membrane",
    Am. Chem. Soc. Sympo. Ser. #180: Washington D.C., 1982.
19. Grot, W.G.F., Munn, G.E. and Walmsley, P.N., 141st Meeting of the
    Electrochemical Society, Houston 1972, Abstract No. 154 and
    J. Electrochemical Soc., 1972, 119, 108c.
20. Grot, W.G.F. Chem. Eng. Tech. 1978, 50, 299.
21. Vaughan, D.J. DuPont Innovation 1973, 4(3), 10.
22. Yeager, H.L., Kippling, B. and Dotson, R.S. J. Electrochem. Soc.,
    1980, 127, 303.
23. Yeager, H.L. Chap. 4, p. 41 in ref. 18.
24. Gierke, , T.D. 152nd Meeting of the Electrochemical Society
    1977, Atlanta, Georgia.
25. Gierke, T.D., Munn, G.E. and Wilson, F.C. J. Polym. Sci. Polym.
    Phys. Ed. 1981, 19, 1687.
26. Roche, E.J., Pineri, M., Duplessix, R. and Levelut, A.M.
    J. Polym. Sci. Polym. Phys. Ed. 1981, 19, 1.
27. Pineri, M., Duplessix, R. and Volino, F. Chap. 12, p. 249 in
    Ref. 18.
28. Fujimura, M., Hashimoto, T. and Kawai, H. Macromolecules 1981,
    14, 1309.
29. Fujimura, M., Hashimoto, T. and Kawai, H. Macromolecules 1982,
    15, 232.
30. Hashimoto, T., Fujimura, M. and Kawai, H. Chap. 11, p. 217 in
    Ref. 18.
31. Lowry, S.R. and Mauritz, K.A. J. Am. Chem. Soc. 1980, 102,
    4665.
32. Falk, M., Can. J. Chem. 1980, 58, 1495 and Chap. 8, p. 139 in
    Ref. 18.
33. Komoroski, R.A. and Mauritz, K.A. J. Am. Chem. Soc. 1978, 100,
    7487.
34. Boyle, N.G., McBrierty, V.J. and Douglass, D.C. Macromolecules
    1983, 16, 75.
35. Boyle, N.G., McBrierty, V.J. and Eisenberg, A. Macromolecules
    1983, 16, 80.
36. Rodmacq, B., Pineri, M. and Coey, J.M.D. Rev. Phys. Appl. 1980,
    15, 1179.
37. Rodmacq, B., Pineri, M., Coey, J.M.D. and Meagher, A. J. Polym.
    Sci. Polym. Phys. Ed. 1982, 20, 603.

38. Rodmacq, B., Coey, J.M.D. and Pineri, M. Chap. 9, p. 171 in
     Ref. 18.
39. Starkweather, H.W. Jr. <u>Macromolecules</u> 1982, 15, 320.
40. Mauritz, K.A. Hora, C.J. and Hopfinger, A.J. in "Ions in
     Polymers"; Ad. Chem. Ser. #187, A. Eisenberg Ed., Chap. 8, 1980,
     p. 123.
41. Gierke, T.D. and Hsu, W.Y. Chap. 13, p. 283 in Ref. 18.
42. Yeager, H.L. Chap. 4, p. 41 in Ref. 18.
43. MacKnight, W.J. and Earnest, T.R. Jr. <u>J. Polym. Sci. Macro-
     molecular Rev.</u> 1981, 16, 41.
44. Handlin, D.L., MacKnight, W.J. and Thomas, E.L. <u>Macromolecules</u>
     1981, 14, 795.
45. Hodge, I.M. and Eisenberg, A. <u>Macromolecules</u> 1978, 11, 289.
46. Yeo, S.C. and Eisenberg, A. <u>J. Appl. Polym. Sci.</u> 1977, 21, 875.
47. Kyu, T. and Eisenberg, A. <u>J. Polym Sci. Polym. Symp</u>. in press
     1984.
48. Kyu, T. and Eisenberg, A. Chap. 6, p. 79 in Ref. 18.
49. Takamatsu, T., Hashiyama, M. and Eisenberg, A. <u>J. Appl. Polym.
     Sci.</u> 1979, 24, 2199.
50. Lundberg, R.D., Makowski, H.S. and Westerman, L. in "Ions in
     Polymers," A. Eisenberg Ed., Advances in Chemistry Series #187
     1980, p. 67.
51. Yeo, R.S. <u>Polymer</u> (London) 1980, 21, 432.
52. Kyu, T. and Eisenberg, A., in preparation.
53. Dotson, R.L., Lynch, R.W. and Hilliard, G.E. in "Proceedings of
     the Symposium on Ion Exchange," R.S. Yeo and R.P. Buck Eds., The
     Electrochemical Society, Pennington, N.J. 1981.
54. Yeager, H.L. Chap. 4 in Ref 18.
55. Suhara, M. and Oda, Y. in "Proceedings of the Symposium on Ion
     Exchange," R.S. Yeo and R.P. Buck Eds., The Electrochemical
     Society, Pennington, N.J., 1981.
56. Mauritz, K.A., Branchick, K.L., Gray, C.L. and Lowry, S.R.
     <u>Am. Chem. Soc. Polym. Prepr.</u>, 1980, 20, 122.
57. Kyu, T. and Eisenberg, A. <u>J. Polym. Sci. Polym. Lett. Ed.</u>
     1983, 21, 589.
58. Kyu, T. Hashiyama, M. and Eisenberg, A. <u>Can J. Chem</u>, 1983, Gl,
     680.
59. Yeo, S.C.   Ph.D. Dissertation, McGill University, 1977.
60. Nakano, T. and MacKnight, W.J. submitted for publication.
61. Rigdhal, M. and Eisenberg, A. <u>J. Polym. Sci. Polym. Phys. Ed.</u>
     1981, 19, 164.
62. McCrum, N.G. <u>J. Polym. Sci.</u> 1959, 34, 355.

Ethanol–Water Separation by Countercurrent Reverse Osmosis

ERIC K. L. LEE, W. C. BABCOCK, and P. A. BRESNAHAN

Bend Research, Inc., Bend, OR 97701-8599

Countercurrent reverse osmosis (CCRO) is a process
design that helps solve a major problem in enriching
ethanol by reverse osmosis: the high osmotic pressure of
concentrated ethanol solutions. The effective osmotic
pressure gradient across a membrane is reduced by
supplying the permeate side of the membrane with a
solution more concentrated in ethanol than the permeate
but less concentrated than the feed. This causes
ethanol to back-diffuse from the recirculation solution
into the membrane. The concentration increase inside
the membrane lowers the concentration difference (and
thus the osmotic pressure difference) between the feed-
solution and membrane phases. Membranes with open
porous sublayers are preferred for use in CCRO because
they allow ethanol to diffuse relatively unhindered
through the sublayer and accumulate inside the membrane.
With a new thin-film-composite membrane, designated 3N8,
it has been shown that CCRO is about seven-fold more
energy-efficient than distillation for enriching 10 vol%
ethanol to 50 vol%. However, this and other reverse-
osmosis membranes developed for desalination cannot be
used at higher ethanol concentrations because of their
low ethanol-water selectivity and their tendency to
degrade.

Ethanol produced by fermentation is conventionally dehydrated by
distillation, an inefficient process that consumes energy equivalent
to a large fraction of the energy content of the product ethanol.(1)
Reverse osmosis (RO) has been considered before for ethanol-water
separation because of its inherent energy efficiency. However, a
difficulty encountered in using RO is the high osmotic pressures
associated with concentrated ethanol solutions. For example, the
osmotic pressure of a 15-vol% ethanol solution is about 960 psi, and
that of a 50-vol% solution is about 3700 psi.(2) Because most

modern RO systems operate at below 1000 psi, concentrating ethanol
beyond about 15 vol% has not been considered possible, according to
previous studies.(2,3)

Countercurrent reverse osmosis (CCRO) is a process design
originally conceived by Loeb and Bloch(4) for overcoming the problem
of high osmotic pressure gradients in the production of concentrated
salt solutions. Essentially, the osmotic pressure across a membrane
is reduced by recirculating, on the permeate side of the membrane, a
solution whose osmotic pressure is slightly below that of the feed.
Only a modest operating pressure would in principle sustain the flow
across the membrane and effect separation.

CCRO may be applied to ethanol enrichment as illustrated in
Figure 1. A fermentation beer containing about 8 to 10 vol% ethanol
is pressurized and fed into a membrane unit. Assuming that the
membrane is preferentially permeable to water, ethanol would be
enriched in the direction of feed solution flow. Part of the
concentrated product solution leaving the feed side of the membrane
unit is depressurized and recirculated to the permeate side, flowing
countercurrent to the feed. Mixing between the recirculation
solution and the permeate brings the permeate-side concentration
(and thus its osmotic pressure) closer to that of the feed. In this
way, the osmotic pressure difference can be kept below the operating
pressure even as the feed solution becomes highly concentrated.

The CCRO concept has not been proven in practice; thus, an
objective of the present work was to demonstrate the process concept
experimentally. Various RO membranes were characterized to
determine if their use for ethanol enrichment by CCRO would be more
energy-efficient than by distillation, and to identify membrane
characteristics that affect the performance of the process.

Principles

Comparison of RO and CCRO. In virtually all RO membranes, a thin,
selective skin layer is supported by a much thicker microporous
sublayer. During RO operation, the composition of the permeate is
determined by the selectivity of the skin layer, the feed solution
composition, and the operating pressure. The concentration of the
permeate is established as the feed solution flows through the skin
layer, and it remains constant inside the sublayer. This
concentration profile is shown in Figure 2a.

The osmotic pressure across the membrane, $\Delta \pi = \pi_2 - \pi_3$,
increases with increasing concentration difference, $c_2 - c_3$, across
the skin layer. If $\Delta \pi$ exceeds the operating pressure, no permeate
will be obtained. Since the osmotic pressure of a 14-vol% ethanol
solution already exceeds 800 psi, for example, an operating pressure
of 800 psi cannot be used to enrich ethanol solutions past 14 vol%
if the membrane exhibits perfect rejection.

Real membranes are not perfectly permselective; the rate of
ethanol permeation across the skin layer of the membrane determines
the actual osmotic pressure gradient. The lower the membrane
selectivity, the less likely it is that the flow of permeate would
be stopped due to high osmotic pressures. However, using a membrane
with poor ethanol rejection necessarily compromises the efficiency
of separation.

CCRO represents a more attractive method of reducing the osmotic pressure gradient. As shown in Figure 2b, an ethanol concentration gradient c_4-c_3 is established across the porous sublayer of the membrane by supplying a relatively concentrated solution to the low-pressure side of the membrane. This concentration gradient causes ethanol to diffuse toward the skin layer against the convective flow of the permeate. An accumulation of ethanol inside the sublayer increases the ethanol concentration c_3 at the skin-sublayer interface and decreases $\Delta\pi$. Controlling the permeate-side concentration in this way decreases the effective osmotic pressure difference and increases the permeate flux. We refer to the flux increase as the "CCRO effect."

CCRO Process Model. The CCRO process is illustrated by the schematic diagram of the membrane unit shown in Figure 3. A model of the process is derived based on the overall mass balance around the entire membrane unit, the local mass balance around a differential section (x--y) of the unit, and the membrane model which correlates the fluxes of water and ethanol within that section to the operating conditions.

The overall mass balance can be written as:

$$V_p = V_f - V_r \qquad (1)$$

and
$$V_p c_p = V_f c_f - V_r c_r, \qquad (2)$$

where c and V represent the ethanol concentration (as volume fraction) and volumetric flow rate, respectively. The subscripts p, f, and r denote product, feed, and recirculation solutions, respectively. Subscripts 2 and 4 denote the feed and permeate sides of the membrane, respectively. External concentration polarization is assumed to be negligible, so that c_2=c_1 and c_4=c_5. The subscript perm stands for the permeate.

The local mass balance within the differential section (delineated by the broken lines x and y in Figure 3) is described by:

$$V_f' = V_{perm} + V_f'' \qquad (3)$$

$$V_r' = V_{perm} + V_r'' \qquad (4)$$

$$V_f' c_2' = V_{perm} c_{perm} + V_f'' c_2'' \qquad (5)$$

$$V_r' c_4' = V_{perm} c_{perm} + V_r'' c_4''. \qquad (6)$$

The superscripts ′ and ″ denote the values of a given variable at the boundaries x and y, respectively. The terms V_{perm} and c_{perm} are functions of membrane properties and are related to J_v and J_s as follows:

$$V_{perm} = J_v A \qquad (7)$$

$$c_{perm} = J_s / J_v, \qquad (8)$$

where A is the membrane area within the section x--y of the membrane unit.

The local mass balance described by Equations 3 through 6 is affected by the recycle ratio, r, defined as the fraction of the
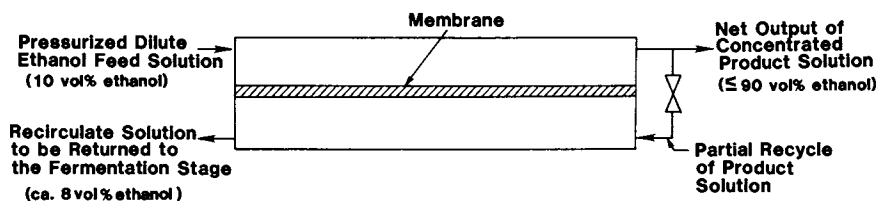
Figure 1.   Diagram of the Countercurrent Reverse-Osmosis Process
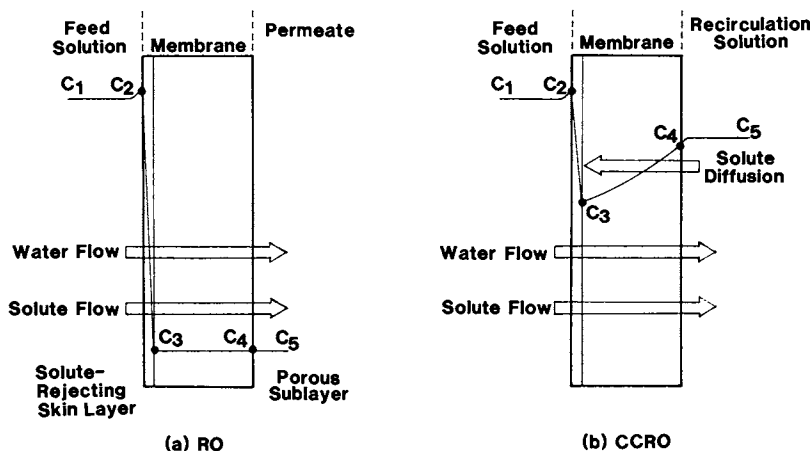
Figure 2.   Comparison of Concentration Profiles Inside a Skinned
             Reverse-Osmosis Membrane Under Reverse-Osmosis and
             Countercurrent Reverse-Osmosis Conditions
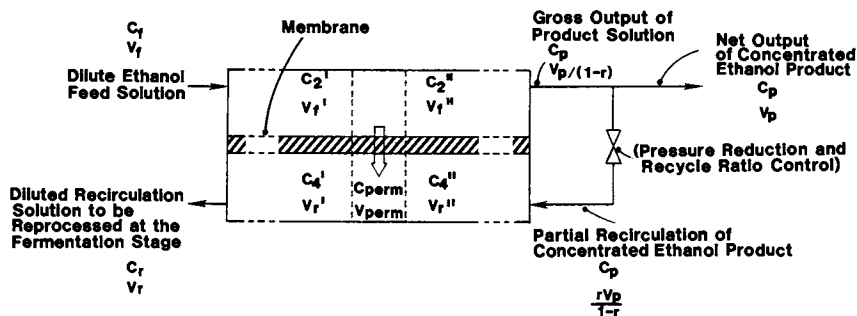
Figure 3.   Schematic Diagram of the Countercurrent Reverse-Osmosis
             Process

gross product solution recirculated to the permeate side. Referring
to Figure 3, if the net product output flow rate is V_p, then the
gross product flow rate at the exit of the membrane unit is $V_p/(1-r)$
and the recycled stream flow rate is $rV_p/(1-r)$.

   The recycle ratio affects the performance of the CCRO process
in two ways. With a high recycle ratio, the osmotic pressure
gradient is more effectively reduced, and the consequent permeate
flux increase means that the desired degree of ethanol enrichment
can be accomplished in a smaller membrane area. However, a higher
recycle ratio also decreases the net product flow rate such that
more feed solution is required to reach a given production goal. At
some optimum recycle ratio, the desired product purity and
productivity is obtained with the minimum membrane area and feed
rate.

Membrane Model. The function of the membrane model is to allow J_v
and J_s to be calculated under a given set of operating conditions.
The properties of both the skin layer and the porous sublayer are
involved in deriving a suitable CCRO membrane model. The material
of the skin layer governs its permselectivity, and the porous
sublayer characteristics determine how effectively the osmotic
pressure gradient across the skin layer could be reduced by
permeate-side recirculation.

   A variety of RO membrane models exist that describe the
transport properties of the skin layer. The solution-diffusion
model([5]) is widely accepted in desalination where the feed solution
is relatively dilute on a mole-fraction basis. However, models
based on irreversible thermodynamics usually describe membrane
behavior more accurately where concentrated solutions are
involved.([6]) Since high concentrations will be encountered in
ethanol enrichment, our present treatment adopts the irreversible
thermodynamics model introduced by Kedem and Katchalsky.([7])

   In this model, the volumetric flux J_v and solute flux J_s
through the skin layer are described by two equations:

$$J_v = L_p \ (\Delta P - \sigma[\pi_2 - \pi_3]) \qquad (9)$$

and $\qquad$ $$J_s = J_v(1-\sigma)(c_2+c_3)/2 + \omega^\prime(c_2-c_3), \qquad (10)$$

where ΔP is the operating pressure. There are three membrane
parameters: L_p, the hydraulic permeability; σ, the reflection
coefficient; and $\omega^\prime$, the solute permeability. The values of these
parameters are obtained from RO experiments in which J_v and c_3
(equal to c_4) are directly measurable. The selectivity of the
membrane is expressed in terms of the rejection:

$$\text{Rejection (\%)} = (1-c_3/c_2) \times 100\%. \qquad (11)$$

Equations 9 and 10 have the same form as the model equations derived
by Kedem and Katchalsky, but they differ in two ways: 1) the use of
$(c_2+c_3)/2$ instead of the logarithmic mean of c_2 and c_3; and 2) the

use of $\omega'(c_2-c_3)$ instead of $\omega(\pi_2-\pi_3)$, as given by those authors. These modifications were made to simplify the subsequent derivation of the CCRO membrane model; some loss of accuracy is expected at high ethanol concentrations, 'at which the osmotic pressure does not vary linearly with concentration.

In the porous sublayer, the net ethanol flux is the difference between convective permeation and back-diffusion:

$$J_s = J_v \, c(x) - D_e \frac{dc(x)}{dx}, \qquad (12)$$

where D_e is the effective diffusivity of ethanol in the porous sublayer, and x is the distance measured from the skin-sublayer interface toward the low-pressure side of the membrane. D_e incorporates the effects of all sublayer characteristics that affect mass transfer of ethanol, such as porosity and tortuosity.

At steady state, the ethanol flow across the skin layer equals that across the porous sublayer. Thus, combining Equations 10 and 12 yields the overall ethanol balance across the entire membrane:

$$J_v(1-\sigma)(c_2+c_3)/2 + \omega'(c_2-c_3) = J_v \, c(x) - D_e \frac{dc(x)}{dx}. \qquad (13)$$

Equation 13 can be integrated with the following boundary conditions:

$$c(x) = c_3 \text{ at } x = 0$$

and $c(x) = c_4$ at $x = t$,

where t is the thickness of the sublayer. Thus:

$$c_3/c_2 = \frac{(1-\sigma)/2 + \omega'/J_v + (c_4/c_2)(Q/1-Q)}{1/(1-Q) - (1-\sigma)/2 + \omega'/J_v} \qquad (14)$$

where $Q = \exp[-J_v K]$. K is the fourth parameter in the membrane model, defined as $K \equiv t/D_e$, and quantifies the diffusional resistance to ethanol in the sublayer of the membrane. With Equation 14, c_3 can be explicitly calculated for known values of J_v and c_4/c_2, the concentration ratio of the recirculation and feed solutions. Assuming osmotic pressure to be proportional to ethanol concentration, Equations 9 and 14 are combined to give

$$J_v = L_p \left\{ \Delta P - \sigma\pi_2 \left[\frac{(1-Qc_4/c_2)/(1-Q) - (1-\sigma)}{1/(1-Q) - (1-\sigma)/2 + \omega'/J_v} \right] \right\} \qquad (15)$$

Equation 15 is an implicit function of J_v in terms of measurable quantities and the four membrane parameters L_p, σ, ω, and K, and it can be solved by numerical methods. Substituting the values of J_v into Equation 14 yields c_3, which in turn allows J_s to be calculated from Equation 10. Then the quantities V_{perm} and c_{perm} can be calculated using Equations 7 and 8.

The value of K is determined from an RO experiment in which the permeate side of the membrane is exposed to a recirculation solution to produce a known c_4/c_2 ratio to simulate CCRO conditions. The measured permeate flux is substituted into Equation 15 to compute the value of K that would match the experimental value of J_v.

Combining the process and membrane models, the overall CCRO system is described by Equations 1 through 8, 10, 11, 14, and 15, and the value of the recycle ratio, r. The performance of the CCRO process is expressed in terms of the total membrane area (which determines the equipment costs), and the input flow rate of the pressurized dilute feed solution (which determines the energy costs). For a given membrane, these two quantities are fixed at a given recycle ratio and operating pressure.

Experimental

Membranes. Seven membranes were evaluated in this work. These were flat-sheet and hollow-fiber membranes originally developed for RO applications. All have the anisotropic, skinned structure depicted in Figure 2.

1. NS-100. This is a polyurea thin-film-composite membrane formed by interfacially crosslinking polyethyleneimine (PEI) with tolylene diisocyanate (TDI) on a microporous polysulfone support membrane. Flat-sheet and hollow-fiber membranes were prepared in our laboratory. The solute-rejecting skin layer was deposited on the lumen surface of the hollow fibers. The fibers were pressurized internally during use.

2. NS-101. This is a polyamide TFC membrane prepared by crosslinking PEI with isophthaloyl chloride. Flat-sheet NS-101 membranes were prepared by a procedure similar to that used for producing NS-100 membranes.

3. TFC-801. Flat-sheet samples of this commercial polyetherurea TFC membrane were supplied by the Fluid Systems Division of UOP Inc. (San Diego, California).

4. Polybenzimidazolone (PBIL). This is an asymmetric membrane(8) that exhibits good rejection of many organic compounds. Flat-sheet samples were provided by Teijin Ltd. (Tokyo, Japan).

5. Cellulose triacetate (CTA). CTA hollow-fiber membranes were obtained from Dow Chemical Company (Midland, Michigan). The solute-rejecting layer is on the

                    outside surface of these fibers, which are
                    pressurized externally.
        6. Poly(vinyl alcohol) (PVA). A commercial flat-sheet PVA
                    film (Mono-Sol Type 1-0015-3, Chris Craft
                    Industries, Inc., Gary, Indiana) was surface-
                    crosslinked with TDI to render it water-insoluble.
        7. 3N8. This is a TFC polyamide membrane developed at Bend
                    Research. It is formed by interfacially
                    crosslinking a monomeric amine on a microporous
                    polysulfone support membrane.

Membrane Testing. The membranes were characterized on an RO test
loop. Hollow-fiber modules were equipped with fittings as shown in
Figure 4 to allow circulation on both sides of the membrane. Flat-
sheet membranes were tested in special cells of the type shown in
Figure 5; recirculation solution could be pumped into a port in the
center of the cell and forced to flow through a sintered stainless
steel support plate to reach the permeate side of the membrane.
     RO tests were conducted at various pressures to measure ethanol
rejection and permeate flux as functions of feed concentration. To
mimic CCRO conditions, a solution equal in concentration to the feed
was used for permeate-side recirculation, and the changes in flux
was monitored as recirculation was switched on and off.

Results and Discussion

Reverse-Osmosis Tests. The performance of the membranes at low
ethanol feed concentrations is summarized in Figure 6. The 3N8,
TFC-801 and NS-100 flat-sheet membranes exhibited the best
selectivity. Notably, the highest ethanol rejection observed was
about 60%--much lower than the rejection of these membranes for
salts. Further tests were conducted at higher feed concentrations;
the results are shown in Figures 7 to 11. The membranes generally
exhibited decreasing rejection and permeate flux with increasing
ethanol feed concentration. Obviously, the increase in osmotic
pressure with increasing concentration offset the effect of lower
rejection, which tends to reduce the osmotic pressure gradient
across the membrane. The net result was a decrease in driving force
for permeation, and thus a decrease in the flux observed. For the
CTA and PBIL membranes, the permeate flux increased somewhat as the
membranes became essentially non-selective at feed concentrations
approaching about 50 vol% ethanol.
     All of the membranes tested degraded to some extent upon
exposure to concentrated ethanol solutions. Degradation was
manifested by lower rejections and higher fluxes when membranes
exposed to high ethanol concentrations were retested at low feed
concentration.
     The hollow-fiber geometry is preferred for CCRO because it is
more convenient to provide circulation on both sides of fibers than
it is for flat-sheet membranes. A number of hollow-fiber NS-100
membrane modules were tested at 250 psi. The fibers were stable for
several days at this operating pressure at feed concentrations up to
25 vol% ethanol. However, higher operating pressure and/or feed
concentration caused these membranes to fail rapidly due to
plasticization weakening of the polysulfone support. The CTA
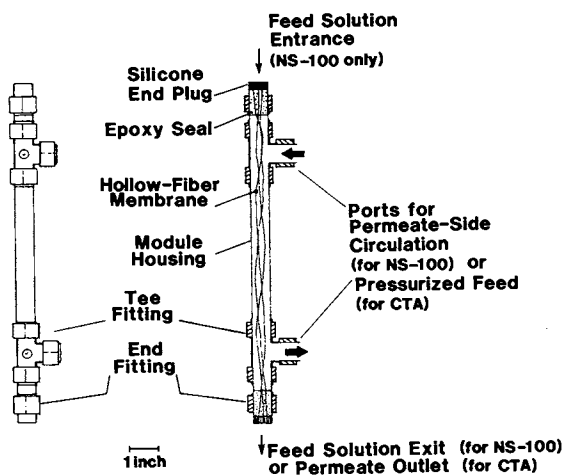
Figure 4.   Construction of a Hollow-Fiber Membrane Module
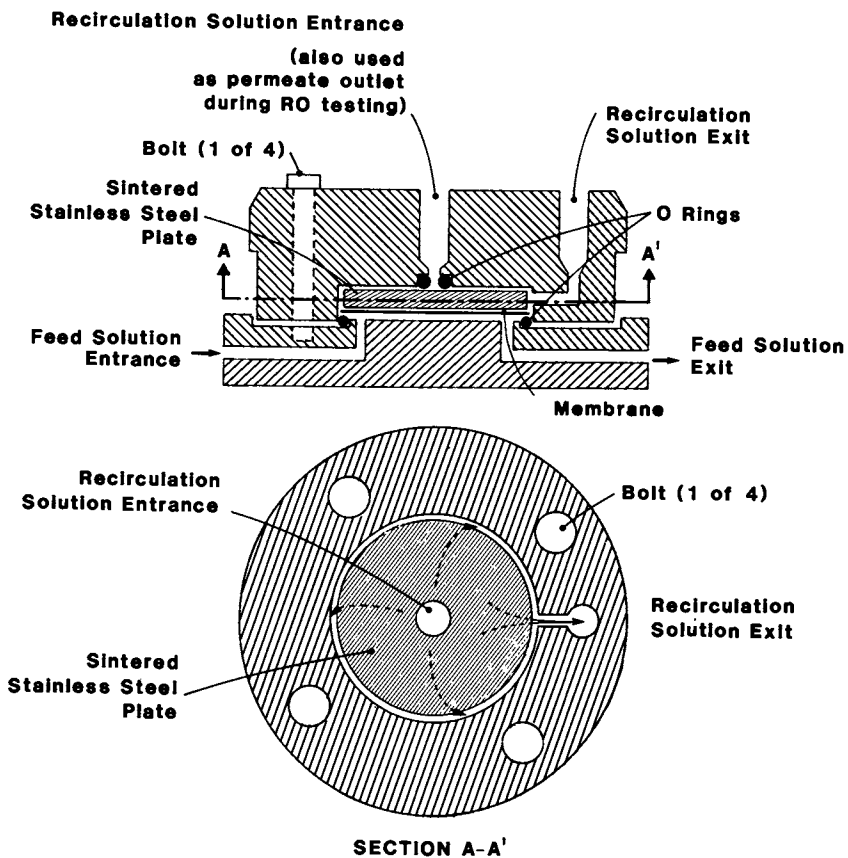
Figure 5.   Flat-Sheet Membrane Test Cell
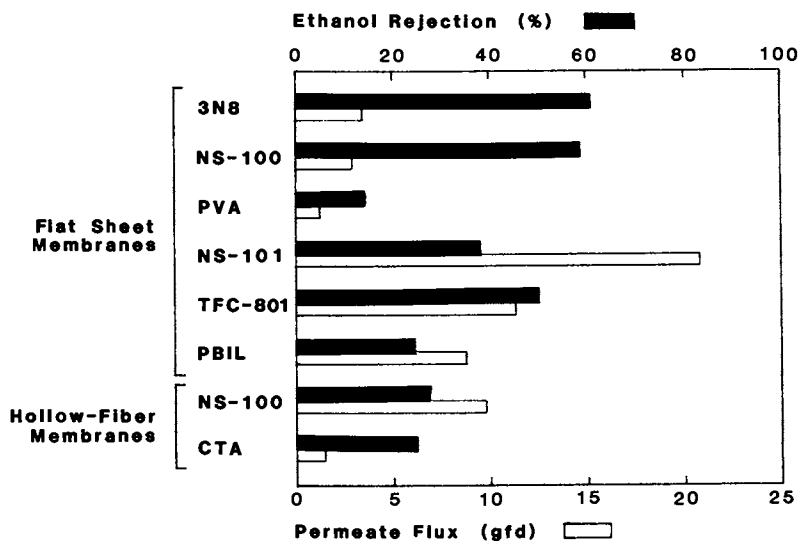
Figure 6.   Average Reverse-Osmosis Performance of Membranes Evaluated

(●Performance after <6 hr exposure to 56% Ethanol)
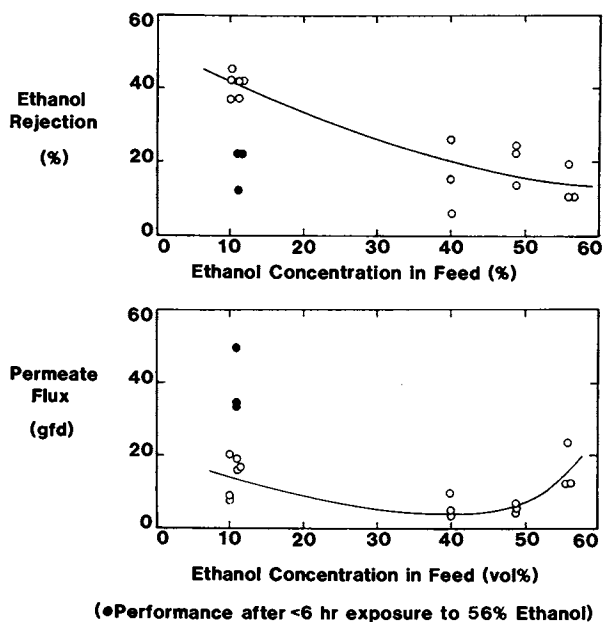
Figure 7.   Effect of Ethanol Feed Concentration on the Reverse-
            Osmosis Performance of Triplicate 3N8 Membrane Samples
            (400 psi, ambient temperature)
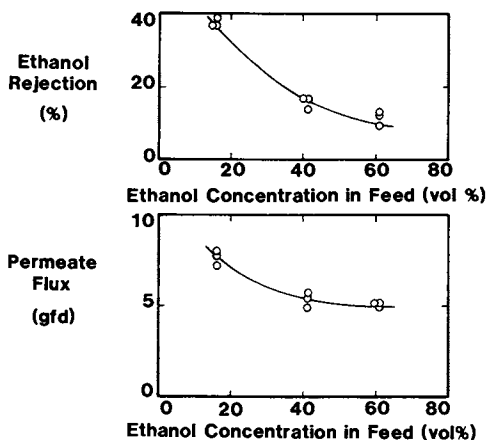
Figure 8. Effect of Ethanol Feed Concentration on the Reverse-
           Osmosis Performance of Triplicate TFC-801 Membranes
           (800 psi, ambient temperature)

(• Performance after <6 hr exposure to 50% ethanol)
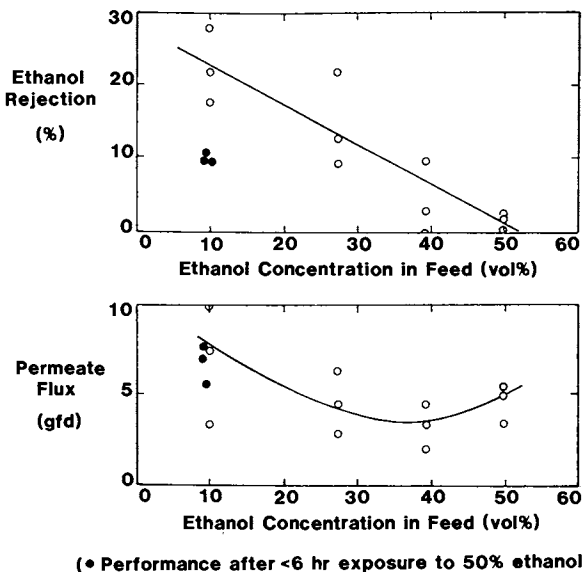
Figure 9. Effect of Ethanol Feed Concentration on the Reverse-
           Osmosis Performance of Triplicate PBIL Membrane Samples
           (400 psi, ambient temperature)
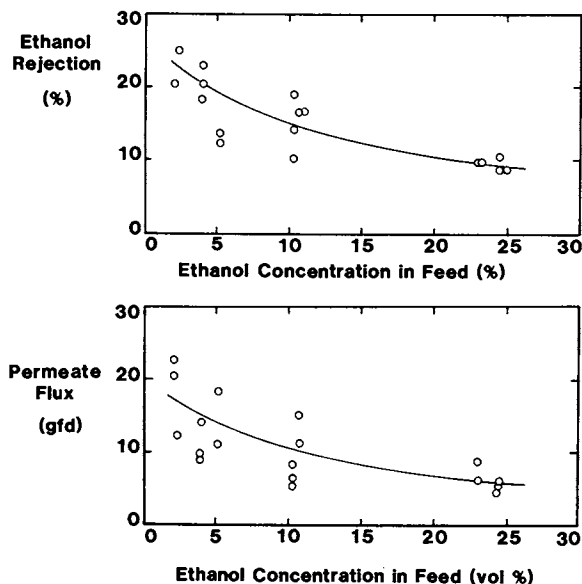
Figure 10.   Effect of Feed Concentration on the Reverse-Osmosis
Performance of NS-100 Hollow-Fiber Modules (250 psi,
ambient temperature)
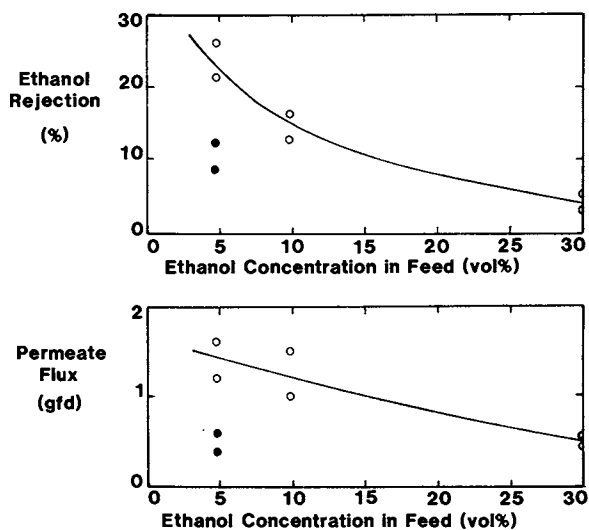
(• Performance after <6 hr exposure to 30% ethanol)

Figure 11.   Effect of Ethanol Feed Concentration on the Reverse-
Osmosis Performance of Duplicate CTA Hollow-Fiber Modules
(400 psi, ambient temperature)

hollow-fiber membranes also degraded rapidly in ethanol solutions more concentrated than about 30 vol%.

Countercurrent Reverse-Osmosis Tests. Flat-sheet 3N8 and TFC-801 membranes were characterized with and without permeate-side recirculation. Other flat-sheet membranes were not tested because of either their low ethanol-water selectivity or their tendency to degrade even in relatively dilute ethanol solutions.

    The test results with triplicate 3N8 flat-sheet membranes are shown in Figure 12. The permeate flux was first measured under RO conditions, then permeate-side recirculation was started and the flux measured again. The concentration of the feed and recirculation solutions was limited to 50-vol% ethanol to minimize artifacts associated with membrane degradation.

    A large CCRO effect was observed in the 3N8 membranes; the permeate fluxes increased by an average of about five-fold with recirculation. The increase in flux corresponded to a decrease in effective osmotic pressure difference from about 340 psi to about 6 psi. When recirculation was stopped, the permeate fluxes decreased immediately, indicating that the CCRO effect was reversible and that the flux increases were not due to membrane damage. The test was repeated with new membrane samples at 800 psi. Under RO conditions the permeate flux averaged 3.8 gfd; under CCRO conditions the average flux increased by about six-fold to 23 gfd. This flux increase was comparable to those observed in the 400 psi experiments.

    The TFC-801 membranes did not exhibit any measurable CCRO effect under equivalent test conditions. These results are consistent with our previous work on osmotic membranes.(9) Thin-film-composite desalination membranes derived from polyamine precursors (such as TFC-801) contain a gel layer within the porous sublayer formed by thermal crosslinking of the polyamine.(10) This gel layer retards the diffusion of ethanol into the membrane from the recirculation solution. Thus the ethanol concentration inside the porous sublayer is not increased effectively by increasing the concentration of the recirculation solution. By contrast, Loeb-Sourirajan-type asymmetric membranes or composite membranes derived from monomeric precursors do not contain any gel layer. Such membranes are better suited to use in the CCRO process.

    The low ethanol rejection and the instability of the hollow-fiber NS-100 membranes preclude the use of this membrane for practical ethanol enrichment. Nevertheless, for the purpose of demonstrating the concept of CCRO using hollow-fiber membranes, CCRO experiments were conducted at the reduced ethanol concentration of 10 vol%. The permeate fluxes of NS-100 modules were measured at 250 psi in the absence and presence of recirculation with a 10-vol% ethanol solution. The results were varied: recirculation brought about flux increases ranging from 5% to about 20%. The limited flux increase may again be explained in terms of the formation of a polyamine gel during NS-100 membrane fabrication. Nevertheless, the flux increase shows that the hollow-fiber geometry is a viable one for CCRO operation.

    The results of the membrane tests suggest three criteria for choosing membranes for ethanol enrichment by CCRO: good selectivity,

resistance to degradation, and a morphology characterized by an open porous sublayer.

Comparative Analysis of CCRO and Distillation

In the following analysis, the energy efficiency of ethanol enrichment by CCRO is estimated for two membranes: 1) 3N8, the only membrane exhibiting a significant CCRO effect; and 2) a hypothetical membrane that is assumed to be completely stable at any ethanol concentration, and which is assumed to exhibit better ethanol/water selectivity than 3N8. In each case the energy consumption is estimated and compared with that required by distillation to produce the same amount and quality of enriched ethanol solution.

Projected CCRO Performance with 3N8 Membrane. The 3N8 membrane is relatively stable in ethanol solutions up to about 50 vol%. Thus, an enrichment range from 10 to 50 vol% ethanol is considered for a CCRO system employing this membrane. There is no existing market for 50-vol% ethanol, but CCRO might serve as an adjunct to distillation by preconcentrating the fermentation beer.

The membrane parameters for 3N8 were determined from the results of RO and CCRO tests shown in Figures 7 and 12, respectively. L_P and σ were obtained by substituting RO fluxes and osmotic pressure differences at various feed concentrations into Equation 9 and solving simultaneously. Then ω' was calculated from Equation 10. The value of ω' was concentration-dependent and was expressed as a linear function in c_2. The results were:

$$L_P = 4.1 \times 10^{-5} \text{ cm}^3/\text{cm}^2\text{-sec-atm}$$
$$\sigma = 0.468$$
$$\omega' = (3.36 \times 10^{-4} - 6.58 \times 10^{-5} c_2) \text{ cm}^3/\text{sec}.$$

From the response of the flux to permeate-side recirculation shown in Figure 12, the value of K was calculated at $c_4/c_2 = 1$ using Equation 15. Thus:

$$K = 1 \times 10^2 \text{ sec/cm}.$$

The value of K is assumed to be constant for the purpose of this projection.

With the four membrane parameters, a computer program of the CCRO process model was used to calculate the required membrane area and pumping energy at different recycle ratios and operating pressures. The basis of the calculation was a net output rate of 1000 gal/hr of 50-vol% ethanol product from a 10-vol% feed. Axial pressure drop inside the membrane unit has not been considered, as it is a function of membrane geometry and system design. The results of the process modelling are illustrated in Figure 13.

As predicted in the Principles section, an optimum recycle ratio exists for each operating pressure where the overall membrane area and feed solution flow rate are minimized. Increasing the operating pressure directly increases the driving force available; thus both the membrane area and feed solution flow rate requirements
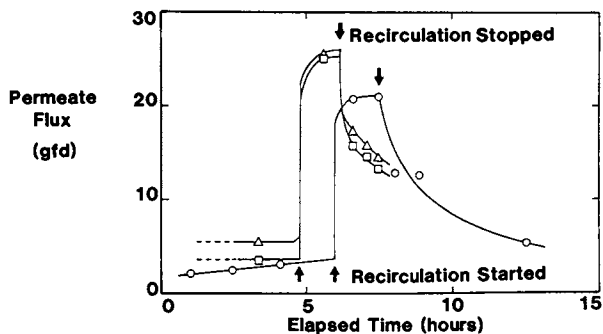
Figure 12. Effect of Permeate-Side Recirculation on the Reverse-
Osmosis Permeate Flux of Triplicate 3N8 Membranes
(400 psi, 50-vol% ethanol feed and recirculation
concentration, ambient temperature)
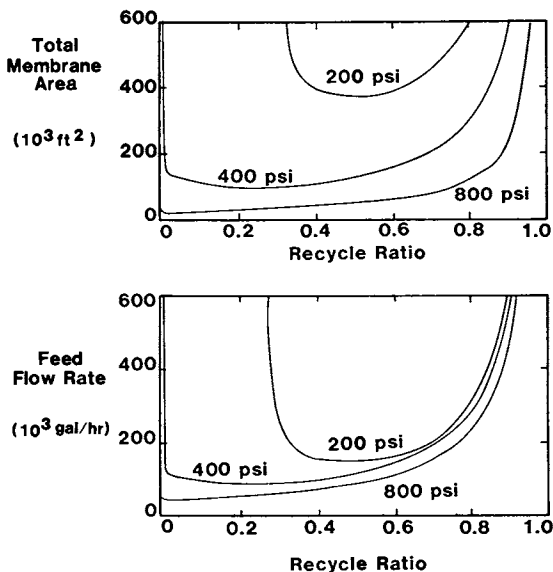
Figure 13. Effect of Recycle Ratio on the Projected Countercurrent
Reverse-Osmosis Performance of 3N8 Membranes at Different
Operating Pressures [Basis: 1000 gal/hr of 50-vol% ethanol
product output.]

are reduced. Furthermore, the optimum recycle ratio is shifted to a
lower value because a smaller amount of recirculation solution would
lower the osmotic pressure gradient as effectively as that
achievable with a higher recycle ratio at a lower operating
pressure. Table I is a summary of the projected CCRO process
performance of the 3N8 membrane.

Table I. Calculated Countercurrent Reverse-Osmosis Performance of
3N8 Membranes at Different Operating Pressures to Enrich a 10-
vol% Ethanol Feed to Produce a 1000 gal/hr Output of 50-vol%
Ethanol Concentrate

Operating Pressure (psi)	Optimum Recycle Ratio	Membrane Area Required (10^3 ft^2)	Feed Solution Flow Rate (10^3 gal/hr)	Power Requirement* (kW)
200	0.5	380	150	296
400	0.25	100	85	335
800	0.015	25	45	355

*Assuming a 70% overall pumping efficiency

The pumping power requirement was calculated from the flow rate
and pressure using the equation:

$$\text{Power Requirement (kW)} = \frac{V_f \text{ (gal/hr) x } \Delta P \text{ (psi)}}{E \text{ x } 145 \text{ x } 10^3 \text{(gal-psi/hr-kW)}}, \quad (16)$$

where E is the overall pumping efficiency, assumed to be 70% in the
calculation.
     The results show that increasing the operating pressure reduces
the required membrane area significantly, yet increases the power
requirement only slightly. The power requirement of 355 kW at 800
psi corresponds to an energy requirement of 0.37 kWh/gal of 50-vol%
ethanol product. Clearly, it would be desirable to operate the CCRO
system at the maximum possible pressure.

Estimated Process Performance with a Hypothetical Membrane. The
CCRO performance of a hypothetical membrane was calculated as an
estimate of the improvement in process performance that may be
realized when better membranes are developed. Assume that a
membrane could be developed to be totally ethanol-resistant and to
also have better selectivity than does 3N8. Specifically, its
transport parameters are assumed to be the same as those of 3N8, but
its ethanol permeability coefficient, ω', is only one-tenth as high.
Because of its better selectivity, the hypothetical membrane would
exhibit higher ethanol rejection and lower fluxes than does 3N8 at
any concentration.
     Table II summarizes the performance of CCRO processes using the
hypothetical membrane to enrich ethanol to two concentrations. The

improved membrane properties resulted in significant energy savings
compared with the less selective 3N8 membrane.

Table II. Calculated CCRO Process Performance of a Hypothetical
    Membrane (see text) at 800 psi for Two Ranges of Ethanol
    Enrichment [Basis: 1000 gal/hr net product output]

| Performance | Range of Ethanol Enrichment | |
Criterion	10 to 50 vol%	10 to 90 vol%
Optimum recycle ratio	0.03	0.22
Membrane area (10^3 ft^2)	17	96
Feed solution flow rate (10^3 gal/hr)	25	145
Power requirement (kW)	200	1140
Energy requirement (kWh/gal)	0.21	1.2

Comparison with Distillation. Conventional distillation produces
ethanol above 90 vol% in concentration. To allow direct comparison
with the CCRO cases discussed above, however, we assumed that the
distillation process is only required to produce ethanol solutions
at concentrations of either 50 vol% or 90 vol%.
    From the vapor-liquid equilibrium data of ethanol-water
mixtures,(11) a 10-to-50 vol% ethanol enrichment by distillation can
be accomplished in a single equilibrium stage. The energy
requirement was calculated as the heat input to a flash evaporator
producing a 50-vol% ethanol distillate. Assumptions were made that
energy would be conserved by heat exchange between the condensing
vapor and the bottoms liquid stream, and that both heat-exchange
operations would be 85% efficient. The calculated net heat input to
the process corresponds to an energy requirement of 1.5 kWh/gal of
50-vol% product. This energy requirement is several times higher
than that of the CCRO process employing 3N8 or the hypothetical
membrane.
    Distillation to 90-vol% ethanol requires multistage operation.
The process calculations were performed according to the Ponchon-
Savarit method.(12)   Assuming the concentration of the ethanol
bottoms stream to be 1 vol%, and a reflux ratio of 1.5 times the
minimum, the heat input to the reboiler corresponds to an energy
requirement of 3.2 kWh/gal of 90-vol% product as distillate, or
about 2.7 times that of a CCRO process employing the hypothetical,
improved membrane.
    On the basis of energy efficiency alone, CCRO appears to be
preferable to distillation. However, the merit of the process can
only be determined when improved membranes similar to that used as
the hypothetical case in our analysis become available, which in
turn will enable a realistic estimate of the capital costs to be
included in the overall cost of ethanol enrichment.

Conclusion

We have demonstrated experimentally that the high osmotic pressure gradients associated with reverse-osmosis enrichment of ethanol can be reduced by adopting the process design of countercurrent reverse osmosis. However, the use of RO membranes in CCRO is limited at present by their inadequate selectivity and poor stability at high alcohol concentrations.

A further requirement of a CCRO membrane is that it should have an open, microporous sublayer structure. Such membranes allow effective diffusion of ethanol into the membrane from a recirculation solution supplied on the permeate side of the membrane. In our survey of various flat-sheet and hollow-fiber membranes, a monomer-derived polyamide composite membrane designated 3N8 was identified which satisfied this requirement. Other membranes tested either exhibited small or no measurable flux increases with permeate-side recirculation and are thus not suited to CCRO applications.

Preliminary analysis suggests that CCRO processes are more energy-efficient than is distillation. However, the overall feasibility of CCRO as an alternative or adjunct to distillation for producing high-purity ethanol also depends on the capital costs associated with the process. The capital cost aspect has not been considered at present because membranes with substantially better performance will be required to make such an analysis meaningful. The merit of CCRO processes therefore requires further verification with improved membranes.

Acknowledgment

Literature Cited

1. Black, C., "Distillation Modelling of Ethanol Recovery and Dehydration Processes for Ethanol and Gasohol," Chem. Eng. Prog., 1980, 76, 78-85.
2. Mehta, G., "Comparison of Membrane Processes with Distillation for Alcohol/Water Separation," J. Membrane Sci., 1982, 12, 1-26.
3. Ohya, H.; Kazama, E; Negishi, Y., "Reverse Osmosis Concentration of Aqueous Ethyl Alcohol Solutions." Kagaku Kogaku Ronbunshi, 1982, 8, 144.
4. Loeb, S.; Bloch, M.R., "Countercurrent Flow Osmotic Process for the Production of Solutions Having a High Osmotic Pressure," Desalination, 1973, 13, 207-215.
5. Lonsdale, H.K.; Merten, U.; Riley, R.L., "Transport Properties of Cellulose Acetate Osmotic Membranes," J. Appl. Polym. Sci., 1965, 9, 1341.

6. Soltanieh, M.; Gill, W.N., "Review of Reverse Osmosis Membranes and Transport Models," Chem. Eng. Comm., 1981, 12, 279-363.
7. Kedem, O.; Katchalsky, A., "The Physical Interpretation of the Phenomenological Coefficients of Membrane Permeability," J. Gen. Physiol., 1961, 45, 143-179.
8. Hara, S.; Mori, K.; Taketani, T.; Noma, T.; Seno, M., "Reverse Osmosis Membranes from Aromatic Polymers," Desalination, 1977, 21, 183-194.
9. Lee, K.L.; Lonsdale, H.K.; Baker, R.W., "Membranes for Power Generation by Pressure-Retarded Osmosis," J. Membrane Sci., 1981, 8, 141-171.
10. Riley, R.L.; Case, P.A.; Lloyd, A.L.; Milstead, C.E.; Tagami, M., "Recent Developments in Thin-Film Composite Reverse Osmosis Membrane Systems," Desalination, 1981, 36, 207-233.
11. Perry, R.H.; Chilton, C.H., Chemical Engineers' Handbook, 5th edition. McGraw-Hill, New York, New York, 1973; p.3-171.
12. Treybal, R.E., Mass Transfer Operations, 2nd edition. McGraw-Hill, New York, New York, 1968; Chapter 9.

Electrically Conductive Membranes Based on Polyacetylene Chemistry

KEN B. WAGENER[1]

Membrana Research Department, Akzona Inc., American Enka Research, Enka, NC 28728

Laminates of porous polymer substrates and polyacetyl-
ene can be produced by first dipping the polymer sub-
strate in a catalyst solution, allowing the solvent to
evaporate, then polymerizing acetylene on the polymer's
surface. Acetylene polymerizes throughout the pore
structure. The polymerization is done in an oxygen-
and water-free environment yielding porous laminates
containing up to 43 weight percent polyacetylene. Non-
porous semicrystalline substrates will not accept near-
ly as much polyacetylene. The laminates retain the
physical properties of the substrate; that is, membrane
properties are not altered. These laminate structures
can be doped with iodine to give conductivities in the
range of 100 to 1000 ohm^{-1} cm^{-1}, whereas all of the
polymers examined in this study are by themselves in-
sulators. The laminates should exhibit magnetic prop-
erties also. Doped polyacetylene, both in the pristine
state and in laminate form, is sensitive to oxygen and
moisture. A two-week exposure of an iodine doped lami-
nate of microporous polypropylene and 18% polyacetylene
causes a loss of up to three orders of magnitude of
conductivity. Recent publications, however, show this
problem might be overcome.

Conductive polymers have been a goal of fundamental polymer research
for many years, mainly because such materials would be lightweight
and presumably moldable into any shape desired. Ten years ago, al-
most every polymer known displayed insulator properties, and re-
search efforts to modify their character met with failure. Since
that time, however, success has been reported in the literature, and
a few conductive polymers do exist now, each with its merits and
drawbacks. Various degrees of conductivity can be achieved princi-
pally by synthesizing an unsaturated, conjugated polymer and doping
it in some fashion. Example polymers are polyphenylene,

[1] Current address: Department of Chemistry, University of Florida, Gainesville, FL 32611.

polyacetylene, polyphenylene sulfide, poly(2,2' bithiophene), TCNQ, polypyrrole, and several organometallic polymers such as polytetramethyltin. The field is scientifically exciting and growing at a rapid pace today [three review articles are cited (1-3)].

Whereas selected unsaturated polymers can be made conductive, making saturated polymers like polyethylene or polypropylene conductive is another matter. Because of their low cost, availability and ease of processing, they are used as electrical insulators, and making them electrically conductive would seem at first thought difficult to do. In one approach, saturated polymers can be made conductive via polyacetylene chemistry by forming composites wherein the conductive phase can be varied in weight percent from 10 to 50 percent (4-5).

Turning to the other aspect of this discussion, today's membranes perform a myriad of separations utilizing one of three mechanisms; that is, mechanical sieving, controlled diffusion, and adsorption, with the first two mechanisms dominating. Driving forces for these separations can be pressure, concentration differential, electrical potential differential or pH differential (a relatively new driving force used in liquid membrane separations). Exemplary applications are:

- Hemodialysis - a controlled diffusion mechanism process driven by concentration differential.
- Desalting sea water via reverse osmosis - a controlled diffusion mechanism process driven by pressure differential.
- Desalting brackish water - a controlled diffusion mechanism process driven by electrical potential.
- Bacteria removal from water via microfiltration - a mechanical sieving process driven by pressure differential.
- Removal of pyrogens from water - an adsorption process driven by pressure differential.
- Removal of valuable elements (for example, uranium) from waste streams via liquid membranes - a diffusion mechanism process driven by pH differential.

To date no one has reported the preparation of "electromembranes". Easily defined, an electromembrane is one which separates with either an electrical or magnetic field. Separations would be the result of placing an electrical potential "barrier" in the path of a composition being separated, or if a full electrical current were allowed to flow, then a magnetic field "barrier" might also cause separations to occur. Driving forces in such separations could be pressure, or as in electrodialysis, electrical potential. Neither of these separation mechanisms (that is, the use of electrical or magnetic environments) has been investigated in detail before, and polyacetylene chemistry offers a novel approach in the development of electromembranes.

Of all the conductive polymers in the current literature, polyacetylene and analogs of this polymer probably have received the widest attention. The polymer is not new (6), having been reported many years ago, yet only in the past ten years has research activity flourished. The reasons for this are simple. In 1974 Shirakawa (7)

and coworkers reported a synthetic technique for creating polyace-
tylene films possessing considerable physical integrity. Prior to
that report, polyacetylene was known as a black powder only, re-
sulting from the instantaneous precipitation of the polymer from
solution. These intractable powders were of considerable scientif-
ic interest but offered little commercial value.

Shortly after Shirakawa's discovery, MacDiarmid and Heeger (8)
described the results of doping these films with both "p" and "n"
type dopants, showing that polymers having a wide range of conduct-
ivity could be created depending upon the nature and the amount of
dopant incorporated. This disclosure sparked an immense effort to
find out more about doped polyacetylenes, both with regard to the
mechanism of its conductivity and to uncover possible applications.
The eight years of research have turned out literally hundreds of
research papers [a polyacetylene review is cited (9)]. Important
results are:

1. Doped polyacetylene conducts electrons via an intrinsic mecha-
nism rather than by an extrinsic one. That is to say, conductivity
of the polymer is due directly to electronic conductivity rather
than to charge carrier motion.

2. "P" doped polyacetylene results in the formation of highly con-
jugated carbenium ions, whereas "n" doped polymer forms highly con-
jugated carbanions. These "holes" and "electrons", respectively,
are thought to move along the polymer backbone.

3. Both cis and trans forms of polyacetylene can be made with the
trans isomer being the most stable.

4. Both types of polyacetylene are highly crystalline, intractible
solids. The morphology of polyacetylene films consists of fibrils
about 200 Angstroms in diameter oriented normal to the surface of
the film.

5. Substitution on polyacetylene reduces the crystallinity of the
polymer and also decreases its conductivity. Solubility increases
with substitution.

6. Conductivities as good as 10^{-4} ohm^{-1} cm^{-1} are possible. Figure
1 shows the range of conductivities that have been achieved (10).

7. Polyacetylene is paramagnetic, having a spin density of 10^{17} to
10^{19} spins/gram, depending upon the degree of crystallinity and oxy-
gen content.

8. Films of polyacetylene can be oriented to create an anisotropic
conductivity response when doped.

9. The conductivity of the doped polymer is quite sensitive to its
environment, with both oxygen and water leading to decay. "N" doped
polymers are extremely sensitive to ambient conditions.

Given that "electromembranes" may have utility, and given that con-
ductive polymer research has advanced considerably in recent times,
it was decided to investigate synthetic methods to create electro-
membranes using microporous membranes as substrates for the deposi-
tion of Ziegler-Natta and Luttinger catalysts, followed by the het-
erogeneous polymerization of acetylene.
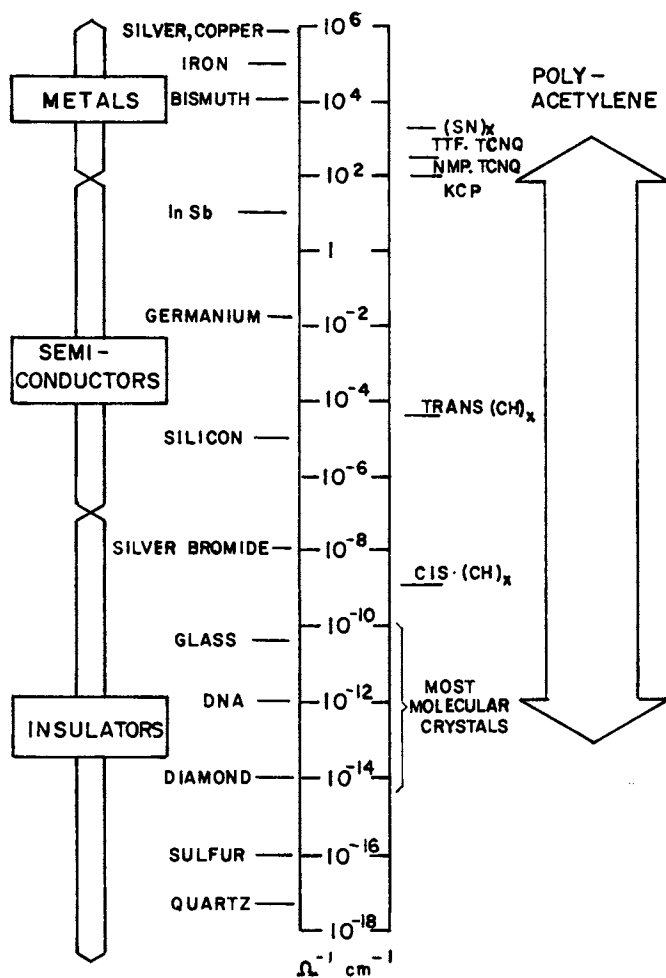
Figure 1.   Conductivity range of polyacetylenes.   Reproduced with
permission from Ref. 10.

Experimental

Procedure 1: Preparation of a Polypropylene/Polyacetylene Structure
        Containing 5.7 wt % Polyacetylene. Acetylene was polymerized
using an aluminum/titanium catalyst system that was prepared as fol-
lows. Approximately 200 mL of freshly distilled toluene (dried over
CaH$_2$) was transferred to a Schlenk tube using a constant argon purge.
The purge involved the use of specially modified ground glass joints
on the Schlenk tube such that contact with air was completely elimi-
nated. A magnetic stirring bar was placed in the tube, again keeping
an argon blanket in place. Distilled titanium tetrabutylate, 17 mL,
was added to the tube and dissolved in the stirred toluene. Neat
triethylaluminum, 27 mL, was then slowly added to the solution,
which resulted in the formation of a very dark color and the evolu-
tion of a gas. Additions were made with dried syringes at ambient
temperatures. The catalyst solution, a Ziegler-Natta catalyst solu-
tion, was aged for approximately three hours.
        Samples of microporous polypropylene were prepared for treat-
ment with the catalyst solution. Microporous polypropylene (0.2
micrometer rated) membrane properties are shown in Table I.

Table I. Microporous Polypropylene
Rated Pore Size 0.2 Micron

Thickness	180 micrometers
Maximum Pore Size	0.55 micrometers
IPA Bubble Point	115 kPa (16.6 psi)
Air Flow	1.3 L/cm^2 min @ 69 kPa (10 psi)
Shrinkage, Machine Direction	1.3%
Shrinkage, Cross Machine Direction	0.4%

An 0.8470-gram sample of the above membrane was placed in a dry box
via an evacuated antechamber. The Schlenk tube containing the cata-
lyst solution described above was moved into the dry box. The fol-
lowing techniques were performed in a nitrogen dry box atmosphere.
        A 10-mL aliquot of the catalyst solution was diluted with 100
mL of freshly distilled toluene in a beaker. The solution was
stirred for five minutes, and then the membrane sample was placed in
the solution. The catalyst solution immediately penetrated the
microporous structure. The sample was allowed to soak for about
five minutes and then was allowed to dry in the box under blowing
nitrogen for 10-15 minutes, giving a membrane with the solid state
catalyst components deposited within the pore structure of the poly-
propylene. Weight of the sample plus the deposited catalyst was
0.8872 grams, or a wt % gain of 4.7%. The sample was placed in an
empty Schlenk tube and removed from the dry box.
        Polymerization of acetylene within the microporous pore struc-
ture was accomplished on a vacuum line in order to assure absolutely
no contact with either oxygen or water. A one-liter gas storage
bulb was mounted on a vacuum line manifold and evacuated as much as
possible (to less than 10^{-5} mm). A stoichiometric excess of acetyl-
ene from a cylinder was introduced into the bulb until a pressure
(measured by a manometer) of 740 mm Hg was attained. The cold
finger of the gas storage bulb was immersed in liquid nitrogen to

freeze the acetylene, and the space above the solid acetylene was
then exposed to high vacuum (a procedure to remove any oxygen or
other gases that might have been present in the acetylene). A
vacuum better than 10^{-5} was achieved.

The bulb was sealed off from the vacuum line, and the acetyl-
ene was allowed to sublime. The pressure in the bulb went to ap-
proximately 600 mm Hg, indicating that dissolved oxygen (or perhaps
another gas) indeed was present in the acetylene stream. This pro-
cedure was repeated twice to bring the total pressure of acetylene
in the storage bulb up to 740 mm Hg. The bulb was left on the vac-
uum line.

At this point, the Schlenk tube containing the sample was
mounted on the vacuum line and evacuated for about 30 minutes,
bringing the pressure down to $<10^{-5}$ mm Hg. The vacuum was sealed
off from the vacuum manifold, thus leaving a pathway between the
mounted gas storage bulb containing acetylene and the Schlenk tube.

By controlling the stopcocks on the vacuum manifold, it was
possible to slowly introduce acetylene from the bulb into the evac-
uated Schlenk tube. Only 15 mL of acetylene was introduced at a
time with intervals of about 5 minutes. During this period, the
sample visually changed, becoming darker with each introduction.
After the procedure was repeated five or six times, the stopcocks
were opened fully, giving a free passageway between the storage
bulb and the Schlenk tube. Polymerization continued, as evidenced
by a slow reduction in the acetylene gas pressure in the system,
and the reaction continued overnight (about 16 hours).

The polymerization was done at room temperature. The sample
eventually changed from the characteristic white color of micro-
porous polypropylene to a deep purple due to the presence of poly-
acetylene.

Once the polymerization was complete, the Schlenk tube was re-
moved from the vacuum line and taken again into the dry box. The
tube was opened and the sample removed. Catalyst was washed from
the sample via repeated rinsings with freshly distilled toluene,
with the washings being continued until the toluene coming from the
sample was colorless. The sample was allowed to dry in the box
until no change in weight (with time) was observed. The final
weight of the microporous polypropylene/polyacetylene structure was
0.9012 grams, or a gain of 0.512 grams of acetylene. Thus, the
weight percentage of polyacetylene in the laminate structure was
5.7%. The structure displayed flexibility equal to that of micro-
porous polypropylene alone.

The structure was then doped to produce a laminate with high
electrical conductivity. Two dopants were investigated, iodine and
nitrosonium hexafluorophosphate.

Doping with iodine was relatively easy. An undoped sample was
placed in a chamber and exposed to flowing argon containing a low
concentration of iodine. The iodine was introduced by passing ar-
gon over iodine crystals prior to entering the sample chamber.
Sample exposure time normally was 4-6 hours. The use of iodine
gave a "p" doped material.

Using such a procedure, a sample of the microporous polypropyl-
ene/polyacetylene structure consisting of 5.7% polyacetylene was
doped to the maximum level.

The electrical conductivity of the sample was measured using the four-probe technique, which has been described in detail in the literature. The technique consisted of mounting a sample of known dimensions on a glass plate with four platinum wires, making contact with the sample using graphite cement (Electrodag 502, Acheson Colloids Co.). A current was applied across the outer two platinum leads, and the voltage across the inner two leads was measured.

Microporous polypropylene has a poor conductivity ($<10^{-16}$ ohm^{-1} cm^{-1}), whereas the microporous polypropylene/polyacetylene laminate doped with iodine had a conductivity of 7.3×10^{-1} ohm^{-1} cm^{-1}, representing an improvement in conductivity of 10^{16}. This final conductivity compares well with that of pure polyacetylene doped with iodine.

The membrane properties of the microporous polypropylene/polyacetylene structure were measured, and a comparison with the original properties is given in Table II.

Table II. Microporous Polypropylene Properties

Property	Microporous Polypropylene Alone	Microporous Polypropylene/ Polyacetylene Structure
Thickness, micrometers	180	182 micrometers
Maximum Pore Size, micrometers	0.55	0.55 micrometers
IPA Bubble Point, kPa (psi)	115 (16.6)	113 (16.4)
N_2 Flow, L/cm^2 min @ 69 kPa (10 psi)	1.3	1.3
IPA Flow, L/cm^2 min	-	4.13
Water Flow, mL/cm^2 min	-	8.29

Clearly, the laminate retained microporous membrane properties, which could have a variety of uses. The microporous nature of the laminate also could be seen in scanning electron micrographs. Little change in structure, as compared with the original membrane, could be detected. Also, there was no detectable change in flexibility.

The conductivity of doped polyacetylene is known to be transient when the polymer is exposed to oxygen and/or water. The structure prepared as described in this example exhibited similar properties. Table III shows how the laminate's conductivity worsens with time.

The structure was also doped using nitrosonium hexafluorophosphate, NOPF$_6$. This technique was simple, and because of the chemistry involved, it yielded a "p" doped system carrying the PF$_6$ anion on the polymer chain. Doping consisted of soaking a piece of the microporous polypropylene/polyacetylene structure in a mixed solvent of nitromethane/methylene chloride (2:3 by volume) containing approximately 1% dissolved NOPF$_6$. The doping time was 4 minutes, which yielded a laminate having a conductivity of 3.8×10^{-2} ohm^{-1} cm^{-1}. Changes in conductivity in air for this doped laminate are given in Table IV.

Table III. Change in the Conductivity of Iodine Doped
    Microporous Polypropylene/Polyacetylene Structure
    Containing 5.7% Polyacetylene Upon Exposure to Air

Time, hr	Conductivity, ohm^{-1} cm^{-1}
0	9.7×10^{-1}
1	7.1×10^{-1}
18	4.8×10^{-1}
42	3.1×10^{-1}
71	2.2×10^{-1}
89	1.7×10^{-1}
186	5.4×10^{-2}
211	4.4×10^{-2}
233	3.5×10^{-2}
259	2.6×10^{-2}
329	1.3×10^{-2}
353	9.6×10^{-3}
384	6.5×10^{-3}

Table IV. Change in the Conductivity of $NOPF_6$ Doped
    Microporous Polypropylene/Polyacetylene Structure
    Containing 5.7% Polyacetylene Upon Exposure to Air

Time, hr	Conductivity, ohm^{-1} cm^{-1}
0	3.8×10^{-2}
1	2.2×10^{-2}
18	1.0×10^{-2}
42	3.0×10^{-3}
71	9.0×10^{-4}
89	7.0×10^{-4}
186	3.8×10^{-5}
211	3.3×10^{-5}
233	1.3×10^{-5}
259	7.5×10^{-6}
329	2.0×10^{-6}

Procedure 2: Preparation of a Microporous Polypropylene/Polyacetyl-
    ene Structure Containing 13.5 wt % Polyacetylene. The proce-
dure followed here was virtually the same as described above except
for the change in the concentration of the catalyst.

A 25-mL aliquot of the original catalyst solution was diluted
with 100 mL of freshly distilled toluene, and a 0.8441-gram sample
of polypropylene membrane, taken from the same lot as that used in
Procedure 1, was soaked in this solution as before. The sample
weighed 0.9328 grams after catalyst pickup, or an increase in weight
of 10.5%.

After acetylene polymerization and washing to remove catalyst,
the sample weighed 0.9763 grams. Thus, the structure contained
13.5% polyacetylene. No change in flexibility was noted, and the
structure was still microporous as shown by SEM photographs. The
laminate was dark with an obvious purple hue.

Doping with iodine improves the conductivity of the structure to
7.3 x 10⁻¹ ohm⁻¹ cm⁻¹; NOPF₆ doping brought the conductivity to
1.03 ohm⁻¹ cm⁻¹. In both cases, conductivity decay in air was simi-
lar to the behavior observed in Procedure 1.

Procedure 3: Preparation of a Microporous Polypropylene/Polyacetyl-
    ene Structure Containing 18.0 wt % Polyacetylene. The proce-
dure followed here was virtually the same as described in Procedure
1 except for a change in the catalyst concentration.

A 50-mL aliquot of the original Shirakawa catalyst was diluted
with 100 mL of freshly distilled toluene, and a 0.9597-gram sample
of polypropylene membrane, taken from the same lot as before, was
soaked in this solution. The sample weighed 1.1266 grams after
catalyst pickup, or an increase in weight of 17.4%.

After acetylene polymerization and washing with toluene to re-
move catalyst, the sample weighed 1.1703 grams. Thus, the structure
contained 18.0% polyacetylene. No change in flexibility was noted,
and the structure was very dark in color with a detectable purple
hue.

Doping with iodine improved the conductivity of the structure
to 1.92 ohm⁻¹ cm⁻¹; NOPF₆ doping brought the conductivity to 1.21
ohm⁻¹ cm⁻¹. In both cases, conductivity decay in air was similar to
the behavior observed in Procedure 1.

Procedure 4: Preparation of a Microporous Polypropylene/Polyacetyl-
    ene Structure Containing 4.3 wt % Polyacetylene. The procedure
followed in this experiment was virtually the same as described in
Procedure 1 except for a change in the catalyst concentration.

A 5-mL aliquot of the original Shirakawa catalyst was diluted
with 100 mL of freshly distilled toluene. A 0.6905-gram sample of
microporous polypropylene membrane, taken from the same lot as used
in Procedure 1, was soaked in this solution. The sample weighed
0.6944 grams after catalyst pickup, or an increase of 0.56%.

After acetylene polymerization and washing to remove catalyst,
the sample weighed 0.7201 grams. Thus, the structure contained 4.3%
polyacetylene. No change in flexibility was noted, and the struc-
ture still is microporous as shown by SEM photographs. Only a light
purple color is evident on the structure.

Doping with either iodine or NOPF₆ did not make the structure
conductive. Apparently a lack of continuity of the polyacetylene
phase existed with this low level of polyacetylene.

Procedure 5: Use of the Luttinger Catalyst System to Create 0.2-
    Micron Rated Microporous Polypropylene/Polyacetylene Structures.
The Luttinger catalyst was prepared as follows. Sodium borohydride,
0.020 grams, was dissolved in 50 mL of absolute ethanol with stir-
ring, and the solution was then cooled to -76°C in a dry ice bath.
To this solution was added 1 mL of a 1.0 wt % solution of cobalt
nitrate in absolute ethanol. The solutions were made under ambient
conditions with no attempt to exclude air or water. However, after
the catalyst was made, an argon blanket was placed over the solution.

Samples of microporous polypropylene taken from the same lot
used for Procedures 1 through 4 were dipped in the catalyst solution
and quickly placed in a chamber full of flowing acetylene. Polymer-
ization occurred immediately.

The structures were doped with iodine using the procedures described previously, and their conductivities were measured as before. Initial conductivity was 1.5×10^{-1} ohm^{-1} cm^{-1}, and the decay in conductivity on exposure to air was similar to that observed in Procedure 1.

The effect of soak time in the Luttinger catalyst was also studied. Samples were dipped quickly once, dipped quickly five times, soaked for 3 seconds, for 5 seconds, for 10 seconds and for 1 minute, then exposed to acetylene. No change in performance was observed.

Procedure 6: Use of the Luttinger Catalyst System to Create 0.1-Micron Rated Microporous Polypropylene/Polyacetylene Structures. In order to investigate the effect of pore size on microporous polypropylene/polyacetylene conductivity, samples of 0.1 micrometer rated microporous polypropylene were treated with the Luttinger catalyst using the method described in Procedure 5. Properties of the sample are shown in Table V.

Table V. Microporous Polypropylene, Rated Pore Size 0.1 Micron

Thickness	100 micrometers
Maximum Pore Size	0.31 micrometers
IPA Bubble Point	207 kPa (30.0 psi)
Air Flow	0.1 L/cm^2 min @ 69 kPa (10 psi)
Shrinkage, Machine Direction	2.4%
Shrinkage, Cross Machine Direction	0.9%

The polymerization procedure was identical to that used in Procedure 5. Initial conductivity is 1.2×10^{-1} ohm^{-1} cm^{-1}, conductivity decay was as before, and no change in membrane performance was observed.

Procedure 7: Preparation of a Microporous Polypropylene/Polyacetylene Structure Using a Dry Box Apparatus Rather than a Vacuum Line to Give Microporous Polypropylene/Polyacetylene Structures Using a Ziegler-Natta Catalyst. This experiment and the one described in Procedure 8 were performed exclusively in a dry box apparatus rather than employing both a dry box and a vacuum line.

A dry box was prepared for the experiment first by purging with nitrogen, then scrubbing the nitrogen within the chamber with the attached atmosphere purification system. Specifications for the purification system claim a reduction of moisture and oxygen down to less than 1 ppm.

Catalyst solutions were prepared in an open beaker on a stirrer plate in the box. Distilled titanium tetrabutylate, 10.2 grams, was poured into a 100-mL beaker containing a stirrer bar, followed by the slow addition of 47 mL of a 25% by weight active solution of triethylaluminum in toluene.

The solution was placed in a 1-liter resin kettle, the top was mounted, and a vacuum was slowly applied to remove the gas that was evolved. The vacuum was kept in place for 20 minutes. The solution was then returned to the beaker.

A sample of microporous Accurel polypropylene membrane was then prepared for exposure to the catalyst system. Characteristics of the membrane are described in Table VI.

Table VI. Microporous Polypropylene Membrane Properties

Thickness	180 micrometers
Maximum Pore Size	0.49 micrometers
Bubble Point	130 kPa (19 psi)
Water Flow	11.28 mL/cm^2 min

A 7.6 cm x 5 cm sample of this membrane was dried overnight in a vacuum oven at 105°C. This sample, which had been transferred to the dry box, was soaked in the catalyst solution for about 3 minutes and then immediately exposed to vacuum in the resin kettle for 10 minutes. After this treatment, the sample was observed to be off-white.

The resin kettle was rigged to allow for a continuous flow of acetylene into it. The vacuum was released to acetylene, thus completely blanketing the sample in one atmosphere of this gas. The sample was exposed to acetylene for about 10 minutes, followed by a nitrogen sweep. During this period, the sample shrank slightly and became somewhat darker.

The sample was removed from the kettle and washed copiously with freshly distilled toluene until it was evident that no further catalyst was being removed.

The sample was placed in an iodine chamber for doping. The sample, which still remained off-white in the dry state, appeared to be conductive as judged by the two-point probe method (instead of the four-point method for measuring resistance). Values as small as 500 ohms were measured when touching the sample with probes approximately 1 cm apart.

The sample exhibited no change in flexibility as compared with untreated microporous polypropylene.

Procedure 8: Preparation of a Microporous Polypropylene/Polyacetyl-
        ene Structure Using a Dry Box Apparatus Rather than a Vacuum
        Line to Give Uniform Structures. The experimental procedure used in this example was essentially the same as that used in Procedure 7. Makeup of the catalyst solution was as before, and the treatment procedure was the same except that a vacuum was not used. Dipping the membrane sample in the catalyst solution, followed by exposure to acetylene was repeated four times.

The appearance of the sample was quite different from that in Procedure 7. After only one exposure, the sample was dark in color, indicating a more uniform deposition of polyacetylene throughout. Multiple exposures gave an even darker membrane.

Conductivity of the sample was identical to that for the sample from Procedure 7. As before, the sample was quite flexible.

Procedure 9: Preparation of a Microporous Polyethylene/Polyacetyl-
        ene Structure Containing 43 wt % Polyacetylene. A sample of microporous polyethylene was prepared for treatment with the catalyst solution. Characteristics of the membrane are described in Table VII.

Table VII. Microporous Polyethylene Membrane Properties

Thickness	130 micrometers
Maximum Pore Size	0.52 micrometers
IPA Bubble Point	121 kPa (17.6 psi)
Water Flow	9.25 mL/cm^2 min
Air Flow	1.15 L/cm^2 min @ 69 kPa (10 psi)

A 0.5600-gram sample of the above membrane was placed in a dry box via an evacuated antechamber. The Schlenk tube containing the catalyst solution described above was moved into the dry box also.

A 50-mL aliquot of the catalyst solution, prepared as in Procedure 1, was diluted with 50 mL of freshly distilled toluene in a beaker. The solution was stirred for 5 minutes, and then the polyethylene sample was placed in the solution. The catalyst solution immediately penetrated the microporous structure; even so, the sample was allowed to soak for 2 minutes. The sample was then allowed to dry in the box under blowing nitrogen for 10-15 minutes, giving a membrane with the catalyst components deposited within the pore structure of the polypropylene. The sample was placed in an empty Schlenk tube and removed from the box.

After acetylene exposure and iodine doping, the conductivity was 11.21 ohm^{-1} cm^{-1}.

Procedure 10: Preparation of a Microporous Polyvinylidene Fluoride/ Polyacetylene Structure Containing 17% Polyacetylene. A 1.2992-gram sample of a microporous polyvinylidene fluoride (PVDF) membrane having properties described in Table VIII was dipped in a catalyst solution prepared as in Procedure 1. The acetylene polymerization was carried out in the same manner as before. Sample weight after catalyst removal was 1.5690 grams; thus, the structure contained 17% polyacetylene. After iodine doping, the conductivity was 1.09 x 10^{-2} ohm^{-1} cm^{-1}. Conductivity after 10 days in air was 4.4 x 10^{-4}ohm^{-1} cm^{-1}, indicating conductivity decay as before.

Table VIII. Microporous PVDF Membrane Properties

Thickness	264 micrometers
Maximum Pore Size	0.52 micrometers
IPA Bubble Point	129 kPa (18.7 psi)
Water Flow	0.09 L/cm^2 min
Air Flow	0.44 mL/cm^2 min @ 69 kPa (10 psi)

Procedure 11: Preparation of a Microporous Polypropylene/Polyacetylene Structure Containing 32% Polyacetylene. A microporous polypropylene sample having membrane properties virtually identical to those in the previous examples was dipped in the catalyst solution of Procedure 1 and exposed to acetylene. The initial weight was 0.9916 grams; after exposure, catalyst removal and drying, the weight was 1.4573 grams. After iodine doping, the conductivity was 1.59 ohm^{-1} cm^{-1}. Following 10 days of air exposure, the conductivity became 4.8 x 10^{-2} ohm^{-1} cm^{-1}.

Procedure 12: Attempt to Prepare a Nylon 6/Polyacetylene Structure.
Samples of nylon 6 membrane prepared by the formic acid process
were dipped into the catalyst solution of Procedure 1, and in doing
so, the membrane appeared to become brittle. Exposure to acetylene
did not result in polymerization, and no weight increase was evident
after the polymerization procedure was completed.

The nylon membrane samples became less brittle upon standing in
air for several days.

Results and Discussion

Conductive Porous Structures Made with the Ziegler-Natta Catalyst
System. Using rather straightforward experimental techniques, it
was possible to render a number of porous structures conductive by
forming a laminate with the porous substrate polymer and doped poly-
acetylene. The laminate was prepared by first loading the porous
substrate with a Ziegler-Natta solution in an inert environment fol-
lowed by evaporation of the solvent (toluene) from the substrate.
This procedure left a uniform solid-state deposit of catalyst
throughout the pore structure. Purified acetylene was then intro-
duced which polymerized instantly and formed a layer of polyacetyl-
ene on the pore walls. Subsequent doping with iodine or nitrosonium
hexafluorophosphate produced a conductive laminate. As shown in
Table IX, porous polypropylene, polyethylene and polyvinylidene
fluoride could be made conductive, whereas nylon 6 could not.

Table IX. Ziegler-Natta Catalysis
Conductivity Data for Several Porous Polymer Substrates

Procedure Number(s) (See Experimental Section)	Polymer Type	Conductivity Range, $ohm^{-1} cm^{-1}$
1 through 4, 7, 8, 11	Polypropylene	10^{-1} to 10^1
9	Polyethylene	10^1
10	Polyvinylidene Fluoride	10^{-2}
12	Nylon 6	Nonconductive

Two different experimental methods were used in this work, one fol-
lowing standard polyacetylene vacuum line/dry box techniques and the
other employing a dry box setup only. Both methods gave similar re-
sults, although rigorous exclusion of contaminants such as oxygen
and water was more difficult to achieve with the all-dry box method.

In the all-dry box method, catalyst was made in the box and
placed in a polymer reaction vessel, which was connected to an
acetylene tank and a vacuum source. The membrane sample was placed
in the bottom of the vessel where it was penetrated by the catalyst
solution, then the membrane was supported on a small frame. The
vessel was closed and vacuum applied to remove the solvent. Once
this was done, the vacuum was opened to acetylene, and the gas was
allowed to flow through the reaction vessel until the polymerization
was complete.

Experimental difficulties with the all-dry box method were
many. Polymerizations were slow or did not occur at all. Successful
experiments occurred only sporadically, and these frustrations led to

the vacuum line method, where it was found that the dry box frustrations probably were caused by oxygen being present in the acetylene.

In the vacuum line method, membrane samples were prepared for exposure to acetylene in the dry box and then placed in a Schlenk tube. The tube was connected to a vacuum line for exposure to purified acetylene. The only real experimental difficulty encountered was too fast a rate of polymerization; in the first experiment, the heat of polymerization actually melted the substrate polymer polypropylene. This problem was overcome by diluting the catalyst system prior to treating the substrate, thus leaving a smaller amount of catalyst on the pore walls. Slower polymerization rates resulted. Smaller quantities of acetylene were introduced in a stepwise manner (only 15 mL at a time) with time between steps to allow for heat dissipation. Once polymerization was complete, the sample was doped in the dry box.

Most of the research was done with 0.2 micrometer rated porous polypropylene (Accurel) membrane, and the concentration of polyacetylene in the composite could be varied from 4 to 43 percent. Larger percentages should be possible. The membranes did not lose their flexibility, and membrane properties such as flux rates and bubble point pressure were not altered (see Experimental Procedure 1). As is the case for polyacetylene alone, the conductivity of these membranes could be varied depending upon the type and amount of dopant. Iodine doped laminates were the most stable of the two doped laminates investigated in this study.

It seems reasonable to expect that any polymer which does not contain an active hydrogen could be used as a substrate in this work. Polyethylene and polyvinylidene fluoride gave reasonable results, both samples retaining their flexibility and possessing a high degree of porosity as observed by scanning electron micrograph photos. Nylon 6 membranes did not behave well, however. The nylon sample became brittle when soaked in the catalyst system and did not increase in weight upon exposure to acetylene, nor was a weight increase observed upon attempted doping. Apparently, acetylene polymerization did not occur at all. Interestingly, the embrittled nylon became more flexible upon standing in air for a couple of days. These observations suggest that the catalyst reacts with nylon, most likely with the amide proton, and the fact that the polymer becomes brittle implies either the polymer loses molecular weight or becomes cross-linked in some fashion. The latter is more likely to be true, and the return of some degree of flexibility to the polymer after exposure to air (water) suggests a reversal of this cross-linking reaction, perhaps as the result of hydrolysis, which would return the amide proton to nylon 6.

Polyacetylene is a colorful polymer. The cis isomer transmits red light, the trans isomer blue, and because these polymers often come in mixtures of cis and trans, various shades of purple result. If well formed films of polyacetylene are made, the surfaces reflect silver and, sometimes, gold. Polyacetylene in powder form appears black. The vacuum line experiments produced membranes which appeared purple when wet with solvent (transmitted light - the membrane is transparent when wet) and silver when dry (reflected light - the membrane is opaque when dry).

The all-dry box procedures resulted in another interesting visual
effect. By controlling the solvent removal step; that is, how long
a vacuum was applied to the polymerization vessel, the location of
the polyacetylene within the membrane structure could be regulated.
For example, sandwich structures could be created by immediately
applying a vacuum to a membrane sample wet with catalyst solution.
This technique caused the solution to move into the center of the
membrane's cross section; thus polyacetylene formed only in the cen-
ter of the cross section as well. The presence of polyacetylene,
then, was hidden by the membrane's surface. Consequently, the sur-
face of the membrane appeared almost white when dry (opaque) but in-
stantly turned very dark when wet with solvent (transparent - poly-
acetylene then could be seen). Upon drying, the membrane again
turned white. The phenomenon could be observed countless times with
the same sample.

Conductive Porous Structures and Films Made with the Luttinger
Catalyst System. The Luttinger catalyst system (11), which is a
combination of sodium borohydride and cobalt nitrate, can be used
to create conductive polymers. It is easier to work with because
inert conditions are not required for all experimental steps. The
procedure is fast and can be used for screening experiments; how-
ever, the polyacetylene that is formed is of lower quality and
would not be suitable for long-term applications. Table X gives
conductivity data for one nonporous and two porous substrates. The
experimental section provides appropriate details.

Table X. Luttinger Catalysis
Conductivity Data for Two Porous Polymer Substrates

Procedure Number(s) (See Experimental Section)	Polymer Type	Conductivity Range ohm^{-1} cm^{-1}
5 and 6	Porous Polypropylene	10^{-1}

Emerging Polyacetylene Chemistry Improvements. The conductivity of
doped polyacetylene is extremely sensitive to oxygen and water, and
the same is true for the conductive laminates described in the pre-
ceding section. Figure 2 demonstrates the effect of ambient condi-
tions (that is, exposure to air) with time, and it is evident from
this plot that the practical utility of polyacetylene laminates will
have to be limited to nonambient conditions unless some method of
stabilization is discovered. Recently, two papers have appeared
describing conditions for doped polyacetylene having improved con-
ductivity stability. Wnek and Guiseppi-Elie (12) show that poly-
acetylene films doped with iodine exhibit significant improvements
in conductivity stability when they are dipped in aqueous chloride
solutions. Schue, et al. (13) report that conductive polyacetylene
films can be made by dipping them in toluene solutions of transition
or lanthanide salts. While the stabilization mechanism is not well
understood, it may be similar in both cases.
     Ion implantation also may offer some degree of stabilization.
Maby and Day (14) have shown that films of polyphenylene sulfide
implanted with inert gases such as krypton exhibit stable
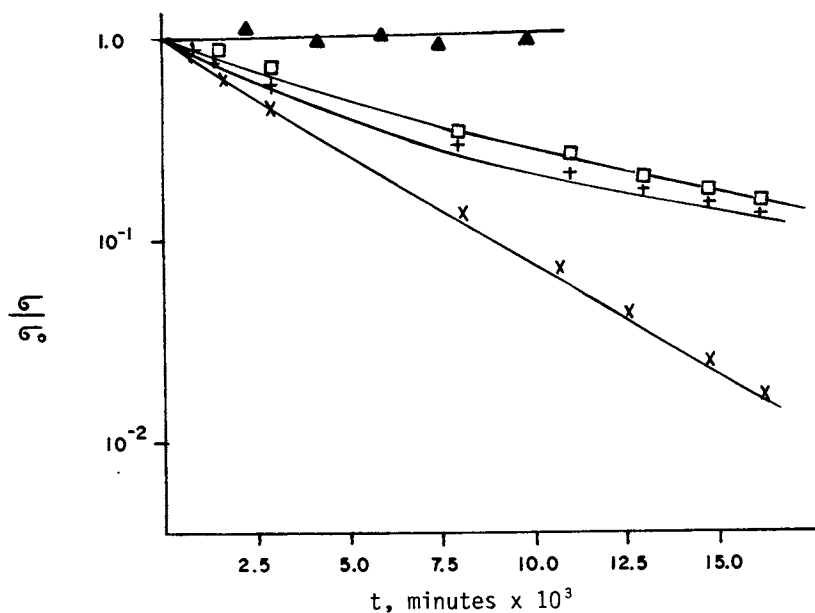
Symbol	Membrane Type, % Polyacetylene	σ_0, Ω^{-1} cm^{-1}
▲	Polypropylene, 18%, ion implanted with Krypton	6×10^{-5}
□	Polyethylene, 43%	11.21
+	Polypropylene, 32%	1.59
X	PVDF, 17%	1.09×10^{-2}

σ_0 = Conductivity at t = 0.
σ = Conductivity after exposure to air.

Figure 2. Conductivity decay of iodine doped Accurel membrane/
polyacetylene laminates.

conductivities for up to a year. Conductivities are not as good, however. Ion implantation also stabilizes the conductivity of the doped laminates described in this report.

Because of the stability problem, polyacetylene may not be the best conductive polymer to pursue. Other polymers, like the poly-pyrroles, might prove more useful in making electromembranes, or, electroless plating of membranes might be the preferred route to making them electrically conductive. It might be possible to elec-troplate laminates of polyacetylene and membranes to make them per-manently conductive. In any event, electromembranes offer a great enough potential to make their pursuit worthwhile.

Acknowledgments

Literature Cited

1. Gill, W.D.; Clarke, T.C.; Street, G.B. Appl. Phys. Commun. 1983, 2, 211-282.
2. Shirakawa, H. Kobunshi 1983, 32, 431-437.
3. Duke, C.B.; Gibson, H.W. Kirk-Othmer Encycl. Chem. Technol., 3rd Ed. 1982, 18, 755-793.
4. Galvin, M.; Wnek, G. Polymer 1982, 23, 795-797.
5. Robner, M.F.; Tripathy, S.K.; Georger Jr., J.; Cholewa, P. Macromolecules 1983, 16, 870-874.
6. Natta, G.; Mazzanit, G.; Corradini, P. Atti. Acad. Nazl. Lincei. Reud. Classe. Sci. Fis. Mat. Nat. 1958, 25, 3-7.
7. Ito, T.; Shirakawa, H.; Ikeda, S. J. Poly. Sci., Poly. Chem. Ed. 1974, 12, 11-16.
8. Chiang, C.; Fincher Jr., C.; Park, Y.; Heeger, A.; Shirakawa, H.; Louis, E.; Gau, S.; MacDiarmid, A. Phys. Rev. Lett. 1977, 39, 1098-1107.
9. MacDiarmid, A.; Heeger, A. Syn. Metals 1979, 1, 101-117.
10. Wnek, G. Ph.D. Thesis, University of Massachusetts, Amherst, 1980, p. 36.
11. Lieser, G.; Wegner, G.; Müller, W.; Enkelmann, V. Makromol. Chem., Rapid Comm. 1980, 1, 621-631.
12. Wnek, G.; Guiseppi-Elie, A. J. Chem. Soc., Chem. Comm. 1983, 63-68.
13. Shue, F.; Giral, L.; Rolland, M.; Adisei, M.; Dubois, J.; Gazard, M. European Patent Application EP69,641, 1983.
14. Mazurek, H.; Day, D.; Maby, E.; Abel, J.; Senturia, S.; Dresselhaus, M.; Dresselhaus, G. J. Poly. Phys. 1983, 21, 537-543.

Biofunctional Synthetic Membranes

MASUO AIZAWA

Institute of Materials Science, University of Tsukuba, Sakura-mura, Ibaraki 305, Japan

The many dramatic developments in biotechnology
over the past few years have enabled great advances
in our ability to mimic the function of biomembranes.
Using a relatively simple case, molecularly
recognizable membranes are synthesized by
amalgamating bioactive substances such as antibodies
within a polymeric membrane matrix. Matrix-bound
biomolecules can retain the function of molecular
recognition in a manner similar to that of the native
form. Molecularly recognizable membranes provide
selectivity for specific substances and find a number
of novel applications including biosensors and
bioreactors. Selection of the membrane matrix is
discussed as part of the materials science of
biofunctional synthetic membranes. In addition,
several biofunctional synthetic membranes are
described.

We may learn from biological membranes how nature has solved some
of the same problems that face synthetic membrane scientists. An
increasing knowledge of the architecture and function of biological
membranes has led a number of synthetic membrane scientists to
incorporate specific and efficient biological membrane constituents
into synthetic membrane matrices. A close look at biological
membranes reveals that the basic structure contributing to the
membrane thickness is the lipid bilayer and the proteins, including
those associated with the polar groups of the membrane surface and
those hydrophobically attached to the lipids of the membrane matrix.
Another important aspect of cell membranes is that they are fluid.
In fact, the plasma membrane can be thought of as a two-dimensional
liquid with a viscosity some ten times that of water.
    These understandings encourage us to utilize the lipid
bilayer as a membrane matrix in which to incorporate biological
molecules. It has been proven that planar bilayer lipid membranes
(BLM) and liposomes may serve as biomimic membrane matrices. They

are, however, noncovalent assemblies of their constituents. Hydrophobic interactions among the lipids serve as organizing forces. The practical consequence of such relatively weak binding forces is that they are mechanically much more fragile than most synthetic membranes and are unable to withstand significant mechanical or chemical disruption. From a practical viewpoint, it is important to develop stable biofunctional synthetic membranes. Various biological molecules have been incorporated into polymer membrane matrices, which are mechanically more stable. During the past ten years it has become possible to obtain a variety of biofunctional synthetic membranes, which have found novel applications.

     This chapter mainly concerns itself with three major fields of biofunctional synthetic membranes: (1) biocatalytic, (2) energy-transducing and (3) information-transducing membranes (Figure 1). A biocatalytic synthetic membrane provides selective catalytic activity. For example, single enzymes or a series of enzyme complexes can be arranged on or within various membrane matrices such that the enzymes retain their native activity. These membranes can be used as membrane bioreactors, which are then linked with separator processes. Some pioneering work has been done on the activity control of membrane-bound enzymes, and the area promises further development. The second area discussed is that of designing an energy-transducing membrane modelled on the photosynthetic primary processes. Photo-transducing biomolecules such as chlorophyll and bacterial rhodopsin have been incorporated into synthetic membranes for the production of energy in a useful form. The third area discussed involves information-transducing membranes which mimic the bio-sensory system. There has been significant progress in the development and application of information-transducing membranes, or "biosensors." One example is the chemoreceptor membrane which incorporates biomolecules such as enzymes and antibodies for molecular recognition. Another example is the presynaptic model membrane which releases neurotransmitters upon electric stimulation.

     In addition to biocatalytic, energy-transducing and information transducing membranes, there are, of course, other types of biofunctional synthetic membranes. However, this review concentrates on these three important biofunctional membranes. The historical background of their development, the molecular mechanism in biological membranes on which biofunctional synthetic membranes are modelled, the methodology of membrane preparation and current trends in the research and development are described.

Biocatalytic Membranes

Incorporation of Biocatalysts into Synthetic Membranes. It is generally accepted that only a few enzymes exist in vivo as a free protein in an aqueous medium, and that most of them either are bound to membranes or to solid-state assemblies or are present in a gel-like surrounding. Enzymes attached to synthetic membrane matrices may serve as specific heterogeneous catalysts that can be used repeatedly, if they are sufficiently stable. In comparison to natural membranes, enzyme-bound synthetic membranes possess the advantage that they are mechanically more stable.

One of the earliest references to enzyme-binding appeared in 1953, although the matrix was not a membrane form. Grubhofer and Schlith (1) described the covalent fixation of carboxy peptidase, diastase, pepsin and ribonuclease to diazotized polyaminostyrene. Since then workers in many laboratories have developed a variety of artificial matrices and enzyme binding methods. Mitz reported the ionic adsorption of catalase to DEAE-cellulose in 1956 (2). In 1963, Bernfeld and Wan (3) entrapped trypsin, papain, amylase and ribonulease in polyacrylamide gels. Quiocho and Richards (4) developed a cross-linking method to immobilize carboxypeptidase A by glutaraldehyde. It was reported by Chang in 1964 (5) that cabonic anhydrase was encapsulated in a microcapsule. In an attempted medical application, Gregoriadis (6) immobilized amyloglucosidase into liposome. It is striking that immobilization techniques have been applied not only to subcellular organella but also to microbial whole cells, thereby involving integrated enzyme processes. Much information, with numerous examples of immobilized biocatalysts and their matrices, is available in a series of reviews and monographs (7-20).

In 1969, Chibata and co-workers (20) succeeded in developing the first industrial process incorporating immobilized enzymes. Since then a number of applications for immobilized biocatalysts have appeared in various areas. Updike and Hicks (21) proposed a novel use for membrane-bound enzymes for an analytical device, an "enzyme electrode," which bases its selectivity on the membrane-bound enzyme. The details appear below in the section on "Information-transducing Membranes."

Matrices for Biocatalytic Synthetic Membranes. Biocatalyst-bound synthetic membranes have been prepared by the following four methods:

1) Covalent attachment of the biocatalyst to the membrane matrix
2) Intermolecular cross-linking of the biocatalyst to form a membrane
3) Entrapment of the biocatalyst within the matrix during membrane preparation
4) Adsorption of the biocatalyst to the membrane matrix

Among the successful membrane matrices are collagen, various cellulose derivatives, polyamides (such as Nylon and polyacrylonitrile) and urethane. In the following paragraphs, a brief discussion of each of those membrane materials is presented.

Collagen Matrix. Suzuki and co-workers developed an electrochemical preparation of enzyme-collagen membranes (22). A similar electro-chemical complexation of enzymes in the collagen fibril network has been studied by Vieth et al. (23). An enzyme solution is added to a solution of calf skin collagen fibrils at pH 3.8 or pH 10.4 at a ratio of 1:10. A pair of platinum electrodes are immersed in the solution. Electrolytic deposition is performed at a constant current, with a current density of 2 to 4 mA cm^{-2} without circulation. The electrolyte is cooled in ice to avoid

enzyme denaturation. The wet membrane formed on the electrode is peeled off and treated with glutaraldehyde if necessary. After washing, the enzyme-membrane is dried in a vacuum oven.

Enzyme-collagen membranes have also been prepared by a simple casting method. A collagen fibril suspension containing enzyme in the pH range 4 to 5 is cast on a Teflon plate at 4°C to form a membrane and dried at room temperature. The membrane is then dipped in 1%(wt/vol) glutaraldehyde solution at pH 7.

Cellulose Derivative Matrix. Four possible methods for preparing cellulosic, enzyme membranes are presented:

1) Cellulose acetate is solubilized in an organic solvent and an enzyme added to the solution. The resulting solution is cast on a glass plate to form an enzyme-containing membrane. This preparation can only be applied to enzymes that retain activity in organic solvents.

2) A solution of cellulose acetate and cellulose bromoacetate is cast onto a glass plate to form a membrane and dried. The membrane is then chemically modified by the following reaction.

Membrane --- $CH_2Br + H_2N(CH_2)_nNH_2 \rightarrow$ Membrane --- CH_2NH--$(CH_2)_nNH_2$
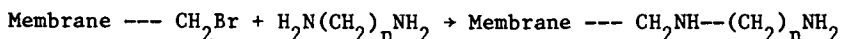
Finally, an enzyme is covalently bound to the membrane via peptide bonding.

3) Aizawa et al. (24) proposed a novel preparation of a composite cellulose membrane. Cellulose acetate, a triamine (1,8-diamino 4-amino methyl octane) and glutaraldehyde are homogeneously mixed in dichloromethane. The solution is cast onto a glass plate. The cross-linking of the triamine by glutaraldehyde takes place within the membrane matrix during drying. The membrane binds the amino group of an enzyme via a Schiff's base reaction when it is subsequently contacted with an enzyme solution.

4) Enzymes or whole cells can be immobilized in ultrafiltration (UF) and reverse osmosis (RO) membranes by several methods. First, cellulose acetate or polysulfone are used to obtain asymmetric membranes by the phase inversion technique. Albumin and glutaraldehyde are then used for cell immobilization within the membranes via co-cross-linking methods (25,26).

Polyurethane. Fukui et al. (27) developed a urethane prepolymer method for immobilizing enzymes, subcellular organella and whole cells. First a prepolymer, which is a copolymer of polyethylene glycol and polypropylene glycol coupled with toluene diisocianate, undergoes cross-linking in the presence of water.

$$R-NCO + OCN-R + H_2O \rightarrow R-NHCONH-R + CO_2$$
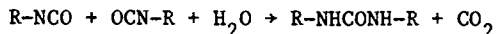
When an enzyme solution or a whole cell suspension is added to a prepolymer solution, gelation occurs to immobilize the biocatalyst.

Other Synthetic Polymeric Films. Various enzymes have been covalently immobilized to the surface of synthetic polymer films. For example, the surface of a Nylon film can be activated either by the partial hydrolysis of the amide bonds or by methylation with dimethyl sulfonic acid. Subsequently, an enzyme is covalently immobilized to the surface (28).

Selective Catalytic Membrane Process Linked with a Separation
Process. Some biological membranes take up specific chemicals,
eliminate wastes and secrete products; that is, they act as a
selective catalytic process linked with a separation process.
Several attempts have been made to mimic such a biocatalytic
process.
     Because a biocatalyst-binding membrane works as a specific,
heterogeneous catalyst that can be used repeatedly, it finds many
applications in chemical processes. Several types of reactors have
been designed to incorporate biocatalyst-binding membranes. A
spiral module reactor has an advantage that pressure-drop is
extremely retarded (29). The chemical engineering of membrane
bioreactors has been reviewed elsewhere (30,31).
     The possibility of using UF and RO membranes filled with
biocatalysts has been demonstrated by Drioli et al. (32).
Immobilization of enzymes or whole cells in UF and RO membranes has
been limited by the need for nonaqueous solvents in the membrane
casting solutions and high temperature annealing, which destroys
the catalytic properties. They utilized Caldariella acidophilla,
an extreme thermophile which grows optimally at 87°C and whose
enzymes are generally stable to protein denaturing agents.
C. acidophilla was immobilized in asymmetric UF membranes by
several methods without loss of enzyme activity. The results
indicated that no marked decrease of activity was observed after 8
to 9 months of wet storage at 4°C. The membrane had a flat sheet
configuration and were tested in standard ultrafiltration systems.
     Several carrier-mediated membrane transport systems have been
demonstrated by utilizing biomolecules. The first system was
reported by Scholander (33) who showed that oxygen diffusion through
a filter paper membrane containing a hemoglobin solution was greatly
accelerated. A number of mechanisms have been suggested for
coupling external energy sources to carrier mediated membranes as a
means of controlling and/or accelerating the flux of permeants
(33). In opposition to passive or facilitated transports, active
transport pumps have also been suggested (34). The membrane was
made of two half-membranes (the first one containing hexokinase,
the second one phosphatase) that were successively met during
transport (Figure 2). Pumping was demonstrated.
     A novel membrane has been designed on the model of the pancreas
to control insulin release in response to changes in the
concentration of glucose (35). The membrane consists of two polymer
membranes. One is a polyacrylamide membrane containing glucose
oxidase (GOD), which recognizes glucose and forms hydrogen
peroxidase. The other is a redox polymer membrane having a
nicotinamide moiety which is oxidized by hydrogen peroxide with a
resulting increase in insulin permeation (Figure 2).
     In the future, the chemical synthesis of a number of
biologically relevant chemicals and pharmaceutics may use membrane
reactor systems utilizing biocatalytic synthetic membranes.
Although few enzyme-membrane systems have actually been developed,
it is possible to design biocatalytic synthetic membranes which
permit enzyme reactions in vectorial sequence. A series of enzyme
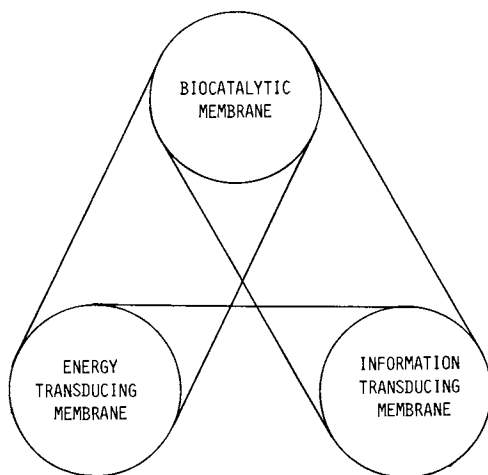
Figure 1.   Scope of the biofunctional synthetic membranes.
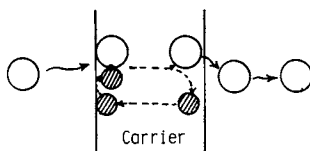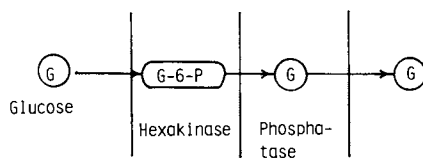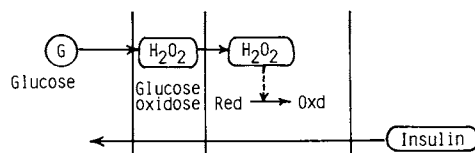
Figure 2.   Biomimetic controlled membrane transport systems.

complexes could be arranged on or within the membrane such that the product or products of one process may be acted upon by an adjacent enzyme-membrane. Membrane transport must be controlled to regulate the total process.

Regulation of the Biocatalytic Function. By compartmentalization of enzymes, by controlling the alternate pathways of metabolism, by feedback controls of a number of different modes, by chemical modification of enzymes, by involving cascade systems, by protolytic modifications of enzymes and by repression and induction, enzymes in metabolic pathways can be maintained at precise levels so that substrates or intermediates can in turn be controlled at physiologically proper concentrations. The behavior of many membrane enzymes is markedly affected by their insertion into the membrane structure. Neighboring molecules (for example, phospholipids and proteins) may play a major role in regulating the catalytic activity of these enzymes. Changes in membrane phospholipids may therefore serve a major regulating function. A number of the regulating enzymes are controlled by having the effectors induce conformational changes in the protecting structures which physically modify the catalytic site of the enzyme. All of these suggestions are profitable in regulating membrane-bound enzyme activity. Some of the more important means of regulating enzyme activity are discussed here (see also Figure 3).

Photocontrol of Enzyme Activity. It has been shown by Suzuki et al. that chemical modification by spiropyran compounds can make an enzyme photoresponsive (36,37). A number of spiropyran compounds undergo photochromism; that is, the reversible photoisomerization of colored (open ring structure) and colorless (closed ring structure) forms. Several enzymes such as α-amylase were modified with a spiropyran compound to produce photoresponsive enzyme activity. The mechanism of photoregulation was indicated by the drastic change in polarity due to photoisomerization of enzyme-bound spiropyran.
     Photocontrol of enzyme activity has also been demonstrated with membrane-bound enzymes. Urease was modified with a spiropyran and immobilized in a collagen membrane matrix. The activity of the modified urease decreased with ultraviolet irradiation and then was restored to the initial activity with visible light irradiation (38). A collagen membrane matrix has also been modified with a spiropyran compound to be photosensitive. Trypsin was immobilized in the photosensitive collagen membrane matrix. The activity of the trypsin membrane under visible light decreased by about 20% in the dark (39). The spiropyran-modified membrane was hydrophilic in the dark and turned hydrophobic under visible light, which may have been responsible for the photo change in the apparent diffusion coefficient of the substrate within the membrane matrix.
     All of these facts suggest that enzyme activity is controllable by a change of environmental conditions with an external energy source.

Electric Field Control of Enzyme Activity. An electric field is expected to be a powerful external source for enzyme activity

control. Because liquid crystals are extremely sensitive to an
electric field, a liquid crystal supported by a collagen membrane
was selected as a membrane matrix for the immobilization of an
enzyme to be activity-controlled by an electric field (40). Lipase
was entrapped in a collagen membrane containing
4-methoxybenzilidene-4'-n'butylaniline (MBBA). The lipase-liquid
crystal membrane was prepared by casting a suspension of collagen
fibril, MBBA and lipase on a Teflon plate and drying at 20°C. The
membrane was treated with a 0.1% glutaraldehyde solution for 30
seconds, washed and dried. An electric field was applied across
the lipase-liquid crystal membrane fixed on a platinum electrode.
The membrane-bound lipase showed that the activity depended on the
electric field.

Temperature Control of Enzyme Activity. The liposomal membrane,
consisting of phospholipids, causes a drastic change in membrane
characteristics at the phase transition temperature. An "enzyme
switch," in which enzyme activity is alternatively changed with an
external, thermal source, has been developed by Matsuoka et al.,
using a liposome which incorporates a conjugate of a purple
membrane and an enzyme (41). Urease was covalently bound to the
purple membrane from Halobacterium halobium while retaining its
activity. The purple membrane-urease conjugate was incorporated
into liposomes of dipalmitoyl phophatidyl choline by sonication.
The liposome-bound urease showed no appreciable activity below a
transition temperature of 42°C. By elevating the temperature above
the transition point, the enzyme activity sharply increased
indicating that urease activity could be switched on and off
repeatedly by temperature changes.

Energy-transducing Membranes

Architecture of Energy-transducing Biomembranes. Membranes play
a central role in the energy-transducing processes of living cells.
Highly specialized membranes are involved in the most fundamental
processes, such as respiration and photosynthesis. In both
processes electron transport is mediated by membrane-bound enzymes
and carriers, the architecture of which is extremely complex.
Membrane architecture in living cells has long enchanted membrane
scientists who intend to assemble energy-transducing artificial
membranes.
     Biophysical chemical studies have suggested that the thylakoid
membrane of the chloroplast consists of an ultrathin layer of lipids
(presumably a lipid bilayer) with sorbed proteins and pigments
organized in a lamellar structure approximately 100 A thick (Figure
4). Although the precise functions of the thylakoid membrane are
still obscure, it is believed that the membrane is the locus of the
primary photophysical and photochemical processes.
     During the last several years, purple membranes formed from
the extreme halophile Halobacterium halobium and its retinal
containing protein, backteriorhodopsin, have attracted the
attention of many groups working in the field of bioenergetics.
Unlike photosynthesis and respiration, the function of
bacteriorhodopsin does not rely on the transport of electrons but

Photocontrol

Electric control

Temperature control
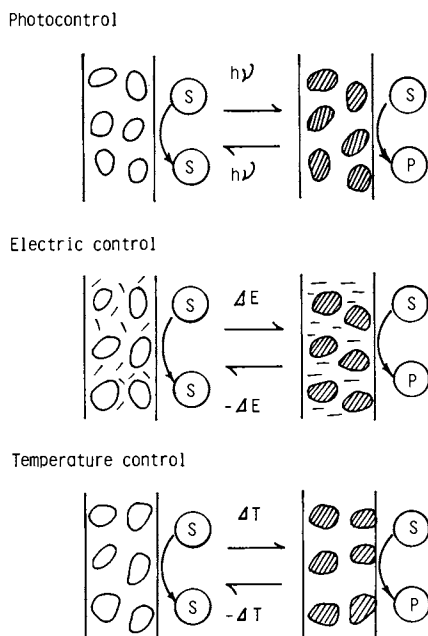
Figure 3. Membrane systems for control of enzymatic activity.
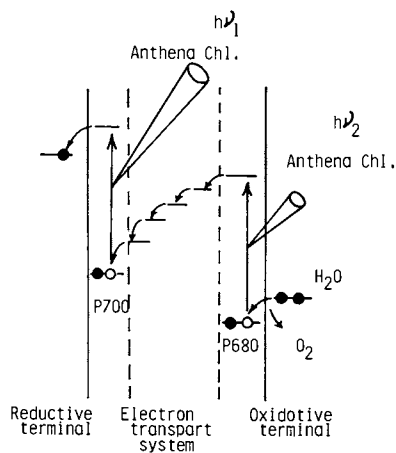
Figure 4. Postulated electron transport systems of a thylakoid membrane.

instead relies on the vectorial transport of proteins which leads
to the establishment of an electrochemical proton gradient across
the cell membrane. The energy for proton translocation is provided
by light which is absorbed by the chromophore of bacteriorhodopsin.

Molecular Organization of Photoenergy-transducing Synthetic
Membranes. Various types of chlorophyll-containing membranes have
been designed for photoenergy conversion primarily on the basis of
the idea that photosynthesis is an electronic process. The process
assumes that two-dimensional chlorophyll arrays are photo-
conductive. The absorption of a photon promotes one electron into
the conduction band and leaves one hole in the valence band. The
excited electrons and holes are free to move around. They are also
considered to be spread out over the whole unit although their
lifetimes and mobilities may be different. In the second scheme,
it is assumed that the electrons can be transferred to an electron
acceptor which is thereby effectively reduced, and the holes can be
transferred to an electron donor which is thereby effectively
oxidized.
     Photosynthetic pigments, specifically chlorophylls, have been
attached to a variety of matrices to convert visible light energy
to electric or chemical energy. The molecular assemblies may be
classified into the following three categories.

Pigmented Bilayer Lipid Membranes. Chlorophyll molecules have been
incorporated into two types of artificial bilayer lipid membrane
systems for the study of photoenergy transduction. The first
consists of a planar bilayer lipid membrane (BLM) separating two
aqueous solutions where photovoltaic effects can be induced. The
second system comprises liposomes which are ideally suited for
studies of photo-induced permeability, spectroscopy and chemical
reactions. For more complete technical details, two pertinent
publications are available (42,43).
     BLMs are made of pure lipid, for example phosphatidyl choline,
or oxidized cholesterol in common salt solutions. Chlorophyll
molecules situated at the biface in the Chl-BLM are tightly
compressed together, and the average area occupied per porphyrin
group is much less than 75 Å^2 (44). We may expect that the
hydrophobic portions (phytyl group) of the molecules extend
inwards, while the hydrophilic heads (porphyrin) and polar lipid
groups are situated at the aqueous solution/membrane interface
(Figure 5). On the basis of this data, it seems probable that the
porphyrin plane of the chlorophyll molecule is oriented at about
45° to the lipid bilayer (45).

Chlorophyll-containing Membrane on an Electrode Surface.
Photoelectrochemical and photovoltaic effects have been noted with
a variety of chlorophyll assemblies deposited on metal or
semiconductor electrode surfaces (Figure 6).
     In the photosynthetic primary processes, electrons are pumped
via two photosystems (photosystem I and II), where light induced
charge separation takes place efficiently in association with
uni-directional electron transport. The oxidative water splitting
reaction is linked to photosystem II; photosystem I is followed by
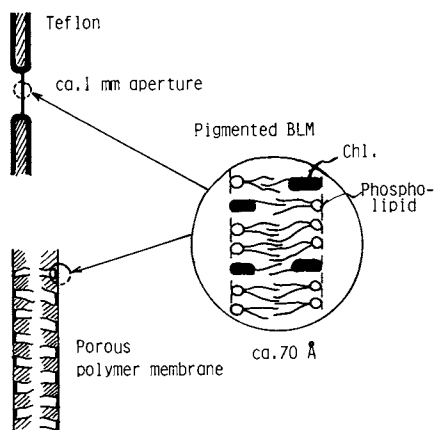
Figure 5. Chlorophyll containing bilayer membrane (BLM).
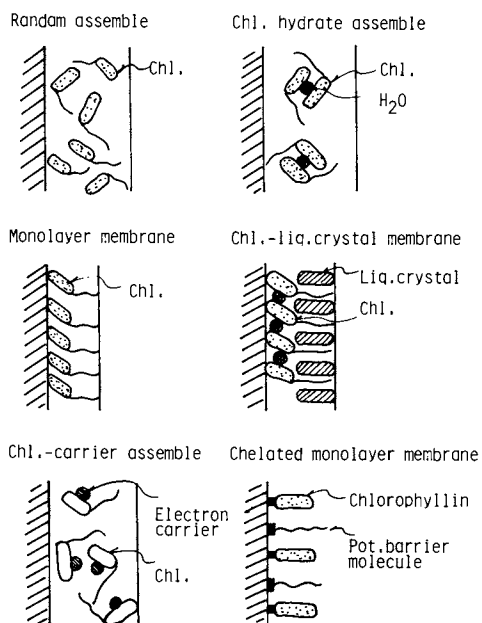
Figure 6. Molecular organizations of chlorophyll membranes deposited on metal or semiconductor electrodes.

the reduction of NADP. The function of photosystem I can thus be
simulated by a photocathode in an electrochemical photocell.
Conversely, photosystem II refers to a photoanode.

An n-type semiconductor electrode modified with a chlorophyll-
containing membrane may act as an efficient photoanode for visible
light conversion. Tributsch and Calvin first employed chlorophylls
and demonstrated anodic sensitized photocurrents under
potentiostatic conditions in aqueous electrolytes (46). The
photocurrent action spectrum of chlorophyll a on ZnO (single
crystal) showed a red band peak at 673 nm, corresponding closely to
the amorphous and monomeric state of chlorophyll a. The anodic
photocurrent increased by the addition of supersensitizers
(reducing agents) to the electrolyte. A maximum quantum efficiency
of 12.5% was obtained in the presence of phenylhydrazine.
Takahashi et al. made a thin membrane of chlorophylls complexed
with electron donors which was deposited on a platinum electrode
(47,48). It should be noted that the chlorophyll electrode behaved
as a photocathode when electron acceptors were co-deposited in
place of the electron donors. The photoactive species could be
attributed to the composite of chlorophyll-oxidant or chlorophyll-
reductant.

To enhance quantum efficiency, various molecular organizations
have been proposed for photoenergy transduction using chlorophyll-
containing membranes (Figure 6). Fong et al. (49) insisted that
hydrated microcrystalline chlorophyll a is superior to the
amorphous aggregate in light-induced charge separation. Hydrated
microcrystalline chlorophyll a was electrochemically deposited onto
a platinum electrode and was then assayed for photoelectrochemical
properties. Of various chlorophyll a hydrates, the dihydrated
Chl a oligomers, $(Chl\ a-2H_2O)_n$, are considered to be the most
powerful redox species for water splitting under far red
excitation. The water splitting reaction was demonstrated with an
illuminated $(Chl\ a-2H_2O)_n$ platinum electrode (50). The authors
indicated that the $(Chl\ a-2H_2O)_n$-platinum electrode is capable of
reducing CO_2 under illumination.

Aizawa et al. (51-54) incorporated chlorophyll molecules into
a liquid crystal thin membrane, which was deposited on a platinum
electrode. The liquid crystal molecules were found to be effective
in the inhibition of intermolecular interaction of chlorophylls and
the formation of the chlorophyll-hydrate, which could enhance the
charge separation in photoexcitation.

Attempts have been made to intersperse a suitable inert
surfactant diluent in the monolayer in order to control the surface
concentration as well as the mean intermolecular separation of
chlorophyll. Among the surfactants which can act as ideal two-
dimensional diluents for a chlorophyll a monolayer, Miyasaka et al.
(55) chose the phospholipid dipalmitoyllecithin (DPL) to enhance
the quantum efficiency. They conclude that a monolayer thick
membrane having well interspersed chlorophyll is most efficient for
the conversion of light energy using chlorophyll-sensitized
semiconductor electrodes. Aizawa et al. (56) introduced various
substances among chlorophyll molecules to prevent the
intermolecular interaction and to improve the photoconversion
properties. A monolayer of Cu chlorophyllin was fixed on the

surface of SnO_2 via heavy metal polynuclear chelation. The mono-
layer membrane was then partially substituted by Cr myristate. It
should be noted that the quantum efficiency was sharply increased
by the presence of Cr myristate. A thin layer of chitosan, in
which Cu chlorophyllin was immobilized, was deposited on the
surface of SnO_2. The chitosan markedly enhanced the quantum
efficiency in the similar manner to myristate. From these results,
a potential barrier substance such as myristate and chitosan
polymer may be considered to prevent effectively the energy
dissipation of surface-bound sensitizer in photoexcitation.

Bacteriorhodopsin-containing Membrane. The preparation of BLM
containing bacteriorhodopsin was first reported by Dancshazy and
Karvaly (57) and Herrmann and Rayfield (58). These membranes
developed a maximum photocurrent of 2×10^{-12} A and a photopotential
of 20 to 60 mV, the action spectrum of which indicated that
bacteriorhodopsin was the species responsible for the photoelectric
effect. Shieh and Packer (59) increased the lifetime of the film
by the addition of polystyrene or polyacrylamide to the membrane
forming solution. Efforts to increase the total surface area of
the artificial membrane have been most successful by attaching
liposomes containing bacteriorhodopsin to Millipore filters (60).
Packer et al. (61) reported that the membrane preparations retained
their photovoltaic response for over a month without significant
loss of activity.

Methodology of Energy-transducing Membrane Formation.
Pigmented BLM. Planar bilayer lipid membranes (BLM) consist of a
variety of lipids from highly purified single phospholipids. BLM
are commonly formed in an aperture in a hydrophobic barrier (for
example, a Teflon cup) separating two aqueous solutions. A droplet
of lipid solution is applied to the aperture. Excess lipid
solution drains into the border and within minutes optically black
spots appear and, enlarge themselves to occupy the majority of
aperture area. Pigmented BLM can be formed from a droplet of lipid
solution containing pigment such as chlorophyll and
bacteriorhodopsin.
      Because BLM made of pure lipid or oxidized cholesterol in
common salt solutions are nonconducting, the physical properties of
BLM are with one exception similar to those of a liquid hydrocarbon
layer of equivalent thickness. The interfacial tension of BLM is
less than 5 dynes cm^{-1}, which is approximately one order of
magnitude lower than that of the hydrocarbon/water interface. This
low interfacial tension is due to the presence of polar groups at
the interface. BLM have negligible permeability for ions and most
polar molecules. Permeability to water is comparable to that of
biological membranes. The permeability to water of Chlorophyll
BLM, as determined by an osmotic flow method, is 50 $\mu m\ s^{-1}$, which
is in·the range of phospholipid BLM but six times larger than that
of oxidized cholesterol BLM.

Pigment Membrane Deposited on a Solid Surface. An amorphous
membrane is generally prepared by solvent evaporation of an organic
solution of chlorophyll or bacteriorhodopsin on a solid substrate

surface. The red absorption peak of a dry amorphous chlorophyll a membrane is approximately 675 to 680 nm, which reflects the formation of dimers and oligomers of chlorophyll a. Chlorophyll a – H_2O microcrystals and other hydrated chlorophyll species are readily obtained by allowing a small amount of water to remain in solutions of chlorophyll a dissolved in a suitable nonpolar organic solvents. Membranes can be formed on a solid surface by solvent evaporation. A chlorophyll a – H_2O microcrystalline membrane has also been prepared by the electrodeposition technique established by Tang and Albrecht (62).

Pigmented Monolayer Membrane on the Solid Surface. Monolayers and mixed monolayers of pigments can be prepared on a neutral aqueous buffer solution surface and deposited, at a controlled surface concentration, onto a solid substrate by the Langmuir-Blodgett technique (63,64). As a typical feature, a monolayer membrane of chlorophyll a possesses absorption peaks at 675-680 nm and 435-440 nm with corresponding optical sensities of 0.008-0.01 and 0.01-0.013 in the red and blue bands, respectively (65).

Photoenergy Transduction. Pigmented BLM elicit large photopotentials under asymmetric conditions, particularly when the membrane is interposed between two solutions containing different redox couples. For example, the presence of $FeCl_3$ on one side and ascorbic acid on the other side resulted in a photopotential of more than 150 mV across a chlorophyll-BLM (66). A variety of redox compounds affecting the photoresponse of the chlorophyll-BLM have been investigated (67,68).
    Bilayer lipid membranes containing chloroplast extracts are almost ideal systems with which to investigate energy transduction and photochemical processes as they occur in the photosynthetic membranes of green plants. Although many of the obtained results are qualitative and preliminary, the pigmented BLM have opened a new vista to the study of the intricate membranous aspects of photosynthesis, particularly the primary events of solar energy conversion (67,68). Gross et al. (69) made a photovoltaic cell using Photosystem I subchloroplast particles (Figure 7). The particles were placed on a filter between two compartments, one of which contained the electron donor $K_4Fe(CN)_6$ and the other the electron acceptor FMN. Upon illumination with white light ($I=80$ W m^{-2}), a potential of 300 mV generated across a 3000 ohm load resistance. Both PS I photochemistry and direct photoreactions of FMN contributed to the process. A power output of 20 µW was observed for a 2 cm^2 filter containing 60 µg chlorophyll. This corresponds to 0.1 W m^{-2}. The power efficiency was 0.13%. The short circuit current was 108 µA (69). Katz et al. reported a photovoltaic cell comprised of a glass cylinder containing two compartments separated by either a polyvinyl chloride membrane or aluminum foil. A chlorophyll-water adduct was impregnated in the membrane or deposited on one side of the Al foil by evaporation from an octane suspension of the adduct. One of the compartments in the cylinder was filled with an electron acceptor solution such as tetramethylphenylenediamine. The second compartment was filled with an electron donor solution such as

sodium ascorbate. Each compartment contained an electrode. In the best cell version--using an aluminum film support for the chlorophyll--a potential difference of 422 mV was observed with a simultaneous current of 2.36 x 10^{-5}A in the external circuit. The efficiency was estimated at about 0.0024%. Tien et al. incorporated chlorophyll-BLM (phosphatidyl choline) into a porous polycarbonate filter (pore size 0.05 to 8 μm) to make a photovoltaic cell.

Ochiai et al. prepared membrane-bound whole chloroplast (70). A chloroplast suspension was mixed with native ferredoxin plus ferredoxin-NADP resuctase which were freshly prepared and co-immobilized with polyvinyl alcohol (PVA-117). The resulting film reduced NADP upon illumination as 0.64 μmole per mg chlorophyll per hr, about 1% yield of recovery. They applied the film to a photovoltaic cell.

Photoelectrochemical conversion from visible light to electric and/or chemical energy has been investigated with chlorophyll thin membranes deposited on semiconductor or metal electrodes (71). Chlorophyll-coated metal (platinum) electrodes derived cathodic photocurrent in acidic electrolyte solutions, although the photocurrent efficiencies tend to be low compared to those of chlorophyll-semiconductor electrodes. The cathodic photoresponse may result from the p-type photoconductive nature of a solid chlorophyll layer and/or the formation of a contact barrier at the metal-chlorophyll interface, which contributes to light-induced carrier separation and leads to photocurrent generation.

A photoelectrochemical cell, reported by Takahashi et al., contained chlorophyll-naphthoquinone-Pt and chlorophyll-anthrahydroquinone-Pt electrodes (47). In a typical experiment, NAD and $Fe(CN)_6^{-4}$, each dissolved in a neutral electrolyte solution, were employed as an acceptor for a photocathode and as a donor for a photoanode, respectively. Upon illumination with white light, the short circuit current was 8 x 10^{-6}A cm^{-2}.

Aizawa et al. showed that chlorophyll-liquid crystal electrodes in acidic buffer solutions gave cathodic photocurrents accompanied by the evolution of hydrogen gas (52). Substitution of the central metal of native chlorophyll (Mg-pheophytin) resulted in a drastic change of photoelectrochemical behavior. A Mn-pheophytin/liquid crystal/Pt electrode generated anodic photocurrent upon illumination. In contrast, Ru-pheophytin/liquid crystal/Pt electrode gave a cathodic photocurrent with a quantum efficiency of approximately 0.5% (54). Fong's work on photoelectrochemical cell has proved that chlorophyll hydrates are photoactive (49).

Chlorophyll-coated semiconductor (n-type ZnO, CdS and SnO_2) electrodes provided dye-sensitized anodic photocurrent with high efficiency (Table I). It was found that the quantum efficiency of the anodic photocurrent in the chlorophyll a/dipalmitoyl lecithin (DPL)/SnO_2 system was enhanced to about 25%, while the chlorophyll a monolayer/SnO_2 gave a quantum efficiency of 3 to 4%. The considerable increase in quantum efficiency may result from the suppression of the self-quenching of chlorophyll molecules (55). Miyasaka et al. (55) concluded that a monolayer-thick film having well interspersed chlorophyll is most efficient for the conversion of light energy using chlorophyll-sensitized semiconductor electrodes. Aizawa et al. (56) have also shown that the use of

Table I. Characteristics of chlorophyll membranes on
metal or semiconductor electrodes

Substrate	Chl. layer	Electrolyte	Photocurrent	Quantum efficiency	Ref.
ZnO	Chl.	Hydroquinone	$6 \times 10^{-7} A/cm^2$ 0.5V/SCE 673 nm	2.5–5%	46
Pt	Chl.a/ lecithin			20–30% 700 nm	
SnO_2	Chl.a monolayer (stearic acid)	Hydroquinone	$0.8 \times 10^{-7} A/cm^2$ 0.1V/SCE 675 nm	12–16%	55
Pt	Chl–Quinone Chl–Hydro- quinone	NAD^+ Cathode $Fe(CN)_6^{4-}$ Anode	Short current $8 \times 10^{-6} A/cm^2$		47
Pt–Pt	Chl.a dihydrate	Phosphate buffer(pH3.0)		0.2% 740 nm	49
Pt	MgChl–LC*	Acetate buffer (pH3.5)	$3 \times 10^{-7} A/cm^2$ 0V/SCE	Cathode	51
	MnChl–LC	$NaOH–Na_2CO_3$ (pH12.3)	$9 \times 10^{-8} A/cm^2$ 0.1V/SCE	Anode	53
	RuChl–LC	Quinone (pH7.0)	$1.3 \times 10^{-6} A/cm^2$ 0v/SCE 630 nm	Cathode 0.5% 630 nm	54

potential barrier molecules between chlorophyll molecules may
enhance the quantum efficiency.

Information-Transducing Membranes

Photoreceptor Membranes.
Visual Processes.   Understanding how the eye transforms light
energy into a signal that can be sent to the brain is an enormous
task. Within a second after light strikes a rhodopsin molecule in
the outer segment of a rod cell, the synapse at the far end of the
rod cell responds and signals the adjacent neuron. The information
is transmitted from one end of the cell to the other by a change in
the electrical behavior of the cell's plasma membrane. In the
absence of light, the current is large; about 10^9 electronic
charges per second. When light interacts with rhodopsin, this dark
current is shut down. A single photon reduces the current by about
3%; that is, more than 2×10^6 charges do not flow because light
closes the gates which normally allow sodium to pass through the
plasma membrane. But rhodopsin itself cannot block those sodium
channels.
     About half of rhodopsin's mass forms seven α-helices, which
are embedded in the lipid bilayer of rod disks. The remaining
polypeptide chains extend into the aqueous environment of the
cytoplasm or the disk interior, linking the helices. Retinal is
bound as a protonated Schiff base to a lysine amino acid residue in
the carboxyl terminal helix. The chromophore is held in a pocket
that is nearly parallel to the membrane surface. When light
strikes rhodopsin, the 11-cis double bond of the protein-bound
retinal isomerizes to the trans form, which leads to the separation
from the protein opsin. To complete the visual cycle, the
all-transretinal slowly isomerizes back to the 11-cis isomer, which
recombines with opsin to reform rhodopsin. However, little is
known about how the isomerization of retinal in rhodopsin triggers
the transduction process (72,73).

Photo-responsive Synthetic Membranes.   Although the visual
information transduction is too complexed to be realized in vitro,
the photoeffects of retinal-containing synthetic membranes have
been investigated. Aizawa et al. (74) prepared a photo-responsive
membrane from a solution of 11-cis retinal, phosphatidyl choline
and triacetyl cellulose. The retinal was assumed to be incorporated
into the molecular assemblies of phosphatidyl choline, which were
dispersed in the triacetyl cellulose membrane matrix. The membrane
responded to visible light by showing a transmembrane potential in
association with the photoisomerization of membrane-bound 11-cis
retinal. On the other hand, a membrane incorporating 11-cis
retinal without phosphatidyl choline exhibited little light-induced
transmembrane potential (75).
     The light-induced transmembrane potential, $\Delta\psi_p$, may be
approximated by Equation 1, (76-78)

$$\frac{F}{RT} \Delta\psi_p = 2(t_L - t_D)\ln\gamma + \frac{2(\gamma-1)}{\gamma}\frac{1}{C_2}\{t_L(1-t_L)\ \theta_L - t_D(1-t_D)\ \theta_D\} \quad (1)$$

Where, θ, t, C_1, C_2, and γ are the charge density of the membrane

phase, the transport number of the anion, the electrolytic concentrations and the concentration ratio ($C_1 > C_2$, $\gamma = C_1/C_2$). The subscripts D and L indicate "in the dark" and "on exposure to light," respectively. Equation 1 indicates that a photopotential should be generated due to a change of t_D and θ_D to t_L and θ_L. The conformational change of the entrapped retinal is thought to cause the phospholipid micelles in the membrane matrix to change the charge density, which leads to a change in the transmembrane potential.

To enhance the photo-induced change of either t or θ of a retinal-containing membrane, several proteins which show an affinity for 11-cis retinal were employed in place of opsin. Retinal was conjugated with proteins such as bovine serum albumin, alcohol dehydrogenase and α-chymotrypsin, and incorporated in a triacetyl cellulose membrane together with phosphatidyl choline. The incorporation of such a hydrophobic protein as albumin markedly enhanced the extent of the photo-induced potential (75). As was evident from the spectroscopic characteristics of the retinal-bound membrane, the membrane-bound 11-cis retinal isomerized on illumination. The photoisomerization of the membrane-bound retinal may be the first event in the photo-response. For example, albumin is bound to retinal so closely that the photoisomerization of retinal may cause albumin to change conformation. Such a change is believed to induce a rearrangement of the phospholipid microspheres so as to increase the negative charge. In the retinal-albumin-phosphatidyl choline membranes, the conjugation of one mole of 11-cis retinal per mole of albumin was found effective enough to enhance the photopotential.

Chemoreceptor Membranes
Receptors and Molecular Recognition. Insight into chemoreceptors in biological systems has triggered the development of biomimetic sensors which can respond selectively and sensitively to specific substances. The word "receptor" refers to a surface membrane component, usually a protein, which regulates some biological event in response to reversible binding of a relatively small ligand.

Recognition between molecules by biological receptors depends on the ability of a surface membrane component to discriminate between different structures. To accomplish a biomimetic chemical sensor or "biosensor," a membrane for molecular recognition must be synthesized on the model of a biological receptor. The receptor membrane for molecular recognition may then be amalgamated in various manners with a device for signal transduction to form a biosensor (Figure 8). Such biosubstances as enzymes, antibodies, lectin, binding proteins, hormone receptors and microbial whole cells, have been incorporated into membrane matrices for molecular recognition. These biosubstances offer a specific molecular space which fits in size and shape into the corresponding molecule to be recognized.

Enzyme-containing Membranes for Molecular Recognition. Updike et al. applied an enzyme-containing synthetic membrane to form an enzyme electrode, that is, an "enzyme sensor," which was the first configuration that realized the concept of a biosensor (79). The
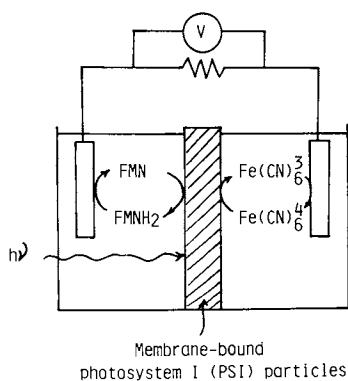
Figure 7.   A photovoltaic cell assemble consisting of a PSI particle
bound membrane.
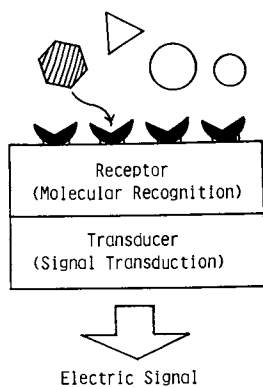
Figure 8.   Functional concept of biosensors using bioactive
substances.

membrane contained glucose oxidase (GOD), which undergoes selective conversion of β-D-glucose with stoichiometric consumption of O_2.

$$\beta\text{-D-Glucose} + O_2 \xrightarrow{\text{GOD}} \text{Gluconic acid} + H_2O_2$$
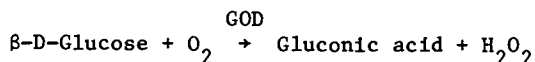
An enzyme sensor for β-D-glucose incorporates a GOD-containing membrane for molecular recognition and a Clark-type oxygen electrode for signal transduction. The sensor output depends on dissolved oxygen in the vicinity of the GOD-containing membrane. When β-D-glucose permeates the membrane, oxygen is consumed due to selective oxidation of glucose. The sensor output decreases in response to β-D-glucose. A similar enzyme sensor for β-D-glucose has been constructed from a GOD-containing membrane and an H_2O_2 electrode.

     In the early stage of investigation, GOD was entrapped in a thin membrane of polyacrylamide gel. The gel membrane provided poor permeability to substrates, which resulted in a slow sensor response. Great effort has been made to improve the membrane matrix (80-82). The response time of the sensor has been reduced to less than 10 seconds (82). Some of these enzyme sensors for glucose have been commercialized.

     In a similar manner, enzyme-containing membranes have been coupled with electrochemical devices such as an oxygen electrode to form enzyme sensors for a variety of biochemical and clinical applications (Table II). Considerable effort has been concentrated on the development of these enzyme sensors (83-86).

     Some enzymes, such as peroxidase, catalyze luminescence reactions.

$$\text{Luminal} + H_2O_2 \xrightarrow{\text{Peroxidase}} \text{Aminophthalate} + N + h\nu$$
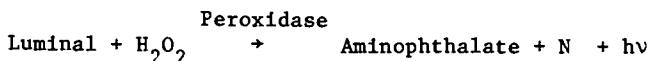
Peroxidase has been immobilized in a membrane matrix (87). The enzyme-containing membrane emitted light in the presence of luminol and H_2O_2. This luminous membrane was applied for the determination of H_2O_2, because the luminescence intensity reflected the concentration of H_2O_2 (87). Many oxidases generate hydrogen peroxide as the result of the oxidation of a substrate. When an oxidase is coupled with a peroxidase-containing membrane, the oxidase reaction can initiate the chemiluminescent reaction. Either substrate or oxidase can be quantified by measuring the chemiluminescence emitted from the peroxidase-containing membrane. Glucose was determined using a membrane containing peroxidase and glucose oxidase (87). Aizawa et al. (88) attached the peroxidase-containing membrane onto an Si photodiode for the determination of H_2O_2. The device is called a "biophotodiode" (88).

Microbial Cell-containing Membranes for Molecular Recognition. Suzuki et al. (87) have proposed a miocrobial sensor which consists of membrane-bound microbial cells and an electrochemical device. The assemblies of microbial sensors are similar to enzyme sensors. Two types of microbial sensors have been developed as presented in Figure 9. The first monitors the respiration activity of membrane-bound microbial cells with a Clark-type oxygen electrode. The

Table II. Membrane materials for enzyme sensors

Membrane matrix	Enzyme	Immobil-ization	Trans-ducer	Deter-minant	Response time	Range (mg/1)
Polyacryl amide	GOD	Entrap	O_2 EL.	Glucose	0.5-3min.	10^2-10^3
	ADH	Entrap	Pt EL.	Ethanol	–	1-10^4
	Tyrosi-nase	Entrap	Pt EL.	Phenol	5-10 min.	0.05-10
Gelatin GA*	GOD	Entrap	O_2 EL.	Glucose	15 s	-5×10^4
Albumin GA	ADH	Cross-link	O_2 EL.	Ethanol	30 s	5-10^3
Collagen	Invert-ase,GOD Mutaro-tase	Entrap	O_2 EL.	Sucrose	5 min.	10^2-5×10^3
	Catalase	Entrap	O_2 EL.	H_2O_2	2 min.	1-100
Polyamide GA	ADH	Covalent	C EL.	Ethanol		
AN*2 GA	LOD	Covalent	O_2 EL.	Lactate	30 s	5-2×10^3
CTA*3 Tiamine*4 GA	GOD	Covalent	O_2 EL.	Glucose	10 s	

*1 GA:glutar aldehyde
*2 AN:acrylonitrile
*3 CTA:cellulose triacetate
*4 Triamine:1,8-diamino-4-aminomethyl octane
ADH:alcohol dehydrogenase, GOD:glucose oxidase
LOD:lactate oxidase

second is based on the electrochemical detection of the metabolites from membrane-bound microbial cells.

Extensive research and development of microbial sensors has been carried out by Suzuki et al. (89–94) and Rechnitz et al. (95–97) (see Table III). Microbial sensors consisting of membrane-bound whole cells and an oxygen electrode were constructed for the determination of substrates such as assimilable sugars, acetic acid, alcohols and ammonia, and for the estimation of biochemical oxygen demand (BOD) (98–104). Glutamic acid was determined with a microbial sensor which consists of membrane-bound whole cells containing glutamate decarboxylase and a carbon dioxide gas electrode. These microbial sensors have been applied and evaluated for on-line measurements in fermentation processes (105,106).

Microbial sensors offer effective tools for microbioassay. They require a much shorter time and less experience as compared with conventional microbioassay methods. A novel primary screening test for a mutagen has been proposed by Suzuki et al. (107). Living cells of the Rec$^+$ and the Rec$^-$ strains were immobilized in different membrane matrices and attached to oxygen electrodes. The bacterial respiratory activity of the Rec$^+$ strain was electrochemically compared with that of the Rec$^-$ strain.

Immunoresponsive Membranes. An immunoresponsive polymer membrane has been developed by Aizawa et al. (108). Cardiolipin was incorporated in a triacetyl cellulose membrane matrix along with cholesterol and phosphatidyl choline. Because cardiolipin reacted with the Wassermann (syphilis) antibody in solution, the membrane surface charge changed with a resulting variation in transmembrane potential. The immunochemically induced potential change depended on the concentration of antibody in solution. It was noted that an antigen-containing membrane responded specifically in transmembrane potential to the corresponding antibody in solution (108).

Castillo et al. (109) and others (110,111) have shown that immune damage to biological membranes can be mimicked in bilayer lipid membranes (BLM). Related experiments have also been carried out on liposomes (112–113). Mountz et al. (114) incorporated complement into the BLM system. The antigen-antibody complex or the complement has no ability to affect the BLM system separately, but when carefully combined they destabilized the BLM even at a much reduced concentraiton.

Janata (115) coated a platinum electrode with a polyvinyl chloride thin film containing Concanavalin A. The electrode responded in electrode potential to the corresponding saccharide. From these findings, an immunosensor has been proposed (Figure 10). Aizawa et al. (116) demonstrated blood analysis for syphilis and blood typing with immunosensors. For the ABO system, the blood group substances (A and B) were extracted from human erythrocytes (A and B) and incorporated into triacetyl cellulose membrane matrices to form immunoresponsive membranes. A pair of immunosensors were assembled using these immunoresponsive membranes. Blood type was determined by measuring the transmembrane potential before and after the agglutination reaction with seum (116). Several other immunosensors have been reported (117–121). Immunosensors provide utlimately high selectivity in the

Table III. Microbial sensors

Determinant	Microbial	Immobil- ization	Transducer	Range (mg/l)	Ref.
Glucose	P. fluorescens	Entrap	O_2 elect.	3-20	88
Assimilable sugars	S. lactofermentum	Adsorptn.	O_2 elect.	20-200	90
Methanol	Undefined	Adsorptn.	O_2 elect.	5-3x10	90
Ethanol	T. brassicae	Adsorptn.	O_2 elect.	5-3x10	91
Acetic acid	T. brassicae	Adsorptn.	O_2 elect.	10-100	92
Formic acid	C. butyricum	Entrap	H_2 elect.	1-300	93
Glutamic acid	E. coli	Adsorptn.	CO_2 elect.	10-800	94
Lysine	E. coli	Adsorptn.	CO_2 elect.	10-100	95
Glutamin	S. flava	Adsorptn.	NH_3 elect.	20-1000	96
Alginine	S. faecium	Adsorptn.	NH_3 elect.	10-170	97
Aspargine	B. cacaveris	Adsorptn.	NH_3 elect.	5-45	98
Nystatin	S. cerevisie	Adsorptn.	O_2 elect.	1-800	99
Nicotinic acid	L. arabinosus	Entrap	pH elect.	0.01-5	100
Vitamin B	L. fermenti	Entrap	H_2 elect.	0.001-0101	101
Cephalos- porins	C. freundii	Entrap	pH elect.	100-500	102
BOD	T. cutaneum	Entrap	O_2 elect.	5-30	103
Cell number			Fuel cell	10^6-10^{11}*	

*cells/ml
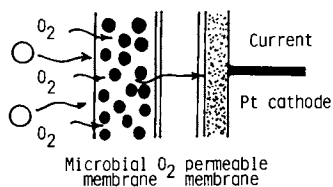
Respiratory Acitivity Monitoring
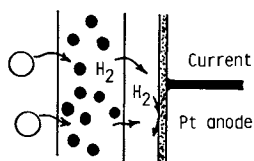
Metabolites Monitoring

Figure 9.   Two types of microbial sensors.
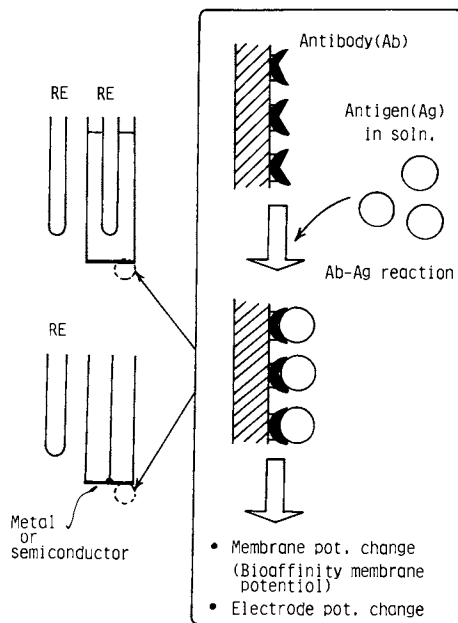
Figure 10.   Principle of immunosensors.

measurements of macromolecules such as proteins and peptides. One
of the unsolved problems is to enhance the sensitivity of the
immunosensors for the ultra-trace analysis of a specific serum
component.
     The use of labelling agents for the measurement of antigens
and antibodies has stimulated the new and expanding field of
immunoassay. Enzyme immunoassay, involving the use of antigen or
antibody labelled with an enzyme, is competing with
radioimmunoassay (RIA) in sensitivity. A novel immunosensor has
been developed by Aizawa et al. on the principle of enzyme
immunoassay (Figure 11), which is dependent on the immunochemical
affinity for selectivity and on the chemical amplification of an
enzyme for sensitivity (122-125). In this case (Figure 12)
catalase, which catalyzes the evolution of oxygen from hydrogen
peroxide, is a labelling enzyme for an antigen, and the
immunosensor is constructed by assembling an antibody-containing
membrane and an oxygen electrode. The antibody-containing membrane
binds both non-labelled antigen to be assayed and enzyme-labelled
antigen which is added to the test solution. The sensor is rinsed
to remove free antigen and contacted with hydrogen peroxide. The
labelling enzyme fixed to the membrane surface is quantified by
counting the enzymatically and quantitatively generated oxygen;
thus the enzyme appears to act as an amplifier (chemical
amplification). Chemical amplification is particularly effective
in ultra-trace analysis. Alpha-fetoprotein (AFP), for instance,
was determined in the concentration range 10^{-11} to 10^{-8} g ml^{-1}
using the immunosensor facilitated with chemical amplification.
Various chemical amplification systems are available to enhance the
sensitivty of biosensors, which should prove of practical
importance in designing biochemical sensing systems (126-129).

Homologous and Heterologous Bioaffinity Membranes. The concept of
a bioaffinity sensor has recently been proposed. A molecule
analogous to the determinant is covalently bound to a proper
membrane matrix, on which a labelled binding protein is complexed
to serve as the receptor as schematically shown in Figure 13.
Labelled binding protein may be released from the matrix to form a
much more stable complex with the determinant in solution, when the
receptor of the sensor is contacted with determinant molecules.
The residual amount of the binding protein depends on the
determinant concentration in solution. Because the principle of
the sensor is based on the binding protein affinity to not only a
specific substance but its analogues, the sensor is termed a
"bioaffinity sensor" (130).
     Avidin, an egg white protein, is a protein capable of binding
biotin (vitamin H). The protein can also bind 2-(4'-hydroxy
phyenylazo) benzoic acid (HABA); however, the binding affinity of
avidin to HABA ($K_a=1.7x10^5$ M^{-1}) is less than that to biotin
($K_a=10^{15}$ M^{-1}). A cellulose composite membrane was prepared from
cellulose triacetate, 1,8-diamino-4-aminomethyloctane and
glutaraldehyde as described above. HABA was covalently bound to
the membrane. Catalase-labelled avidin was complexed with
membrane-bound HABA. The membrane was then amalgamated with an
oxygen electrode to form a bioaffinity sensor. The membrane
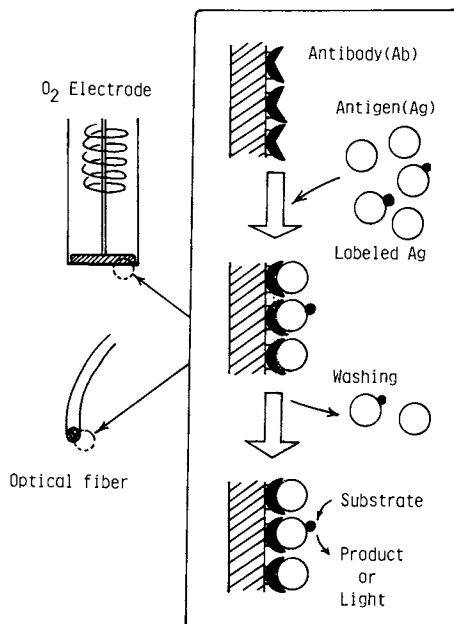
Figure 11. Principle of enzyme immunosensors.
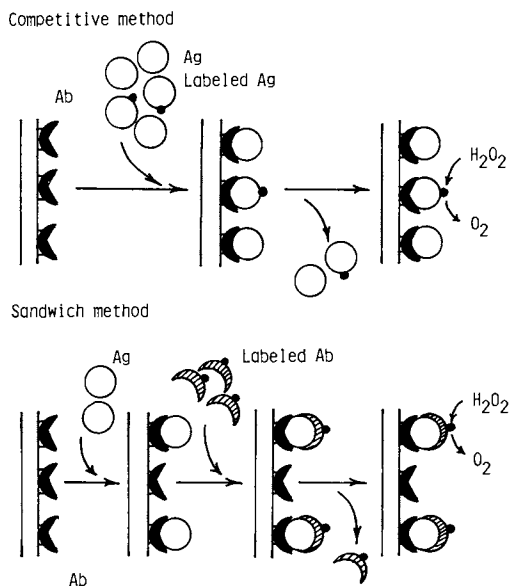
Figure 12. Procedures of immunoassays with the enzyme immunosensors.

released catalase-labelled avidin in response to biotin in solution
(131). The residual molecular complex on the membrane surface
correlated with biotin concentration in the range 10^{-8} to 10^{-5} g
ml^{-1}.

Bioaffinity sensors appear promising, particularly in the
selective determination of molecules not as large as protein.
Selective determinations of thyroxine (3,5,3',5'-tetraiodothyronine:
T_4) and insulin were performed with bioaffinity sensors (130-135).
Schultz et al. (136) reported affinity sensors for monitoring
various metabolites in blood plasma by optical means. Concanavalin
A, a protein with specific binding character for glucose, was
immobilized on the inside surface of a hollow dialysis fiber.
Fluorescein-labelled dextran was selected as the competitive
labelled ligand. The sensor was completed by inserting a single
optical fiber in the lumen of the dialysis fiber, thus allowing
measurement of the unbound FITC-dextran. Sensitivity to glucose in
the physiological range was obtained.

Membranes for Chemical Communication.
Chemical Communication. Living cells in human bodies communicate
with each other mainly by means of chemical messengers, a process
termed "chemical communication." For simplicity, the chemical
messengers may be classified into two broad categories: long-range
messengers and short-range messengers. The long-range messengers
such as hormones are synthesized by specialized glands, released
into the blood and circulated intact to their target organs. On
the other hand, the short-range messengers are small chemicals
produced by nerve cells (neurons) and are released only a few
angstroms or microns from their target cells. They are called
"neurotransmitters." In addition, intermediate range messengers,
called "modulators," may be defined.

Synapses are chemical communication units typical of the
short-range messengers. The extent and orientation of nerve
terminal branching results in synapses of various configurations.
The nerve ending or presynaptic membrane, is separated from the
postsynaptic membrane by a gap of 20 to 60 nm. Neurotransmitters
such as acetyl choline are packed in quanta of less than 10^4
molecules contained in vesicles in the presynaptic membrane. An
electric pulse (impulse) generated at the nerve ending, transfers
through the axon and reaches the presynaptic membrane. The impulse
stimulates the presynaptic membrane to release the packed
neurotransmitter. The presynaptic membrane transduces the electric
signal into chemical information. In contrast, the postsynaptic
membrane generates the electric pulse in response to the
neurotransmitter that is released from the presynaptic membrane.

Presynaptic Model Membranes (Figure 14). Aizawa et al. reported an
electrically stimulated release of neurotransmitter from a
synthetic membrane, which was modelled on a presynaptic membrane
(137). In recent years, research has progressed rapidly on new
types of conductive polymers including polyacetylene, polypyrrole
and polythienylene (138,139). These polymers become conductive by
incorporation of electron acceptors or donors, a process called
"doping." Although there are several doping methods,
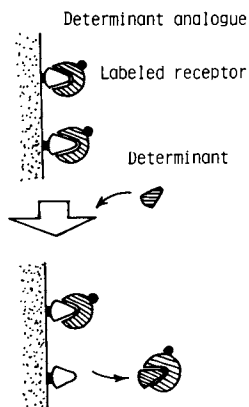
Figure 13. Principle of bioaffinity sensors.
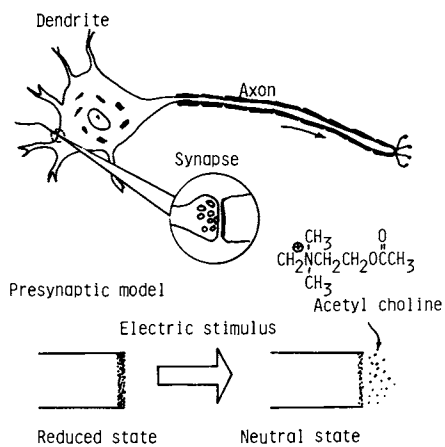
Figure 14. Presynaptic model using conducting polymer membranes.

electrochemical doping has the advantage that the doping level can be electrically controlled.

A polyacetylene membrane was first applied to mimic a presynaptic membrane. An Ohmic contact was formed on the back side of a polyacetylene membrane. The potential of the polyacetylene was controlled with a potentiostat. In an acetonitrile solution containing acetyl choline, polyacetylene was found to be electrochemically reduced with resulting incorporation of acetyl choline into the matrix. The polyacetylene membrane was initially controlled at a potential to incorporate the neurotransmitter. The neurotransmitter remained entrapped within the membrane matrix when the polyacetylene membrane was kept at a proper potential. Timed release of the neurotransmitter was performed with the polyacetylene membrane. When the polyacetylene membrane was stimulated by an electric pulse, the entrapped acetyl choline was released from the matrix (137). A graphite membrane showed properties similar to the polyacetylene membrane in the timed release of acetyl choline (140).

Aizawa et al. have extended the idea that the electrically stimulated release of neurotransmitters may be accomplished with the electrochemical undoping of a conductive polymer membrane. They have also demonstrated the timed release of neurotransmitter amino acids such as glutamic acid with a polypyrrole membrane (140).

Miller et al. designed a chemically modified electrode to release neurotransmitters upon call (141). They coated them with polymers consisting of a stable polystyrene backbone linked to cationic isonicotinamide groups with cathodically cleavable amide bonds. Upon cleavage, these bonds released the neurotransmitters glutamic acid, γ-aminobutyric acid and dopamine.

As suggested by Miller, these devices likely will be useful not only for neurotransmitter studies, but also for other applications needing release of chemicals from a surface at an appropriate moment in response to an electric signal. In addition, using these devices for chemical communication will provide a bioaccessible interface which may find applications in connecting biosystems to non-biosystems.

Concluding Remarks

Many a biofunctional synthetic membranes have been developed, although they are far behind the actual biological membranes. There will be a significant growth in the use of the biofunctional synthetic membranes. Recent progress in molecular engineering should help to promote the materials science of the biofunctional synthetic membranes and thereby increase the use of biofunctional synthetic membranes.

Literature Cited

1. Grubhofer, N.; Griffin, E. G., Naturwiss. 1953, 40, 508.
2. Mitz, M. A. Science 1956, 123 1076.
3. Bernfeld, P.; Wan, J. Science 1963, 142 678.

4. Quiocho, F. A.; Richards, F. M. Proc. Natl. Acad. Sci. 1964, 52, 833.
5. Chang, T.M.S. Science 1964, 146, 524.
6. Gregoriadis, G.; Leathwood, P. D.; Ryman, B. E. FEBS Lett. 1971, 14, 95.
7. Silman, I. H.; Katchalski, E. Ann. Rev. Biochem 1966, 35, 873.
8. Katchalski, E.; Silman, I. H.; Goldman, R. Adv. Enzymol. 1971, 34, 445.
9. Smiley, K. L.; Strandberg, G. W. Adv. Appl. Microbiol. 1972, 15, 13.
10. Mosbach, K., FEBS Lett. 1976, 62, E80.
11. Jakoby, W. B.; Wilchek, M., Eds. Methods Enzymol., 34, Academic Press: New York, 1974.
12. Chibata, I., Ed. Immobilized Enzymes, Kodansha, 1975.
13. Fukui, S.; Tabushi, I.; Kunitake, T. Bioorganic Chemistry Kodansha, 1976.
14. Chibata, I.; Tosa, T.; Matsuo Y. Affinity Chromatography Kodansha 1976.
15. Mosbach, K., Ed. Methods Enzymol. 44 Academic Press: New York, 1976.
16. Weetall, H. H.; Suzuki, S., Eds. Immobilized Enzyme Technology Plenum Press: New York, 1975.
17. Zaborsky, O. Immobilized Enzymes, CRC Press (1972).
18. Fukui, S.; Chibata, I.; Suzuki, S., Eds., Enzyme Engineering Tokyo Kagaku Dojin, 1981.
19. Suzuki, S., Ed. Biomass Energy Conversion Kodansha, 1983.
20. Chibata, I.; Tosa, T. Hokko to Kogyo 1977, 35, 281.
21. Updike, S. J.; Hicks, G. P. Nature 1967, 214, 986: Science 1967, 158, 270.
22. Karube, I.; Suzuki, S. Biochem. Biophys. Res. Commun. 1972, 47, 51.
23. Venkatasubramanian, K.; Vieth, W. R.; Wang, S. S. J. Ferment. Technol. 1972, 50, 600.
24. Aizawa, M.; Morioka, A.; Suzuki, S. Anal. Chim. Acta 1980, 115, 61.
25. Drioli, E.; Iorio, G.; Morinari, R.; Rosa, M.; Gambacorta, A.; Esposito, E. Biotechnol. Bioeng. 1981, 23, 221.
26. Drioli, E.; Iorio, G.; Rosa, M.; Gambacora, A.; Nicolaus, B. Enzyme Engineering, VI (Ed. Chibata, I., et al.) Plenum Press: New York, 1982; p. 209.
27. Fukushima, S.; Nagai, T.; Fujita, K.; Tanaka, A.; Fukui, S. Biotechnol. Bioeng. 1978, 20, 1465.
28. Inman, D. J.; Hornby, W. E. Biochem. J. 1972, 129, 255: Campbell, J.; Hornby, W. E.; Morris, D. L. Biochim. Biophys. Acta 1975, 384, 307.
29. Maeda, H. Membrane 1984, 9, 14.
30. Fukushima, T. In Enzyme Engineering; Fukui, S. et al., Eds.; Tokyo Kagaku dojim; Tokyo: 1981; p. 285.
31. Michaels, A. S. Desalination 1980, 35, 329.
32. Drioli, E.; Iorio, G.; Morinari, R.; Rosa, M.; Gambacorta, A.; Esposito, E. J. Membrane Sci. 1980, 6, 345.

33. Scholander, P. F. Science 1960, 131, 585; Smith, K. A.; Meldon, J. K.; Colton, C. K. AIChE. J. 1973, 19, 102; Schultz, J. S.; Doddard, J. D.; Suchdeo, S. R. AIChE. J., 20, 417.
34. Selegny, E.; Broun, C.; Thomas, D. J. Memb. Biol. 1972, 8, 313.
35. Ishihara, K.; Kobayashi, M.; Shinohara, I. Macromol. Chem. Rapid Commun. 1983, 4, 327.
36. Namba, K.; Suzuki, S. Chem. Lett. 1975, 947.
37. Aizawa, M.; Namba, K.; Suzuki, S. Arch. Biochem. Biophys. 1977, 180, 41: 182, 305.
38. Suzuki, S.; Karuba, I.; Nakamoto, Y.; Namba, K. Enzyme Engineering III (Ed., Pye, K.; Weetall, H. H.) Plenum Press: New York, 1978, p. 163: Karuba, I.; Nakamoto, Y.; Namba, K.; Suzuki, S. Biochim. Biophys. Acta 1976, 429, 975.
39. Karube, I.; Nakamoto, Y.; Suzuki, S. Biochim. Biophys. Acta 1976, 445, 774: Nakamoto, Y.; Karube, I.; Terakawa, S.; Nishida, M.; Suzuki, S. J. Ferment. Technol. 1977, 55, 409.
40. Karube, I.; Yugeta, Y.; Suzuki, S. Biotechnol. Bioeng. 1977, 19, 1493.
41. Matsuoka, H.; Suzuki, S.; Aizawa, M.; Kimura, Y.; Ikegami, A. J. Appl. Biochem. 1981, 3, 437.
42. Tien, H. T. Bilayer Lipid Membranes (BLM): Theory and Practice, M. Dekker (1974).
43. Bangham, A. D.; Hill, M. W.; Miller, N.G.A. In Methods in Membrane Biology (E. D. Korn, Ed.), Vol. 1, Ch. 1, Plenum Press: New York, 1974.
44. Tien, H. T. Nature 1968, 219, 272: J. Phys. Chem. 1968, 72, 4512.
45. Steinemann, A.; Stark, G.; Laeuger, P. J. Memb. Biol. 1972, 9, 177: Cherry, R. J.; Hsu, K.; Chapman, D. Biochim. Biophys. Acta 1972, 288, 12: Weller, H.; Tien, H. T. Biochim. Biophys. Acta.
46. Tributtsch, H.; Calvin, M. Photochem. Photobiol. 1971, 14, 95.
47. Takahashi, F.; Kikuchi, R. Biochim. Biophys. Acta 1976, 430, 490.
48. Takahashi, F.; Aizawa, M.; Kikuchi, R.; Suzuki, S. Electrochim. Acta 1977, 22, 289.
49. Fong, F. K.; Winograd, N. J. Am. Chem. Soc. 1976, 98, 2287.
50. Fruge, D. R.; Fong, G. D.; Fong, F. K. J. Am. Chem. Soc. 1979, 101, 3694.
51. Aizawa, M.; Hirano, M.; Suzuki, S. Electrochim. Acta 1978, 23, 1185.
52. Aizawa, M.; Hirano, M.; Suzuki, S. J. Memb. Sci. 1978, 4, 251.
53. Aizawa, M.; Hirano, M.; Suzuki, S. Electrochim. Acta 1979, 24, 89.
54. Aizawa, M.; Yoshitake, J.; Suzuki, S. Mol. Cryst. Liq. Cryst. 1981, 70, 129.
55. Miyasaka, T.; Watanabe, T.; Fujishima, A.; Honda, K. J. Am. Chem. Soc. 1978, 100, 6657.
56. Aizawa, M.; Shinohara, H.; Watanabe, S. Denki Kagaku 1982, 50, 854.
57. Dancshazy, Z.; Karvaly, B. FEBS Lett. 1976, 72, 136.

58. Herrmann, T. R.; Rayfield, G. W. Biochim. Biophys. Acta 1976, 443, 623.
59. Shieh, P.; Packer, L. Biochem. Biophys. Res. Commun. 1976, 71, 603.
60. Skulachev, V. P. FEBS Lett. 1977, 64, 23.
61. Packer, L.; Konishi, T.; Shieh, P. In Living Systems as Energy Converters; R. Buvet et al., Eds.; Elsevier: 1977; p. 119.
62. Tang, C. W.; Albrecht, A. C. Mol. Cryst. Liq. Cryst. 1974, 25, 53.
63. Langmuir, I.; Schafer, V. J. J. Am. Chem. Soc. 1937, 59, 2075.
64. Hanson, E. A. Rec. Trav. Botan. Neerl. 1939, 36, 180.
65. Bellamy, W. D.; Gaines, G. L.; Tweet, A. G. J. Chem. Phys. 1963, 39, 2528.
66. Shieh, P.; Tien, H. T. J. Bioenerg. 1974, 6, 45.
67. Tien, H. T. In Photosynthesis in Relation to Model Systems; J. Baker, Ed.; Elsevier: 1979; p. 116.
68. Hong, F. T. Photochem. Photobiol. 1976, 24, 155.
69. Gross, E. L.; Youngman, D. R.; Winemiller, S. L. Photochem. Photobiol. 1978, 28, 249.
70. Ocjiai, H.; Shibata, H.; Matsuo, T.; Hashinokuchi, K.; Inamura, I. Agric. Biol. Chem. 1978, 42, 683.
71. Miyasaka, T.; Honda, K In ACS Symposium Series: Photoeffects at Semiconductor-Electrolyte Interfaces American Chemical Society: Washington, D.C., 1980; p. 1.
72. Mueller, P.; Pugh, E. N., Jr. Proc. Natl. Acad. Sci. 1983, 80, 1892.
73. O'Brien, D. F. Science 1982, 218, 961.
74. Aizawa, M.; Tomono, S.; Suzuki, S. J. Memb. Sci. 1977, 2, 289.
75. Aizawa, M.; Tomono, S.; Suzuki, S. J. Memb. Sci. 1980, 6, 235.
76. Kato, S.; Aizawa, M.; Suzuki, S. J. Memb. Sci. 1976, 1, 289.
77. Kato, S.; Aizawa, M.; Suzuki, S. J. Memb. Sci. 1977, 2, 39.
78. Kato, S.; Aizawa, M.; Suzuki, S. J. Memb. Sci. 1978, 3, 29.
79. Updike, S. J.; Hicks, G. P. Nature 1967, 264, 986.
80. Nagy, L. H.; Guibault, G. G. Anal. Chim. Acta 1973, 66, 443.
81. Thevenot, D. R.; Sternberg, R.; Coulet, P. R.; Laurent, J.; Gautheron, D. C. Anal. Chem. 1979, 51, 96.
82. Koyama, M.; Sato, Y.; Aizawa, M.; Suzuki, S. Anal. Chim. Acta 1980, 116, 307.
83. Guilbault, G. G. Handbook of Enzymatic Methods of Analysis M. Dekker: 1976.
84. Suzuki, S., Ed. Ion and Enzyme Electrodes Kodansha: 1974.
85. Suzuki, S., Ed. Biosensors Kodansha: 1984.
86. Aizawa, M. In Chemical Sensors; T. Seiyama, J. Shiokawa, S. Suzuki, and K. Fueki, Eds.; Elsevier: 1983; p. 683.
87. Ikariyama, Y.; Aizawa, M.; Suzuki, S. J. Solid-Phase Biochem. 1980, 5, 223.
88. Aizawa, M.; Ikariyama, Y.; Kuno, K. Anal. Lett. (in press).
89. Karube, I.; Mitsuda, S.; Matsunaga, T.; Suzuki, S. J. Ferment. Technol. 1977, 55, 243.

90. Hikuma, M.; Kubo, T.; Yasuda, T.; Karube, I.; Suzuki, S. Biotechnol. Bioeng. 1979, 21, 2845.
91. Hikuma, M.; Kubo, T.; Yasuda, T.; Karube, I.; Suzuki, S. Anal. Chim. Acta 1979, 109, 33.
92. Matsunaga, T.; Karube, I.; Suzuki, S. Europ. J. Appl. Microbiol. Biotechnol. 1980, 10, 235.
93. Hikuma, M.; Kubo, T.; Yasuda, T.; Karube, I.; Suzuki, S. Anal. Chim. Acta 1980, 116, 61.
94. Hikuma, M.; Obana, H.; Yasuda, T.; Karube, I.; Suzuki, S. Anal. Chim. Acta 1980, 116,   .
95. Rechnitz, G. A.; Rechel, T. L.; Kobos, R. K.; Meyerhoff, M. E. Science 1978, 199, 440.
96. Rechnitz, G. A.; Kobos, T. L.; Riechel, R. K.; Gebauer, C. R. Anal. Chim. Acta 1977, 94, 357.
97. Kobos, R. K.; Rechnitz, R. G. Anal. Lett. 1977, 10, 751.
98. Hikuma, M.; Kubo, T.; Yasuda, T.; Karube, I.; Suzuki, S. Anal. Chim. Acta.
99. Karube, I.; Matsunaga, T.; Suzuki, S. Anal. Chim. Acta 1979, 109, 39.
100. Matsunaga, T.; Karbue, I.; Suzuki, S. Anal. Chim. Acta 1978, 99, 233.
101. Matsunaga, T.; Karube, I.; Suzuki, S. Anal. Chim. Acta 1978, 98, 25.
102. Matsunaga, T.; Seijo, H.; Watanabe, T.; Karube, I.; Satoh, I.; Suzuki, S. Anal. Chim. Acta 1979, 106, 369.
103. Hikuma, M.; Suzuki, H.; Yasuda, T.; Karube, I.; Suzuki, S. Europ. J. Appl. Microbiol. Biotechnol. 1979, 37, 117.
104. Matsunaga, T.; Karube, I.; Suzuki, S. Appl. Environ. Microbiol. 1979, 37, 117.
105. Suzuki, S.; Karube, I. Appl. Biochem. Bioeng. 1981, 3, 145.
106. Hikuma, M.; Yasuda, T.; Karube, I.; Suzuki, S. Ann. N.Y. Acad. Sci. 1981, 369, 307.
107. Karube, I.; Matsunaga, T.; Nakahara, T.; Suzuki, S. Anal. Chim. Acta 1981, 53, 1024.
108. Aizawa, M.; Kato, S.; Suzuki, S. J. Memb. Sci. 1977, 2, 125.
109. Castillo, J. Del; Rodriguez, A.; Romero, C. A.; Sanchez, V. Science 1966, 153, 185.
110. Michaelis, D. W.; Abramowitz, A. S.; Hammer, C. H.; Mayer, M. M. Proc. Natl. Acad. Sci., U.S.A. 1976, 73, 2852.
111. Rosentreich, D. L.; Blumenthal, R. J. Immunol., 1977, 118, 129.
112. Wobschall, D.; Mecheon, C. Biochim. Biophys. Acta 1975, 413, 317.
113. Wolf, D. E.; Schlessinger, J.; Elson, E. L.; Webb, W. W.; Blumenthal, R.; Henkart, P. Biochemistry 1977, 16, 3476.
114. Mountz, J. D.; Tien, H. T. J. Bioenerg. Biomembranes 1978, 10, 139.
115. Janata, J. J. Am. Chem. Soc. 1975, 97, 2914.
116. Aizawa, M.; Kato, S.; Suzuki, S. J. Memb. Sci. 1980, 7, 1.
117. Aizawa, M.; Suzuki, S.; Nagamura, Y.; Shinohara, R.; Ishiguro, I. J. Solid-Phase Biochem. 1979, 4, 25.
118. Aizawa, M.; Suzuki, S.; Nagamura, Y.; Shinohara, R.; Ishiguro, I. Chem. Lett. 1977, 779.

119. Aizawa, M.; Suzuki, S.; Nagamura, Y.; Shinohara, R.; Ishiguro, I. Kobunshi Ronbunshu 1977, 34.
120. Yamamoto, N.; Nagasawa, Y.; Sawai, M.; Suda, T.; Tsubomura, H. J. Immunol. Method. 1979, 22, 309.
121. Yamamoto, N.; Nagasawa, Y.; Shuto, S.; Tsubomura, H.; Sawai, M.; Okumura, H. Clin. Chem. 1980, 26, 1569.
122. Aizawa, M.; Morioka, A.; Matsuoka, H.; Suzuki, S. J. Solid Phase Biochem. 1976, 1, 319.
123. Aizawa, M.; Morioka, A.; Suzuki, S. J. Memb. Sci. 1978, 4, 221.
124. Aizawa, M.; Morioka, A.; Suzuki, S.; Nagamura, Y. Anal. Biochem. 1979, 94, 22.
125. Aizawa, M.; Morioka, A.; Suzuki, S. Anal. Chim. Acta 1980, 115, 61.
126. D'Oraizio; Rechnitz, G. A. Anal. Chem. 1977, 49, 2083.
127. Boitieux, J. L.; Desnel, G.; Thomas, D. Clin. Chem. 1979, 25, 318.
128. Shiba, K.; Umezawa, Y.; Watanabe, T.; Ogawa, S.; Fujiwara, S. Anal. Chem. 1980, 52, 1610.
129. Aizawa, M.; Suzuki, S. Jap. J. Appl. Phys., 1983, 21(1), 219.
130. Ikariyama, Y.; Aizawa, M. Proc. 2nd Sensor Symp., 1982, 97.
131. Ikariyama, Y.; Aizawa, M. Proc. Intl. Meeting Chemical Sensors, 1983, 693.
132. Ikariyama, Y.; Aizawa, M. Proc. 3rd Sensor Symp., 1983, 17.
133. Aizawa, M.; Ikariyama, Y. Toyoshima, T. J. Chem. Soc. Jap. 1983, 819.
134. Aizawa, M.; Ikariyama, Y.; Toyoshima, T. Kobunshi Ronbunshu (in press).
135. Aizawa, M.; Ikariyama, Y.; Kuno, K. Anal. Lett. (in press).
136. Schultz, J. S.; Mansouri, S.; Goldstein, I. J. Diabetes Care 1982, 5, 235.
137. Aizawa, M.; Shinohara, H.; Shirakawa, H. Proc. Ann. Meeting Electrochem. Soc. Japn., 1983, p. 223: Denki Kagaku 1983, 51, 951.
138. Shirakawa, H.; Yamabe, T., Eds. Synthetic Metals Kagaku Dojin: 1980.
139. Chem. Soc. Hapn., Ed. Chemistry of Low Dimensional Conducting Compounds, Gakkai Shuppan Center: 1983.
140. Aizawa, M.; Shinohara, H.; Shirakawa, H. Ann. Meeting Electrochem. Soc. Japn., 1983, p. 151.
141. Miller, L. L.; Lau, A.N.K.; Zinger, B.; Lente, M. V. J. Am. Chem. Soc., 1983, 105, 5271.

Author Index

Aizawa, Masuo, 447
Babcock, W. C., 409
Bateman, Blaine R., 119
Bresnahan, P. A., 409
Cabasso, Israel, 305
Cadotte, John E., 273
Chern, R. T., 25
Feldhoff, Pamela W., 99
Finken, Heinz, 245
Gerlach, K., 229
Hiatt, W. C., 229
Hoehn, H. H., 81
Hopfenberg, H. B., 25
Josefiak, C., 229
Kamide, Kenji, 197
Kesting, R. E., 131
Klein, Elias, 99
Koros, W. J., 25

Krause, Sonja, 351
Kyu, Thein, 365
Lee, Eric K. L., 409
Lloyd, Douglas R., 1,47
Manabe, Sei-ichi, 197
Meluch, Timothy B., 47
Noble, Richard D., 119
Smolders, C. A., 327
Spencer, H. Garth, 295
Stannett, V. T., 25
Strathmann, H., 165
Tkacik, Gabriel, 339
Vitzthum, G. H., 229
Vugteveen, E., 327
Wagener, K. B., 229,429
Ward, Richard A., 99
Way, J. Douglas, 119
Zeman, Leos, 339

Subject Index

A

Acetylene, polymerization, 433-34
Acrylic polymers, 105
Aliphatic acid esters of wood,
    apparent melting
    temperatures, 153,154t
Amalgamation of primary
    particles, 201,204f
Amorphous polymers, 55
Annealing
  cellulose acetate blend
      membranes, 262,264,266f
  porous membranes, 148-49
Apparent solubilities
  glassy polymers, 33,34t
  penetrants in glassy
      polymers, 35,36f
Aromatic polyamide membranes, 81-96
Asymmetric membranes
  characterization methods, 327-38
  gas separations, 245-70
  morphology, 88-91
  permeation properties, 89

B

Bacteriorhodopsin-containing
    membrane, 459
Bilayer lipid membranes,
    pigmented, 456,457f,459
Binary system with limited
    miscibility, kinetic and ther-
    modynamic descriptions, 183-85
Binodal-spinodal phase diagram,
    polymer-solvent-nonsolvent
    system, 230-32
Bioaffinity membranes, homologous and
    heterologous, 471,473,474f
Biocatalytic function,
    regulation, 453-54
Biocatalytic membranes, 448-54
Biofunctional synthetic
    membranes, 447-75
Biomimetic-controlled membrane tran-
    sport systems, 452f
Biosensors, functional concept using
    bioactive substances, 464,465f
Blushing, phase inversion
    membranes, 161-62

483

Author Index

Aizawa, Masuo, 447
Babcock, W. C., 409
Bateman, Blaine R., 119
Bresnahan, P. A., 409
Cabasso, Israel, 305
Cadotte, John E., 273
Chern, R. T., 25
Feldhoff, Pamela W., 99
Finken, Heinz, 245
Gerlach, K., 229
Hiatt, W. C., 229
Hoehn, H. H., 81
Hopfenberg, H. B., 25
Josefiak, C., 229
Kamide, Kenji, 197
Kesting, R. E., 131
Klein, Elias, 99
Koros, W. J., 25

Krause, Sonja, 351
Kyu, Thein, 365
Lee, Eric K. L., 409
Lloyd, Douglas R., 1,47
Manabe, Sei-ichi, 197
Meluch, Timothy B., 47
Noble, Richard D., 119
Smolders, C. A., 327
Spencer, H. Garth, 295
Stannett, V. T., 25
Strathmann, H., 165
Tkacik, Gabriel, 339
Vitzthum, G. H., 229
Vugteveen, E., 327
Wagener, K. B., 229,429
Ward, Richard A., 99
Way, J. Douglas, 119
Zeman, Leos, 339

Subject Index

A

Acetylene, polymerization, 433-34
Acrylic polymers, 105
Aliphatic acid esters of wood,
    apparent melting
    temperatures, 153,154t
Amalgamation of primary
    particles, 201,204f
Amorphous polymers, 55
Annealing
  cellulose acetate blend
    membranes, 262,264,266f
  porous membranes, 148-49
Apparent solubilities
  glassy polymers, 33,34t
  penetrants in glassy
    polymers, 35,36f
Aromatic polyamide membranes, 81-96
Asymmetric membranes
  characterization methods, 327-38
  gas separations, 245-70
  morphology, 88-91
  permeation properties, 89

B

Bacteriorhodopsin-containing
    membrane, 459
Bilayer lipid membranes,
    pigmented, 456,457f,459
Binary system with limited
    miscibility, kinetic and ther-
    modynamic descriptions, 183-85
Binodal-spinodal phase diagram,
    polymer-solvent-nonsolvent
    system, 230-32
Bioaffinity membranes, homologous and
    heterologous, 471,473,474f
Biocatalytic function,
    regulation, 453-54
Biocatalytic membranes, 448-54
Biofunctional synthetic
    membranes, 447-75
Biomimetic-controlled membrane tran-
    sport systems, 452f
Biosensors, functional concept using
    bioactive substances, 464,465f
Blushing, phase inversion
    membranes, 161-62

483